



HAL
open science

Développement de molécules anti-tumorales pour le traitement du gliome sur la base de dérivés de toxines animales

Lucie Dardevet

► **To cite this version:**

Lucie Dardevet. Développement de molécules anti-tumorales pour le traitement du gliome sur la base de dérivés de toxines animales. Médecine humaine et pathologie. Université Grenoble Alpes, 2016. Français. NNT : 2016GREAV047 . tel-01819702

HAL Id: tel-01819702

<https://theses.hal.science/tel-01819702>

Submitted on 20 Jun 2018

HAL is a multi-disciplinary open access archive for the deposit and dissemination of scientific research documents, whether they are published or not. The documents may come from teaching and research institutions in France or abroad, or from public or private research centers.

L'archive ouverte pluridisciplinaire **HAL**, est destinée au dépôt et à la diffusion de documents scientifiques de niveau recherche, publiés ou non, émanant des établissements d'enseignement et de recherche français ou étrangers, des laboratoires publics ou privés.

THÈSE

Pour obtenir le grade de

DOCTEUR DE L'UNIVERSITÉ GRENOBLE ALPES

Spécialité : **Sciences du médicament**

Arrêté ministériel : 7 août 2006

Présentée par

Lucie DARDEVET

Thèse dirigée par **Michel DE WAARD**

préparée au sein du **l'Institut des Neurosciences de Grenoble**
dans **l'École Doctorale Chimie et Sciences du Vivant**

Développement de molécules anti-tumorales pour le traitement du gliome sur la base de dérivés de toxines animales

Thèse soutenue à huis-clos le : **27 Octobre 2016**

devant le jury composé de :

Mme, Chrystelle, BRETON

Professeur des Universités de l'université Grenoble Alpes, Présidente

Mr, Bernard, LEBLEU

Professeur Emérite de l'université de Montpellier, Rapporteur

Mr, Jean-Pierre, POUGET

Chargé de recherche à l'Institut de Recherche en Cancérologie de
Montpellier, Rapporteur

Mr, Jean-Marc, SABATIER

Directeur de recherche au sein de l'UMRs-1097 Aix Marseille Université,
Examineur

Mr, Michel, DE WAARD

Directeur de recherche à l'institut du thorax à Nantes, Directeur de Thèse



« La vérité de demain se nourrit de l'erreur d'hier »
Antoine de Saint-Exupéry

Remerciements

Je remercie tout d'abord mon directeur de thèse, **Michel De Waard** pour m'avoir proposé ce sujet de thèse et accueilli au sein de son équipe. Grâce à vous j'ai pu travailler avec une grande autonomie et être impliqué dans d'autres projets menés au sein de l'équipe.

Je tiens aussi à remercier le Labex ICST (Laboratory of Excellence in Ion Channel Science and Therapeutics) pour m'avoir attribué une bourse afin de réaliser ces travaux.

J'exprime tous mes remerciements à l'ensemble des membres de mon jury : **Christelle Breton, Bernard Lebleu, Jean-Pierre Pouget, Jean-Marc Sabatier**. Merci d'avoir accepté d'évaluer mon travail.

Au cours de cette thèse j'ai eu l'occasion de collaborer avec plusieurs personnes que je ne peux pas toutes citer, mais je souhaiterais remercier **Sonia Aroui, Mayeul Collot, Ryan Arrant** et **Julien Pêcher**, pour leur aide technique et leur conseil scientifique.

Je remercie aussi les membres de l'équipe 3 du GIN pour leur accueil. **Céline, Élodie, Marwa, Nadia, Christelle, Gaëtan, Mohamad** et **Manu**, vous avez fait du laboratoire un endroit chaleureux où j'ai beaucoup apprécié travailler. Merci de votre soutien et de votre aide, je vous souhaite le meilleur pour la suite.

Impossible de ne pas remercier **Nath**, la meilleure secrétaire gestionnaire que j'aurais pu avoir. Merci pour ton soutien et ton aide administratif ou non-administratif, mais surtout pour ton amitié. Ton bureau a été pour moi un petit refuge qui va me manquer. Je te dis : « À plus dans le bus ! »

Un grand merci aussi à l'équipe 1 de l'institut, mon équipe d'adoption sur la fin de cette thèse. Merci de m'avoir accueilli lorsque je cherchais un bureau pour rédiger, et de m'avoir invité à participer à vos activités extra-laboratoire (sortie ski, soirée jeux société). Vous m'avez montré qu'une équipe de laboratoire peut ressembler beaucoup à une grande famille.

Durant ces quelques années passées au GIN, j'ai eu le plaisir de faire partie des **Neurodocs**, groupe de doctorant participant à la vie de l'institut. À tous, je voudrais vous dire que j'ai vraiment apprécié ces moments passés avec vous que ce soit pour l'organisation d'événements : pique-nique de l'institut, les deux éditions du meeting européen de neurosciences pour doctorants ou pour simplement décompresser après le travail.

Cette thèse a aussi été l'occasion pour moi de faire la connaissance de personnes formidables, qui méritent chacune mes plus profonds remerciements.

Céline, que te dire à part merci, tu fus l'un des premiers visages amicaux que j'ai vus quand je suis arrivée au laboratoire. Travailler avec toi a été « Fantastique ». Je te suis reconnaissante pour tous ces moments passés ensemble, au labo et en dehors. Merci pour ton soutien, merci de me montrer qu'il y a mieux ailleurs et qu'il y a vraiment de la lumière au bout du tunnel. Je te souhaite de tout cœur le meilleur pour le futur tu l'as amplement mérité.

Élodie, je t'ai connu comme stagiaire de M2, maintenant tu es la maman de mon adorable filleule ! Tu as fait beaucoup pour moi, été là en cas de besoin, m'aider à maîtriser ma peur des chiens (coucou Euka !), mais aussi et surtout partager ton grain de folie avec moi. Merci de me rappeler d'être le grand enfant que je suis. Alors à toi et à ta petite famille simplement merci d'être là.

Julie, ma copine de labo, merci de répondre toujours présente quand j'ai besoin de parler (râler), j'espère te rendre la pareille quand tu en auras besoin. Merci pour toutes ces discussions, fou rire, repas, soirée ciné partagées. Toute cette aventure qu'est la thèse aurait été bien différente sans toi. Alors bon courage pour la fin de ta thèse, c'est la dernière étape !

Manu, même si tu es arrivé à la fin de ma thèse, ça été un plaisir de travailler avec toi, toujours de bonne humeur et prêt à aider. Merci pour ton aide mais surtout pour tous ces moments de complicité et ces fous rires partagés à la paillasse, certains ont été salutaires. Je te souhaite à toi et à ta famille le meilleur pour la suite.

Et parce qu'il n'y a pas que la thèse et le laboratoire dans la vie d'un doctorant, et que je ne saurais probablement pas la personne que je suis sans eux, un énorme merci à ma famille. Votre soutien inconditionnel, vos encouragements et votre présence à mes côtés me sont essentiels. Je sais que je ne vous rends pas toujours la tâche facile, alors merci d'être là prêt à tous pour m'aider. Je vous aime.

Maman, papa, je sais que vous avez subi avec moi cette dernière année, merci d'avoir toujours cru en moi souvent plus que moi-même. À mes sœurs, **Marie-Charlotte** et **Mathilde**, merci de votre soutien et d'être les personnes que vous êtes, vous m'avez apporté beaucoup plus que vous ne le pensez.

Listes des principales abréviations

Abu :	Acide Aminobutyrique
AChE :	Acétylcholine Estérase
ADN :	Acide Désoxyribonucléique
ANSM :	Agence nationale de sécurité du médicament
ARN :	Acide Ribonucléique
ATP :	Adénosine Triphosphate
BHE :	Barrière Hémato-Encéphalique
CFTR :	Cytic Fibrosis Transmembrane Conductance Regulator
CPP :	Cell Penetrating Peptide
CTX :	Chlorotoxine
EGFR :	Epidermal Growth Factor Receptor
EMA :	European Medicines Agency
FACS :	Fluorescence-Activated Cell Sorting
FDA :	Food and Drug Administration
FITC :	Isothiocyanate de Fluorescéine
Fmoc :	9-Fluorenylmethoxycarbonyl
GFP :	Green Fluorescence Protein
GSH :	Forme réduite du glutathion
GST :	Forme oxydé du glutathion
IC ₅₀ :	Concentration D'inhibition 50%
ICK :	Inhibition Cystin-Knot
IRM :	Imagerie à Résonance Magnétique
IV :	Intraveineuse
LD ₅₀ :	Léthal Dose 50% ou médiane léthal dose
MCa :	Maurocalcine
MMP-2 :	Matrice Metalloprotéase MMP-2
MTT :	Thiazolyl Blue Tetrazolium Blue
NLS :	Nuclear Localisation Sequence
PEG :	Polyethylene Glycol
PTD :	Protein Transduction Domaine
ROS :	Espèce Réactives de l'Oxygène
RyR :	Récepteur A La Ryanodine
TAT :	Trans-Activator of Transcription
VIH-1 :	Virus de l'Immunodéficience Humaine de Type 1

Table des matières

Listes des principales abréviations	7
Table des figures	12
Liste des tableaux	13
Introduction.....	15
Rappel bibliographique.....	21
<u>Chapitre 1 : La maurocalcine.....</u>	<u>23</u>
I. Les peptides de pénétration cellulaire	23
a. Définition et découverte.....	23
b. Classification.....	25
c. Voies d'entrées dans la cellule	27
d. Intérêt clinique des CPP.....	32
II. La maurocalcine, un CPP à part entière.....	35
a. Description et découverte.....	35
b. Effet pharmacologique.....	36
c. La MCa en tant que CPP.....	37
<u>Chapitre 2 : Toxine de ciblage : Chlorotoxine.....</u>	<u>39</u>
I. Chlorotoxine.....	39
a. Découverte et présentation	39
b. Effet biologique.....	40
c. Les chlorotoxine-like peptides.....	42
II. Chlorotoxine et chlorotoxine-like peptide : applications thérapeutiques	45
a. Agent de marquage.....	45
b. Agent thérapeutique.....	48
<u>Chapitre 3 : Glioblastome et anticancéreux.....</u>	<u>51</u>
I. Le glioblastome	51
a. Description et impact.....	51

<i>b. Prise en charge thérapeutique</i>	52
<i>c. Les futurs traitements</i>	54
II. La doxorubicine.....	57
<i>a. Présentation, historique</i>	57
<i>b. Mécanisme d'action</i>	57
<i>c. Les résistances à la doxorubicine</i>	59
III. Le cisplatine et ses dérivés	61
<i>a. Présentation, historique</i>	61
<i>b. Mécanismes d'action</i>	62
<i>c. Les résistances au cisplatine</i>	63
<u>Chapitre 4 : La chimie click</u>	<u>65</u>
I. La chimie click : concept	65
<i>a. Généralités</i>	65
<i>b. Les réactions clicks</i>	67
<i>c. Huisgen 1.3 dipolar cycloaddition</i>	68
II. Les applications de la chimie click en biologie	70
<i>a. Découvertes / synthèses de nouvelles molécules</i>	70
<i>b. Bioconjugaison</i>	71
<i>c. Sciences de polymères</i>	73
Travaux de thèse.....	75
<u>Chapitre 1 : Administration ciblés de doxorubicine</u>	<u>77</u>
I. Introduction.....	77
II. Conclusions.....	114
<u>Chapitre 2 : La maurocalcine comme vecteur d'un dérivé du cisplatine.</u>	<u>115</u>
I. Introduction.....	115
II. Conclusions.....	133
<u>Chapitre 3 : La maurocalcine, vecteur de doxorubicine</u>	<u>134</u>
I. Introduction.....	134
II. Matériels et méthodes.....	135
<i>a. Modélisation moléculaire</i>	135

<i>b. Synthèse peptidique.....</i>	<i>135</i>
<i>c. Couplage de la doxorubicine-alkyne avec les vecteurs</i>	<i>136</i>
<i>d. Culture cellulaire.....</i>	<i>136</i>
<i>e. Etude microscopies.....</i>	<i>136</i>
<i>f. Evaluation de la pénétration des composés</i>	<i>137</i>
<i>g. Essai de toxicité et cytométrie en flux.....</i>	<i>137</i>
<i>h. Test MTT.</i>	<i>138</i>
III. Résultats.....	138
<i>a. Conception et synthèse des nouveaux composés</i>	<i>138</i>
<i>b. Evaluation de l'efficacité in vitro des nouveaux composés synthétisés.....</i>	<i>139</i>
<i>c. Caractérisation des nouveaux composés à base de doxorubicine.....</i>	<i>142</i>
IV. Conclusions	145
Conclusions et perspectives	147
Annexes	155
<u>Article 1:</u> Cell Penetration Properties of a Highly Efficient Mini Maurocalcine Peptide.....	157
<u>Article 2:</u> Quantitative evaluation of the cell penetrating properties of an iodinated Tyr-L-maurocalcine analog	181
<u>Article 3:</u> Chlorotoxin: A Helpful Natural Scorpion Peptide to Diagnose Glioma and Fight Tumor Invasion.....	193
<u>Article 4:</u> H-Rubies, a new family of red emitting fluorescent pH sensors for living cells.....	219
<u>Article 5:</u> In cellulo phosphorylation induces pharmacological reprogramming of maurocalcin, a cell-penetrating venom peptide.....	231
Références	263

Table des figures

Figure 1 : <i>Distribution des CPP en fonction de leur charge nette (D'après Milletti, 2012 (modifié))</i>	25
Figure 2 : <i>Modèle de la micelle inversée</i>	29
Figure 3 : <i>Illustration de la translocation selon les modèles de « barrel - Stave » et de « carpet ». (D'après Lundberg and Langel, 2003 (modifié))</i>	30
Figure 4 : <i>Mécanisme d'entrée des CPP (D'après Durzyńska et al., 2015 (Modifié))</i>	31
Figure 5 : <i>Applications des CPP comme vecteur</i>	32
Figure 6 : <i>A. Séquence peptidique de la MCa ; B. Représentation tridimensionnel de la MCa ; C. Scorpio maurus palmatus (crédit photo : Stuart Summerfield)</i>	35
Figure 7 : <i>Activation du RyR par la MCa</i>	36
Figure 8 : <i>A. Séquence peptidique de la CTX ; B. Représentation tridimensionnelle de la CTX ; C. Scorpion Leiurus quinquestriatus</i>	39
Figure 9 : <i>Structure chimique de la doxorubicine</i>	57
Figure 10 : <i>Structure des dérivés du platine commercialisé dans le monde</i>	61
Figure 11 : <i>Mécanisme d'action du cisplatine</i>	62
Figure 12 : <i>Classification des différentes click réaction, (d'après Hein et al., 2008a)</i>	66
Figure 13 : <i>A. Click réaction énergétiquement favorable ; B. Exemple d'une cycloaddition catalysé par le cuivre et comparaison structurale et électronique d'une liaison peptidique et d'une liaison 1,2,3 triazole. D'après (Kolb and Sharpless, 2003)</i>	68
Figure 14 : <i>Mécanisme réactionnel de la cycloaddition dipolaire de Huisgen, D'après (Bock et al., 2006; Hein et al., 2008)</i>	69
Figure 15 : <i>Représentation schématique du couplage entre la tacrine et un fragment alkyne dans le site actif de l'AChE. (Moorhouse and Moses, 2008)</i>	71
Figure 16 : <i>Application de la bioconjugaison par cycloaddition d'azide et acétylène. D'après (Kolb and Sharpless, 2003)</i>	72
Figure 17 : <i>Synthèse de la M_{CaUF1,9} et de la D-MCa et couplage avec la doxorubicine-alkyne</i> ..	139
Figure 18 : <i>Toxicité de la doxorubicine, doxorubicine alkyne, doxorubicine D-MCa et doxorubicine M_{CaUF1,9}</i>	141
Figure 19 : <i>Localisation cellulaire de la doxorubicine, doxorubicine alkyne, doxorubicine D-MCa et doxorubicine M_{CaUF1,9} chez des cellules F-98</i>	142

Figure 20 : Localisation cellulaire de la doxorubicine, doxorubicine alkyne, doxorubicine D-MCa et doxorubicine M _{CaUF1,9} chez des cellules MDA-MB-435s	143
Figure 21 : Localisation cellulaire de la doxorubicine, doxorubicine alkyne, et doxorubicine D-MCa chez des cellules MDA-MB-231	143
Figure 22 : Pénétration de la doxorubicine, doxorubicine alkyne, doxorubicine D-MCa et doxorubicine M _{CaUF1,9} chez des cellules F-98 (A.), MDA-B-435s (B.) et MDA-MB-231 (C.), après deux heures d'incubations.....	144

Liste des tableaux

Tableau 1 : Exemple de CPP avec leur origine et séquence.....	24
Tableau 2 : Définition des différentes voies de pénétration dans une cellule.....	28
Tableau 3 : Complexe à base de CPP en essai clinique.....	34
Tableau 4 : Alignement des structures primaires de la CTX et des chlorotoxine-like peptides	43
Tableau 5 : Exemples de complexes CTX-cargo et leurs applications	47

Introduction

De nos jours, il est de plus en plus difficile pour la recherche Pharmaceutique de développer/mettre sur le marché de nouvelles molécules thérapeutiques. Des problèmes économiques, avec la chute dans le domaine public de brevets de nombreux « blockbuster », ou de l'essentiel du catalogue de certaines industries, viennent impacter les moyens financiers mis à disposition pour la recherche et le développement de nouveaux composés. À ces problèmes, se rajoutent le durcissement du cahier des charges que doivent remplir les futurs médicaments. Et bien sûr, il reste toujours aussi difficile d'identifier et de développer un nouveau médicament.

En effet, identifier, une molécule comme étant active sur une cible d'intérêt, n'est que la 1^{ère} étape du développement d'un médicament, et elle est loin d'être l'étape limitante. Ainsi de nombreux hits sont abandonnés, condamnés à rester dans un placard malgré leurs activités car ils ne possèdent pas les caractéristiques nécessaires à la poursuite des recherches (faibles solubilités, incapacités à franchir les membranes, effets secondaires trop importants, efficacité moindre que les molécules concurrentes, plus-value discutable...). À ces « défauts » des molécules, se rajoutent la difficulté d'atteindre la cible. Avec l'avancée de la recherche fondamentale, on possède une meilleure connaissance des maladies et la liste des cibles pour agir sur ces maladies augmente. Cependant ces cibles sont pour certaines difficiles à atteindre de par leurs localisations intracellulaires. À ces problèmes de développement s'ajoutent les problèmes après mise sur le marché. En effet l'apparition de mécanismes de résistance (inactivation, pompe à efflux...) diminue d'autant la durée de vie des médicaments, et donc rend la recherche pharmaceutique encore plus chère et difficile.

Ainsi une grande partie de la recherche appliquée publique se consacre au développement de nouveaux systèmes de vectorisation. Ces systèmes regroupent à la fois de nouvelles formulations galéniques (microémulsions, liposomes..), de nouvelles techniques d'administration (technologie sonique pour perméabiliser la BHE), la création de nanoparticules (nanovecteurs), mais aussi l'utilisation de peptides de pénétration cellulaire, et la découverte de molécules de ciblage afin d'améliorer la vectorisation ciblée de composés.

Le glioblastome est un cancer touchant le cerveau, dont le traitement est rendu difficile par sa localisation et la présence de la BHE. C'est dans l'optique d'améliorer sa prise en charge que mes travaux de thèse se sont déroulés. Les objectifs de ces travaux de thèse étaient

l'utilisation de toxines animales comme vecteurs peptidiques d'anticancéreux connus afin d'en améliorer leur pénétration et rétention dans la cellule ou afin de cibler leur administration précisément aux cellules cancéreuses. Pour ceux faire j'ai concentré mes efforts sur la maurocalcine et ses analogues (pour la pénétration et rétention) et sur la chlorotoxine et ses analogues (pour le ciblage).

La maurocalcine et ses analogues sont étudiés et caractérisés dans le laboratoire au cours de ces dernières années comme des peptides de pénétration cellulaire ayant un intérêt dans l'administration de composés variés. L'utilisation d'analogues de la maurocalcine comme de ses substances actives permet de modifier leur pharmacocinétique, leur biodistribution et contrer les mécanismes de résistance, et ce uniquement en améliorant leur pénétration et leur rétention dans les cellules. La chlorotoxine est connue depuis quelques années comme ayant la particularité de cibler les cellules cancéreuses de gliome. Des toxines présentant des analogies de séquence et structurale ont été identifiées et utilisées au cours de mes travaux afin de trouver un analogue de la chlorotoxine pour vectoriser un agent anticancéreux. Pour déterminer l'intérêt de ces toxines en tant que vecteurs, elles ont été couplées à des anticancéreux : analogue du cisplatine et à la doxorubicine. Le couplage de la doxorubicine a été réalisé de façon innovante en utilisant la chimie click. L'efficacité antitumorale, la distribution, l'internalisation de ces composés ont été testées. Pour les analogues de la chlorotoxine, une caractérisation de ces peptides a été réalisée au préalable avant le couplage et la création d'un nouveau composé.

Ce manuscrit présente les résultats obtenus aux cours de ma thèse sur ces différents projets. Ces résultats seront précédés d'un rappel bibliographique pour en faciliter leur compréhension. En annexe à la fin du manuscrit, seront regroupés l'ensemble des publications auxquelles j'ai participé.

Rappel bibliographique

Chapitre 1 : La maurocalcine

I. Les peptides de pénétration cellulaire

a. Définition et découverte.

La membrane plasmique représente pour la plupart des molécules une barrière infranchissable. Son passage représente un enjeu clef dans la découverte et le développement de nouvelles molécules thérapeutiques. En effet, seule une molécule sur 10 000 passera tous les stades de développement et arrivera sur le marché (LEEM).

Pendant longtemps, il a été considéré comme impossible que des peptides ou protéines arrivent à franchir cette barrière sans l'existence d'un récepteur membranaire spécifique. Frankel et Pabo furent les premiers à constater que cette barrière n'était pas si infranchissable. En 1988, ils observèrent que la protéine TAT (pour Trans-activator of transcription) du virus de l'immunodéficience humaine (VIH-1) était capable de pénétrer dans des cellules en culture pour s'accumuler dans le noyau, aucun récepteur spécifique n'étant lié à la pénétration de cette protéine (Frankel and Pabo, 1988). Peu de temps après, en 1991, une observation semblable a été réalisée sur *antennapedia homeodomain*, un facteur de transcription de *Drosophila melanogaster* (Qian et al., 1989; Joliot et al., 1991; Derossi et al., 1994; Gehring et al., 1994). Ces découvertes successives ont conduit à l'identification des premiers peptides de pénétration cellulaire. Depuis, plus d'une centaine de peptides capables de se transduire dans les cellules ont été décrits (**Tableau 1**).

Plus de 20 ans après la découverte de cette nouvelle classe de peptides, il est toujours difficile de donner une définition générale de ces peptides. On peut les retrouver mentionné sous le nom de peptides de pénétration cellulaires (CPP pour « cell penetrating peptide » en anglais, ou de « protein transduction domain » (PTD anglais de domaine de transduction protéique), ou encore sous le terme de Trojan peptide en référence au cheval de Troie. Ils regroupent de petits peptides de 5 à 30 acides aminés environ d'origine naturelle ou synthétique (Brasseur and Divita, 2010; Bechara and Sagan, 2013; Reissmann, 2014). Ils sont capables de franchir la membrane plasmique par des mécanismes nécessitant ou non de l'énergie sans l'intervention d'un quelconque récepteur et en étant peu toxiques. Les CPP suscitent un réel intérêt de la part de la communauté scientifique car ils peuvent faire pénétrer dans les cellules, les cargos (molécules, liposomes, nanoparticules...) qui leurs sont rattachés (Foerg and Merkle, 2008; Brasseur and Divita, 2010; Milletti, 2012; Reissmann, 2014). Comme aucun récepteur spécifique n'est impliqué dans la pénétration, l'internalisation du peptide avec son cargo se fait de manière non spécifique, ce qui peut être problématique si un ciblage est

Peptide	Origine	Séquence	Références
<i>Les peptides cationiques</i>			
TAT	VIH-1 TAT	GRKKRRQRRRQ	(Green et al., 1989)
Penetratine	Homoprotéine de <i>Drosophila antennapedia</i>	RQIKIWFQNRRMKWKK	(Balayssac et al., 2006)
Polyarginine	Peptide de synthèse	(R) _n n=6-12	(Tünnemann et al., 2008)
MCa	Toxine de scorpion	GDCLPHLKLCKENKDCCKKCKRRGTNIEKRCR	(Estève et al., 2005b)
<i>Amphiphiles primaires</i>			
pVEC	VE- cadherine	LLIILRRRIRKQAHASK	(Elmqvist et al., 2001)
Pep-1	NLS de SV40 + Séquence riche en tryptophane	KETWWETWWTEWSQPKKKRKV	(Morris et al., 2001)
MPG	NLS de SV40 + glycoprotéine 41 du VIH	GALFLGWLGAAGSTMGAWSQPPKKRKV	(Morris et al., 1997)
MPrPp (1-28)	Prion protéine signal + motif KKRPKP	MANLGYWLLALFVTMWTDVGLCKRKP	(Lundberg et al., 2002)
<i>Amphiphile à hélice α</i>			
Transportan	Galanine + Mastoparan	GWTLNSAGYLLGKINLKALAALAKKIL	(Pooga et al., 1998)
MAP	Peptide de synthèse	KLALKLALKALKAAALKLA	(Oehlke et al., 1998)
<i>Amphiphile à feuillet β</i>			
VT5	Peptide de synthèse	DPKGDPKGVTVTVTVTGKGDPKPD	(Oehlke et al., 1997)
<i>Amphiphile riche en proline</i>			
Bac7	Cathelicidin bovine	RRIRPRPRLPRPRPLPFPRPG	(Sadler et al., 2002)
Pyrrhocoricin	Peptide antimicrobien	VDKGSYLPRPTPPRIYNRN	(Otvos, et al., 2004)
(PPR) _n	Peptide de synthèse	(PPR) ₃ , (PPR) ₄ , (PPR) ₅ , (PPR) ₆	(Daniels and Schepartz, 2007)
<i>Hydrophobes</i>			
K-FGF	Facteur de croissance de Sarcofibroblaste de Kaposi	AAVALLPAVLLALLAP	(Lin et al., 1995)
FGF 12	Facteur de croissance de fibroblaste	PIEVCMYREP	(Nakayama et al., 2011)
Bip	?	VPTLK (PMLKE, VPALR, VSALK, IPALK)	(Gomez et al., 2007, 2010)

Tableau 1 : Exemple de CPP avec leur origine et séquence.

souhaité (Vivès et al., 2008). Même si l'internalisation n'est pas spécifique, elle peut varier selon le type cellulaire et le cargo attaché au CPP. Jusqu'à présent leurs utilisations comme vecteurs a largement fait ses preuves *in vitro* (sur des cellules en cultures) (Heitz et al., 2009). L'existence de tests précliniques et cliniques montre le potentiel de ces composés (voir paragraphe I. d).

b. Classification

Il existe une grande diversité dans la famille des CPP. Il n'y a pas vraiment d'homologies de séquences même si certains CPP présentent des caractéristiques structurales identiques ou proches. La grande variété dans l'origine des CPP fait que l'on trouve aussi bien des peptides avec des séquences cationiques, anioniques ou neutres, et des degrés d'hydrophobicité et de polarité différentes. Il est possible de classer les peptides suivant deux classifications différentes. La première selon leurs propriétés physico-chimiques, la seconde selon leurs origines (Milletti, 2012; Reissmann, 2014). Ainsi dans la classification physicochimique, les CPP sont répartis en 3 classes (**Figure 1**):

- Les peptides cationiques
- Les amphiphiles
- Les hydrophobes

Les peptides anioniques n'ont pas de groupe spécifique et sont répartis au cas par cas avec les amphiphiles ou les hydrophobes. Ils sont assez rares, puisque pendant longtemps on a pensé qu'une charge nette positive était obligatoire pour l'interaction avec la membrane et la pénétration (Martín et al., 2011).

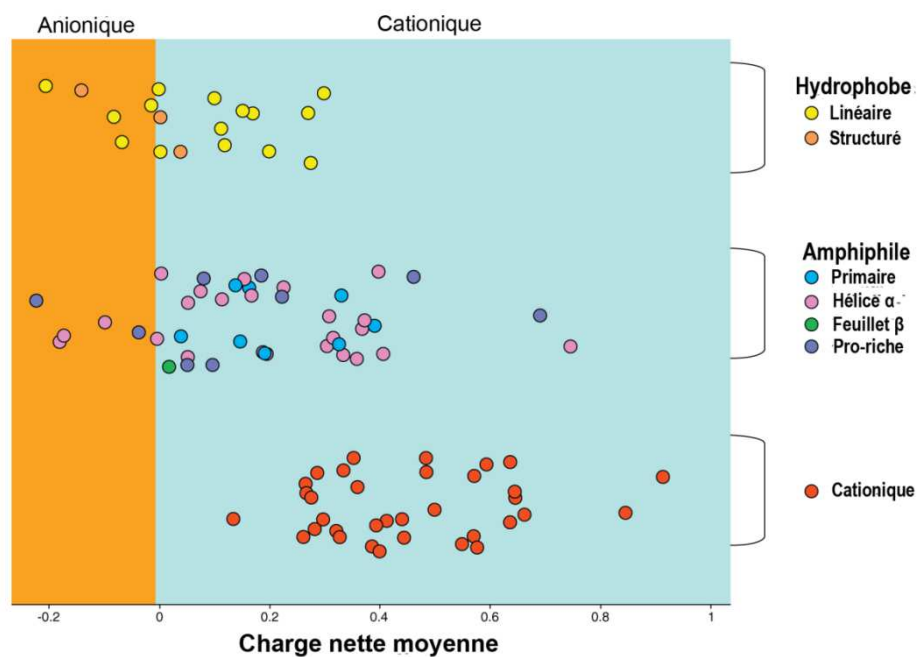


Figure 1 : Distribution des CPP en fonction de leur charge nette (D'après Milletti, 2012 (modifié))

Plus de 83% des CPP ont une charge nette positive (Milletti 2012), mais ne sont regroupés dans les peptides cationiques que les peptides dont la pénétration repose uniquement sur la présence de charges positives. Huit charges positives seraient nécessaires à une pénétration efficace des CPP cationiques (Madani et al., 2011). Cela n'empêche pas d'autres résidus d'être cruciaux pour la pénétration (c'est le cas de la pénétratine W14F). Parmi les peptides cationiques, on retrouve les deux CPP historiques, TAT et pénétratine (dérivée de l'antennapedia homeodomain) et leurs dérivés, ainsi que les polyarginines peptides. Dans ce sous-groupe, on retrouve aussi les séquences de localisation au noyau (NLS : nuclear localisation sequence). Ce sont de petits peptides avec des motifs riches en arginine, lysine ou proline qui peuvent être transportés dans le noyau via les pores nucléaires en emmenant avec elles les protéines qui lui sont complexées. La majorité des NLS ne sont pas de remarquables peptides de pénétration, mais qui lorsqu'ils sont associés à une séquence hydrophobe donnent des CPP amphiphiles très intéressants (Morris et al., 1997, 2001; Mueller et al., 2008; Oglecka et al., 2008; Milletti, 2012).

Les CPP amphiphiles sont sous-divisés en 4 classes :

- Les CPP amphiphiles primaires : qui sont souvent des peptides chimériques issus de l'association d'un NLS à une séquence hydrophobe. On retrouve aussi des peptides dérivés de protéines naturelles (exemple : MPrPp (1-28) basés sur la protéine prion associée au motif KKRPK) (Oglecka et al., 2008).
- Les CPP à hélices alpha amphiphiles qui comme leur nom l'indique regroupent les CPP contenant une hélice alpha amphiphile ayant une face très hydrophobe et l'autre face pouvant être chargée (positivement ou négativement) ou polaire. Une simple mutation ponctuelle ou délétion peut entraîner une diminution de la pénétration (Scheller et al. 1999; Soomets et al. 2000; Milletti 2012).
- Les CPP à feuillets Beta amphiphiles ; eux possèdent un feuillet hydrophobe associé à un feuillet hydrophile exposé au solvant. Une étude a montré que pour VT5 la présence de feuillets beta est nécessaire pour avoir une bonne pénétration (Oehlke et al. 1997; Milletti 2012).
- Les CPP amphiphiles riches en proline ; la présence importante de proline impose au peptide une structure secondaire bien précise : (polyproline II (PPII) hélice prolongée gauche de 3.0 résidu par tour) (Milletti 2012).

La dernière classe est celle des CPP hydrophobes. Peu de CPP font actuellement partie de cette classe. Un CPP est considérée comme hydrophobe s'il ne contient que des résidus apolaires avec une faible charge nette ou s'il possède un motif hydrophobe ou des résidus hydrophobes essentiels à la pénétration (Milletti 2012).

La seconde méthode de classification est plus simple puisqu'elle est basée sur l'origine des CPP. Cependant elle est de plus en plus déséquilibrée et obsolète à cause du nombre croissant de CPP synthétisés en laboratoire. Cette classification permet de distinguer les peptides d'origines naturelles, des peptides chimériques et des peptides de synthèse. Rapidement, les peptides d'origines naturelles regroupent tous les CPP issus de protéines naturelles (TAT, penetratin, maurocalcine...). Les CPP chimériques sont issus de la fusion de deux peptides d'origines différentes comme par exemple le transportan qui est issu de la fusion d'un neuropeptide la galanin1-13 et du peptide mastoparam issu du venin de guêpe. Enfin il reste les peptides synthétiques, dont les plus connus sont les polyarginines. Cette classe regroupe l'ensemble des CPP obtenus par synthèse chimique après observation des propriétés physico-chimiques des 1^{er} CPP décrits.

c. Voies d'entrées dans la cellule

Il est impossible de parler des peptides de pénétration cellulaire sans aborder les différents mécanismes d'absorption de la cellule. Un composé a différents moyens pour pénétrer dans une cellule, mais attention, certains d'entre eux conduisent à la dégradation du composé dans les lysosomes. Les différentes voies d'entrée étant variées, plus ou moins compliquées, je ne détaillerai que ceux intervenant dans la pénétration des CPP. Cependant l'ensemble de ces mécanismes est brièvement décrits dans le Tableau 2.

Les voies d'entrée utilisées par les CPP pour pénétrer dans une cellule sont difficiles à étudier. En effet la pénétration d'un CPP peut varier en fonction du type cellulaire, du cargo lui étant attaché, et de la concentration utilisée. De plus, il apparait clairement qu'un même CPP peut utiliser plusieurs voies d'entrée dans la cellule. Ainsi il n'est actuellement accepté que deux types d'internalisation possible pour les CPP :

- La translocation : processus énergie-indépendant (diffusion directe, modèle de la micelle inversée, le modèle de « barrel-stave », et le modèle de « Carpet »).
- L'endocytose : processus énergie-dépendant (macropinocytose, l'endocytose clathrine-dépendante, l'endocytose dépendante des calvéoles/raft lipidiques, et l'endocytose clathrine calvéoline indépendante)

Les principales différences entre les deux types d'internalisations sont bien évidemment le mode de pénétration mais surtout la libération du CPP dans le cytosol. Dans le cas des voies d'entrée par translocation, le peptide se retrouve immédiatement dans le cytosol après avoir passé la membrane plasmique ; alors que dans les cas d'endocytose, le peptide se retrouve dans une vésicule dont il doit s'échapper pour atteindre le cytoplasme.

La diffusion directe est basée sur l'interaction des groupements guanidium des arginines du CPP avec les groupements phosphates des phospholipides de la membrane. Cette interaction va permettre de masquer les charges du peptide, atténuer sa polarité et ainsi

Nom	Description	Caractéristique	Réf.	
Phagocytose	Permet l'ingestion de particules volumineuses. Elle est réalisée par des cellules spécifiques (macrophages, neutrophiles et les cellules dendritiques). Procédé qui fait partie intégrante du système immunitaire de l'organisme. Il nécessite la reconnaissance de la particule par la cellule à l'aide de récepteurs membranaires. Il se produit alors un réarrangement du cytosquelette de la cellule conduisant à la croissance de la membrane plasmique afin d'englober la particule et de former un phagosome. La particule est ensuite détruite et des petits éléments de cette particule vont être exposés à la surface de la cellule immunitaire afin de stimuler les autres cellules immunitaires (Lymphocytes)	Spécifique à certains types cellulaires Formation de phagosome Ingestion puis dégradation de grosses particules (par exemple bactérie) Croissance de la membrane plasmique Consomme beaucoup d'énergie	(Desjardins, 2003; Tollis et al., 2010; Vercauteren et al., 2011)	
Pinocytose	Macropinocytose	Responsable de l'internalisation des fluides et de macromolécules dans différents types cellulaires. Elle implique un mouvement membranaire afin de générer une excroissance membranaire qui va ensuite se replier sur le contenu extérieur pour former une large vésicule hétérogène : le macropinosome. Ce processus permet l'internalisation de facteurs de croissance par la cellule.	Présent dans tout type cellulaire Formation de macropinosome Déformation puis mouvement de la membrane plasmique Endocytose de facteurs de croissance	(Kerr and Teasdale, 2009; Mercer and Helenius, 2009; Gold et al., 2010)
	Dépendante de la clathrine	Intervient dans tout type cellulaire. Elle permet l'absorption par la cellule de composés essentiels (cholestérol, transferrine, lipoprotéines). Elle nécessite la présence de récepteurs membranaires spécifiques à un ligand (cholestérol, transferrine...). Elle peut être décomposée en plusieurs étapes : (i) la fixation du ligand sur son récepteur, (ii) la concentration de récepteurs liés à leur ligand dans une invagination de la membrane. (iii) Recrutement de clathrine au niveau intracellulaire de l'invagination pour recouvrir la vésicule en formation. (iv) accentuation de l'invagination de la vésicule avec l'assemblage de clathrine se terminant par la libération d'un endosome encapsulé de clathrine concentré en molécule d'intérêt.	Présent dans tout type cellulaire Formation d'endosome recouvert de clathrine Nécessite la présence de récepteurs membranaires Invagination de la membrane provoquée par l'assemblage de clathrine Endocytose de composé essentiel à la survie de la cellule.	(Conner and Schmid, 2003; Sahay et al., 2010)
	Dépendante de la calvéoline	La calvéole est décrite comme une invagination de la membrane en forme de flacon. Elle est constituée de calvéoline (protéine transmembranaire) et est riche en cholestérol et sphingolipides. Le virus simien 40 (SV40) utilise cette voie pour infecter les cellules et a donc été utilisé pour l'étudier. Après s'être liée à la membrane via un récepteur, le composé lié au récepteur va se diffuser dans la membrane jusqu'à être piégé dans une calvéole. S'en suit une cascade de signalisation qui va entraîner le recrutement d'actine qui va former des plaques autour de la calvéole. La dynamine va alors s'assembler au col de la calvéole et va provoquer la libération de la vésicule de calvéole. Cette dernière va ensuite perdre les polymères d'actine à sa surface. Cette voie permet entre autre l'internalisation de l'albumine.	<ul style="list-style-type: none"> - Présent dans de nombreux types cellulaires (muscles lisse, fibroblaste, adipocytes, cellule endothélial) - Formation d'endosomes composés de calvéole - Nécessite la présence d'un récepteur - Invagination de la membrane due à la calvéole 	(Pelkmans et al., 2001; Conner and Schmid, 2003; Kumari et al., 2010)
	Clathrine et calvéoline indépendante	Cette voie représente une alternative à la voie liée à la clathrine et à la calvéoline. Elle regroupe un ensemble d'autres voies mettant en jeu d'autres protéines capables de former des vésicules. Comme par exemple les flotillines et les tétraspanines qui vont permettre une endocytose indépendante du niveau de cholestérol membranaire.	- Encore en cours de caractérisation et sujet à débat.	(Conner and Schmid, 2003; Kumari et al., 2010)

Tableau 2 : Définition des différentes voies de pénétration dans une cellule

permettre sa diffusion à travers la membrane. Cette diffusion est possible grâce au potentiel membranaire et nécessite la présence d'un nombre minimum d'arginine et d'une charge nette positive (Bechara and Sagan, 2013)

Le modèle de micelle inversée a été pour la première fois décrit pour expliquer la translocation de la penetratin (Derossi et al., 1996). Dans ce modèle, les résidus basiques du CPP vont interagir avec les phospholipides de la membrane entraînant l'interaction des résidus hydrophobes avec la membrane. Il va alors se produire une déstabilisation de la bicouche lipidique avec invagination de la membrane. La réorganisation des lipides voisins va aboutir à la formation d'une micelle inversée entourant le CPP. Une disruption de la membrane va alors conduire à la libération du peptide dans le cytosol (**Figure 2**) (Lundberg and Langel, 2003).

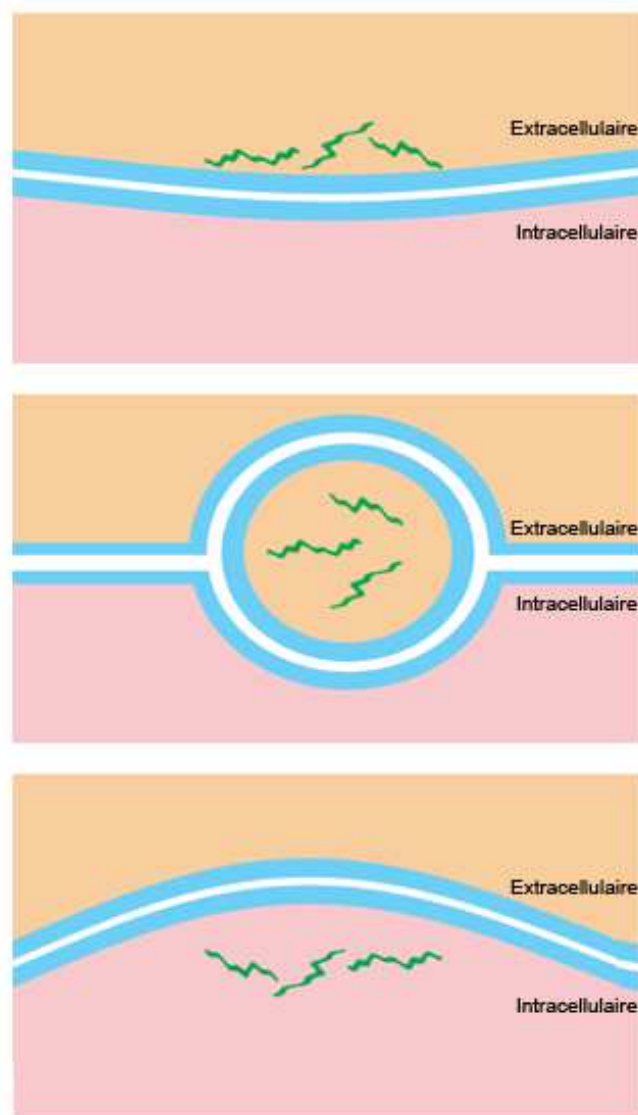


Figure 2 : Modèle de la micelle inversée, les peptides (en vert) interagissent avec la membrane plasmique, entraînant la formation d'une micelle autour des peptides, avant leurs relargages dans le cytoplasme.

Dans le modèle de « barrel-stave », les CPP vont dans un 1^{er} temps se lier à la membrane plasmique. Les molécules de CPP vont alors s'associer pour former un pore transitoire sous la forme d'un tonneau, laissant ainsi diffuser les autres molécules dans la cellule (Gazit et al., 1994; Yeaman and Yount, 2003; Sanderson, 2005). Ce type d'internalisation va nécessiter la présence d'une hélice alpha amphiphile ou hydrophobe, et/ou d'un feuillet beta (Shai and Oren, 2001). (**Figure 3**)

Selon le modèle de « carpet », les peptides vont s'accumuler à la surface de la membrane plasmique sur leur longueur en la recouvrant comme un tapis. Cette accumulation de peptides va conduire à une perturbation locale de la membrane plasmique, provoquant l'apparition de perforations dans la membrane permettant aux peptides de passer (Shai and Oren, 2001; Yeaman and Yount, 2003; Sanderson, 2005). (**Figure 3**)

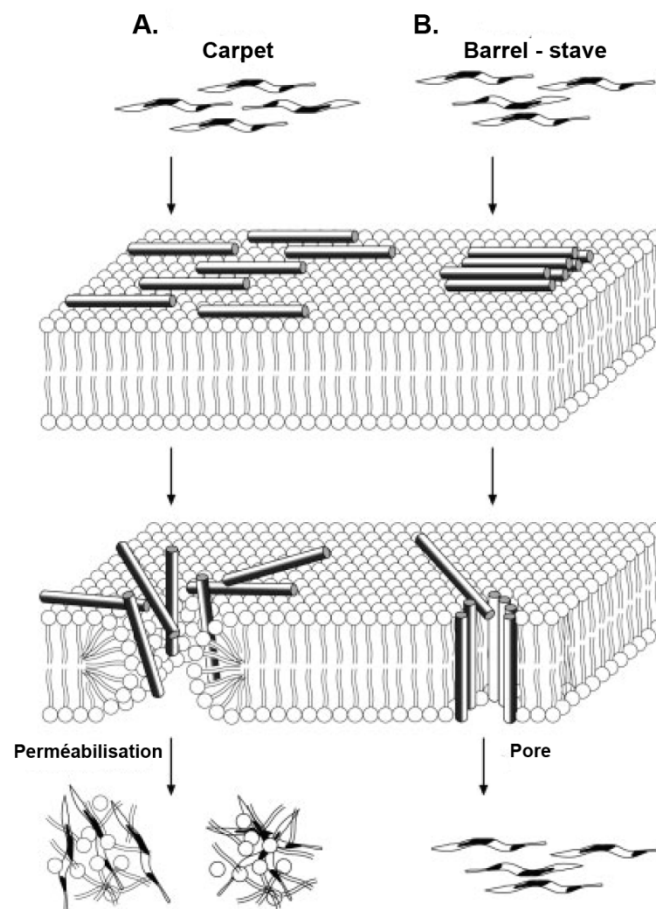


Figure 3 : Illustration de la translocation selon les modèles de « barrel - Stave » et de « carpet ». (D'après Lundberg and Langel, 2003 (modifié))

L'endocytose est un processus d'internalisation de composés et de fluides nécessitant de l'énergie. Comme décrit dans le Tableau 2, il existe différentes voies d'endocytose. L'endocytose des CPP peut être décomposée en 2 étapes : l'entrée par endocytose suivie de l'échappement de la vésicule d'endocytose. Les conditions pour cet échappement ne sont pas encore connues.

La macropinocytose qui permet l'endocytose par la cellule de grandes quantités de fluides a été décrite dans de nombreuses études comme la route prioritaire d'entrée des CPP (Nakase et al., 2004; Wadia et al., 2004; Kaplan et al., 2005; Fretz et al., 2006; Khalil et al., 2006) et notamment pour les polyarginines (Duchardt et al., 2007; Nakase et al., 2007). L'endocytose dépendante de la clathrine a été montrée comme impliquée dans le mécanisme de pénétration de la penetratin, de TAT, lorsque la concentration est importante et d'autre CPP après inhibition de son fonctionnement (Säälk et al. 2004). L'endocytose dépendante de la calvéoline est elle aussi impliquée dans la pénétration des CPP (Duchardt et al., 2007). Elle semble être prioritaire à faible concentration de CPP. (**Figure 4**)

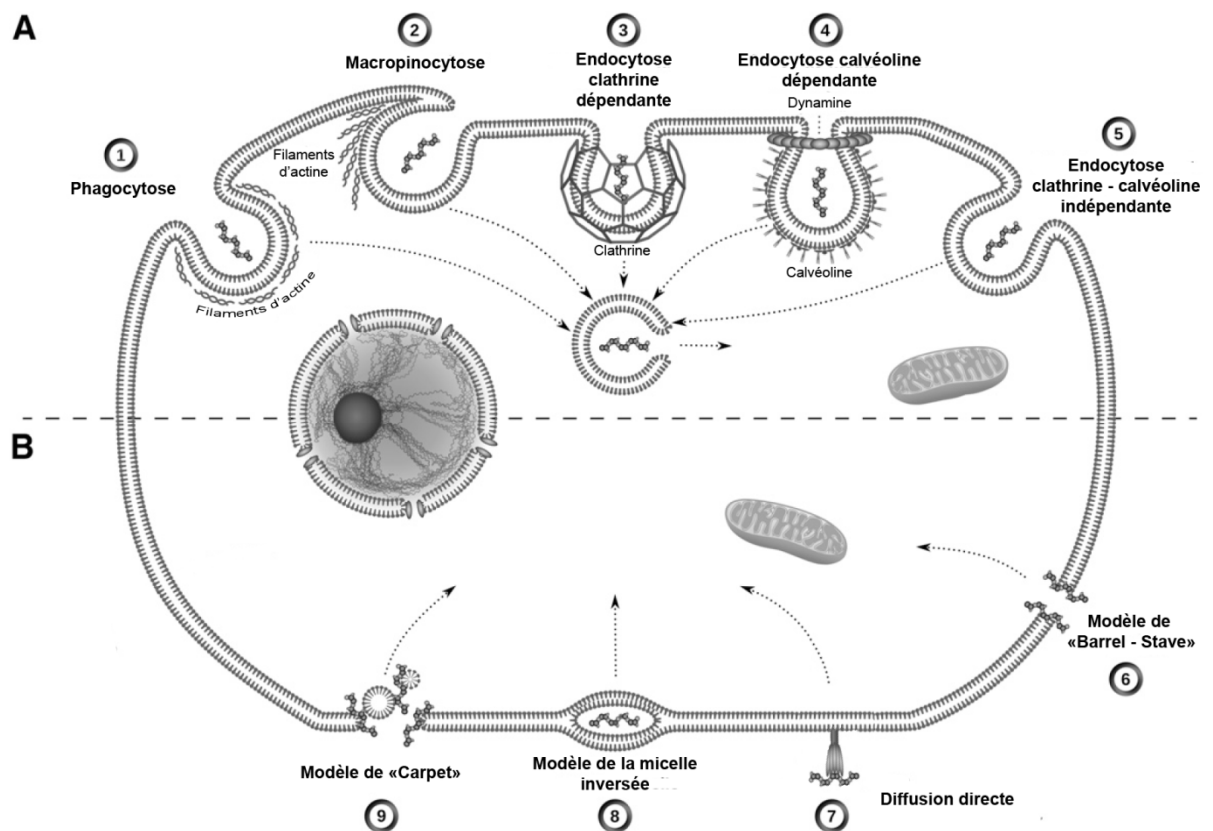


Figure 4 : Mécanisme d'entrée des CPP, A. Mécanismes énergie dépendant ; B. Mécanismes énergie indépendant. (D'après Durzyńska et al., 2015 (Modifié))

d. Intérêt clinique des CPP.

Les CPP offrent de grandes possibilités dans le domaine thérapeutique, leurs utilisations pouvant aller de la « simple » recherche pour comprendre le fonctionnement d'une maladie, à l'administration d'un éventail varié de cargos. Ainsi jusqu'à présent, les CPP ont été utilisés pour transporter : des peptides, des enzymes, des protéines, des anticorps, des acides nucléiques et leurs mimes, de l'ADN, des plasmides, des agents thérapeutiques, des fluorochromes, des nanoparticules, tous pour des applications variées (imagerie, cancer, transfection...). Il serait trop long de faire ici une liste ou de développer l'ensemble de ces applications. Une liste non exhaustive des différents types de cargos délivrés peut être trouvée dans le **Figure 5**.

Les CPP sont utilisés pour :

- améliorer la pénétration d'un composé dans les cellules (tumeurs par exemple)
- améliorer la rétention d'un composé dans une cellule (cellule tumorale par exemple)
- atteindre des zones difficiles d'accès (par exemple le passage de la barrière hémato-encéphalique).

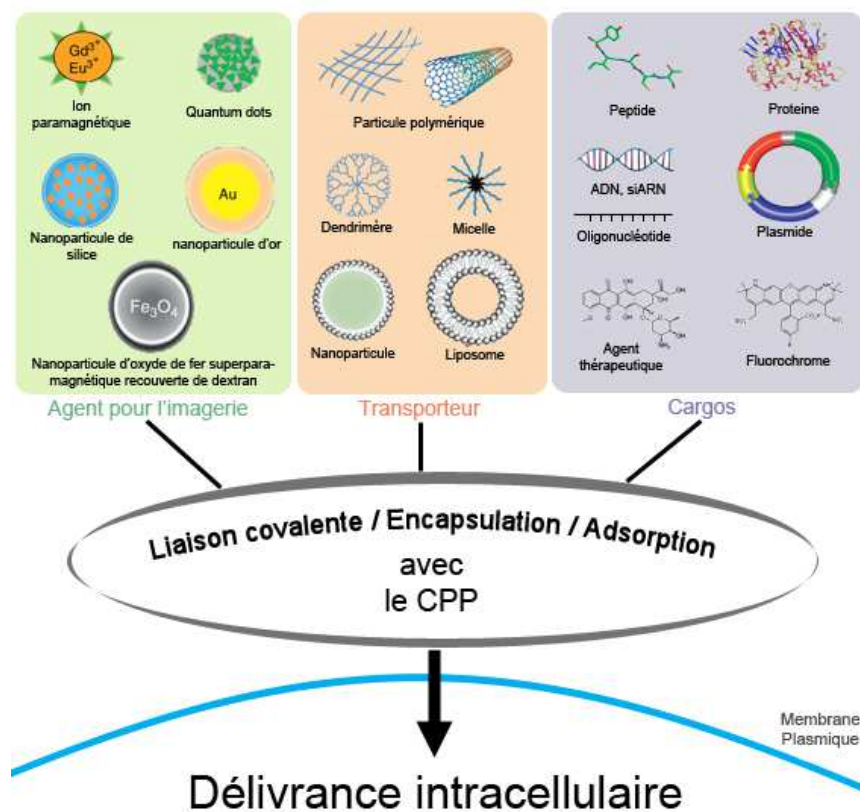


Figure 5 : Applications des CPP comme vecteur

Bien que leurs intérêts en clinique soient grands, il n'y a pour l'instant aucun CPP-médicament qui ait été approuvés par la FDA, mais l'on retrouve des CPP dans des essais précliniques et cliniques (**Tableau 3**) ce qui traduit bien leurs potentiels (Shi et al., 2014). Cependant, leur développement en produits pharmaceutiques n'est pas garanti. En effet, il y a plusieurs aspects qu'il faudrait étudier avant de voir les CPP couramment utilisés comme vecteurs de médicaments, Le premier étant de mieux caractériser leur pénétration (mécanisme, efficacité, cinétique...) en fonction du type cellulaire afin de pouvoir comparer l'efficacité, l'intérêt des différents CPP dans différentes conditions. En effet, bien qu'il y ait un nombre croissant d'applications décrites, elles concernent très souvent les même CPP, avec comme peptides de références TAT et penetratin. On retrouve aussi souvent les polyarginines.

Il faut ensuite s'intéresser au potentiel effet toxique ou secondaire de l'utilisation de ces peptides, étudier aussi une éventuelle réponse immunitaire, et la biodisponibilité d'un tel composé. Et enfin, il faut impérativement contrôler la pénétration non sélective de ces composés avant d'envisager une utilisation massive *in vivo*.

Malgré tout cela, les CPP représentent dans la cancérologie, un intérêt important, ayant conduit récemment à l'émergence d'un groupe de CPP : les « tumor penetrating peptides », (ex iRGD, iNGR, lyp-1, Omomyc...). Ces peptides permettent la délivrance profondément au sein de tissu tumoral de petites molécules ou nanovecteurs (Sugahara et al., 2009; Savino et al., 2011; Alberici et al., 2013; Yang et al., 2014).

Même s'il reste encore du travail, je ne doute pas de voir apparaître sur le marché des CPP.

Nom	CPP	Cargo	Indication	Phase clinique (année)	Entreprise	Réf.
PsorBan	R8	Cyclosporine A	Psoriasis	2 arrêté (2007)	CellGate	(Lebleu et al., 2008)
RT-001	Lysine-riche peptide encadré par deux peptides TAT ₄₉₋₅₇	Toxine botulique	Cosmétique	2 (2013)	Revenance therapeutics	(Brandt et al., 2010)
AZX-100	PTD ₄	Heat shock protéine 20	Prévention et réduction des cicatrices	2 (2012)	Capstone therapeutics	(Lopes et al., 2009)
KAI-9803	TAT ₄₇₋₅₇	Inhibiteur de la protéine kinase C _δ	Infarctus du myocarde	2 (2011)	Amgen	(Miyaji et al., 2011)
KAI-1678	TAT ₄₇₋₅₇	Inhibiteur de la protéine kinase C _ε	Blessure de la colonne vertébrale	2 (2011)	Amgen	(Cousins et al., 2013)
AVI-5126	6-aminohexanoicacid-spaced oligoarginine [(R-Ahx-R) ₄]	Antisense PMO	Maladie cardiovasculaire et pontage coronarien	2 arrêté (2009)	Sarepta	(Hosseini et al., 2012)
AVI-5038	?	Antisense PMO	Dystrophie musculaire de ducheme	Préclinique (2012)	Sarepta	(Goyenvallé and Davies, 2011)
ISS P-002	TAT	V2- deleted Env protéines	Infection au VIH	1 (2014)	Novartis et l'institut supérieur de la santé d'Italie	(ISS P-002) ClinicalTrials.gov
DTS-108	Vectocell	SN38	cancer	Préclinique	Diatos SA et Drais Pharmaceuticals	(Meyer-Losic et al., 2008)
XG-102	TAT ₄₈₋₅₇	Kinase C-Jun-N-terminal	Inflammation	1 (2012)	Xigen	(Wang et al., 2003)
p28	p28	p28 (inhibiteur de l'ubiquitination de p53)	Tumeur solide résistante	1 (2013)	CDG therapeutics	(Warso et al., 2013)
AM111	TAT ₄₈₋₅₇	Inhibiteur de la kinase C-Jun-N-terminal	Déficit auditif	2 (2013)	Auris Medical et Xigen	(Omotehara et al., 2011)

Tableau 3 : Complexe à base de CPP en essai clinique

II. La maurocalcine, un CPP à part entière.

a. Description et découverte

La maurocalcine (MCa) est un peptide de 33 acides aminés extraite du venin de scorpion *Scorpio maurus palmatus* qui fut identifiée pour la 1ère fois en 2000 (Fajloun et al., 2000). Il s'agit d'un peptide ayant un fort caractère basique avec 11 acides sur 33 chargés positivement. Grâce à une structure 3D particulière, élucidée par 1H-RMN en 2000 (Mosbah et al., 2000), l'ensemble de ces charges se retrouve localisé sur la même face du peptide. On retrouve ce phénomène aussi chez d'autres CPP tel que TAT, ou la pénétratine (Ram et al., 2008). La MCa doit sa structure 3D à trois ponts disulfures (Cys³-Cys¹⁷, Cys¹⁰-Cys²¹; Cys¹⁶-Cys³²), qui assure son repliement et la formation d'un motif ICK (« inhibitor cystin knot »). On retrouve aussi dans sa structure secondaire des motifs consensus habituellement retrouvés dans les toxines de scorpions : 1 hélice alpha, et 3 feuillets beta) (**Figure 6**).

La MCa a été découverte grâce à son activité pharmacologique activatrice sur le récepteur à la ryanodine. C'est l'observation de cette activation qui a conduit à l'étude de la MCa en tant que CPP.

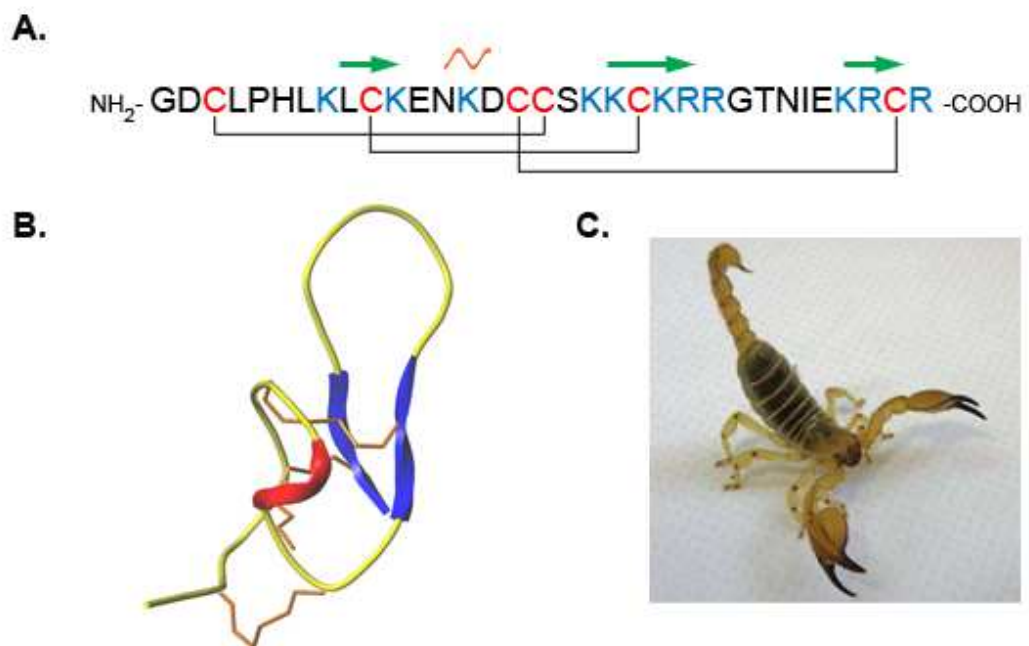


Figure 6 : A. Séquence peptidique de la MCa, en rouge les cystéines, en bleu les acides aminés basiques, les flèches vertes correspondent au feuillet β et en orange apparait l'hélice α ; **B. Représentation tridimensionnelle de la MCa** ; **C. Scorpio maurus palmatus** (crédit photo : Stuart Summerfield).

b. Effet pharmacologique

La MCa possède une homologie de séquence de 82% avec l'imperatoxine A, qui est connue pour agir sur les récepteurs à la ryanodine. Les 1ères études sur la MCa ont porté sur son effet pharmacologique sur le RyR.

Le RyR est un canal calcique se situant sur la membrane du réticulum endoplasmique. Il existe plusieurs isotopes du RyR : RyR1 essentiellement retrouvé dans les cellules du muscle squelettique, le RyR2 spécifique du muscle cardiaque et enfin RyR3 qui lui est ubiquitaire. Les RyR sont impliqués dans la mobilisation des stocks de calcium internes du réticulum endoplasmique permettant la contraction musculaire. Ces canaux doivent leur nom à leurs fortes affinités pour la ryanodine un alcaloïde naturel. La MCa agit sur deux isoformes, RyR1 et RyR2 (Altafaj et al., 2007). La MCa se lie au récepteur sur sa face cytoplasmique. Elle va stabiliser l'ouverture du canal, et augmenter l'affinité du canal pour la ryanodine. La fixation de la MCa va induire un relargage massif de calcium par le réticulum sarcoplasmique en diminuant le seuil d'activation du canal et en augmentant son seuil d'inhibition (**Figure 7**).

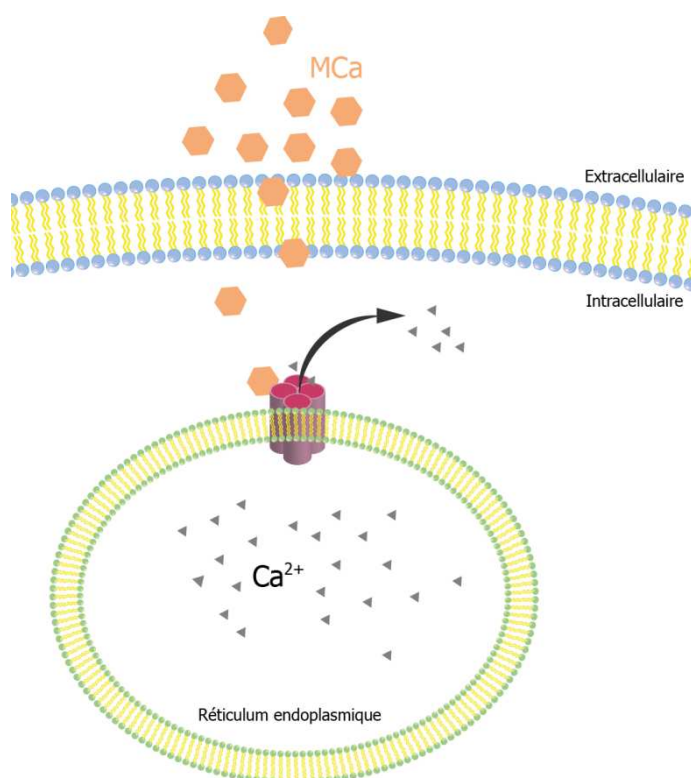


Figure 7 : Activation du RyR par la MCa

Cet effet de la MCa se produit immédiatement suite à son ajout dans le milieu extracellulaire. Cela traduit la capacité de ce peptide à franchir la membrane plasmique très rapidement et a donc conduit à la poursuite de son étude en tant que CPP.

c. La M_{Ca} en tant que CPP

La première étude sur la capacité de la M_{Ca} à traverser la membrane cellulaire date de 2005. Estève et collaborateur ont montré que la M_{Ca} biotinylé était capable de transloquer à travers la membrane plasmique et d'emmener avec elle des cargos (Estève et al., 2005a). Ils ont réalisé cette étude sur différentes lignées cellulaires et ont observé la pénétration de la M_{Ca} marquée à la Cy3, un fluorochrome dans différentes conditions : à température ambiante ou 4°C (inhibition de l'endocytose), avec ou sans inhibiteurs d'endocytose. Cette étude a montré que la M_{Ca} pénètre dans la cellule sans utiliser les voies d'endocytose. L'hypothèse d'une pénétration de la M_{Ca} par translocation est cohérente avec le délai de son effet sur le RyR (après une minute seulement). Cette hypothèse a été confirmée par Boisseau et collaborateur. Ils ont montré que la pénétration de la toxine était dose-dépendante et dépendait du potentiel membranaire de la cellule (Boisseau et al., 2006). Ces deux études ont donc permis de trouver chez la M_{Ca} des caractéristiques communes aux CPP, et donc d'affirmer que la M_{Ca} en faisait partie.

Cependant la M_{Ca} présente un inconvénient majeur par rapport aux autres CPP : elle possède une activité pharmacologique. Or il est préférable pour un vecteur d'être inactif. Afin de pouvoir utiliser la M_{Ca} comme vecteur, des travaux ont été conduits pour identifier la séquence porteuse de l'activité pharmacologique de la M_{Ca}. Il a ainsi été montré que l'Arg 24, était nécessaire à l'activité du RyR (Mabrouk et al., 2007). La synthèse d'un analogue linéaire de la M_{Ca} a montré que la structure tridimensionnelle de la toxine est nécessaire à son activité (Ram et al., 2008). A partir de ces résultats plusieurs stratégies ont été mises en place pour conduire à la synthèse d'analogues inactifs de la M_{Ca} gardant toujours leurs propriétés de pénétration (Poillot et al., 2012). La M_{Ca} linéaire fut le 1^{er} analogue de la M_{Ca} entièrement CPP développé. Afin de l'obtenir, les 6 cystéines présentes dans la forme native de la toxine ont été remplacées par de l'acide aminobutyrique (Abu). Une cystéine en C-terminal a été rajoutée pour permettre le couplage du cargo. Le plus gros des travaux de caractérisation de la M_{Ca} en tant que CPP a été réalisé avec la M_{Ca} linéaire. Elle a notamment été couplée à des fluorochromes via le complexe biotin-streptavidin ou via une cystéine extra numéraire. Elle a aussi été utilisée pour la délivrance de quantum dots. Une version iodée grâce à l'addition d'une tyrosine en position N-terminale a permis d'étudier sa répartition *in vitro* dans la cellule, mais aussi ses caractéristiques *in vivo* (stabilité, répartition, élimination) comparée à la toxine native iodée (Tisseyre et al., 2014). Son utilisation en tant que vecteur de molécule active a aussi été vérifiée par le couplage de doxorubicine au peptide. Via un crosslinker, la doxorubicine a été couplée à la M_{Ca} linéaire. Aroui et al. ont pu montrer que ce complexe était actif mais surtout qu'il permettait de « contourner » les mécanismes de résistance des cellules cancéreuses, et de récupérer ainsi une sensibilité à la doxorubicine (Aroui et al., 2009a, 2009b, 2009c). C'est dans la poursuite de ces travaux, que se situe mon travail de thèse. En effet même si on resensibilise

les cellules résistantes, les cellules sensibles à la doxorubicine répondent moins bien au complexe qu'à la doxorubicine seul. Il y a donc des améliorations à apporter.

Malheureusement bien que la M_{Ca} linéaire soit un bon CPP, elle ne constitue pas une approche viable puisque sa stabilité *in vivo* est diminuée dû à l'absence de structure tridimensionnelle (Perret et al., 2015). Les travaux sur l'amélioration/ la synthèse de nouveaux CPP dérivés de la M_{Ca} ont donc été poursuivis par la synthèse d'un analogue dextrogyre de la M_{Ca}. Il s'agit de la M_{Ca} native entièrement synthétisée avec des acides aminés dont le carbone alpha est dextrogyre. On conserve ainsi les propriétés de pénétration puisque l'on garde la même séquence. Cependant, on perd complètement l'activité biologique, puisque la M_{Ca} ne peut plus se fixer sur le RyR. De plus la D-M_{Ca} présente une stabilité *in vivo* plus élevée que la M_{Ca} linéaire et native (Poillot et al., 2010). Bien que cet analogue soit très intéressant sur le papier, sa synthèse reste contraignante et chère. Une nouvelle approche visant à améliorer la M_{Ca} linéaire a donc été menée. Il a été identifié que les acides aminés basiques de la M_{Ca} sont indispensables pour la translocation de la toxine dans les cellules. Ils garantissent en effet une bonne interaction avec la membrane plasmique (Mabrouk et al., 2007). Partant de cette constatation, la M_{Ca} linéaire a été tronquée en plusieurs petits fragments contenant les charges positives afin d'obtenir de petits CPP variants de la M_{Ca} capables de pénétrer dans les cellules (Poillot et al., 2012; Tisseyre et al., 2013). Certains de ces petits peptides ont montré qu'ils pénétraient plus efficacement dans les cellules que la M_{Ca} linéaire.

Les précédents travaux ont montré le potentiel de la M_{Ca} comme CPP. C'est dans l'idée de développer son utilisation pour l'administration de molécules thérapeutiques qu'une partie de mon travail de thèse s'inscrit.

Chapitre 2 : Toxine de ciblage : Chlorotoxine

I. Chlorotoxine

a. Découverte et présentation

La chlorotoxine (CTX) est un petit peptide de 36 acides aminés issu du venin de scorpion *Leiurus quinquestriatus*. Elle a été isolée en 1991 et doit son nom à son activité pharmacologique sur les canaux chlore des cellules épithéliales de colon de rat (DeBin and Strichartz, 1991). Cependant, ces dernières années, la CTX est surtout connue et étudiée pour ses propriétés de ciblage des tumeurs cérébrales. La CTX a une structure compacte maintenue par 4 ponts disulfures suivant le motif : C₁-C₄ ; C₂-C₆ ; C₃-C₇ ; C₅-C₈. Elle possède trois feuillets β antiparallèles placés à proximité d'une hélice α . (**Figure 8**)

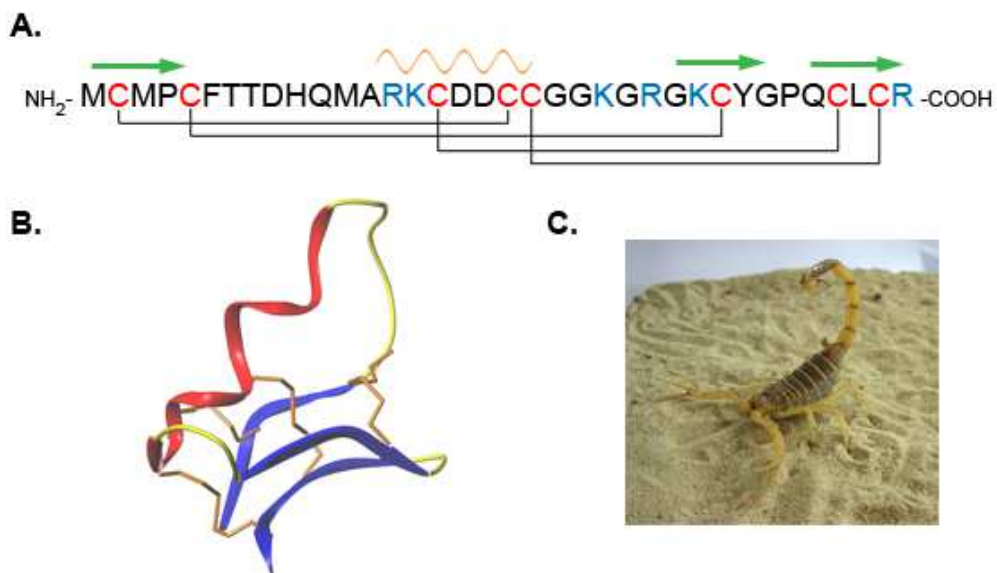


Figure 8 : A. Séquence peptidique de la CTX, avec en rouge les cystéines, en bleu les acides aminés basique, les flèches verte représentent les feuillets β et l'onde en orange l'hélice α ; **B. Représentation tridimensionnelle de la CTX** ; **C. Scorpion *Leiurus quinquestriatus***

Avec sa structure compacte, il a été proposé que la CTX soit capable de passer la barrière hémato-encéphalique. Cependant il n'y a pas assez de données à ce jour pour affirmer cette hypothèse ou la réduire à un simple passage de la barrière hématoencéphalique tumorale. Il a été toutefois montré que la CTX était capable de diffuser en profondeur dans les tumeurs alors que d'autres agents ciblant comme les anticorps n'y arrivent pas (Mamelak and Jacoby, 2007; Veisoh et al., 2007). La composition en acide aminés de la CTX présente aussi de

nombreux intérêts pour un chercheur. En effet, elle est facilement marquable grâce à la présence d'une tyrosine unique en position 29 et de lysines permettant son marquage via des crosslinker. Cela a permis d'étudier sans trop de modifications, sa cible ou son récepteur, ses propriétés pharmacologiques et d'étudier son mode d'action. Ainsi l'ajout d'iode sur Tyr²⁹ a permis d'identifier les sites de liaisons et d'affinité de la CTX sur des cellules de gliomes en cultures. Il a pu être montré ainsi que la Tyr²⁹ n'est pas essentielle pour l'activité du peptide. C'est grâce à cette ¹²⁵I-CTX que Soroceanu et al ont démontré que la toxine était capable de marquer spécifiquement les cellules cancéreuses sur une biopsie de patient (Soroceanu et al., 1998). Ils ont aussi montré qu'après injection IV de ¹³¹I-CTX chez des souris porteuses d'une tumeur cérébrale humaine, il y avait une accumulation spécifique du composé dans la tumeur. Ce qui a permis de démontrer que la CTX était capable d'atteindre les cellules tumorales dans le cerveau. Quelques années plus tard une autre équipe : Lyons et al, a montré qu'en plus de marquer les cellules de gliomes, la CTX marquait aussi spécifiquement les cellules tumorales de la même origine neuroectodermique, augmentant ainsi le potentiel thérapeutique de la molécule (Lyons et al., 2002).

b. Effet biologique

En tant que composant du venin, la CTX induit une paralysie chez les insectes ayant été piqués par le scorpion. Lorsqu'elle est injectée chez les vertébrés aucune toxicité n'est observée. La cible liant donc la CTX à la surface des cellules chez les vertébrés n'est donc pas liée à une fonction essentielle à la survie de la cellule. Il a été observé à de nombreuses reprises que si la CTX n'a pas d'effet sur un tissu sain, elle en avait en revanche sur les cellules de gliomes. De nombreuses études ont montré un effet anti-migratoire et anti-invasif de la CTX (Soroceanu et al., 1999; Deshane et al., 2003; Olsen et al., 2003; Sontheimer et al., 2006; Sontheimer, 2008; Veisheh et al., 2009c; Lui et al., 2010). A l'heure actuelle, il y a 3 cibles de la CTX décrites : les canaux chlore (découverts en 1er), la matrice metalloprotéase MMP-2 et l'annexine A2. L'ensemble de ces cibles sont compatibles avec la capacité / particularité de la CTX à marquer les cellules cancéreuses et à inhiber la migration et l'invasion de ces dernières.

De façon historique la CTX a d'abord été identifiée comme agissant sur les canaux chlore (DeBin et al., 1993). La toxine serait capable de bloquer les canaux chlore de faible conductance et a été longtemps utilisée comme outil pharmacologique pour l'étude des canaux chlore. C'est au cours d'une de ces études que Ulrich et al 1998, ont fait la découverte d'un courant chlore spécifique sensible à la CTX dans des coupes de gliomes humains. Après des investigations plus poussées, il a été démontré que la CTX interagit avec un canaux chlore de la famille des CIC (Sontheimer et al., 2006). Une exposition prolongée à la CTX entrainerait l'internalisation du canal. L'hypothèse de ce canal chlore comme récepteur de la CTX est très intéressante, car même si les gliomes présentent une variabilité génétique importante, il semble avoir en commun la surexpression de canaux chlore, ces derniers n'étant que faiblement voire non exprimés dans les tissus sains (Ullrich and Sontheimer, 1997; Olsen et al., 2003; Turner

and Sontheimer, 2014). Ce canal chlore pourrait jouer un rôle dans le changement de forme de la cellule cancéreuse, lui permettant ainsi de migrer et d'envahir le tissu sain (Rouzai-Dubois et al., 2000). Ainsi la CTX agirait en inhibant les échanges Cl^- , limitant le changement de forme de la cellule, prévenant ainsi l'invasion du tissu sain par les cellules cancéreuses, ce qui correspond aux observations d'effets anti-migration, anti-invasion de la CTX.

Cependant l'ensemble de ces arguments en faveur d'un canal chlore comme récepteur sont contrebalancés par des données négatives : une inhibition du canal avec une affinité inférieure à celle attendue (Ullrich et al., 1998), et l'identification de 2 sites de liaison avec des affinités différentes chez des lignées cellulaires de gliome *in vitro* (Soroceanu et al., 1998). Ce dernier résultat nous laisserait penser à l'existence de plusieurs récepteurs membranaires de la CTX. C'est pourquoi lorsque Deshane et al. ont publié en 2003 un article expliquant que la chlorotoxine en plus d'interagir avec le canal chlore CIC-3, interagirait avec un complexe protéique contenant entre autre la matrix metalloprotéase MMP-2, le problème de l'identification de la cible de la CTX semblait résolu (Deshane et al., 2003). En effet la matrix metalloprotéase MMP-2, est une enzyme de la famille des métalloprotéases qui est exprimée uniquement dans les gliomes et autres types de tumeurs mais pas dans les tissus sains. Cette enzyme a été associée avec la dégradation de la matrice extracellulaire, générant des espaces au travers desquels les cellules anticancéreuses vont pouvoir envahir les tissus sains environnants. Tous les types de tumeurs sur-exprimant la MMP-2 fixent la CTX. Cette corrélation semble confirmer la présence de la MMP-2 dans le complexe protéique liant la toxine. Cependant, on ne sait toujours pas comment un peptide de cette taille pourrait interagir simultanément avec un complexe protéique. Mais l'idée que la CTX se lie à un récepteur qui va par la suite entrainer l'internalisation d'un complexe contenant à la fois CIC-3 et MMP-2 est possible et expliquerait les résultats obtenus par Veisheh et al avec leurs nanoparticules marquées à la CTX (Veisheh et al., 2007). En réalisant une expérience de pulldown avec une nanoparticule fonctionnalisée avec de la CTX et de la MMP-2 recombinante ils n'ont pas réussi à observer une liaison spécifique entre les deux composés.

Alors que l'on pensait la question de la cible de la CTX résolue une publication en 2009 est venue relancer les débats (Kesavan et al., 2009). En effet cette équipe a montré que la CTX est capable de se fixer à l'annexin A2. Il s'agit d'une protéine dépendante du calcium liant les phospholipides; elle est retrouvée à la fois dans les tissus cancéreux mais aussi dans les cellules endothéliales. Elle interviendrait dans plusieurs fonctions cellulaires comme, l'angiogenèse, l'apoptose, la migration, la prolifération, l'invasion et la cohésion tissulaire.

Pour l'heure on a peu de données décrivant la liaison de la CTX sur ces 3 cibles (et particulièrement sur l'annexin A2) et malheureusement il semble que l'élucidation du mystère concernant le récepteur de la toxine reste complet tant qu'aucune étude structure-activité fonction ne sera réalisée.

c. Les chlorotoxine-like peptides

Bien que l'on ait plus de données sur l'utilisation de la CTX que sur son mécanisme d'action, il a déjà été lancé des études afin de trouver d'autres peptides/ toxines de scorpion possédant des caractéristiques identiques à celle de la CTX. Ainsi en se basant sur une homologie de séquence et d'action, plusieurs peptides ont été identifiés comme de potentiels analogues de la chlorotoxine (Tableau 4). Cependant seulement quatre d'entre eux, partagent avec la CTX une activité sur les canaux chlore. Il s'agit de :

- AaCTx, extrait du venin de scorpion : *Androctonus australis* (Rjeibi et al., 2011).
- BmKCT, extrait du venin de scorpion : *Buthus martensii Karsch* (Zeng et al., 2000; Fu et al., 2005).
- GaTx1 et GaTx2, extrait du venin de scorpion : *Leiurus quinquestriatus* (Fuller et al., 2007; Thompson et al., 2009).

L'AaCTx est un petit peptide de 34 acides-aminés ayant une homologie de séquence de 61% avec la CTX. Tout comme cette dernière, elle possède 8 cystéines formant des ponts disulfures selon le même modèle. Douze acides aminés diffèrent avec la CTX, ce qui conduit à une charge net de l'AaCTx de +4 alors que celle de la CTX est de +3. La neurotoxicité de la toxine a été évaluée par Rjeibi et al. Ils ont montré que l'injection intra-ventriculaire de 1 µg de toxine chez la souris n'était pas toxique (Rjeibi et al., 2011). La dose utilisée lors de cette étude étant élevée, il en a été conclu que l'AaCTx était non-toxique pour les mammifères. L'effet de la toxine sur la migration et l'invasion cellulaire de gliome a montré qu'elle était moins active que la chlorotoxine, avec pour l'AaCTx une IC₅₀ de 125 µM (migration) et 10 µM (invasion) alors que pour les deux processus la CTX agit pour des concentrations proches de 600 nM (Soroceanu et al., 1999; Rjeibi et al., 2011). Rjeibi et al n'ont pas trouvé d'effet de la toxine sur les protéines de la matrice extracellulaire (Fibronectine, fibrinogène, vitronectine, laminine et collagène de type IV), ils supposent que AaCTx agit via les canaux chlore. Pour l'heure, la toxine n'a pas été utilisée pour l'administration ciblée de composés.

Contrairement à AaCTx, BmKCT est l'analogue de la CTX qui est le plus étudié. Il est extrait du venin d'un scorpion chinois *Buthus martensii karsh* dont il a été montré qu'il avait un effet sur la croissance des tumeurs de glioblastomes et induirait l'apoptose des cellules cancéreuses. Pour l'instant, l'ensemble des molécules actives du venin n'a pas été caractérisé (Goudet et al., 2002; Wang and Ji, 2005). Il s'agit d'un peptide de 36 acide-aminés qui a une homologie de séquence avec la chlorotoxine de 68%. En 2005, Fu et al ont déterminé la toxicité de cette toxine: LD₅₀ de 4,3 mg/kg chez la souris. Afin de déterminer les propriétés de BmKCT et d'évaluer son potentiel thérapeutique, de nombreuses études ont été réalisées : toxicité comparée cellule de gliome / astrocyte, patch-clamp analyse, et étude histologique. BmKCT inhibe la croissance cellulaire des cellules SHG-44 de façon dose dépendante avec un IC₅₀ de 0,28 µM alors que l'IC₅₀ chez les astrocytes normaux est de 8 µM. Il existe donc une spécificité

Toxine	Structure primaire	Taille	Identité	Motif des ponts disulfures	Espèces
Chlorotoxin	MC ₁ MPC ₂ FTTDH QMARK C ₃ DDC ₄ C ₅ G GK-G RGKC ₆ Y GPQC ₇ L C ₈ -R--	36 AA	100%	C ₁ -C ₄ ,C ₂ -C ₆ ,C ₃ -C ₇ ,C ₅ -C ₈	<i>Leiurus quinquestriatus quinquestriatus</i>
I₃	MC ₁ MPC ₂ FTTDH QTARR C ₃ RDC ₄ C ₅ GGR-G R-KC ₆ F G-QC ₇ L C ₈ GYD	36 AA	82%	C ₁ -C ₄ ,C ₂ -C ₆ ,C ₃ -C ₇ ,C ₅ -C ₈	<i>Buthus eupeus</i>
I₄	MC ₁ MPC ₂ FTTDH NMAKK C ₃ RDC ₄ C ₅ GGN-- -GKC ₆ F GPQC ₇ L C ₈ NR	35 AA	82%	C ₁ -C ₄ ,C ₂ -C ₆ ,C ₃ -C ₇ ,C ₅ -C ₈	<i>Buthus eupeus</i>
Bs-8	RC ₁ KPC ₂ FTTDP QMSKK C ₃ ADC ₄ C ₅ G GK-G KGKC ₆ Y GPQC ₇ L C ₈	35 AA	80%	C ₁ -C ₄ ,C ₂ -C ₆ ,C ₃ -C ₇ ,C ₅ -C ₈	<i>Buthus indicus</i>
I₅	MC ₁ MPC ₂ FTTDP NMANK C ₃ RDC ₄ C ₅ GGG-K K--C ₆ F GPQC ₇ L C ₈ NR	35 AA	79%	C ₁ -C ₄ ,C ₂ -C ₆ ,C ₃ -C ₇ ,C ₅ -C ₈	<i>Buthus eupeus</i>
I_{5A}	MC ₁ MPC ₂ FTTDP NMAKK C ₃ RDC ₄ C ₅ GGN-G K--C ₆ F GPQC ₇ L C ₈ NR	35 AA	79%	C ₁ -C ₄ ,C ₂ -C ₆ ,C ₃ -C ₇ ,C ₅ -C ₈	<i>Buthus eupeus</i>
GaTx1	-C ₁ GPC ₂ FTTDH QMEQK C ₃ AEC ₄ C ₅ GGI-G K--C ₆ Y GPQC ₇ L C ₈ NR	34 AA	79%	C ₁ -C ₄ ,C ₂ -C ₆ ,C ₃ -C ₇ ,C ₅ -C ₈	<i>Leiurus quinquestriatus hebraeus</i>
BmKCT	-C ₁ GPC ₂ FTTDA NMARK C ₃ REC ₄ C ₅ GGI-G K--C ₆ F GPQC ₇ L C ₈ NRI	35 AA	76%	C ₁ -C ₄ ,C ₂ -C ₆ ,C ₃ -C ₇ ,C ₅ -C ₈	<i>Buthus martensii</i>
Bm12-b	-C ₁ GPC ₂ FTTDA NMARK C ₃ REC ₄ C ₅ GGN-G K--C ₆ F GPQC ₇ L C ₈ NRE	35 AA	76%	C ₁ -C ₄ ,C ₂ -C ₆ ,C ₃ -C ₇ ,C ₅ -C ₈	<i>Buthus martensii</i>
Lqh-8/6	RC ₁ SPC ₂ FTTDQ QMTKK C ₃ YDC ₄ C ₅ G GK-G KGKC ₆ Y GPQC ₇ I C ₈ APY	38 AA	72%	C ₁ -C ₄ ,C ₂ -C ₆ ,C ₃ -C ₇ ,C ₅ -C ₈	<i>Leiurus quinquestriatus hebraeus</i>
I₁	MC ₁ MPC ₂ FTTTP DMAQQ C ₃ RAC ₄ C ₅ KGR-G K--C ₆ F GPQC ₇ L C ₈ GYD	36 AA	71%	C ₁ -C ₄ ,C ₂ -C ₆ ,C ₃ -C ₇ ,C ₅ -C ₈	<i>Buthus eupeus</i>
Neurotoxin P2	-C ₁ GPC ₂ FTTDP YTESK C ₃ ATC ₄ C ₅ GGR-G K--C ₆ V GPQC ₇ L C ₈ NRI	35 AA	70%	C ₁ -C ₄ ,C ₂ -C ₆ ,C ₃ -C ₇ ,C ₅ -C ₈	<i>Androctonus mauretanicus mauretanicus</i>
Lepidopteran	RC ₁ GPC ₂ FTTDP QTQAK C ₃ SEC ₄ C ₅ GRK-G G-VC ₆ K GPQC ₇ I C ₈ GIQ	37 AA	63%	C ₁ -C ₄ ,C ₂ -C ₆ ,C ₃ -C ₇ ,C ₅ -C ₈	<i>Buthus tamulus</i>
AaCtx	MC ₁ IPC ₂ FTTNP NMAAK C ₃ NAC ₄ C ₅ GSRRG S--C ₆ R GPQC ₇ I C ₈	34 AA	61%	C ₁ -C ₄ ,C ₂ -C ₆ ,C ₃ -C ₇ ,C ₅ -C ₈	<i>Androctonus australis</i>
Bs-14	-C ₁ GPC ₂ FTKDP ETEKK C ₃ ATC ₄ C ₅ GGI-G R--C ₆ F GPQC ₇ L C ₈ NRGY	36 AA	61%	C ₁ -C ₄ ,C ₂ -C ₆ ,C ₃ -C ₇ ,C ₅ -C ₈	<i>Buthus indicus</i>

Tableau 4 : Alignement des séquences peptidiques de la CTX et des chlorotoxine-like peptides, les alignements ainsi que le pourcentage d'identité ont été obtenu en utilisant @TOME v2 (Pons and Labesse, 2009), le motif des ponts disulfures si connue

d'action de cette toxine. De plus l'étude histologique chez la souris a montré que BmKTC ciblait de façon spécifique le cerveau, le cœur et le squelette. Grâce aux études de patch clamp cellule entière, que BmKTC était capable d'inhiber les courants chlores des cellules SGH-44(Fu et al., 2007). Comme pour la CTX, il a été montré que la toxine peut se lier à la MMP-2 (Fu et al., 2006, 2011). Toutes ces similitudes avec la CTX ont mené au développement d'un composé basé sur BmKCT pour traiter, marquer les cellules cancéreuses (Fu et al., 2012a). Un brevet a même été déposé pour utiliser BmKCT comme un peptide de délivrance d'anti-tumoraux (Dahe, 2007).

GaTx1 et GaTx2 sont deux toxines extraites du venin du scorpion *Leiurus quinquestriatus hebraeus*. GaTx1 est un peptide de 34 résidus d'acide aminé ayant une homologie de séquence de 79%. Elle est connue pour agir sur le canal « cystic fibrosis transmembrane conductance regulator » (CFTR). C'est un récepteur de la famille des ABC, mais qui possède aussi une activité intrinsèque sur les canaux chlore. Ce récepteur est connu pour son implication dans la fibrose kystique. GaTx1 est un inhibiteur réversible spécifique des canaux CFTR qui se lie sur la face cytoplasmique du récepteur. Ce peptide est actuellement utilisé comme un outil moléculaire pour comprendre le rôle fonctionnel de CFTR (Fuller et al., 2007). GaTx2 est un peptide de 29 acides aminés qui a une faible homologie de séquence avec CTX (38 %). Cependant, cette toxine est décrite comme agissant sur les canaux chlore CIC-2. Ces canaux appartiennent à la même famille que les canaux CIC-3 et sont aussi surexprimés à la membrane des cellules cancéreuses (Ullrich et al., 1998; Thompson et al., 2009). Le rôle physiologique de CIC-2 n'est pas encore défini, mais il est raisonnable de penser qu'il a un rôle semblable à CIC-3 dans l'invasion cellulaire et la migration des cellules de gliome. GaTx2 inhibe CIC-2 en ralentissant son activation et l'inhibition résultante est dépendante du voltage. De façon intéressante, GaTx2 a été décrit plus tôt en 1997 sous le nom de leiuopeptide II sans être plus caractérisé (Buisine et al., 1997). Il est raisonnable de penser que GaTx2 peut être utilisé comme outil pharmacologique pour étudier et déterminer le rôle des canaux CIC-2. Mais comme ces canaux sont surexprimés chez les cellules de gliome, il est envisageable de l'utiliser comme toxine de ciblage des gliomes, mais cela reste à tester.

En dehors de ces quatre toxines, deux autres toxines animales valent la peine d'être mentionnées. D'abord, Lqh-8/6 isolé du venin du scorpion *Leiurus quinquestriatus hebraeus* et Bs14 isolé du venin du scorpion *Buthus indicus*. Ce sont des peptides de 38 et 36 acides aminés, respectivement, partageant une homologie de séquence de 72% et 61% respectivement et de structure avec la CTX (8 résidus cystéine conduisant à un repliement identique). L'ensemble de ces données suggère une action sur des canaux chlore, cependant aucune étude n'a encore été menée. Ce qui nous laisse espérer que ces deux peptides sont de nouveaux analogues de la CTX.

II. Chlorotoxine et chlorotoxine–like peptide : applications thérapeutiques

a. *Agent de marquage*

La première option thérapeutique dans le traitement du glioblastome est l'ablation/ le retrait de la masse tumorale. Malheureusement, les glioblastomes sont des tumeurs extrêmement invasives et non donc pas de contour clairement délimité. C'est un problème pour les chirurgiens lorsqu'ils veulent délimiter clairement la tumeur pour en déterminer son volume et retirer entièrement la masse tumorale. Le glioblastome est un cancer agressif, si l'ensemble des cellules cancéreuses n'est pas retiré lors de l'opération, inexorablement une nouvelle masse tumorale va se développer à partir des cellules restantes. C'est pour cela qu'il est très important d'être capable de visualiser précisément la masse tumorale et ces bords en particulier. L'existence de toxines comme la chlorotoxine ciblant les cellules cancéreuses de glioblastome est source d'espoir et d'inspiration pour le développement de sondes de marquage. De plus ces toxines étant synthétisables chimiquement et facilement modifiables, elles sont un outil potentiel à la fois pour l'imagerie et pour la thérapie. Sur la base de ce principe, trois types de composés ont été conçus. Le premier type est composé de CTX couplée de façon covalente à un fluorochrome, Cy5.5. Cet outil devrait permettre à un chirurgien de directement visualiser des cellules cancéreuses en temps réel pendant la résection de la tumeur (Veiseh et al., 2007; Akcan et al., 2011; Stroud et al., 2011). Le deuxième type de composé est de la CTX couplée à un ligand contrastant pour l'imagerie à résonance magnétique (IRM) (Hockaday et al., 2005; Veiseh et al., 2005; Sun et al., 2008a). Finalement, le troisième type de complexe est une nanoparticule multifonctionnelle, avec un agent de contraste pour l'IRM ou un fluorochrome associé à un agent thérapeutique ou non. La nanoparticule est fonctionnalisée avec de la CTX pour le ciblage (Veiseh et al., 2005, 2009c, 2010; Meng et al., 2007; Sun et al., 2008b). Jusqu'à présent la CTX est le peptide de ciblage du glioblastome le plus développé pour cette approche. De ce fait les exemples développés par la suite seront des composés à base de CTX.

L'application la plus connue de la CTX comme agent de marquage est le « Tumor pain » (Veiseh et al., 2007). Il s'agit de CTX marquée avec un fluorochrome la Cy5,5. L'intérêt de ce composé repose dans le choix du fluorochrome, en effet, la Cy5,5 présente la particularité d'émettre des photons qui sont peu absorbés par l'eau et l'hémoglobine, permettant ainsi son utilisation en bloc opératoire. Le couplage du marqueur à la toxine est effectué via une liaison entre le NHS ester de la Cy5,5 et une amine d'une des lysines présente dans la CTX (Veiseh et al., 2007). Le problème avec ce protocole c'est que l'on se retrouve avec un mélange de toxine marqué à la Cy5,5 à différentes positions. Cela rend son utilisation telle quelle en clinique coûteuse puisqu'il faudrait maintenir entre chaque lot le même ratio des différents marquages du peptide. Afin de remédier à ce problème Akcan et collaborateur, ont simplement remplacé les lysines 15 et 23 par une alanine ou une arginine ne laissant alors plus qu'une seule position

possible pour le marquage (Akcan et al., 2011). Les lysines en positions 15 et 23 ont été choisies puisqu'elles réagissaient peu avec la Cy5,5. La même équipe a aussi réalisé le même mono-marquage sur une forme non mutée cyclique de la CTX. L'ensemble de ces composés ont montré qu'ils gardaient leur capacité à cibler les cellules cancéreuses. Des études de toxicité et de bio-distribution chez la souris, ont permis de mettre en évidence une élimination rénale du produit, l'absence de toxicité majeure, ainsi qu'une distribution homogène du composé dans l'organisme après injection IV (Veiseh et al., 2007). A côté de ces essais le groupe d'Olson a étudié la stabilité de la CTX. Seulement 30% de CTX est dégradée après incubation pendant 24h dans du sérum humain à 37°C (Akcan et al., 2011). Cela traduit une bonne résistance de la toxine au peptidase, qui est intéressante pour le développement de produits à durée de vie longue.

Un des examens le plus courant pour déterminer la localisation et le volume de la masse tumorale est l'IRM. Cependant même en utilisant un bon agent de contraste, il n'est pas possible de visualiser précisément les bords de la tumeur. C'est dans l'optique d'améliorer le ciblage de ces produits de contraste que Huang et collaborateur créèrent une macromolécule : « L-Lysine dendritique macromolécule », capable de chélater le gadolinium et de fixer la CTX. Ainsi ils ont obtenu un nouvel agent de contraste avec un temps de rétention dans la cellule tumorale accru. L'utilisation de cette agent a aussi permis d'augmenter la force du signal enregistré au cours d'un IRM (Huang et al., 2011a). Les nanoparticules sont aussi utilisées comme agents de contraste et même si elles montrent une meilleure résolution des bords de la tumeur que le gadolinium, elles semblent plus marquer le système réticulo-endothelial entourant la tumeur que les cellules tumorales elles-mêmes. Afin d'améliorer leur ciblage, des nanoparticules au noyau de fer ont été fonctionnalisées avec de la chlorotoxine. Leurs essais *in vitro* et *in vivo* ont montré une amélioration du ciblage des nanoparticules. Aucune toxicité de ces nanoparticules fonctionnalisées n'a été observée.

Mais le point le plus intéressant concernant ces nanoparticules, c'est que toutes les molécules de PEG ne sont pas fonctionnalisées par la CTX. Il en reste des libres. Il est donc possible d'ajouter d'autres caractéristiques à ces nanoprobés et ainsi créer des nanoparticules multifonctionnelles (Veiseh et al., 2005, 2009c; Meng et al., 2007). Les premières particules créées sur ce modèle par Veiseh et collaborateur sont des particules avec un noyau fer coater avec des molécules de PEG. Ces molécules de PEG ont été fonctionnalisées à la fois par de la CTX et aussi par de la Cy5,5 (Veiseh et al., 2005). L'intérêt de ce double marquage réside dans la possibilité de comparer les images IRM préopératoire avec les images intra opératoires. Le composé ayant montré un temps de rétention par les cellules cancéreuses d'environ 5 jours, il serait possible de faire le suivi opératoire IRM sans avoir à réinjecter de produit. Une nanoparticule semblable a aussi été synthétisée mais présente un moindre intérêt clinique puisqu'à la place de la Cy5,5 c'est du isothiocyanate de fluorescéine (FITC) qui a été fixé. Les propriétés optiques du FITC ne lui permettent pas d'être utilisé *in vivo* (Meng et al., 2007).

Evidemment l'existence de composés multifonctionnels, ne se limite pas juste à la détection des cellules cancéreuses ; il a été envisagé/développé des composés à base de CTX permettant à la fois le diagnostic, suivi de la tumeur et son traitement. Je reviendrais sur ce sujet dans la section suivante. C'est à cause de l'existence de ce potentiel double effet de la CTX que je n'ai pas encore abordé le cas de la CTX marquée à l'iode 131 : ¹³¹I-TM601. En effet ce composé d'abord pour la radiothérapie, s'est montré efficace pour visualiser la tumeur. Comme pour les nanoparticules multifonctionnelles, j'aborderai ce composé dans la section suivante. Le **Tableau 5** regroupe les différents composés à base CTX qui ont été développés jusqu'à présent que ce soit à visée thérapeutique ou pour l'imagerie.

Types de liaison	Cargo	Application	Références
Directe	<i>Iode</i> ¹²⁵ I, ¹³¹ I	Radiothérapie et Imagerie	(Soroceanu et al., 1998; Hockaday et al., 2005; Shen et al., 2005; Mamelak and Jacoby, 2007; Yin et al., 2007; Jacoby et al., 2010; Wu et al., 2010; Huang et al., 2011a)
	<i>Fluorochromes</i> Cy5.5 Oregon green	Imagerie et détection	(Soroceanu et al., 1998; Veiseh et al., 2007; Kesavan et al., 2009)
	<i>Agent thérapeutique</i> Platinum Anticancéreux	Thérapeutique	(Graf et al., 2012; Nicolaidis et al., 2013)
	<i>Biotine</i>	Immunomarquage	(Soroceanu et al., 1998)
	<i>Oxide nitrique</i>	Adjuvant thérapeutique	(Safdar et al., 2013)
Véhicule	<i>Nanoparticules</i> Noyau de super-oxyde de fer	Agent de contraste IRM	(Akcan et al., 2011)
	Nanoprobe multifonctionnelle + Fluorochrome (Cy5.5, FITC, Alexa fluor)	Agent de contraste IRM et imagerie	(Veiseh et al., 2005, 2009b; Huang et al., 2011a)
	Nanoprobe multifonctionnelle + cADN ou siARN	Agent de contraste IRM et thérapeutique	(Veiseh et al., 2009c; Kievit et al., 2010)
	Nanoprobe multifonctionnelle + Methotrexate	Thérapeutique et agent de contraste IRM	(Meng et al., 2007)
	PEI core +cADN +Fluorochrome	Thérapeutique et imagerie	(Veiseh et al., 2009a; Huang et al., 2011b)
	<i>Liposome</i> Chargé en doxorubicine	Thérapeutique	(Xiang et al., 2011)
	<i>Dendrigraft de polylysine</i> avec du Gadolinium	Agent de contraste IRM	(Stroud et al., 2011)
	<i>Capsule vide de l'hépatite B</i>	Vecteur thérapeutique	(Kasai et al., 2012)

Tableau 5 : Exemples de complexes CTX-cargo et leurs applications

b. Agent thérapeutique

La prise en charge thérapeutique des gliomes passe aussi par la radiothérapie associée ou non à de la chimiothérapie. L'utilisation de la chlorotoxine ou de chlorotoxin like peptide dans l'administration de thérapeutique représente un potentiel important. Puisque l'objectif de tout médicament est d'atteindre sa cible et uniquement sa cible, les propriétés de ciblage sont très importantes, d'autant plus dans le traitement des cancers. Ce ciblage va ainsi permettre de limiter les toxicités et effets indésirables du composé. (**Tableau 5**)

Le 1^{er} agent thérapeutique à base de CTX développé est le ¹³¹I-TM601. Il s'agit du nom commercial d'un dérivé synthétique de la CTX (=TM601) marqué à l'iode 131 sur la tyrosine 29. Assez rapidement après la découverte du potentiel thérapeutique de la CTX, de nombreux brevets ont été déposés pour en contrôler son utilisation. Ainsi ¹³¹I-TM601 a fait l'objet d'un grand nombre de publication (Hockaday et al., 2005; Shen et al., 2005; Mamelak et al., 2006; Mamelak and Jacoby, 2007; Yin et al., 2007; Kesavan et al., 2009; Jacoby et al., 2010; Wu et al., 2010; Zhai et al., 2011). Depuis 2002, ¹³¹I-TM601 est en essai clinique aux États-Unis. Les résultats de phase 1 ont permis de déterminer l'innocuité, la biodistribution, la tolérance et la dosimétrie du composé après injection intra-cavitaire chez des patients adultes atteints de gliome de haut grade (Mamelak et al., 2006). L'injection intra-cavitaire correspond à une mono-injection de 10mCi du composé (0,25 à 1mg de CTX) dans la cavité laissée après la résection chirurgicale de la tumeur. Les résultats ont montré une bonne tolérance du composé sur la période d'observation de 180 jours. Comme espéré, le produit s'accumule au niveau des marges de résection de la tumeur, permettant la délivrance localisée des radiations, de façon à ce que le tissu sain ne soit pas affecté. Aucune mort ou toxicité majeure liée à ¹³¹I-TM601 ayant été observée, la FDA a autorisé le projet à se poursuivre en phase 2-3 (Mamelak et al., 2006; Mamelak and Jacoby, 2007; Wu et al., 2010). Cependant il est à noter que 3 des 18 patients, ont développé des effets indésirables (fièvre, faible œdème cérébral, infection de la cavité tumorale...) qui ont été attribués à la méthode d'injection (utilisation d'un réservoir Ommaya). En parallèle de ces essais, le même groupe a réalisé des tests avec une injection intra-veineuse de ¹³¹I-TM601 mais cette fois-ci pour une application en imagerie et non en thérapeutique (Hockaday et al., 2005). Une injection de ¹³¹I-TM601 permet de visualiser la tumeur par scintigraphie, mais semble aussi marquer l'estomac. Jusqu'à présent TM601 est le seul composé à base de CTX qui ait des résultats d'essai clinique chez l'homme publiés.

En plus de ces études sur l'utilisation de CTX iodé, beaucoup de travail a été fourni sur la vectorisation ciblé d'agent thérapeutique (anti-tumoraux, cDNA, siRNA...) via des nanoparticules (Sun et al., 2008b; Veiseh et al., 2009a, 2010; Kievit et al., 2010; Huang et al., 2011b; Fu et al., 2012b). Deux types de nanoparticules peuvent être distingués en fonction de leur noyau. Il peut être soit à base de polymère (polyéthylèneimine ou de poly(amidoamine)) ou à base de super-oxyde de fer. Les nanoparticules à base de polymère ont été utilisées avec succès pour l'administration de cADN à des cellules cancéreuses (Veiseh et al., 2009a; Huang et

al., 2011b). Ces composés représentent une alternative à l'utilisation de virus comme vecteur pour la transfection de cellule *in vivo*. Les nanoparticules au noyau composé de fer, présentent un double avantage puisqu'il s'agit des nanoparticules multifonctionnelles abordées dans la section précédente. Elles peuvent donc être utilisées à la fois pour visualiser la tumeur par IRM mais aussi pour la soigner, avec un avantage en plus pour les nanoparticules au cœur de fer super-paramagnétique qui peuvent être utilisées comme dans les thérapies hyperthermiques contre les cellules cancéreuses. Ainsi deux nouveaux composés ont été développés, il s'agit de nanoparticules à noyaux de fer fonctionnalisées avec de la CTX et aussi par du méthotrexate ou un siARN (Sun et al., 2008b; Veisoh et al., 2010). Ces deux agents s'accumulent dans les cellules de gliome et ont permis l'augmentation de la toxicité du méthotrexate pour la particule fonctionnalisée avec l'agent anticancéreux et un effet inhibiteur correct pour celle au siARN. Une autre équipe a utilisé ces nanoparticules pour transférer des cellules cancéreuses avec un plasmide codant pour une « green fluorescence protein » (GFP). Ils ont ainsi prouvé que ces particules représentaient un vecteur de transfection viable de cellule anticancéreuse (Kievit et al., 2010). Bien que ces résultats soient extrêmement prometteurs, il faudra malheureusement devoir attendre longtemps avant de voir un tel composé sur le marché. En effet, très peu de médicaments à base de nanoparticule existent et sont développés pour une mise sur le marché en raison d'une faible connaissance des dangers de l'usage de telles particules *in vivo* (devenir de la particule une fois dans l'organisme).

Heureusement les nanoparticules ne sont pas les seuls vecteurs fonctionnalisables disponibles. Xiang et collaborateur ont conçu avec succès un liposome chargé en doxorubicine et fonctionnalisé avec de la CTX (Xiang et al., 2011). L'utilisation de ce vecteur a conduit à une meilleure accumulation de doxorubicine dans les cellules cancéreuses suivie d'une augmentation de sa toxicité.

La CTX a aussi été utilisée directement comme agent thérapeutique grâce au couplage par liaison covalente avec un agent thérapeutique (Graf et al., 2012; Safdar and Taite, 2012; Safdar et al., 2013). Graf et collaborateur ont synthétisé un complexe composé de CTX lié à du platini(IV). Ce composé a été créé pour être un analogue aussi efficace que le cisplatine. En effet bien que le cisplatine soit un anti cancéreux efficace et largement utilisé, il a de nombreux effets secondaires. Ce nouveau complexe de platine offre une toxicité similaire à celle du cisplatine tout en amenant des propriétés de ciblage ; ce composé est très prometteur mais des études supplémentaires sont nécessaires pour pouvoir caractériser complètement ce nouveau composé. Une étude récente présente une approche originale de l'utilisation de la CTX dans la prise en charge thérapeutique des gliomes. En effet cette fois, au lieu de coupler un agent anticancéreux à la CTX, c'est un adjuvant le mono-oxyde d'azote qui a été utilisé (Safdar et al., 2013). Safdar et collaborateur, ont en effet couplé l'oxyde d'azote à la CTX afin de former un diazeniumdiolate donneur d'oxyde d'azote (Safdar and Taite, 2012). Ce composé va alors induire une chemo-sensibilité chez la cellule cible. Ainsi lors du traitement par du temozolomide

ou de la carmustine des cellules tumorales, on va observer une augmentation de leur toxicité chez les cellules traitées avec NO-CTX. Bien que le mécanisme d'action de l'oxyde d'azote ne soit pas encore élucidé, cet article ouvre l'esprit à de nouvelles approches thérapeutiques pour améliorer les molécules existantes.

Deux autres approches méritent d'être mentionnées ici sur l'utilisation de la CTX en thérapeutique. Il s'agit des travaux de Veiseh et collaborateur ainsi que ceux de Kasai et collaborateur. En effet pour le premier, ils ont conçu une nouvelle nanoparticule à noyau de fer, recouverte de PEG fonctionnalisé avec de la CTX et de l'Alexa fluor 680 (Veiseh et al., 2009b). Si on s'arrête ici dans la description du composé il est difficile de comprendre pourquoi il est développé dans la section sur l'utilisation en thérapeutique de la CTX et pas dans la section précédente sur l'imagerie. En fait, cette particule possède deux caractéristiques qui font d'elle un potentiel agent thérapeutique. La première est la composition de son noyau, il s'agit d'une nanoparticule de fer superparamagnétique qui va pouvoir être utilisée dans les thérapeutiques par action thermique. La deuxième correspond à une observation qui a été faite par l'équipe de Veiseh lors des tests des particules. La seule présence de la CTX comme agent de ciblage a aussi des effets anti-migratoires et invasifs sur la tumeur. Ainsi à défaut de tuer les cellules cancéreuses, ces nanoparticules les empêchent de se déplacer et d'envahir le tissu sain. L'équipe de Kasai, a elle crée un nouveau vecteur à base de CTX. Ils sont partis d'une capsule vide du virus de l'hépatite B sur laquelle ils ont fixé un fragment FC d'un anticorps (Kasai et al., 2012). C'est sur ce fragment d'anticorps que la CTX a été couplée. Ces particules vont se fixer préférentiellement sur les cellules de gliomes et vont inhiber la migration et l'invasion de ces dernières. Comme il s'agit d'une capsule vide il est possible d'envisager de la remplir d'un agent toxique pour la cellule cancéreuse.

Il est clair que les propriétés de ciblage de la CTX représentent un potentiel énorme pour le développement de thérapie ciblée pour le gliome. TransMolecular Incorporation (l'entreprise possédant les brevets de TM601) est convaincu de l'intérêt de l'utilisation de la CTX dans le traitement du gliome. Il estime une augmentation de deux ans de la durée de vie des patients avec un traitement à base de TM601. Lorsque l'on prend en compte l'agressivité de ce type de cancer ainsi que les données de survie à 5 ans actuelle pour les patients, on ne peut que constater l'avance considérable que cela représente dans le traitement de cette pathologie.

Chapitre 3 : Glioblastome et anticancéreux

I. Le glioblastome

a. Description et impact

Les glioblastomes ou gliomes de grade 4, représentent 65% des gliomes (tumeurs cérébrales primitives) (Lévy et al., 2014). Rapidement, les gliomes sont des tumeurs cérébrales issues des cellules gliales. En temps normal, ces cellules sont des constituants essentiels du tissu cérébral. Elles ont un rôle de soutien pour les cellules nerveuses, en leur fournissant nutriments et énergie. Elles jouent aussi un rôle important dans le maintien de la barrière hématoencéphalique. Il existe différents types de cellules gliales avec pour chacune différentes fonctions (McPherson, 2013) :

- Les astrocytes : apportent les nutriments et supportent les neurones
- Les oligodendrocytes : fournissent la myéline aux neurones
- La microglie : constitue les cellules gliales qui « mangent » les neurones morts et les pathogènes
- Les cellules de l'épendyme, qui forment les parois des ventricules et qui produisent le liquide cébrospinal.

Les gliomes regroupent l'ensemble des tumeurs provenant de la cancérisation de ces cellules d'où la diversité de leur nom en fonction de leurs origines (astrocytome, oligodendrogliome, glioblastome...). Malheureusement, leur traitement est difficile en raison de l'organe touché, de leur nature infiltrant et de leur faible radiosensibilité. Le pronostic est souvent défavorable et varie en fonction du type de tumeur, de l'âge du patient et de sa localisation dans le cerveau.

Les glioblastomes sont issus des astrocytes et correspondent à la forme la plus agressive et la plus commune des tumeurs cérébrales primitives. Elles se différencient histologiquement des autres grades de gliomes grâce à la présence de cellules nécrosées au cœur de la tumeur, la présence de nombreux vaisseaux sanguins à sa périphérie et la composition hétérogène en cellules avec des cellules de types différents (Glioblastoma (GBM) | American Brain Tumor Association). Comme la tumeur est issue de cellule gliale, elle va très facilement diffuser et infiltrer le tissu sain. La croissance de la tumeur avec des projections tentaculaires est d'autant plus rapide que les cellules la composant se divisent rapidement et sont largement alimentées en nutriments grâce à la densité élevée de vaisseaux sanguins, ce qui rend difficile son ablation chirurgicale (Glioblastoma (GBM) | American Brain Tumor Association; McPherson, 2013).

On dénombre en France environ 2 000 nouveaux cas par an (Lévy et al., 2014). Et l'incidence de ces tumeurs est en augmentation (1/33 330 par an). Elles touchent préférentiellement les adultes (70% des cas entre 45 et 70 ans) et plus les hommes que les femmes (Orphanet: Glioblastome). Il existe deux types de glioblastomes en fonction de leur origine : (i) les glioblastomes primaires, tumeurs *de novo*, c'est la forme la plus commune et la plus agressive. Elle se développe rapidement et avec une évolution rapide (2-3 mois) ; (ii) les glioblastomes secondaires, il s'agit de tumeurs qui ont souvent commencé par une tumeur de grade inférieur et qui ont évolué lentement vers un grade 4 très agressif. On les retrouve souvent chez des personnes autour des 45 ans. Leur évolution est plus lente (Glioblastoma (GBM) | American Brain Tumor Association). La durée médiane de survie est entre 12 et 15 mois (Lévy et al., 2014).

La symptomatologie des glioblastomes va varier en fonction de la zone du cerveau touchée. Cependant on va retrouver quelques symptômes communs : céphalée d'apparition récente et vomissements (dûs à l'augmentation de la pression intracrânienne induit par le développement de la tumeur), associés à des troubles du comportement ou des déficits neurologiques focaux (Orphanet: Glioblastome). On peut aussi parfois observer des crises d'épilepsie. Le diagnostic du glioblastome et son traitement sont relativement urgents puisque ce type de tumeur évolue très vite. Le diagnostic repose sur une IRM afin d'évaluer l'emplacement, la taille de la tumeur et ensuite si possible une biopsie de la masse tumorale. La biopsie va permettre de déterminer le type (grade de la tumeur). Cette étude histologique va être accompagnée d'exams de biologie moléculaire : recherche de la méthylation de la O(6)-methylguanine-DNA methyltransferase (MGMT), marqueur prédictif de sensibilité au témozolamide (Lévy et al., 2014). En fonction du résultat de ce test, de la localisation et de la taille de la tumeur, et de l'âge du patient, au cours de la réunion de concertation pluridisciplinaire, un plan thérapeutique adapté sera mis en place.

b. Prise en charge thérapeutique

L'approche thérapeutique va varier en fonction de l'âge du patient. Deux cas peuvent être identifiés : un patient de moins de 70 ans et un patient de plus de 70 ans.

Ainsi le traitement standard pour un patient de moins de 70 ans repose dans un premier temps sur de la chirurgie avec l'exérèse la plus large possible de la tumeur sans entraîner de déficit cognitif majeur (Stummer et al., 2011). La qualité de l'exérèse est un facteur pronostic majeur, il existe des techniques différentes afin d'aider les chirurgiens à mieux visualiser la tumeur (IRM fonctionnelle préopératoire, IRM en tenseur de diffusion préopératoire, bistouri à ultra-sons, microscope opératoire, loupes binoculaires, neuronavigation, cartographie per-opératoire, échographie per-opératoire, examen extemporané) (Chauffert, 2012). Une résection fluoroguidée est en cour de diffusion en France. Elle consiste à administrer au patient un composé : 5-ALA quelque heures avant l'opération ; ce

composé va permettre de rendre fluorescentes les cellules tumorales, et ainsi permettre de mieux visualiser les bords de la tumeur (Stummer et al., 2006; Jacquesson et al., 2013). Suivant la localisation de la tumeur, une chirurgie éveillée avec cartographie de stimulation peut être utilisée afin d'éviter de créer des déficits majeurs dans les zones fonctionnelles (aire du langage, de la mémoire...) (De Witt Hamer et al., 2012). Malheureusement parfois même avec l'ensemble de ces aides techniques une résection complète de la tumeur n'est pas possible ; dans le meilleur des cas une résection partielle de la tumeur sera réalisée et dans le pire une simple biopsie sera effectuée. La qualité de la résection est évaluée par IRM dans les 48 hrs suivant l'intervention.

Les glioblastomes étant des tumeurs très infiltrantes, même la résection la plus large possible de la tumeur va laisser des cellules tumorales dans le tissu sain. Il est donc nécessaire, afin d'améliorer le pronostic, d'associer l'exérèse tumorale à un protocole de chimioradiothérapie. Le protocole standard est celui de Stupp et collaborateur : radiothérapie de 60 Gy en 30 fractions et six semaines, associée à du témozolomide à la dose de 75 mg/m²/j pendant 42 jours consécutifs, puis six cycles de 150–200 mg/m²/j de j1–j5 débutant tous les 28 jours (Stupp et al., 2005; Lévy et al., 2014). La mise en place de ce protocole a permis de faire passer la survie à 5 ans de 1,9% (en cas de radiothérapie seule) à 9,8%. La durée médiane de survie a elle augmentée de 2,5 mois (Stupp et al., 2009; Lévy et al., 2014). La chimiothérapie adjuvante (six cycles de témozolomide à la dose de 150–200 mg/m²/j de j1–j5 débutant tous les 28 jours) est souvent en pratique clinique prolongée au-delà de ces six cycles. Une étude a montré une augmentation de la survie liée à un plus grand nombre de cycles réalisés (Roldán Urgoiti et al., 2012). Cependant des études prospectives sont nécessaires pour déterminer quel patient bénéficierait le plus de cette augmentation du nombre de cycles (Darlix et al., 2013). Lorsqu'il y a eu résection totale ou quasi-totale de la masse tumorale, il est possible de mettre en place un implant imprégné de carmustine (Gliadel) dans la cavité opératoire. Si son utilisation seule montre un intérêt et une augmentation de la survie, sans augmentation des effets indésirables (Chauffert, 2012) et que sa combinaison avec le protocole de Stupp est possible (Chauffert, 2012), il n'y pas d'étude randomisée qui permette d'en évaluer son effet sur la survie du patient. Il est important aussi de noter que l'implantation de Gliadel est un critère d'exclusion pour la plupart des essais thérapeutiques testant de nouveaux composés.

L'essai du protocole de Stupp a été réalisé sur des patients de moins de 70 ans (Stupp et al., 2005). De ce fait la prise en charge des patients plus âgés diffère légèrement et est plus dû à un avis d'expert qu'à des résultats d'études. De plus, chez les patients de cet âge, il y a souvent présence d'autres pathologies, d'un état général plus altéré et d'une fragilité plus importante. Il y a donc une grande diversité dans les plans thérapeutiques. Ainsi la chirurgie va être proposée mais l'existence de facteurs pronostics défavorables (indice de Karnofsky¹

¹ L'échelle de Karnofsky court de 100 à 0, où 100 représente la pleine santé et 0 la mort, elle permet au médecin d'évaluer la capacité de survie d'un patient à la chimiothérapie.

inférieur à 80%, broncho-pneumopathie chronique obstructive, déficit moteur ou cognitif, trouble phasique, taille tumorale supérieure à 4 cm) peuvent conduire à l'abstention chirurgicale (Chauffert, 2012; Lévy et al., 2014). L'intérêt de la résection par rapport à la biopsie fait actuellement l'objet d'une étude randomisée (Chauffert, 2012; Lévy et al., 2014). Suivant l'état générale et neurologique du patient, il va lui être proposé : (i) une chimioradiothérapie selon le protocole de Stupp standard ; (ii) une radiothérapie seule ; ou (iii) du témozolomide seul (Lévy et al., 2014). La radiothérapie seule correspond soit à une dose de 50 Gy en 25 fractions de 2 Gy (plus efficace que les soins palliatifs) (Keime-Guibert et al., 2007; Chauffert, 2012), soit en une dose de 40,5 Gy en 15 fractions de 2,7 Gy (mêmes résultats que pour une dose de 60 Gy en 30 fractions) (Roa et al., 2004; Chauffert, 2012). La présence de la méthylation de la MGMT peut aider à choisir entre un protocole de radiothérapie seule ou de témozolomide seul. Des études ont montré qu'il y avait une survie globale plus longue avec chimiothérapie lorsque la méthylation était présente : 9,7 contre 6,8 mois. Et en absence de méthylation, c'est la radiothérapie qui permet d'augmenter la probabilité de survie sans progression (Malmström et al., 2012; Wick et al., 2012; Lévy et al., 2014).

Les glioblastomes sont des tumeurs à forts risques de récurrences. Ces récurrences sont généralement locales, proches de la zone irradiée (80 à 86% ont lieu dans le volume irradié dans les deux ans suivant le diagnostic initial) (Lévy et al., 2014). Il n'y a pas de standard de traitement pour les récurrences, Plusieurs choix sont possibles, la décision sera prise au cas par cas au cours de réunions de concertation pluridisciplinaire. Parmi ces options de traitement on retrouve (Lévy et al., 2014) :

- la chirurgie qui semble allonger la médiane de survie, mais dont l'efficacité dépend toujours de la qualité de la résection
- La ré-irradiation en conditions stéréotaxiques, qui permet d'obtenir une durée de survie médiane de 8 à 12,4 mois. Sa seule limitation est le risque de radio-nécrose.
- La chimiothérapie et la thérapie ciblée, il n'y a pas de protocole standard. Les composés utilisés sont le témozolomide, le bévécizumab, l'erlotinib associé au bévécizumab.

c. Les futurs traitements

Avec leurs incidences faibles (2 000/an pour le glioblastome, 53 913/an pour la prostate et 54 062/an pour le cancer du sein), le glioblastome fait partie des maladies rares. Cependant, beaucoup de travaux sont réalisés afin d'améliorer son dépistage et sa prise en charge. Ainsi on compte actuellement 109 essais cliniques nationaux et 5 essais cliniques internationaux (Orphanet: Glioblastome), 32 projets de recherche recensés et 16 projets de recherche multicentrique traitant du glioblastome. Une recherche sur pubmed avec les termes glioblastoma[MH] OR glioblastoma[ti] aboutit à 19 503 réponses. Détailler l'ensemble des travaux effectués pour améliorer le dépistage et la prise en charge du glioblastome serait trop

long et peu intéressant dans le cadre de ma thèse. Je vais donc me concentrer sur les travaux les plus porteurs d'espoir en clinique.

Un des axes principaux dans la recherche contre le glioblastome et comme dans beaucoup de cancers est l'immunothérapie. En effet, l'immunothérapie semble détenir à elle seule la solution « miracle » pour guérir le cancer. La majorité des essais cliniques actuels est basée sur l'utilisation de composés issus de l'immunothérapie. Il est important de faire la différence entre les thérapies ciblées qui vont utiliser des composés dirigés contre une cible particulière et l'immunothérapie, qui consiste en l'utilisation du système immunitaire et de ces outils (antigène, cellules immunitaire...) afin de « relancer » le système immunitaire du patient.

On peut ainsi distinguer 3 approches d'immunothérapie différentes. La première correspond à la création de vaccins contre le glioblastome. Le principe est le même que pour un vaccin classique contre un agent pathogène extérieur. Il va être présenté au système immunitaire un antigène spécifique du glioblastome afin d'induire une réponse du système immunitaire. Dans le meilleur des cas ce dernier est activé et va pouvoir identifier et éliminer les cellules tumorales. Le vaccin anti-glioblastome le plus avancé est un vaccin dirigé contre le variant III du néo-antigène tumoral EGFR (« tumor-restricted neo-antigen EGFR variant III » ; EGFRvIII) (Okonogi et al., 2015). EGFRvIII est une forme mutante active du récepteur au facteur de croissance épidermal (epidermal growth factor receptor ; EGFR) exprimée chez 33% des glioblastomes et jamais dans les tissus sains. Un vaccin à base de cet antigène est actuellement en essai clinique de phase III (Ampie et al., 2015). L'essai clinique de phase II de ce composé a permis de déterminer l'immunogénicité du composé, la survie sans progression et la survie en général après traitement. L'étude a été réalisée sur des patients nouvellement diagnostiqués et ayant subi une résection chirurgicale supérieure à 95% et ne présentant aucun signe de progression tumorale après traitement par chimioradiothérapie standard. Une seule réaction allergique a été observée. A part ça, seule une irritation cutanée au niveau du point d'injection a été observée parmi les patients. L'utilisation du vaccin a montré une augmentation de la survie sans progression et de la survie en générale, respectivement, 14.2 et 26 mois contre 6.3 et 15 mois pour les patients non traités (Ampie et al., 2015; Okonogi et al., 2015). L'utilisation d'un tel vaccin semble très prometteuse. Cependant il reste encore à caractériser l'association de cette vaccination avec le traitement standard par chimioradiothérapie.

La seconde approche consiste à l'utilisation d'inhibiteurs des checkpoints immunitaires (immune checkpoint inhibiteur) (Ampie et al., 2015; Okonogi et al., 2015). Les checkpoints immunitaires vont permettre dans un organisme sain d'éviter les emballements immunitaires qui pourraient induire des dommages dans les tissus sains. Lors de son développement, le glioblastome va utiliser ce système pour éviter l'activation des lymphocytes T. Les cellules de glioblastomes vont favoriser l'apparition de nouveaux checkpoints immunitaires en exposant le système immunitaire de façon chronique à ses antigènes. Cela va forcer le système immunitaire à tolérer la présence de la tumeur. L'utilisation d'inhibiteurs de ces checkpoints immunitaires spécifiques du glioblastome devrait permettre une réactivation des lymphocytes T et donc une

disparition de la tolérance du système immunitaire vis-à-vis du glioblastome (Ampie et al., 2015; Okonogi et al., 2015). Beaucoup de protéines impliquées dans ces checkpoints ont été identifiées, pour l'instant un seul composé est en essai clinique pour comparer son efficacité à celle de l'avastin (bevacizumab) dans la prise en charge de récurrences de glioblastomes. Ce composé, le nivolumab est un anticorps anti-PD-1. PD-1 est une protéine impliquée dans la régulation négative de l'activité des cellules T (Ampie et al., 2015). Elle a été montrée comme étant exprimée dans les lymphocytes T_{régulateur}. Son expression est dépendante de l'activation du lymphocyte. Le nivolumab a déjà montré son efficacité en association avec un autre anticorps inhibiteur de checkpoint immunitaire (ipilimumab) chez des patients atteints de mélanome (Ampie et al., 2015).

Enfin la troisième approche en immunothérapie peut apparaître sous le nom d'ingénierie des lymphocytes T. Il s'agit en fait d'un transfert adoptif de lymphocyte T qui ont été modifiés afin d'exprimer un récepteur d'antigène chimérique (CAR) (Ampie et al., 2015). L'activation de ce récepteur chimérique ne dépend plus du complexe d'histocompatibilité, ce qui permet de contourner les mécanismes de régulation négative du système immunitaire mis en place par le glioblastome. L'intérêt de l'utilisation de telles cellules vient du fait que en plus d'être actives directement contre les cellules tumorales, elles peuvent recruter d'autres composants intervenant de la réponse immunitaire. Il y a actuellement plusieurs essais cliniques en cours pour déterminer l'efficacité et la sûreté de l'utilisation de telles cellules (Ampie et al., 2015).

L'immunothérapie semble présenter à l'heure actuelle le meilleur espoir pour le traitement des glioblastomes. Et cela majoritairement car l'utilisation du système immunitaire permet de contourner les difficultés rencontrées avec la localisation et les caractéristiques de la tumeur. En effet le cerveau est protégé par la barrière hématoencéphalique, ce qui permet de le protéger des agressions extérieures. Cependant en cas de maladie cette barrière devient un obstacle quasi-infranchissable pour les agents thérapeutiques. L'utilisation du système immunitaire permet de s'affranchir de cette barrière. Une autre difficulté réside dans le fait que une fois la barrière franchie, les molécules se retrouvent dans le cerveau, un organe particulièrement fragile avec de faible capacité de régénération, ainsi tout dommage sur le tissu sain devient rapidement problématique. L'agent anticancéreux parfait pour le glioblastome est à la fois capable de passer la barrière hématoencéphalique mais aussi de cibler les cellules cancéreuses. A l'heure actuelle, l'utilisation du système immunitaire du patient semble être la seule approche qui présente ces deux avantages. Cependant il y a actuellement beaucoup d'équipes qui travaillent sur la création de systèmes de vectorisation plus ou moins complexes qui une fois optimisés devrait permettre l'administration d'agents cancéreux classiques dans le cadre du traitement du glioblastome. C'est dans cette optique que ces travaux de thèse ont été menés.

II. La doxorubicine

a. Présentation, historique

La doxorubicine ou adriamycine est un antibiotique cytotoxique de la famille des anthracyclines, obtenue à partir de la bactérie *Streptomyces peucetius var. caesi* avant d'être synthétisée chimiquement. La doxorubicine a une structure chimique particulière commune à tous les anthracyclines. On distingue deux parties (**Figure 9**) :

- Une partie aglycone : composée d'un noyau tétracyclique hydrophobe formant quasiment un plan. Ce noyau est fonctionnalisé par des fonctions quinones et hydroquinones ainsi qu'une chaîne latérale.
- Un sucre rattaché à l'aglycone par le C7

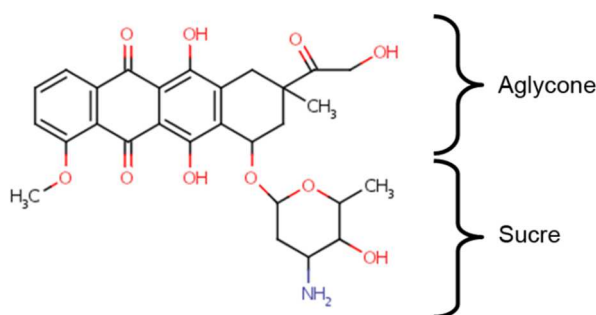


Figure 9 : Structure chimique de la doxorubicine

C'est cette structure particulière qui va permettre à la doxorubicine de s'intercaler dans l'ADN entre deux paires de bases de la double hélice.

La doxorubicine est utilisée depuis 1974 comme anticancéreux. Elle est encore très utilisée notamment dans la prise en charge des cancers de l'ovaire, du sein, de la vessie, de certains lymphomes et des tumeurs solides de l'enfant. Cependant, elle possède une cardiotoxicité importante, dont la prévention repose sur le non dépassement d'une dose cumulée de 550 mg/m². Un autre problème rencontré avec l'utilisation de la doxorubicine est l'apparition de résistances importantes en cas de rechute. De plus à cause de leur capacité à s'intercaler dans le double brin d'ADN, la doxorubicine est un carcinogène connu.

Un autre avantage de la doxorubicine est que la présence de ce noyau tétracyclique lui confère des propriétés de fluorescence.

b. Mécanisme d'action

Le mécanisme d'action de la doxorubicine n'est pas encore complètement résolu. La doxorubicine peut effectuer son action anti-cancéreuse notamment via l'inhibition de la topoisomérase II, l'intercalation dans l'ADN, et la formation de radicaux libres.

L'intercalation dans l'ADN est le premier mécanisme de l'action anti-tumorale attribué à la doxorubicine. Elle a été étudiée par diffraction des rayons X. La partie aglycone de la molécule va s'intercaler entre deux paires successives de nucléotides. Le sucre ainsi que le cycle de l'aglycone à laquelle il est rattaché dépasse dans le petit sillon de l'ADN. Cela va permettre de stabiliser la molécule dans l'ADN (Frederick et al., 1990; Gewirtz, 1999). La doxorubicine s'intercale préférentiellement dans un doublet GC s'il est précédé d'une adénine ou d'une thymine (Wang and Kang, 1999). La présence de la doxorubicine dans la molécule d'ADN va empêcher les enzymes responsables de la transcription de l'ADN (Wang et al., 1987).

Les topoisomérases sont des enzymes essentiels qui contrôlent l'enroulement de la molécule d'ADN. Elles sont les cibles de nombreux agents cytotoxiques. Il existe deux types de topoisomérases :

- Les topoisomérases de type I, qui clivent un seul brin de la molécule d'ADN afin de permettre la rotation du brin intact autour du brin coupé. Elles sont impliquées dans la séparation des brins d'ADN lors de la réplication (topoisomérase I)
- Les topoisomérases de type II clivent les deux brins de la molécule d'ADN transitoirement. Elles sont impliquées dans la séparation de l'enchevêtrement des molécules d'ADN lors de la réplication. (topoisomérase II)

La topoisomérase II est une protéine à plusieurs sous unités. La catalyse de l'ADN par la topoisomérase II se décompose en 6 étapes (Burden and Oshero, 1998) :

- *1^{ère} étape* : liaison à l'ADN, La topoisomérase se lie à l'ADN au niveau de séquences préférentielles même si cette préférence est faible. Cette étape ne requière pas la présence de cofacteur.
- *2^{ème} étape* : la coupure de l'ADN, grâce à la présence d'une tyrosine dans son site actif, la topoisomérase va former un complexe de clivage entraînant une coupure double brin de l'ADN en générant des extrémités cohésives de 4 paires de base. Le complexe de clivage est transitoire, pas stable dans le temps.
- *3^{ème} étape* : Liaison de deux molécules d'ATP. La topoisomérase va alors changer de conformation pour permettre le passage d'un double brin d'ADN au travers de l'espace créé par le complexe de clivage.
- *4^{ème} étape* : Fermeture de la molécule d'ADN, par soudage des extrémités cohésives générées au cours de l'étape 2.
- *5^{ème} étape* : Libération de la molécule d'ADN.
- *6^{ème} étape* : régénération de l'enzyme grâce à l'hydrolyse de deux molécules d'ATP.

La doxorubicine agit lors de l'étape 2. Elle va interagir avec le complexe de clivage, le stabiliser en formant une liaison covalente entre les brins d'ADN clivé et l'enzyme. Ce qui aboutit à la formation de coupures simples ou doubles brin de la molécule d'ADN (Burden and Oshero,

1998). La toxicité de la doxorubicine va dépendre du nombre, de la localisation et de la persistance des cassures créées. On remarquera aussi que l'action sur les topoisomérases est plus toxique au cours de la phase S du cycle cellulaire de la cellule.

Le site d'action de la doxorubicine n'est pas uniquement localisé dans le noyau. En effet la doxorubicine est capable de générer des espèces réactives d'oxygène (ROS). Deux voies sont à l'origine de cette production de ROS (Keizer, 1990; Minotti et al., 1999, 2004) :

- La chélation d'ions métalliques (du fer par exemple)
- Via le cycle redox, avec la réduction monoélectrique enzymatique des fonctions quinones.

La doxorubicine va conduire à la formation de diverses formes de ROS (doxorubicine radicalaire, H_2O_2 , $O_2^{\cdot-}$, OH^{\cdot} ...) en quantités supérieures à la capacité de détoxification de la cellule. Cette présence en surnombre de ROS va conduire à l'oxydation de composés cellulaires (lipides, protéines, ADN, ARN...) perturbant ainsi leurs structures et fonctions. Cette perte de fonction et la modification du statut oxydatif de la cellule conduira cette dernière à la mort. La production de ROS par la doxorubicine est étudiée avec intérêt puisqu'elle pourrait être à l'origine de la toxicité cardiaque de la molécule (Wold et al., 2005; Zhang et al., 2012). En effet les cellules cardiaques sont beaucoup plus sensibles au ROS du fait de leur faible capacité de détoxification.

Bien que découverte il y a très longtemps, l'ensemble des mécanismes d'actions de la doxorubicine n'est encore que partiellement résolue. Je n'ai décrit ici que trois mécanismes sur les différents connus. Il existe un certain nombre de revues abordant plus en détails les différents mécanismes d'action de la doxorubicine et leurs importances quant à l'action anti-tumorale de la molécule.

c. Les résistances à la doxorubicine

Comme pour de nombreux anti-cancéreux, leur activité est mise en péril par l'existence de mécanismes de résistance. Ce phénomène de résistance est souvent mis en évidence lors de rechute du cancer traité à la doxorubicine. Pour cette dernière, on peut distinguer deux types de résistances : (i) associé à une diminution de la concentration intracellulaire de doxorubicine ; (ii) non associé à une diminution de la concentration intracellulaire de doxorubicine (Nielsen et al., 1996).

Dans le premier cas, la diminution de la concentration intracellulaire de la doxorubicine est due à l'expression par la cellule de pompe à reflux (Dano, 1973; Juliano and Ling, 1976). Il s'agit de protéines transmembranaires qui vont expulser hors de la cellule les molécules de doxorubicine qui pénètrent dans la cellule. Un exemple de pompe à efflux très connu est la glycoprotéine membranaire P-gp (Juliano and Ling, 1976; Kartner et al., 1983). Elle fait partie de la très grande famille des transporteurs ABC (ATP-binding cassette). Elle est composée de deux domaines transmembranaires, de deux sites de liaisons à l'ATP localisés sur deux boucles intracellulaires. Les extrémités de la protéine sont intracellulaires. On la retrouve naturellement

exprimée dans certains organes chez l'Homme : le foie, le rein, les intestins, la barrière hémato-encéphalique, le placenta. Elle a pour cible des constituants naturels variés à la structure hydrophobe, neutre ou cationique. Bien que très étudié, le fonctionnement de la P-gp n'est pas totalement résolu (Borst et al., 2000). Elle permettrait l'expulsion de la doxorubicine grâce à un phénomène de Flip-flop. Le substrat interagirait avec les domaines transmembranaires de la protéine. L'hydrolyse d'une molécule d'ATP induirait le changement de conformation de la P-gp qui libèrerait alors le substrat soit directement à l'extérieur de la cellule soit dans le feuillet externe de la membrane. L'hydrolyse d'une deuxième molécule d'ATP permettrait le retour à son état d'origine de la P-gp.

Dans le cas où la résistance de la cellule n'est pas liée à une diminution de la concentration intracellulaire de la doxorubicine, on observe l'apparition de mécanismes d'adaptation. Afin de survivre à l'exposition à la doxorubicine, la cellule va augmenter ses mécanismes de détoxification, et la réparation de l'ADN. On peut aussi observer des modifications de la topoisomérase II et une inhibition des processus d'apoptose.

L'augmentation des mécanismes de détoxification est obtenue par une surexpression des enzymes de détoxification (Nielsen et al., 1996; McLellan and Wolf, 1999). Ces enzymes vont permettre à la cellule tumorale de réparer et d'éliminer les dégâts des ROS produits par la doxorubicine. Le principal système de détoxification impliqué dans la résistance à la doxorubicine est le système dépendant du glutathion. Le statut redox de la cellule est maintenu par la neutralisation des ROS par la forme réduite du glutathion : GSH. En effet le GSH va réagir spontanément ou non avec des ROS et, en s'oxydant, les neutraliser. On obtient alors du glutathion sous forme oxydé (GST) qui ne représente pas de risque oxydatif pour la cellule.

L'implication des mécanismes de réparation de l'ADN ou une tolérance de la cellule vis-à-vis de ces lésions n'est pas encore pleinement élucidée. Jusqu'à présent, les connaissances sur ce sujet porte à croire en l'existence d'un déficit en un système qui détecterait de façon plus efficace les complexe ADN-topoisomérase II. La cellule détectant moins ces complexes, elles ne les perturbent plus, n'entraînant ainsi plus la formation de lésions (coupures) sur l'ADN (Nielsen et al., 1996; Larsen and Skladanowski, 1998).

Enfin des modifications de la topoisomérase II ont aussi été corrélées avec l'apparition d'une résistance à la doxorubicine ou autres inhibiteurs de topoisomérase II. Ces modifications peuvent être soit quantitatives, avec une diminution de l'expression de la topoisomérase II (Dingemans et al., 1998). Elles peuvent aussi être qualitatives avec des mutations entraînant la modification des régions de liaison à l'ATP ou du site catalytique (Dingemans et al., 1998; Larsen and Skladanowski, 1998), ou une modification de la localisation cellulaire obtenue par épissage alternatif. Cet épissage peut entraîner la perte de la séquence d'adressage au noyau et donc l'obtention d'une enzyme cytoplasmique (Feldhoff et al., 1994).

III. Le cisplatine et ses dérivés

a. Présentation, historique

Le cisplatine est un agent alkylant dont les effets furent découverts par hasard par Barnett Rosenberg en 1965. C'est un sel de platine de nom chimique : (SP-4-2)-diamminedichloroplatinum(II) (**Figure 10**) (Kelland et al., 1999; Kelland, 2007; Apps et al., 2015). Depuis sa mise sur le marché en 1978, plus de 25 dérivés ont été synthétisés. Seuls deux (carboplatine et oxaliplatine) ont obtenu une autorisation de mise sur le marché mondial. Trois autres (nedaplatine, lobaplatine, heptaplatin) ont obtenu une mise sur le marché dans un seul pays uniquement, respectivement Japon, Chine et Corée (**Figure 10**) (Apps et al., 2015).

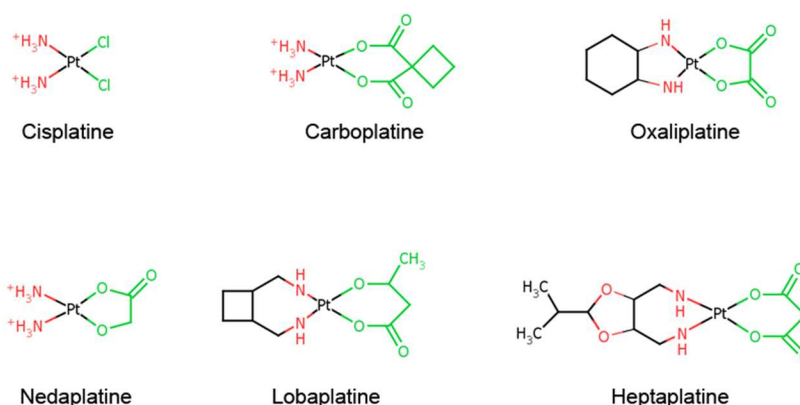


Figure 10 : Structures des dérivés du platine commercialisés dans le monde. Le ligand transporteur apparaît en rouge et le ligand labile apparaît en vert.

Les composés de cette famille ont une structure constituée autour d'un atome de platine. Cet atome va être lié de façon symétrique à deux types de ligands : (i) les ligands transporteurs, ou (ii) les ligands labiles (**Figure 10**). Tous les composés à base de platine sont en fait des pro-drogues. Afin de pouvoir exercer leurs activités, il faut qu'il y ait remplacement des ligands labiles par des molécules d'eau. Le cisplatine et ses dérivés sont des anti-cancéreux encore très utilisés de nos jours. Environ 50% des protocoles de chimiothérapie contiennent un dérivé du platine d'après Martindale et la base de données Australienne EviQ (Apps et al., 2015). Ils sont utilisés notamment dans les cancers des ovaires, du col de l'utérus, des testicules, de l'œsophage, de la vessie, de l'estomac. Ils sont souvent utilisés en association avec d'autres molécules anticancéreuses. Bien que couramment administrés, il existe deux inconvénients majeurs à leur utilisation. Le premier est l'existence d'effets secondaires graves : néphrotoxicité, neurotoxicité, myelosuppression, hépatotoxicité, vomissements et diarrhées (Kelland et al., 1999; Thomas and Chatelut, 2007). Ces effets secondaires peuvent être suffisamment importants pour entraîner une diminution des doses utilisées (Apps et al., 2015).

Ceci facilite l'apparition de résistance. L'existence de ces mécanismes de résistances est le deuxième inconvénient à leurs utilisations.

b. Mécanismes d'action

Les dérivés du platine vont conduire à l'apoptose de la cellule tumorale en se liant de façon covalente à l'ADN et ainsi former des adduits. Cependant comme expliqué au point précédent, les molécules administrées par voie IV ne sont que des pro-drogues. Il faut attendre leurs pénétrations dans la cellule pour que la molécule se retrouve dans des conditions favorables pour échanger ces ligands labiles contre des molécules d'eau (Kelland, 2007; Thomas and Chatelut, 2007; Apps et al., 2015). Le composé ainsi formé va alors pénétrer dans le noyau et interagir avec la molécule d'ADN. Les adduits formés vont être reconnus par les mécanismes de réparation à l'ADN et la cellule va entrer en apoptose (**Figure 11**).

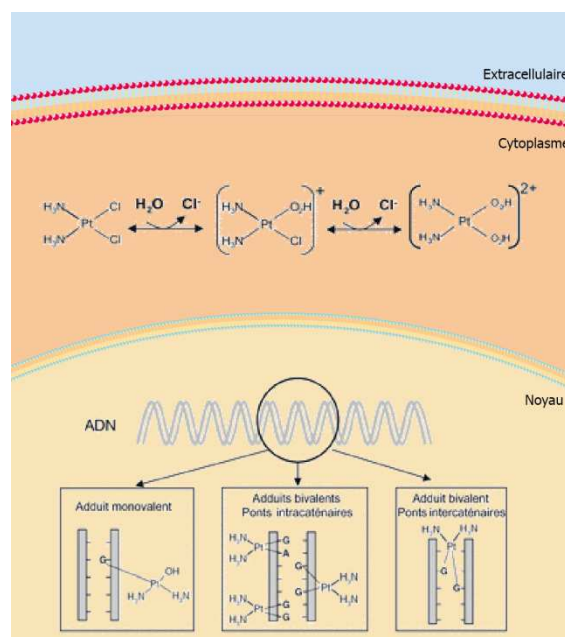


Figure 11 : Mécanismes d'action du cisplatine

Les étapes conduisant à la formation des adduits à l'apoptose ne sont pas encore élucidées. Ils existent trois types d'adduits différents (**Figure 11**):

- Les adduits monovalents : le composé à base de platine va réagir avec une seule base de l'ADN.
- Les adduits de liaisons intra-brins : un composé platine va réagir avec deux bases de l'ADN sur un même brin.
- Les adduits de liaison inter-brins : cette fois-ci l'atome de platine effectue deux liaisons covalentes avec deux bases de l'ADN de brins différents.

c. Les résistances au cisplatine

Il existe 4 mécanismes de résistances connus pour les dérivés du platine. Les deux premiers agissent avant que les composés n'aient pu atteindre le noyau et donc l'ADN (Kelland, 2007; Rabik and Dolan, 2007; Thomas and Chatelut, 2007). Le premier correspond à une diminution de la concentration de molécules anti-tumorales due à une diminution de l'entrée et aussi à une augmentation de l'efflux. Pendant longtemps, on pensait que les composés à base de platine pénétraient dans la cellule par diffusion passive. Or récemment, il a été supposé l'implication d'un transporteur du cuivre CTR1 comme possible voie d'entrée dans la cellule. Les molécules à base de platine rentrent en compétition avec le cuivre pour pénétrer dans la cellule. Quand il y a peu de cuivre, les composés à base de platine rentrent en plus grande quantité. Il a aussi été montré qu'une surexposition au cisplatine entraînait une diminution de l'expression de ce transporteur (Holzer and Howell, 2006; Rabik and Dolan, 2007; Ishida et al., 2010). Il existe aussi une augmentation de l'expulsion hors de la cellule des molécules. Deux transporteurs participent à ce phénomène. Le premier est impliqué dans l'homéostasie du cuivre ; comme pour lors de l'entrée, le cisplatine va être reconnu par cette protéine « spécifique » du cuivre et va donc être expulsé hors de la cellule. Le deuxième transporteur est une pompe à efflux membre de la superfamille ABC ; il s'agit de MRP2. Elle est exprimée à la membrane plasmique et va fonctionner sur le même principe que la P-gp. Une corrélation entre le niveau d'expression de MRP2 et la résistance à la cisplatine a été observée dans un rapport récent (Rabik and Dolan, 2007).

Le deuxième mécanisme correspond à la neutralisation du cisplatine via le glutathion. En effet, le cisplatine va réagir très facilement avec les fonctions thiols de certains composés. C'est ainsi qu'une grande partie de la dose administrée par IV se retrouve très rapidement fixée aux protéines du plasma. On observe ce même phénomène avec le glutathion à l'intérieur des cellules. En absence de résistance, le stock cellulaire de glutathion n'est pas suffisant pour en diminuer son efficacité ; juste suffisant pour perturber l'équilibre redox de la cellule. Mais la cellule se met à surexprimer les enzymes responsables du piégeage des ROS, de façon concomitante, le cisplatine va être piégé par le glutathion de façon beaucoup plus importante et ne pourra donc pas atteindre le noyau (Rabik and Dolan, 2007; Thomas and Chatelut, 2007; Apps et al., 2015).

Les deux autres mécanismes interviennent après l'action toxique du cisplatine. Il s'agit d'une augmentation de la tolérance et/ou de la réparation de l'ADN. L'augmentation de la tolérance de la cellule à la présence d'adduits est liée en partie à la présence d'ADN polymérase plus permissives. En effet, elles vont détecter la présence d'adduit et au lieu de s'arrêter, elles vont rajouter des nucléotides en face de l'adduit. Il n'y aura alors pas de signalement de lésions de l'ADN et donc pas de signal induisant l'apoptose (Rabik and Dolan, 2007; Thomas and Chatelut, 2007). La déficience des systèmes identifiant et signalant les lésions à l'ADN est aussi responsable de la tolérance de la cellule aux adduits. Enfin, l'utilisation

importante du cisplatine, va aussi conduire la cellule tumorale à s'adapter et à augmenter l'efficacité des systèmes de réparation de l'ADN (NER, BRCA). Ces systèmes vont détecter les adduits, couper l'ADN avant et après la liaison, éliminant ainsi l'adduit de la séquence d'ADN qui sera ensuite réparée par une ADN polymérase (Rabik and Dolan, 2007).

C'est l'existence de ces mécanismes variés de résistance au cisplatine qui a poussé la communauté scientifique à créer de nouveaux analogues et de nouvelles méthodes d'administration.

Chapitre 4 : La chimie click

I. La chimie click : concept

a. Généralités

La chimie click prend exemple sur la nature pour créer de nouvelles molécules. En effet, la nature est capable de créer un grand nombre de molécules très diverses. Un grand nombre d'entités chimiques peuvent être découpées en plusieurs morceaux qui sont reliés les uns aux autres par des liaisons carbone hétéroatomes. Cependant, ces morceaux sont constitués de liaisons carbone-carbone que seule la nature arrive à créer facilement. La chimie click n'a pas pour but /ambition l'élaboration de telles liaisons. Elle se concentre sur la création de liaisons carbone-hétéroatome entre divers fragments (Kolb et al., 2001; Kolb and Sharpless, 2003; Moses and Moorhouse, 2007).

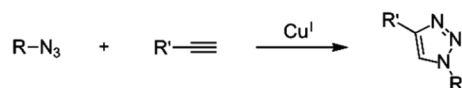
Ces liaisons sont créées grâce à des réactions ayant des caractéristiques précises. Elles doivent être modulaires, rapides et faciles à mettre en place, à très hauts rendements, et générer seulement des sous-produits inoffensifs pouvant être éliminés par des méthodes non-chromatographiques. De plus ces réactions doivent être stéréospécifiques. Le milieu réactionnel doit être simple, les matières premières ainsi que les réactifs doivent être faciles à trouver. L'utilisation d'un solvant n'est pas obligatoire, dans tous les cas il doit être facilement éliminable. Les différentes réactions utilisées peuvent être regroupées en quatre catégories (Kolb et al., 2001; Kolb and Sharpless, 2003; Moses and Moorhouse, 2007; Hein et al., 2008) :

- des réactions de cycloadditions dont celles de la famille des Diels-Alder transformations.
- des réactions de substitutions nucléophiles conduisant à l'ouverture d'un cycle.
- des réactions chimiques de type non aldoliques sur des fonctions carbonyle.
- des réactions sur des doubles liaisons carbone-carbone : surtout des réactions d'oxydation.

L'ensemble de ces réactions est regroupé sous le terme de « click réaction » (**Figure 12**).

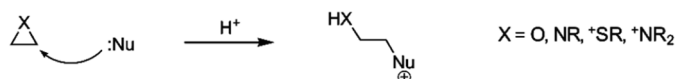
Les matières premières nécessaires à ces réactions sont fournies aux chimistes par l'industrie pétrolière. En effet, les matières premières utilisées lors de synthèses ayant recouru à la chimie click sont des oléfines et des composés acétyléniques. Ces composés possèdent des doubles liaisons carbone-carbone qui sont de très bons réactifs. Ces molécules peuvent être facilement modifiées via des réactions d'oxydation et d'addition. Ces matières premières renferment de l'énergie qui va être utilisée lors de la réaction. En résumé, les réactifs apportent une partie de l'énergie nécessaire à la réaction (Kolb et al., 2001; Kolb and Sharpless, 2003; Moses and Moorhouse, 2007; Hein et al., 2008) .

Cycloadditions

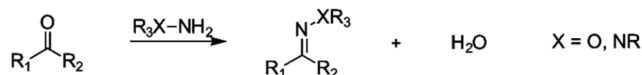


Husigen 1,3-dipolar cycloaddition d'azides et alkynes

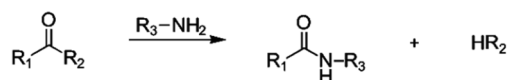
Ouverture de cycle par attaque d'un nucléophile



Chimie du carbonyle de type non aldolique

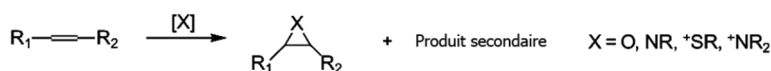


formation d'hydrazone/ oxime d'éther



formation d'Amide/ isourea

Additions sur double liaison carbon-carbone



Format de cycle à trois atomes



Certaines additions de Michael

Figure 12 : Classification des différentes click réaction, avec Nu = nucléophile et EWC = « electron withdrawing group » ou groupe électro-attractif (d'après Hein et al., 2008a)

Le solvant, le plus couramment utilisé est l'eau. En effet l'équipe du professeur Sharpless a constaté que de nombreuses réactions se déroulaient sans problème pour donner un seul produit dans l'eau chaude. La solubilité des réactifs dans l'eau n'entre pas en compte. En effet, l'énergie libre de telles molécules est augmentée lorsqu'elles ne sont pas solubles dans l'eau, ce qui a pour conséquence d'augmenter leurs réactivités. De plus, l'eau est un solvant neutre, il ne va pas interférer avec les réactifs. L'eau empêche aussi les différentes fonctions telles que les fonctions hydroxy et amides d'interférer avec les réactions clicks, ce qui va avoir pour conséquence de supprimer toutes les étapes de protection et de déprotection de ces fonctions. Enfin l'eau est un solvant qui présente l'avantage d'avoir une température d'évaporation facile à obtenir, et c'est aussi un solvant très intéressant de par sa capacité à

stocker de grandes quantités d'énergie (Kolb et al., 2001; Kolb and Sharpless, 2003; Moses and Moorhouse, 2007; Hein et al., 2008).

b. Les réactions clicks

Les réactions de cycloadditions, sont les plus utilisées des réactions clicks. Ces réactions de cycloadditions se rapportent majoritairement aux 1, 3 dipolar cycloadditions (**Figure 13**). Elles regroupent aussi les hétéro Diels-Alder cycloadditions (Moses and Moorhouse, 2007; Colombo and Peretto, 2008; Hein et al., 2008; Moorhouse and Moses, 2008). C'est cette classe de réaction, et plus particulièrement la : « Huisgen 1,3 dipolar cycloaddition (HDC) of azides and terminal alkynes », qui est la plus utilisée (Hein et al., 2008; Gregoritz and Brandl, 2015). En effet, la grande majorité des publications sur les applications de la chimie click font référence à cette réaction. De plus, elle peut être considérée comme la click réaction type : elle remplit tous les critères et est facile à mettre en place. Comme il s'agit de la réaction la plus utilisée, elle va être abordée en détail dans la sous-partie suivante.

Les autres réactions clicks sont moins utilisées que les cycloadditions. Mais ce n'est pas pour autant qu'elles ne présentent aucun intérêt. Par exemple, les réactions nucléophiles conduisant à l'ouverture de cycles peuvent être utilisées pour former les fonctions azides ou alkynes sur une molécule. Ces réactions d'ouvertures de cycles regroupent notamment les ouvertures de cycles tendus à hétéroatomes tels que les époxydes, les aziridines, les cycles sulfates... (**Figure 13**) (Moses and Moorhouse, 2007; Colombo and Peretto, 2008; Hein et al., 2008; Moorhouse and Moses, 2008).

Les réactions chimiques de type non-aldolique sur des fonctions carbonyle renferment elles des réactions telles que la formation d'oxime d'éthers, d'hydrazones et d'hétérocycles aromatiques (Kolb et al., 2001; Kolb and Sharpless, 2003; Moses and Moorhouse, 2007; Colombo and Peretto, 2008; Hein et al., 2008) (**Figure 13**).

Pour les réactions sur des doubles liaisons carbone-carbone, on retrouve surtout des réactions d'oxydation telles que l'époxidation, la dihydroxylation... et certaines réactions d'addition de Michael (**Figure 13**) (Kolb et al., 2001; Kolb and Sharpless, 2003; Moses and Moorhouse, 2007; Colombo and Peretto, 2008; Hein et al., 2008).

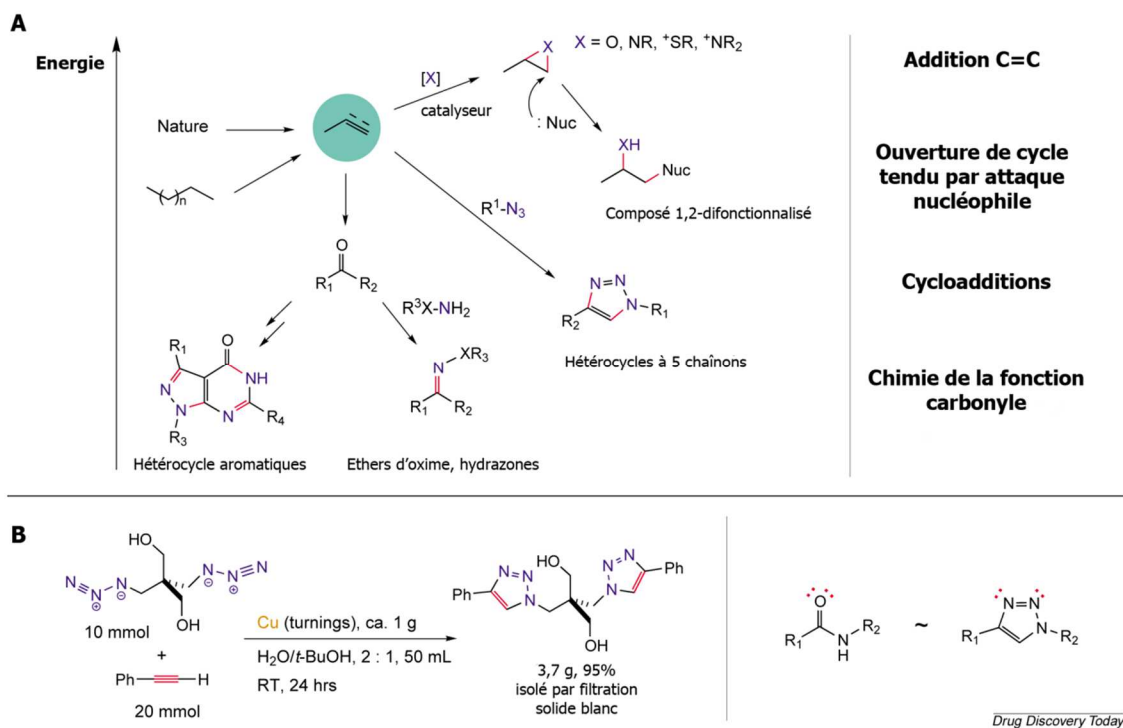


Figure 13 : A. Réaction click énergétiquement favorable, en rouge les liaisons nouvellement formées. **B. Exemple d'une cycloaddition catalysée par le cuivre et comparaison structurale et électronique d'une liaison peptidique et d'une liaison 1,2,3 triazole.** D'après (Kolb and Sharpless, 2003).

c. Huisgen 1.3 dipolar cycloaddition

Cette réaction permet l'obtention d'hétérocycles 1, 2, 3 triazolés disubstitués. Elle peut être réalisée dans de nombreuses conditions expérimentales (Moses and Moorhouse, 2007; Hein et al., 2008) :

- des températures allant de 0 à 160°C
- une large variété de solvants (dont l'eau)
- à différentes valeurs de pH (5 à 12)

L'étape de purification ne consiste généralement qu'en une étape de filtration. De plus, cette réaction n'est pas affectée par des problèmes d'encombrements stériques. Les autres avantages de cette réaction viennent du fait que les fonctions azides et alkynes terminales sont faciles à obtenir (Breinbauer and Köhn, 2003; Hein et al., 2008; Tron et al., 2008). Le produit obtenu lui aussi présente des avantages. En effet, les cycles 1, 2, 3 triazolés imitent les propriétés des liaisons peptidiques (place des atomes et propriétés électroniques) mais sans être sensibles au clivage par hydrolyse. Cette réaction n'est utilisée qu'en présence d'un catalyseur. En fonction de la nature de ce dernier, le produit obtenu varie (Hein et al., 2008) :

- Si le catalyseur utilisé contient du cuivre, comme dans l'exemple suivant, on obtient alors un 1, 2, 3 triazolés disubstitué en 1,4.
- Si on utilise un complexe au ruthenium alors on obtiendra un 1, 2, 3 triazolés disubstitué en 1, 5.

En général, les mécanismes réactionnels des cycloadditions se font par processus concertés. Cependant, d'après des études expérimentales, il a été montré que pour cette réaction il ne s'agissait pas d'un mécanisme concerté. Le mécanisme détaillé ci-dessous est celui de la « CuI catalysed Huisgen dipolar cycloaddition ». Ce schéma a été réalisé d'après des résultats expérimentaux (Hein et al., 2008).

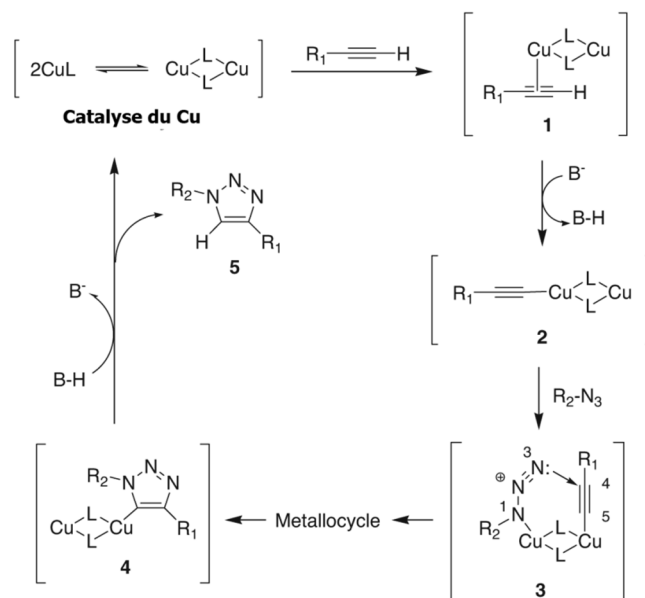


Figure 14 : Mécanisme réactionnel de la cycloaddition dipolaire de Huisgen, L représente les ligands qui peuvent être très variable. D'après (Bock et al., 2006; Hein et al., 2008).

La première étape de cette synthèse est la complexation de l'atome de cuivre par une des liaisons pi de l'alkyne. Il y a ensuite déprotonation de l'alkyne pour former un Cu-acétylide. Cette déprotonation est rendue possible car la complexation de l'atome de cuivre a conduit la diminution du pKa de l'alkyne de départ. De ce fait, cette protonation peut se réaliser dans un solvant aqueux sans l'ajout d'une base.

Dans l'étape suivante, le doublet libre de l'azote (N1) va réagir avec le deuxième atome de cuivre du Cu-acétylide. Cette étape va conduire à un réarrangement électronique au niveau des atomes d'azotes de l'azide. Ce réarrangement va conduire à une attaque nucléophile de l'azide sur la triple liaison de l'alkyne. Il va alors se former un métallo-cycle qui va évoluer vers la formation d'un hétérocycle à 5 atomes.

La dernière étape de cette synthèse est la protonation du cycle, conduisant à la régénération du catalyseur et à la libération du produit. L'utilisation d'une telle réaction a permis la création d'une librairie de molécules très variées.

II. Les applications de la chimie click en biologie

a. *Découvertes / synthèses de nouvelles molécules*

- Synthèses de molécules leader / bibliothèques de molécules.

La création de bibliothèques de molécules avec l'aide de la chimie click peut être divisée en deux parties. En effet on peut distinguer les bibliothèques obtenues à partir d'un seul produit de départ qui va subir des modifications (chimie combinatoire), de celle appelée « convergent click librairies » (Moorhouse and Moses, 2008).

Les bibliothèques découlant de la modification d'une molécule servant de modèle sont nombreuses et ont amené à la découverte de molécules intéressantes pour la recherche médicale. Ainsi, Lexion Pharmaceuticals a utilisé la chimie click pour produire une librairie de molécules contenant 200000 composés différents, chacun étant pur à plus de 85% (Kolb and Sharpless, 2003). La synthèse de ces composés a été réalisée à partir de petits blocks non commerciaux. Des réactions telles que l'ouverture de cycle par attaque nucléophile ont été utilisées pour la création de cette librairie. Une des molécules leader de cette librairie a conduit à la découverte d'un agoniste des récepteurs gamma, responsable de l'activation de la prolifération des peroxysomes (peroxisome proliferator-activated receptor γ agonist) (Kolb and Sharpless, 2003). Plus récemment, des chercheurs ont créé une librairie de molécules en prenant comme point de départ la molécule de zanamivir dans le but de trouver de nouvelles molécules pour le traitement de la grippe aviaire. 16 molécules ont été synthétisées ; certaines possédaient une activité plus faible que le zanamivir et une seule était à peu près aussi active que la molécule de départ. Il existe plein d'autres exemples de ce type de librairie ayant contribué à la découverte de nouvelles molécules actives (Moorhouse and Moses, 2008).

Les « convergent click librairies » ont aussi conduit à la découverte de nouveaux composés. Dans ces bibliothèques, la synthèse des produits se fait par couplage de plusieurs petites entités complexes. Cela a pour conséquence d'augmenter la diversité des molécules produites (Moorhouse and Moses, 2008).

- *In situ* chimie click.

Cette technique correspond à la synthèse guidée de façon irréversible d'une molécule cible. On va par exemple chercher à synthétiser un inhibiteur d'une enzyme (Manetsch et al., 2004; Krasiński et al., 2005; Moorhouse and Moses, 2008; Mamidyala and Finn, 2010). Pour se faire, on va mettre dans notre milieu réactionnel une certaine concentration d'enzymes puis des fragments de molécules se liant au site actif de l'enzyme. Ces fragments devront contenir de façon individuelle une fonction azide et une fonction alkyne terminale. Ces deux fonctions devront se trouver à proximité dans le site actif. L'enzyme va alors synthétiser par elle-même son inhibiteur. Cette technique de synthèse de molécules d'intérêts a été mise au point par le

professeur Sharpless et ces collègues (Manetsch et al., 2004). Pour mettre en évidence ce phénomène, ils ont utilisé comme enzyme l'acétylcholine estérase (AChE) (**Figure 15**).

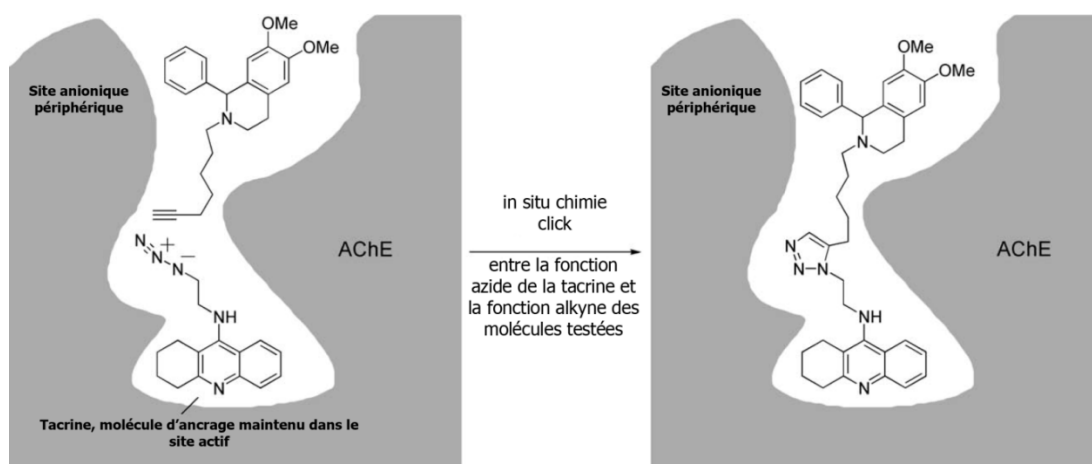


Figure 15: Représentation schématique du couplage entre la tacrine et un fragment alkyne dans le site actif de l'AChE (Moorhouse and Moses, 2008).

Cette technique est à l'origine de nombreuses publications dans le domaine de recherche de ligands de diverses enzymes, une des récentes correspond à la recherche d'un inhibiteur d'une enzyme bactérienne : une chitinase (Hirose et al., 2009; Mamidyala and Finn, 2010).

Bien que la découverte de nouvelles molécules d'intérêts médicales soit l'un des domaines dans laquelle l'utilisation de la chimie click est très répandue, les applications de cette stratégie de synthèse sont très variées allant de la synthèse d'inhibiteurs, de ligands spécifiques à un récepteur, à la synthèse d'anticorps (Kraśiński et al., 2005; Moorhouse and Moses, 2008; Hirose et al., 2009; Mamidyala and Finn, 2010; Millward et al., 2013).

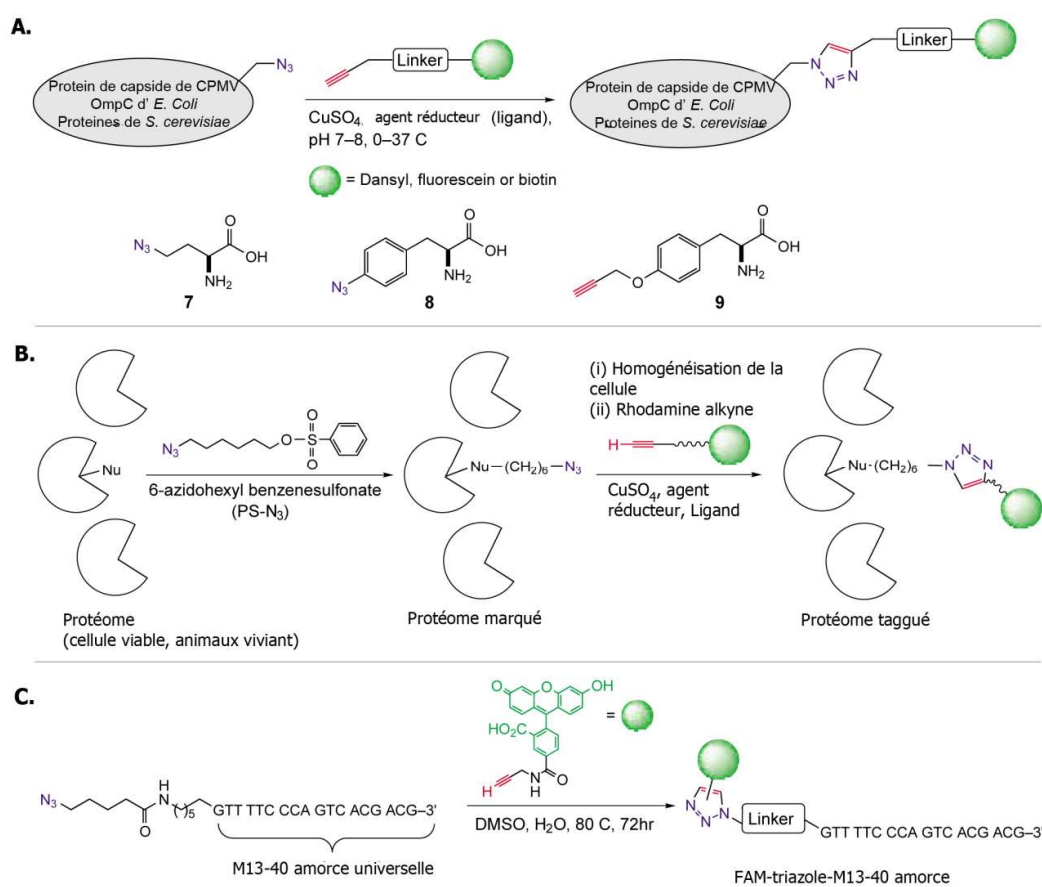
b. Bioconjugaison

La bioconjugaison consiste à la modification *in vivo* ou *in vitro* de molécules biologiques sur des cellules vivantes dans des conditions physiologiques. L'utilisation de la chimie click dans ce domaine est due aux propriétés de la « Copper-catalysed azide-alkyne union » (Breinbauer and Köhn, 2003). En effet, de par la grande inertie des réactifs de départ et de la capacité de cette réaction de se dérouler sans problème dans des conditions biologiques, cette réaction est parfaite pour ce type d'application. Cette réaction a été utilisée pour marquer des organismes vivants ou des protéines. Grâce à l'utilisation de cette méthode, le professeur Finn et son équipe ont réussi à étiqueter sans dommage les particules composant la capsid du « Cowpea mosaic virus » (CMPV) (Breinbauer and Köhn, 2003; Kolb and Sharpless, 2003).

L'application de la chimie click au domaine de la bioconjugaison permet aussi le marquage de l'ADN. Cette application peut être utilisée pour le séquençage de fragments d'ADN en utilisant la méthode de Sanger. Pour ce faire, il suffit de rajouter dans le milieu PCR une

base purique modifiée (contenant une fonction azide rajouté à l'aide d'un « linker ») (Kolb and Sharpless, 2003; Seo et al., 2003; Ami and Fujimoto, 2008).

On peut aussi utiliser cette réaction pour réaliser un ABPP (Activity-based protein profiling) (Breinbauer and Köhn, 2003; Moses and Moorhouse, 2007). Il s'agit d'une méthode chimique qui utilise des sondes se liant au site actif des protéines pour marquer ces protéines et suivre leur taux d'expression ainsi que leur fonction. La sonde utilisée porte à son extrémité une fonction azide. Cette dernière réagira avec la fonction acétylène du révélateur, marquant ainsi la protéine ayant fixée la sonde. Cette méthode a déjà permis la détection de nombreuses molécules. Cette technique a démontré qu'elle était aussi efficace que les méthodes traditionnelles pour déterminer le taux d'expression de la glutathion S-transférase (GSTO 1-1) dans les cas de cancer du sein (Kolb and Sharpless, 2003).



Drug Discovery Today

Figure 16 : Application de la bioconjugaison par cycloaddition d'azide et acétylène. A. Virus, cellule, et marquage de protéine ; B. Profil d'activité protéique *in vivo* ; C. Séquençage de l'ADN par la méthode de Sanger. D'après (Kolb and Sharpless, 2003).

Dans la **Figure 16** sont résumées toutes les applications de bioconjugaison utilisant la cycloaddition d'une fonction azide et acétylène.

c. Sciences de polymères

- Les polymères thérapeutiques.

Les polymères thérapeutiques regroupent tous les différents types de polymères pouvant être utilisés comme vecteurs non viraux (Binder and Sachsenhofer, 2007; Hein et al., 2008). Bien que la chimie click ait été développée pour être un outil important dans la recherche de nouvelles molécules d'intérêt thérapeutique, l'application pour laquelle elle est le plus utilisée est la chimie des polymères. En effet, la majorité des publications contenant les mots clés « Click chemistry » a pour sujet la synthèse de polymères. Comme pour les autres applications, la réaction la plus utilisée est la réaction de cycloaddition permettant la formation d'un hétérocycle 1,2,3 triazolé (Opsteen and van Hest, 2007; Billiet et al., 2009). Toutes ces publications abordent différents points de la synthèse des polymères allant de la synthèse de blocs de copolymères à celle de la synthèse de dendrimères. Il serait trop long de décrire toutes les utilisations de la chimie click dans ce type de synthèse, c'est pourquoi il ne sera abordé que les aspects généraux de certaines de ces utilisations (Binder and Sachsenhofer, 2007; Dijk, 2009; Ma et al., 2015).

L'apparition du concept de chimie click a grandement modifié la synthèse de nouveaux blocs de copolymères. En effet, c'est l'un des moyens les plus efficaces pour relier deux substances ensemble et de répéter cette étape de lier des homopolymères pour former des blocs de copolymères. L'utilisation de la chimie click dans ce domaine a permis d'utiliser un plus large panel de composés, qui ne pouvait être employés avec les anciennes méthodes (Billiet et al., 2009).

La chimie click a aussi un rôle dans la synthèse de dendrimères. Elle en a grandement simplifié leurs synthèses. Elle a rendu plus facile leurs applications (Binder and Sachsenhofer, 2007).

- Synthèse de nanoparticules pour la délivrance de composés.

Ces nanoparticules sont des systèmes de délivrances de substances médicamenteuses ou non. On retrouve sous ce terme : les nanoparticules d'or, les liposomes, les micelles... Ces systèmes de livraisons de molécules présentent un grand intérêt dans le domaine pharmaceutique (Brennan et al., 2006; Binder and Sachsenhofer, 2007; Gole and Murphy, 2007; Hein et al., 2008). La chimie click est notamment utilisée pour la modification de la surface des liposomes pour en améliorer leur propriété. Deux études sont parues sur ce sujet, celle du professeur Hassane est particulièrement intéressante. Le professeur Hassane et ses collègues ont reporté une nouvelle stratégie pour la fixation de mannose sur la surface de liposomes via la chimie click (Hassane et al., 2006; Hein et al., 2008). Le résultat de cette étude a montré que de tels liposomes pouvaient servir de véhicules pour des substances ayant une cible bien particulière comme les cellules dendritiques humaines.

Travaux de thèse

Chapitre 1 : Administration ciblée de doxorubicine

I. Introduction

Les glioblastomes, comme abordés lors des rappels bibliographiques, sont des cancers difficiles à prendre en charge. Une majorité des travaux de recherche menée pour améliorer leurs prises en charge repose sur l'administration ciblée de médicaments. Avec la découverte de la CTX, une alternative à l'utilisation de l'immunothérapie semble viable et prometteuse. Dès lors, l'identification de peptides semblables à la CTX est devenue un enjeu important. Actuellement un seul analogue de la CTX montre un intérêt il s'agit de BmKCT. De très récents travaux ont montré un potentiel comparable pour ce peptide à celui de la CTX (Xu et al., 2016). Au cours de mon travail de thèse, j'ai travaillé à la caractérisation de 3 autres peptides : Lqh8/6, Bs 14 et le lepidopteran. Ces 3 peptides sont issus de venins de scorpions comme la CTX et partagent avec cette dernière une forte homologie de séquences (61% à 72%). Il nous a donc semblé intéressant de les étudier afin de déterminer s'ils pouvaient être utilisés pour l'administration ciblée de médicaments. Le but de cette caractérisation était d'identifier parmi ces 3 peptides, celui qui était le plus intéressant et de réaliser des essais d'administration de doxorubicine avec ce composé.

Ce travail a été mené en parallèle avec mes autres travaux de thèse basés sur une autre toxine : la maurocalcine et avec le même fil conducteur, à savoir l'utilisation d'un système de couplage « cargo-vecteur » universel. C'est pour cela que nous avons à nouveau eu recours à la chimie click afin de coupler la doxorubicine au meilleur des trois peptides. En effet, l'utilisation de la chimie click pour réaliser le couplage présente deux intérêts majeurs : (i) la réaction de couplage azide/alkyne choisi est spécifique, ne génère pas de sous-produit et permet la plupart du temps l'utilisation de solvant simple ; (ii) la synthèse d'un vecteur unique « universel » avec une fonction azide qui pourra être couplé à tout cargo possédant la fonction alkyne (fluorochrome, agent thérapeutique, nanoparticule, quantum dot...). Cependant un inconvénient majeur de cette stratégie est la nécessité de modifier le cargo pour introduire la fonction alkyne. Si l'introduction de la fonction azide sur le peptide peut se faire facilement au cours de la synthèse par l'introduction d'un acide aminé modifié porteur de la fonction, la modification du cargo nécessite plus de travail. Il faut en effet identifier une fonction chimique facilement modifiable et qui n'est pas essentiel à l'activité du cargo.

Les résultats obtenus sur ce projet sont présentés sous la forme du draft d'un article qui sera soumis dès l'obtention des résultats des essais *in vivo*.

Use of the Lqh-8/6-doxorubicin conjugate for the targeted treatment of Glioma

Lucie Dardevet^{1,2,3}, Feten Najloui^{1,4,5}, Sonia Aroui⁶, Mayeul Collot⁷, Céline Tisseyre^{2,3},
Michael Pennington⁸, Jean-Maurice Mallet⁷ & Michel De Waard^{1,4,9*}

¹ INSERM, UMR1087, LabEx Ion Channels Science and Therapeutics, Institut du Thorax, Nantes, F-44000 France.

² INSERM U1216, Grenoble Neuroscience Institute, Grenoble, France ;

³ Université Grenoble Alpes, Grenoble, France

⁴ CNRS, UMR6291, Nantes, F-44000 France.

⁵ Institut Pasteur of Tunisia, 1007 Tunis, Tunisia.

⁶ Unité de recherche UR 12ES08 "Signalisation Cellulaire et Pathologies" 5019 Monastir, Tunisia.

⁷ CNRS, UMR 7203, Ecole Normale Supérieure, 75231 Paris Cedex 05, France.

⁸ Peptides International, Inc., Louisville, KY 40299 U.S.A.

⁹ Smartox Biotechnology, 38400 Saint-Martin d'Hères, France.

*To whom correspondence should be sent : E-mail : michel.dewaard@uni-nantes.fr; Phone : +00 33 660763375.

Abstract

Animal toxins isolated from venoms target cell surface receptors with high affinity and selectivity. These receptors are generally over-expressed in cancer cells. Herein, we identified Lqh-8/6 as a toxin homolog of chlorotoxin a useful peptide for the diagnosis and treatment of glioma. Lqh-8/6 and two analogues were chemically synthesized for the first time and evaluated for their ability to label, detect and prevent glioma growth *in vitro* and *in vivo*. We demonstrate that a biotinylated version of Lqh-8/6 allows both the labeling of glioma cell lines and detection of glioma in brain sections of glioma allograft Fisher rats. Lqh-8/6 has intrinsic anti-invasive properties but is non-toxic to glioma cells. To enhance the anti-tumor properties of Lqh-8/6, we chemically coupled doxorubicin to the glioma targeting peptide using click chemistry. This required the successful chemical synthesis of Lqh-8/6-azide and doxorubicin-alkyne without impairment of the toxic function of doxorubicin. The toxin-drug conjugate efficiently promotes apoptosis of glioma cells *in vitro* and contributes to the prevention of glioma growth *in vivo*. This example contributes to the concept that animal venom peptides constitute exquisite warheads for toxin conjugates, a parallel to the popular concept of antibody-drug conjugates for the treatment of cancer.

Introduction

Gliomas are primary brain tumors derived from glial cells [1]. Fifty five percent of these gliomas are represented by glioblastomas (GBM) that is the most aggressive form of glioma [2,3]. The median survival time of patients affected by GBM is 12-15 months [4]. Just in the USA, 12,120 new cases of patients affected by GBM are diagnosed each year (estimate for 2016) [2]. GBM are derived from astrocytes [2,3]. The core of GBM tumor mass is composed of highly undifferentiated tumor cells that end up in necrosis, whereas the boundaries of the tumor mass are more heterogeneous in terms of dedifferentiation level. Neovascularization is more pronounced at the boundaries of the tumor mass and significant levels of healthy tissue infiltration are evidenced [2,3]. There is no preventive diagnosis possible and generally patients consult owing to the appearance of a neurological disorder. The nature of the deficit will of course depend on the exact localization of the tumor in a given brain region. Final diagnosis is established by MRI and biopsy coupled to histopathology characterization if possible [1–3,5].

Patient treatment will involve first the exeresis of the tumor mass by a neurosurgeon which is complicated by two factors: (i) the localization and size of the tumor that do not always allow the removal of the tumor mass, and (ii) the difficulty for the surgeon to identify with precision the boundaries of the tumor mass owing to the infiltrating nature of GBM [6]. The patient medical management will also involve a combination of chemotherapy associated to irradiation [4,6,7]. Temolozomide is generally the golden standard for chemotherapy in treating GBM [8,9]. Thanks to these medical efforts, the percentage of patients that pass the five-year survival time rises from 1.9 to 9.8% [10]. In comparison, with the progress of oncology treatment, patients affected by prostate and breast cancers have now a five-year survival time above 50%. There is thus considerable progress to be made for the treatment of GBM. Reasons for failure of successful GBM management involve (i) incomplete resection during surgery, (ii) limited passage of the temolozomide through the blood brain barrier, and (iii) the weak radiosensitivity of GBM cells [4].

There is thus a clear need for the development of innovative therapies and management of GBM patients. There are several research and clinical initiatives throughout the world that attempt to fill the gap still existing in the management of GBM compared to other cancer types. One initiative called “Orphanet” (www.orpha.net), that classified GBM as an orphan disease due to its low occurrence in the general population, list the worldwide ongoing projects. There are currently 114 clinical assays ongoing of which 5 are international, 32

listed research projects and 16 multicentric projects in the world [11]. Most of the efforts are concentrated on immunotherapy, which is a heavy trend in the management of several cancer types [12,13]. The most advanced projects include anti-GBM vaccination and immune checkpoint inhibitors [12]. While most industrial efforts focus on immunotherapy, there are wealth of projects in academia that concentrate their efforts on tumor vectorization for the targeted delivery of anti-tumor agents. Two trends have appeared: (i) the use of GBM targeting peptides (GTP) and (ii) the use of Tumor Penetrating Peptides (TPP). The later are meant to not only penetrate into tumor cells but also to possess some preferential GBM targeting properties. Alternatively, TPP may also carry a function that annihilates a GBM pathway that is selectively present only in GBM cells, so that the cell targeting function is not essential [14–17].

One particular GTP has encountered a frank success: chlorotoxin. Chlorotoxin is a 36 amino acid peptide from the venom of Israeli scorpion *Leiurus quinquestriatus quinquestriatus* folded according to a $\alpha\beta\beta\beta$ motif and connected internally by four disulfide bridges [18,19]. It was first used as a pharmacological tool, like many other toxins before, for the study and characterization of chloride channels (ClC-3, small-conductance Cl⁻ channels) [20–24]. Soon thereafter, with the understanding that there is a specific chloride current present in glioma cells (GCC, Glioma-specific Chloride Channels), blocked by chlorotoxin, it was discovered that chlorotoxin was capable to target glioma, GBM, melanoma, small cell lung carcinoma, neuroblastoma and medulloblastoma cancer cells (all of neuroectodermal origin) [25,26]. It should be mentioned however that the membrane receptor of chlorotoxin still needs formal confirmation because it was also found to bind onto Matrix Metalloprotease MMP-2 and annexin-A2 [27,28]. The compound was patented by TransMolecular Inc. in 2002 for its GBM targeting properties. Since then, many derivatives have been produced with the aim to cover various applications in oncology. Examples include: (i) TM-601, ¹³¹I-chlorotoxin up to phase III clinical trials (phase I/II completes in 2003 and authorization for phase III in 2006), (ii) the infrared-sensitive Cy5.5-chlorotoxin to help surgeons delineate the boundaries of the GBM tumors [29], and (iii) a variety of functionalized nanoparticles [30–34]. Chlorotoxin was also used a toxin-drug conjugate, that mirrors the use of antibody-drug conjugates [35,36]. It was conjugated to a chelator of platinum for the efficient delivery of platinum into GBM cells and the induction of apoptosis. Since the acquisition of the chlorotoxin patent license or patent itself by Morphotek Inc., a subsidiary of EISA Corp., little information is now published on the commercial and clinical fate of chlorotoxin.

Because chlorotoxin has become so popular for the study of GBM treatment and diagnosis, researchers have neglected to look for the existence chlorotoxin-related toxins that would present the same diagnostic and therapeutic potential than chlorotoxin. This would however be advantageous to circumvent the intellectual property rights and further our understanding of the structural determinants that make chlorotoxin so efficient. A closer look at the taxonomy of scorpion species indicates the existence of two subspecies of *Leiurus quinquestriatus* and presupposes the existence of several chlorotoxin-like toxins [37]. A sequence homology search using chlorotoxin as entry reveals the existence of fifteen known scorpion toxins that present at least 61% sequence identity with chlorotoxin (**Table 1**). All these toxins possess between 34 and 38 amino acids. They are all connected according to a C₁-C₄, C₂-C₆, C₃-C₇ and C₅-C₈ disulfide bridging pattern. The amino acid regions that present the greatest diversities are the C-terminus and the domain between C₅ and C₇. BmKCT, a peptide from the venom of the scorpion *Buthus martensi*, with 76% sequence identity with chlorotoxin, was recently shown to inhibit cell division and migration of GBM cells and to possess anti-angiogenic properties [38,39], clearly indicating that the search of functional homologs of chlorotoxin is not vain. By using the program @TOME V2 [40], we built homology models for all these toxins (**Figure 1**). A clear compact structural homology is evident from these toxin representations with the presence of α -helix combined with an antiparallel three-stranded β -sheet (see also [41]). One of the most conserved analogues is Lqh-8/6, a toxin isolated from the venom of a subspecies of *Leiurus quinquestriatus* (*hebraeus* instead of *quinquestriatus*). It has 72% sequence identity with chlorotoxin, which is less than the sequence identities of BmKCT, I₃, I₄, I₅, I_{5A} and Bs-8. However, one distinguishing feature of Lqh-8/6 is that many substitutions are conservative (Lys¹⁴, Lys²⁵ and Ile³⁴ instead of Arg¹⁴, Arg²⁵, and Leu³⁴, respectively). In addition, there is a sequence extension at the C-terminus that lowers the sequence homology compared to other toxins. Finally, the comparison of the modelled structures illustrates that Lqh-8/6 most closely resembles the structure of chlorotoxin.

Herein, we chemically synthesized Lqh-8/6 for the first time by solid-phase peptide synthesis by producing two variants, a biotinylated one and an analogue compatible with click chemistry for the grafting of an anti-tumor agent. We demonstrate the ability of the peptide to selectively bind to GBM rat F98 cells both *in vitro* and *in situ* from brain slices of rats containing F98 allografts. We also show that Lqh-8/6 does not present cell toxicity and does not affect cell migration. However, it significantly reduces cell invasion. We chemically synthesized for the first time doxorubicin-alkyne for the click chemistry conjugation to azide-

Lqh-8/6. The resulting conjugate produces significant GBM rat F98 cell death and human U-87 caspase-3 dependent cell apoptosis. *In vivo*, the Lqh-8/6-doxorubicin significantly delays tumor growth from F98 allografts implanted in the striatum of Fisher rats.

Materials and Methods

Chemicals

N- α -Fmoc-L-aminoacid and Wang-Tentagel resin and reagents used for peptide synthesis were obtained from Iris Biotech (Markterditz, Germany). Analytical grade quality solvents (acetonitrile (ACN), dimethylformamide (DMF), N-methylpyrrolidone (NMP), trifluoroacetic acid (TFA)) were from Acros Organics (Illkirch, France). For Western blotting, the antibodies used were: anti-caspase-3 (H-277) and anti- β -actin (B-6) (Santa Cruz Biotechnology Inc., Heidelberg, Germany), anti-Bax (Merk Millipore, Darmstadt, Germany), anti-Bim (BD transduction Laboratories, Erembodegem, Belgique), peroxidase-conjugated goat anti-rabbit and anti-mouse antibodies (Jackson Immunoresearch Laboratories, West Grove, USA). z-VAD-fmk and z-DEVD-fmk used to study apoptosis were obtained from Sigma Aldrich (Lyon, France). Doxorubicin hydrochloride was a gift from Peptides International (Louisville, Kentucky, USA). Hoescht 34580, concanavalin A-rhodamine, concanavalin A-alexa 647, and Cy5- or Cy3-streptavidin (strep-C5 or strep-Cy3) were purchased from ThermoFisher Scientific (Waltham, Massachusetts, USA). Thiazolyl Blue Tetrazolium Bromide (MTT) was obtained from Sigma Aldrich. LIVE/DEAD[®] Viability/Cytotoxicity Kit for mammalian cells was used for toxicity measurements (ThermoFisher). The CytoSelect[™] 96-Well Cell Migration and Invasion Assay Combo Kit, 8 μ m, was to evaluate cell migration and invasion (Cell Biolabs Inc., San Diego, California, USA).

Molecular modelling

Using the Sybyl X 1.3 software (Tripos Inc., St. Louis, Missouri, USA) and the Protein Data Bank (PDB) structure of chlorotoxin (code 1CHL) and @Tome2 web server (40), we generated 3D models of Lqh8/6, Bs-14, I3, GaTx1, BmKCT, Bm12-b, Neurotoxin P2, AaCTx and Lepidopteran. Several steps of minimization and control of the stereochemistry were performed to obtain a model for each molecule. The parameters of the minimization were as follows: field force: MMFF94, charge: MMFF94, method: Powell without initial optimization, terminate point: gradient = 0.5 kcal/(mol.Å).

Peptide Syntheses

Chemical syntheses of the various peptides (Lqh-8/6, Lqh-8/6-biotin (Lqh-8/6_b), Lqh-8/6-azide, chlorotoxin, Bs-14, Bs-14-biotin (Bs-14_b), lepidopteran and lepidopteran-biotin (lepidopteran_b) were performed as previously described ([42]). Biotins were added at the N-termini of peptide sequences. Briefly, peptides were chemically synthesized by the solid-phase method using an automated peptide synthesizer (CEM[®] Liberty, Orsay, France). Peptide chains were assembled stepwise on 0.24 mEq of Fmoc-L-Arg(Pbf)-Wang-Tentagel resin using 0.24 mmol of N- α -fluorenylmethyloxycarbonyl (Fmoc) L-amino-acid derivatives. The side-chain protecting groups were: trityl for Cys and Asn, tert-butyl for Ser, Thr, Glu and Asp, Pbf for Arg and tert-butylcarbonyl for Lys. Reagents were at the following concentrations: Fmoc-amino-acids (0.2 M Fmoc-AA-OH in DMF), activator (0.5 M 2-(1H-benzotriazole-1-yl)-1,1,3,3-tetramethyluronium hexafluorophosphate in DMF), activator base (2 M diisopropylethylamine in NMP) and deprotecting agent (5% piperazine/0.1 M 1-hydroxybenzotriazole in DMF), as advised by the PepDriver software (CEM[®]). After peptide chain assemblies, resins were treated 4 hrs at room temperature with a mixture of TFA/water/triisopropylsilane (TIS)/dithiothreitol (DTT) (92.5/2.5/2.5/2.5; v/v/v/v). The peptide mixtures were then filtered and the filtrates were precipitated by adding cold tert-butylmethyl ether. The crude peptides were pelleted by centrifugation (10.000 \times g, 15 min) and the supernatants were discarded. The peptides were purified by Reverse-phased High Pressure Liquid Chromatography (RP-HPLC) using a Vydac C18 column (218TP1010, 4 μ m, 250 \times 100 mm) using a 10–60% ACN linear gradient containing 0.1% TFA. Crude peptides were then oxidized/folded in 0.1 M Tris.HCl buffer at pH 8.3 for 48 hrs before purification of the folded/oxidized peptides by RP-HPLC using a Vydac C18 column (218TP104, 5 μ m, 250 \times 46 mm) again with a 10-60% ACN linear gradient with 0.1% TFA. Correct oxidations of the synthesized peptides were checked by MALDI-TOF mass spectrometry.

Cell culture

Undifferentiated malignant glioma rat (F98) and differentiated malignant glioma rat (RG-2) cell lines (from American Type Culture Collection (ATCC)) were maintained at 37°C in 5% CO₂ in DMEM/F-12 nutrient medium (Invitrogen, Cergy Pontoise, France) supplemented with 2% (v/v) fetal bovine serum (FBS, Invitrogen) and 100 μ g/mL streptomycin and 100 units/mL penicillin (Invitrogen). Human glioblastoma (U-87) cell line (from ATCC) were maintained at 37°C in 5% CO₂ in low-glucose (1 g/L) Dulbecco's modified Eagle's medium (DMEM) (Invitrogen) supplemented with 10% fetal bovine serum (Invitrogen), 100 μ g/mL

streptomycin and 100 units/mL penicillin (Invitrogen). All cell media were changed every 2 or 3 days. All experiments were carried out on cells having initial viability exceeding 95%. After seeding (96- and 24-well plates or 8-well Labtek slides), cells were incubated overnight to adhere at the surface and then treated with drugs at different concentrations and time intervals.

Confocal microscope imaging of GBM cells

For analysis of the cell entry of Cy5-labeled-peptides in living F98 cells, cell cultures were incubated with the fluorescent peptides (in DMEM/F-12 nutrient medium only) for 5 min, 30 min or 2 hrs, and then washed twice with phosphate-buffered saline (PBS) alone. Cell nuclei were stained with 60 $\mu\text{g/mL}$ Hoechst 34580 for 5 min before the cell cultures were washed with PBS. The plasma membrane was stained with 50 $\mu\text{g/mL}$ concanavalin A-rhodamine for 5 min. Cells were washed once more. Live cells were then immediately analysed by confocal laser scanning microscopy using a Zeiss LSM operating system. Hoechst 34580 (λ_{ex} 405 nm), rhodamine (λ_{ex} 561 nm) and Cy5 (λ_{ex} 633 nm) were sequentially excited and emission fluorescence were collected. For the 5 min incubation time with fluorescent peptides, the staining of the cell nuclei and plasma membrane were performed simultaneously. For analysis of the subcellular distribution of doxorubicin and doxorubicin-alkyne in living cells, cell cultures were incubated 2 hrs with the compounds in DMEM/F-12 nutrient medium lacking FBS, and then washed twice with PBS. Cell nuclei and plasma membrane staining were performed as described in the previous paragraph, except that concanavalin A-alexa 647 was used instead of concanavalin A-rhodamine. Live cells were then immediately analysed by confocal laser scanning microscopy with doxorubicin and doxorubicin-alkyne being excited at λ_{ex} 590 nm.

Cy5-peptide labeling of GBM F98 cells in culture

50 μL of streptavidin-Cy5 (16 μM) and 39.4 μL of biotinylated peptides (81 μM) were mixed in 310 μL of DMEM/F-12 nutrient medium only. The mixtures were vortexed and incubated during 1 hr at room temperature to produce the fluorescent peptides. They were used as such for cell labeling in cell cultures.

Synthesis of doxorubicin-alkyne

To a solution of doxorubicin hydrochloride (21 mg, 36.26 μmol) in methanol (10 mL) was added triethylamine (20 μL , 144.4 μmol , 4 eq) followed by propargyl chloroformate (10 μL ,

108.7 μmol , 3 eq). The solution was stirred at room temperature for 5 min. The solvents were then evaporated and the product solubilized in dichloromethane (DCM), washed with HCl (1 M) and a saturated solution of NaHCO_3 . The organic phase was dried over MgSO_4 , filtered and evaporated to give 22 mg of pure doxorubicin-alkyne (97% yield) as an orange solid.

Conjugation of doxorubicin-alkyne to Lqh-8/6-azide

Lqh-8/6-azide (3 mg, 0.69 μmol , 1 eq) was dissolved in 300 μL water/DMF (1:1) and 660 μL of doxorubicin-alkyne (10 mM in methanol/DCM, 1/1, v/v) were added (10 eq). Then, 34.5 μL $\text{CuSO}_4 \cdot 5\text{H}_2\text{O}$ (100 mM in water, 5 eq) and 34.5 μL sodium ascorbate (100 mM in water, 5 eq) were added to the mixture. The solution was sonicated and bathed at 35°C for 2 days. The solution was then purified by RP-HPLC using a Vydac C18 column (218TP104, 5 μm , 250 \times 46 mm). Elution of doxorubicin-Lqh-8/6 was performed with a 5-90% acetonitrile linear gradient containing 0.1% TFA. The pure fraction was lyophilized and quantified. 3.3 mg of doxorubicin-Lqh-8/6 was purified representing a theoretical yield of 90%. Doxorubicin-Lqh-8/6 was characterized by MALDI-TOF mass spectrometry.

Excitation and emission spectra of doxorubicin and doxorubicin-alkyne

Solutions of doxorubicin (180 μM) and doxorubicin-alkyne (370 μM) were prepared in water/dimethylsulfoxide (DMSO) (1/1, v/v). The absorbance spectra were obtained using a spectrophotometer (Pherastar FS, BMG Labtech, Champigny-sur-Marne, France). Using the wavelength of maximal absorbance of doxorubicin and doxorubicin-alkyne, the fluorescence emissions were recorded.

Stereotaxic implantation of F98 cells in Fisher rat brain striatum

2 months-old male Fisher rats were anesthetized by inhalation of isoflurane (induction by isoflurane 4% in air, followed by anesthesia maintenance by isoflurane 2% in air). The cranium were then shaved before placing the rats in a stereotaxic frame. After disinfecting the scalp, an incision followed by resection of the subcutaneous tissue was made. Trepanning of the skull was realized 3.5 mm to the right of the median line with a needle of 25G. The implantation of F98 cells was performed by a slow injection (0.5 $\mu\text{L}/\text{min}$) of 5 μl of solution (10^3 F98 cells in PBS) using a Hamilton syringe connected to a pump. This injection was made 5.5 mm below the external surface of the skull. After slow removal of the syringe, the burr hole was filled with Horsley's wax and the scalp stitched with absorbable thread. Rats were placed in an incubator until awakening and then monitored for 2 hrs before going back

into the care facility. The tumor-growth was monitored by RMI. Animals were euthanized when their condition was judged too painful to keep them alive. Their brains were removed and instantaneously frozen in a bath of cold isopropane, removed and stored at -80°C before use.

Cy3-peptide labeling of F98 GBM tumors in brain slices of allograft rats

Frozen sections (8 μ m thick) were fixed in cold methanol (100%) for 8 min at -20°C, then washed in PBS and saturated with 10% FBS (Gibco) in PBS for 60 min. The sections are incubated overnight with Lqh-8/6_b at 4°C. The next day, the tissues are washed 3 times with PBS, then fixed for 2 min with 4% PFA 60% acetone and 20 mM HEPES, washed with PBS and incubated with Cy3-streptavidin (1/1000; Amersham) and with Hoechst 33258 (1/1000; Sigma-Aldrich) for 2 hrs at room temperature. Brain sections were digitized using a DMI6000 microscope (LEICA, Nanterre, France) which was equipped with a 20x dry objective and a EMCCD Quantem camera that was driven by the MetaMorph software (Roper Scientific, France).

Migration and invasion assays

These assays were performed according to the manufacturer's protocol (CytoSelect™ 96-Well Cell Migration and Invasion Assay Combo Kit, 8 μ m; Cell Biolabs Inc.). Boyden chambers contained or not an extracellular matrix (ECM) depending on the type of measurement required: (i) invasion (with ECM) or (ii) migration (without ECM). GBM F98 cells were seeded in Boyden chambers at a density of 0.5×10^6 cells/mL in a culture medium without FBS. Peptides were added immediately in the upper chamber for 24 hrs at 37°C. The lower chamber contained culture medium with FBS that acts as chemoattractant. Cells that reached the inner part of the Boyden chamber 24 hrs later were detached. The invasive or migratory cells, depending on the chamber type, are then lysed and quantified using CyQuant GR fluorescent Dye. The fluorescence of the lysates were read using a plate reader at λ_{ex} 480 nm / λ_{em} 520 nm (Pherastar FS).

MTT assays

Cells were seeded into 96-well plates at a density of 8,000 cells/well. After 24 hrs of culture, the cells were incubated for 72 hrs at 37 °C with chlorotoxin, Lqh8/6, Bs-14, or lepidopteran at various concentrations. Control wells containing cell culture medium with or without cells, both without peptide addition, were included in each experiment. 0.1% saponin was used as

toxic agent for comparison. The cells were then incubated with MTT for 30 min. Conversion of MTT into purple-colored MTT formazan by the living cells indicates the extent of cell metabolism. The crystals were dissolved with DMSO and the optical density was measured at 540 nm using a microplate reader (Pherastar FS) for quantification of cell viability. All assays were run in triplicate.

GBM cell viability assays by flow cytometry

Cells were seeded into 24-well plates at a density of 10,000 cells/well. After 24 hrs of culture, cells were incubated for 72 hrs at 37°C with chlorotoxin, Bs-14, lepidopteran, Lqh-8/6, doxorubicin, doxorubicin-alkyne or doxorubicin-Lqh-8/6 at various concentrations. Negative and positive controls consisted of untreated and 0.1% saponin-treated cells, respectively. After incubation, cells were washed with PBS and detached with 500 µl trypsin/EDTA (ThermoFisher). Cells were centrifuged at 200 g for 5 min and resuspended in 500 µL of staining mix (DMEM/F-12 nutrient medium without FBS with 31 nM calcein and 1 µM ethidium homodimer). Cell suspensions were incubated for 15 min at room temperature and then analyzed by flow cytometry. Flow cytometry analyses were performed using a C6 Flow cytometer (Accuri, BD Biosciences, Pont de Claix, France). Cells were gated by forward/side scattering from a total of 10,000 events. Data obtained were analyzed using the Accuri CFlow software (Accuri).

Apoptosis pathway induced by Lqh-8/6, doxorubicin-alkyne and Lqh-8/6-doxorubicin in U-87 cells

Hoechst staining of cells - 1×10^4 cells were grown on coverslips into a 6-well plate and incubated with Lqh-8/6 (1 µM), doxorubicin (10 µM) or Lqh-8/6-doxorubicin (10 µM). Thereafter, cells were fixed with 4% paraformaldehyde for 30 min at room temperature and washed twice with PBS. Chilled methanol (-20°C) was added to each well for 10 min at room temperature followed by 2–3 washes with PBS. Cells were then stained with Hoechst 33258 (5 mg/mL) for 10 min, washed with PBS and then examined by a Zeiss fluorescent microscope. Cells with condensed, fragmented nuclei and having brighter fluorescence were considered as apoptotic cells. The percentage of apoptotic cells was calculated from the ratio of apoptotic cells to total cells counted. At least 300 cells were counted for each condition.

Western immunoblotting analyses - Cells were incubated for the indicated time and concentration of compounds and cultured in Petri dishes to about 75% confluence in serum-free medium supplemented with 0.1% BSA. The incubated cells were washed twice with cold

PBS and scrapped in ice-cold lysis buffer (10 mM Tris pH 7.5, 0.5 mM EDTA pH 8.0, 0.5 mM DTT, 0.5% CHAPS, 10% glycerol) supplemented with a cocktail of protease inhibitors. After 30 min on ice, cell debris were removed by centrifugation at 10,000 g at 4°C for 20 min. Proteins were quantified using the DC Protein Assay (Bio-Rad) according to the manufacturer's specifications. Twenty µg of protein lysate were incubated in loading buffer (60 mM Tris-HCl, pH 6.8, 0.18 M β-mercaptoethanol, 2% SDS, 10% glycerol, and 0.005% bromophenol blue), boiled and separated on a polyacrylamide gel by SDS-PAGE under reducing conditions. The proteins were electro-transferred overnight or 2 hrs at 4°C to polyvinylidene difluoride (PVDF) membrane (Hybond-P, Amersham Biosciences). Membranes were blocked for at least 1 hr in Tris-buffered saline (TBS), 5% BSA and 0.5% Tween 20 and then probed with the appropriate primary antibodies (1:1000) in 5% BSA, 0.1% Tween 20, and 0.05% sodium azide in TBS for 1 hr at room temperature or overnight at 4°C and thereafter incubated with the appropriate secondary peroxidase-labeled antibody (1:20,000) for 1 hr at room temperature. Enhanced chemiluminescence (ECL, Amersham Pharmacia Biotech) was used for protein detection. The ECL staining was quantified by densitometry with ImageJ software (National Institutes of Health, USA).

Results

Lqh-8/6_b efficiently labels GBM tumor cells

Based on the sequence homology of Lqh-8/6 with chlorotoxin, we expected that Lqh-8/6 should be able to bind onto a surface receptor of GBM cells. The peptide was synthesized in its biotinylated version, Lqh-8/6_b, and coupled to strep-Cy5 *in vitro*. Live F98 cells were incubated 5 min, 30 min or 2 hrs with 3 µM Lqh-8/6_b-strep-Cy5, their nuclei and plasma membrane stained with Hoescht 34580 and concanavalin A-rhodamine, respectively. As shown by confocal microscopy, Lqh-8/6_b-strep-Cy5 labeled F98 cells *in vitro* and induced a time-dependent internalization of the ligand / receptor complex (**Figure 2A**). Interestingly, toxin labeling at 5 min reveals cell surface clustering of the receptor. No labeling of the nucleus was evident suggesting that the fluorescence remained restricted to the cytoplasm/endosomes. Similar experiments using Bs-14_b-strep-Cy5 and lepidopteran_b-strep-Cy5 produced comparable F98 cell surface staining and time-dependent internalization of the toxin receptors (**Supplementary Figure 1**). These data indicate that Lqh-8/6 (72% sequence identity with chlorotoxin), Bs-14 (61% sequence identity) and lepidopteran (63% sequence

identity) all have the ability to bind to a surface receptor of F98 GBM cells in spite of limited sequence identities. To check the specificity of this labeling, Lqh-8/6_b-strep-Cy3 staining was performed on 8 μm-thick coronal brain slices from Fisher rats that were previously injected with F98 cells in the striatum and in which the tumor developed for 25 days. As shown, on these coronal slices a predominant staining by Lqh-8/6_b-strep-Cy3 was evident in the tumor zone (**Figure 2B**). This zone was confirmed by the evidence of a high density of nuclei due to the lack of cell extensions such as neurites. Lqh-8/6_b-strep-Cy3 staining also illustrates the presence of positive cells further outside the tumor zone. Their presence is probably explained by the high invasiveness of this tumor cell type, especially 25 days after tumor development. These findings illustrate the value of a fluorescent derivative of Lqh-8/6 for tumor painting GBM cells *in situ*.

Lqh-8/6 lacks intrinsic cell toxicity

Next, we assessed whether Lqh-8/6 presents any intrinsic cell toxicity. Both MTT tests and cell viability assays by FACS were performed on F98 cells *in vitro* after 72 hrs incubation with the toxins. Both tests demonstrate that Lqh-8/6, like chlorotoxin, presents no intrinsic toxicity up to 33 μM (**Figure 3A**). Similarly, Bs-14 and lepidopteran also are non-toxic to F98 cells *in vitro* demonstrating that the F98 cell surface toxin receptors are not required for cell survival and metabolism (**Supplementary Figure 2A**).

Lqh-8/6 affects invasion but spares migration

To test the effect of Lqh-8/6 on cell migration and invasion, we used Boyden chambers without and with ECM at the bottom of the chamber. As shown, Lqh-8/6 has no effect on F98 cell migration at low (1 μM) and high (10 μM) concentrations (**Figure 3B**), a result confirmed for lepidopteran and to a lower extent for Bs-14 (**Supplementary Figure 2B**). Concerning invasion by F98 cells in control conditions, 0.8% of cells showed a propensity to cross the Boyden chamber after ECM degradation. Interestingly, Lqh-8/6 was capable of inhibiting F98 cell invasion at both concentrations tested (1 and 10 μM), indicating that the toxin efficiently inhibits ECM degradation by F98 cells (**Figure 3C**). The extent of inhibition reached $74 \pm 9.8\%$ (n=3) at 10 μM Lqh-8/6. Lepidopteran was slightly more efficient than Lqh-8/6 at 1 μM to block cell invasion, while Bs-14 showed more limited efficacy at both concentrations (**Supplementary Figure 2C**). These findings are consistent with earlier claims that chlorotoxin acts by potentially binding on MMP-2, an important player for ECM degradation.

Altogether these data demonstrate that Lqh-8/6, like chlorotoxin and other toxin analogs, have limited inherent anti-tumor efficacies (lack of cell toxicity and no inhibition of migration). However, they have moderate to significant effects on cell invasion, combined to potent GBM targeting properties. In the next steps, we improved the anti-tumor properties of Lqh-8/6 by grafting onto it a potent cytotoxic agent while continuing to exploit the targeting properties of the peptide for selective delivery to F98 GBM cells.

Chemical synthesis and characterization of a click chemistry-compatible doxorubicin analogue

Doxorubicin is an anthracycline generally used for the treatment of solid cancers. It is a DNA intercalating agent and inhibitor of topoisomerase type II (both nuclear targets), but also a Reactive-Oxygen Species (ROS)-generating compound (mainly cytoplasmic target), all promoting cell apoptosis. However it possesses significant secondary effects, and namely produces cardiomyopathy, a condition that limits its long-term use. It would therefore benefit from a grafting to a vectoring agent thereby limiting unwanted effects on healthy tissues. Doxorubicin has two chemical functions that have been used in the past while keeping its activity intact to some extent [43–48]. These include: the alcohol function of the aglycone moiety or the amino group of the daunosamine moiety (**Figure 4A**). Earlier evidence seems to suggest that doxorubicin loses more activity if the alcohol function is functionalized rather than the amine function probably by interfering with the intercalating properties of doxorubicin [45]. To render doxorubicin compatible for chemical grafting on Lqh-8/6 we turned towards click chemistry for its ease of use and reproducibility. We chemically produced doxorubicin-alkyne in one step by mixing doxorubicin with propargyl chloroformate in the presence of trimethylamine (**Figure 4A**). The resulting product was purified by RP-HPLC and verified by MALDI-TOF MS (**Figure 4B**). Doxorubicin-alkyne has a molecular weight (MW) of 625.4 Da (648.3 Da with a Na⁺ adduct), compared to doxorubicin which has a MW of 543.5 Da. ¹H-NMR spectrum of doxorubicin-alkyne confirms the expected structure of the synthetic product (**Figure 4C**). This change in structural properties is susceptible to alter the chemical properties of doxorubicin. We first checked whether the chemical modification had an impact on the spectral properties of doxorubicin (**Figure 4D**). As shown, the spectrum of absorbance of doxorubicin-alkyne was not significantly modified compared to the spectrum of absorbance of doxorubicin. In contrast, the intensity of emission fluorescence was significantly reduced by a factor of 4-fold at the peak of emission without change in the

wavelength-dependence of the emission. This modification of the spectral emission properties will therefore limit our capacity of detection of doxorubicin-alkyne in cells.

Next, we therefore evaluated the cell-inducing toxicity and subcellular distribution properties of doxorubicin-alkyne compared to doxorubicin alone in various GBM cells. A 72 hrs incubation of F98, RG-2 or U-87 GBM cells with 10 μ M doxorubicin or doxorubicin-alkyne produces significant cell toxicity as assessed by the cell viability assay (**Figure 5A**). On rat F98 cells, the alkyne modification slightly reduced the cell toxicity of doxorubicin: $18 \pm 3\%$ survival (n=6 wells and N=6 x 5,000 cells, doxorubicin-alkyne) *versus* $2.4 \pm 0.6\%$ survival (n=6 wells and N=6 x 5,000 cells, doxorubicin). However, the opposite observation was made for rat RG-2 and human U-87 cells with doxorubicin-alkyne being slightly more potent than doxorubicin ($2.9 \pm 0.3\%$ (doxorubicin-alkyne) *versus* $5.1 \pm 0.8\%$ (doxorubicin) for RG-2, and $43.7 \pm 2.1\%$ (doxorubicin-alkyne) *versus* $29.6 \pm 5.3\%$ (doxorubicin) for U-87 in similar conditions). Of note, human U-87 GBM cells seem intrinsically more resistant to doxorubicin treatment compared to rat cell line GBM models. These data confirm that the toxicity of doxorubicin is largely preserved in spite of the chemical modification. Slight differences in cell toxicity efficiencies of doxorubicin-alkyne can tentatively be explained by alterations in the cell toxicity contribution of the different doxorubicin targets (nucleus *versus* cytoplasm). In spite of the limited emission efficiency of doxorubicin-alkyne, we managed to examine the relative nuclear / cytoplasm subcellular distribution of the alkyne-modified doxorubicin and compared it to the distribution of parent doxorubicin (**Figure 5B-E**). As shown, doxorubicin-alkyne was essentially present in the cytoplasm of F98 cells and less in the nucleus ($76.7 \pm 5.0\%$, nuclear/cytoplasm ratio = 0.31), whereas the opposite was true for doxorubicin ($40 \pm 7\%$, nuclear/cytoplasm ratio = 1.6). A similar trend for a more pronounced cytoplasmic localization of doxorubicin-alkyne was observed for U-87 cells (nuclear/cytoplasm ratio = 0.23 compared to 0.86 for unmodified doxorubicin). Reasons for these changes may include (i) a greater size of doxorubicin-alkyne making it more difficult to cross nuclear pores, or (ii) a less pronounced DNA-intercalating efficacy. Whatever the reasons for these changes, it is concluded that doxorubicin-alkyne remains a valid anti-tumor agent that is now compatible for click chemistry coupling onto Lqh-8/6.

Coupling of doxorubicin-alkyne to Lqh-8/6-azide produces an efficient peptide-drug conjugate

To follow up on the click chemistry coupling of doxorubicin-alkyne onto Lqh-8/6, we first modified the later by grafting an azide function. We chose to add this function onto the N-

terminus because a N-terminal biotinylated version of Lqh-8/6 was found efficient in labeling F98 cells (**Figure 2**). We therefore synthesized Lqh-8/6-azide by incorporating an additional Gly residue at the N-terminus preceded by Aha (an Ala onto which an azide function has been added) (**Figure 6A,B**). The chemical synthesis was performed using Fmoc chemistry and the peptide was folded/oxidized similarly to Lqh-8/6 or Lqh-8/6_b (**Figure 6C**). MALDI-TOF MS was used to assess that the proper mass was obtained ($[M+H]^+ = 4348.1$ Da) (**Figure 6C, inset**). The Huisgen 1.3 dipolar cycloaddition was used to couple Lqh-8/6-azide to a five-fold excess of doxorubicin-alkyne (**Figure 6D**). CuSO₄ was used as Cu(I) donor and sodium ascorbate as activator. The final product was purified by RP-HPLC (**Figure 6E**) and characterized by MALDI-TOF MS (**Figure 6E, Inset**).

Next, the conjugated Lqh-8/6-doxorubicin peptide was evaluated with the cell viability assay by FACS for its ability to induce cell death in various GBM cell lines (rat F98, rat RG-2 and human U-87). For the sake of comparison with Lqh-8/6-doxorubicin, the effects of Lqh-8/6-azide and doxorubicin-alkyne alone were evaluated also in parallel. As shown, while Lqh-8/6-azide has no toxicity *per se*, similarly to Lqh-8/6 alone, the conjugate displayed significant cell toxicity on all three cell lines (**Figure 7**). Of interest, the concentration-dependence of the toxic effects of the conjugate parallels the concentration-dependence of the toxic effects of doxorubicin-alkyne, but always showed a shift towards higher concentrations. This is expected since doxorubicin is now attached to a peptide that also needs to enter into GBM cells. The IC₅₀ values measured for the conjugate were $0,84 \pm 0,05$ μ M (F98), $4,14 \pm 0,03$ μ M (RG-2) and $16,6 \pm 0,05$ μ M (U-87). In comparison, values observed for doxorubicin-alkyne alone were $0,34 \pm 0,02$ μ M (F98), $1,67 \pm 0,02$ μ M (RG-2) and $9,3 \pm 0,06$ μ M (U-87), thus representing decreases in efficacies of 2,47-, 2,48- and 1,8-fold, respectively.

Lqh-8/6-doxorubicin induces GBM cell death by apoptosis

We investigated whether Lqh-8/6-doxorubicin cell toxicity could be attributed to the induction of apoptosis. As shown in **Figure 8A**, U-87 cells treated with 10 μ M Lqh-8/6-doxorubicin or 10 μ M doxorubicin-alkyne for 24 hrs displayed similar typical morphologic features of apoptotic cells with chromatin condensation and nuclei fragmentation as visualized by fluorescence microscopy after DNA staining with Hoechst 33342. These morphologic changes were not observed in the case of Lqh-8/6-azide. Coherent with these observations, it was found that both Lqh-8/6-doxorubicin and doxorubicin-alkyne induce an increase in the percentage of apoptotic cells: $26.8 \pm 2.0\%$ for Lqh-8/6-doxorubicin and $27.5 \pm 2.0\%$ for doxorubicin-alkyne alone as compared to untreated cells ($3.5 \pm 1\%$) or cells treated with Lqh-

8/6-azide ($4.5 \pm 1.3\%$) (**Figure 8B**). In order to investigate whether doxorubicin-alkyne or Lqh-8/6-doxorubicin-induced apoptosis is mediated by caspases, we first used two caspase inhibitors: a broad-spectrum caspase inhibitor, z-VAD-fmk, and a caspase-3/-7-specific inhibitor, z-DEVD-fmk. Pretreatment of U-87 cells with these caspase inhibitors ($100 \mu\text{M}$) strongly inhibited apoptosis, suggesting that doxorubicin-alkyne and Lqh-8/6-doxorubicin-induced apoptotic cell death is largely dependent on caspase activation (**Figure 8C**). Furthermore, the proteolytic activation of caspase-3 was examined. Lqh-8/6-azide did not induce caspase-cleavage, whereas $10 \mu\text{M}$ of doxorubicin-alkyne or Lqh-8/6-doxorubicin caused activation of caspase-3 after 24 hrs, as indicated by the detection of the cleavage fragments (p20 and p17 fragments) (**Figure 8D**). The activation of caspase-3 in doxorubicin-alkyne and Lqh-8/6-doxorubicin treated cells ($10 \mu\text{M}$) was further confirmed by the cleavage of its known substrate PARP with the appearance of a 89 kD cleavage fragment (**Figure 8D**). Moreover, we studied the impact of these compounds on the expression levels of pro-apoptotic proteins (Bax and Bim) in U-87 cells by Western blotting. An important up-regulation of Bax and Bim levels were observed in U-87 cells treated 24 hrs with $10 \mu\text{M}$ of doxorubicin-alkyne or Lqh-8/6-doxorubicin (**Figure 8E**). Taken together, these results demonstrate that Lqh-8/6-doxorubicin induce apoptosis with equivalent efficiency than doxorubicin-alkyne alone.

Discussion

Herein, a @TOMEV2 search for toxins presenting sequence homologies with chlorotoxin, a well-studied peptide for its usefulness in characterizing, diagnosing and treating glioma, revealed the existence of several new scorpion venom peptides that may possess properties akin to chlorotoxin. A total of 14 sequences were identified to possess significant homologies ($\geq 61\%$). Among these sequences, two had previously been recognized as possessing anti-migration and anti-proliferation properties: AaCtx (Rjeibi et al., 2011) and BmKCT [49]. These two toxins ranked 7th and 13th in terms of sequence homology with chlorotoxin indicating that all the retrieved sequences have the potential to be potent glioma-labeling peptides. With the exception of the N- (before C₁) and C-termini (after C₈), the only region that showed amino acid insertions or deletion within the toxin sequences is the one located between C₅ and C₇. Most of the observed differences occur between C₅ and C₆ suggesting that this region may not be essential for the activity of the toxins. Three new toxins were chemically synthesized for the first time: Lqh-8/6, lepidopteran and Bs-14. These

additional syntheses now bring to five the total number of toxins that have been chemically produced on this list of 15 toxins (**Table 1**). Lqh-8/6 originated from a scorpion that is phylogenetically very close of the scorpion from which chlorotoxin was identified. Lepidopteran and Bs-14, together with AaCtx, were last on the list of sequence homologies and also belong to the same scorpion than BmKCT. All toxins synthesized had the ability to bind onto and integrate into GBM cells validating this search for analogues of chlorotoxin. Quite surprisingly, there is no structure-activity relationship studies published for chlorotoxin or some of its closest analogues. This may be due to the lack of a clearly identified membrane receptor. However, it is obvious that such information would tremendously facilitate the identification of novel toxins possessing chlorotoxin glioma-labeling properties. In the future, chemical engineering work, aimed at functionalizing Lqh-8/6, may help performing reverse pharmacology experiments for the identification of the GBM receptor recognizing Lqh-8/6. The identification of the receptor for this toxin could also help the understanding of the mechanism of GBM invasion on which this toxin is intrinsically active.

Similarly to chlorotoxin, there is no doubt that various types of functionalization may be done on Lqh-8/6 to exploit its specific labeling of GBM cells. As such, many analogues carrying appropriate tags can be envisioned: (i) a fluorescent tag, emitting in the near infrared (such as Cy5.5), for tumor painting during surgery or diagnosis on biopsies, (ii) a chelating agent for contrast agents for MRI, and (iii) a radionuclide such as ^{123}I iodine, technetium-99m for tumor treatment. There are also chelating agents with mixed properties that can be grafted onto Lqh-8/6. These agents are versatile in the sense that they accept either a fluorescent lanthanide (terbium, europium) for diagnosis or a short wavelength radionuclide for therapeutic treatment, minimizing the cost of production of Lqh-8/6 analogues. Finally, it is worth mentioning that Lqh-8/6 may also be functionally coupled to nanoparticles for the development of multimodal functions. Examples in the case of chlorotoxin are numerous [50–53]. Herein, we have provided evidence that functionalization with biotin / streptavidin or doxorubicin through click chemistry does not hinder GMB receptor recognition by Lqh-8/6 thereby indicating that the development of these future analogues should not be problematic. In that respect, the mastering of the click chemistry for the grafting of doxorubicin onto Lqh-8/6 serves as a good experimental basis for the grafting of other components of functions onto Lqh-8/6 also by click chemistry without requiring the synthesis of a new peptide. In addition, the Lqh-8/6_b-strep-Cy5 or Cy3 can also be useful for the treatment of human biopsies in the future.

As many venom-derived toxins, Lqh-8/6 was found to possess no intrinsic cell toxicity, at least with mammalian cell lines. By itself, it also possesses low anti-tumor properties. Nevertheless, it showed potent inhibition of cell invasion which is an interesting property to exploit. The most important effect of Lqh-8/6 was its capacity to specifically label GBM cells. Like for chlorotoxin before, it will be of interest to determine whether Lqh-8/6 also labels tumor cells of the same neuroectodermal origin. This cell targeting properties was exploited to selectively target an anti-cancer compound to GBM cells. This project required two innovations: (i) the development of a doxorubicin analogue compatible with click chemistry and that preserves, at least partially, its toxic mode of action, and (ii) the chemical synthesis of an Lqh-8/6 analogue, also compatible with click chemistry, and that would conjugate efficiently to doxorubicin-alkyne with high yield, and again without perturbing the activity of doxorubicin. On all counts these requirements were successful. The choice of the linker, an additional N-terminal flexible Gly residue along with Aha, turned to be sufficient to preserve doxorubicin action without further optimization. Coupling to doxorubicin conferred to Lqh-8/6 a GBM toxicity that was not observed with the native peptide. In that sense, the conjugation process is a success. It was also sufficient to provide an *in vivo* efficacy to Lqh-8/6-doxorubicin on GBM allografted rats. The mechanism of cell death induction clearly involves cell apoptosis. Inasmuch as antibody-drug conjugates, these data confirm the existence of a bright future for toxin-conjugates in the treatment of cancers. This strategy presents the immense advantage to avoid some of the negative secondary effects that lead to a reduction of the use of doxorubicin in the clinics. Conjugation to a targeting peptide should significantly reduce the cardiotoxicity of doxorubicin [54–56]. This example illustrates the benefit of the approach in providing a second potential clinical life to a known anti-tumor agent. In addition, the strategy employed also presents the added benefit of reducing the time of development for FDA approval if clinical assays demonstrate the viability of the approach. While these results were positive, there is room for improvement in the future. The efficacy of Lqh-8/6-doxorubicin on GBM cells *in vitro* was found to be less than doxorubicin-alkyne alone. This reduction in efficacy is probably linked to a reduced delivery of the doxorubicin moiety with the cytoplasm/nucleus of GBM cells. The cause of this reduced delivery is probably the use of a non-cleavable linker between Lqh-8/6 and doxorubicin. Future developments may imply the use of different types of linkers, such as a pH-sensitive hydrazine bond that should more readily liberate doxorubicin in the more acidic environment of the tumor [57–60]. An ester bond is another alternative that relies on intracellular esterases. Finally, without further modifications, endosome disruption agents may facilitate the escape

of a fraction of the toxin-conjugate from the endosomes. Their use is however limited *in vivo*. The search for a cleavable linker may hopefully yield a toxin-conjugate that has a toxicity profile on GBM cells identical to doxorubicin for the next generation of toxin-conjugates. Another versatile option for improvement concerns the toxic moiety that is grafted onto Lqh-8/6. While doxorubicin seems as a pertinent choice in the case of the GBM cell lines tested, other toxic moieties can be envisioned as well further illustrating the versatility of this toxin-conjugate approach, useful for personalized medicine. Along the toxic moieties of interest, let's cite other topoisomerase inhibitors, ¹³¹I, alkylating agents such as platinum (themselves conjugated), pro-apoptotic peptides, anti-microtubule agents, antimetabolites, and other cytotoxic compounds. The choice of these compounds will be linked to the intrinsic sensitivity of GBM cells to these unconjugated agents, to the benefit of the coupling and the feasibility of the conjugation.

In conclusion, this study adds credit to the concept that animal venom peptides can be used as warheads for the delivery of anti-tumor agents. They present the unusual benefit to be extremely stable *in vivo*. Peptides from venoms have been shown to possess half lives in plasma that exceed 10 hrs which is excessively long for a peptide. The reason for this stability lies behind millions of years of evolution and the existence of a very stable disulfide-bridge organized fold. While we developed the example of a toxin that presents sequence homology with chlorotoxin, there is significant hope that other toxins may possess similar virtuous targeting properties on unrelated cancers. These latter's generally overexpress a repertoire of ion channels and G protein coupled receptors and this is exactly what animal venom toxins target in Nature with exquisite selectivity and affinity.

Figure legends

Table 1: Alignment of primary amino acid sequences of chlorotoxin-like peptides. Alignments were performed by using @TOME V2. Percentage sequence of identities is given as compared to chlorotoxin by using @TOME V2. Disulfide bridge patterns are also indicated.

Figure 1: Representation of the 3D structures of chlorotoxin and chlorotoxin-like peptides. The 3D structure of chlorotoxin and I5A were obtained from their pdb files: 1CHL (chlorotoxin) and 1SIS (I5A). All other structures are models built by homology with chlorotoxin using @TOME V2 and modeller for Lqh-8/6, Bs-14, I3, GaTx1, BmKCT, Bm12-b, neurotoxin P2, AaCTx and lepidopteran. All toxins present an anti-parallel β -sheet structure and most an alpha helix (with the exception of BmKCT and Bm12-b).

Figure 2: GBM F98 labelling with Lqh-8/6_b. (A) Confocal microscopy images illustrating the cell surface labelling and penetration of Lqh-8/6_b-strep-Cy5 into glioma F98 cells (red color). Incubation times were 5, 30 min and 2 hrs. Images were taken immediately after washout of the extracellular peptide. The plasma membrane is labeled with concanavalin-A-rhodamine (green color) and the nucleus with Hoechst 34580 (blue color). (B) Brain slices of F98 tumors in allograft Fischer rats labeled with Lqh-8/6_b-strep-Cy3.

Figure 3: Functional effects of chlorotoxin and Lqh-8/6 onto F98 cells in culture. (A) Lack of cell toxicity of chlorotoxin and Lqh-8/6 as assessed by MTT assay and FACS. FACS toxicity results are represented by full lines, whereas MTT results are shown with dashed lines. (B) Effect of chlorotoxin and Lqh-8/6 on F98 cell migration. (C) Effect of chlorotoxin and Lqh-8/6 on F98 cell invasion. *, $p \leq 0.07$; **, $p \leq 0.05$.

Figure 4: Synthesis and characterization of doxorubicin alkyne. (A) Chemical synthesis of doxorubicin-alkyne. The aglycone moiety is shown in orange, while the daunosamine moiety is represented in blue. (B) RP-HPLC purification and mass spectra characterization of doxorubicin-alkyne. (C) $^1\text{H-NMR}$ characterization of doxorubicin-alkyne. (D) Spectral properties of doxorubicin and doxorubicin-alkyne.

Figure 5: Cell toxicity on GBM cells and subcellular distribution of doxorubicin-alkyne.

(A) Cell toxicity of 10 μ M doxorubicin and doxorubicin-alkyne incubated 72 hrs with various cell lines. (B) Cell localization of doxorubicin and doxorubicin-alkyne in F98 cells at 3 μ M (2 hrs incubation time). Doxorubicin and doxorubicin-alkyne are shown in green. The plasma membrane is labeled with concanavalin-A-alexa fluor 647 (red color) and the nucleus with Hoechst 34580 (blue color). (C) Cell localization of doxorubicin and doxorubicin-alkyne in U-87 as in (B). (D) Quantification of the cell localization of doxorubicin and doxorubicin-alkyne in F98 cells. (E) Quantification of cell localization of doxorubicin and doxorubicin-alkyne in U-87 cells.

Figure 6: Synthesis of Lqh-8/6-azide and chemical coupling to doxorubicin-alkyne.

(A) Amino acid sequence and disulfide bridge arrangement of Lqh-8/6-azide. Note the additional N-terminal Gly residue and Aha residue aimed at spacing the peptide and doxorubicin moieties. (B) Chemical structure of Aha. (C) RP-HPLC purification and MALDI-TOF MS of folded/oxidized Lqh-8/6-azide. (D) Huisgen cycloaddition of Lqh-8/6-azide and doxorubicin-alkyne to produce Lqh-8/6-doxorubicin. (E) RP-HPLC purification and MALDI-TOF MS of Lqh-8/6-doxorubicin.

Figure 7: GBM cell toxicity of Lqh-8/6-doxorubicin conjugate compared to the toxicities of Lqh-8/6-azide and doxorubicin-alkyne.

(A) Concentration-dependence of the various compounds on F98 cell toxicity. 72 hrs chronic incubation. (B) As in (A), but on RG-2 cells. (C) As in (A and B), but on U-87 cells.

Figure 8: Lqh-8/6-doxorubicin induces U-87 cell apoptosis.

(A) Hoechst-stained U-87 cells showing morphological changes induced in the cell nuclei. Apoptotic cells show condensed and fragmented nuclei. (B) Percentage of apoptotic cells induced by the various treatments for 24 hrs at 10 μ M. (C) Effects of a broad-spectrum caspase inhibitor, z-VAD-fmk, and a caspase-3/-7-specific inhibitor, z-DEVD-fmk, on the percentage of apoptotic cells for the different treatments. (D) Caspase 3 and PARP cleavage induced by doxorubicin-alkyne and Lqh-8/6-doxorubicin. Total proteins were extracted and detected by Western blot analysis using antibodies against C-Caspase-3 and PARP. (E) Up-regulation of Bax and Bim levels in U-87 cells by 10 μ M doxorubicin-alkyne or Lqh-8/6-doxorubicin.

Supplementary Figure 1: GBM F98 labelling with Bs-14_b or lepidopteran_b. (A) Confocal microscopy images illustrating the cell surface labeling and penetration of Bs-14-strep-Cy5 into glioma F98 cells (red color). Incubation times were 5, 30 min and 2 hrs. Images were taken immediately after washout of the extracellular peptide. The plasma membrane is labeled with concanavalin-A-rhodamine (green color), the nucleus is labeled with Hoechst 34580 (blue color). (B) Confocal microscopy images illustrating the penetration of lepidopteran_b-strep-Cy5 into glioma F98 cells. Same conditions as in (A).

Supplementary Figure 2: Functional effects of Bs-14 and lepidopteran onto F98 cells in culture. (A) Lack of cell toxicity of Bs-14 and lepidopteran as assessed by MTT assay and FACS. FACS toxicity results are represented by full lines, whereas MTT results are shown with dashed lines. (B) Effect of Bs-14 and lepidopteran on F98 cell migration. (C) Effect of Bs-14 and lepidopteran on F98 cell invasion. *, $p \leq 0.07$; **, $p \leq 0.05$.

Table 1: Primary sequence alignments of chlorotoxin-like peptides. Alignments were performed by using @TOME V2. Percentage sequence of identity is given as compared to chlorotoxin by using @TOME V2. Disulfide Bridge pattern is given when known.

Toxin	Primary sequence	Length	Identity	Disulfide bridge pattern	Species
Chlorotoxin	MC ₁ MP ₂ C ₂ FT ₁ TDH Q ₁ MARK C ₃ DD ₂ C ₄ C ₅ GGK-G R ₁ GK ₂ C ₃ Y GPQC ₇ L C ₈ -R--	36 AA	100%	C ₁ -C ₄ ,C ₂ -C ₆ ,C ₃ -C ₇ ,C ₅ -C ₈	<i>Leiurus quinquestriatus quinquestratus</i>
I ₃	MC ₁ MP ₂ C ₂ FT ₁ TDH Q ₁ TARR C ₃ RDC ₄ C ₅ GGR-G R-KC ₆ F G-QC ₇ L C ₈ GYD	36 AA	82%	C ₁ -C ₄ ,C ₂ -C ₆ ,C ₃ -C ₇ ,C ₅ -C ₈	<i>Buthus eupeus</i>
I ₄	MC ₁ MP ₂ C ₂ FT ₁ TDH N ₁ MARK C ₃ RDC ₄ C ₅ GGN-- -GK ₆ F GPQC ₇ L C ₈ NR	35 AA	82%	C ₁ -C ₄ ,C ₂ -C ₆ ,C ₃ -C ₇ ,C ₅ -C ₈	<i>Buthus eupeus</i>
Bs-8	RC ₁ KPC ₂ FT ₁ TD ₁ P Q ₁ MSKK C ₃ AD ₂ C ₄ C ₅ GGG-K K ₆ K ₇ C ₈ Y GPQC ₇ L C ₈	35 AA	80%	C ₁ -C ₄ ,C ₂ -C ₆ ,C ₃ -C ₇ ,C ₅ -C ₈	<i>Buthus sindicus</i>
I ₅	MC ₁ MP ₂ C ₂ FT ₁ TD ₁ P N ₁ MANK C ₃ RDC ₄ C ₅ GGG-K K--C ₆ F GPQC ₇ L C ₈ NR	35 AA	79%	C ₁ -C ₄ ,C ₂ -C ₆ ,C ₃ -C ₇ ,C ₅ -C ₈	<i>Buthus eupeus</i>
I _{5A}	MC ₁ MP ₂ C ₂ FT ₁ TD ₁ P N ₁ MARK C ₃ RDC ₄ C ₅ GGN-G K--C ₆ F GPQC ₇ L C ₈ NR	35 AA	79%	C ₁ -C ₄ ,C ₂ -C ₆ ,C ₃ -C ₇ ,C ₅ -C ₈	<i>Buthus eupeus</i>
GaTx1	-C ₁ GP ₂ C ₂ FT ₁ TDH Q ₁ MEQK C ₃ AEC ₄ C ₅ GGI-G K--C ₆ Y GPQC ₇ L C ₈ NR	34 AA	79%	C ₁ -C ₄ ,C ₂ -C ₆ ,C ₃ -C ₇ ,C ₅ -C ₈	<i>Leiurus quinquestriatus hebraeus</i>
BmKCT	-C ₁ GP ₂ C ₂ FT ₁ TD ₁ A N ₁ MARK C ₃ REC ₄ C ₅ GGI-G K--C ₆ F GPQC ₇ L C ₈ NR1	35 AA	76%	C ₁ -C ₄ ,C ₂ -C ₆ ,C ₃ -C ₇ ,C ₅ -C ₈	<i>Buthus marrensi</i>
Bm12-b	-C ₁ GP ₂ C ₂ FT ₁ TD ₁ A N ₁ MARK C ₃ REC ₄ C ₅ GGN-G K--C ₆ F GPQC ₇ L C ₈ NR1	35 AA	76%	C ₁ -C ₄ ,C ₂ -C ₆ ,C ₃ -C ₇ ,C ₅ -C ₈	<i>Buthus marrensi</i>
Lqh-8/6	RC ₁ SPC ₂ FT ₁ TD ₁ Q Q ₁ MTKK C ₃ YDC ₄ C ₅ GGG-K K ₆ K ₇ C ₈ Y GPQC ₇ L C ₈ APY	38 AA	72%	C ₁ -C ₄ ,C ₂ -C ₆ ,C ₃ -C ₇ ,C ₅ -C ₈	<i>Leiurus quinquestriatus hebraeus</i>
I ₁	MC ₁ MP ₂ C ₂ FT ₁ TRP D ₁ MAQD C ₃ RAC ₄ C ₅ KGR-G K--C ₆ F GPQC ₇ L C ₈ GYD	36 AA	71%	C ₁ -C ₄ ,C ₂ -C ₆ ,C ₃ -C ₇ ,C ₅ -C ₈	<i>Buthus eupeus</i>
Neurotoxin P2	-C ₁ GP ₂ C ₂ FT ₁ TD ₁ P YTESK C ₃ ATC ₄ C ₅ GGR-G K--C ₆ V GPQC ₇ L C ₈ NR1	35 AA	70%	C ₁ -C ₄ ,C ₂ -C ₆ ,C ₃ -C ₇ ,C ₅ -C ₈	<i>Androctonus mauritanicus mauritanicus</i>
Lepidopteran	RC ₁ GPC ₂ FT ₁ TD ₁ P Q ₁ TQAK C ₃ SEC ₄ C ₅ GRK-G G-VC ₆ K GPQC ₇ L C ₈ GIQ	37 AA	63%	C ₁ -C ₄ ,C ₂ -C ₆ ,C ₃ -C ₇ ,C ₅ -C ₈	<i>Buthus lamulus</i>
AaC1x	MC ₁ IPC ₂ FT ₁ TNP N ₁ MAAK C ₃ NAC ₄ C ₅ GSRRG S--C ₆ R GPQC ₇ L C ₈	34 AA	61%	C ₁ -C ₄ ,C ₂ -C ₆ ,C ₃ -C ₇ ,C ₅ -C ₈	<i>Androctonus australis</i>
Bs-14	-C ₁ GP ₂ C ₂ FT ₁ KD ₁ P ETEKK C ₃ ATC ₄ C ₅ GGI-G R--C ₆ F GPQC ₇ L C ₈ NRGY	36 AA	61%	C ₁ -C ₄ ,C ₂ -C ₆ ,C ₃ -C ₇ ,C ₅ -C ₈	<i>Buthus sindicus</i>

Figure 1:

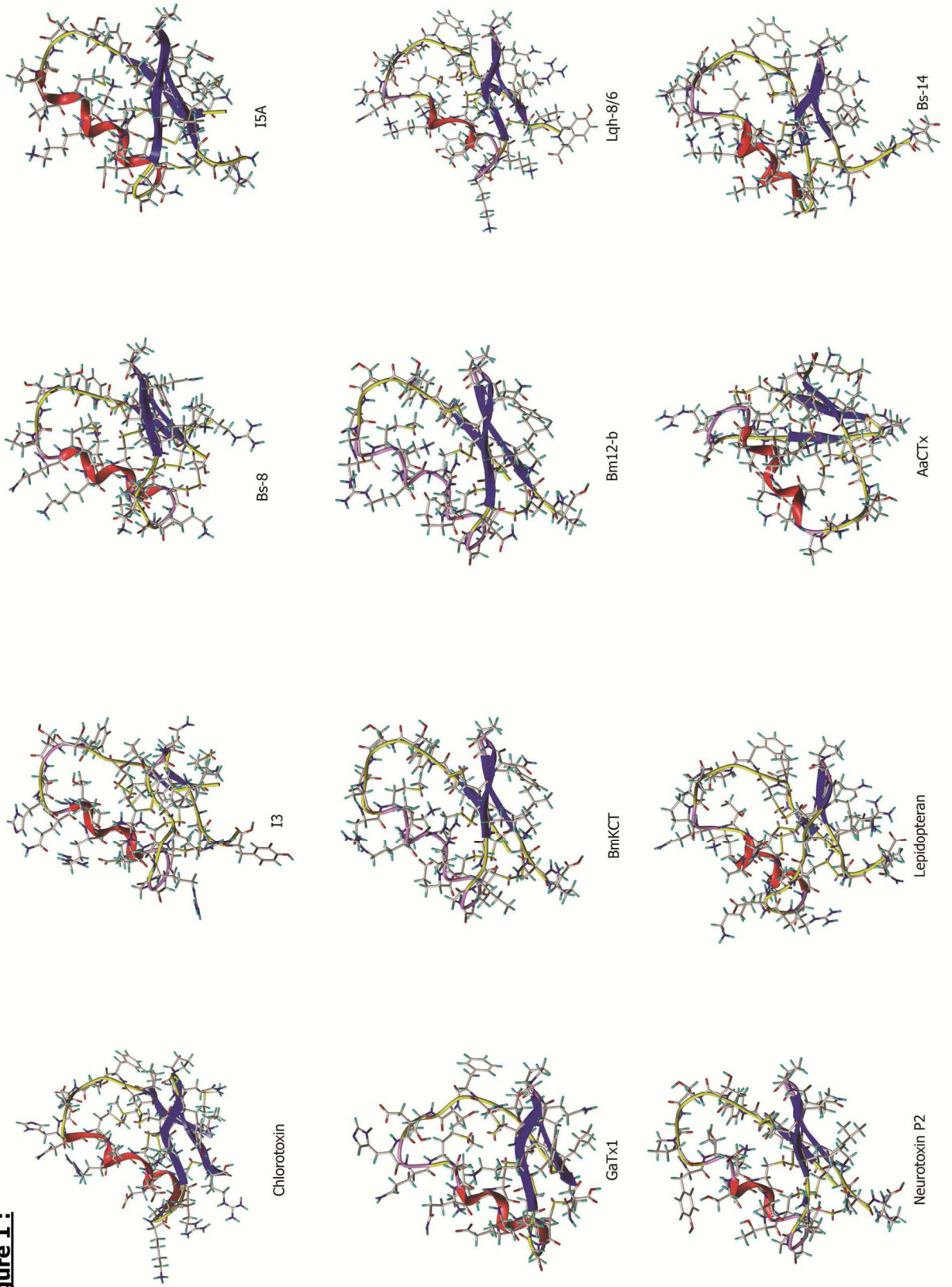
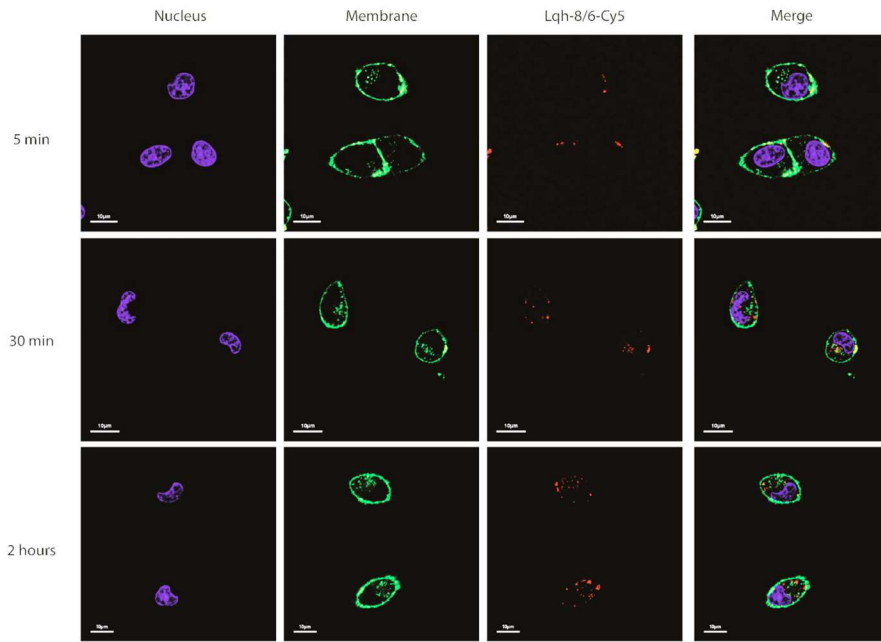


Figure 2 :

A.



B.

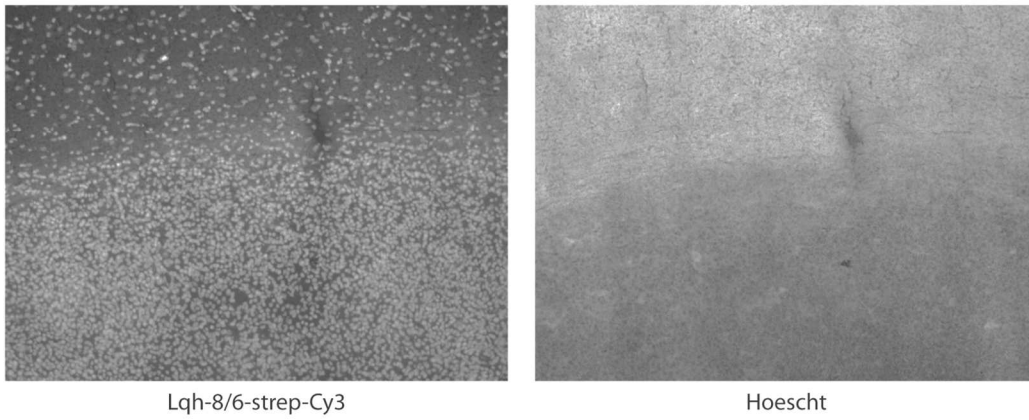
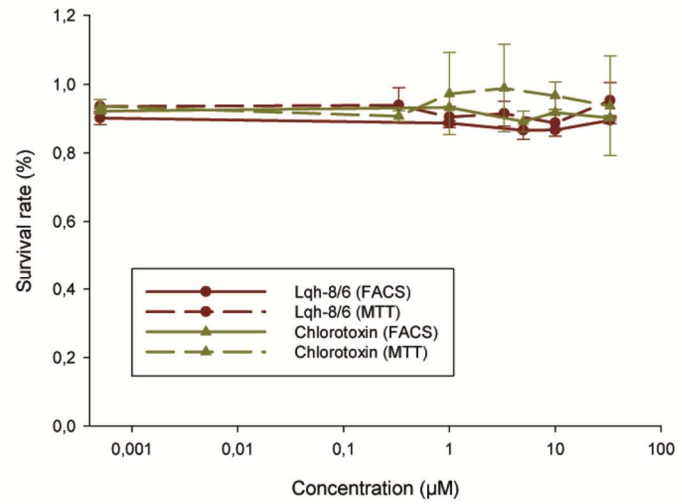
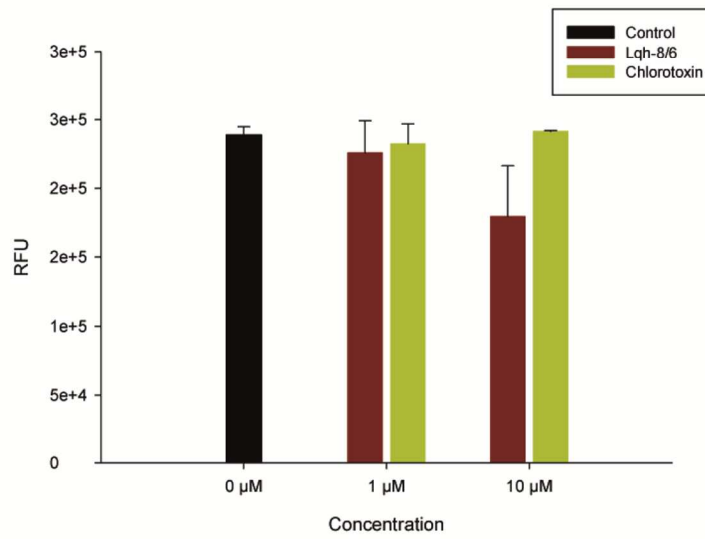


Figure 3 :

A.



B.



C.

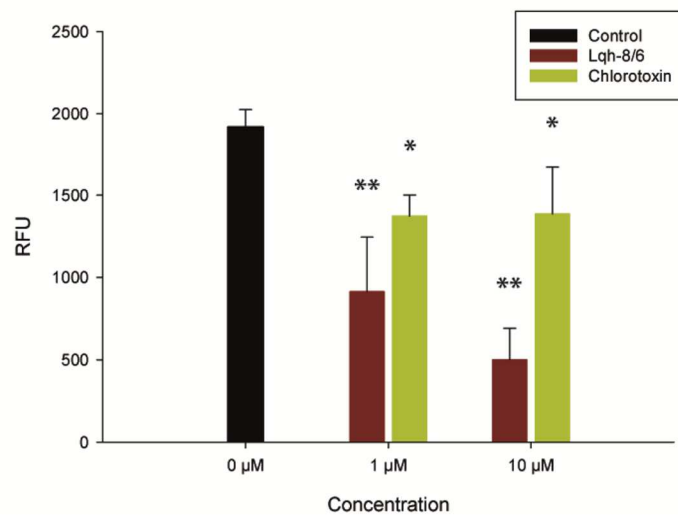
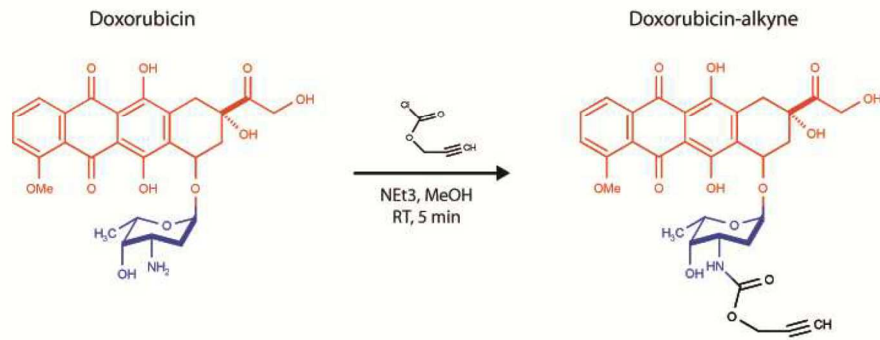
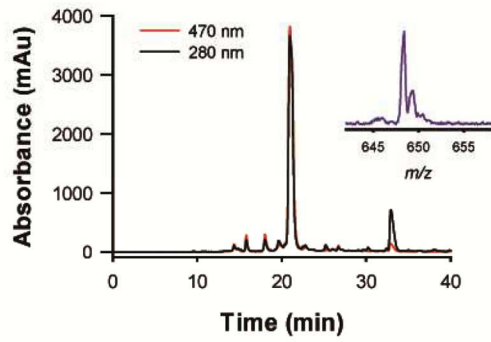


Figure 4 :

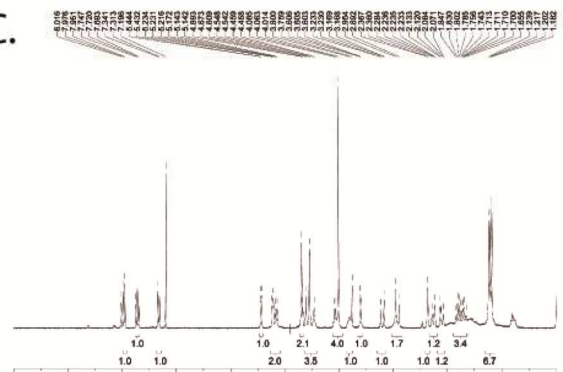
A.



B.



C.



D.

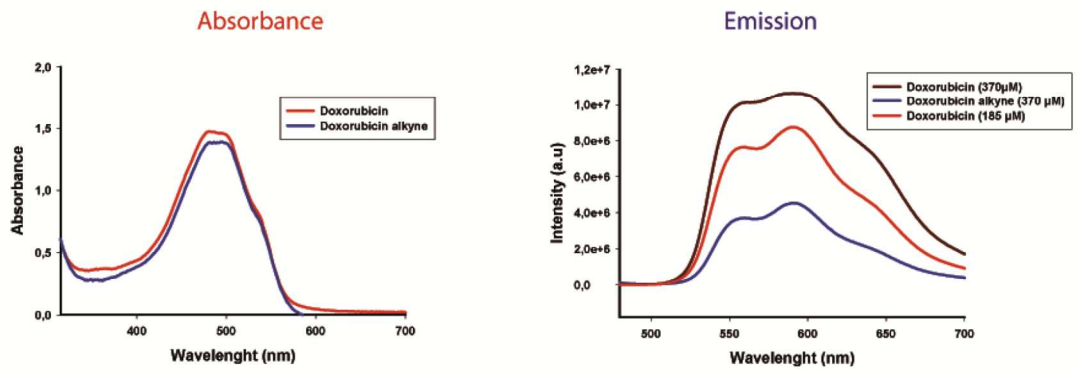


Figure 5:

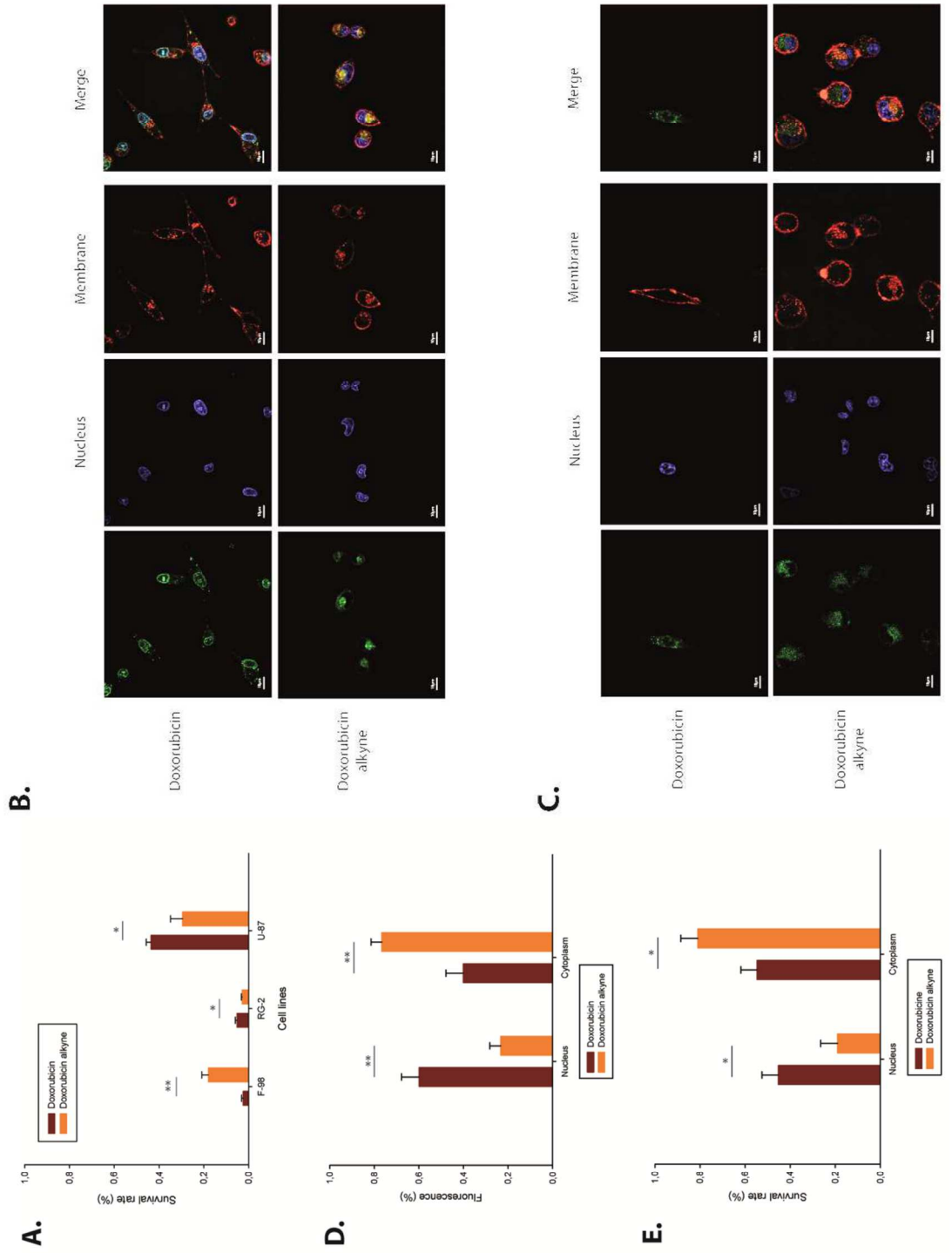


Figure 6 :

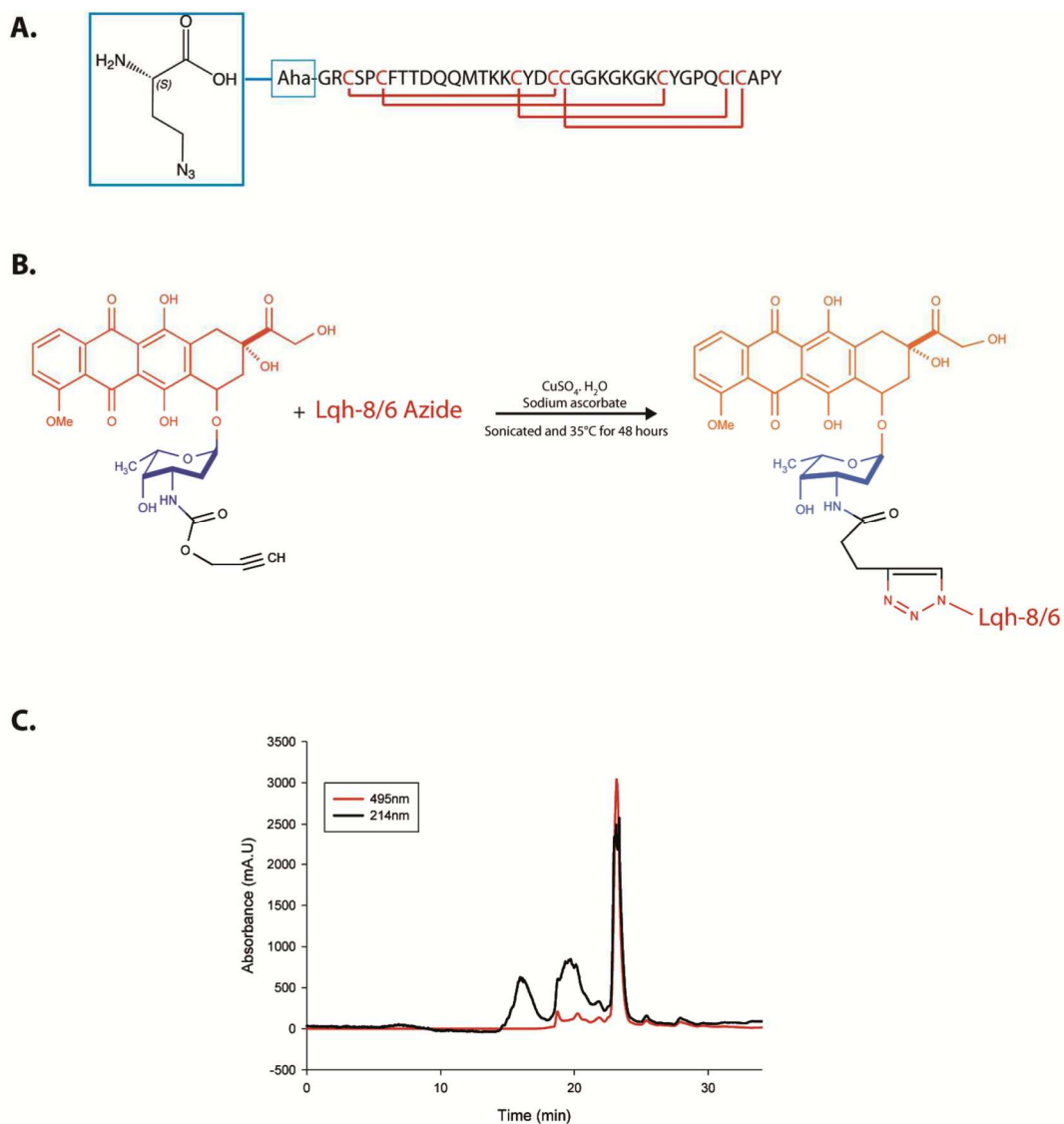


Figure 7 :

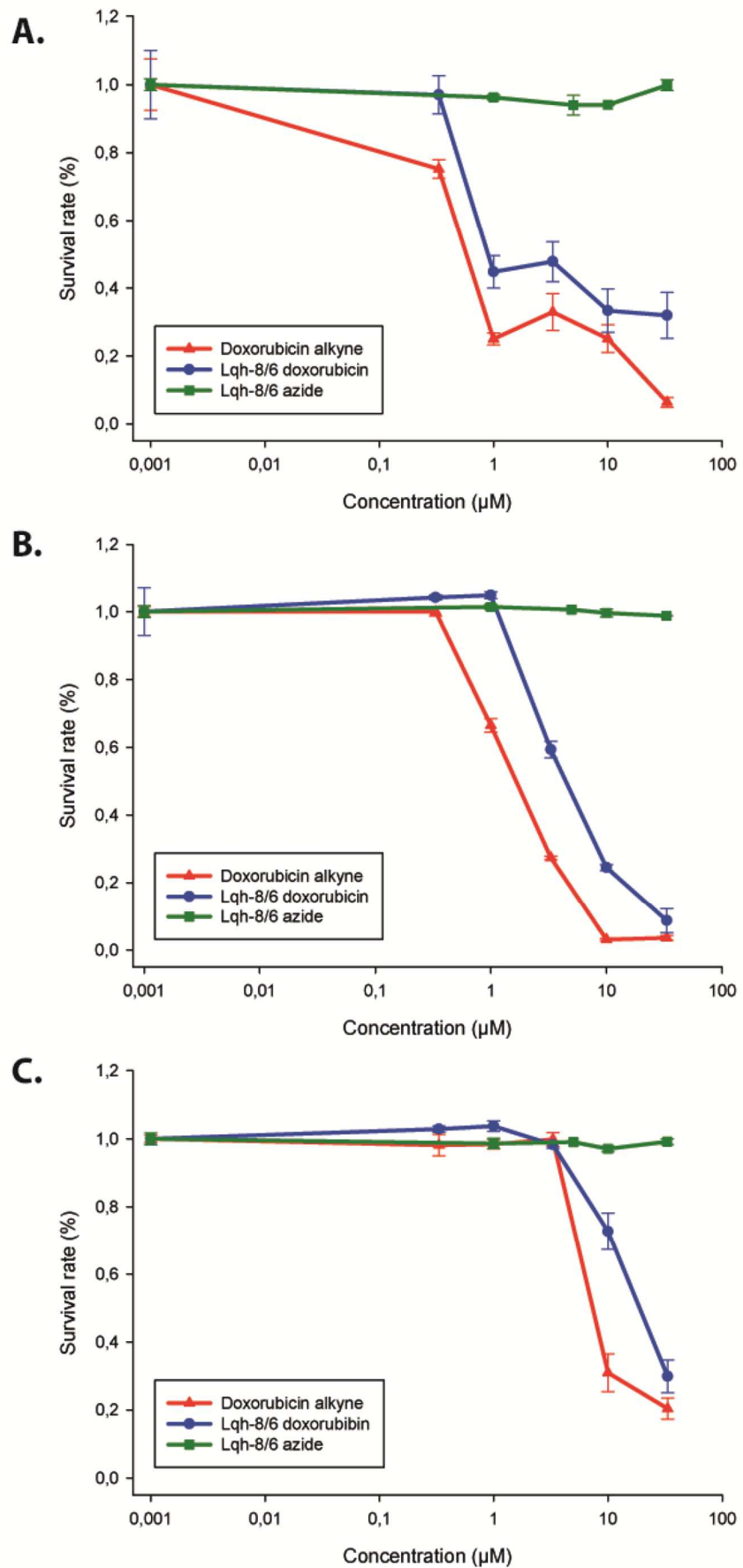
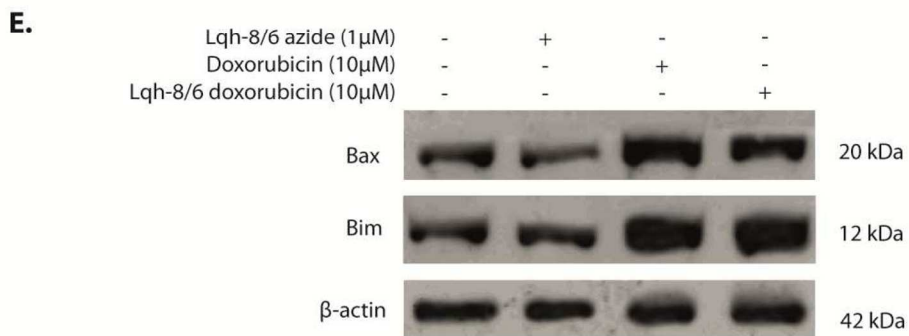
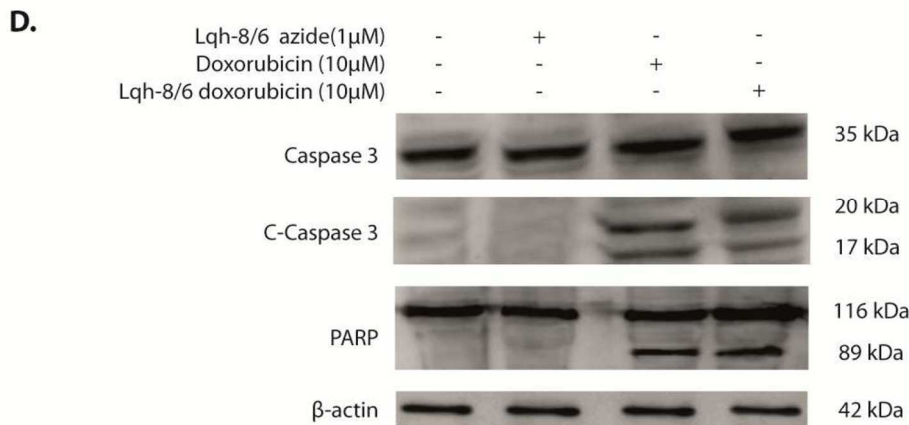
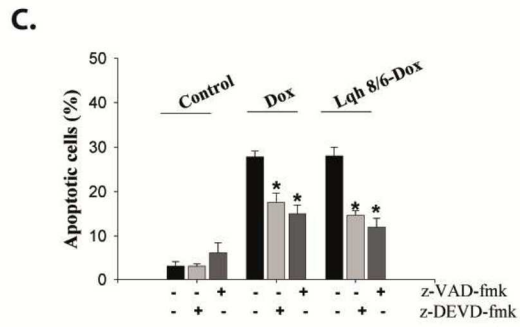
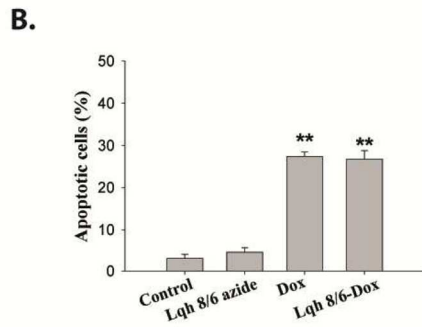
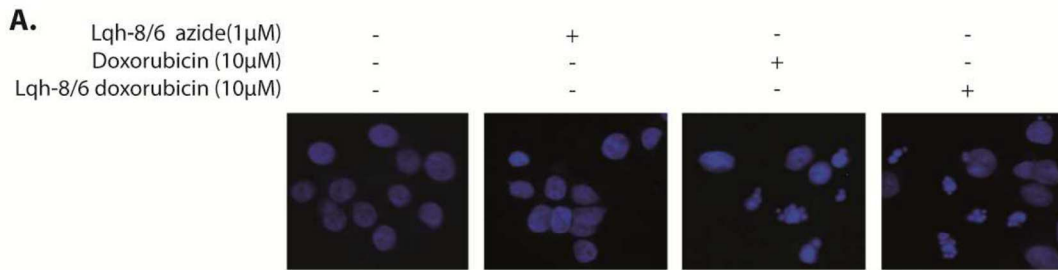
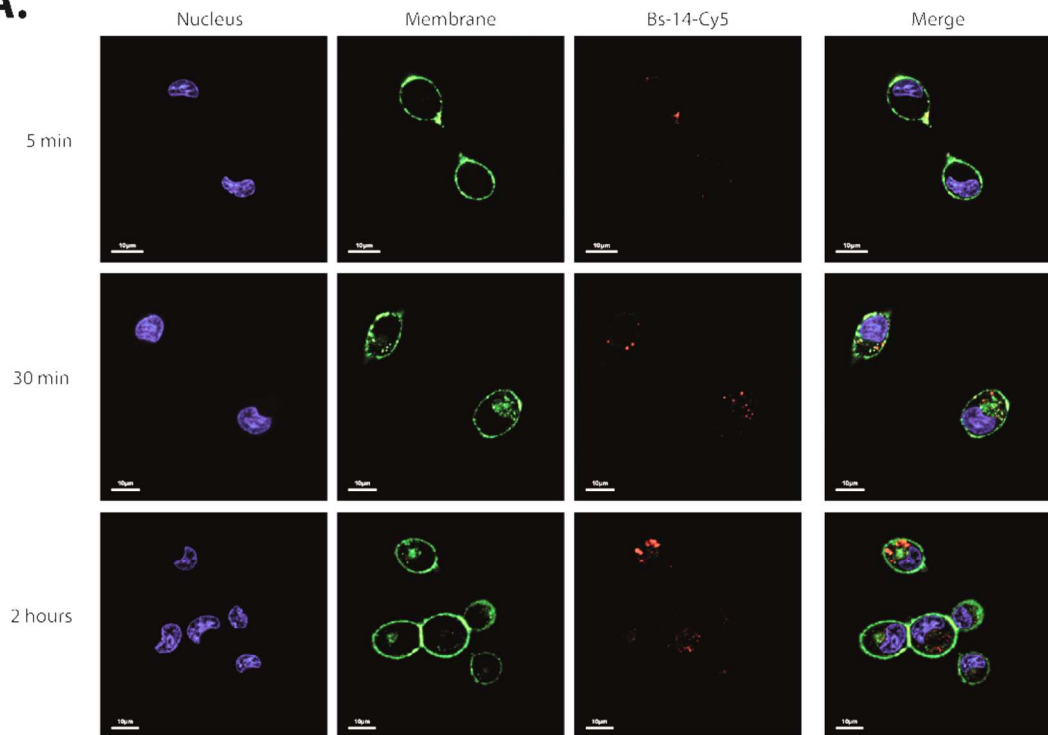


Figure 8 :

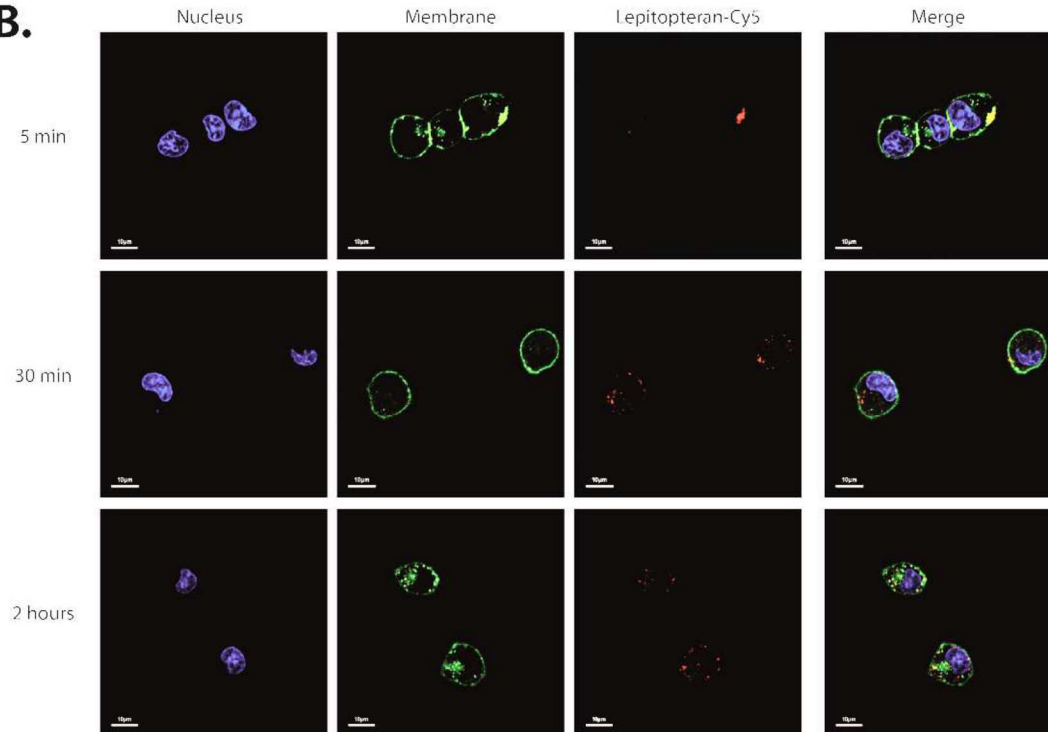


Supplementary figure 1 :

A.

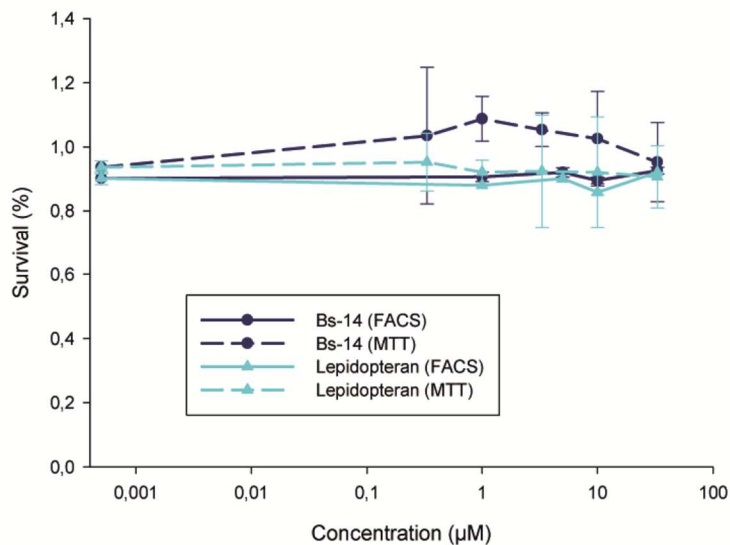


B.

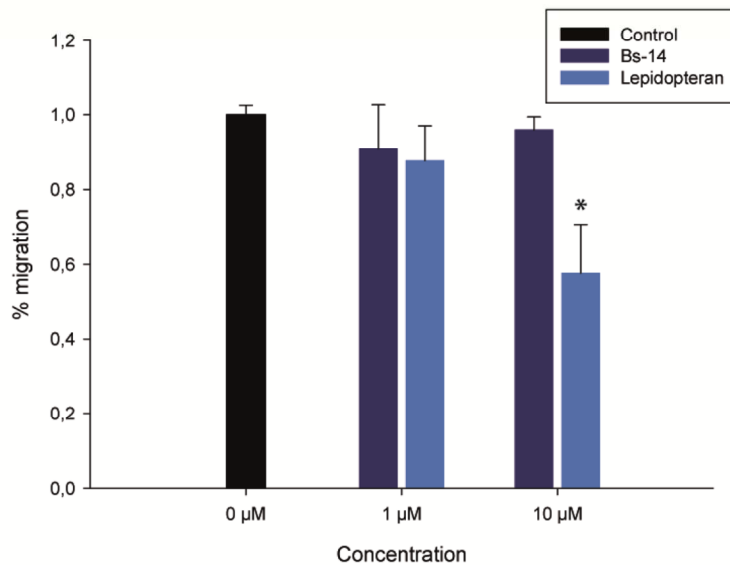


Supplementary figure 2:

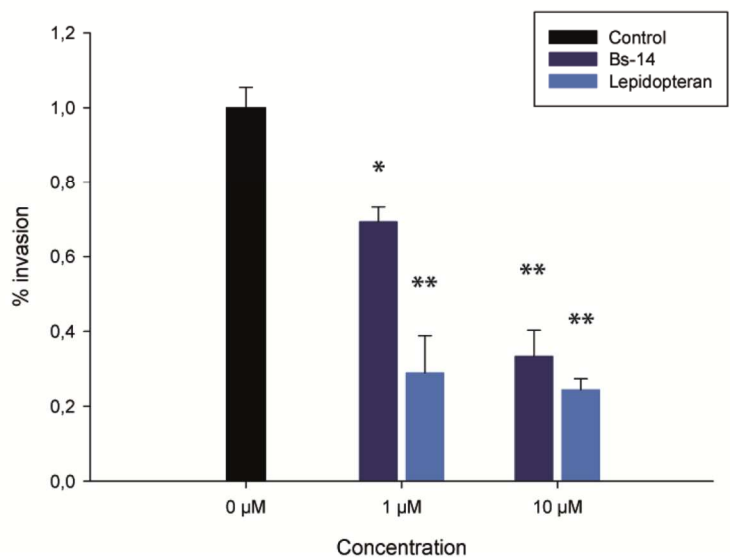
A.



B.



C.



References

- 1 McPherson, C. (2013) Glioma Brain Tumors. *Mayf. Clin. Spine Inst.*
- 2 Glioblastoma (GBM) | American Brain Tumor Association. . [Online]. Available: <http://www.abta.org/brain-tumor-information/types-of-tumors/glioblastoma.html>. [Accessed: 19-Jan-2016]
- 3 Brandes, A. a. *et al.* (2008) Glioblastoma in adults. *Crit. Rev. Oncol. Hematol.* 67, 139–152
- 4 Lévy, S. *et al.* (2014) Prise en charge des gliomes. *Cancer/Radiothérapie* 18, 461–467
- 5 Behin, A. *et al.* (2003) Primary brain tumours in adults. *Lancet* 361, 323–331
- 6 Stummer, W. *et al.* (2011) Cytoreductive surgery of glioblastoma as the key to successful adjuvant therapies: new arguments in an old discussion. *Acta Neurochir. (Wien)*. 153, 1211–8
- 7 Stupp, R. and Regg, C. (2003) New drugs and combinations for malignant glioma. *Forum (Genova)*. 13, 61–75
- 8 Stupp, R. *et al.* (2005) Radiotherapy plus concomitant and adjuvant temozolomide for glioblastoma. *N. Engl. J. Med.* 352, 987–96
- 9 Hottinger, a. F. *et al.* (2012) Decision making and management of gliomas: Practical considerations. *Ann. Oncol.* 23,
- 10 Stupp, R. *et al.* (2009) Effects of radiotherapy with concomitant and adjuvant temozolomide versus radiotherapy alone on survival in glioblastoma in a randomised phase III study: 5-year analysis of the EORTC-NCIC trial. *Lancet Oncol.* 10, 459–466
- 11 Orphanet: Glioblastome. . [Online]. Available: http://www.orpha.net/consor/cgi-bin/OC_Exp.php?Lng=FR&Expert=360. [Accessed: 19-Jan-2016]
- 12 Ampie, L. *et al.* (2015) Immunotherapeutic advancements for glioblastoma. *Front. Oncol.* 5, 12
- 13 Okonogi, N. *et al.* (2015) Topics in chemotherapy, molecular-targeted therapy, and immunotherapy for newly-diagnosed glioblastoma multiforme. *Anticancer Res* 35, 1229–1235
- 14 Feron, O. (2010) Tumor-Penetrating Peptides : 2, 1–6
- 15 Sugahara, K.N. *et al.* (2009) Tissue-penetrating delivery of compounds and nanoparticles into tumors. *Cancer Cell* 16, 510–20
- 16 Savino, M. *et al.* (2011) The action mechanism of the Myc inhibitor termed Omomyc may give clues on how to target Myc for cancer therapy. *PLoS One* 6, e22284
- 17 Alberici, L. *et al.* (2013) De Novo Design of a Tumor-Penetrating Peptide. *Cancer Res.* 73, 804–812
- 18 Mouhat, S. *et al.* (2004) Diversity of folds in animal toxins acting on ion channels. *Biochem. J.* 378, 717–26
- 19 DeBin, J.A. *et al.* (1993) Purification and characterization of chlorotoxin, a chloride channel ligand from the venom of the scorpion. *Am. J. Physiol.* 264, C361–369
- 20 Veiseh, O. *et al.* (2009) Inhibition of tumor-cell invasion with chlorotoxin-bound superparamagnetic nanoparticles. *Small* 5, 256–264
- 21 Soroceanu, L. *et al.* (1999) Modulation of glioma cell migration and invasion using Cl(-) and K(+) ion channel blockers. *J. Neurosci.* 19, 5942–5954
- 22 Ullrich, N. *et al.* (1998) Expression of voltage-activated chloride currents in acute slices of human gliomas. *Neuroscience* 83, 1161–1173
- 23 Olsen, M.L. *et al.* (2003) Expression of voltage-gated chloride channels in human glioma cells. *J. Neurosci.* 23, 5572–5582
- 24 Debin, J. a and Strichartz, G.R. (1991) Short Communications Chloride Channel

- Inhibition By the Venom of the. *Toxicon* 29, 1403–1408
- 25 Soroceanu, L. *et al.* (1998) Use of Chlorotoxin for Targeting of Primary Brain Tumors. *Cancer Res.* 58, 4871–4879
- 26 Lyons, S. a. *et al.* (2002) Chlorotoxin, a scorpion-derived peptide, specifically binds to gliomas and tumors of neuroectodermal origin. *Glia* 39, 162–173
- 27 Deshane, J. *et al.* (2003) Chlorotoxin inhibits glioma cell invasion via matrix metalloproteinase-2. *J. Biol. Chem.* 278, 4135–4144
- 28 Kesavan, K. *et al.* (2009) Annexin A2 Is a Molecular Target for TM601, a Peptide with Tumor-targeting and Anti-angiogenic Effects. *J. Biol. Chem.* 285, 4366–4374
- 29 Veiseh, M. *et al.* (2007) Tumor paint: A chlorotoxin: Cy5.5 bioconjugate for intraoperative visualization of cancer foci. *Cancer Res.* 67, 6882–6888
- 30 Kievit, F.M. *et al.* (2010) Chlorotoxin labeled magnetic nanovectors for targeted gene delivery to glioma. *ACS Nano* 4, 4587–4594
- 31 Huang, R. *et al.* (2011) Targeted delivery of chlorotoxin-modified DNA-loaded nanoparticles to glioma via intravenous administration. *Biomaterials* 32, 2399–2406
- 32 Veiseh, O. *et al.* (2009) A ligand-mediated nanovector for targeted gene delivery and transfection in cancer cells. *Biomaterials* 30, 649–657
- 33 Veiseh, O. *et al.* (2005) Optical and MRI multifunctional nanoprobe for targeting gliomas. *Nano Lett.* 5, 1003–1008
- 34 Akcan, M. *et al.* (2011) Chemical re-engineering of chlorotoxin improves bioconjugation properties for tumor imaging and targeted therapy. *J. Med. Chem.* 54, 782–787
- 35 Graf, N. *et al.* (2012) Platinum(IV)-chlorotoxin (CTX) conjugates for targeting cancer cells. *J. Inorg. Biochem.* 110, 58–63
- 36 Nicolaides, N.C. *et al.* Multifunctional AGENTS. . 26-Mar-(2013)
- 37 Smertenko, A. *et al.* (2001) TOXIN EVOLUTION IN SCORPION VENOM: EVIDENCE FOR TOXIN DIVERGENCE UNDER STRONG NEGATIVE SELECTION IN *LEIURUS QUINQUESTRATUS* SUBSPECIES. *J. Toxicol. Toxin Rev.* 20, 229–244
- 38 Xu, T. *et al.* (2016) Identification of two novel Chlorotoxin derivatives CA4 and CTX-23 with chemotherapeutic and anti-angiogenic potential. *Sci. Rep.* 6, 19799
- 39 Fan, S. *et al.* (2010) BmKCT toxin inhibits glioma proliferation and tumor metastasis. *Cancer Lett.* 291, 158–166
- 40 Pons, J.L. and Labesse, G. (2009) @TOME-2: A new pipeline for comparative modeling of protein-ligand complexes. *Nucleic Acids Res.* 37,
- 41 Adjadj, E. *et al.* (1997) Solution structure of Lqh-8/6, a toxin-like peptide from a scorpion venom--structural heterogeneity induced by proline cis/trans isomerization. *Eur. J. Biochem.* 246, 218–27
- 42 Tisseyre, C. *et al.* (2014) Quantitative evaluation of the cell penetrating properties of an iodinated Tyr-I-maurocalcine analog. *Biochim. Biophys. Acta - Mol. Cell Res.* 1843, 2356–2364
- 43 Liang, J.F. and Yang, V.C. (2005) Synthesis of doxorubicin-peptide conjugate with multidrug resistant tumor cell killing activity. *Bioorg. Med. Chem. Lett.* 15, 5071–5
- 44 Ché, C. *et al.* (2010) New Angiopep-modified doxorubicin (ANG1007) and etoposide (ANG1009) chemotherapeutics with increased brain penetration. *J. Med. Chem.* 53, 2814–24
- 45 Meyer-Losic, F. *et al.* (2006) Improved therapeutic efficacy of doxorubicin through conjugation with a novel peptide drug delivery technology (Vectocell). *J. Med. Chem.* 49, 6908–16
- 46 Ai, S. *et al.* (2011) Biological evaluation of a novel doxorubicin-peptide conjugate for

- targeted delivery to EGF receptor-overexpressing tumor cells. *Mol. Pharm.* 8, 375–86
- 47 Rousselle, C. *et al.* (2000) New advances in the transport of doxorubicin through the
blood-brain barrier by a peptide vector-mediated strategy. *Mol. Pharmacol.* 57, 679–86
- 48 Rousselle, C. *et al.* (2000) New Advances in the Transport of Doxorubicin through the
Blood-Brain Barrier by a Peptide Vector-Mediated Strategy. *Mol. Pharmacol.* 57, 679–
686
- 49 Fan, S. *et al.* (2010) BmKCT toxin inhibits glioma proliferation and tumor metastasis.
Cancer Lett. 291, 158–66
- 50 Mu, Q. *et al.* (2016) Gemcitabine and Chlorotoxin Conjugated Iron Oxide
Nanoparticles for Glioblastoma Therapy. *J. Mater. Chem. B. Mater. Biol. Med.* 4, 32–
36
- 51 Tamborini, M. *et al.* (2016) A Combined Approach Employing Chlorotoxin-
Nanovectors and Low Dose Radiation To Reach Infiltrating Tumor Niches in
Glioblastoma. *ACS Nano* 10, 2509–20
- 52 Zhao, L. *et al.* (2015) Chlorotoxin-conjugated nanoparticles for targeted imaging and
therapy of glioma. *Curr. Top. Med. Chem.* 15, 1196–208
- 53 Fu, Y. *et al.* (2012) Chlorotoxin-conjugated nanoparticles as potential glioma-targeted
drugs. *J. Neurooncol.* 107, 457–62
- 54 Hopewell, J.W. *et al.* (2001) Preclinical evaluation of the cardiotoxicity of PK2: A
novel HPMA copolymer–doxorubicin–galactosamine conjugate antitumour agent.
Hum. Exp. Toxicol. 20, 461–470
- 55 Yeung, T.K. *et al.* (1991) Reduced cardiotoxicity of doxorubicin given in the form
of N-(2-hydroxypropyl) methacrylamide conjugates: an experimental study in the rat.
Cancer Chemother. Pharmacol. 29, 105–111
- 56 Injac, R. and Strukelj, B. (2008) Recent Advances in Protection against Doxorubicin-
induced Toxicity. *Technol. Cancer Res. Treat.* 7, 497–516
- 57 Di Stefano, G. *et al.* (2004) A novel method for coupling doxorubicin to
lactosaminated human albumin by an acid sensitive hydrazone bond: synthesis,
characterization and preliminary biological properties of the conjugate. *Eur. J. Pharm.
Sci.* 23, 393–7
- 58 Koren, E. *et al.* (2012) Multifunctional PEGylated 2C5-immunoliposomes containing
pH-sensitive bonds and TAT peptide for enhanced tumor cell internalization and
cytotoxicity. *J. Control. Release* 160, 264–73
- 59 Du, J.-Z. *et al.* (2011) Tailor-made dual pH-sensitive polymer-doxorubicin
nanoparticles for efficient anticancer drug delivery. *J. Am. Chem. Soc.* 133, 17560–3
- 60 Prabakaran, M. *et al.* (2009) Amphiphilic multi-arm-block copolymer conjugated with
doxorubicin via pH-sensitive hydrazone bond for tumor-targeted drug delivery.
Biomaterials 30, 5757–66

II. Conclusions

Depuis la découverte de la CTX, beaucoup de travaux ont été conduits sur l'utilisation de cette toxine dans la lutte contre le glioblastome. Concentrant ainsi l'attention, il y a encore à ce jour peu d'articles publiés sur l'existence d'autres peptides présentant les mêmes caractéristiques. Cependant la découverte d'un tel peptide représente un véritable potentiel pour améliorer la prise en charge des glioblastomes mais aussi d'autres cancers. Avec ce projet nous avons voulu identifier de nouveaux peptides d'origine naturelle présentant des caractéristiques identiques. Après avoir sélectionné trois candidats sur la base de leur homologie de séquences et de structure, nous avons commencé à caractériser ces peptides, à comparer leurs propriétés à celle de la CTX. Si l'on regarde les résultats présentés concernant la caractérisation, il apparaît clairement qu'il s'agit uniquement d'un début. Cependant l'absence de toxicité des peptides, l'effet anti-invasif de Lqh8/6 et du lepidopteran associé à leur capacité à pénétrer dans la cellule et à diffuser dans le cytoplasme, représente autant de résultats encourageants pour la suite de ce projet. Il est évident que la prochaine étape dans la caractérisation de ces peptides est la vérification du ciblage des cellules cancéreuses sur une des coupes histologiques humaines. En effet sans la capacité de ciblage, l'utilisation de ces peptides dans le traitement des glioblastomes sera compromise malgré l'efficacité observée lors de l'administration de Lqh-8/6 doxorubicine. Des essais de toxicité et de pénétration sur des lignées astrocytaires saines doivent aussi être réalisés afin de compléter les résultats obtenus jusqu'à présent. De plus les résultats des essais *in vitro* viendront aussi parachever les résultats présentés dans ma thèse.

La Lqh-8/6 doxorubicine permet d'apporter la preuve de concept que l'utilisation d'un système de couplage « universel » basé sur la chimie click est très intéressante. En effet les résultats de toxicité, bien que montrant un effet de la Lqh-8/6 doxorubicine, il reste moindre que celui de la doxorubicine alkyne et de la doxorubicine. Il reste donc du travail à réaliser afin d'optimiser ce composé sans doute en se concentrant sur le couplage. L'utilisation d'un autre anticancéreux ayant une activité uniquement cytoplasmique est aussi une possibilité à envisager.

Le travail réalisé sur ce projet au cours de ma thèse représente le premier pas vers le développement d'un nouveau système de délivrance de composés actifs pour le traitement des glioblastomes et des autres tumeurs cancéreuses de la même origine neuro-ectodermique..

Chapitre 2 : La maurocalcine comme vecteur d'un dérivé du cisplatine.

Article : Un nouveau conjugué : Platine-maurocalcine induit l'apoptoses des cellules de glioblastome Humain en agissant sur la voie ROS-ERK/AKT-p53.

I. Introduction

Comme nous l'avons vu dans la présentation de la maurocalcine, de nombreux travaux ont été conduits au sein du laboratoire pour trouver le variant le plus intéressant comme vecteur de composé. Seul trois papiers ont été publiés présentant l'intérêt du couplage de la MCa à la doxorubicine. Dans le but d'approfondir ces résultats, nous avons choisi de tester le couplage d'un autre anticancéreux, un dérivé du cisplatine. En effet, les dérivés du cisplatine et ce dernier font partie de l'arsenal thérapeutique pour traiter les glioblastomes. Suite à la parution de travaux de Damian et collaborateur (Damian et al., 2010), nous avons décidé d'utiliser leurs nouveaux dérivés du platine, le MBL-III-7. Il a l'avantage d'être facilement synthétisable et de pouvoir se coupler au peptide au cours de la synthèse peptidique. Ce sont deux avantages très importants puisque pour ce projet nous avons retenu deux analogues de la MCa comme vecteur : un variant tronqué linéaire constitué des neuf premiers acides aminés de la MCa : la MCa_{UF1-9} et un variant taille complète la D-MCa. Il nous fallait donc trouver une méthode de couplage applicable pour ces deux vecteurs et qui n'augmentait pas le coût de production. Comme la D-MCa est un peptide de 33 acides aminés ayant une structure secondaire maintenue par 3 ponts disulfures, l'utilisation d'une cystéine surnuméraire et un couplage via une liaison disulfure ou maleimide était une stratégie trop coûteuse. La possibilité de coupler l'agent thérapeutique sur le vecteur au cours de la synthèse peptidique présente un véritable avantage.

Lors des travaux préliminaires sur ces deux composés, j'ai comparé leurs activités sur des cellules F-98 (cellules de glioblastome de rat). Ces résultats non présentés dans l'article, ont permis de déterminer que bien que nous ayons une activité pour le composé utilisant la D-MCa comme vecteur, on ne retrouve pas d'effet similaire pour le composé utilisant le MCa_{UF1-9} comme vecteur. La suite des travaux, ayant pour objectif de déterminer s'il y a une augmentation de la toxicité pour le composé vectorisé par rapport au cisplatine et sur les mécanismes de toxicité, a été réalisée en collaboration avec d'autres laboratoires. Afin de pouvoir poursuivre mes travaux sur mes autres projets de thèse, seule la synthèse chimique et les résultats préliminaires ont été réalisés au laboratoire. Ce sont les résultats de ces travaux qui ont abouti à la publication de l'article suivant.

A Novel Platinum–Maurocalcine Conjugate Induces Apoptosis of Human Glioblastoma Cells by Acting through the ROS-ERK/AKT-p53 Pathway

Sonia Aroui,^{*,†} Lucie Dardevet,^{‡,§} Wafa Ben Ajmia,[⊥] Madryssa de Boisvilliers,[⊗] Florian Perrin,[⊗] Amel Laajimi,[†] Ahcène Boumendjel,^{§,||} Abderraouf Kenani,[†] Jean Marc Muller,[⊗] and Michel De Waard^{‡,§,#}

[†]Laboratoire de Biochimie, Unité de recherche UR 12ES08 “Signalisation Cellulaire et Pathologies”, Faculté de Médecine de Monastir, Université de Monastir, 5019 Monastir, Tunisia

[‡]LabEx Ion Channels, Science and Therapeutics, INSERM U836, Grenoble Neuroscience Institute, 38042 Grenoble Cedex 09, France

[§]University Grenoble Alpes, 38000 Grenoble, France

[⊥]Toxicology-Microbiology and Environmental Health Unit (UR11ES70), Faculty of Sciences, University of Sfax, Sfax 3072, Tunisia

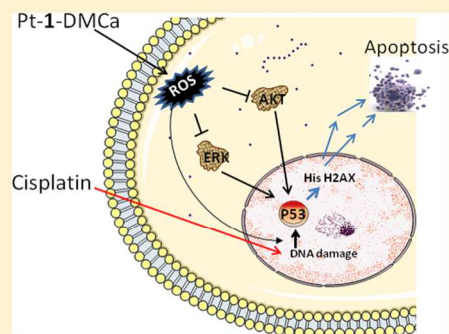
^{||}CNRS 5063, Département de Pharmacochimie Moléculaire, Université Joseph Fourier, 38400 Saint-Martin d'Hères, France

[⊗]Equipe émergente “Récepteurs, régulations et cellules tumorales” (2RCT), Université de Poitiers, 1 rue Georges Bonnet, TSA 51106, 86073 Poitiers Cedex 9, France

[#]Smartox Biotechnology, 570 Rue de la Chimie, 38400 Saint-Martin d'Hères, France

ABSTRACT: Glioblastoma multiforme (GBM) is a highly malignant and aggressive primary brain tumor. In spite of an arsenal of therapeutic interventions, the prognosis of glioblastoma remains very poor. Cisplatin-based therapy is one of the most important chemotherapy treatments for GBM, although its efficacy is limited by drug resistance and undesirable side effects. In the present study, we designed a chimera molecule containing the platinum binding moiety MBL-III-7 (1) attached N-terminal to the sequence of D-maurocalcine (D-MCa), a protease-resistant and highly efficient cell-penetrating peptide (CPP) derived from the Tunisian chactid scorpion toxin, L-MCa. The concept behind this design is that MCa, through its cell retention properties, should reduce cell expulsion of the platinum complex and increase its efficiency. The anti-cancer properties of the synthesized platinum analogue Pt-MBL-III_7-D_MCa (Pt-1-DMCa) were assessed in human glioblastoma cells (U87) by assaying cell viability and apoptosis. The new molecule exhibited enhanced anti-cancer efficacy compared to cisplatin, especially at low doses. By inducing intracellular oxidative stress, Pt-1-DMCa potentiated platinum-induced DNA damage and led to enhanced p53 phosphorylation, followed by increased activation of both mitochondrial and death receptor pathways. Decreased phosphorylated AKT and ERK levels were associated with the apoptosis induced by the novel synthesized cisplatin analogue. Our results suggested that a chimera between platinum and a maurocalcine-derived CPP is a highly successful anti-cancer compound that works by targeting the intracellular redox system. Pt-1-DMCa is an interesting candidate for a preclinical assessment of platinum-based therapy in GBM treatments and possibly other cancer types.

KEYWORDS: platinum/peptide conjugate, maurocalcine, cisplatin, apoptosis, ROS, AKT, ERK



INTRODUCTION

Development of drug delivery systems has been a topic of international efforts to improve cancer treatments.^{1,2} The efficacies of many well-known anti-cancer drugs are usually limited by their poor bio-availabilities, which may include their low capacities to cross cell membranes.³ Among the strategies developed to overcome these limitations is their conjugation to a convenient carrier that is able to improve the cell uptake of the drug. Cell-penetrating peptides (CPPs) are now considered as peptide-based delivery systems to transport a large variety of

cell-membrane permeable and impermeable cargoes into cells, ranging from small peptides and proteins to nucleic acids and nanoparticles.^{4,5} CPPs have been used successfully to boost the bioavailability of anti-cancer drugs, enhancing their cytotoxic activity while in many cases reducing their dosage and

Received: July 2, 2015

Revised: October 5, 2015

Accepted: October 14, 2015

Published: October 14, 2015

secondary effects.^{6,7} One of the most efficient CPPs described in the past decade is L-maurocalcin (L-MCa), a 33-mer peptide that was initially isolated from the venom of a Tunisian chactid scorpion, *Scorpio maurus palmatus*.⁸ The peptide has a peculiar target for a venom toxin: an intracellular calcium channel, the ryanodine receptor (RyR). This channel is inserted into the membrane of the endoplasmic reticulum and controls Ca²⁺ release from intracellular stores. The binding site for L-MCa has been located in the cytoplasmic region of the predicted topology of RyR, meaning that L-MCa delivery occurs into the cytoplasm. In terms of structure, the peptide contains an inhibitor cystine knot motif with three disulfide bridges connected according to the model Cys³–Cys¹⁷, Cys¹⁰–Cys²¹, and Cys¹⁶–Cys³². L-MCa shares many structural and functional properties with some efficient CPPs because (i) the peptide is heavily charged (12 of the 33 residues of the peptide are positively charged) and (ii) it interacts with critical membrane components needed for cell penetration, such as negatively charged lipids and proteoglycans.^{9,10} Most importantly, L-MCa and several of its analogues were shown to act as efficient vectors for the delivery of proteins, peptides, nanoparticles, and drugs inside cells.^{10,11}

Because of its pharmacological activity which may represent a burden for *in vivo* applications, several strategies have been developed to define analogues that lack pharmacological activity while preserving cell penetration.^{10,12,13} Recently, we produced D-maurocalcin (D-MCa), a diastereoisomer of L-MCa which has cell penetration properties similar to those of L-MCa but without any pharmacological activity.¹⁴ Moreover, the new peptide analogue loses the protease sensitivity of L-MCa, making it the first folded/oxidized CPP built with D-amino acids designed on the basis of an animal toxin amino acid sequence.¹⁴ In the present work, to gain insight into the efficacy of D-MCa as a vector for the efficient delivery of anti-cancer drugs, we decided to couple it to a platinum chelator and investigate the anti-tumor properties of the new complex.

Platinum-based therapeutic drugs, notably cisplatin and carboplatin, have been used in chemotherapy to treat cancer cells and a wide spectrum of solid malignancies.^{5,16} The prominent cytotoxic mode of action of these compounds involves the formation of intra-strand cross-link DNA adducts which then activates particular apoptosis signal transduction pathways. However, these drugs lack partial efficacy mainly because of low uptake by cancer cells and possibly also because the drug is repelled by the multidrug resistance protein of these cells.¹⁷ Also, it should be mentioned that many cancer types are insensitive to platinum-induced apoptosis owing to numerous resistance mechanisms such as the overexpression of the Bcl-2 family of anti-apoptosis proteins, the inactivation of p53 and mitogen-activated protein kinases (MAPKs), and development of AKT phosphorylation.^{18,19} Consequently, patients are treated with higher doses of cisplatin, exposing them to higher risks of side effects such as nephrotoxicity, neurotoxicity, and ototoxicity.²⁰ The relative insensitivity of cancer cells to cisplatin leads to chemo-resistance and therapeutic failure.

Thus far, the great incidence of chemo-resistance is still the major limitation in the clinical efficacy of cisplatin as an anti-cancer drug.²¹ In this context, other platinum anti-tumor agents are still required not only in order to broaden the spectrum of activity but also to improve clinical effectiveness and to overcome the side effects of platinum-based chemotherapy. Herein, our approach is to combine the properties of two different moieties within a single compound to create a more

effective platinum-based drug with some reduced drawbacks of cisplatin. We covalently coupled **1**, a platinum chelating agent, to D-MCa as a CPP to improve platinum delivery into cancer cells and force the retention of the anti-tumor agent once delivered into the cytoplasm.

Glioblastoma multiforme (GBM) is a highly malignant and aggressive primary brain tumor in adults. In spite of joint efforts to improve current therapies, the prognosis of glioblastoma remains very poor. So far, the treatment of glioblastoma still represents one of the most challenging concerns in clinical oncology.²² Enhancing the potency of platinum drugs in glioblastoma could be an alternative therapeutic strategy. In the present study, the anti-cancer properties of the synthesized Pt-1-DMCa were assessed in human glioma cells (U87) as an *in vitro* model. The platinum derivative displayed the expected cytotoxic properties and induced apoptosis at doses lower than those needed for cisplatin. The novel platinum analogue induced inhibition of protein kinase B (also called AKT) and extracellular signal-regulated kinase (ERK) phosphorylation associated with activated apoptosis signal cascades involving both the mitochondrial (intrinsic) and the death receptor (extrinsic) pathways. In contrast, cisplatin activates only the mitochondrial apoptosis pathway.

Our data also indicate that ROS accumulation in treated cells could be a crucial factor for the strengthening effect of Pt-1-DMCa. We conclude that the synthesized product has more effective anti-tumor activity than cisplatin, especially at low doses, and represents an interesting candidate molecule for platinum-based therapy in preclinical application.

METHODS

Chemicals. *N*- α -Fmoc-D-amino-acid, Wang-tentagel resin, and reagents used for peptide synthesis were obtained from Iris Biotech. Solvents were analytical-grade products from Acros Organics. Cisplatin, Hoechst 33258, dihydrorhodamine 123 (DHR123), 5,50,6,60-tetrachloro-1,10,3,30-tetraethylbenzimidazolylcarbocyanine iodide (JC-1), propidium iodide (PI), and *N*-acetyl-L-cysteine (NAC) were purchased from Sigma-Aldrich (St. Louis, MO, USA). Cell Titer 96_Aqueous One Solution Reagent (MTS) was obtained from Promega. Tetramethylrhodamine ethyl ester (TMRE) solution was purchased from Abcam. For Western blotting, the antibodies used and their suppliers were anti-caspase-3 (H-277), anti-Hsc70 (B-6), anti- β -actin (Santa Cruz Biotechnology, Inc.); anti-caspase-8 (Alexis), anti-caspase-9, ERK, p-ERK, and anti-cleaved poly-[ADP-ribose]polymerase (cleaved PARP) (Cell Signaling); Akt, p-Akt (S473), anti-Bcl-2 (Calbiochem); anti-Bcl-xL (BD Transduction Laboratories); anti-Bax (R&D Systems); and anti-p53, anti-p-p53, anti-p-His H2A.X (ser139), and anti-GAPDH (Abcam). Peroxidase-conjugated goat anti-rabbit and anti-mouse antibodies were from Jackson ImmunoResearch Laboratories (West Grove, PA, USA). For immunofluorescence, antibodies used were monoclonal anti-DR4 and anti-DR5 (Alexis Biochemicals). The antioxidant NAC, LY294002, and U0126 and SYBR green 1 dye were obtained from Invitrogen, USA.

Cell Culture. Human normal astrocyte SVGp12 and glioma U87 cells were obtained from the American Type Culture Collection (Rockville, MD, USA) and maintained in Dulbecco's modified Eagle's medium (DMEM, Lonza), containing 10% fetal bovine serum (FBS) and 10 000 units/mL streptomycin and penicillin. Cells were incubated at 37 °C in a humidified atmosphere containing 5% CO₂. Medium was changed every 2

or 3 days. All experiments were carried out on cells having viability more than 95%. After seeding, cells were incubated overnight to adhere and then treated with drugs at different concentrations and time intervals.

Synthesis of MBL-III-7 (1), the Platinum Chelator Moiety. *N*-Fmoc MBL-III-7 or *N*-Fmoc-(3-Fmoc-aminopropyl)glycine was produced as previously described by Damian et al.²⁵ We began by synthesizing *tert*-butyl *N*-(3-aminopropyl)glycinate (2) by mixing *tert*-butyl bromoacetate (3) and 1,3-diaminopropane (4) (Figure 1A). The next step

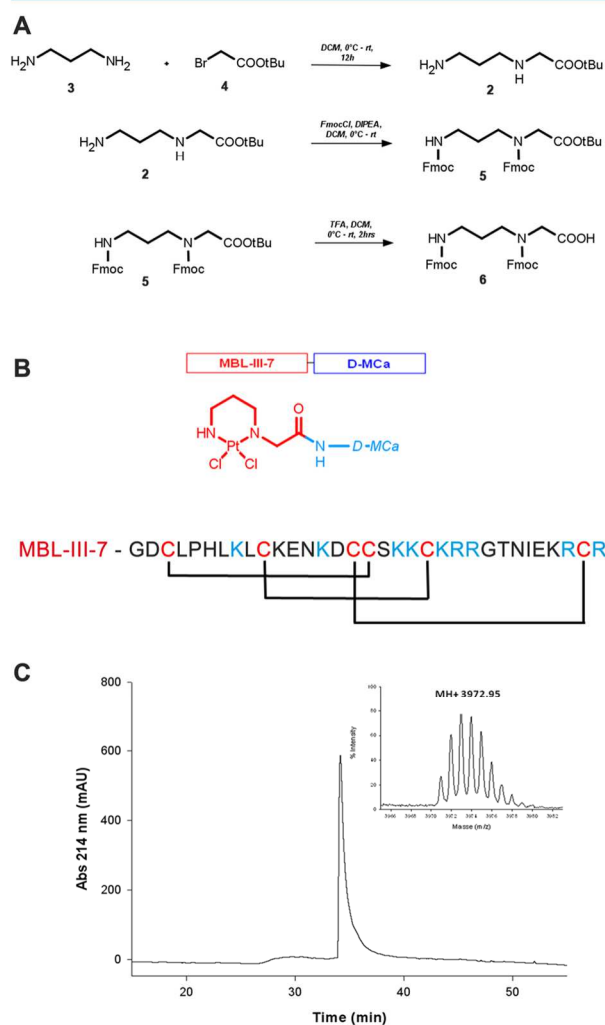


Figure 1. Synthesis and purification of the Pt-1-DMCa conjugate. (A) Synthesis of the MBL-III-7. (B) Amino acid sequences of D-MCa (single letter code) and chemical structure of MBL-III-7 bound to D-MCa. The positions of half-cystine residues are highlighted in red. Basic amino acids are highlighted in blue. (C) HPLC spectrum of 1-DMCa after folding with mass spectrometry analysis.

was to add protecting groups (Fmoc) to the two amine functions in order to obtain *tert*-butyl *N*-Fmoc-(3-Fmoc-aminopropyl)glycinate (5). The last step was to remove the *tert*-butyl protecting group of the carboxylic function by adding TFA dropwise to a cooled 0 °C solution of compound 5 in DCM. This yielded compound 6, which is used in solid-phase peptide synthesis.

Synthesis of the MBL-III-7 (1)/D-MCa Chimera. D-MCa was first chemically synthesized by the solid-phase method using an automated peptide synthesizer (CEM Liberty).^{23,24} The *N*-Fmoc-1 was then conjugated to the *N*-terminal sequence of protected D-MCa similarly to a classical protected amino acid. The resin was first swollen for 2 h in dimethylformamide (DMF). The peptide chain and chimera were assembled stepwise on 0.24 mequiv of Fmoc-D-Arg-Pbf-Wang-Tentagel resin using 0.24 mmol of *N*- α -fluorenylmethylloxycarbonyl (Fmoc) *D*-amino-acid derivatives. The side-chain protecting groups were trityl for Cys and Asn; *tert*-butyl for Ser, Thr, Glu, and Asp; Pbf for Arg; and *tert*-butylcarbonyl for Lys. Reagents were at the following concentrations: *N*-Fmoc-1 (0.2 M in DMF), Fmoc-amino acids (0.2 M Fmoc-AA-OH in DMF), activator (0.5 M HBTU in DMF), activator base (2 M diisopropylethylamine in *N*-methylpyrrolidone), and deprotection agent (5% piperazine/0.1 M 1-hydroxybenzotriazole in DMF) as advised by PepDriver (CEM Liberty). After coupling, resins were treated 4 h at room temperature with a mixture of trifluoroacetic acid/water/triisopropylsilane/dithiothreitol (DTT) (92.5/2.5/2.5/2.5). The conjugate was then filtered and the filtrate precipitated by adding cold *tert*-butyl methyl ether. The crude conjugate was pelleted by centrifugation (10000g, 15 min) and the supernatant discarded. The conjugate was then purified by HPLC using a Vydac C18 column (218TP1010, 250 \times 4.6 mm). Elution of the peptide was performed with a 10–60% acetonitrile linear gradient containing 0.1% trifluoroacetic acid. The peptide was dissolved in 200 mM Tris-HCl buffer, pH 8.3, at a final concentration of 1 mM and stirred for 72 h at room temperature under air for oxidation and folding. Oxidized 1-DMCa was purified by HPLC using a Vydac C18 column (218TP1010, 250 \times 4.6 mm). Elution of 1-DMCa was performed with a 10–60% acetonitrile linear gradient containing 0.1% trifluoroacetic acid. The purified fraction was analyzed by analytical reversed-phase HPLC (Vydac C18 column 218TP104, 250 \times 4.6 mm) and lyophilized. For platination, a solution of K₂PtCl₄ (10 equiv, 0.05 M) in DMF/H₂O (9/1, v/v) was added to the peptide and shaken in the dark for 30 h. Products were purified by HPLC to eliminate non-conjugated K₂PtCl₄. The final compound produced is named Pt-1-DMCa.

Determination of Cell Viability. Cell viability was determined on SVGp12 and glioma U87 cells using the 3-(4,5-dimethylthiazol-2-yl)-5-(3-carboxymethoxyphenyl)-2-(4-sulfophenyl)-2*H*-tetrazolium (MTS) Cell Proliferation Colorimetric Assay kit from Promega.²⁶ Cells were seeded onto a 96-well plate at 500 cells per well and allowed to adhere overnight. After treatment with Pt-1-DMCa or 1-DMCa without platinum or cisplatin at various concentrations for different times, 20 μ L of the tetrazolium substrate was added to each well of the plate. Plates were incubated at 37 °C for 2 h, after which the absorbance at 490 nm was measured. All experiments were done in triplicate and repeated at least three independent times.

Phosphatidylserine Externalization Assay. The apoptotic rates of cells were determined by annexin V-FITC and PI dual staining kit (APOAF, Sigma-Aldrich) according to the manufacturer's instructions. In brief, cells were treated with Pt-1-DMCa (20 μ M) or cisplatin (40 μ M) for 4 h, and then the medium was replaced with a fresh one and cultured again for a further 48 h. Adherent and floated cells (5 \times 10⁴/flask) were collected, washed by cold PBS solution, and resuspended in annexin-binding buffer containing FITC-conjugated annexin V

and PI in appropriate concentrations for 15 min at room temperature. The cells were then subjected to analysis by flow cytometry (FACS Calibur, BD Bioscience), and 10 000 events from each sample were acquired to ensure adequate data.

Hoechst Staining of Cells. A total of 1×10^4 cells were grown on coverslips into a six-well plate and incubated with Pt-1-DMCa ($20 \mu\text{M}$) or cisplatin ($40 \mu\text{M}$). Thereafter, cells were fixed with 4% paraformaldehyde for 30 min at room temperature and washed twice with PBS. Chilled methanol (-20°C) was added to each well for 10 min at room temperature, followed by two or three washes with PBS. Cells were then stained with Hoechst 33258 (5 mg/mL) for 10 min, washed with PBS, and then examined by a Zeiss fluorescent microscope. Cells with condensed, fragmented nuclei and having brighter fluorescence were considered as apoptotic cells.

Determination of DNA Fragmentation. DNA integrity in treated cells was assessed by the DNA ladder assay. Cells were seeded at a density of 5×10^6 cells/flask and incubated with Pt-1-DMCa ($20 \mu\text{M}$) or cisplatin ($40 \mu\text{M}$), and then the medium was replaced with a fresh one and cultured again for a further 48 h. After incubation, cells were harvested and washed with PBS, and DNA was isolated by Promega "DNA Purification from Mammalian Cell Lines" kit as described by the manufacturer's guidelines. DNA was quantitated spectrophotometrically, and an equal amount of DNA (1 mg) was loaded onto 2% agarose gel containing $5 \mu\text{g/mL}$ of ethidium bromide. The agarose gel was run at 1.5 V/cm in Tris-borate/EDTA electrophoresis buffer. Approximately 1 mg of DNA was loaded in each well, visualized under UV light, and photographed.

Single-Cell Gel Electrophoresis (Comet Assay). Single-cell gel electrophoresis for detection of DNA damage was performed using the comet assay reagent kit as described previously.²⁸ U87 cells were cultured and treated with Pt-1-DMCa ($20 \mu\text{M}$) or cisplatin ($40 \mu\text{M}$) for 4 h, and then the medium was replaced with a fresh one and cultured again for a further 48 h. The cells were then dissociated 0.5 or 4 h after irradiation for single-cell gel electrophoresis at 19 V (300 mA , 40 min) and analyzed by neutral comet assay (Trevigen, Gaithersburg, MD) according to the manufacturer's instructions. SYBR green-stained DNA comets were visualized and photographed under a Zeiss fluorescent microscope.

Western Immunoblotting Analysis. Cells were incubated for the indicated time and concentration of compounds and cultured in Petri dishes to about 75% confluence in serum-free medium supplemented with 0.1% bovine serum albumin (BSA). The incubated cells were washed twice with cold PBS and scrapped in ice-cold lysis buffer (10 mM Tris pH 7.5, 0.5 mM EDTA pH 8.0, 0.5 mM DTT, 0.5% CHAPS, 10% glycerol) supplemented with a cocktail of protease inhibitors. After 30 min on ice, cell debris were removed by centrifugation at $10000g$ at 4°C for 20 min. Proteins were quantified using the DC Protein Assay (Bio-Rad) according to the manufacturer's specifications. A total of $20 \mu\text{g}$ of protein lysate was incubated in loading buffer (60 mM Tris-HCl, pH 6.8, 0.18 M β -mercaptoethanol, 2% SDS, 10% glycerol, and 0.005% bromophenol blue), boiled, and separated on a polyacrylamide gel by SDS-PAGE under reducing conditions. The proteins were electro-transferred overnight or 2 h at 4°C to a polyvinylidene difluoride (PVDF) membrane (Hybond-P, Amersham Biosciences). Membranes were blocked for at least 1 h in Tris-buffered saline (TBS), 5% BSA, and 0.5% Tween 20 and then probed with the appropriate primary antibodies

(1:1000) in 5% BSA, 0.1% Tween 20, and 0.05% sodium azide in TBS for 1 h at room temperature or overnight at 4°C and thereafter incubated with the appropriate secondary peroxidase-labeled antibody (1:20,000) for 1 h at room temperature. Enhanced chemiluminescence (ECL, Amersham Pharmacia Biotech) was used for protein detection. The ECL staining was quantified by densitometry with ImageJ software (National Institutes of Health, USA).

Assessment of Mitochondrial Membrane Potential ($\Delta\psi\text{m}$). The $\Delta\psi\text{m}$ was determined using two fluorescent probes in separate assays, JC-1 and TMRE. JC-1 is a lipophilic molecule that penetrates the cell and accumulates in mitochondria. In non-treated cells with well-polarized mitochondria, JC-1 can form aggregates that are excited by a 488 nm laser (FL-2) and display orange fluorescence. When $\Delta\psi\text{m}$ is decreased, JC-1 present in mitochondria tends to exist as monomers that emit green fluorescence on FL-1 after excitation (decrease in the orange fluorescence). Thus, $\Delta\psi\text{m}$ can be estimated by simultaneous measurement of the fluorescence of JC-1 aggregates and monomers on the FL2 and FL1 detection channel of a flow cytometer, respectively.²⁷ Briefly, treated cells were loaded with JC-1 probe as described and then analyzed by flow cytometry. TMRE is a cell-permeable, positively charged, red-orange dye that readily accumulates in active mitochondria due to their relative negative charge. Depolarized or inactive mitochondria have decreased membrane potential and fail to sequester TMRE. The depletion of $\Delta\psi\text{m}$ was then monitored qualitatively with TMRE by a Zeiss fluorescent microscope.

Measurement of Intracellular Reactive Oxygen Species (ROS). The ability of Pt-1-DMCa to generate ROS in GBM cells was assessed by DHR123. Briefly, 2×10^6 cells were treated by Pt-1-DMCa or cisplatin for 4 h, and then the medium was replaced with a fresh one and cultured again for a further 48 h. Cells were then incubated with $2.5 \mu\text{g/mL}$ DHR123, a non-fluorescent cell-permeable dye, for 30 min in the CO_2 incubator. DHR123 upon oxidation by ROS generated in the cell is converted to rhodamine 123 (Rh123). The cells were collected and washed with PBS, and ROS generation was measured by the fluorescence intensity (FL-1, 530 nm) of 10 000 cells using a FACS Calibur flow cytometer (BD Biosciences). For fluorescence microscopy, DHR123 incubated cells were then washed three times in PBS for 5 min, fixed for 30 min in 4% paraformaldehyde at room temperature, and washed twice with PBS. Counterstaining of nuclei was performed by incubating cells with Hoechst 33258 (5 mg/mL) for 10 min, washed with PBS, and mounted onto glass slides using Permafluor aqueous mounting media. Rh123 and Hoechst fluorescence were examined by a Zeiss fluorescent microscope with fluorescein and UV filters, respectively.

Statistical Analyses. Results are expressed as mean \pm standard errors (mean \pm SEM). All analyses were carried out with GraphPad Prism 6.0 for Windows (GraphPad Software, San Diego, CA). Significant differences between the effects of the treatments were determined by one-way ANOVA, followed by Tukey's post hoc test for multiple comparisons with statistical significance of $p < 0.05$.

■ RESULTS

Synthesis of the Pt-1-DMCa Conjugate. In order to produce the novel platinum-peptide conjugate, we first initiated the synthesis of *N*-Fmoc MBL-III-7 (**1**) as described in the Methods section (Figure 1A). The compound was then coupled at the N-terminal position of the D-MCa amino acid

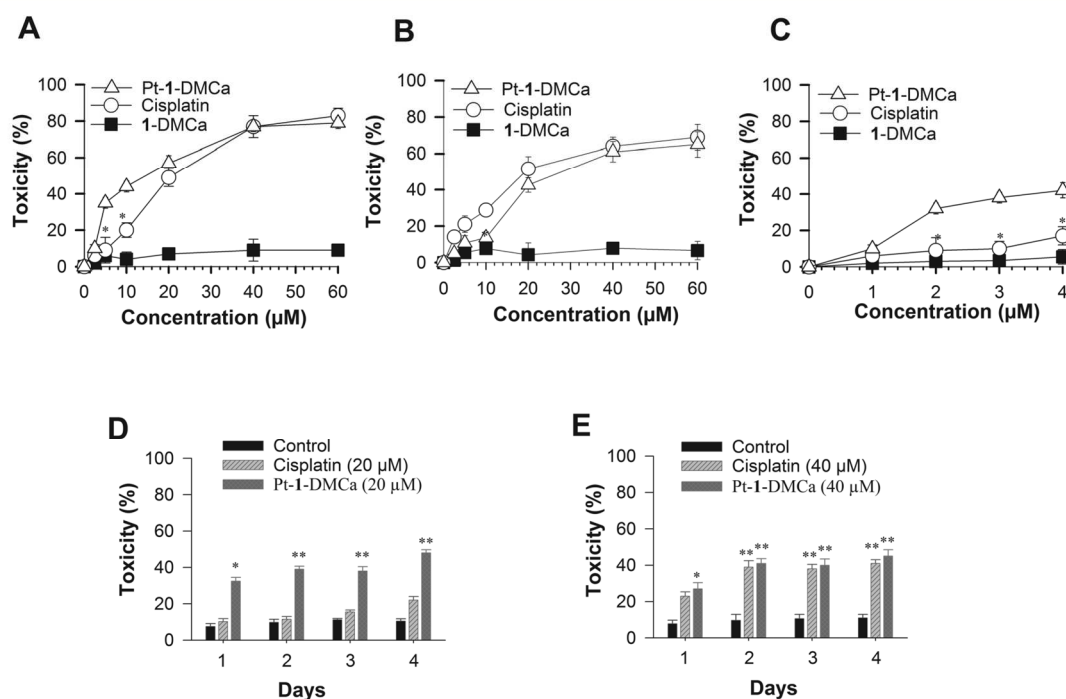


Figure 2. Cell death induction by 1-DMCa, cisplatin, and Pt-1-DMCa in SVGP12 and glioma U87 cells. (A) Compounds were applied at various concentrations on U87 cells for 48 h before performing the MTS assay, as described in the Methods section. (B) SVGP12 cells were treated with various concentrations of Pt-1-DMCa, cisplatin, or 1-DMCa for 48 h before performing the MTS assay. (C) Cytotoxicity was assessed by 5 μM of all compounds after 4 h treatment, removing the medium, and cultured again for 1, 2, 3, and 4 days. (D) 20 μM of Pt-1-DMCa or cisplatin was used to treat the cells for 4 h, removing the medium, and cultured again for 1, 2, 3, and 4 days before performing the MTS assay. Data are representative of two independent experiments carried out in triplicate. Results are presented as mean \pm SD. Significant differences between stimulated Pt-1-DMCa and cisplatin cells are indicated by a star, $^*(P < 0.05)$ (A and B). Significant differences between stimulated cells (Pt-1-DMCa or cisplatin) and control cells are indicated by stars, $^*(P < 0.05)$ and $^{**}(P < 0.01)$ (B and C).

sequence using the solid-phase synthesis, and the resulting product was termed 1-DMCa. After cleavage from the resin and deprotection, the crude non-folded 1-DMCa compound was folded/oxidized to yield the three disulfide bridges normally seen in D-MCa. A schematic representation of 1-DMCa shows what the primary structure of the compound looks like (Figure 1B). 1-DMCa was then purified to homogeneity by RP-HPLC (Figure 1C) and the proper mass of the compound checked by MALDI TOF MS (Figure 1C, inset). The detected mass ($M + H$)⁺ of 3972.95 Da does indeed correspond to the theoretical mass of folded/oxidized 1-DMCa, indicating that the platinum vector was pure and correctly assembled. Finally, we produced Pt-1-DMCa by adding a solution of K_2PtCl_4 to purified folded/oxidized 1-DMCa. The resulting conjugate was then purified again by HPLC to eliminate non-conjugated K_2PtCl_4 . The final compound is termed Pt-1-DMCa.

Pt-1-DMCa Causes Cytotoxicity in Astrocytes and in Glioma U87 Cells. To investigate the cytotoxic effect of the Pt-1-DMCa conjugate and to compare it with that of cisplatin in U87 GBM cells, MTS assays were performed after treating the cells, or not, with several concentrations of each drug for variable durations (Figure 2). As shown in Figure 2A, 1-DMCa alone had negligible cytotoxicity against this cell line, including at high concentration (60 μM). These results are in line with the reported absence of toxicity of D-MCa¹⁴ and indicate that MBL-III-7 (1) conjugation to D-MCa does not generate by itself a toxic compound. In contrast, 48 h treatments with either

Pt-1-DMCa or cisplatin induce cell cytotoxicity in the cell line in a concentration-dependent manner (Figure 2A). The cell toxicity after treatment with the novel platinum-conjugate Pt-1-DMCa (concentration from 1 to 60 μM) ranged from 10.9 to 79.6%. The average IC_{50} value of the conjugate determined from three independent experiments in U87 cells was 12.7 ± 2 μM , whereas the average IC_{50} value for cisplatin was 23.5 ± 3.4 μM . Interestingly, the Pt-1-DMCa platinum conjugate appears to possess a marked cytotoxic effect at lower concentrations that is not observed with cisplatin (below or equal to 10 μM). At higher concentrations, however, the cytotoxicity of Pt-1-DMCa was similar to that of cisplatin. In addition, we examined the cytotoxic effects of both compounds on a normal non-tumor cell line such as SVGP12. Pt-1-DMCa seems to possess a negligible cytotoxic effect on SVGP12 since it did not exceed 13.6% at concentrations below or equal to 10 μM (Figure 2B). In contrast, in the case of cisplatin, cytotoxicity starts at low concentrations and reaches greater levels (28.7%) than with Pt-1-DMCa, suggesting that the latter has a more selective effect on cancerous cells.

To further study the toxicity of both drugs on U87 cells, their effects were analyzed at the concentration of 5 μM for prolonged times (1–4 days). At this concentration Pt-1-DMCa exerted a significant effect that was not observed for cisplatin. In these conditions, up to $42 \pm 4.2\%$ of the cells were not viable in the presence of the platinum conjugate, while in the presence of cisplatin only $17 \pm 5\%$ of the cells died at 4 days (Figure 2B).

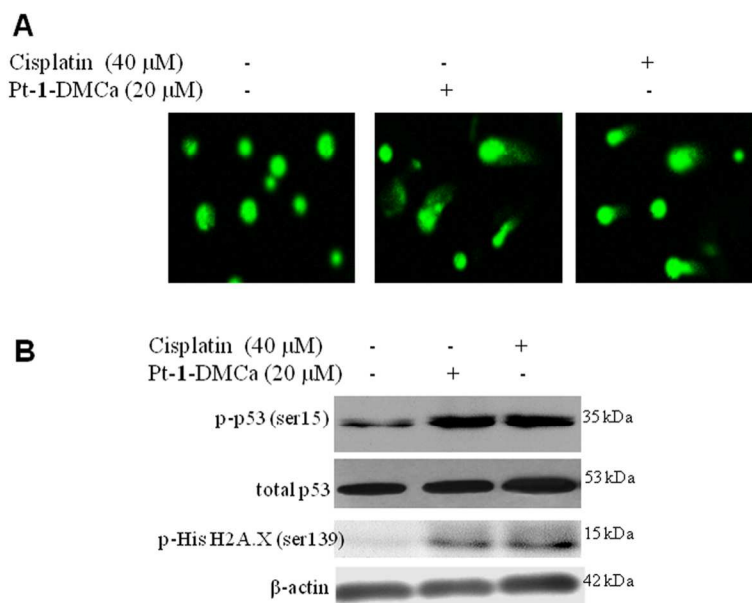


Figure 3. DNA damage induction by cisplatin and Pt-1-DMCa in U87 cells. (A) Pt-1-DMCa and cisplatin-induced DNA damage is evidenced by Comet assay as described in the [Methods](#) section. Appearance of a DNA tail reflects the DNA damages in cells. (B) Western blot analysis of the expression levels of phosphorylation of p53, histone H2A, and total p53 in U87 cells. β -Actin is used to confirm the equal protein loading in the protein extracts. Similar results were obtained from two independent experiments.

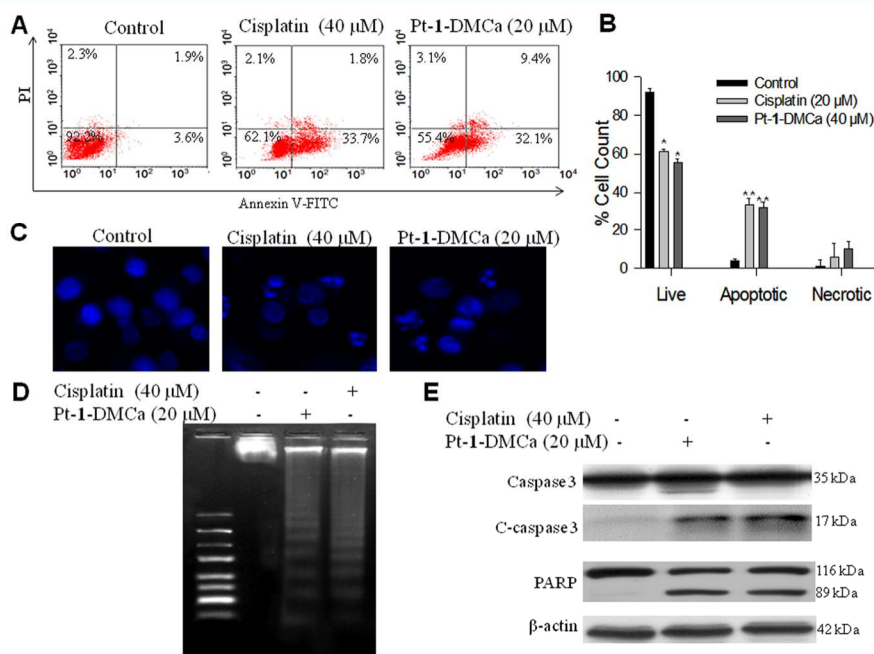


Figure 4. Apoptosis induction by cisplatin and Pt-1-DMCa in U87 cells. Cells were treated with cisplatin (40 μ M) and Pt-1-DMCa (20 μ M) for 4 h, removing the medium, and cultured again for further 48 h. (A) Cells were stained with Annexin V/PI, and then the apoptosis was determined using flow cytometry. (B) Graph showing percentage of viable, apoptotic, and necrotic cells assessed using annexinV/PI dual staining. (C) Hoechst-stained U87 cells showing morphological changes induced in nucleus. Apoptotic cells show condensed and fragmented nuclei. (D) DNA fragmentation resolved on 2% agarose gel. DNA markers of 10,000–250 bp and 700–25 bp were used to assess the laddering pattern. (E) U87 cells were treated as described before, and total proteins were extracted and detected by Western blot analysis using antibodies against C-Caspase-3 and PARP. Data are presented as mean \pm SD, and significant differences from the control are indicated by stars, * ($P < 0.05$) and ** ($P < 0.01$).

In addition, the effect of each drug was assessed after a short-term exposure (4 h) at higher concentration (20 and 40 μ M) followed by 1–4 days incubation of the cells after removal of

the drugs. Treatment with 20 μ M Pt-1-DMCa induced from 32.5 \pm 1.6% to 48 \pm 2% of cell killing between 1 and 4 days (Figure 2C). In contrast, in the same conditions, 20 μ M of

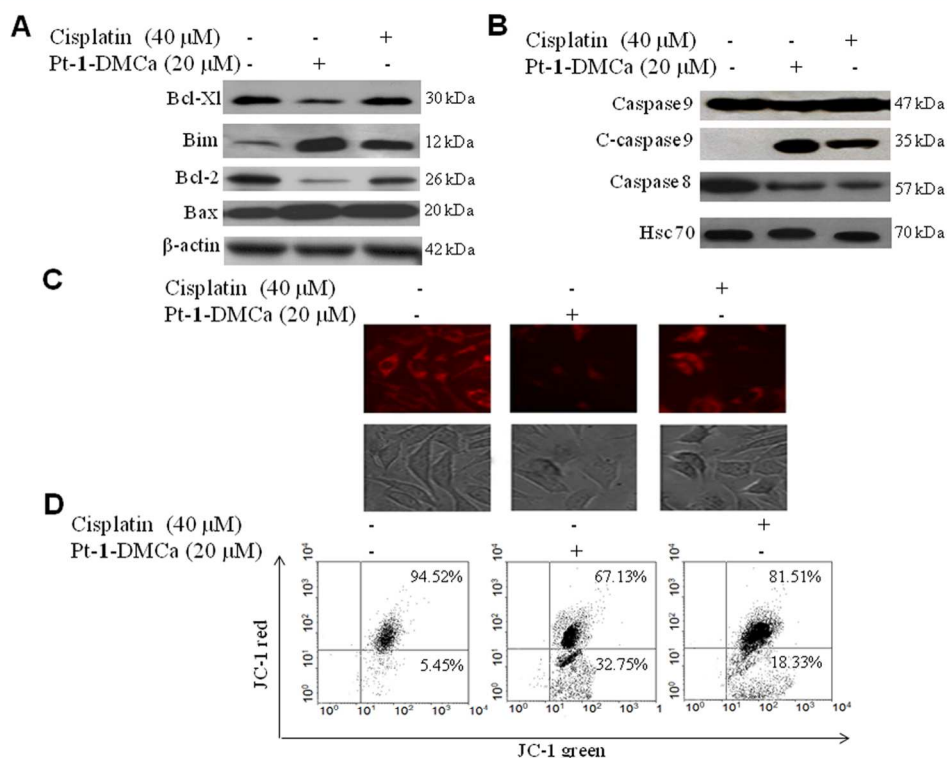


Figure 5. Pt-1-DMCa and cisplatin-induced alteration in the expression level of Bcl-2 family proteins, activation of caspases, and mitochondrial membrane depolarization. Cells were treated with cisplatin (40 μ M) and Pt-1-DMCa (20 μ M) as described before. (A) Western blot analysis of the expression levels of Bcl-xl, Bim, Bcl-2, and Bax in U87 cells. (B) Western blot analysis of the cleaved caspase-9 and -8 induced by cisplatin and Pt-1-DMCa. β -Actin and Hsc-70 are used to confirm the equal protein loading in the protein extracts. (C) Treated cells were stained with the mitochondria-selective dye TMRE and then analyzed by fluorescence microscope. (D) Treated cells were harvested and stained with the mitochondria-selective dye JC-1 and then analyzed by flow cytometry. Percentage of cells losing $\Delta\Psi_m$ and emitting green fluorescence is represented in the bottom of the right region. Similar results were obtained from two independent experiments.

cisplatin produced a low toxicity (from $10.2 \pm 1.6\%$ to $22 \pm 2\%$). However, rising the concentration of these drugs to 40 μ M led to similar effects of both compounds on cytotoxicity (from $23 \pm 2\%$ to $41 \pm 2.1\%$ for cisplatin and from $27 \pm 3.2\%$ to $45 \pm 2\%$ for Pt-1-DMCa) (Figure 2D).

Pt-1-DMCa Causes DNA Damage in U87 Cells.

Production of DNA damage is the main known mechanism by which platinum and its analogues induce cell apoptosis. In this work, we examined whether Pt-1-DMCa or cisplatin could generate DNA damage and subsequently activate proteins such as histone H2A.X and p53, involved in response to this phenomenon (Figure 3). Comet assay was chosen to assess the DNA damage induced by each compound in experimental conditions similar to those of Figure 2C,D. The chosen concentrations (20 μ M for the conjugate and 40 μ M for cisplatin) generated similar toxic effects in GBM cells. Comet tails reflecting DNA damage could be observed in cells treated with cisplatin or Pt-1-DMCa, suggesting a common action of both compounds on DNA fragmentation (Figure 3A). To further confirm the effect caused by Pt-1-DMCa and cisplatin on DNA, the expression levels of several DNA damage related signaling proteins, phospho-histone H2A.X, phospho-p53, and total p53, were assessed by Western blot. Increased phosphorylation levels of p53 and histone H2A.X were observed with 20 μ M Pt-1-DMCa and 40 μ M cisplatin (Figure 3B). Phosphorylation of these proteins is well known to occur

in response to DNA damage.²⁹ These data demonstrate that both compounds act through DNA damage.

Pt-1-DMCa Induces U87 Cell Apoptosis. We next investigated whether Pt-1-DMCa toxicity was related to the induction of apoptosis in U87 cells. First, we performed annexin V/PI staining to detect the apoptotic cell state in cells treated for 4 h with drugs then washed and cultured for 48 h in fresh medium. A significant increase of the number of apoptotic cells was observed in cells after exposure to 20 μ M Pt-1-DMCa ($32.1 \pm 3.2\%$) and 40 μ M cisplatin ($33.7 \pm 1.7\%$) (Figure 4A). A limited number of necrotic cells were observed in these experimental conditions (Figure 4B). Hoechst staining revealed the occurrence of cell shrinkage and rounding, chromatin condensation, and nuclei fragmentation after treatment with 20 μ M Pt-1-DMCa or 40 μ M cisplatin (Figure 4C). Moreover, treatments with Pt-1-DMCa and cisplatin in the same conditions resulted in inter-nucleosomal DNA fragmentation, as evidenced by the formation of a DNA ladder in agarose gel (Figure 4D). To further confirm that the platinum compounds induce U87 cell apoptosis, caspase-3 and PARP cleavage were analyzed by Western blotting. In agreement, treatment of cells by the indicated concentrations of Pt-1-DMCa and cisplatin resulted in an increased cleavage of both caspase-3 and PARP, indicating that these compounds are activated (Figure 4E).

Pt-1-DMCa Induces Apoptosis by Activating the Intrinsic Mitochondrial Pathway. Apoptosis can be triggered by two basic signaling mechanisms: the extrinsic

pathway triggered by TNF/TRAIL family factors and the intrinsic mitochondrial pathway.³⁰ In order to characterize the molecular events initiated by the platinum analogue and cisplatin, the impact of these compounds on the expression levels of pro-survival (Bcl-Xl and Bcl-2) and pro-apoptotic (Bax and Bim) proteins were investigated in U87 cells by Western blotting. Again, the 4 h treatment followed by 48 h growth in normal conditions was adopted. Obvious decreases of Bcl-XL and Bcl-2 expression were observed in cells treated with Pt-1-DMCa, while only Bcl-2 expression decreased with cisplatin treatment. In addition, the inhibition of Bcl-2 expression was more accentuated with Pt-1-DMCa ($65 \pm 7.5\%$) than with cisplatin treatment ($32.6 \pm 5.5\%$). Concerning the pro-apoptotic proteins, an important up-regulation of Bim level was observed in cells treated with $20 \mu\text{M}$ Pt-1-DMCa and to a lesser extent with $40 \mu\text{M}$ cisplatin (Figure 5A). To investigate whether the drug-induced apoptosis involves initiating caspases, we examined the proteolytic activation of caspase-8 and -9. The results reveal that caspase-9 was cleaved and activated by $20 \mu\text{M}$ Pt-1-DMCa or $40 \mu\text{M}$ cisplatin. In the case of caspase-8 both drugs triggered a decreased level of the native form of this protein indicating a degradation and activation of this protease (Figure 5B). These variations in expression of these different apoptotic proteins are consistent with an activation of the intrinsic mitochondrial pathway. Loss of mitochondrial membrane potential ($\Delta\Psi\text{m}$) is a crucial event in the apoptotic process. It gives rise to the release of different apoptogenic factors from mitochondria into the cytoplasm.³¹ Thus, we investigated the change of $\Delta\Psi\text{m}$ in U87 cells by both TMRE staining assay (Figure 5C) and JC-1 flow cytometry analysis (Figure 5D). The results showed that $20 \mu\text{M}$ Pt-1-DMCa or $40 \mu\text{M}$ cisplatin induced a loss of mitochondrial membrane potential. In the TMRE assay, the signal observed by fluorescence microscopy was strongly attenuated in Pt-1-DMCa-treated cells and to a lesser extent in cisplatin treatment. When analyzed by JC-1 flow cytometry, a greater effect of Pt-1-DMCa ($27.5\text{--}32.8\%$) was observed on the loss of mitochondrial potential than with cisplatin ($16.9\text{--}18.3\%$).

Pt-1-DMCa Induces Apoptosis by Activating the Extrinsic TNF/TRAIL Pathway. The cell surface expressions of the TRAIL receptors DR4 and DR5 were analyzed in U87 cells by flow cytometry and fluorescence immunocytochemistry. Increased expressions of these receptors is a crucial event upstream the extrinsic TNF/TRAIL pathway. Expressions of DR4 and DR5 were observed at low levels in the control GBM cells (Figure 6A,B). Furthermore, Pt-1-DMCa, but not cisplatin, triggered a higher expression of both receptors at the cell membrane as well as their redistribution into membrane patches as suggested by fluorescence microscopy (Figure 6A) and flow cytometry data (Figure 6B). These data are consistent with an involvement of the TNF/TRAIL pathway in the effect of Pt-1-DMCa-mediated cell apoptosis but not of the cisplatin-induced apoptosis.

Pt-1-DMCa Increases ROS Generation in U87 Cells. ROS accumulation is considered to be a pivotal phenomenon related to the apoptotic mechanisms induced by DNA damage.^{29,32} The generation of ROS was evaluated using the DHR123 fluorescent probe which is rapidly absorbed by cells and converted to Rh123 in the presence of ROS. Cells exposed to $20 \mu\text{M}$ Pt-1-DMCa exhibited increased fluorescence intensity in flow cytometry experiment (Figure 7A) indicating an intracellular ROS production in the U87 cells. This response was not observed in cells treated with $40 \mu\text{M}$ cisplatin. These

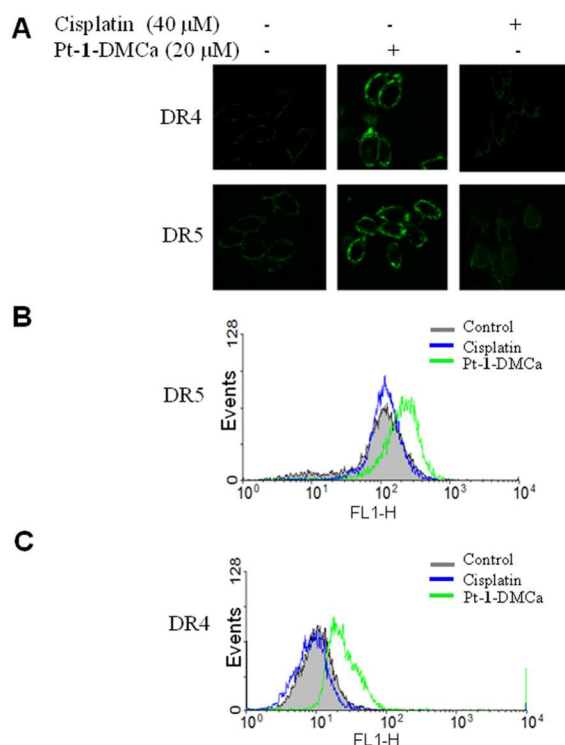


Figure 6. Contribution of TRAIL receptors to apoptotic signaling. (A) Immunostaining analyzed by fluorescence microscopy of DR4 and DR5 in U87 cells exposed to vehicle (control), cisplatin ($40 \mu\text{M}$), or Pt-1-DMCa ($20 \mu\text{M}$) as described in the Methods section. Cell surface expression of TRAIL receptors DR4 and DR5 in U87 cells was analyzed by flow cytometry. Cells were incubated with anti-DR4 (B) or anti-DR5 (C) or with mouse IgG1 followed by Alexa-488 goat anti-mouse IgG.

results were consistent with those observed by fluorescence microscopy (Figure 7B). To confirm whether ROS generation is a necessary event in the induction of apoptosis by the new platinum conjugate, several ROS scavengers, GSH, NAC, and Trolox, were tested for cell cytotoxicity. The results reveal that scavenging of ROS strongly reversed the effects of the conjugate on cell viability (Figure 7C). The effect of the ROS scavenger NAC on the expression of the activated p-53 and histone H2A.X proteins was assessed by Western blotting. The data indicate that the NAC completely reversed the effect of $20 \mu\text{M}$ of the conjugate on the phosphorylation of both proteins showing the involvement of ROS production in this response (Figure 7D).

Pt-1-DMCa Induces Apoptosis by Inhibiting AKT Phosphorylation. Numerous protein kinases are key regulators of cell proliferation and survival processes. One of them, AKT, is linked to the status of p53 pathways in different cell types.³³ Inhibition of Akt signaling could contribute to the regulation of Mdm2, producing an enhancement of p53 expression.³⁴ Since the activation of the p53 pathway by our platinum conjugate could possibly be related to the involvement of AKT in cell apoptosis, we analyzed the effect of platinum conjugate and cisplatin on Ser⁴⁷³ AKT phosphorylation level during different periods of time ranging from 0 to 24 h. Remarkably, diminution of phospho-AKT (Figure 8A,C) level as well as of the ratio phospho-AKT/AKT (Figure 8B,D)

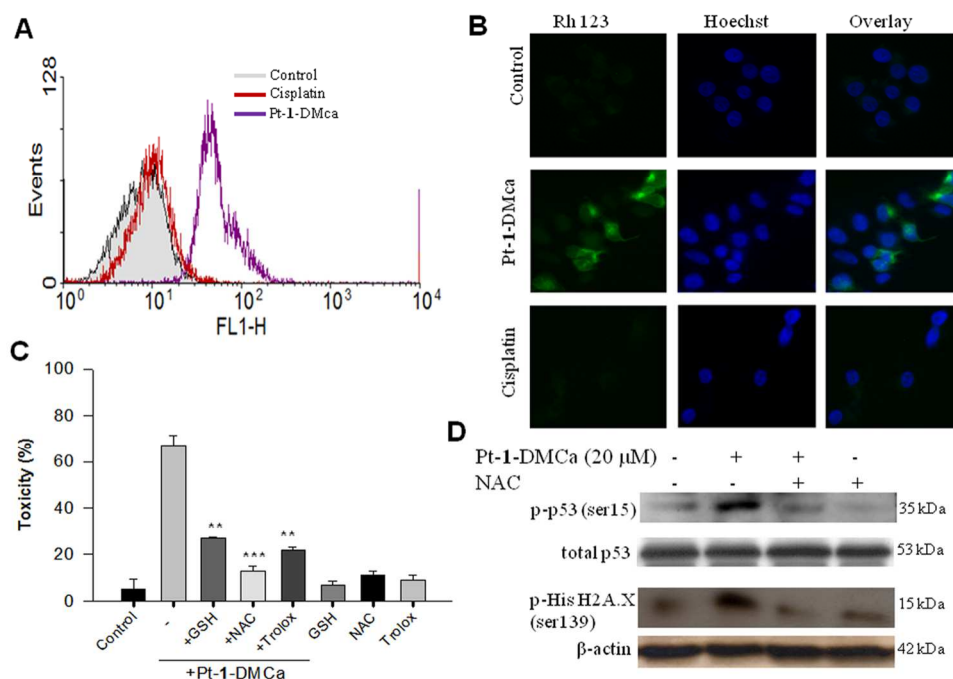


Figure 7. Roles of ROS in apoptosis induced by cisplatin and Pt-1-DMCa. (A,B) U87 cells were treated with cisplatin ($40 \mu\text{M}$) or Pt-1-DMCa ($20 \mu\text{M}$) as described in the Methods section, and ROS generation was measured by flow cytometry or by fluorescence microscopy using DHR123. (C) U87 cells were pretreated with 5 mM NAC/GSH/Trolox for 3 h and further treated with Pt-1-DMCa ($20 \mu\text{M}$) and cisplatin ($40 \mu\text{M}$) before performing the MTS assay. (D) Cell lysates were subjected to Western blot analysis. Protein expression levels of phosphorylated histone H2A.X, phosphorylated p53, and total p53 were determined. Equal protein loading was confirmed by analysis of β -actin in the protein extracts.

starting from 2 h treatment was observed in cells exposed to $20 \mu\text{M}$ Pt-1-DMCa but not to $40 \mu\text{M}$ cisplatin. In contrast, no significant changes of total AKT protein were detected in response to both drugs. These results indicate that the efficient inhibition of AKT phosphorylation by our novel platinum-analogue, which was not found with cisplatin, could also result in strengthened anti-cancer effects. To confirm the importance of the inhibition of phospho-AKT, the effect of LY294002, an inhibitor of PI3-kinase which is an upstream regulator of phospho-AKT, was first checked to assess the consequences of inhibition of phospho-AKT on cell viability in the same experimental conditions reported in Figure 2C,D. The results showed that $20 \mu\text{M}$ LY294002 alone or in combination with $20 \mu\text{M}$ Pt-1-DMCa led to a significant cytotoxicity (Figure 8E). Also, the Western blotting assay indicates that the inhibitor significantly reduces the phospho-AKT level in cells treated by $20 \mu\text{M}$ Pt-1-DMCa and enhances this inhibition effect in cells treated by $40 \mu\text{M}$ cisplatin after 24 h (Figure 8F). In this case, cisplatin acts similarly to the Pt-1-DMCa. Taken together, these results indicate that inhibition of phosphorylation of AKT contributes to the apoptosis induced by Pt-1-DMCa but not by cisplatin.

Pt-1-DMCa Induces Apoptosis by Inhibiting ERK Phosphorylation. Activation of the MAPK pathways is commonly recognized to be associated with the resistance to cisplatin in many cancer cells, such as ERK.³⁵ ERK phosphorylation can interfere with apoptosis at several levels. It can prevent the activation of caspases and induce the expression of anti-apoptotic factors such as Mcl-1 and Bcl-2. In this study, experiments were conducted to assess the effects of Pt-1-DMCa on the MAPK pathway in GBM cells. Decreased levels of phosphorylated ERK and decreased phospho-ERK/

ERK ratio were detected in cells treated with $20 \mu\text{M}$ Pt-1-DMCa (Figure 8A,B) but not in cells exposed to $40 \mu\text{M}$ cisplatin (Figure 8C,D) for different periods of time ranging from 0 to 24 h. In all conditions tested, total ERK protein remained globally stable. The phosphorylation level started to decrease after 2 h and was strongly inhibited after 24 h. Phospho-ERK inhibition may represent an early event in the apoptosis process as for the inhibition of phospho-AKT. The specific effect of the conjugate on inhibition of ERK phosphorylation represents another functional advantage of Pt-1-DMCa as a potential anti-cancer effect. To analyze the importance of inhibition of ERK phosphorylation on U87 cells apoptosis, U0126, an inhibitor of MEK, the upstream kinase of phospho-ERK, was tested in the same experimental condition than in Figure 1C,D. Alone or combined with $20 \mu\text{M}$ Pt-1-DMCa or $40 \mu\text{M}$ cisplatin, an important cytotoxicity was observed with all these treatments (Figure 8E). Furthermore, the Western blotting assay showed that U0126 significantly inhibits phospho-ERK level in cells treated by $20 \mu\text{M}$ Pt-1-DMCa and enhances this inhibition effect in cells treated by $40 \mu\text{M}$ cisplatin after 24 h (Figure 8F). In this case, cisplatin acts similarly to Pt-1-DMCa. These results indicate that inhibition of ERK phosphorylation plays an important role in the apoptosis induced by Pt-1-DMCa but not by cisplatin.

DISCUSSION

MCa is an additional member of the exponentially growing list of reported CPPs. It is, however, one of the rare CPPs that (i) is fully natural and (ii) presents a well-defined three-dimensional structure, and (iii) whose cell penetration can be straightforwardly assessed by intracellular Ca^{2+} release. Since the initial demonstration that MCa can serve as a vector for the

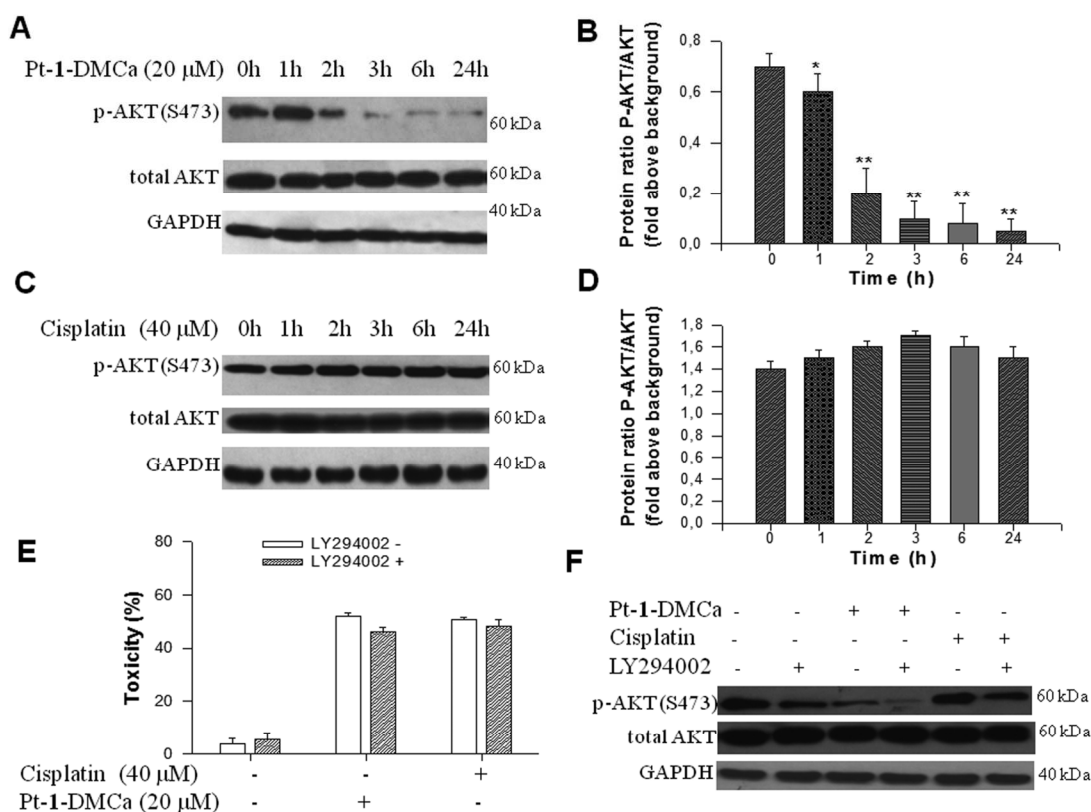


Figure 8. Pt-1-DMCa induces apoptosis with the involvement of AKT signaling pathway. (A,C) Time-dependent effects of Pt-1-DMCa or cisplatin on the phosphorylation and expression level of AKT. Cells were treated with or without Pt-1-DMCa (20 μ M) and cisplatin (40 μ M) for 1–24 h, respectively. (B,D) Comparison of total AKT and phospho-AKT levels on treated cells. Quantification of the western band intensity was performed using the Image G software. (E,F) Effect of LY294002 (PI3K inhibitor) on growth inhibition induced by cisplatin and Pt-1-DMCa. Cells were pretreated with 20 μ M LY294002 for 1 h and then cultured for another 4 h with Pt-1-DMCa or cisplatin, and then the medium was removed and replaced by a fresh one for 48 h incubation. Cell viability was assessed by the MTS assay, and the cell lysates were subjected to Western blot analysis. Equal protein loading was confirmed by analysis of GAPDH in the protein extracts. All data are expressed as means \pm SD of duplicates. Bars with different characters are statistically different at $P < 0.05$.

intracellular delivery of fluorescent streptavidin,^{12,13} accumulating data have highlighted the biotechnological value of this CPP, including for the cell delivery of nanoparticles. Besides being an exceptionally useful CPP for the delivery of cargoes, MCa can also be used as a potent retention agent in cells.^{14,24,36} This principle was used in the case of the covalent coupling to doxorubicin, an anti-tumor agent, allowing bypassing the chemo-resistance of breast cancer cells.^{37,38} Several new MCa analogues were then designed in order to bypass the native pharmacological activity of MCa that all retained excellent cell-penetrating properties.³⁷ It is in this spirit that the D-MCa analogue was designed with the added advantage of conferring protease resistance to the compound.²³ Therefore, a platinum conjugate of a chimera molecule 1-DMCa was herein synthesized, and its efficacy was evaluated in glioblastoma cells. The aim of this work was obviously to use the proven cell retention properties of D-MCa to improve the toxicity of the delivered platinum. Cytotoxicity of Pt-1-DMCa was compared to the reference compound cisplatin in human U87 cells, one of the most widely used cell line for glioblastoma studies. It is also known for its high resistance toward cisplatin therapeutic treatment³⁹ making this investigation particularly relevant.

Our data demonstrated that Pt-1-DMCa alters the sensitivity of U87 cell to platinum treatment while minimally affecting non

tumor cells as compared to cisplatin, indicating that it may eventually possess a better therapeutic index. We found that the cytotoxicity of the Pt-1-DMCa conjugate in U87 GBM cells was detectable after treatment of U87 cells at low concentrations from 5 to 10 μ M for which cisplatin had negligible effects. Furthermore, long-term 5 μ M drug treatment for 1–4 days of these cells confirms that the conjugate confers greater cytotoxic effects than cisplatin. These observations suggest that long exposures at relatively low Pt-1-DMCa concentration may represent a viable strategy for inducing GBM cell death. The reason for this difference of efficacy at low concentrations is not established but we can tentatively assume that the ability of MCa analogues to accumulate in cells against the concentration gradient combined to the cell retention properties of this vector may significantly contribute to the process.^{36,40}

To study the efficacy of platinum accumulation after short-term exposure to the drugs, U87 cells were treated for 4 h with 20 μ M Pt-1-DMCa or 40 μ M cisplatin, then washed and cultured again for 1–4 days. In these conditions, 20 μ M Pt-1-DMCa demonstrated greater cytotoxic effect than cisplatin administered at the same concentration. However, this difference was no longer significant at 40 μ M cisplatin. These data suggest that this strategy of conjugation of platinum with

1-DMCa is advantageous since it could enhance platinum delivery and retention in this GBM cell line. Possible reasons for the enhanced efficacy of Pt-1-DMCa could be attributed to (i) the enhanced uptake and accumulation of platinum due to the CPP properties of DMCA, leading to a more efficient and long lasting cytotoxicity, (ii) specific interactions of the platinum conjugate with the plasma membrane components, and (iii) specific modulation by Pt-1-DMCa of signaling pathways involved in cell death. Consequently, we have chosen the concentrations of 20 μM Pt-1-DMCa and 40 μM cisplatin that presents comparable cytotoxicity to assess the effects of the two drugs in terms of the mechanisms related to DNA damage and apoptosis induction.

Comet assay indicates that both drugs produce DNA damage and fragmentation, p53 and histone H2A.X phosphorylation, suggesting that the novel platinum conjugate retains the crucial role of platinum on DNA breakage. Cisplatin is a strong, widely used anti-cancer therapeutic drug that causes DNA damage and programmed cell death and acts in a p53-dependent pathway.^{41,42} It is well-known that DNA fragmentation results in p53 activation and subsequent induction of apoptosis, resulting in the activation of caspases through the implication of the mitochondrial (intrinsic) pathway and the death receptor TNF/TRAIL (extrinsic) cascade.⁴³ The first pathway implicates an alteration of mitochondrial membrane permeability transition and subsequent release of cytochrome *c* from mitochondria to the cytoplasm resulting in caspase-9 cleavage and downstream caspases activation.⁴⁴ One of them, caspase-3, mediates PARP cleavage and DNA fragmentation, leading to cell death.^{30,35} The second pathway involves activation of death receptors such as Fas or TRAIL-R's DR4 and DR5. This results in the formation of a death-signaling complex (DISC) with recruitment of the Fas-associated death domain (FADD) adaptors and activation of procaspase-8, leading to cleavage of procaspase-3 without implication of the mitochondria. The activation of both signaling pathways promotes synergistic apoptotic effects. The present study demonstrates that Pt-1-DMCa or cisplatin induced comparable apoptotic effects as well in the generation of apoptotic cells as for the induction of DNA fragmentation or the activation of caspases-3, -8, and -9.

To investigate further the molecular mechanisms triggered by Pt-1-DMCa or cisplatin, the expression levels of anti-apoptotic (Bcl-XL and Bcl-2) and pro-apoptotic (Bax and Bim) proteins were studied in U87 cells. Clinical data revealed that members of the anti-apoptotic Bcl-2 family are associated with cisplatin resistance and tumor reappearance.^{45,46} Ongoing research trials support a rationale for targeting platinum-resistant tumors with Bcl-2 family antagonists.^{21,45} In our experiments Pt-1-DMCa induced a sustained decrease of the expression of the Bcl-2 and Bcl-XL expression and an increase of Bax and Bim expression. Thus, the platinum conjugate displays pro-apoptotic effects in cells in which survival pathways are exacerbated.

In addition to its effect on the intrinsic pathway, our data from this study demonstrate that Pt-1-DMCa promotes stronger responses than cisplatin on the extrinsic pathway by greatly increasing DR4 and DR5 death receptors' expression levels. Therefore, the novel platinum conjugate induces, in addition to the intrinsic apoptotic pathway, a specific effect on the TNF/TRAIL associated mechanism.

It is well documented that ROS generation by several anti-cancer drugs can cause DNA damage, p53 activation, and apoptosis.⁴⁵ Interestingly, ROS have been shown to induce p53

activation, presumably by causing oxidative DNA damage.^{47,48} Since Pt-1-DMCa or cisplatin was able to potentially induce p53 activation, it may be assumed that this effect occurs through an increase of ROS production, subsequently leading to p53 activation and apoptosis in GBM cells. Here again, a specific effect of Pt-1-DMCa on ROS accumulation was observed in our experiments. These data argue for a possible involvement of ROS as upstream molecular components in the apoptotic effect of Pt-1-DMCa in U87 GBM cells.

Different protein kinase pathways coordinate cell proliferation and survival. Among them, AKT and MAPK are main signaling molecules correlated with the activation of the p53 pathways in different cells and tissue types.⁴⁹ Simultaneously, a family of serine-threonine protein kinases, MAPKs, play significant roles in relation to the p53 pathway in different cancer cells.³⁹ Generally, kinases of the MAPK family, including c-JUN N-terminal kinase/stress-activated protein kinases (JNK/SAPKs), ERK, and p38 kinase, are triggered by oxidative stress, UV irradiation, or osmotic shock and are usually involved in the induction of apoptosis.³⁵ ERKs also play key roles in cell growth and survival and are generally overexpressed in many cancer cell types.⁴⁹ The PI3K/Akt signaling pathway is also activated or overexpressed in human ovarian cancer and is a determinant in chemo-resistance to cisplatin.⁵¹ Different studies have demonstrated that the anti-cancer effect of other anti-cancer drugs like trastuzumab, tamoxifen, doxorubicin, and paclitaxel involved an inhibition of the MAPK and PI3K/AKT resulting in a p53-mediated apoptosis.^{52,53} In our study, Pt-1-DMCa, but not cisplatin, decreased AKT and ERK phosphorylation in U87 GBM cells. Introduction of the AKT inhibitor LY294002 and the ERK inhibitor U0126 significantly enhanced AKT and ERK phosphorylation in the case of Pt-1-DMCa but not cisplatin. In addition, these effects were observed in cells treated by cisplatin only in the presence of one inhibitor or the other, which is another argument in favor of the specific effects of the Pt-1-DMCa in these two signaling pathways. These results are consistent with reports describing that many stimuli induce apoptosis in human GBM cells through ROS-mediated inhibition of PI3K/AKT/ERK signaling pathways.^{32,54,55} Moreover, the state of the cellular redox system is reportedly linked to the activities of the PI3/AKT and MAPK pathways, and to their associated downstream effectors.^{57,58} The Pt-1-DMCa that specifically inhibits the AKT and/or MAPK pathways displays another real advantage compared to cisplatin as a potential anti-cancer drug.

In conclusion, in the present study, the Pt-1-DMCa conjugate presents a few properties that distinguish it from cisplatin in U87 GBM cells in the experimental conditions used: (i) it shows cytotoxic effects at lower doses than those needed for cisplatin, (ii) it activates the extrinsic apoptosis pathway and implicates the production of ROS which should facilitate DNA damage in addition to the effects of platinum, and (iii) it inhibits the activity of ERK and AKT cascades. These additional properties, not observed with cisplatin, indicate that the conjugate displays interesting anti-cancer properties, including for cisplatin-resistant cancer cells. In future prospects, it will be of interest to investigate the effects of Pt-1-DMCa on the enzymes implicated in ROS production in GBM cells, such as iNOS. Moreover, ROS inhibitors may be used to assess the involvement of oxidative metabolism on the AKT and ERK pathways. AKT and ERK pathway inhibitors would allow demonstrating the link between inhibition of these cascades and p53 inhibition.

AUTHOR INFORMATION

Corresponding Author

*E-mail: sonia_aroui2002@yahoo.fr.

Notes

The authors declare no competing financial interest.

ACKNOWLEDGMENTS

The present work was supported by grants from DGRST (Appui 467 à la Recherche Universitaire de base, ARUB, UR 12ES08) Tunisia. M.D.W. acknowledges financial support of the Agence Nationale de La Recherche (grant number ANR-11-LABX-0015). The authors are grateful to Dr. Jacqueline Bréard (INSERM U749, Faculté de Pharmacie, 5 rue J.B. Clément, 92290 Châtenay-Malabry, France) for kindly providing anti-ERK, anti-Bcl-2, and anti-Bcl-XL antibodies.

REFERENCES

- Alvarez-Lorenzo, C.; Concheiro, A. Smart drug delivery systems: from fundamentals to the clinic. *Chem. Commun.* **2014**, *50* (58), 7743–7765.
- Kleiner, L. W.; Wright, J. C.; Wang, Y. Evolution of implantable and insertable drug delivery systems. *J. Controlled Release* **2014**, *181*, 1–10.
- Thanki, K.; Gangwal, R. P.; Sangamwar, A. T.; Jain, S. Oral delivery of anticancer drugs: challenges and opportunities. *J. Controlled Release* **2013**, *170* (1), 15–40.
- Foged, C.; Nielsen, H. M. Cell-penetrating peptides for drug delivery across membrane barriers. *Expert Opin. Drug Delivery* **2008**, *5* (1), 105–117.
- Gasparini, G.; Bang, E. K.; Molinard, G.; Tulumello, D. V.; Ward, S.; Kelley, S. O.; Roux, A.; Sakai, N.; Matile, S. Cellular uptake of substrate-initiated cell-penetrating poly(disulfide)s. *J. Am. Chem. Soc.* **2014**, *136* (16), 6069–6074.
- Bechara, C.; Sagan, S. Cell-penetrating peptides: 20 years later, where do we stand? *FEBS Lett.* **2013**, *587* (12), 1693–1702.
- Zhang, X. X.; Eden, H. S.; Chen, X. Peptides in cancer nanomedicine: drug carriers, targeting ligands and protease substrates. *J. Controlled Release* **2012**, *159* (1), 2–13.
- Fajloun, Z.; Kharrat, R.; Chen, L.; Lecomte, C.; Di Luccio, E.; Bichet, D.; El Ayeb, M.; Rochat, H.; Allen, P. D.; Pessah, I. N.; De Waard, M.; Sabatier, J. M. Chemical synthesis and characterization of maurocalcine, a scorpion toxin that activates Ca₂⁺ release channel/ryanodine receptors. *FEBS Lett.* **2000**, *469* (2–3), 179–185.
- Mabrouk, K.; Ram, N.; Boisseau, S.; Strappazzon, F.; Rehim, A.; Sadoul, R.; Darbon, H.; Ronjat, M.; De Waard, M. Critical amino acid residues of maurocalcine involved in pharmacology, lipid interaction and cell penetration. *Biochim. Biophys. Acta, Biomembr.* **2007**, *1768* (10), 2528–2540.
- Ram, N.; Aroui, S.; Jaumain, E.; Bichraoui, H.; Mabrouk, K.; Ronjat, M.; Lortat-Jacob, H.; De Waard, M. Direct peptide interaction with surface glycosaminoglycans contributes to the cell penetration of maurocalcine. *J. Biol. Chem.* **2008**, *283* (35), 24274–24284.
- Aroui, S.; Ram, N.; Appaix, F.; Ronjat, M.; Kenani, A.; Pirollet, F.; De Waard, M. Maurocalcine as a non toxic drug carrier over comes doxorubicin resistance in the cancer cell line MDA-MB 231. *Pharm. Res.* **2009**, *26* (4), 836–45.
- Mabrouk, K.; Ram, N.; Boisseau, S.; Strappazzon, F.; Rehim, A.; Sadoul, R.; Darbon, H.; Ronjat, M.; De Waard, M. Critical amino acid residues of maurocalcine involved in pharmacology, lipid interaction and cell penetration. *Biochim. Biophys. Acta, Biomembr.* **2007**, *1768* (10), 2528–2540.
- Ram, N.; Aroui, S.; Jaumain, E.; Bichraoui, H.; Mabrouk, K.; Ronjat, M.; Lortat-Jacob, H.; De Waard, M. Direct peptide interaction with surface glycosaminoglycans contributes to the cell penetration of maurocalcine. *J. Biol. Chem.* **2008**, *283* (35), 24274–24284.
- Poillot, C.; Dridi, K.; Bichraoui, H.; Pecher, J.; Alphonse, S.; Douzi, B.; Ronjat, M.; Darbon, H.; De Waard, M. D-Maurocalcine, a Pharmacologically Inert Efficient Cell-penetrating Peptide Analogue. *J. Biol. Chem.* **2010**, *285* (44), 34168–34180.
- Stephens, I. E. L.; Bondarenko, A. S.; Gronbjerg, U.; Rossmeis, J.; Chorkendorff, I. Understanding the electrocatalysis of oxygen reduction on platinum and its alloys. *Energy Environ. Sci.* **2012**, *5* (18), 6744–6762.
- Kostova, I. Platinum complexes as anticancer agents. *Recent Pat. Anti-Cancer Drug Discovery* **2006**, *1* (1), 1–22.
- Klein, A. V.; Hambley, T. W. Platinum drug distribution in cancer cells and tumors. *Chem. Rev.* **2009**, *109* (10), 4911–4920.
- Boulikas, T.; Vougiouka, M. Cisplatin and platinum drugs at the molecular level (Review). *Oncol. Rep.* **2003**, *10* (6), 1663–1682.
- Galluzzi, L.; Senovilla, L.; Vitale, I.; Michels, J.; Martins, I.; Kepp, O.; Castedo, M.; Kroemer, G. Molecular mechanisms of cisplatin resistance. *Oncogene* **2012**, *31* (15), 1869–1883.
- Sprauten, M.; Darrah, T. H.; Peterson, D. R.; Campbell, M. E.; Hannigan, R. E.; Cvanarova, M.; Beard, C.; Haugnes, H. S.; Fossa, S. D.; Oldenburg, J.; Travis, L. B. Impact of long-term serum platinum concentrations on neuro- and ototoxicity in cisplatin-treated survivors of testicular cancer. *J. Clin. Oncol.* **2012**, *30* (3), 300–307.
- Siddik, Z. H. Cisplatin: mode of cytotoxic action and molecular basis of resistance. *Oncogene* **2003**, *22* (47), 7265–7279.
- Bleeker, F. E.; Molenaar, R. J.; Leenstra, S. Recent advances in the molecular understanding of glioblastoma. *J. Neuro-Oncol.* **2012**, *108* (1), 11–27.
- Poillot, C.; Dridi, K.; Bichraoui, H.; Pecher, J.; Alphonse, S.; Douzi, B.; Ronjat, M.; Darbon, H.; De Waard, M. D-Maurocalcine, a Pharmacologically Inert Efficient Cell-penetrating Peptide Analogue. *J. Biol. Chem.* **2010**, *285* (44), 34168–34180.
- Poillot, C.; Bichraoui, H.; Tisseyre, C.; Bahemberae, E.; Andreotti, N.; Sabatier, N. J.; Ronjat, M.; De Waard, M. Small efficient cell-penetrating peptides derived from scorpion toxin maurocalcine. *J. Biol. Chem.* **2012**, *287* (21), 17331–17342.
- Damian, M. S.; Hedman, H. K.; Elmroth, S. K. C.; Diederichsen, U. Synthesis and DNA interaction of platinum complex/peptide chimera as potential drug candidates. *Eur. J. Org. Chem.* **2010**, *2010* (32), 6161–6170.
- Cochaud, S.; Meunier, A. C.; Monvoisin, A.; Bensalma, S.; Muller, J. M.; Chadéneau, C. Neuropeptides of the VIP family inhibit glioblastoma cell invasion. *J. Neuro-Oncol.* **2015**, *122* (1), 63–73.
- Troiano, L.; Ferraresi, R.; Lugli, E.; Nemes, E.; Roat, E.; Nasi, M.; Pinti, M.; Cossarizza, A. Multi parametric analysis of cells with different mitochondrial membrane potential during apoptosis by polychromatic flow cytometry. *Nat. Protoc.* **2007**, *2* (11), 2719–2727.
- Du, S.; Bouquet, S.; Lo, C. H.; Pellicciotta, I.; Bolourchi, S.; Parry, R.; Barcellos-Hoff, M. H. Attenuation of the DNA Damage Response by Transforming Growth Factor-Beta Inhibitors Enhances Radiation Sensitivity of Non-small Cell Lung Cancer Cells In Vitro and In Vivo. *Radiation Oncology International Journal of biology physics.* *Int. J. Radiat. Oncol., Biol., Phys.* **2015**, *91* (1), 91–99.
- Zhang, Y.; Zheng, S.; Zheng, J.-S.; Wong, K.-H.; Huang, Z.; Ngai, S.-M.; Zheng, W.; Wong, Y.-S.; Chen, T. Synergistic Induction of Apoptosis by Methylseleninic Acid and Cisplatin, The Role of ROS-ERK/AKT-p53 Pathway. *Mol. Pharmaceutics* **2014**, *11* (4), 1282–1293.
- Milane, L.; Trivedi, M.; Singh, A.; Talekar, M.; Amiji, M. Mitochondrial biology, targets, and drug delivery. *J. Controlled Release* **2015**, *207*, 40–58.
- Rayman, M. P. Selenium in cancer prevention: a review of the evidence and mechanism of action. *Proc. Nutr. Soc.* **2005**, *64* (4), S27–S42.
- Zhang, L.; Wang, H.; Xu, J.; Zhu, J.; Ding, K. Inhibition of cathepsin S induces autophagy and apoptosis in human glioblastoma cell lines through ROS-mediated PI3K/AKT/mTOR/p70S6K and JNK signaling pathways. *Toxicol. Lett.* **2014**, *228* (3), 248–259.
- Astle, M. V.; Hannan, K. M.; Ng, P. Y.; Lee, R. S.; George, A. J.; Hsu, A. K.; Haupt, Y.; Hannan, R. D.; Pearson, R. B. AKT induces senescence in human cells via mTORC1 and p53 in the absence of

DNA damage: implications for targeting mTOR during malignancy. *Oncogene* **2012**, *31* (15), 1949–1962.

(34) Jiang, P.; Du, W.; Mancuso, A.; Wellen, K. E.; Yang, X. Reciprocal regulation of p53 and malic enzymes modulates metabolism and senescence. *Nature* **2013**, *493* (7434), 689–693.

(35) Boldt, S.; Weidle, U. H.; Kolch, W. The role of MAPK pathways in the action of chemotherapeutic drugs. *Carcinogenesis* **2002**, *23* (11), 1831–1838.

(36) Tisseyre, C.; Ahmadi, M.; Bacot, S.; Dardevet, L.; Perret, P.; Ronjat, M.; Fagret, D.; Usson, Y.; Ghezzi, C.; De Waard, M. Quantitative evaluation of the cell penetrating properties of an iodinated Tyr-L-maurocalcine analog. *Biochim. Biophys. Acta, Mol. Cell Res.* **2014**, *1843* (10), 2356–2364.

(37) Poillot, C.; De Waard, M. Potential of cell penetrating peptides for cell drug delivery. *Med. Sci.* **2011**, *27* (5), S27–S34.

(38) Aroui, S.; Brahim, S.; Hamelin, J.; De Waard, M.; Bréard, J.; Kenani, A. Conjugation of doxorubicin to cell penetrating peptides sensitizes human breast MDA-MB 231 cancer cells to endogenous TRAIL-induced apoptosis. *Apoptosis* **2009**, *14* (11), 1352–1365.

(39) Eisele, G.; Weller, M. Targeting apoptosis pathways in glioblastoma. *Cancer Lett.* **2013**, *332* (2), 335–345.

(40) Ahmadi, M.; Bacot, S.; Poillot, C.; Desruet, M.-D.; Perret, P.; Riou, L.; Cestele, S.; Couvet, M.; Bourgoin, S.; Seve, M.; De Waard, M.; Ghezzi, C. Selective mono-radioiodination and characterization of a cell-penetrating peptide: L-Tyr-Maurocalcine. *Radiochim. Acta* **2014**, *102* (11), 1047–1057.

(41) Tomasini, R.; Seux, M.; Nowak, J.; Bontemps, C.; Carrier, A.; Dagorn, J. C.; et al. P53INP1 is a novel p73 target gene that induces cell cycle arrest and cell death by modulating p73 transcriptional activity. *Oncogene* **2005**, *24* (55), 8093–8104.

(42) Gong, J. G.; Costanzo, A.; Yang, H. Q.; Melino, G.; Kaelin, W. G.; Jr; Levrero, M.; et al. The tyrosine kinase c-Abl regulates p73 in apoptotic response to cisplatin-induced DNA damage. *Nature* **1999**, *399* (2), 806–809.

(43) Whibley, C.; Pharoah, P. D.; Hollstein, M. p53 polymorphisms: cancer implications. *Nat. Rev. Cancer* **2009**, *9* (2), 95–107.

(44) Li, M. X.; Dewson, G. Mitochondria and apoptosis: emerging concepts. *F1000Prime Rep.* **2015**, *1* (7), 42.

(45) Crawford, N.; Chacko, A. D.; Savage, K. I.; McCoy, F.; Redmond, K.; Longley, D. B.; Fennell, D. A. Longley. Platinum resistant cancer cells conserve sensitivity to BH3 domains and obatoclax induced mitochondrial apoptosis. *Apoptosis* **2011**, *16* (3), 311–320.

(46) Michaud, W. A.; Nichols, A. C.; Mroz, E. A.; Faquin, W. C.; Clark, J. R.; Begum, S.; Westra, W. H.; Wada, H.; Busse, P. M.; Ellisen, L. W.; Rocco, J. W. Bcl-2 blocks cisplatin-induced apoptosis and predicts poor outcome following chemoradiation treatment in advanced oropharyngeal squamous cell carcinoma. *Clin. Cancer Res.* **2009**, *15* (5), 1645–1654.

(47) Pal, H. C.; Sehar, I.; Bhushan, S.; Gupta, B. D.; Saxena, A. K. Activation of caspases and poly (ADP-ribose) polymerase cleavage to induce apoptosis in leukemia HL-60 cells by *Inula racemosa*. *Toxicol. In Vitro* **2010**, *24* (5), 1599–1609.

(48) Lawrence, N. J.; McGown, A. T.; Nduka, J.; Hadfield, J. A.; Pritchard, R. G. Cytotoxic Michael-type amine adducts of alpha-methylene lactones alantolactone and isalantolactone. *Bioorg. Med. Chem. Lett.* **2001**, *11* (5), 429–431.

(49) Tanel, A.; Averill-Bates, D. A. P38 and ERK mitogen-activated protein kinases mediate acrolein-induced apoptosis in Chinese hamster ovary cells. *Cell. Signalling* **2007**, *19* (5), 968–977.

(50) Johnson, G. L.; Lapadat, R. Mitogen-activated protein kinase pathways mediated by ERK, JNK, and p38 protein kinases. *Science* **2002**, *298* (5600), 1911–1912.

(51) Woo, M. G.; Xue, K.; Liu, J.; McBride, H.; Tsang, B. K. Calpain-mediated Processing of p53-associated Parkin-like Cytoplasmic Protein (PARC) Affects Chemosensitivity of Human Ovarian Cancer Cells by Promoting p53 Subcellular Trafficking. *J. Biol. Chem.* **2012**, *287* (6), 3963–3975.

(52) Clark, A. S.; West, K.; Streicher, S.; Dennis, P. A. Constitutive and inducible Akt activity promotes resistance to chemotherapy, trastuzumab, or tamoxifen in breast cancer cells. *Mol. Cancer Ther.* **2002**, *1* (9), 707–717.

(53) Diarra-Mehrpour, M.; Arrabal, S.; Jalil, A.; Pinson, X.; Gaudin, C.; Pietu, G.; Pitaval, A.; Ripoche, H.; Eloit, M.; Dormont, D.; Chouaib, S. Prion protein prevents human breast carcinoma cell line from tumor necrosis factor alpha-induced cell death. *Cancer Res.* **2004**, *64* (2), 719–727.

(54) Drake, E. N. Cancer chemoprevention: selenium as a prooxidant, not an antioxidant. *Med. Hypotheses* **2006**, *67* (2), 318–322.

(55) Letavayova, L.; Vlckova, V.; Brozmanova, J. Selenium: from cancer prevention to DNA damage. *Toxicology* **2006**, *227* (1–2), 1–14.

(56) Vousden, K. H.; Lu, X. Live or let die: the cell's response to p53. *Nat. Rev. Cancer* **2002**, *2* (8), 594–604.

(57) Wang, J.; Yuan, L.; Xiao, H.; Xiao, C.; Wang, Y.; Liu, X. Momordin Ic induces HepG2 cell apoptosis through MAPK and PI3K/Akt-mediated mitochondrial pathways. *Apoptosis* **2013**, *18* (6), 751–765.

(58) Kim, Y. M.; Kim, K. E.; Koh, G. Y.; Ho, Y. S.; Lee, K. J. Hydrogen peroxide produced by angiopoietin-1 mediates angiogenesis. *Cancer Res.* **2006**, *66* (12), 6167–6174.

ERRATUM : A Novel Platinum–Maurocalcine Conjugate Induces Apoptosis of Human Glioblastoma Cells by Acting through the ROS-ERK/AKT-p53 Pathway

Sonia Aroui,^{*,†} Lucie Dardevet,^{‡,§} Wafa Ben Ajmia,[⊥] Madryssa de Boisvilliers,[⊙] Florian Perrin,[⊙] Amel Laajimi,[†] Ahcène Boumendjel,^{§, //} Abderraouf Kenani,[†] Jean Marc Muller,[⊙] and Michel De Waard^{‡,§,#}

[†]Laboratoire de Biochimie, Unité de recherche UR 12ES08 “Signalisation Cellulaire et Pathologies”, Faculté de Médecine de Monastir, Université de Monastir, 5019 Monastir, Tunisia

[‡]LabEx Ion Channels, Science and Therapeutics, INSERM U836, Grenoble Neuroscience Institute, 38042 Grenoble Cedex 09, France

[§]University Grenoble Alpes, 38000 Grenoble, France

[⊥]Toxicology-Microbiology and Environmental Health Unit (UR11ES70), Faculty of Sciences, University of Sfax, Sfax 3072, Tunisia

^{//} CNRS 5063, Département de Pharmacochimie Moléculaire, Université Joseph Fourier, 38400 Saint-Martin d’Hères, France

[⊙]Equipe émergente “Récepteurs, régulations et cellules tumorales” (2RCT), Université de Poitiers, 1 rue Georges Bonnet, TSA 51106, 86073 Poitiers Cedex 9, France

[#]Smartox Biotechnology, 570 Rue de la Chimie, 38400 Saint-Martin d’Hères, France

After publication of the article, we identified errors in the article body, concerning the reference in the text to the result of figure 2. It also appears, that figure 9, showing the results on the study of phosphorylation of ERK is missing since the results are referenced in the text as in figure 8. You will find below the correction to the relevant section and the figure 9.

▪ Results

Pt-1-DMCa Causes Cytotoxicity in Astrocytes and in Glioma U87 Cells.

To investigate the cytotoxic effect of the Pt-1-DMCa conjugate and to compare it with that of cisplatin in U87 GBM cells, MTS assays were performed after treating the cells, or not, with several concentrations of each drug for variable durations (Figure 2). As shown in Figure 2A, 1-DMCa alone had negligible cytotoxicity against this cell line, including at high concentration (60 μ M). These results are in line with the reported absence of toxicity of D-MCa14 and indicate that MBL-III-7 (1) conjugation to D-MCa does not generate by itself a toxic compound. In contrast, 48 h treatments with either Pt-1-DMCa or cisplatin induce cell cytotoxicity in the cell line in a concentration-dependent manner (Figure 2A). The cell toxicity after treatment with the novel platinum-conjugate Pt-1- DMCa (concentration from 1 to 60 μ M) ranged from 10.9 to 79.6%. The average IC₅₀ value of the conjugate determined from three independent experiments in U87 cells was 12.7 \pm 2 μ M, whereas the average IC₅₀ value for cisplatin was 23.5 \pm 3.4 μ M. Interestingly, the Pt-1-DMCa platinum conjugate appears to possess a marked cytotoxic effect

at lower concentrations that is not observed with cisplatin (below or equal to 10 μM). At higher concentrations, however, the cytotoxicity of Pt-1-DMCa was similar to that of cisplatin. In addition, we examined the cytotoxic effects of both compounds on a normal non tumor cell line such as SVGp12. Pt-1-DMCa seems to possess a negligible cytotoxic effect on SVGp12 since it did not exceed 13.6% at concentrations below or equal to 10 μM (Figure 2B). In contrast, in the case of cisplatin, cytotoxicity starts at low concentrations and reaches greater levels (28.7%) than with Pt-1-DMCa, suggesting that the latter has a more selective effect on cancerous cells.

To further study the toxicity of both drugs on U87 cells, their effects were analyzed at the concentration of 5 μM for prolonged times (1–4 days). At this concentration Pt-1-DMCa exerted a significant effect that was not observed for cisplatin. In these conditions, up to $42 \pm 4.2\%$ of the cells were not viable in the presence of the platinum conjugate, while in the presence of cisplatin only $17 \pm 5\%$ of the cells died at 4 days (Figure 2C). In addition, the effect of each drug was assessed after a short term exposure (4 h) at higher concentration (20 and 40 μM) followed by 1–4 days incubation of the cells after removal of the drugs. Treatment with 20 μM Pt-1-DMCa induced from $32.5 \pm 1.6\%$ to $48 \pm 2\%$ of cell killing between 1 and 4 days (Figure 2D). In contrast, in the same conditions, 20 μM of cisplatin produced a low toxicity (from $10.2 \pm 1.6\%$ to $22 \pm 2\%$). However, rising the concentration of these drugs to 40 μM led to similar effects of both compounds on cytotoxicity (from $23 \pm 2\%$ to $41 \pm 2.1\%$ for cisplatin and from $27 \pm 3.2\%$ to $45 \pm 2\%$ for Pt-1-DMCa) (Figure 2E).

Pt-1-DMCa Causes DNA Damage in U87 Cells.

Production of DNA damage is the main known mechanism by which platinum and its analogues induce cell apoptosis. In this work, we examined whether Pt-1-DMCa or cisplatin could generate DNA damage and subsequently activate proteins such as histone H2A.X and p53, involved in response to this phenomenon (Figure 3). Comet assay was chosen to assess the DNA damage induced by each compound in experimental conditions similar to those of Figure 2D,E. The chosen concentrations (20 μM for the conjugate and 40 μM for cisplatin) generated similar toxic effects in GBM cells. Comet tails reflecting DNA damage could be observed in cells treated with cisplatin or Pt-1-DMCa, suggesting a common action of both compounds on DNA fragmentation (Figure 3A). To further confirm the effect caused by Pt-1-DMCa and cisplatin on DNA, the expression levels of several DNA damage related signaling proteins, phospho-histone H2A.X, phospho-p53, and total p53, were assessed by Western blot. Increased phosphorylation levels of p53 and histone H2A.X were observed with 20 μM Pt-1-DMCa and 40 μM cisplatin (Figure 3B). Phosphorylation of these proteins is well known to occur in response to DNA damage.²⁹ These data demonstrate that both compounds act through DNA damage.

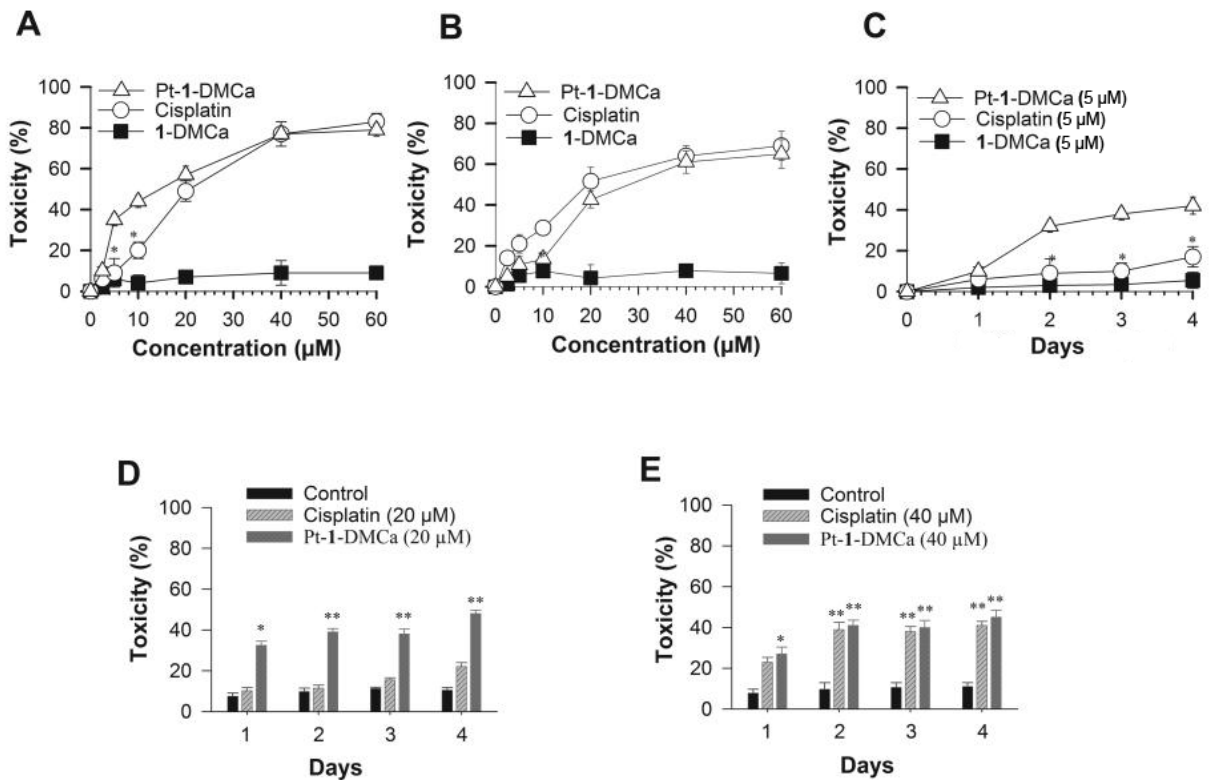


Figure 2 : Cell death induction by 1-DMCa, cisplatin, and Pt-1-DMCa in SVGp12 and glioma U87 cells. (A) Compounds were applied at various concentrations on U87 cells for 48 h before performing the MTS assay, as described in the Methods section. (B) SVGp12 cells were treated with various concentrations of Pt-1-DMCa, cisplatin, or 1-DMCa for 48 h before performing the MTS assay. (C) Cytotoxicity was assessed by 5 µM of all compounds after 4 h treatment, removing the medium, and cultured again for 1, 2, 3, and 4 days. (D) 20 µM of Pt-1-DMCa or cisplatin was used to treat the cells for 4 h, removing the medium, and cultured again for 1, 2, 3, and 4 days before performing the MTS assay. (E) 40 µM of Pt-1-DMCa or cisplatin was used to treat the cells for 4 h, removing the medium and cultured again for 1, 2, 3, and 4 days before performing the MTS assay. Data are representative of two independent experiments carried out in triplicate. Results are presented as mean \pm SD. Significant differences between stimulated Pt-1-DMCa and cisplatin cells are indicated by a star, *($P < 0.05$) (A,B and C). Significant differences between stimulated cells (Pt-1-DMCa or cisplatin) and control cells are indicated by stars, *($P < 0.05$) and **($P < 0.01$) (D and E).

Pt-1-DMCa Induces Apoptosis by Inhibiting ERK Phosphorylation.

Activation of the MAPK pathways is commonly recognized to be associated with the resistance to cisplatin in many cancer cells, such as ERK.³⁵ ERK phosphorylation can interfere with apoptosis at several levels. It can prevent the activation of caspases and induce the expression of anti-apoptotic factors such as Mcl-1 and Bcl-2. In this study, experiments were conducted to assess the effects of Pt-1-DMCa on the MAPK pathway in GBM cells. Decreased levels of phosphorylated ERK and decreased phospho-ERK/ERK ratio were detected in cells treated with 20 µM Pt-1-DMCa (Figure 9A,B) but not in cells exposed to 40 µM cisplatin (Figure 9C,D) for different periods of time ranging from 0 to 24 h. In all conditions tested, total ERK protein remained globally stable. The phosphorylation level started to decrease after 2 h and was strongly inhibited after 24 h. Phospho-ERK inhibition may represent an early event in the apoptosis process as for the inhibition of phospho-AKT. The specific effect of the conjugate on inhibition of ERK phosphorylation represents another functional advantage of Pt-1-DMCa as a

potential anti-cancer effect. To analyze the importance of inhibition of ERK phosphorylation on U87 cells apoptosis, U0126, an inhibitor of MEK, the upstream kinase of phospho-ERK, was tested in the same experimental condition than in Figure 1C,D. Alone or combined with 20 μ M Pt-1-DMCa or 40 μ M cisplatin, an important cytotoxicity was observed with all these treatments (Figure 9E). Furthermore, the Western blotting assay showed that U0126 significantly inhibits phospho-ERK level in cells treated by 20 μ M Pt-1-DMCa and enhances this inhibition effect in cells treated by 40 μ M cisplatin after 24 h (Figure 9F). In this case, cisplatin acts similarly to Pt-1-DMCa. These results indicate that inhibition of ERK phosphorylation plays an important role in the apoptosis induced by Pt-1-DMCa but not by cisplatin.

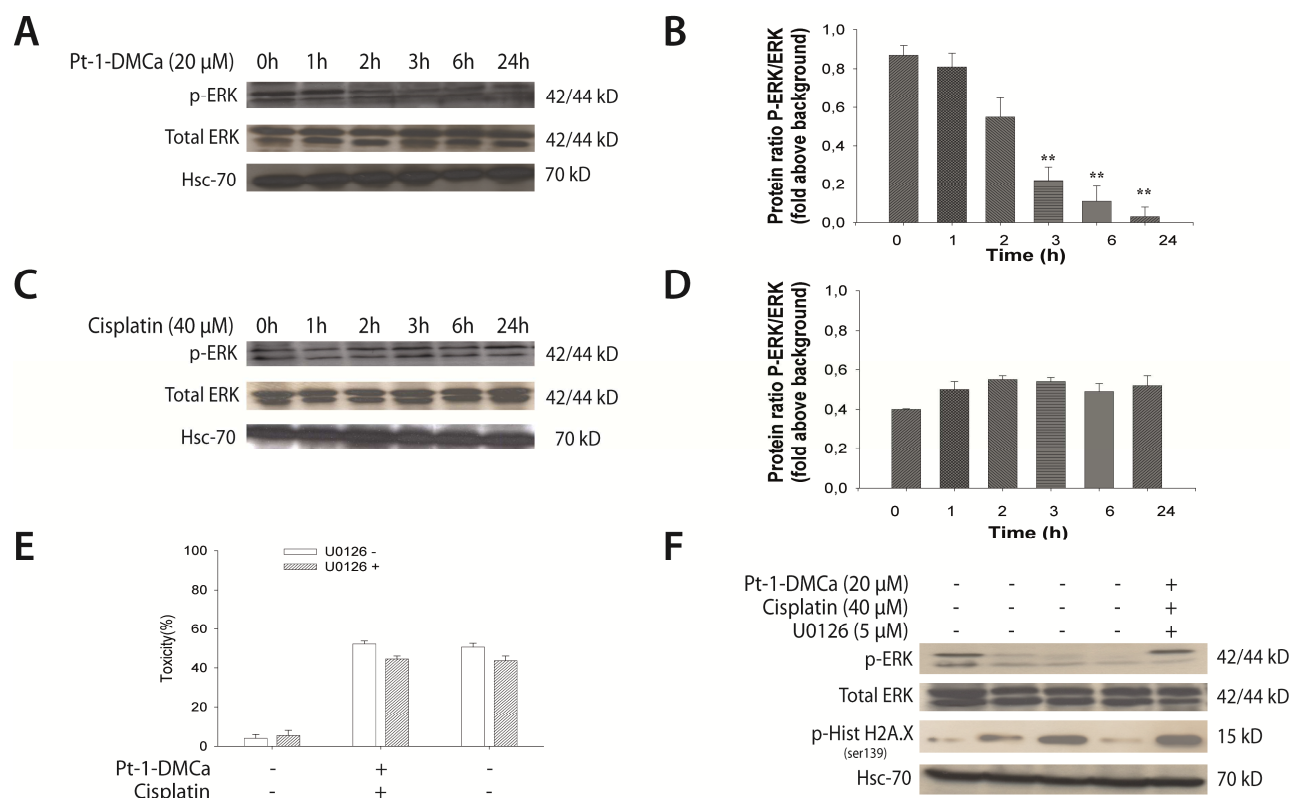


Figure 9 : Contribution of ERK to apoptosis induced by Pt-1-DMCa and cisplatin. (A, B) Time dependent Effect of Pt-1-DMCa and cisplatin on the phosphorylation and expression level of ERK for 1-24 h, respectively. (C, D) Comparison of total ERK and phospho-ERK levels on treated cells. Quantification of the western band intensity was performed using the Image G software. (E) Effect of U0126 (MEK inhibitor) on growth inhibition induced by Pt-1-DMCa and cisplatin. Cells were pretreated with 5 μ M U0126 for 1 h and then cultured in presence of Pt-1-DMCa for 72 h. Cell viability was determined by the MTS assay. All data are expressed as means \pm SD of triplicates. Bars with different characters are statistically different at P < 0.05 level. (F) Cell lysates were subjected to Western blot analysis to determine the effect of U0126 on ERK and histone H2A phosphorylation. Equal protein loading was confirmed by analysis of Hsc70 in the protein extracts.

II. Conclusions

Dans cette étude, nous avons montré que notre composé Pt-1-DMCa présente des propriétés différentes de celle du cisplatine :

- Une activité cytotoxique à plus faible dose,
- L'induction de l'apoptose via la production d'espèces réactives de l'oxygène (ROS), augmentant les dégâts à l'ADN induit par le platine,
- L'induction de l'apoptose par la voie intrinsèque et extrinsèque
- L'inhibition des voies AKT et ERK.

L'ensemble de ces propriétés ayant été observé chez une lignée cellulaire connue pour présenter une résistance au cisplatine, rend notre nouveau composé intéressant pour l'administration d'anticancéreux à base de platine.

Bien que ces résultats soient très positifs, il reste encore des questions en suspens concernant le mécanisme d'action de ce composé. Il serait en effet intéressant de déterminer plus précisément l'action de Pt-1-DMCa sur les enzymes responsables de la production de ROS, et déterminer comment cette augmentation des ROS entraîne l'inhibition de voies AKT et ERK. De plus si l'on reprend les résultats préliminaires, il serait utile de déterminer les raisons de l'efficacité de la D-MCa comme vecteur par rapport à la M_{CaUF1-9}. Même si l'utilisation de la D-MCa fonctionne et offre au composé en plus de son activité une résistance aux protéases ; la synthèse de la D-MCa n'en est pas moins coûteuse et plus complexe qu'un peptide linéaire. Afin de réduire le coût de cette stratégie, il serait intéressant de pouvoir déterminer les raisons de l'efficacité de la D-MCa pour essayer de la remplacer par un analogue de la M_{Ca} qui serait plus facile et moins coûteux à produire.

Chapitre 3 : La maurocalcine, vecteur de doxorubicine

I. Introduction

Comme abordée dans le chapitre précédent, la M_{Ca} est un bon vecteur de substances anticancéreuses. Dans l'optique de créer un vecteur « universel » de composés au sein de cellules, j'ai poursuivi au cours de ma thèse les travaux du laboratoire sur l'administration de doxorubicine via la M_{Ca}. Comme de préalables travaux ont déjà montré l'efficacité du couplage de la doxorubicine via une liaison covalente (Aroui et al., 2009a; Poillot and De Waard, 2011), nous sommes restés sur cette idée de couplage via liaison covalente, mais au lieu d'utiliser un cross-linker, ou les réactions de couplage traditionnel (maleimide, formation de liaison disulfure), nous avons opté pour une approche plus originale : la chimie click. Cela nous a permis d'utiliser la même doxorubicine modifiée que pour le couplage avec la Lqh-8/6.

L'utilisation de la doxorubicine dans cette preuve de concept présente 2 intérêts : (i) la doxorubicine étant fluorescente par elle-même, il est donc possible d'évaluer sa pénétration et localisation dans la cellule ; (ii) elle a déjà été utilisée dans le laboratoire couplé à la M_{Ca}, ce qui nous offre un point de comparaison. Ainsi dans le cadre de ce projet nous avons décidé d'évaluer l'intérêt de cette stratégie, en caractérisant les nouveaux composés formés puis en évaluant leurs toxicités sur différentes lignées cellulaires. Afin de ne pas me répéter, je ne reviendrai pas sur la synthèse de la doxorubicine alkyne et sur ses caractéristiques optiques. Ces points ayant été abordés dans le chapitre 1. Afin de compléter les travaux effectués et décrits dans le chapitre précédent, nous sommes partis des deux même vecteurs : D-M_{Ca} et M_{Ca}_{UF1,9}.

L'intérêt de la vectorisation de la doxorubicine via un variant de la M_{Ca} est d'en améliorer sa pénétration dans les cellules cancéreuses et les tissus difficiles d'accès (cerveau protégé par la BHE...), mais aussi de traiter de façon efficace des tumeurs complexes composées de cellules sensibles à la doxorubicine et des cellules résistantes à la doxorubicine. C'est avec ces deux objectifs en tête que nous avons choisi de réaliser les tests *in vitro* sur des cellules F-98 (présentée plus tôt) et sur deux lignées cellulaires de cancer du sein : les MDA-MB-435s (sensibles à la doxorubicine) et les MDA-MB-231 (résistantes à la doxorubicine).

II. Matériels et méthodes

a. *Modélisation moléculaire*

En utilisant le logiciel Sybyl X 1.3 (Tripos Inc., St. Louis, MO, USA), et les structures PDB de la D-MCa (code 2KQL) et de la L-MCa (code 1C6W) et de la doxorubicine (code 1DA9), une représentation 3D des nouveaux composés a été réalisée. En utilisant la fonction mutation build de sybyl, les séquences de la D-MCa et de la L-MCa ont été modifiées pour correspondre au vecteur utilisé. En utilisant la fonction draw, les vecteurs et la doxorubicine ont pu être fusionnés en créant un cycle triazolé entre les deux structures.

b. *Synthèse peptidique*

La synthèse des toxines a été réalisée par synthèse peptidique en phase solide comme décrit précédemment (Poillot et al., 2010). N- α -Fmoc-L-acide-aminé, Wang-Tentagel résine et autres réactifs utilisés ont été obtenus chez Iris Biotech. Les solvants utilisés étaient de grade analytique et produit par Acros Organics. Brièvement, les peptides ont été chimiquement synthétisés en utilisant un synthétiseur de peptide automatisé (CEM © liberty). La chaîne peptidique a été assemblée un acide aminé à la fois à partir de 0.24 mEq de Fmoc-L-Arg (Pbf) - wang-tentagel résine pour la MCaUF1-9 en utilisant 0.24 mmol des dérivées N- α -fluorenylméthoxy-carbonyl (Fmoc) L-amino-acide. Pour la D-MCa la résine utilisée fut de la Fmoc-D-Arg-Pbf-Wang-Tentagel résine (0.24 mEq) using 0.24 mmol of N- α -fluorenylméthoxy-carbonyl (Fmoc) D-amino-acide. Les groupes de protection des chaînes latérales utilisés sont : trityl pour Cys et Asn, tert-butyle pour Ser, Thr, Glu et Asp, Pbf (2,2,4,6,7-pentaméthyl-dihydrobenzofuran-5-sulfonyl) pour Arg et tert-butylcarbonyl pour Lys. Les réactifs étaient aux concentrations suivantes: Fmoc-amino-acide [0.2 M Fmoc-AA-OH dans diméthylformamide (DMF)], l'activateur (0.5 M 2-(1H-benzotriazole-1-yl)-hexafluorophosphate 1,1,3,3-tétraméthyluronium dans DMF), l'activateur base [2 M diisopropylethylamine dans N-méthylpyrrolidone (NMP)] et l'agent de déprotection (5 % piperazine/0.1 le M de 1-hydroxybenzotriazole dans DMF), comme conseillé par PepDriver (CEM ©). Une fois la chaîne peptide synthétisée, les résines ont été traitées 4 heures à température ambiante avec un mélange d'acide trifluoroacétique/l'eau/triisopropylsilane (TSI)/dithiothreitol (DTT) (92.5/2.5/2.5/2.5). Le mélange peptidique est alors filtré et le filtrat est précipité à froid par l'ajout de tert-butylméthyl éther. Les peptides bruts sont récupérés par centrifugation (10.000 \times G, 15 minute) et le surnageant est éliminé. Les peptides synthétisés sont ensuite purifiés par HPLC, utilisation d'une colonne Vydac C18 (218TP1010, 25 \times 10 cm). L'élution des peptides a été exécutée avec un gradient de 10-60 % acetonitrile contenant 0.1 % d'acide trifluoroacétique (TFA). Les fractions purifiées ont été analysées par RP-HPLC analytique (Vydac C18 la colonne 218TP104, 25 \times 4.6 cm). Tous les peptides ont été caractérisés par spectrométrie de masse MALDI-TOF.

c. Couplage de la doxorubicine-alkyne avec les vecteurs

Afin de réaliser le couplage par chimie click le vecteur M_{Ca}-azide (1 eq) a été dissous dans du DMF et la doxorubicine-alkyne en solution dans du méthanol/DCM (1/1) a été ajouté (10 eq). Ensuite une solution aqueuse de CuSO₄.5 H₂O (5 eq) et une solution aqueuse d'ascorbate de Sodium (5 eq) ont été ajoutées. Le mélange a ensuite été soniqué à 35°C pendant 2 jours. La solution a ensuite été purifiée par HPLC en utilisant une colonne Vydac C18 (218TP1010, 25×10 cm). L'élution de la doxorubicine-M_{Ca} a été réalisée en utilisant un gradient de 5-90% d'acétonitrile et 0,1% TFA. Le complexe a été identifié grâce à l'absorbance simultanée du complexe à 214 nm (liaison peptidique) et 495 nm (doxorubicine). La fraction d'intérêt est ensuite purifiée et quantifiée (rendement théorique de 90%). Une analyse par spectrométrie de masse (MALDY-TOF) a permis de caractériser le produit.

d. Culture cellulaire

Afin d'évaluer la toxicité des composés développés, des cellules indifférenciées de gliome de rat (F-98), deux lignées de cellule humaine de cancer du sein (MDA-MB-435s et MDA-B-231). Les cellules F-98 ont été maintenues en culture à 37°C, 5% CO₂ dans du milieu DMEM/F-12 supplémenté avec 2% (v/v) de sérum de veau fœtal et 100 µg/mL de streptomycine et 100 unités/mL de pénicilline (Invitrogen). Les lignées de cancer de sein ont été maintenues en culture à 37°C, 5% CO₂ dans du milieu DMEM avec une forte concentration de glucose (5 g/l) supplémenté avec 10% (v/v) de sérum de veau fœtal, 100 mM de MEN et 100 µg/mL de streptomycine et 100 unités/mL de pénicilline (Invitrogen). Le milieu de culture est changé tous les deux jours. Toutes les expériences ont été réalisées sur des cellules ayant une viabilité de 95%. Après ensemencement, les cellules sont incubées à 37°C et 5% de CO₂ sur la nuit avant d'être utilisées pour les différentes expérimentations.

e. Etude de microscopies

Afin d'étudier la pénétration et la répartition des composés synthétisés, de la doxorubicine, doxorubicine-alkyne, j'ai réalisé une série d'expériences d'imagerie confocale. Les cellules ont étéensemencées dans des labteks à une densité de 1000 cellules/puits. Après les avoir laissé sur la nuit à l'incubateur, les cellules ont été incubées pendant deux heures avec 10 µM de doxorubicine, doxorubicine-alkyne, doxorubicine-DM_{Ca} ou de doxorubicine-M_{Ca}_{UF1,9} dans du milieu de culture sans FBS. Après les deux heures d'incubation, les cellules sont rincées 2 fois avec du PBS. Les cellules ont été marquées dans du PBS avec 60 µg/mL Hoechst 34580 (Molecular Probes Invitrogen, Cergy Pontoise, France) pendant 5 min afin de visualiser les noyaux des cellules. Les cellules ont ensuite été lavées avec du PBS avant d'être marquées dans du PBS contenant 50 µg/mL concanavalin A-Alexa 647 (Molecular Probes Invitrogen, Cergy Pontoise, France) pendant 5 min afin d'observer la membrane plasmique des cellules. On a de nouveau rincé les cellules avec du PBS. Avant de les ré-incuber dans du milieu de culture sans FBS et phénol red. Les cellules ont été immédiatement analysées en microscopie confocale en

utilisant un système Zeiss LSM. Hoechst 34580 (405 nm), Alexa 647 (668 nm) et la doxorubicine (590 nm) ont été excités et leur émission enregistré séquentiellement. Le réglage du laser permettant la détection de la doxorubicine a été réalisé en utilisant des cellules contrôles non incubées avec un composé contenant de la doxorubicine. Les paramètres ont été réglés au niveau le plus haut n'entraînant pas l'apparition d'une fluorescence chez ces cellules. Une fois le réglage effectué, le temps de la manipulation n'a plus été modifié. Après la prise d'images d'au minimum 50 cellules, les images ont été analysées en utilisant image J, et le rapport fluorescence dans le cytoplasme sur celles dans le noyau a permis de déterminer la localisation préférentielle des composés.

f. *Evaluation de la pénétration des composés*

Les différentes lignées cellulaires ont étéensemencées dans des plaques 24 puits à une densité de 50 000 cellules/puits. Après 24 hrs de culture, les cellules ont été incubées avec des concentrations diverses des différents composés (doxorubicine, doxorubicine-alkyne, doxorubicine-DMCa, doxorubicine-MCa_{UF1,9} dans du milieu de culture sans sérum à 37°C pour 2 hrs). Les cellules ont été alors lavées avec du PBS pour enlever l'excès extracellulaire de composé et ont été traitées avec 500 µL de trypsine (Invitrogen) pendant 3 min à 37°C pour détacher les cellules de la surface et centrifugées à 500 g dans du milieu de culture avec sérum avant resuspension dans du PBS. Les cellules ont été immédiatement analysées par cytométrie en flux utilisant un BD Accuri C6 cytomètre (BD Biosciences, Pont de Claix, la France). Les données ont été obtenues et analysées utilisant le logiciel CFlow (BD Biosciences). Les cellules vivantes ont été consignées par forward/side scattering et un total de 10,000 événements ont été enregistrés.

g. *Essai de toxicité et cytométrie en flux*

Afin d'évaluer la toxicité des composés par cytométrie en flux, le kit LIVE/DEAD® Viability/Cytotoxicity, for mammalian cells (life technologies) a été utilisé. Les cellules ont étéensemencées dans des plaques 24 puits à une densité de 7500 cellules/puits. Après 24 heures de culture les cellules ont été incubées pour 24, 48, 72 hs à 37°C avec la doxorubicine, la doxorubicine-alkyne et la doxorubicine-DMCa. Une condition contrôle correspondant aux cellules incubées avec le véhicule a été ajoutée à chaque expérience. Après incubation, le milieu de culture contenant les composés est éliminé et les cellules sont rincées avec du PBS. 500 µL de Trypsine/EDTA (Invitrogen) a été utilisé pour détacher les cellules. Les cellules ainsi détachées furent centrifugées dans du milieu de culture contenant du FBS, à 500 g pendant 5 min. Le surnageant est éliminé et les cellules sont resuspendues dans du milieu de culture sans phénol red et FBS contenant 31 nM calcéine et 1 µM d'homodimer d'éthidium. La calcéine permet de marquer les cellules vivantes et l'homodimer d'éthidium marque les cellules mortes. La suspension cellulaire est incubée dans ce milieu pour 15 min à température ambiante et à l'abri de la lumière avant d'être analysée en cytométrie de flux (C6 Flow cytometer (Accuri)). Les

cellules ont été identifiées en utilisant forward/side scattering et un total de 10,000 événements ont été enregistrés. Les données obtenues ont été analysées en utilisant le logiciel Accuri CFlow (Accuri).

h. *Test MTT.*

Les cellules des différentes lignées cellulaires ont été ensemencées dans une plaque 96 puits à une densité de 8.10^4 cellules/puits. Après un jour de culture, les cellules ont été incubées pour 72 hrs à 37°C avec de la doxorubicine, doxorubicine-alkyne, doxorubicine-DMCa ou doxorubicine-MCa_{UF1,9} à des concentrations différentes. Pour chaque expérience des conditions contrôles ont été ajoutées, 6 puits ne contenant que du milieu de culture (blanc), 6 puits contenant des cellules traitées uniquement avec le véhicule (contrôle positif) et 6 puits contenant des cellules traitées avec 0,1% de saponine (contrôle négatif). Les cellules ont été alors incubées avec du MTT pendant 30 min. La conversion du MTT en MTT formazan par les cellules vivantes indique la mesure de viabilité cellulaire, l'état de leur métabolisme. Les cristaux ont été dissous avec du DMSO et la densité optique a été mesurée à 540 nm en utilisant un lecteur de microplaque (PHERAstar fsx; GMG Labtech.). Tous les essais ont été réalisés en triplicat.

III. Résultats

a. *Conception et synthèse des nouveaux composés*

Afin de rendre, nos deux vecteurs peptidiques chimie-click compatibles, nous leur avons rajouté lors de la synthèse peptidique à leur extrémité N-terminal deux acides aminés. Comme pour la synthèse de la Lqh-8/6 azide, une glycine extra-numéraire a été rajoutée entre le premier acide aminé de la séquence peptidique et l'acide aminé modifié porteur de la fonction azide (**Figure 17A**). La présence de cette glycine supplémentaire va permettre d'apporter à la fois de la flexibilité au complexe et de diminuer la gêne stérique des vecteurs peptidiques sur la doxorubicine. L'acide aminé modifié porteur de la fonction azide utilisée est le même que celui utilisé pour la Lqh-8/6 azide. Une fois la D-MCa azide et la MCa_{UF1,9} azide synthétisés le couplage à la doxorubicine alkyne a été réalisé selon la même réaction chimique qu'avec Lqh-8/6 azide (**Figure 17B**). Après purification par RP-HPLC et caractérisation par analyse de masse, nous avons obtenu nos deux nouveaux composés anticancéreux (**Figure 17C, D**) :

- La doxorubicine D-MCa
- La doxorubicine MCa_{UF1,9}

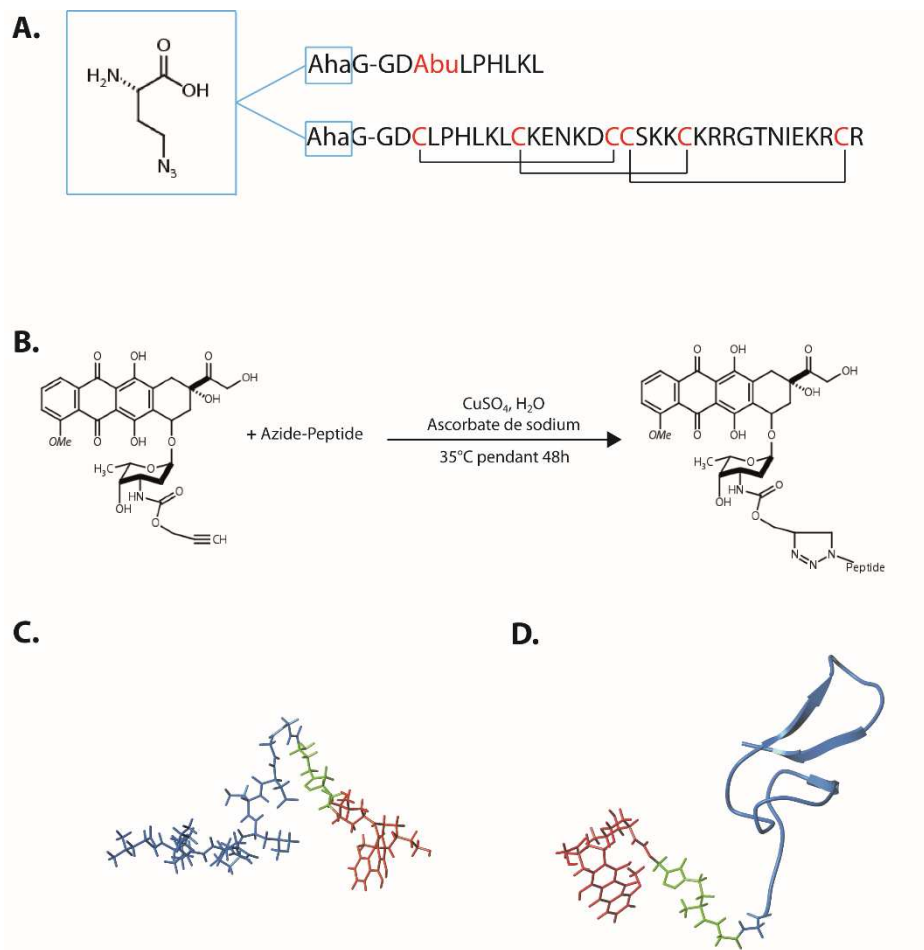


Figure 17 : Synthèse de la M_{Ca}UF_{1,9} et de la D-M_{Ca} et couplage avec la doxorubicine-alkyne ; A. Séquence peptidique de la M_{Ca}UF_{1,9}, et de la D-M_{Ca}, avec la structure de l'acide aminé porteur de la fonction azide en encart ; B. Réaction chimique de couplage de la doxorubicine alkyne aux deux vecteurs ; C. Modélisation moléculaire de la doxorubicine M_{Ca}UF_{1,9}, en bleu la M_{Ca}UF_{1,9}, en vert la glycine surnuméraire et le cycle triazolé couplant la doxorubicine au vecteur, en rouge la doxorubicine ; D. Modélisation moléculaire de la doxorubicine D-M_{Ca}, en bleu la D-M_{Ca}, en vert la glycine surnuméraire et le cycle triazolé couplant la doxorubicine au vecteur, en rouge la doxorubicine.

b. Evaluation de l'efficacité *in vitro* des nouveaux composés synthétisés

Afin d'évaluer les composés nouvellement synthétisés, j'ai observé leur toxicité sur les trois lignées cellulaires à des concentrations et temps d'incubation différents. Dans un premier temps la toxicité des composés a été évaluée par FACS via le kit d'Invitrogen. Pour des fins de comparaison, la toxicité de la doxorubicine et la doxorubicine alkyne ont été évaluées en parallèle. L'absence de toxicité des variants de la maurocalcine ayant déjà été démontrée dans le laboratoire, je n'ai pas reproduit la manipulation avec les vecteurs seuls.

Après 72 hrs d'incubation, chez les cellules F-98 et MDA-MB-435s, on observe pour l'ensemble des composés que la concentration-dépendance de la toxicité présente le même

profil mais avec une plus grande toxicité de la doxorubicine (**Figure 18A** et B). Ainsi sur chez les cellules F-98, les IC_{50} sont de $0,39 \pm 0,02 \mu\text{M}$ doxorubicine, $0,84 \pm 0,05 \mu\text{M}$ doxorubicine alkyne, $2,36 \pm 0,03 \mu\text{M}$ doxorubicine D-MCa, et $1,92 \pm 0,02 \mu\text{M}$ doxorubicine $\text{MCa}_{\text{UF1,9}}$. Chez les MDA-MB435s, les IC_{50} sont de $11,7 \pm 0,03 \mu\text{M}$ doxorubicine, $21,19 \pm 0,04 \mu\text{M}$ doxorubicine alkyne, $19,66 \pm 0,02 \mu\text{M}$ doxorubicine D-MCa, et $\geq 33\mu\text{M}$ doxorubicine $\text{MCa}_{\text{UF1,9}}$. On constate que les F-98 sont plus sensibles à la doxorubicine sous toutes ces formes que les cellules MDA-MB-435s. Par contre le shift de toxicité observé entre la doxorubicine et la doxorubicine alkyne est très probablement lié à la modification chimique réalisée sur cette dernière pour la rendre chimie click compatible. Les différences de toxicité entre la doxorubicine alkyne et la doxorubicine couplé au vecteur peut être imputable à plusieurs phénomènes : (i) la gêne stérique provoquée par la présence du vecteur, (ii) l'efficacité de pénétration du nouveau complexe.

Par contre de façon très intéressante le couplage de la doxorubicine aux deux vecteurs entraine une récupération de la sensibilité à la doxorubicine des cellules MDA-MB-231 (**Figure 18C**). On retrouve des IC_{50} supérieur à $33 \mu\text{M}$ pour la doxorubicine et la doxorubicine alkyne et de $6,34 \pm 0,03 \mu\text{M}$ et $28,01 \pm 0,02 \mu\text{M}$, respectivement pour la doxorubicine D-MCa et doxorubicine $\text{MCa}_{\text{UF1,9}}$. La D-MCa semble être un vecteur plus performant que la $\text{MCa}_{\text{UF1,9}}$, cela pourrait s'expliquer par une moins bonne compensation de l'hydrophobicité de la doxorubicine par le petit variant de la MCa.

Afin de confirmer ces résultats, j'ai par la suite évalué la toxicité de ces composés par MTT. De façon surprenante, les résultats obtenus semblent montrer une plus grande toxicité des composés en général quelque-soit la lignée cellulaire (**Figure 18D, E** et F). De plus, il semble que les cellules MDA-MB-231 ne soient que légèrement moins sensibles à la doxorubicine que les MDA-MB-435s, et on n'observe plus une re-sensibilisation des MDA-MB-231 à la doxorubicine lorsqu'elle est couplée à un vecteur (**Figure 18F**). Ces différences de toxicité peuvent s'expliquer par la différence entre les deux tests réalisés. L'analyse par FACS se base sur la perméabilisation membranaire pour détecter les cellules mortes, alors que le MTT se base sur l'activité métabolique de la cellule. De ce fait on peut se demander si les résultats obtenus par MTT, ne montrent pas à la fois un effet létal des composés ainsi qu'un effet sur le métabolisme de la part de ces composés.

L'obtention de ces résultats contradictoires, montre l'importance de déterminer le mécanisme de toxicité de ces molécules, d'étudier les voies d'apoptose impliquées... Malheureusement par manque de temps, je n'ai pas eu le temps de réaliser ces études.

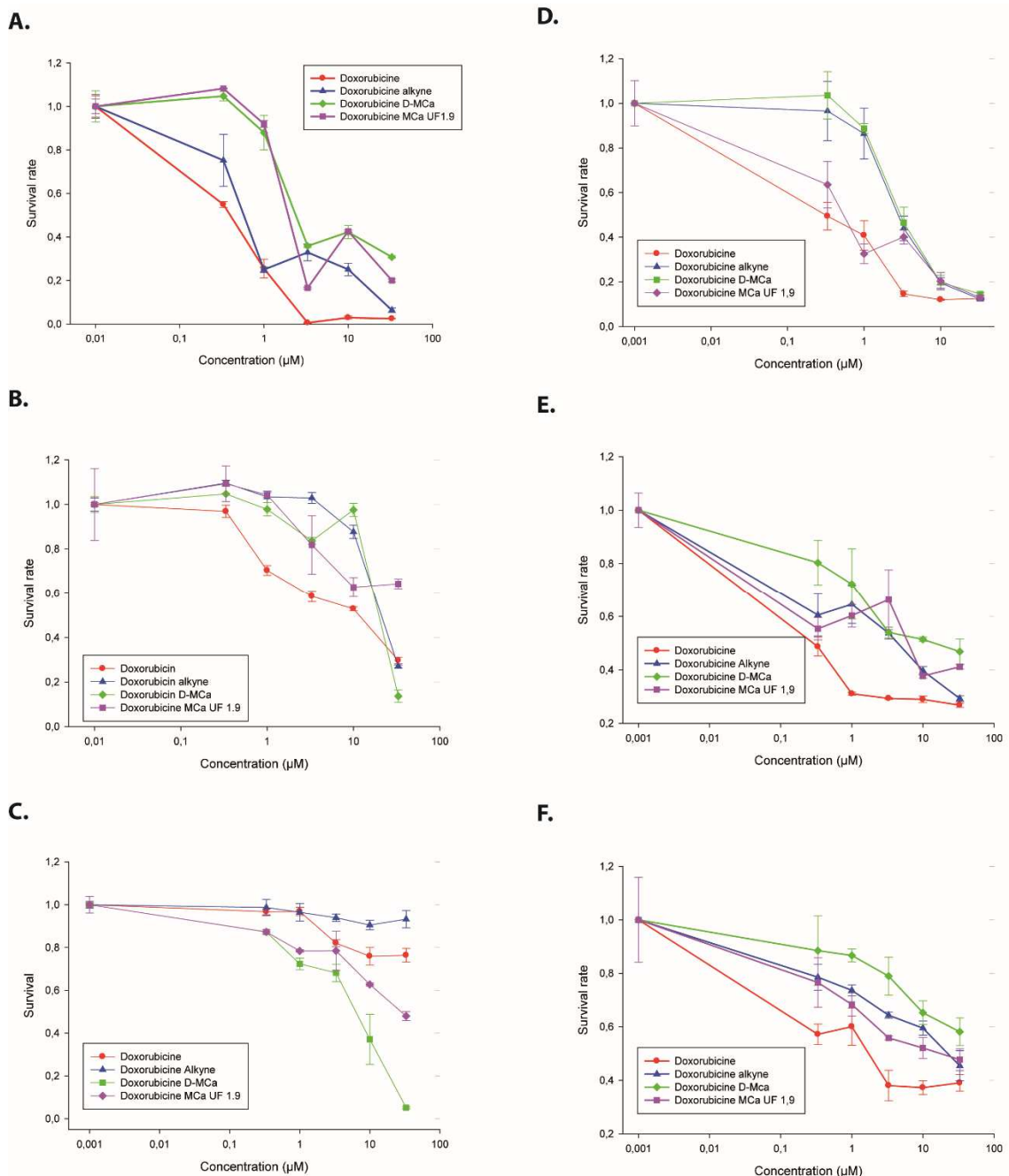


Figure 18 : Toxicité de la doxorubicine, doxorubicine alkyne, doxorubicine D-MCa et doxorubicine MCa_{UF1,9}. **A.** Concentration-dépendance de la toxicité des composés sur des cellules F-98 après 72 hrs d'incubation par FACS; **B.** Concentration-dépendance de la toxicité des composés sur des cellules MDA-MB-435s après 72 hrs d'incubation par FACS; **C.** Concentration dépendance de la toxicité des composés sur des cellules MDA-MB-231 après 72 hrs d'incubation par FACS; **D.** Concentration dépendance de la toxicité des composés sur des cellules F-98 après 72 hrs d'incubation par MTT; **E.** Concentration-dépendance de la toxicité des composés sur des cellules MDA-MB-435s après 72 hrs d'incubation par MTT; **F.** Concentration-dépendance de la toxicité des composés sur des cellules MDA-MB-231 après 72 hrs d'incubation par MTT.

c. Caractérisation des nouveaux composés à base de doxorubicine

Afin de mieux caractériser les effets des nouveaux composés, et d'expliquer la différence d'efficacité de ces derniers, j'ai dans un premier temps regardé s'il y avait une modification de la répartition cellulaire. Chez les F-98, on observe une nette différence de répartition, la doxorubicine est le seul composé qui s'accumule préférentiellement dans le noyau (**Figure 19**). La doxorubicine alkyne, doxorubicine D-MCa et doxorubicine $MCa_{UF1,9}$ s'accumulent majoritairement dans le cytoplasme. Cette différence de localisation peut-être à l'origine de la plus faible toxicité de ces trois composés par rapport à la doxorubicine.

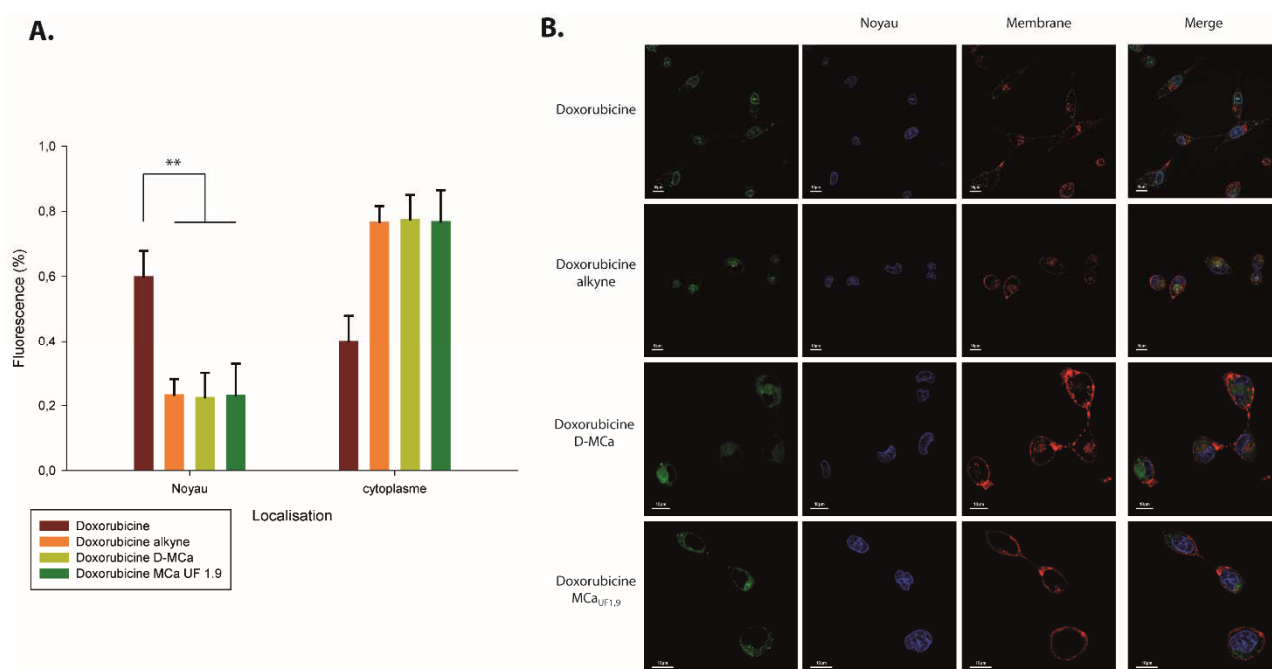


Figure 19 : Localisation cellulaire de la doxorubicine, doxorubicine alkyne, doxorubicine D-MCa et doxorubicine $MCa_{UF1,9}$ chez des cellules F-98 ; A. Quantification de la répartition cellulaire de la doxorubicine, doxorubicine alkyne, doxorubicine D-MCa et doxorubicine $MCa_{UF1,9}$ chez des cellules F-98 ; **B.** Localisation cellulaire de la doxorubicine, la doxorubicine alkyne, doxorubicine D-MCa et doxorubicine $MCa_{UF1,9}$ dans les cellules F-98 à 3 μ M (2 heures d'incubation). Doxorubicine, la doxorubicine alkyne, doxorubicine D-MCa et doxorubicine $MCa_{UF1,9}$ sont représentés en vert . La membrane plasmique est marquée avec de la concanavaleine -A- alexa Fluor 647 (couleur rouge) et le noyau avec Hoechst 34580 (couleur bleu).

On observe ce même déplacement de l'accumulation vers le cytoplasme pour les deux lignées du cancer du sein (**Figure 20**, **Figure 21**). Cependant ce phénomène est moins marqué dans ces deux lignées. Pour les cellules MDA-MB-231 seuls des résultats partiels sont présentés (absence de données pour la $MCa_{UF1,9}$) dus à un problème technique qui m'a empêché d'acquérir les images avant la fin de ma thèse (**Figure 21**). Cependant je pense que l'on peut s'attendre à un même déplacement de l'accumulation du composé dans le cytoplasme. En effet la taille du composé et les données dans les autres lignées cellulaires tendent vers un mauvais passage de la membrane nucléaire pour atteindre le noyau.

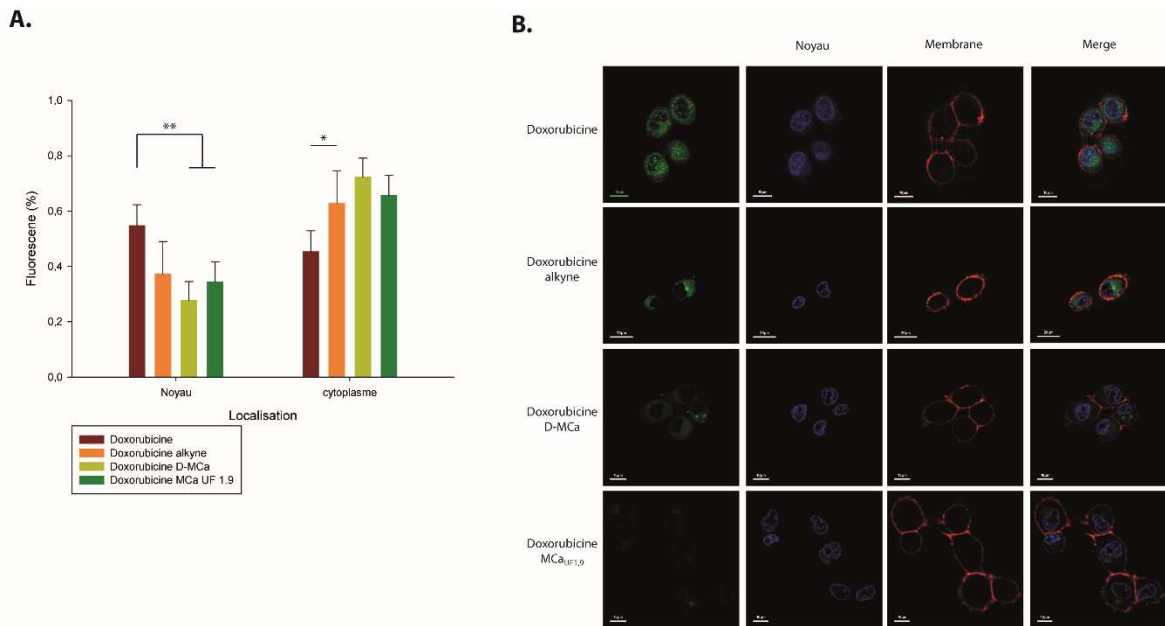


Figure 20 : Localisation cellulaire de la doxorubicine, doxorubicine alkyne, doxorubicine D-MCa et doxorubicine MCA_{UF1,9} chez des cellules MDA-MB-435s ; A. Quantification de la répartition cellulaire de la doxorubicine, doxorubicine alkyne, doxorubicine D-MCa et doxorubicine MCA_{UF1,9} chez des cellules MDA-MB-435s ; **B.** Localisation cellulaire de la doxorubicine, la doxorubicine alkyne, doxorubicine D-MCa et doxorubicine MCA_{UF1,9} dans les cellules MDA-MB-435s à 3 μ M (2 heures d'incubation). Doxorubicine, la doxorubicine alkyne, doxorubicine D-MCa et doxorubicine MCA_{UF1,9} sont représentés en vert. La membrane plasmique est marquée avec de la concanavaleine -A- alexa Fluor 647 (couleur rouge) et le noyau avec Hoechst 34580 (couleur bleu).

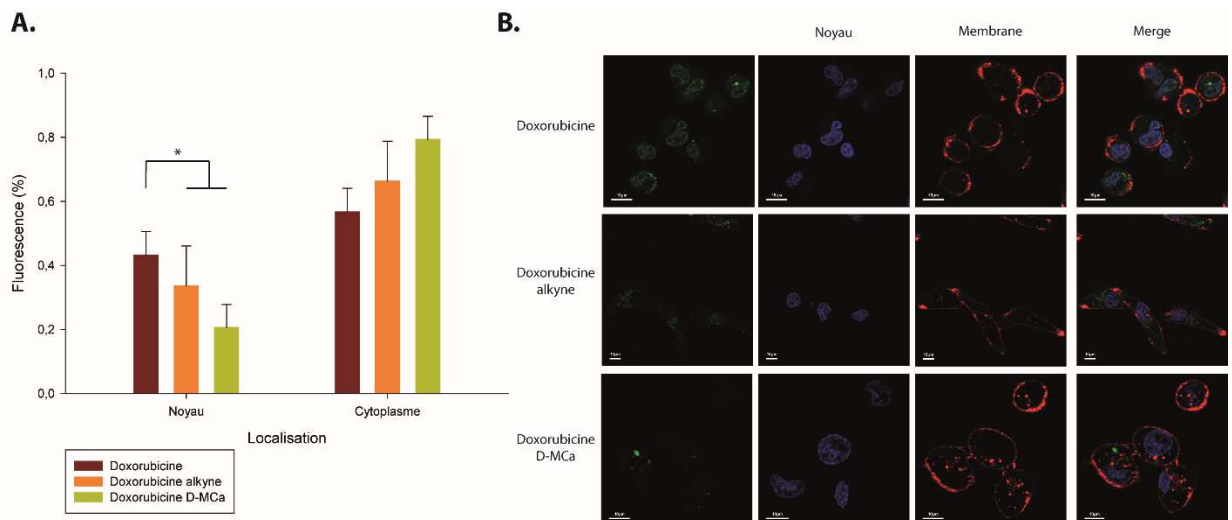


Figure 21 : Localisation cellulaire de la doxorubicine, doxorubicine alkyne, et doxorubicine D-MCa chez des cellules MDA-MB-231 ; A. Quantification de la répartition cellulaire de la doxorubicine, doxorubicine alkyne, et doxorubicine D-MCa chez des cellules MDA-MB-231 ; **B.** Localisation cellulaire de la doxorubicine, la doxorubicine alkyne, et doxorubicine D-MCa dans les cellules MDA-MB-231 à 3 μ M (2 heures d'incubation). Doxorubicine, la doxorubicine alkyne, et doxorubicine D-MCa sont représentés en vert. La membrane plasmique est marquée avec de la concanavaleine -A- alexa Fluor 647 (couleur rouge) et le noyau avec Hoechst 34580 (couleur bleu).

Après avoir vérifié la répartition cellulaire des composés, j'ai étudié la pénétration des composés dans les cellules des différentes lignées (**Figure 22**)

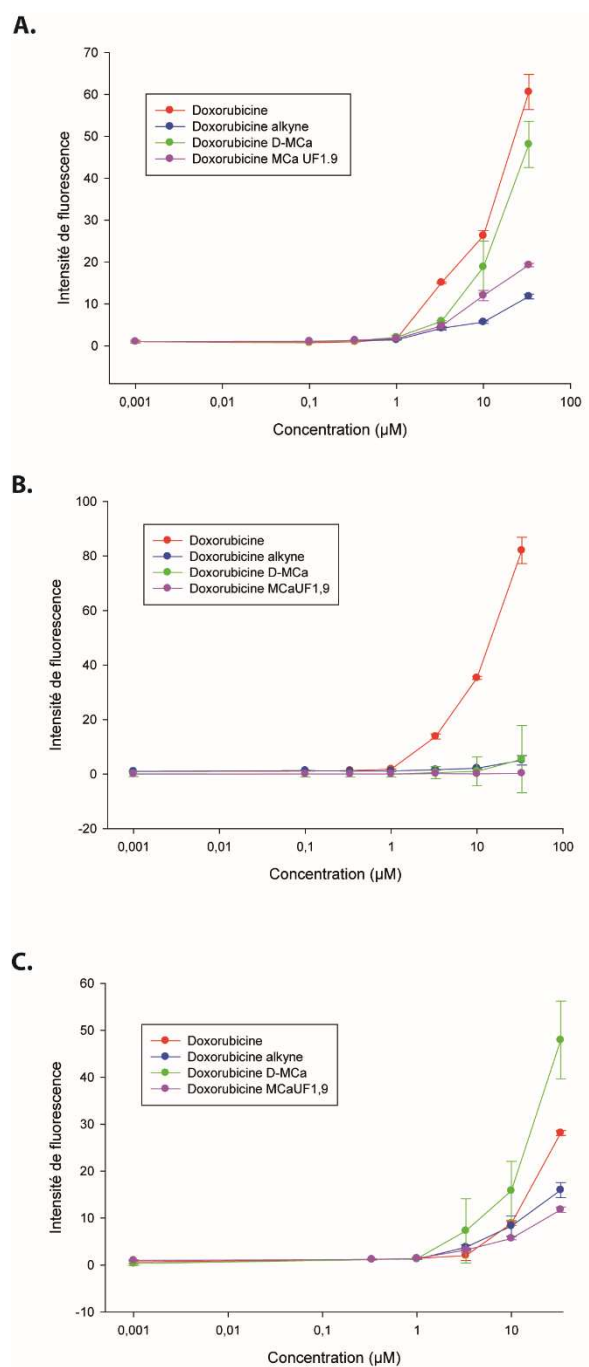


Figure 22 : Pénétration de la doxorubicine, doxorubicine alkyne, doxorubicine D-MCa et doxorubicine MCA_{UF1,9} chez des cellules F-98 (**A.**), MDA-B-435s (**B.**) et MDA-MB-231 (**C.**), après deux heures d'incubations.

Lorsque l'on regarde rapidement ces données on constate rapidement que la pénétration des différentes molécules varie grandement en fonction de la lignée cellulaire. Par ordre de pénétration décroissante, on retrouve chez les cellules F-98 : la doxorubicine, doxorubicine D-MCa, doxorubicine MCA_{UF1,9} et enfin la doxorubicine alkyne. Chez les cellules MDA-MB-435s,

l'ordre est légèrement différent avec: la doxorubicine, doxorubicine D-MCa et la doxorubicine alkyne avec une pénétration comparable, et en dernière position doxorubicine $\text{MCA}_{\text{UF1,9}}$. Enfin, chez les cellules MDA-MB-231, on a un classement bien différent avec en première position doxorubicine D-MCa, suivis de la doxorubicine puis de la doxorubicine alkyne et en dernière position doxorubicine $\text{MCA}_{\text{UF1,9}}$. Si l'on compare ces résultats avec les résultats de toxicité de la **Figure 18**, on ne retrouve pas forcément le même ordre dans les composés. Même si le composé qui pénètre le mieux semble être toujours le plus actif. La différence d'activité des composés ne peut donc pas être simplement expliquée par une différence de pénétration.

IV. Conclusions

Les travaux décrits dans ce chapitre sont incomplets et vont nécessiter du travail complémentaire avant de pouvoir être publiés. En effet même si nous avons avec succès produit de nouveaux composés anticancéreux, et montrés que la chimie click est une méthode de couplage viable dans la recherche biomédicale, il reste encore de la place pour l'amélioration. De façon identique à ce qui a été dit pour la Lqh-8/6 dans le chapitre 1, mes travaux de thèse ne sont qu'une preuve de concept, qu'une vague idée du potentiel que représente l'utilisation des toxines animales et de leurs variants en médecine. Si l'on associe les résultats obtenus avec ceux obtenus avec la Lqh-8/6, il apparaît clairement que l'utilisation d'un système de couplage universel et très spécifique est possible et pourrait représenter un atout dans le développement de nouvelles molécules et dans la re-valorisation d'anciennes molécules comme la doxorubicine.

Cependant, bien qu'encourageant ces résultats doivent être complétés par des études des mécanismes d'action ainsi que par des essais *in vivo*, avant de pouvoir être publié. De plus une fois ce travail effectué, il serait très intéressant d'utiliser un autre anticancéreux ou une autre molécule active pour démontrer la pluri-potence de l'utilisation de CPP comme vecteur d'agent thérapeutique.

Une autre approche qui peut aussi être envisagée c'est une amélioration des variants de la MCa utilisés comme vecteur. Jusqu'à présent dans le laboratoire, on ne s'est concentré qu'autour de l'idée de trouver le variant complet ou non de la MCa qui présente le plus d'intérêt comme vecteur sans en modifier sa séquence. Et même s'il est vrai que l'utilisation du vecteur le plus petit et le plus simple possible (pas de ponts disulfures...) soit très intéressante d'un point de vue financier, les variants longs, voir complet de la MCa présente l'avantage d'être modifiable afin d'intégrer par exemple facilement des séquences d'adressage au noyau. Il est aussi facile d'imaginer la possibilité de fusion la MCa et la séquence responsable du ciblage des glioblastome de la CTX, et d'étudier l'efficacité de ce nouveau vecteur à la fois ciblant et pénétrant.

Conclusions et perspectives

Au cours de cette thèse, j'ai étudié le potentiel thérapeutique de différentes toxines animales issues de venins de scorpion. Depuis longtemps la nature a fourni à l'Homme des composés servants de base à de nombreux médicaments. Jusqu'à présent les toxines animales sont majoritairement utilisées comme agent pharmacologique (Zhang et al., 2007; Soman et al., 2009). La découverte de la M_{Ca} et de la CTX a entrouvert la porte pour l'usage de toxines comme vecteurs de substances thérapeutiques d'intérêt.

La M_{Ca} est une toxine de scorpion qui est depuis longtemps étudiée dans le laboratoire. Au départ, les travaux portaient uniquement sur l'utilisation de la M_{Ca} pour l'étude du récepteur à la ryanodine. C'est au cours de ces travaux que les propriétés de la M_{Ca} ont été découvertes. Dès lors plusieurs travaux de thèse ont été menés pour caractériser et découvrir le potentiel de la M_{Ca} et de ses analogues comme vecteur. Les travaux que j'ai conduits au cours de ma thèse sont la suite logique de ces précédents efforts de faire des variants de la M_{Ca} des vecteurs de substances d'intérêt. Ainsi deux variants de la M_{Ca} : la D-M_{Ca} et la M_{Ca}_{UF1,9} ont été choisis pour ma thèse. Comme montré dans des travaux précédents, ces deux variants possèdent chacun des propriétés, des caractéristiques pouvant représenter un avantage lors de leur utilisation. La D-M_{Ca} possède une structure plus importante de par sa taille mais aussi une plus grande stabilité *in vivo* grâce à la présence des ponts disulfures (Poillot et al., 2010). La M_{Ca}_{UF1,9} est quant à elle de petite taille mais a une plus faible stabilité *in vivo*, cependant ce CPP présente une pénétration cellulaire augmentée en milieu acide (Poillot et al., 2012; Tisseyre et al., 2013), ce qui présente un avantage puisque le milieu extracellulaire tumoral possède un pH plus faible que celui du tissu sain.

L'un de mes deux projets de thèse portant sur l'utilisation d'analogues de la M_{Ca} comme vecteurs de substances actives correspond à une étape essentielle pour la poursuite du développement de ces composés. Afin d'évaluer pleinement leurs potentiels nous avons retenu deux anticancéreux : le cisplatine et la doxorubicine pour être couplés aux peptides. Pour ces molécules, nous avons dû avoir recours à des méthodes de couplage non conventionnelles. Contrairement à ce qui est réalisé dans la majorité des cas nous n'avons pas utilisé d'agents de couplage vendus dans le commerce.

Pour les composés à base de platine nous avons reproduit les travaux de Damian et al, en utilisant nos deux vecteurs à base de M_{Ca}. Une fois nos nouveaux vecteurs synthétisés,

nous avons testé leurs efficacités anticancéreuses sur des lignées de glioblastomes animales puis humaines. De façon intéressante seul le composé à base de D-MCa a montré une efficacité comparable à celle du cisplatine. Et les résultats obtenus sur les voies d'apoptose entraînant l'effet toxique du composé, ont mis en évidence un mode d'action différent du cisplatine. Il serait intéressant de poursuivre ces travaux pour comprendre pourquoi le petit variant de la MCa couplé au dérivé de la platine n'est pas actif, et ainsi croiser ces résultats avec ceux obtenus avec les composés à base de doxorubicine et de MCa.

En effet, l'autre versant de ce projet de thèse sur la MCa, portait sur le couplage des deux même variants la D-MCa et la MCa_{UF1,9} à de la doxorubicine via de la chimie click. Cette fois-ci aussi, la méthode de couplage utilisée est innovante. Après avoir modifié chimiquement la doxorubicine et ajouté une fonction alkyne aux vecteurs, nous avons pu réaliser le couplage. Il m'a alors été possible d'évaluer la toxicité de ces composés sur différentes lignées cellulaires. Sur des cellules très sensibles (F-98) à sensibles (MDA-MB 435s) je n'ai pas observé une plus grande efficacité des nouveaux composés synthétisés. J'ai néanmoins observé de façon similaire à ce que Aroui et al avait trouvé, une re-sensibilisation de cellules résistantes à la doxorubicine (MDA-MB-231) (Aroui et al., 2009a, 2009c). Ces résultats sont à nuancer puisque lorsque que l'on change de test incluant non seulement la mort mais aussi le ralentissement / blocage du métabolisme, on ne conserve pas cette re-sensibilisation. Ces travaux sur la vectorisation de la doxorubicine par la MCa sont à poursuivre en étudiant de façon précise les mécanismes d'action des nouveaux composés et en les comparant à ceux de la doxorubicine. Les données sur la pénétration cellulaire des composés ainsi que sur leurs répartitions cellulaires, indiquent que l'on a bien des composés qui pénètrent dans la cellule et qui s'accumulent préférentiellement dans le cytoplasme. Déterminer l'implication de l'inhibition des topoisomérases et des ROS dans la toxicité de ces composés permettrait de savoir si ce changement de répartition se traduit bien par une modification des mécanismes d'action. Il reste encore beaucoup de travail à effectuer *in vitro* et *in vivo* avant de pouvoir pleinement conclure sur la viabilité de telles molécules. Cependant les résultats que j'ai obtenus jusqu'à présent sont encourageants.

La MCa n'est pas la seule toxine qui a fait l'objet de mon attention pendant cette thèse. Mon second projet de thèse portait sur l'administration ciblée d'anticancéreux en utilisant une toxine. La CTX est la première toxine qui a montré des propriétés de ciblage des cellules cancéreuses, la rendant extrêmement intéressante comme agent thérapeutique pour le traitement des cancers. Après avoir identifié plusieurs toxines présentant une homologie de séquence avec la CTX, nous en avons sélectionné trois : la Lqh-8/6, Bs-14 et le lepidopteran sur lesquelles j'ai concentré mes efforts. Outre cette homologie de séquence, ces toxines ont montré des propriétés identiques à celles de la CTX. Lors des tests j'ai montré l'innocuité de ces trois toxines, leurs capacités à pénétrer et diffuser dans le cytoplasme de cellules, ainsi que l'effet anti-invasif de la Lqh-8/6 et du lepidopteran. Ces résultats sont un premier pas dans la caractérisation de ces peptides mais aussi dans la compréhension des propriétés de ciblage de

la CTX et de la Lqh-8/6. Au cours de ces travaux seules les capacités de ciblage de la Lqh-8/6 ont été testées sur des coupes de cerveaux de rats Fisher ayant développés un glioblastome après implantation de cellule F-98. Il serait intéressant de réaliser cette même expérience avec les deux autres toxines et la CTX sur des coupes humaines et de comparer leurs propriétés de ciblage.

Parce que la Lqh-8/6 est l'équivalent de la CTX trouvé chez un scorpion phylogénétiquement le plus proche (Smertenko et al., 2001) et qu'elle présente un effet anti-invasif comparable à la CTX, nous l'avons choisi pour la suite du projet. Après avoir synthétisé une nouvelle Lqh-8/6 azide, j'ai pu, en utilisant la chimie click, lui coupler la doxorubicine alkyne. Les résultats de la toxicité de la Lqh-8/6 doxorubicine sont très encourageants. Il montre un effet toxique du composé qui est certes moindre que celui de la doxorubicine alkyne et de la doxorubicine mais qui est présent. Pour un composé non optimisé, c'est un très bon point de départ.

La Lqh-8/6 doxorubicine et les MCa doxorubicine sont des preuves de concept de l'intérêt de l'utilisation d'un système de couplage « universel » basé sur la chimie click. Les résultats que j'ai obtenus au cours de ma thèse ne sont que les bases d'un tel système. Beaucoup de possibilités sont à présent envisageables à partir de ce système. En effet, en modifiant le cargo couplé à ces toxines, il est possible de passer d'une application thérapeutique à une application plus centrée sur l'imagerie, simplement en remplaçant la doxorubicine par un marqueur fluorescent par exemple. De même, au cours de mes travaux de thèse j'ai travaillé avec la doxorubicine parce qu'elle présente l'avantage d'être fluorescente, ce qui permet de la suivre en microscopie ou au FACS. Mais c'est aussi un anticancéreux qui est souvent utilisé dans la recherche pour tester de nouveaux moyens de vectorisation, ce qui permet d'avoir une base de données importante sur les fonctions chimiques modifiables pour l'adapter à la chimie click. Au vue des données obtenues avec la doxorubicine, concernant la localisation des peptides, il est assez facilement envisageable de remplacer la doxorubicine par un autre anticancéreux ayant un mécanisme d'action principal se situant dans le cytoplasme.

De même, il est aussi possible de poursuivre les travaux menés au cours de ma thèse en optimisant les vecteurs. Une des difficultés dans la prise en charge thérapeutique des cancers et particulièrement pour les glioblastomes est d'arriver à délivrer l'agent anticancéreux aux cellules cancéreuses en touchant le moins possible les tissus sains. L'utilisation de la CTX ou de la Lqh-8/6 permet de réduire l'impact du traitement sur les tissus sains en ciblant les cellules cancéreuses. L'intérêt de l'utilisation d'un CPP comme les analogues de la MCa pour la vectorisation d'anticancéreux repose sur la très bonne rétention cellulaire et tissulaire de ces peptides, ce qui permettrait, associé à une méthode d'administration ciblée, de traiter l'ensemble d'une tumeur en provoquant un minimum de dégâts au tissu sain entourant la tumeur. Maintenant en modifiant ces peptides, en les faisant fusionner pour associer leurs points forts on pourrait alors obtenir un vecteur idéal. De plus, il existe aussi la possibilité d'ajouter à ces vecteurs une séquence d'adressage au noyau afin de passer outre

l'accumulation dans le cytoplasme observé avec la doxorubicine. On n'aurait alors aucune limitation dans le choix de l'anticancéreux à coupler au vecteur.

Les travaux menés au cours de cette thèse confirment le potentiel des toxines animales et montrent l'intérêt des vecteurs peptidiques dans la recherche biomédicale. L'utilisation de ces toxines comme vecteurs de substances d'intérêt permettrait de redonner une seconde vie à des molécules délaissées actuellement car ne correspondant plus aux critères de sécurité des différentes agences du médicament (FDA, EMA, ANSM ...). Mais elle serait aussi un atout pour le développement de nouvelles molécules puisqu'on ne demanderait plus à une seule molécule de posséder de façon intrinsèque toutes les caractéristiques nécessaires à son utilisation chez l'Homme. Il est donc nécessaire de continuer de travailler sur ces projets afin de prendre pleinement conscience du potentiel de ces toxines.

Annexes

Article 1:
**Cell Penetration Properties of a Highly
Efficient Mini Maurocalcine Peptide**

Article publié dans le journal Pharmaceuticals en 2013

Article

Cell Penetration Properties of a Highly Efficient Mini Maurocalcine Peptide

Céline Tisseyre^{1,2,3,†}, Eloi Bahembera^{1,2,3,†}, Lucie Dardevet^{1,2,3}, Jean-Marc Sabatier⁴, Michel Ronjat^{1,2,3} and Michel De Waard^{1,2,4,5,*}

¹ Unité Inserm U836, Grenoble Institute of Neuroscience, Université Joseph Fourier, La Tronche, Chemin Fortuné Ferrini, Bâtiment Edmond Safra, 38042 Grenoble Cedex 09, France

² Labex Ion Channel Science and Therapeutics, Nice, France

³ Université Joseph Fourier, Grenoble, France

⁴ Inserm U1097, Parc scientifique et technologique de Luminy, 163, avenue de Luminy, 13288 Marseille cedex 09, France

⁵ Smartox Biotechnology, Biopolis, 5 Avenue du Grand Sablon, 38700 La Tronche, France

† These authors contributed equally to this work.

* Author to whom correspondence should be addressed; E-Mail: michel.dewaard@ujf-grenoble.fr; Tel.: +33-4-56-52-05-63; Fax: +33-4-56-52-06-37.

Received: 23 February 2013; in revised form: 6 March 2013 / Accepted: 7 March 2013 /

Published: 18 March 2013

Abstract: Maurocalcine is a highly potent cell-penetrating peptide isolated from the Tunisian scorpion *Maurus palmatus*. Many cell-penetrating peptide analogues have been derived from the full-length maurocalcine by internal cysteine substitutions and sequence truncation. Herein we have further characterized the cell-penetrating properties of one such peptide, MCa_{UF1-9}, whose sequence matches that of the hydrophobic face of maurocalcine. This peptide shows very favorable cell-penetration efficacy compared to Tat, penetratin or polyarginine. The peptide appears so specialized in cell penetration that it seems hard to improve by site directed mutagenesis. A comparative analysis of the efficacies of similar peptides isolated from other toxin members of the same family leads to the identification of hadrucalcin's hydrophobic face as an even better CPP. Protonation of the histidine residue at position 6 renders the cell penetration of MCa_{UF1-9} pH-sensitive. Greater cell penetration at acidic pH suggests that MCa_{UF1-9} can be used to specifically target cancer cells *in vivo* where tumor masses grow in more acidic environments.

Keywords: maurocalcine; hadrucalcin; toxin; cell penetrating peptide; F98 cells; glioma; analogs

1. Introduction

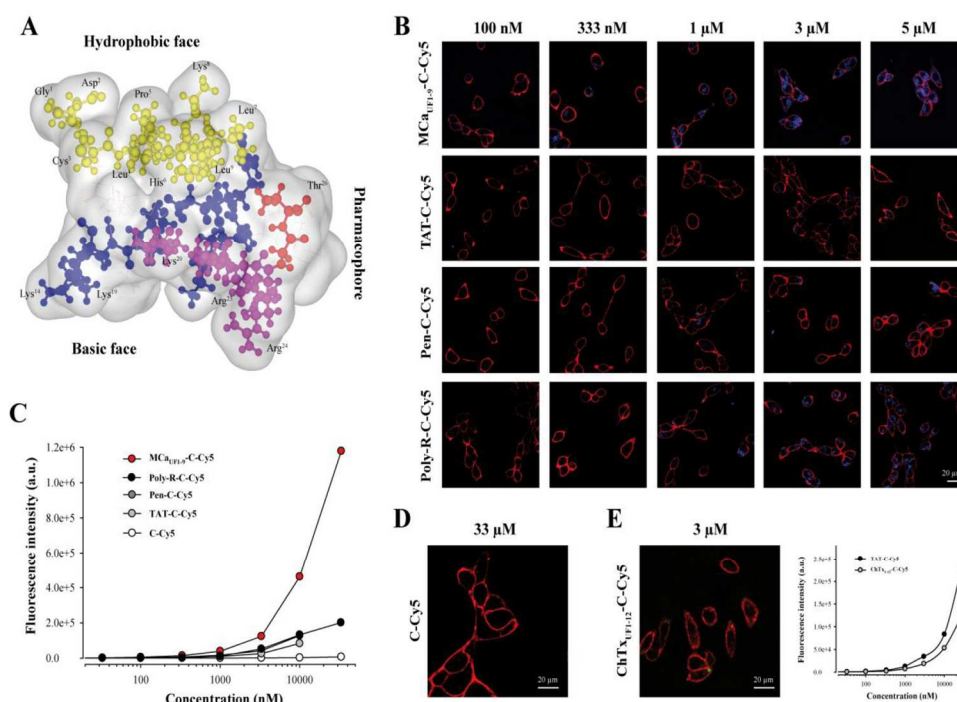
Maurocalcine (MCA) is a 33 amino acid residue peptide that was isolated in 2000 from the venom of the Tunisian chactid scorpion *Scorpio maurus palmatus* [1]. It folds according to an 'Inhibitor Cystine Knot' (ICK) motif [2] and contains three disulfide bridges connected by the following pattern: C₁-C₄, C₂-C₅ and C₃-C₆ [3]. Based on high amino acid sequence and pharmacological target similarities, MCA belongs to a larger family of scorpion toxins that also includes imperatoxin A (from *Pandinus imperator*) [4], opicalcine 1 and opicalcine 2 (from *Opisthophthalmus carinatus*) [5], hemicalcin [6] and hadrucalcin [7]. All these peptides act on ryanodine receptors resulting in pharmacological activation. These receptors are calcium channels located in the membrane of the endoplasmic reticulum. They control Ca²⁺ release from internal stores and therefore a large number of cell functions [7–10]. Binding of MCA on the ryanodine receptor type 1 occurs on protein cytoplasmic domains. Because MCA acts within seconds, once applied to the extracellular medium, it was soon obvious that it had to cross the plasma membrane very efficiently in order to activate the ryanodine receptor [11]. An additional curiosity of MCA lies into the fact that there is an intriguing sequence homology with a domain of the L-type voltage-gated calcium channel from the skeletal muscle (domain A). This channel lies in the plasma membrane, while domain A is found underneath the membrane in the cytoplasm within a loop that has been recognized as extremely important for the process of excitation-contraction coupling [12,13]. While the role of domain A in excitation-contraction coupling is still unclear, it is however surprising and stimulating to observe that peptides containing domain A sequence act with quite a lot of similarities to MCA on the ryanodine receptor type 1 [14,15]. According to the ¹H-NMR solution structure, MCA is rigidly structured by the three disulfide bridges and contains three β-strands, comprising the following stretches of amino acid residues: 9–11 (strand 1), 20–23 (strand 2), and 30–33 (strand 3). MCA has an incredibly stable structure since it cannot be denatured, even at high temperatures up to 100 °C or extreme pH values [16]. Interestingly, the peptide is highly enriched in basic amino acid residues, more than a third of the amino acids being either lysine (seven out of 33) or arginine residues (four out of 33). The histidine residue at position 6 is susceptible, depending of the environmental pH, to introduce an additional positive charge to the peptide by protonation. Interestingly, stretches of positively charged residues seem to confound with the three MCA β-strands. The 3D structure of MCA also strikingly highlights the asymmetrical distribution of the positive charges at its surface: one face is highly basic, while the opposite face is rather hydrophobic. If, in addition, one depicts the amino acid residues important for the ryanodine receptor activation [17], then it appears that the peptide can be schematically represented with three domains: one hydrophobic head that tops the peptide, a larger second face, mainly basic, and a third side domain that contains the pharmacophore (Figure 1A).

Besides its Ca²⁺ channel activity, MCA is also used as a cell-penetrating peptide (CPP). Its properties have been investigated in detail. It was soon discovered that MCA could act as vector for the cell penetration of a variety of cargoes, including proteins [11], peptides [18], small dyes [16,19],

drugs [20–23] or nanoparticles [24,25]. The mechanism of cell penetration most likely includes a combination of membrane translocation (direct passage to the cytoplasm) and endocytosis, mostly macropinocytosis (indirect access to the cytoplasm through leakage from late endosomes) [16,19,26,27].

Figure 1. The hydrophobic domain of MCa is an efficient CPP. **(A)** Schematic representation of MCa 3D structure. The hydrophobic domain (from amino acid residue 1 to 9) is shown on top. Residues are in yellow. Shown also are the basic face (basic amino acid residues are in blue or in pink) and the pharmacophore (residues identified as interacting with the ryanodine receptor are in red or in pink). Pink residues belong both to the pharmacophore and the basic face. **(B)** Confocal microscopy images illustrating the penetration of four different peptides labeled with Cy5 at various concentrations into glioma F98 cells (blue color). Incubation times were 2 h for each peptide/concentration. Images were taken immediately after washout of the extracellular peptide. The plasma membrane is labeled with concanavalin-A-rhodamine (red color). **(C)** Dose-dependent penetration of each peptide-cargo complex in F98 cells as assessed by flow cytometry. A control Cys-Cy5 is also provided. **(D)** Absence of cell penetration of 33 μM Cys-Cy5 (a single Cys residue linked to Cy5—abbreviated C-Cy5) evaluated by confocal microscopy. **(E)** Lack of cell penetration of 3 μM ChTX_{UF1-12}-C-Cy5 as determined by confocal microscopy (right panel). Quantitative analysis of F98 ChTX_{UF1-12}-C-Cy5 fluorescence as determined by flow cytometry. Internalization of the ChTX_{UF1-12}-C-Cy5 peptide is lower than TAT-C-Cy5 but not negligible.

Figure 1



Even if the mechanism(s) of penetration of CPP are subject to debate [28,29], because of the rapidity of action of MCa on the ryanodine receptor, it appears clearly that one way of penetration of

MCa can be membrane translocation. Furthermore, MCa has the ability to bind onto glycosaminoglycans, including heparin and heparan sulfates, with micromolar affinity. However, cell penetration still occurs according to both mechanisms of penetration in cells devoid of glycosaminoglycans, suggesting that glycosaminoglycans do not preferentially direct MCa's cell penetration towards endocytosis [26]. In contrast, these cell surface receptors appear to be helpful as peptide sinks for increased peptide delivery into cells. More relevant to cell penetration is the fact that MCa binds to a number of membrane lipids, mostly negatively charged ones [26,27], as observed for other CPP [28]. Binding seems to occur with higher affinity (100 nM) in close agreement with the concentration of MCa required for cell penetration. In addition, MCa analogues that penetrate better than wild-type MCa also exhibit a greater affinity for membrane lipids and *vice versa*. Endocytosis becomes predominant with some large cargoes. Conversely, small cargoes seem to have less interference with a translocation mode of entry of CPP. These observations tend to indicate that endocytosis may become the preferential mode of cell entry of MCa if coupled to bulky cargoes that are expected to increase the duration of residency at the plasma membrane. However, although MCa is an extremely efficient vector for cell penetration of impermeable cargoes, it is of limited usefulness in its native conformation. Indeed, complex disulfide bridging may hamper the attachment of some cargoes. The size of the CPP is greater than those used in the literature. Finally, the native pharmacological activity is generally undesirable for most applications, so like other CPPs before, modification of the native MCa was made in order to ease its use *in vivo* as a new delivery system [30]. Canceling MCa's pharmacological activity turned out to be quite simple due to the fact that structural requirements involved in binding onto the ryanodine receptor are more stringent than for cell penetration. Several chemical strategies turned out to be successful including point mutations [17], blocking MCa's folding by preventing disulfide bridge formation [18], and producing a D-diastereomer MCa [16]. The second strategy had the advantage to produce a MCa analogue that was simpler to produce since the oxidation/folding step was no longer necessary. However, the resulting peptide turned out to be slightly less efficient in cell penetration than the folded/oxidized MCa, indicating that the correct positioning in space of the various structural determinants of MCa is important to optimize cell penetration. In addition, the unfolded MCa CPP was still thirty three amino acid residues in length. Quite recently, in an attempt to further delimitate the cell penetrating properties of MCa to smaller sequences, a number of unfolded truncated MCa-derived peptides were synthesized and assessed for cell penetration properties [19]. Surprisingly, all truncated peptides turned out to be more efficient than the unfolded full-length MCa for cell penetration, suggesting that each structured domain within the folded/oxidized MCa may provide a specific contribution to the cell penetration of the wild-type peptide. The shortest peptides were nine residues in length and included both the N-terminal and the C-terminal sequences. One of the peptides, MCa_{UF1-9}, stood out as atypical since the net charge of the peptide was 0 and its cell penetration properties differed to some extent from the significantly more basic other MCa-derived truncated peptides. Penetration of this peptide occurred at polarized ends of CHO cells. The peptide also showed greater residency times within the plasma membrane. Its penetration did not rely at all on macropinocytosis for cell entry (at least when coupled to a dye as cargo). Finally, penetration of this peptide occurs at lower extracellular concentrations than the more basic peptides derived from MCa [19]. Altogether the properties of MCa_{UF1-9} seemed interesting enough to warrant a more in-depth investigation of its cell penetration properties. We therefore

compare herein the properties of this peptide to well-reputed CPP (Tat, penetratin and poly-R) or analogous peptides derived from other toxins of the calicin family. We investigated the properties of a number of point mutated M_{CaUF1-9} analogues, and more specifically the pH-sensitivity of its penetration in order to design pH-sensitive CPP. The data point to new very powerful CPP with unprecedented efficacies and demonstrate the pH-sensitivities of several of our analogues for cell penetration.

2. Results and Discussion

2.1. A Peptide Derived from the Hydrophobic Face of M_{Ca} Behaves as a Highly Competitive CPP

A schematic representation of M_{Ca} illustrates that the amino acid sequence 1 to 9 tops the rest of the peptide (yellow residues) and defines an independent more hydrophobic face (Figure 1A). The opposite side of the peptide is highly basic (blue and pink residues) and defines therefore a basic face. Some of the residues involved in binding onto the ryanodine receptor have been defined in the past [17]. They include important residues such as Arg²³ and Arg²⁴ and define the pharmacophore side (residues in red and in pink). Therefore the pharmacophore and basic regions overlap to some degree.

We compared the efficacy of M_{CaUF1-9} for cell penetration within the glioma rat cell line F98 to other very popular peptides, comprising TAT, penetratin (Pen) and poly-Arg (poly-R). All peptides included an additional C-terminal Cys residue that was labeled with the Cy5 fluorochrome which served the purpose of cargo in this study. Of note, the extra Cys residue in M_{CaUF1-9}-C-Cy5 is at its natural position as in the folded/oxidized M_{Ca} (Cys¹⁰) where it is linked to Cys²¹ by a disulfide bridge. In contrast, Cys³ of M_{CaUF1-9} was replaced by an isosteric 2-aminobutyric acid (Abu) residue to avoid mislabeling by Cy5 in the middle of the sequence. A series of confocal microscopy images were taken immediately after a 2 h incubation of F98 cells with various concentrations of the four peptides tested (M_{CaUF1-9}-C-Cy5, TAT-C-Cy5, Pen-C-Cy5 and poly-R-C-Cy5). As shown, cell penetration of M_{CaUF1-9}-C-Cy5 is perceptible at concentrations as low as 100 nM, whereas none of the other peptides showed penetration at this concentration (Figure 1B). Penetration was then dose-dependent for all peptides. It was more marked at 333 nM for M_{CaUF1-9}-C-Cy5 and started to show up for Poly-R-C-Cy5, while still absent for TAT-C-Cy5 and Pen-C-Cy5. At 1 μM all peptides showed some degree of penetration, the least efficient peptide being TAT-C-Cy5. At 5 μM, F98 cells incubated with TAT-C-Cy5 showed levels of fluorescence that were more or less comparable to those obtained with M_{CaUF1-9}-C-Cy5 at 333 nM. These data qualitatively indicated that M_{CaUF1-9}-C-Cy5 behaved better than those three popular CPP as far as F98 cells are concerned. Similar results were obtained with CHO cells indicating that these differences in performances between the four peptides do not depend on the cell type studied (data not shown). With regard to cell distribution of the peptides, we did not notice any obvious differences in distribution suggesting that the peptides may all borrow the same mechanisms of cell penetration. However, a more complete investigation on this issue is needed before one comes to a firm conclusion. To more quantitatively compare the CPP, we investigated fluorescence levels by flow cytometry (Figure 1C). The data confirmed the confocal microscopy analyses showing that M_{CaUF1-9}-C-Cy5 behaves more potently than other CPP. The following order of penetration efficiency was observed: M_{CaUF1-9}-C-Cy5 >> Poly-R-C-Cy5 = Pen-C-Cy5 > TAT-C-Cy5. At 10 μM, M_{CaUF1-9}-C-Cy5

penetrates 5.5-fold better than TAT-C-Cy5, 3.6-fold better than Pen-C-Cy5, and 3.5-fold better than Poly-R-C-Cy5.

2.2. Randomly Defined Control Peptides Delimit the Threshold Level of an Acceptable Cell Penetration

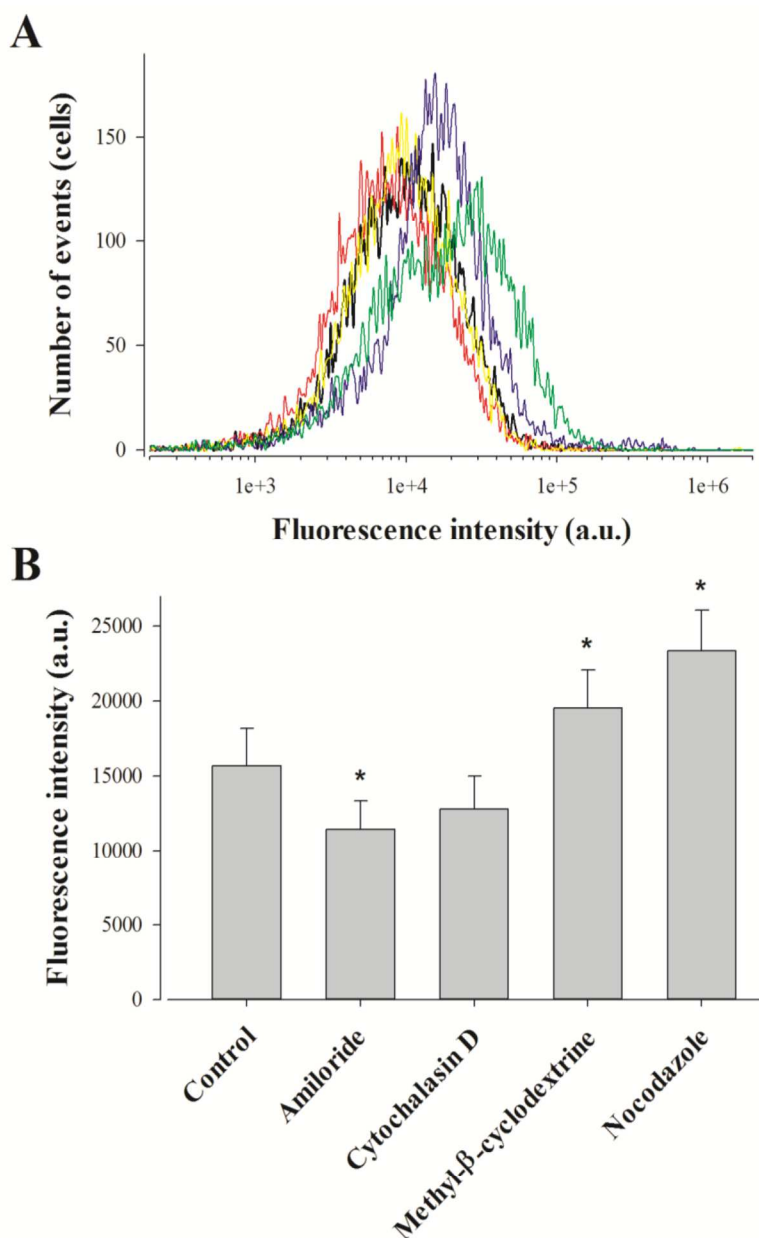
Our data also illustrate that the control linker-cargo, a single Cys residue linked to Cy5 (C-Cy5), does not penetrate at all into F98 cells (at concentrations up to 33 μM), demonstrating the peptide specificity of cell entry (Figure 1C and D). Another control was also tested, based on a fragment of charybdotoxin (ChTx), a voltage-gated potassium channel blocker, not known previously for cell penetration aptitude. The peptide encompasses the 12 first amino acids of ChTx. Internal Cys residues were replaced by Abu, an additional Cys residue was added at the C-terminus and the resulting peptide labeled with Cy5 as well to yield ChTx_{UF1-12}-C-Cy5. Confocal microscopy images do not show any evidence of cell penetration if F98 cells are incubated 2 h with 3 μM ChTx_{UF1-12}-C-Cy5 (Figure 1E). However, if a more sensitive and quantitative approach is taken to examine the levels of fluorescence, it becomes obvious that F98 cells take up a defined amount of ChTx_{UF1-12}-C-Cy5. This is unlikely to represent the level of binding of this peptide to some cell-surface potassium channels as this fragment is not known to bind potassium channels. In contrast, it may indicate the propensity of some cell types to internalize peptides that present even low affinity for the plasma membrane. A comparison with our least-performing peptide TAT-C-Cy5 indicates that ChTx_{UF1-12}-C-Cy5 is less efficient than TAT-C-Cy5, although significant. At 10 μM , the cell entry of this non-conventional CPP is 1.57-fold less than TAT. These findings may question the relevance of some studies reporting the discovery of “new” CPP or alternatively may suggest that ChTx_{UF1-12} can also be considered as a poorly performing CPP.

2.3. Pharmacological Blockade of Endocytosis in F98 Cells Affects Poorly M_{CaUF1-9} Cell Entry

Punctiform distribution of M_{CaUF1-9}-C-Cy5 may be interpreted as a cell entry that is mainly based on a form of endocytosis. This point was assessed by FACS analyses using various drugs at the 2 h cell entry timepoint of 1 μM M_{CaUF1-9}-C-Cy5 in F98 cells. We tested amiloride, a macropinocytosis inhibitor, methyl- β -cyclodextrin to deplete membrane cholesterol and inhibit lipid raft-dependent pathways, nocodazole to prevent microtubule formation, and cytochalasin D to stop F-actin elongation, required for macropinocytosis and clathrin-dependent endocytosis [31]. Amiloride only affected M_{CaUF1-9}-C-Cy5 cell entry in F98 cells very mildly, with an average inhibition of 27% indicating an entry partly based on macropinocytosis (Figure 2).

The 18.5% inhibition observed by cytochalasin D, while being non-significant, was in agreement with the contribution of macropinocytosis to the cell entry of the peptide. Quite surprisingly, both methyl- β -cyclodextrin and nocodazole produced 24.7 and 48.9% increases in the cell entry of M_{CaUF1-9}-C-Cy5. The lack of inhibition by methyl- β -cyclodextrin indicates that caveolae-mediated endocytosis is not involved in the entry of this peptide. The observed increase in cell penetration may indicate on the contrary that one preferential route of cell entry by translocation may be in lipid rafts. Preventing the loss of lipid rafts by blocking endocytosis at this level would increase the surface area devoted to lipid rafts and hence peptide entry.

Figure 2. Effect of endocytosis inhibitors on $\text{MCA}_{\text{UF1-9}}$ peptide penetration in F98 cells. (A) Representative FACS data showing the effect of amiloride (red curve), cytochalasin D (yellow curve), methyl- β -cyclodextrine (blue curve) and nocodazole (green curve) on 1 μM $\text{MCA}_{\text{UF1-9}}$ -C-Cy5 cell entry (black curve). (B) Average fluorescence intensities for the cell entry of 1 μM $\text{MCA}_{\text{UF1-9}}$ -C-Cy5 in F98 cells without and with endocytosis inhibitors. * $p \leq 0.1$.

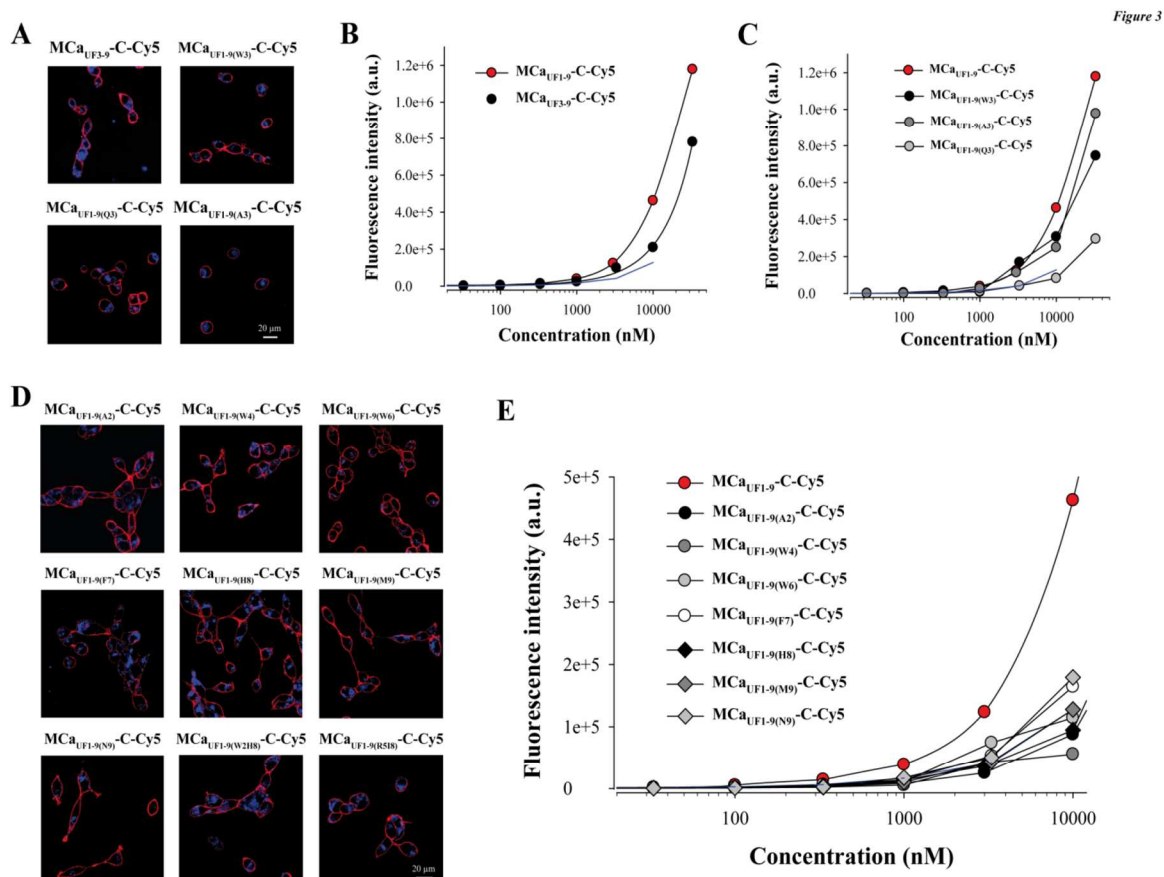


Similarly, it is possible that microtubules hinder cell penetration explaining why blocking their formation may help peptide entry to this large extent. These observations demonstrate that while the intracellular distribution of $\text{MCA}_{\text{UF1-9}}$ -C-Cy5 in F98 cells looks punctiform, this is not necessarily the consequence of a cell entry by endocytosis.

2.4. Point Mutation of MCa_{UF1-9} Fails to Optimize The Cell Penetrating Properties of This Peptide

Next, we attempted to design a number of MCa_{UF1-9} peptide analogues in order to get some hints on what structural determinants may be important for the efficacy of this peptide in cell penetration. At the N-terminal side of Cys³ (replaced by Abu) of MCa_{UF1-9} , there are two residues that appear of minor importance (Gly¹ and Asp²). Removing these two residues yields MCa_{UF3-9} . As shown, MCa_{UF3-9} -C-Cy5 still accumulates very well in F98 cells (Figure 3A,B).

Figure 3. Structural determinants of MCa_{UF1-9} peptide penetration. (A) Confocal images illustrating the penetration of 3 μ M MCa_{UF3-9} -C-Cy5, $MCa_{UF1-9(W3)}$ -C-Cy5, $MCa_{UF1-9(Q3)}$ -C-Cy5 or $MCa_{UF1-9(A3)}$ -C-Cy5 into F98 cells. 2 h incubation time before washout and imaging. (B) Effect of N-terminal peptide truncation on cell penetration efficacy of MCa_{UF1-9} -C-Cy5 as assessed by flow cytometry. (C) Effect of point mutation at position 3 on the cell penetration efficacy of MCa_{UF1-9} -C-Cy5. (D) Confocal images illustrating the penetration of 3 μ M single or double point mutated MCa_{UF1-9} -C-Cy5 peptide into F98 cells. (E) Effect of single point mutations on the cell penetration efficacy of MCa_{UF1-9} -C-Cy5 as assessed by flow cytometry.



At the quantitative level, there was a 1.25-decrease in cell penetration efficacy at 3 μ M, indicating that these two residues were most likely not essential for cell penetration. This deletion brings the size of this efficient CPP down to seven amino acid residues which is remarkably short. At position 3 of the

wild-type M_{Ca} there is normally a Cys residue that engages itself into a disulfide bridge. The lateral chain of this residue is therefore not exposed towards the outside face of the molecule and is unlikely to play a role in cell penetration. M_{Ca}_{UF1-9} contains an Abu residue instead of a Cys residue and the peptide is quite efficient for cell penetration. We nevertheless probed this position by replacing the Abu residue by Trp, Gln or Ala. As shown, none of these replacements at position 3 within M_{Ca}_{UF1-9}-C-Cy5 hindered the cell penetration of these analogues (Figure 3A). At 3 μ M, M_{Ca}_{UF1-9(W3)}-C-Cy5 penetrated 1.36-fold better than M_{Ca}_{UF1-9}-C-Cy5, while M_{Ca}_{UF1-9(A3)}-C-Cy5 penetrated 1.08-fold less well, indicating little variations (Figure 3C). In contrast, when Gln was put at position 3 in the sequence, the resulting M_{Ca}_{UF1-9(Q3)}-C-Cy5 peptide behaved similarly to TAT but 2.94-fold less well than M_{Ca}_{UF1-9}-C-Cy5 suggesting that a Gln may hinder the cell penetration process. Next, we made a series of single (seven peptide) or double (two peptide) point mutated analogues to probe the functional importance of these M_{Ca} residues. As shown, all mutated M_{Ca}_{UF1-9}-C-Cy5 analogues produced evident cell penetration at 3 μ M, indicating that none of the substitutions were powerful enough to fully prevent cell penetration (Figure 3D). However, according to flow cytometry analyses, none of the mutated peptides performed better than M_{Ca}_{UF1-9}-C-Cy5 (Figure 3E). Taking TAT-C-Cy5 as a standard, M_{Ca}_{UF1-9(A2)}-C-Cy5, M_{Ca}_{UF1-9(W4)}-C-Cy5 and M_{Ca}_{UF1-9(H8)}-C-Cy5 behaved slightly less well. In contrast, M_{Ca}_{UF1-9(F7)}-C-Cy5 and M_{Ca}_{UF1-9(M9)}-C-Cy5 still behaved better than TAT-C-Cy5. Double mutants (M_{Ca}_{UF1-9(W2H8)}-C-Cy5 and M_{Ca}_{UF1-9(R5I8)}-C-Cy5 were also closely similar to TAT-C-Cy5 (not shown). Overall, these data indicate that M_{Ca}_{UF1-9} peptide has been optimized for cell penetration with many amino acid residues playing an important role for cell entry. At this stage it would be difficult to point to one single residue as being more important than another one within the sequence.

2.5. Analogous Hydrophobic Domains of Other Toxin Members of the Calcin Family Are Also Excellent CPP

The inability to produce M_{Ca}_{UF1-9} peptides with greater cell penetration efficacies tends to indicate that sequence variation of this hydrophobic domain needs to be considered more cautiously to design optimized peptides. Interestingly, M_{Ca} belongs to a larger family of peptides that have, most of them, never been assessed for cell penetration. Results have been presented indicating that imperatoxin A also behaves as a CPP [32]. All these peptides are structured similarly to M_{Ca}, with a similar hydrophobic face topping a more basic face (Figure 4A). All peptides that have been tested are also active on the ryanodine receptor [6,7,33], indicating the presence of a similar pharmacophore. A close examination of the amino acid sequence of the hydrophobic domain reveals only minor sequence diversity among these peptides (Figure 4B). The nine first residues of hemicalcin are identical to M_{Ca}. Imperatoxin A, opicalcin 1 and opicalcin 2 differ from M_{Ca} only by residue 9 (an arginine instead of a leucine residue).

The most differing peptide sequence is the one derived from hadrucalcin with two extra N-terminal residues. Interestingly, the sequence SerGluLys replaces the Gly¹ residue of M_{Ca}, but Asp² of M_{Ca} is conserved. Also, four internal substitutions are noticeable. Leu⁴, Pro⁵, Lys⁸ and Leu⁹ of M_{Ca} are substituted by Iso, Lys, Gln and Arg, respectively. Finally, Had_{UF1-11} has an additional basic amino acid compared to M_{Ca}_{UF1-9}. We next evaluated the ability of these peptides to accumulate into F98 cells. At 1 μ M, it was obvious, according to confocal imaging, that Imp_{UF1-9}-C-Cy5 (equivalent to

Opi_{UF1-9}-C-Cy5 or Opi_{2UF1-9}-C-Cy5) is less efficient for cell penetration than MCa_{UF1-9}-C-Cy5 and Had_{UF1-11}-C-Cy5 (Figure 4D). Interestingly, a similar deletion of the two first amino terminal residues of Had_{UF1-9}-C-Cy5 yielded a peptide, MCa_{UF3-11}-C-Cy5 with excellent penetration capabilities. Evaluation of dose-dependent penetration by flow cytometry demonstrated that Imp_{UF1-9}-C-Cy5 penetrates quantitatively in a similar way than TAT-C-Cy5. For the first time, we also show that Had_{UF1-11}-C-Cy5 and Had_{UF3-11}-C-Cy5 both penetrate better than MCa_{UF1-9}-C-Cy5 (Figure 4C).

Figure 4. Cell penetration properties of the hydrophobic domains of toxins from the calcin family. **(A)** Real or modeled 3D structures of MCa (PDB access code 1C6W), imperatoxin A (access code 1IE6), hemicalcin (model), opicalcin 1 (model), opicalcin 2 (model) and hadrucalcin (model). Residues in blue describe the hydrophobic domain investigated in this study. Red residues are all amino acids that differ from MCa's amino acid sequence. Residues in green are cystine residues. **(B)** Amino acid sequences of the hydrophobic domains of each member of the calcin family. The third Cys residue is systematically replaced by Abu in our synthetic peptides and is represented in grey color. Residues in blue are those that differ from MCa_{UF1-9} amino acid sequence. This sequence alignment defines three groups of peptides with similar N-terminal sequences. **(C)** Comparative cell penetration efficacies of the peptides derived from members of the calcin family as assessed by dose-response curves from flow cytometry data. TAT-C-Cy5 data are indicated by a blue dashed line for comparison. **(D)** Confocal images illustrating the cell penetration of each peptide of the calcin family after incubation of 1 μ M of the peptides with F98 cells during 2 h. A significantly lower cell penetration is observed for Imp_{UF1-9}-C-Cy5 compared to the two hadrucalcin-derived peptides (Had_{UF1-11}-C-Cy5 and Had_{UF3-11}-C-Cy5).

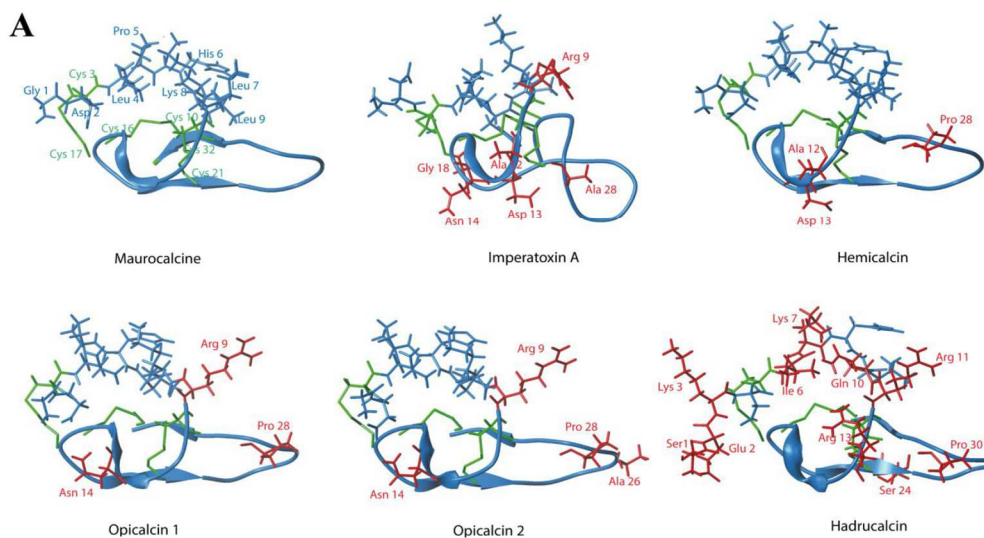
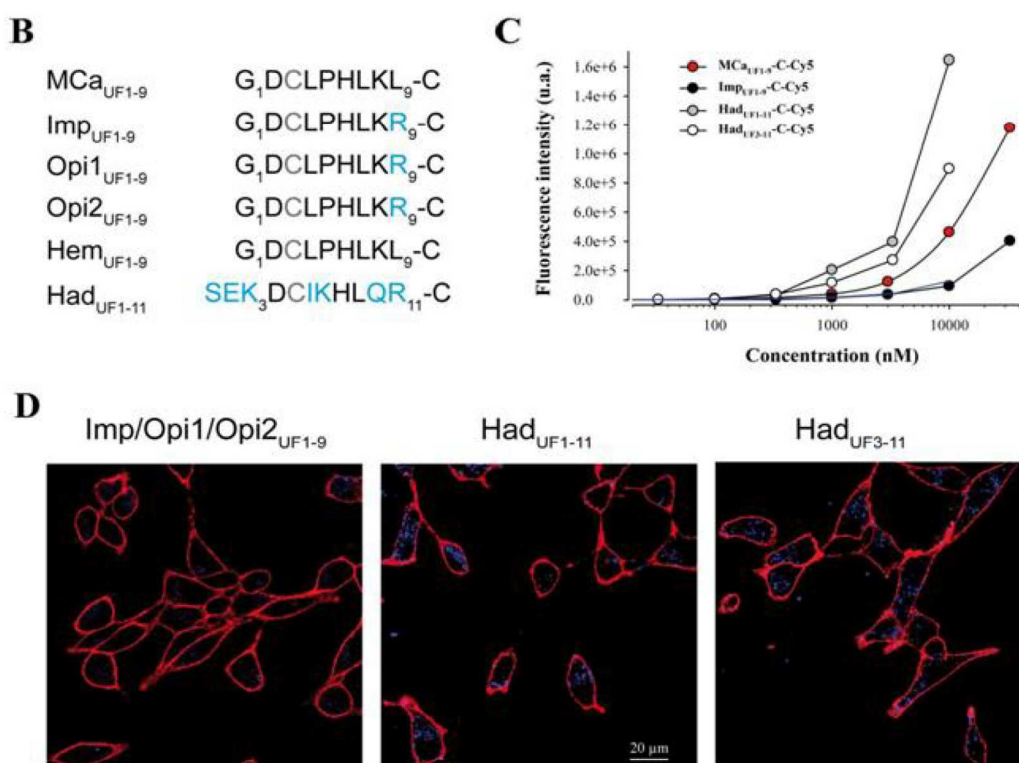


Figure 4. Cont.



This indicates that a series of very selective set of amino acid substitutions are required to improve MCa_{UF1-9} cell penetration properties. They also demonstrate that the calxin family can accommodate some variation in cell penetration efficacy for the activation of the ryanodine receptor. Nevertheless, it remains to be investigated whether the additional basic face and pharmacophore region are necessary to improve the characteristics of cell penetration of imperatoxin A, opicalcin 1 or opicalcin 2. In any case, it is obvious that Had_{UF1-11} is a remarkable cell penetration peptide by the extent of its efficacy compared to the popular peptides challenged in Figure 1.

2.6. Cell Penetration of MCa_{UF1-9} is pH-sensitive Owing to the Presence of an His Residue in its Amino Acid Sequence

Close examination of the amino acid sequence of MCa reveals that it contains a histidine residue at position 6. This residue is therefore also present in MCa_{UF1-9}. According to Figure 2 data, this histidine residue contributes to some extent to the cell penetration efficacy of MCa_{UF1-9}-C-Cy5. The imidazole sidechain of histidine has a pKa of approximately 6.0, while overall the pKa of the amino acid is 6.5. However, this value is susceptible to be influenced by the direct amino acid environment of this residue. In any case, it can be considered that at physiological conditions, relatively small changes in pH value is susceptible to alter the average charge of MCa_{UF1-9}. At a pH value lower than 6, the imidazole ring is essentially protonated. Protonation of the His residue at position 6 may affect the cell penetration efficacy of MCa_{UF1-9}-C-Cy5. To test this idea, the extracellular pH value was varied between 5.0 and 8.0 during the 2 h incubation of F98 cells with MCa_{UF1-9}-C-Cy5 and the total

accumulated fluorescence level evaluated by FACS. The data were normalized to the value at pH 5.0. As shown, decreasing pH values results in higher fluorescence values and therefore greater accumulation of the peptide in F98 cells (Figure 5A).

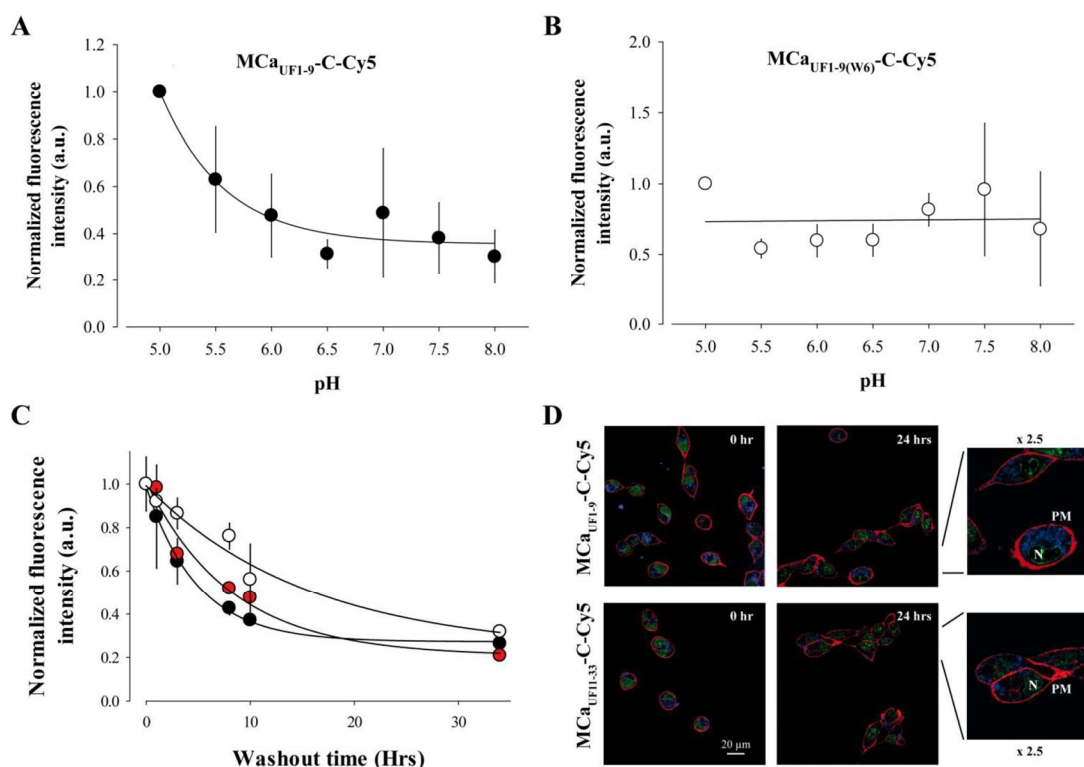
A fit of the data with a decreasing exponential suggests that the peptide enters into F98 cells with a 2.8-fold lower efficacy than at acidic pH values. Half of this decrease in efficacy occurs for a variation in pH from 5.0 to 5.7 indicating that the pKa value of this histidine residue within $\text{MCA}_{\text{UF1-9}}\text{-C-Cy5}$ may be close to 5.7. The involvement of His⁶ in this pH-dependence of the cell penetration of the peptide is demonstrated by the lack of pH-dependence in cell penetration of the mutant peptide $\text{MCA}_{\text{UF1-9(W6)}}\text{-C-Cy5}$ in which His⁶ is replaced by Trp⁶ (Figure 5B). Overall, these data indicate that protonation of His⁶, provided by acidic environments, results in improved $\text{MCA}_{\text{UF1-9}}\text{-C-Cy5}$ cell delivery. In that respect, it is important to note that F98 cells are from rat glioma and that the extracellular pH within the glioma tumors masses in the brain has been predicted to be acidic [34]. Our finding therefore suggests that the $\text{MCA}_{\text{UF1-9}}$ peptide may be useful to more specifically deliver anti-tumor drugs within glioma.

2.7. Long-Lasting Cell Retention of $\text{MCA}_{\text{UF1-9}}$

One property of CPP is that they enter quite rapidly into cells. However, the persistence of their intracellular accumulation is seldom looked after. We investigated this question with three peptides. We used $\text{MCA}_{\text{UF1-9}}\text{-C-Cy5}$, a non or poorly charged peptide depending on the protonation level of His⁶, $\text{MCA}_{\text{UF11-33}}\text{-C-Cy5}$, a highly charged peptide mainly encompassing the two C-terminal thirds of MCA , and $\text{Had}_{\text{UF3-11}}\text{-C-Cy5}$ which is less hydrophobic than $\text{MCA}_{\text{UF1-9}}\text{-C-Cy5}$. One could expect that hydrophobic peptides may more readily escape from the cell interior than charged peptides. To test this idea, F98 cells were loaded 2 h with 1 μM of each of these peptides, extensively washed, maintained in culture for a variable duration (between 0 and 34 h, washout time), treated with trypsin and the fluorescence level remaining in the cells estimated by FACS (Figure 5C).

As shown and quite remarkably, the fluorescence levels of the accumulated peptides fade away only slowly with time indicating that the cell entry of the peptides are faster than their cell exit (Figure 5C,D). Time constant of half exit were estimated to be 5 h for $\text{MCA}_{\text{UF1-9}}\text{-C-Cy5}$, 8 h and 20 min for $\text{MCA}_{\text{UF11-33}}\text{-C-Cy5}$ and 16 h and 40 min for $\text{Had}_{\text{UF3-11}}\text{-C-Cy5}$. After 34 h, cells still contained 27, 21 and 23% of $\text{MCA}_{\text{UF1-9}}\text{-C-Cy5}$, $\text{MCA}_{\text{UF11-33}}\text{-C-Cy5}$ and $\text{Had}_{\text{UF3-11}}\text{-C-Cy5}$ fluorescence, respectively. These values are suspected to be higher in fact since 34 h is enough to register at least one cell division cycle. This property of persistence indicates that $\text{MCA}_{\text{UF1-9}}$, but also $\text{MCA}_{\text{UF11-33}}$ and $\text{Had}_{\text{UF3-11}}$, can be used both as CPP and retention agents for drugs that may freely enter into cells but would also freely escape from them. We have previously used such a property to fight against chemo-resistance of the breast tumor cell line MDA-MB-231 by coupling doxorubicin to a non-folded version of MCA [20,22,23]. Confocal microscopy images of the cell distribution of both peptides tested indicate that the distribution of the peptides does not evolve with washout time (Figure 5D). The distribution remains mostly punctiform (with an evolution towards what may seem smaller dots), internal and hardly invades the nucleus.

Figure 5. pH-dependence and persistence of the cell penetration of $\text{MCA}_{\text{UF1-9}}\text{-C-Cy5}$. **(A)** Effect of extracellular pH variation on the cell penetration efficacy of $1 \mu\text{M}$ $\text{MCA}_{\text{UF1-9}}\text{-C-Cy5}$ in F98 cells (2 h incubation). Mean of $n = 3$ experiments \pm S.D. Mean FACS results were normalized before averaging. Data were fitted by a decreasing exponential of the type $y = y_0 + a.e^{-bx}$ where $y_0 = 0.36 \pm 0.05$, $a = 0.64 \pm 0.09$ and $b = 1.76 \pm 0.61$. **(B)** Effect of extracellular pH variation on the cell penetration of $1 \mu\text{M}$ $\text{MCA}_{\text{UF1-9}}(\text{W6})\text{-C-Cy5}$ in F98 cells (2 h incubation). The pH-insensitive Trp^6 replaces the pH-sensitive His^6 in this mutant peptide. **(C)** Persistence of the fluorescence signal in F98 cells preincubated 2 h with $1 \mu\text{M}$ $\text{MCA}_{\text{UF1-9}}\text{-C-Cy5}$ (net charge 0 if His^6 is unprotonated, black symbol), the positively charged $\text{MCA}_{\text{UF11-33}}\text{-C-Cy5}$ (net charge +7, red symbol) or the mildly charged $\text{Had}_{\text{UF3-11}}\text{-C-Cy5}$ peptide (net charge +2 if His^8 is unprotonated, white symbol). FACS results were normalized to 1 at $t=0$ min at the start of the washout of the CPP. Data were fitted with a decreasing exponential function with $1/\tau = 0.20 \pm 0.01 \text{ h}^{-1}$ ($\text{MCA}_{\text{UF1-9}}\text{-C-Cy5}$), $0.12 \pm 0.03 \text{ h}^{-1}$ ($\text{MCA}_{\text{UF11-33}}\text{-C-Cy5}$) et $0.06 \pm 0.02 \text{ h}^{-1}$ ($\text{Had}_{\text{UF3-11}}\text{-C-Cy5}$), where τ is the time constant of the decrease in the mean cell fluorescence level. The non-decreasing fraction of fluorescence was equal to 0.27 ± 0.14 ($\text{MCA}_{\text{UF1-9}}\text{-C-Cy5}$), 0.21 ± 0.07 ($\text{MCA}_{\text{UF11-33}}\text{-C-Cy5}$) and 0.23 ± 0.13 ($\text{Had}_{\text{UF3-11}}\text{-C-Cy5}$). **(D)** Corresponding confocal images illustrating that the intracellular distribution of the peptides did not change with time. The 2.5-fold image enhancement also shows a close to complete lack of nucleus invasion by the peptides. The images also show that the two peptides do not differ in the type of intracellular distribution 3.5 h after washout of the extracellular peptides.



2.8. Discussion

While all M_{Ca} truncations and/or disruptions of disulfide bridges produce a loss of the 3D structure, M_{Ca}_{UF1-9} is more susceptible than other truncated peptides to preserve some of the structural characteristics that it may possess within the full-length M_{Ca} as it encloses by itself the entire hydrophobic face of M_{Ca}. At this stage, one may only speculate as to why M_{Ca} presents one hydrophobic face diametrically opposite to a highly charged basic face. It may present a strong advantage for the peptide if it has to deal with both a hydrophilic environment (extracellular space and cytoplasm) and a hydrophobic one (membrane lipids). Besides it may be essential to the mechanism of cell translocation if the peptide needs to cope with the amphiphilic nature of membrane lipids. The strong dipole moment of the peptide, resulting from the existence of these two different faces, probably orients the peptide in its interaction with the plasma membrane. The highly basic nature of M_{Ca} should also speed up the peptide entry through electrochemical attraction if one considers that it diffuses freely through the plasma membrane, in a similar way that Na⁺ or Ca²⁺ ions would do when permeating through adequate ion channels while attracted by the inside negative membrane potential. Such a mechanism, if proven, would result in peptide accumulation against the concentration gradient. What the effect of a physical separation between these two peptide entities (hydrophobic face and basic face) might be on the cell penetration mechanism remains however unclear. One may notice at this point that M_{Ca}_{UF1-9}-C-Cy5 and M_{Ca}_{UF11-33}-C-Cy5 produce quite similar intracellular punctiform distributions in F98 cells arguing that they share nonetheless similar mechanisms of cell penetration. This was also the case for the other CPP investigated in this study (poly-R-C-Cy5, Tat-C-Cy5 and Pen-C-Cy5). It is of interest to note however that the cell distribution of fluorescent D-M_{Ca}, a full-length and well-structured analogue of M_{Ca}, is mostly diffuse [16] suggesting that combining the hydrophobic and basic faces of the molecule to shorten the residency time in the plasma membrane may represent a significant advantage in cell penetration.

The most interesting information that we could gather from our mutagenesis program of M_{Ca}_{UF1-9}-C-Cy5 was that the two first amino acid residues were the most dispensable for its penetration properties. This truncation approach led to the design of a 7-mer CPP that has greater potency than most popular CPPs on the market. Investigating the cell penetrating properties of peptides derived from the hydrophobic face of other peptides members of the calcin family turned out as a more interesting approach than mutagenesis. Most of these peptides differ by only a few amino acid residues, with the notable exception of hadrucalcin. Coherent with the mono-substitution we performed at amino acid 9 of M_{Ca}_{UF1-9}-C-Cy5, the cell penetration properties of Imp_{UF1-9}-C-Cy5, Opi1_{UF1-9}-C-Cy5 and Opi2_{UF1-9}-C-Cy5, all presenting Arg⁹ instead of Leu⁹, were reduced to some extent compared to M_{Ca}_{UF1-9}-C-Cy5. Remarkably, multiple amino acid substitution as demonstrated within Had_{UF1-11}-C-Cy5 resulted in an important and unexpected improvement of cell penetration. Similarly to M_{Ca}_{UF1-9}-C-Cy5, removing the two first N-terminal amino acid residues of Had_{UF1-11}-C-Cy5 produced a peptide with quite significant levels of cell penetration. The core of the sequence, the one we assume to be important for cell penetration (after Abu³ in M_{Ca}_{UF1-9}), contains no less than 4 substitutions (Leu⁴ by Ile, Pro⁵ by Lys, Lys⁸ by Gln, and Leu⁹ by Arg). This indicates that quite elaborate alterations need to be done to M_{Ca}_{UF1-9} sequence to further improve its cell penetrating properties. In any case, these findings (i) define a novel CPP with unprecedented efficacy, and (ii)

open the door for the design of hadrucalcin/MCa chimeras 1 μ M M $\text{Ca}_{\text{UF1-9}}$ -C-Cy5 fluorescence at any given concentration and never in terms of starting concentration at which cell entry was observed. These observations suggest that the affinity of these peptides for plasma membrane components remains unaltered.

Since we are interested in developing a number of applications in oncology for MCa analogues, we also investigated the role of His⁶ in cell entry into the glioma F98 cells. Of great interest for future applications, we found that protonation of His⁶, occurring at more acidic pH, but in a range compatible with pH values observed in glioma, produced a three-fold more potent peptide for cell penetration. We assume that protonated His⁶ may form a salt bridge with Asp² in the non-structured M $\text{Ca}_{\text{UF1-9}}$. It is likely that, without this salt bridge, the negative charge carried by Asp² may disfavor cell penetration of M $\text{Ca}_{\text{UF1-9}}$. This observation on the importance of protonation in peptide cell penetration will be useful for the future design of new MCa analogues in which important basic amino acid residues may be substituted by His residues in order to further improve the tumor-selectivity of these potent CPP. Interesting positions will include Lys¹⁹, Lys²⁰, Lys²² and Arg²⁴ all shown to contribute to the cell penetration efficacy of the full length MCa [17].

3. Experimental

3.1. Reagents

N- α -Fmoc-L-aminoacids, Wang-Tentagel resin and reagents used for peptide syntheses were obtained from Iris Biotech (Marktredwitz, Germany). Solvents were analytical grade products from Acros Organics (Geel, Belgium). Cy5 maleimide mono-reactive dye was purchased from GE Healthcare (Saclay, France).

3.2. Peptide Syntheses

Chemical syntheses of truncated toxin peptides were performed as previously described [16]. Briefly, peptides were chemically synthesized by the solid-phase method [35] using an automated peptide synthesizer (CEM[®] Liberty 12, Matthews, NC, USA). Peptide chains were assembled stepwise on 0.24 meq of Fmoc-D-Arg-Pbf-Wang-Tentagel resin using 0.24 mmol of *N*- α -fluorenylmethyloxycarbonyl (Fmoc) L-amino-acid derivatives. The side-chain protecting groups were: trityl for Cys and Asn, *tert*-butyl for Ser, Thr, Glu and Asp, Pbf for Arg and *tert*-butylcarbonyl for Lys. Reagents were at the following concentrations: Fmoc-amino-acids [0.2 M Fmoc-AA-OH in dimethylformamide (DMF)], activator (0.5 M 2-(1H-benzotriazole-1-yl)-1,1,3,3-tetramethyluronium hexafluorophosphate in DMF), activator base [2 M diisopropylethylamine in *N*-methylpyrrolidone (NMP)] and deprotecting agent (5% piperazine/0.1 M 1-hydroxybenzotriazole in DMF), as advised by PepDriver (CEM[®]). After peptide chain assembly, resins were treated 4 h at room temperature with a mixture of trifluoroacetic acid/water/triisopropylsilane (TIS)/dithiothreitol (DTT) (92.5/2.5/2.5/2.5). The peptide mixtures were then filtered and the filtrates were precipitated by adding cold *tert*-butylmethyl ether. The crude peptides were pelleted by centrifugation (10,000 \times g, 15 min) and the supernatants were discarded. Truncated toxin analogues were purified by HPLC using a Vydac C18 column (218TP1010, 25 \times 10 cm). Elutions of the peptides were performed with a 10–60% acetonitrile

linear gradient containing 0.1% trifluoroacetic acid. The purified fractions were analyzed by analytical RP-HPLC (Vydac C18 column 218TP104, 25 × 4.6 cm). All analogues were characterized by MALDI-TOF mass spectrometry.

3.3. Peptide Labeling With Cy5

Each peptide was labeled with Cy5 according to the manufacturer's protocol (GE Healthcare). Peptides were dissolved at 200 µg/mL in 1 M NaHCO₃ buffer, pH 9.3. 500 µL of solubilized peptides were added to Cy5-maleimide containing tubes. The mixtures were incubated during 2 h at room temperature and then purified by HPLC using an analytical Vydac C18 column. Elution of the Cy5-labeled peptides was performed with a 5–90% acetonitrile linear gradient containing 0.1% trifluoroacetic acid. The pure peak fractions were lyophilized and peptides quantified by UV spectrophotometer at 650 nm.

3.4. Cell Culture

Undifferentiated malignant glioma rat (F98) cell line (from ATCC) was maintained at 37 °C in 5% CO₂ in DMEM/F-12 nutrient medium (Invitrogen, Cergy Pontoise, France) supplemented with 2% (v/v) heat-inactivated fetal bovine serum (Invitrogen) and 100 µg/mL streptomycin and 100 units/mL penicillin (Invitrogen).

3.5. Confocal Microscopy

For analysis of the cell entry of Cy5-labeled-truncated toxin peptides in living cells, cell cultures were incubated with the fluorescent peptides (in DMEM/F-12 nutrient medium only) for 2 h, and then washed twice with phosphate-buffered saline (PBS) alone. The plasma membrane was stained with 50 µg/mL rhodamine-conjugated concanavalin A (Invitrogen, Cergy Pontoise, France) for 5 min. Cells were washed once more. Live cells were then immediately analyzed by confocal laser scanning microscopy using a Zeiss LSM operating system. Rhodamine (561 nm) and Cy5 (633 nm) were sequentially excited and emission fluorescence were collected.

3.6. Fluorescence Activated Cell Sorting Analyses

F98 cells were incubated with various concentrations of Cy5-labeled peptides in DMEM/F-12 culture medium without serum at 37 °C for 2 h. The cells were then washed with PBS to remove excess extracellular peptide and treated with 0.48 mM versene (Invitrogen) for 5 min at 37 °C to detach cells from the surface, and centrifuged at 200 g in DMEM/F-12 culture medium before suspension in PBS. For experiments concerning endocytosis inhibitors, F98 cells were initially preincubated in DMEM/F-12 culture medium without serum for 30 min at 37 °C with different inhibitors of endocytosis: (i) 100 µM amiloride, (ii) 5 µg/mL cytochalasin D (10 µM), (iii) 20 µM nocodazole, or (iv) 5 mM methyl-β-cyclodextrin (all from Sigma, Lyon, France). The cells were then incubated for 2 h at 37 °C with 1 µM MCa_{UF1-9}-C-Cy5 in the presence of each drug. Flow cytometry analyses were performed with live cells using an Accuri C6 flow cytometer (BD Biosciences, Le Pont

de Claix, France). Data were obtained and analyzed using CFlow Sampler (BD Biosciences). Live cells were gated by forward/side scattering from a total of 10,000 events.

3.7. Molecular Modeling

Using Sybyl X 1.3 (Tripos Inc., St. Louis, MO, USA) and PDB structure of MCa (code 1C6W) and imperatoxin A (code 1IE6), we generated 3D models of opicalcin 1 and 2, hemicalcin and hadrucalcin. There is a sequence homology (76% up to 91%) between these proteins. Based on previous reports [6,7], we replaced some amino acid of MCa sequence to obtain the corresponding ones for the four different proteins. Several steps of minimization and control of the stereochemistry were performed to obtain a model for each molecule.

4. Conclusions

In this manuscript, we have demonstrated that MCa_{UF1-9}-C-Cy5 starts to show detectable penetration in glioma F98 cells at concentrations as low as 33 nM (5-fold increase over control) as detected by FACS. The process is visible at 100 nM by confocal microscopy and a comparative analysis reveals that it is highly competitive compared to TAT, penetratin or Poly-R CPP. One analogue turns out to be extremely competitive, MCa_{UF3-9}, owing to its performance, length and ease of synthesis. Nevertheless, we also demonstrate that engineered optimization of its cell penetrating properties is hard to achieve but that Mother Nature has provided an elegant solution to this problem by selecting itself the best amino acid substitutions under the form of new calcin analogues. In that respect, the hydrophobic domain of hadrucalcin outperforms that of MCa. We evidence for the first time the possibility to modulate peptide cell penetration by external pH provided that His residues are strategically incorporated within the amino acid sequence. This finding enlarges the potential application of these peptides to the treatment of glioma. Additionally, the observation that the residency time of these peptides in glioma F98 cells is quite long suggest that these peptides may be best used when injected once inside a solid tumor rather than by intravenous route.

Acknowledgements

We acknowledge financial support to MDW by Inserm and by the Nanofret grant and LabEx ICST of the Agence Nationale de la Recherche (ANR). MDW is a recipient of a contrat d'interface from Inserm and Grenoble Hospital. EB has a fellowship from ANR. We also thank the Région Rhône Alpes for the financial support of CT by an Emergence grant.

References

1. Fajloun, Z.; Kharrat, R.; Chen, L.; Lecomte, C.; di Luccio, E.; Bichet, D.; El Ayeb, M.; Rochat, H.; Allen, P.D.; Pessah, I.N.; *et al.* Chemical synthesis and characterization of maurocalcine, a scorpion toxin that activates Ca²⁺ release channel/ryanodine receptors. *FEBS Lett.* **2000**, *469*, 179–185.
2. Mouhat, S.; Jouirou, B.; Mosbah, A.; de Waard, M.; Sabatier, J.M. Diversity of folds in animal toxins acting on ion channels. *Biochem J.* **2004**, *378*, 717–726.

3. Mosbah, A.; Kharrat, R.; Fajloun, Z.; Renisio, J.G.; Blanc, E.; Sabatier, J.M.; El Ayeb, M.; Darbon, H. A new fold in the scorpion toxin family, associated with an activity on a ryanodine-sensitive calcium channel. *Proteins* **2000**, *40*, 436–442.
4. Zamudio, F.Z.; Gurrola, G.B.; Arevalo, C.; Sreekumar, R.; Walker, J.W.; Valdivia, H.H.; Possani, L.D. Primary structure and synthesis of imperatoxin A (iptx(a)), a peptide activator of Ca²⁺ release channels/ryanodine receptors. *FEBS Lett.* **1997**, *405*, 385–389.
5. Zhu, S.; Darbon, H.; Dyason, K.; Verdonck, F.; Tytgat, J. Evolutionary origin of inhibitor cystine knot peptides. *FASEB J.* **2003**, *17*, 1765–1767.
6. Shahbazzadeh, D.; Srairi-Abid, N.; Feng, W.; Ram, N.; Borchani, L.; Ronjat, M.; Akbari, A.; Pessah, I.N.; de Waard, M.; El Ayeb, M. Hemicalcin, a new toxin from the iranian scorpion hemiscorpius lepturus which is active on ryanodine-sensitive Ca²⁺ channels. *Biochem. J.* **2007**, *404*, 89–96.
7. Schwartz, E.F.; Capes, E.M.; Diego-Garcia, E.; Zamudio, F.Z.; Fuentes, O.; Possani, L.D.; Valdivia, H.H. Characterization of hadrucalcin, a peptide from hadrurus gertschi scorpion venom with pharmacological activity on ryanodine receptors. *Br. J. Pharmacol.* **2009**, *157*, 392–403.
8. Altafaj, X.; France, J.; Almassy, J.; Jona, I.; Rossi, D.; Sorrentino, V.; Mabrouk, K.; de Waard, M.; Ronjat, M. Maurocalcine interacts with the cardiac ryanodine receptor without inducing channel modification. *Biochem. J.* **2007**, *406*, 309–315.
9. Szappanos, H.; Smida-Rezgui, S.; Cseri, J.; Simut, C.; Sabatier, J.M.; de Waard, M.; Kovacs, L.; Csernoch, L.; Ronjat, M. Differential effects of maurocalcine on Ca²⁺ release events and depolarization-induced Ca²⁺ release in rat skeletal muscle. *J. Physiol.* **2005**, *565*, 843–853.
10. Gurrola, G.B.; Arevalo, C.; Sreekumar, R.; Lokuta, A.J.; Walker, J.W.; Valdivia, H.H. Activation of ryanodine receptors by imperatoxin A and a peptide segment of the II-III loop of the dihydropyridine receptor. *J. Biol. Chem.* **1999**, *274*, 7879–7886.
11. Esteve, E.; Mabrouk, K.; Dupuis, A.; Smida-Rezgui, S.; Altafaj, X.; Grunwald, D.; Platel, J.C.; Andreotti, N.; Marty, I.; Sabatier, J.M.; *et al.* Transduction of the scorpion toxin maurocalcine into cells. Evidence that the toxin crosses the plasma membrane. *J. Biol. Chem.* **2005**, *280*, 12833–12839.
12. Tanabe, T.; Beam, K.G.; Adams, B.A.; Niidome, T.; Numa, S. Regions of the skeletal muscle dihydropyridine receptor critical for excitation-contraction coupling. *Nature* **1990**, *346*, 567–569.
13. Tanabe, T.; Beam, K.G.; Powell, J.A.; Numa, S. Restoration of excitation-contraction coupling and slow calcium current in dysgenic muscle by dihydropyridine receptor complementary DNA. *Nature* **1988**, *336*, 134–139.
14. Altafaj, X.; Cheng, W.; Esteve, E.; Urbani, J.; Grunwald, D.; Sabatier, J.M.; Coronado, R.; de Waard, M.; Ronjat, M. Maurocalcine and domain a of the II-III loop of the dihydropyridine receptor Ca_v1.1 subunit share common binding sites on the skeletal ryanodine receptor. *J. Biol. Chem.* **2005**, *280*, 4013–4016.
15. Chen, L.; Esteve, E.; Sabatier, J.M.; Ronjat, M.; de Waard, M.; Allen, P.D.; Pessah, I.N. Maurocalcine and peptide a stabilize distinct subconductance states of ryanodine receptor type 1, revealing a proportional gating mechanism. *J. Biol. Chem.* **2003**, *278*, 16095–16106.

16. Poillot, C.; Dridi, K.; Bichraoui, H.; Pecher, J.; Alphonse, S.; Douzi, B.; Ronjat, M.; Darbon, H.; de Waard, M. D-maurocalcine, a pharmacologically inert efficient cell-penetrating peptide analogue. *J. Biol. Chem.* **2010**, *285*, 34168–34180.
17. Mabrouk, K.; Ram, N.; Boisseau, S.; Strappazon, F.; Reham, A.; Sadoul, R.; Darbon, H.; Ronjat, M.; de Waard, M. Critical amino acid residues of maurocalcine involved in pharmacology, lipid interaction and cell penetration. *Biochim. Biophys. Acta* **2007**, *1768*, 2528–2540.
18. Ram, N.; Weiss, N.; Texier-Nogues, I.; Aroui, S.; Andreotti, N.; Pirollet, F.; Ronjat, M.; Sabatier, J.M.; Darbon, H.; Jacquemond, V.; *et al.* Design of a disulfide-less, pharmacologically-inert and chemically-competent analog of maurocalcine for the efficient transport of impermeant compounds into cells. *J. Biol. Chem.* **2008**, *283*, 27048–27056.
19. Poillot, C.; Bichraoui, H.; Tisseyre, C.; Bahemberae, E.; Andreotti, N.; Sabatier, J.M.; Ronjat, M.; de Waard, M. Small efficient cell-penetrating peptides derived from scorpion toxin maurocalcine. *J. Biol. Chem.* **2012**, *287*, 17331–17342.
20. Aroui, S.; Brahim, S.; de Waard, M.; Breard, J.; Kenani, A. Efficient induction of apoptosis by doxorubicin coupled to cell-penetrating peptides compared to unconjugated doxorubicin in the human breast cancer cell line MDA-MB 231. *Cancer Lett.* **2009**, *285*, 28–38.
21. Aroui, S.; Brahim, S.; de Waard, M.; Kenani, A. Cytotoxicity, intracellular distribution and uptake of doxorubicin and doxorubicin coupled to cell-penetrating peptides in different cell lines: A comparative study. *Biochem. Biophys. Res. Commun.* **2010**, *391*, 419–425.
22. Aroui, S.; Brahim, S.; Hamelin, J.; de Waard, M.; Breard, J.; Kenani, A. Conjugation of doxorubicin to cell penetrating peptides sensitizes human breast MDA-MB 231 cancer cells to endogenous trail-induced apoptosis. *Apoptosis* **2009**, *14*, 1352–1365.
23. Aroui, S.; Ram, N.; Appaix, F.; Ronjat, M.; Kenani, A.; Pirollet, F.; de Waard, M. Maurocalcine as a non-toxic drug carrier overcomes doxorubicin resistance in the cancer cell line MDA-MB 231. *Pharm. Res.* **2009**, *26*, 836–845.
24. Ram, N.; Texier-Nogues, I.; Pernet-Gallay, K.; Poillot, C.; Ronjat, M.; Andrieux, A.; Arnoult, C.; Daou, J.; de Waard, M. *In vitro* and *in vivo* cell delivery of quantum dots by the cell penetrating peptide maurocalcine. *Int. J. Biomed. Nanosci. Nanotechnol.* **2011**, *2*, 12–32.
25. Stasiuk, G.J.; Tamang, S.; Imbert, D.; Poillot, C.; Giardiello, M.; Tisseyre, C.; Barbider, E.L.; Fries, P.H.; de Waard, M.; Reiss, P.; Mazzanti, M. Cell-permeable In(III) chelate-functionalized InP quantum dots as multimodal imaging agents. *ACS Nano* **2011**, *5*, 8193–8201.
26. Ram, N.; Aroui, S.; Jaumain, E.; Bichraoui, H.; Mabrouk, K.; Ronjat, M.; Lortat-Jacob, H.; de Waard, M. Direct peptide interaction with surface glycosaminoglycans contributes to the cell penetration of maurocalcine. *J. Biol. Chem.* **2008**, *283*, 24274–24284.
27. Boisseau, S.; Mabrouk, K.; Ram, N.; Garmy, N.; Collin, V.; Tadmouri, A.; Mikati, M.; Sabatier, J.M.; Ronjat, M.; Fantini, J.; *et al.* Cell penetration properties of maurocalcine, a natural venom peptide active on the intracellular ryanodine receptor. *Biochim. Biophys. Acta* **2006**, *1758*, 308–319.
28. Jones, A.T.; Sayers, E.J. Cell entry of cell penetrating peptides: Tales of tails wagging dogs. *J. Control. Release* **2012**, *161*, 582–591.
29. Lindgren, M.; Hallbrink, M.; Prochiantz, A.; Langel, U. Cell-penetrating peptides. *Trends Pharmacol. Sci.* **2000**, *21*, 99–103.

30. Lundberg, P.; Langel, U. A brief introduction to cell-penetrating peptides. *J. Mol. Recognit.* **2003**, *16*, 227–233.
31. Mano, M.; Teodosio, C.; Paiva, A.; Simoes, S.; Pedroso de Lima, M.C. On the mechanisms of the internalization of s4(13)-pv cell-penetrating peptide. *Biochem. J.* **2005**, *390*, 603–612.
32. Gurrola, G.B.; Capes, E.M.; Zamudio, F.Z.; Possani, L.D.; Valdivia, H.H. Imperatoxin A, a cell-penetrating peptide from scorpion venom, as a probe of Ca-release channels/ryanodine receptors. *Pharmaceuticals (Basel)* **2010**, *3*, 1093–1107.
33. El-Hayek, R.; Lokuta, A.J.; Arevalo, C.; Valdivia, H.H. Peptide probe of ryanodine receptor function. Imperatoxin A, a peptide from the venom of the scorpion *pandinus imperator*, selectively activates skeletal-type ryanodine receptor isoforms. *J. Biol. Chem.* **1995**, *270*, 28696–28704.
34. Garcia-Martin, M.L.; Herigault, G.; Remy, C.; Farion, R.; Ballesteros, P.; Coles, J.A.; Cerdan, S.; Ziegler, A. Mapping extracellular pH in rat brain gliomas *in vivo* by 1H magnetic resonance spectroscopic imaging: Comparison with maps of metabolites. *Cancer Res.* **2001**, *61*, 6524–6531.
35. Merrifield, R.B. Solid-phase peptide synthesis. *Adv. Enzymol. Relat. Areas Mol. Biol.* **1969**, *32*, 221–296.

© 2013 by the authors; licensee MDPI, Basel, Switzerland. This article is an open access article distributed under the terms and conditions of the Creative Commons Attribution license (<http://creativecommons.org/licenses/by/3.0/>).

Article 2:

Quantitative evaluation of the cell penetrating properties of an iodinated Tyr-L-maurocalcine analog

Article publié dans le journal Biochimica et Biophysica Acta en 2014



Quantitative evaluation of the cell penetrating properties of an iodinated Tyr-L-maurocalcine analog[☆]

Céline Tisseyre^{a,b}, Mitra Ahmadi^{b,c}, Sandrine Bacot^{b,c}, Lucie Dardevet^{a,b}, Pascale Perret^{b,c}, Michel Ronjat^{a,b}, Daniel Fagret^{b,c}, Yves Usson^{b,e}, Catherine Ghezzi^{b,c}, Michel De Waard^{a,b,d,*}

^a INSERM, U836, Grenoble Institute of Neuroscience, LabEx Ion Channels, Science and Therapeutics, Grenoble, France

^b Université Joseph Fourier, Grenoble, France

^c INSERM, U1039, Radiopharmaceutiques Biocliniques, Grenoble, France

^d Smartox Biotechnologies, Grenoble, France

^e CNRS, UMR5525, TIMC-IMAG, Grenoble, France

ARTICLE INFO

Article history:

Received 3 January 2014

Received in revised form 27 February 2014

Accepted 17 March 2014

Available online 22 March 2014

Keywords:

Maurocalcine

Cell penetrating peptide

Radiiodination

Quantitative evaluation

Drug delivery

ABSTRACT

L-Maurocalcine (L-MCa) is the first reported animal cell-penetrating toxin. Characterizing its cell penetration properties is crucial considering its potential as a vector for the intracellular delivery of drugs. Radiolabeling is a sensitive and quantitative method to follow the cell accumulation of a molecule of interest. An L-MCa analog containing an additional N-terminal tyrosine residue (Tyr-L-MCa) was synthesized, shown to fold and oxidize properly, and successfully radiiodinated to ¹²⁵I-Tyr-L-MCa. Using various microscopy techniques, the average volume of the rat line F98 glioma cells was evaluated at 8.9 to $18.9 \times 10^{-7} \mu\text{l}$. ¹²⁵I-Tyr-L-MCa accumulates within cells with a dose-dependency similar to the one previously published using 5,6-carboxyfluorescein-L-MCa. According to subcellular fractionation of F98 cells, plasma membranes keep less than 3% of the peptide, regardless of the extracellular concentration, while the nucleus accumulates over 75% and the cytosol around 20% of the radioactive material. Taking into account both nuclear and cytosolic fractions, cells accumulate intracellular concentrations of the peptide that are equal to the extracellular concentrations. Estimation of ¹²⁵I-Tyr-L-MCa cell entry kinetics indicate a first rapid phase with a 5 min time constant for the plasma membrane followed by slower processes for the cytoplasm and the nucleus. Once inside cells, the labeled material no longer escapes from the intracellular environment since 90% of the radioactivity remains 24 h after washout. Dead cells were found to have a lower uptake than live ones. The quantitative information gained herein will be useful for better framing the use of L-MCa in biotechnological applications. This article is part of a Special Issue entitled: Calcium Signaling in Health and Disease. Guest Editors: Geert Bultynck, Jacques Haiech, Claus W. Heizmann, Joachim Krebs, and Marc Moreau.

© 2014 Elsevier B.V. All rights reserved.

1. Introduction

Crossing cellular membranes represents a major hurdle in current drug development. Cell-penetrating peptides (CPP) are molecular vectors that enter cells and allow the intracellular delivery of a number of bioactive molecules such as drugs, peptides, proteins, oligonucleotides/cDNA/RNA, and nanoparticles [1–3]. Originally isolated from the venom of the scorpion *Scorpio maurus palmatus* [4], L-maurocalcine (L-MCa) is a highly basic, positively charged, 33-mer peptide that efficiently binds to the ryanodine receptor in skeletal muscles and promotes channel opening and calcium release from the sarcoplasmic reticulum. The binding site of L-MCa on the

ryanodine receptor has been identified as cytoplasmic [5], suggesting that cytoplasmic application is required for its pharmacological effect. The fast kinetics (few seconds) at which extracellular application of L-MCa triggers internal Ca^{2+} release indicates that the peptide should be able to easily translocate through the plasma membrane [6]. According to ¹H NMR analysis, the peptide presents three disulfide bridges (Cys³–Cys¹⁷, Cys¹⁰–Cys²¹ and Cys¹⁶–Cys³²) and folds along an inhibitor cysteine knot pattern [4,7]. It contains three β-strands from amino acid residues 9–11 (strand 1), 20–23 (strand 2), and 30–33 (strand 3) with strands 2 and 3 forming an antiparallel β-sheet (Fig. 1A). Several lines of experimental evidence indicate that L-MCa is a member of the exponentially growing family of CPPs [6,8–13]. The peptide is highly efficient in entering a variety of cell types compared to other popular CPP such as TAT or penetratin. It presents a low toxicity profile (absence of toxicity at concentrations above 10 μM) [8], penetrates at lower concentrations [14], and efficiently accumulates into the cytoplasm which is a highly desirable feature for many biotechnological applications that require the use of CPP. Therefore, a quantitative

[☆] This article is part of a Special Issue entitled: Calcium Signaling in Health and Disease. Guest Editors: Geert Bultynck, Jacques Haiech, Claus W. Heizmann, Joachim Krebs, and Marc Moreau.

* Corresponding author at: INSERM, U836, Grenoble Neuroscience Institute, Site Santé de la Tronche, Bâtiment Edmond J. Safra, 38042 Grenoble Cedex 09, France. Tel.: +33 456 520 563; fax: +33 456 520 637.

E-mail address: michel.dewaard@ujf-grenoble.fr (M. De Waard).

assessment of the cell penetration properties of L-MCa is of great importance considering its potential as a vector for the improved delivery of therapeutic compounds. Radiolabeling represents the most sensitive and quantitative method to follow the quantitative entry of a cell penetrating peptide of interest. Radioiodination is a widely used method for radiolabeling of chemical compounds since the presence of iodine would poorly affect the structural properties of the molecule of interest. Specifically, ^{125}I radiolabeling is commonly performed for *in vitro* radioligand interaction and *in vivo* biodistribution studies [15,16]. For the purpose of radiolabeling of L-MCa, we synthesized an analog with an extra amino-terminal tyrosine residue, termed Tyr-L-MCa, that still possesses the pharmacological properties of wild-type L-MCa. Next, we quantitatively investigated the cell penetration properties of the radioiodinated Tyr-L-MCa using the rat F98 glioma cell

line and a precise evaluation of cell volume by Digital Holographic Microscopy (DHM) or by confocal microscopy (CM). The results of the present study will be useful for future *in vivo* biodistribution studies of MCa.

2. Material and methods

2.1. Materials

N- α -Fmoc-L-amino acid, Wang-Tentagel resin and reagents used for peptide synthesis were obtained from Iris Biotech. Solvents were analytical grade products from Acros Organics. Acetonitrile was High Performance Liquid Chromatography (HPLC) gradient grade from Fischer Scientific and trifluoroacetic acid (purity $\geq 98\%$) from Fluka

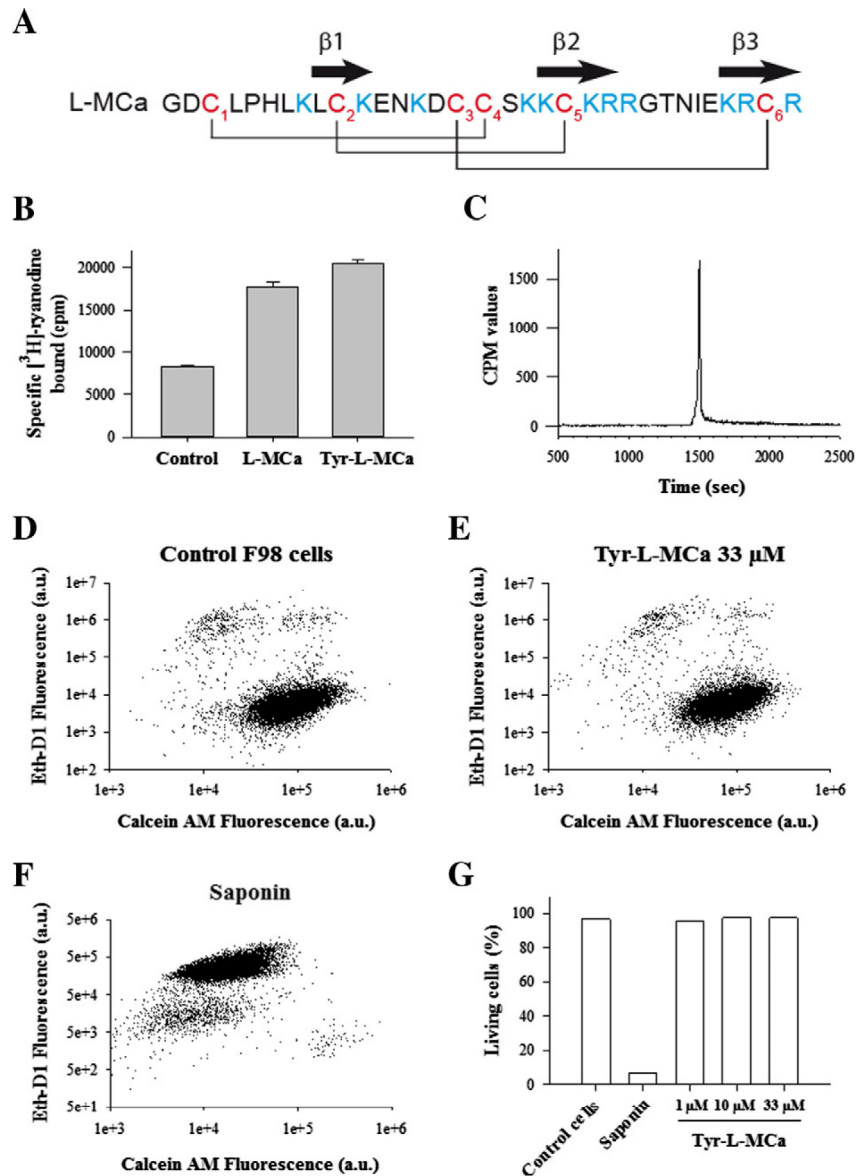


Fig. 1. Properties of the Tyr-L-MCa analog. (A) Primary structure of L-MCa. The disulfide bridge connectivity is shown by lines connecting the six semi-cystine residues. The positions of the three β -strands are indicated by arrows. Blue residues denote basic amino acids. (B) Stimulation of ^3H -ryanodine binding onto SR vesicles. Experimentally, binding was performed at $\text{pCa} = 5$ which explains why L-MCa stimulation of binding is limited. No significant differences were observed between the efficacies of L-MCa and Tyr-L-MCa. (C) RP-HPLC profile of ^{125}I -Tyr-L-MCa after radiolabeling. Note the homogeneous labeling of the peptide by ^{125}I . (D) Cell viability assay by flow cytometry for control F98 cells. The ethidium-D1 fluorescence level measures cell death level. (E) Cell viability assay by flow cytometry for F98 cells after 2 h incubation with 33 μM Tyr-L-MCa. (F) Cell viability assay by flow cytometry for F98 cells after 5 min incubation with 0.1% saponin. Note the extensive cell death produced by saponin. (G) Proportion of live F98 cells for control, saponin and Tyr-L-MCa conditions.

and lactoperoxidase of bovine milk (80 IU/mg) were from Sigma-Aldrich, hydrogen peroxide 30% in water (w/w) from Carlo Erba and Na¹²⁵I (3.7 GBq/ml) from Perkin Elmer. DMEM F-12 medium with or without phenol red, fetal bovine serum, Trypsin-EDTA, rhodamine-conjugated concanavalin A and live/dead viability/cytotoxicity kit were obtained from Invitrogen. Protease inhibitors (cOmplete Min, EDTA-free) were from Roche diagnostics.

2.2. Synthesis of Tyr-L-MCa by solid-phase

Tyr-L-MCa with an extra N-terminal tyrosyl residue was synthesized to allow L-MCa radioiodination. Chemical synthesis of Tyr-L-MCa was performed as previously described [17] with the following modifications. Briefly, Tyr-L-MCa was chemically synthesized by the solid-phase peptide synthesis (SPPS) method [18] using an automated peptide synthesizer (CEM® Liberty). The peptide chain was assembled stepwise on 0.24 mEq of Fmoc-L-Arg(Pbf)-Wang-Tentagel resin using 0.24 mmol of N- α -fluorenylmethyloxycarbonyl (Fmoc) L-amino-acid derivatives. The side-chain protecting groups were Trityl for Cys and Asn, *tert*-butyl for Ser and Tyr, Thr, Glu and Asp, Pbf for Arg, and *tert*-butylcarbonyl for Lys. Reagents were at the following concentrations: 0.2 M Fmoc-amino-acids (Fmoc-AA-OH in dimethylformamide (DMF)), 0.5 M activator (2-(1H-benzotriazole-1-yl)-1,1,3,3-tetramethyluronium hexafluorophosphate in DMF), 2 M activator base (diisopropylethylamine in N-methyl-pyrrolidone) and deprotecting agent (5% piperazine/0.1 M 1-hydroxybenzotriazole in DMF), as advised by PepDriver (CEM®). After peptide chain assembly, the resin was treated with a mixture of trifluoroacetic acid/water/triisopropylsilane/1,4-dithiothreitol (92.5/2.5/2.5/2.5) for 4 h at room temperature. The peptide mixture was then filtered to eliminate the resin and the filtrate was precipitated by adding cold *t*-butylmethyl ether. The crude peptide was pelleted by centrifugation (10,000 \times g, 15 min) and the supernatant was discarded. The crude and reduced Tyr-L-MCa was submitted to oxidation for disulfide bridge formation in 0.1 M Tris/HCl buffer at pH 8.2 during 3 days at room temperature. Oxidized/folded Tyr-L-MCa was then purified by HPLC using a Vydac C18 column (218TP1010, 250 \times 10 mm). Elution of the peptide was performed with a 10–60% acetonitrile linear gradient containing 0.1% trifluoroacetic acid (TFA) over 40 min. The purity of the collected fraction was analyzed by reversed phase (RP)-HPLC using analytical C18 column (Vydac, 218TP104, 10 μ m, 250 \times 4.6 mm). Tyr-L-MCa was characterized by MALDI-TOF mass spectrometry. Samples were mixed 1:1 (v/v) with 10 mg/ml α -cyano-4-hydroxycinnamic acid (HCCA) before spotted onto a MALDI target plate. Mass spectrometry analyses were performed on a 4800 MALDI-TOF/TOF instrument (ABSciex). MS spectra were acquired in positive ion reflector mode over a mass range of 800–6000 m/z.

2.3. Radiolabeling of Tyr-L-MCa using lactoperoxidase

¹²⁵I-Tyr-L-MCa was prepared using a direct iodination procedure with lactoperoxidase/H₂O₂ system as oxidant. Briefly, 37 MBq of ¹²⁵I were added to 10 μ g of Tyr-MCa in phosphate buffer (50 mM, pH 7.4). The reaction was allowed to proceed for 30 min at room temperature after addition of lactoperoxidase and H₂O₂ at a final concentration of 0.5 μ M and 25 μ M respectively. Radioiodinated Tyr-L-MCa was analyzed by HPLC immediately and radiochemical purity higher than 95% was achieved, thereby obviating the need for a purification step. A single peak of radioiodinated ¹²⁵I-Tyr-L-MCa was observed. The compound was stable for over 48 h. A similar labeling was performed with Na¹²⁷I according to the same procedure. In these conditions, the compound was shown to be monoiodinated (not shown). The resulting compounds, ¹²⁵I-Tyr-L-MCa and ¹²⁷I-Tyr-L-MCa, were mixed in order to obtain a specific activity of 0.4 MBq/nmol of Tyr-L-MCa (activimeter Capintec).

Hereafter, we shall speak about ¹²⁵I-Tyr-L-MCa although it reflects a mixture of ¹²⁵I-Tyr-L-MCa and ¹²⁷I-Tyr-L-MCa.

2.4. F98 glioma cell culture

All experiments were performed using the F98 glioblastoma cancer cell line (undifferentiated malignant glioma rat cell line from ATCC) maintained at 37 °C in 5% CO₂ in DMEM F-12 medium supplemented with 2% (v/v) heat-inactivated fetal bovine serum and 10,000 units/ml streptomycin and penicillin. Cells were plated on 24 well plates (Falcon; 700,000 cells/well) and grown 24 h until they reach 90% confluence.

2.5. Cell counting

To get a precise estimate of the cell number present in each well at the time where cell penetration experiments are performed with ¹²⁵I-Tyr-L-MCa, F98 cells were counted by flow cytometry analyses with live cells using a Becton Dickinson Accuri C6 flow cytometer (BD Biosciences). Data were obtained and analyzed using BD Accuri C6 software. Live cells were gated by forward/side scattering.

2.6. Evaluation of F98 cell death

Cells were incubated with or without various concentrations of Tyr-L-MCa during 2 h. Cells were washed with PBS and washes were conserved. They were then treated with 0.05% trypsin-EDTA for 5 min at 37 °C to detach them from the support. Cells were collected and resuspended in DMEM-F12 with 2% fetal bovine serum along with the initial washes. For one series of control cells, 0.1% saponin was added just before centrifugation to induce cell death. All cell conditions (control, Tyr-L-MCa and saponin) were centrifuged at 800 \times g during 5 min. The pellets were resuspended in 200 μ l of staining mix according to Invitrogen recommendations. Cells were left in the dark for 15 min at room temperature before analyses by flow cytometry using the LIVE/DEAD® Viability/Cytotoxicity Kit of Invitrogen. This kit quickly discriminates live from dead cells by simultaneously staining with green-fluorescent calcein-AM to indicate intracellular esterase activity and red-fluorescent ethidium homodimer-1 to indicate loss of plasma membrane integrity. Similar results were obtained with ¹²⁵I-Tyr-L-MCa.

2.7. Estimation of F98 cell volume by Digital Holographic Microscopy or confocal microscopy

Digital Holographic Microscopy (DHM) is an interferometric technique that makes possible the imaging and measurement of the phase retardation through transparent biological specimen [19]. Because it is based on the interference of coherent light (λ 658 nm) a high precision (nm order) can be obtained in optical thickness measurements. Under the hypothesis of invariance of the refractive index within the cytosol, it may be admitted that the measured optical thickness is a good estimate of the quantity of matter traversed by light [20]. Therefore, the average F98 cell volume was estimated by integrating the optical thickness over the projected area of each cell.

To evaluate the F98 cell volume by confocal microscopy, cell plasma membranes were stained with 50 μ g/ml concanavalin A-rhodamine for 5 min. Next, cells were washed with phosphate buffered saline (PBS) and incubated in DMEM without phenol red. Live cells were then immediately analyzed by confocal laser scanning microscopy using a Zeiss LSM operating system. Rhodamine was sequentially excited (at 561 nm) and emission fluorescence (at 590 nm) was collected. Stacks of 17 to 22 confocal images were taken by steps of 1 μ m on the z-axis to cover the entire depth of the cells. Globally, F98 cells were quite thick but some images of the stacks may not contain any information. Next, a dedicated Image J macro was developed to reconstruct the 3-D

F98 cell image to calculate the global volume using the stained plasma membrane boundaries.

2.8. Quantitative evaluation of the cell penetration of ^{125}I -Tyr-L-MCa

F98 cells were incubated with various concentrations of radioiodinated ^{125}I -Tyr-L-MCa (33 nM to 10 μM) in DMEM F-12 culture medium (200 to 400 μl per well) without serum or antibiotics at 37 °C for 2 h to allow cell penetration. For the estimation of the kinetics of cell entry of the compound, the time of incubation could be shortened as indicated. Each concentration contained 2.5% of ^{125}I -radiolabeled peptide and 97.5% of ^{127}I -labeled peptide to diminish the quantity of radioactive peptide to handle. After incubation, the cells were washed twice with PBS to remove excess extracellular peptide. They were then treated with 0.05% trypsin-EDTA for 5 min at 37 °C to (i) degrade any remaining extracellular ^{125}I -Tyr-L-MCa and (ii) detach F98 cells from the surface. Cells were collected and resuspended in DMEM-F12 with 2% fetal bovine serum. Cells were centrifuged at 800 $\times g$ during 5 min. The pellet was resuspended in PBS and cells were then centrifuged a second time in the same conditions. Of note, for each one of the centrifugation and washing steps, resuspended cells were transferred to new tubes to eliminate any extracellular radioiodinated ^{125}I -Tyr-L-MCa or trypsin-induced fragment that may be potentially present by sticking to the plastic. Cells were resuspended in 1 ml of lysis buffer (in mM: Tris 20, NaCl 150, DTT 1, sucrose 250, pH 8.0 along with protease inhibitors) and incubated on ice for 5 min. Next, cells were mechanically disrupted using a potter. Subcellular fractionation was performed as follows. First, the cell lysates were centrifuged at 900 $\times g$ for 20 min and the pellet containing the cell nuclei (F98-N) was collected. Next, the supernatant was collected and centrifuged at 50,000 $\times g$ for 60 min. The pellet containing the plasma membrane was kept (F98-PM) along with the supernatant that represents the cytoplasm (F98-C). Both pellets were resuspended in 500 μl distilled water for counting. This subcellular fractionation method separates membrane-bound (F98-PM) from intracellular ^{125}I -Tyr-L-MCa (F98-N + F98-C) providing an estimate of cell penetration of the peptide into the cytoplasm. Counting of radioactivity was carried out by gamma-well counter.

2.9. Determination of the intracellular concentration of ^{125}I -Tyr-L-MCa

Knowing the precise cell number per well, the average cell volume and the specific activity of ^{125}I -Tyr-L-MCa, we were able to convert counts per min to intracellular peptide concentration. The concentration of radioiodinated Tyr-L-MCa is provided in μM and was calculated according to the equation $f_0 = ((\text{cpm}/\text{cell number})/a)/b/\text{cell volume}$. The value **a** is a constant value of the gamma-well counter ($a = 35515679$ to convert cpm values in MBq). The value **b** is the specific activity of Tyr-L-MCa that has been used for the preparation of dilutions. Only the added values of F98-N and F98-C radioactivity were taken into account to quantify cell penetration. F98-PM values were discarded.

2.10. Kinetic of cellular leakage of ^{125}I -Tyr-L-MCa

F98 cells were incubated with 1 μM of ^{125}I -Tyr-L-MCa in DMEM F-12 culture medium without serum or antibiotics at 37 °C for 2 h. The cells were then washed three times with PBS to remove excess extracellular peptide, and then completed with DMEM F-12 medium. At different times (0, 1, 2, 3, 4, 5, 6 and 24 h), a sample of 100 μl of medium was taken for radioactivity counting and replaced by 100 μl of fresh complete medium. The value obtained was corrected by a factor of 4 (100 μl taken out of 400 μl of medium). A control was performed without cells to demonstrate that the plastic of the wells did not release any radioactivity. The quantity of radioactivity released by the cells was evaluated as a ratio of total cell radioactivity as determined previously.

2.11. [^3H]-ryanodine binding on ryanodine receptors from skeletal muscle heavy SR vesicles

Heavy sarcoplasmic reticulum (SR) vesicles were prepared as described [11]. Protein concentration was measured by the Biuret method. Heavy SR vesicles (1 mg/ml) were incubated at 37 °C for 2 h in an assay buffer composed of 10 nM [^3H]-ryanodine, 150 mM KCl, 2 mM EGTA, 2 mM CaCl_2 ($p\text{Ca} = 5$), and 20 mM MOPS, pH 7.4. 200 nM L-MCa or Tyr-L-MCa was added prior to the addition of heavy SR vesicles. [^3H]-ryanodine bound to heavy SR vesicles was measured by filtration through Whatman GF/B glass filters followed by three washes with 5 ml of ice-cold washing buffer composed of 150 mM NaCl, 20 mM HEPES, pH 7.4. [^3H]-ryanodine retained on the filters was measured by liquid scintillation. Nonspecific binding was measured in the presence of 80 μM unlabeled ryanodine. The data are presented as mean \pm S.E. Each experiment was performed in triplicate.

3. Results

3.1. Tyr-L-MCa: a functional MCa analog for iodination

L-MCa itself lacks a tyrosine residue for radio-iodination of the peptide. To this end, we produced a new analog of L-MCa with an extra amino-terminal tyrosine residue. Earlier observations had demonstrated that N-terminal-modified analogs of L-MCa could be easily produced since the addition of an extra-biotinylated lysine residue is without impact on the proper folding/oxidation of the peptide [9]. MS analyses (MALDI-TOF technique) of crude and folded/oxidized Tyr-L-MCa provide experimental molecular masses ($M + H$)⁺ of 4026.9 and 4020.8 Da, respectively. The shift in experimental molecular mass of 6.1 Da upon folding/oxidation is in agreement with the engagement of all six cysteine residues in the formation of three disulfide bridges. Since the activity of L-MCa is strictly dependent on the proper/folding of the peptide [21] and that this activity is not altered by N-terminal modification [6,9], it is expected that Tyr-L-MCa should have preserved its pharmacological effect. Fig. 1B illustrates that this is indeed the case. As shown, Tyr-L-MCa turned as potent as L-MCa itself in stimulating the binding of [^3H]-ryanodine onto skeletal muscle ryanodine receptors from SR vesicles. Next, since Tyr-L-MCa remained functional, the peptide was enzymatically iodinated using the lactoperoxidase/ H_2O_2 system. Under the experimental conditions described radiochemical purity higher than 95% was achieved. This was further illustrated in the HPLC profile of the compound (Fig. 1C). ^{125}I -Tyr-L-MCa remained stable for over 24 h. ^{127}I iodination was also used to prepare ^{127}I -Tyr-L-MCa instead of ^{125}I -Tyr-L-MCa to lower the specific activity and the quantity of radioactivity to handle. Modeling experiments illustrates the relative position of the extra iodinated tyrosine residue onto L-MCa (Fig. 2).

3.2. Tyr-L-MCa lacks cell toxicity and is partially degraded by trypsin treatment

We first assessed that Tyr-L-MCa does not induce cell death that may alter the evaluation of cell penetration. For that purpose, we used rat glioma F98 cells because we plan to use L-MCa as a vector for the delivery of chemo-active drugs in later studies. As shown by flow cytometry, incubating F98 cells 2 h with 33 μM Tyr-L-MCa does not induce any specific cell death compared to the control condition (Fig. 1D, E). The control condition contained about 3.3% of dead cells compared to the 2.6% of the Tyr-L-MCa condition. In contrast, 5 min incubation with 0.1% saponin has a drastic effect on cell survival since the proportion of dead cells reached 93.4% (Fig. 1F). Similar results were obtained for a set of Tyr-L-MCa concentration that all indicate that this vector is non-toxic for F98 cells (Fig. 1G). Similar observations were made with F98 cells incubated with ^{125}I -Tyr-L-MCa indicating that gamma radiation did not

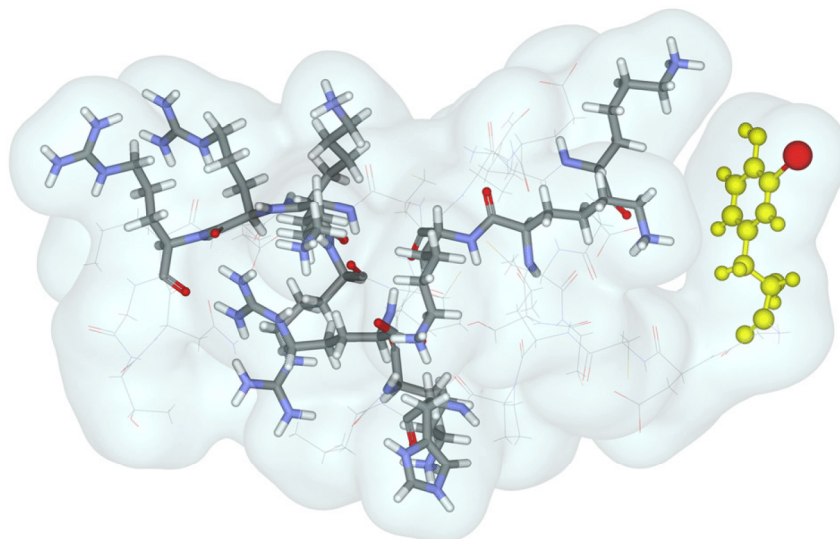


Fig. 2. Modeled 3D structure of ^{125}I -Tyr-L-MCa. The structure was modeled starting with L-MCa as a structural basis (1C6W from the Protein Database). The extra tyrosine residue is in yellow and the iodine on the tryptophan ring in red. The positively charged amino acid residues of L-MCa are also highlighted.

add a layer of cell toxicity in the frame of our experiments (data not shown).

3.3. Cell penetration properties of ^{125}I -Tyr-L-MCa

Production of the ^{125}I -Tyr-L-MCa compound with high radiochemical purity is an opportunity to quantify the cell penetration of L-MCa into cells. Earlier labeling of L-MCa with a fluorescence indicator provided only semi-quantitative information [11]. We first designed a subcellular fractionation protocol that was aimed at minimizing the contribution of any external membrane-attached ^{125}I -Tyr-L-MCa radioactivity associated to F98 cells. This protocol includes trypsin treatment, many cell washes, and a systematic transfer of the biological material to new plastic tubes in order to avoid possible attachment of any external ^{125}I -Tyr-L-MCa to plastic surfaces. Trypsin treatment was kept to the minimum because its first aim is to detach cells from the surface. Longer exposure would result in better external ^{125}I -Tyr-L-MCa degradation but also in cell damaging which is not desirable. Fig. 3 illustrates that indeed a 5 min trypsin digestion after F98 cell incubation with ^{125}I -Tyr-L-MCa results in only limited peptide degradation. The appearance on the HPLC elution profile of a new leftward-shifted peak, which is superimposed to the remnant

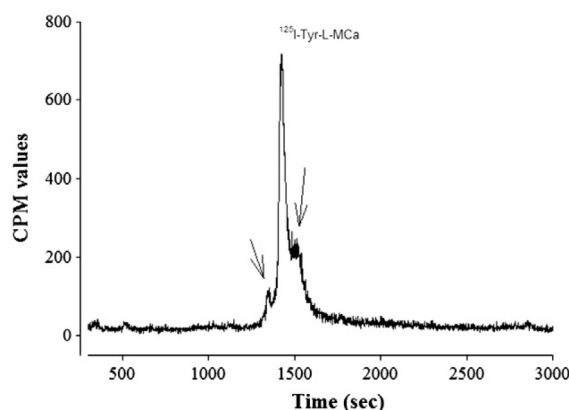


Fig. 3. RP-HPLC profile of ^{125}I -Tyr-L-MCa following 5 min of incubation with trypsin. The major peak is the intact ^{125}I -Tyr-L-MCa, while the peaks denoted by the arrows reflect degraded products.

peak of the original ^{125}I -Tyr-L-MCa compound, indicates that the trypsin-mediated degradation is only partial. To further minimize the potential quantitative contribution of any cell membrane-bound ^{125}I -Tyr-L-MCa, the plasma membrane was quantified as a separate entity and the radioactivity associated to this subcellular fraction was excluded from our calculations of L-MCa cell entry and accumulation. However, as we shall see later, the radioactivity associated with the plasma membrane was extremely low indicating little accumulation of the peptide in membrane fractions which further strengthens the reliance on the protocol used to quantify cell entry.

The entire study was performed on the rat glioblastoma cancer cell line F98 maintained in culture. To assess the cell concentration achieved by the ^{125}I -Tyr-L-MCa, we first determined two important parameters: i) the cell number in each well and ii) the average volume of F98 cells. The cell number in each culture well was established by FACS counting. The average cell number was $403,754 \pm 23,434$ per well ($n = 4$ wells). This includes 96.7% of live cells and 3.3% of dead cells as defined in Fig. 1D. Next, we evaluated the average cell volume using two different techniques: DHM and cell volume reconstruction through the acquisition of stacks of confocal images. Fig. 4A illustrates the optical thickness image produced by DHM with gray levels coding for the optical thickness. The surface reconstruction of the optical thicknesses is shown in Fig. 4B. The volume of F98 cells can be obtained by integration of the optical thickness inside the cell areas. A histogram illustrating individual cell volume was constructed (Fig. 4C). Fitting the data provides an average cell volume of $8.9 \times 10^{-7} \pm 0.2 \times 10^{-7} \mu\text{l}$ ($n = 130$ cells). We also used z-stacks of CM images to reconstruct cell volumes, again by focusing on individual cells. The boundaries of cells were provided by concanavalin-A rhodamine staining of the plasma membranes. Using this CM method instead of DHM, we come up with an average F98 cell volume of $18.9 \times 10^{-7} \mu\text{l}$ ($n = 95$ cells). There is thus a 2.12-fold difference in volume estimation using these two methods. DHM is likely a more precise technique for volume estimation and we will rely on the average DHM value to calculate the intracellular concentration of ^{125}I -Tyr-L-MCa. However, when applicable, the concentration values will also be provided using the CM cell volume evaluation method in parentheses.

First, we investigated how dead cells may affect the uptake of ^{125}I -Tyr-L-MCa. The peptide being extremely basic it is possible that dead cells, by exposing their DNA or their protein content, may overly contribute to the measured signal. We therefore purposely compared

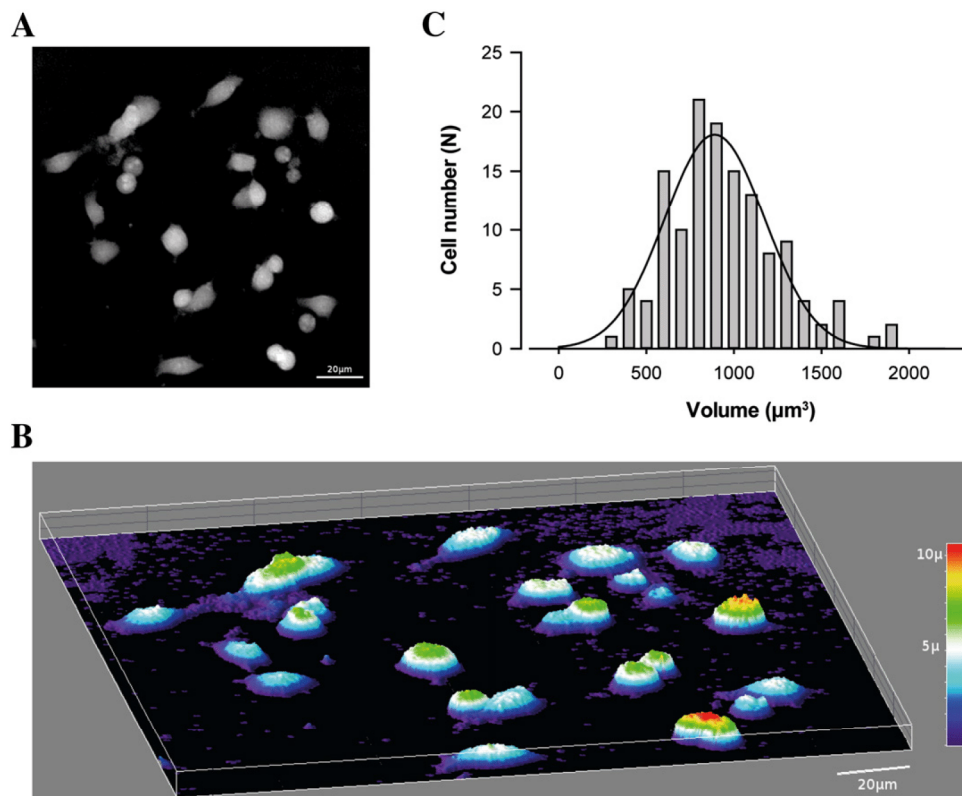


Fig. 4. Estimation of the average volume of F98 glioblastoma cells by DHM. (A) Optical thickness image produced by DHM, the gray levels are coding for the optical thickness. (B) Surface reconstruction of the optical thicknesses. (C) Histogram showing the distribution of individual cell volumes, obtained by integrating the optical thickness inside the cell areas. Only individual cells were used to evaluate cell volumes since touching cells could lead to overestimation. Cell fragments were also avoided for this analysis.

the amount of accumulated radioactivity in live cells incubated 2 h with $33 \mu\text{M}$ ^{125}I -Tyr-L-MCa with the amount found in dead cells, the cell death being promoted by 0.1% saponin. As shown in Fig. 5A, dead cells accumulate a surprisingly high level of radioactivity in each of the subcellular fractions. In each case however, the level of activity was lower than in live cells, indicating that cell death should not affect the measurements on live cells significantly. Fig. 5A also illustrates that the plasma membrane is the subcellular fraction that accumulates the least radioactivity compared to the cytoplasm and the nucleus. At this external concentration, the plasma membrane represents 9.4% of the accumulated radioactivity. In contrast, the cytoplasm and the nucleus of live cells accumulate each 25.6% and 64.7%, respectively. These proportions were however altered in dead cells with respective accumulations of 15.7% (plasma membrane), 45.1% (cytoplasm) and 32.2% (nucleus). The comparatively good accumulation of ^{125}I -Tyr-L-MCa in the cytoplasmic fraction of dead cells is probably linked to the effect of saponin on the plasma membrane. Since saponin should not affect the membrane of the nucleus, we still observe a quantitative difference in the accumulation of ^{125}I -Tyr-L-MCa radioactivity in dead cells compared to live ones. The result also indicates that the intracellular concentration of ^{125}I -Tyr-L-MCa should not exceed by far the extracellular concentration of the compound since passive accumulation within permeabilized cells resembles the accumulation within live cells.

We examined the concentration-dependent uptake of ^{125}I -Tyr-L-MCa by live F98 cells using extracellular concentrations ranging from 3.3 nM to $10 \mu\text{M}$ for a 2 hour-incubation time. We then assessed the cumulated radioactivity within each subcellular fraction. As shown in Fig. 5B, evident accumulation of ^{125}I -Tyr-L-MCa occurs essentially within the cytoplasm and the nucleus at a concentration as low as 300 nM. Increasing extracellular concentrations of the ^{125}I -Tyr-L-MCa also produce

increasing elevations of the radioactivity within each fraction with similar dose-dependent profiles. In the result shown here, there was almost no accumulation within the plasma membrane fraction. There is no sign of saturation in full agreement with earlier observations using L-MCa tagged with fluorescent dyes [10,11]. The cell count, the average DHM-assessed F98 cell volume and the specific activity of ^{125}I -Tyr-L-MCa have been used to convert the experimental cpm data into average cell concentrations of ^{125}I -Tyr-L-MCa. Only cumulated cpm values from the cytoplasm and the nucleus were taken into account since the radioactivity associated to the plasma membrane fraction could bear some ^{125}I -Tyr-L-MCa from the outer leaflet of the membrane that would not be digested by the trypsin treatment as shown earlier. Obviously, this may lead to underestimation of the total accumulated ^{125}I -Tyr-L-MCa in F98 cells but this was preferable to a slightly overestimated concentration, the plasma membrane accounting for only a small fraction of the total radioactivity (<10% at all concentrations tested and for each experiment we performed). According to the method, we show a close correspondence in the intracellular concentration of ^{125}I -Tyr-L-MCa compared to the extracellular concentration (Fig. 5C). For instance at $1 \mu\text{M}$ external ^{125}I -Tyr-L-MCa, F98 cells accumulated $2.41 \mu\text{M}$ of the peptide according to DHM volume estimation ($1.14 \mu\text{M}$ according to CM-based volume estimation). Examining the internal concentration of ^{125}I -Tyr-L-MCa as a function of the external concentration indicates that the concentration ratio (internal/external) is higher at lower external concentrations than at high external concentrations. This was marked at 10 nM where penetration is barely detected with this cell penetrating peptide. Fitting the experimental data with a decreasing exponential curve yields a concentration ratio of 2.45 according to DHM data (or 1.15 according to CM data) (Fig. 5C, inset).

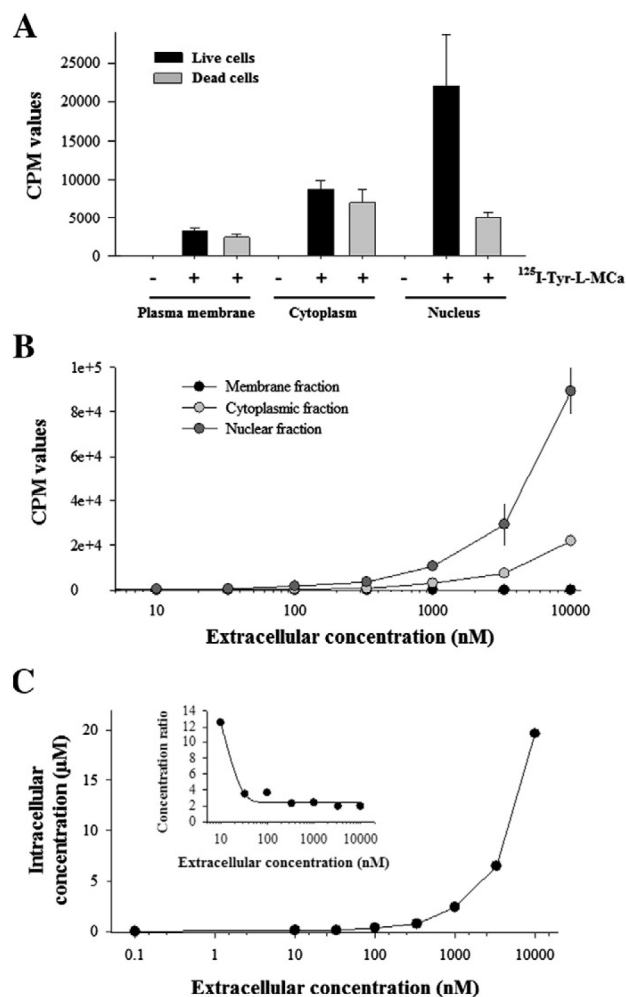


Fig. 5. Estimation of the accumulation properties of ^{125}I -Tyr-L-MCa in F98 cells. (A) Total radioactivity accumulated in subcellular fractions of live and dead cells (plasma membrane, cytoplasm, and nucleus). Radioactivity was also measured for control live cells in the absence of ^{125}I -Tyr-L-MCa. No significant counts could be measured. Extracellular concentration of ^{125}I -Tyr-L-MCa used: 33 μM . 2 h incubation. (B) Concentration dependent accumulation of ^{125}I -Tyr-L-MCa in subcellular fractions of live cells. 2 h of incubation with the radiochemical compound. (C) Evaluation of the internal concentration of ^{125}I -Tyr-L-MCa reached after 2 h incubation of live F98 cells as a function of the external concentration of ^{125}I -Tyr-L-MCa. Inset: ratio of concentration as a function of the external ^{125}I -Tyr-L-MCa. The data were fitted with the following equation $y = y_0 + a \cdot e^{-bx}$ where $y_0 = 2.45 \pm 0.31$, $a = 27.1 \pm 8.6$ and $b = 0.098 \pm 0.031$.

3.4. Kinetics of entry and exit of ^{125}I -Tyr-L-MCa into and from F98 cells

For a ^{125}I -Tyr-L-MCa accumulation in the nucleus, the peptide needs first to cross the plasma membrane, then to accumulate within the cytoplasm, and should afterwards travel to the nucleus of F98 cells. This sequence of events requires that the kinetics of accumulation within each subcellular fraction should follow a logic time gradient. This point was investigated by incubating F98 cells with 1 μM ^{125}I -Tyr-L-MCa for various durations, fractionating the cells and counting the radioactivity associated to each fraction (Fig. 6). As shown, the time constant for radioactivity accumulation in the plasma membrane is $\tau = 5$ min (Fig. 6A). This value rises to $\tau = 10$ min for the cytoplasm (Fig. 6B), which remains quite rapid, and to $\tau = 20$ min for the accumulation in the nuclear fraction of F98 cells (Fig. 6C).

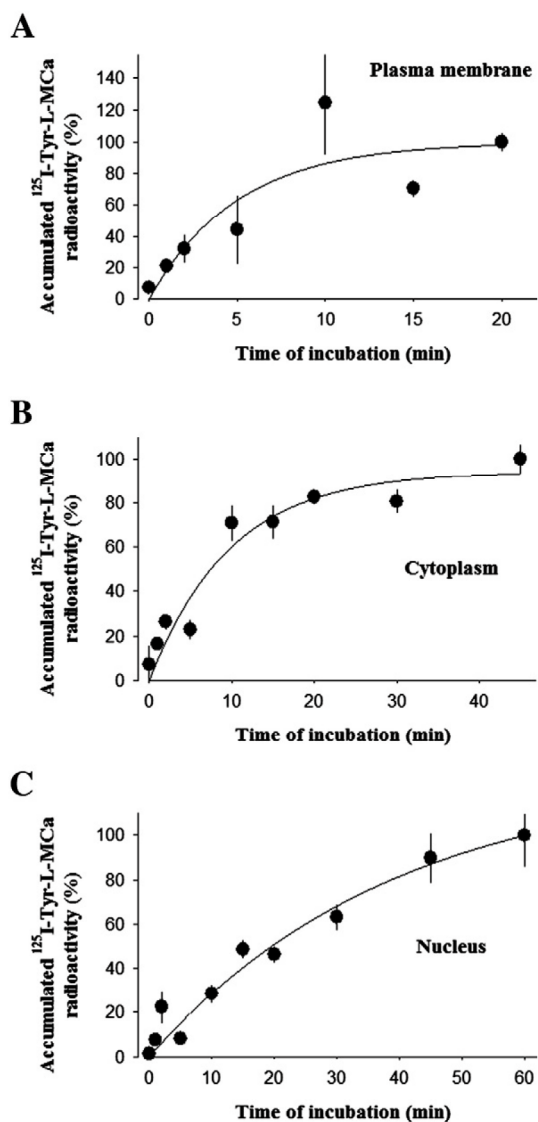


Fig. 6. Kinetics of ^{125}I -Tyr-L-MCa accumulation within the different subcellular compartments of F98 cells. (A) Kinetics of ^{125}I -Tyr-L-MCa accumulation within the plasma membrane fraction of F98 cells. The data were fitted with the equation $y = a \times (1 - e^{-bx})$ where $a = 99.8 \pm 19.7$ and $b = 0.20 \pm 0.12 \text{ min}^{-1}$. (B) Kinetics of ^{125}I -Tyr-L-MCa accumulation within the cytoplasmic fraction of F98 cells. Parameters after fitting were: $a = 94.2 \pm 8.1$ and $b = 0.10 \pm 0.02 \text{ min}^{-1}$. (C) Kinetics of ^{125}I -Tyr-L-MCa accumulation within the nuclear fraction of F98 cells. Parameters after fitting were: $a = 127.6 \pm 23.5$ and $b = 0.025 \pm 0.007 \text{ min}^{-1}$. For all these experiments we used 1 μM of ^{125}I -Tyr-L-MCa.

^{125}I -Tyr-L-MCa is heavily charged (net positive charge = +8) indicating that it may be attracted to the internal face of the plasma membrane because of the existence of the negative membrane potential. It can be envisioned that while the cell entry of the peptide is facilitated because of this membrane potential, the same negative charges residing in the cell may prevent the cell escape of the peptide. We investigated this issue by examining the gradual release of radioactivity within the external medium. As shown, F98 cells are extremely reluctant to release the radioactivity once accumulation has occurred (Fig. 7). It is only after 24 h of washout time that about 8.9% of the radioactivity is released by the cells.

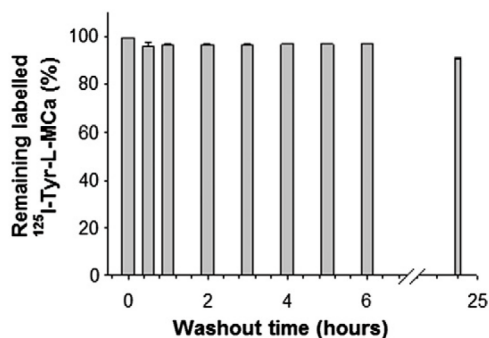


Fig. 7. Kinetics of cell exit rate of ¹²⁵I-Tyr-L-MCa from F98 cells. Time-dependent exit of ¹²⁵I-Tyr-L-MCa from F98 cells expressed as a percentage of total intracellular labeled peptide.

4. Discussion

L-MCa is the first example of a folded and oxidized animal peptide toxin acting as a CPP [6,8–12,14,21–24]. Since CPPs hold great promises in the field of drug delivery, it was therefore of great importance to determine the precise cell entry characteristics of L-MCa. Radiolabeling represents the most sensitive and quantitative method to quantify the cell entry of a molecule of interest. To this aim we produced Tyr-L-MCa that, as expected from earlier evidence, preserved proper folding and oxidation, as well as the original pharmacological properties of L-MCa and the resistance to proteolytic cleavage. The position of the extra tyrosine residue ensured that iodination occurred in a convenient way, without accessibility problems and without introducing structural disturbances within the native sequence. Compared to other reporting methods, the addition of an iodinated Tyr residue at the N-terminus of L-MCa keeps structural alterations of the peptide to a minimum.

For the first time, compared to all our earlier investigations using fluorochromes as reporters [10,11,14,21], we were able to extract valuable quantitative information on the cell penetration properties of ¹²⁵I-Tyr-L-MCa. For that purpose, we used the rat glioblastoma F98 cell line and several critical parameters to assess the penetration properties. First, we precisely defined the specific activity of ¹²⁵I-Tyr-L-MCa that allowed us to establish a precise correlation between measured cpm values and peptide quantities. Then, we used DHM to evaluate the cell volume and transform peptide quantities into intracellular concentrations. Finally, an adequate biochemical protocol combined to cell sub-fractionation helped defined cell compartments and informed on the relative cell distribution of ¹²⁵I-Tyr-L-MCa. It was striking to observe that very little radioactivity is associated to the plasma membrane fraction. This is coherent with earlier observations using MCa analogs coupled to fluorescent dyes. These vector/cargo couples were in most cases not observed at the plasma membrane level on images gathered by confocal microscopy, except on some occasions [10]. It was however possible that the lipophilic environment of the membrane could quench the fluorescence of these dyes. Our data using iodinated Tyr-L-MCa demonstrates that the plasma membrane is not a compartment of peptide accumulation on or in the cells. This indicates that the residency time of ¹²⁵I-Tyr-L-MCa within the plasma membrane is very low, a finding that is consistent with the fast kinetics of cell accumulation within the membrane. While the plasma membrane is an obligatory route of cell entry for ¹²⁵I-Tyr-L-M, the peptide must use unstable modes of interaction with the plasma membrane components. The transient nature of these interactions argues for a rapid crossing followed by a dilution process within the cytoplasm. The kinetics of accumulation within the cytoplasm is itself quite rapid (time constant of 10 min) but the degree of accumulation is significantly greater than in the plasma membrane. An interesting observation is the accumulation of the peptide within the nucleus, to a great proportion, indicating that the peptide that is transferred from the

cytoplasm to the nucleus had to be freely moving in the cytoplasm and could not be trapped within endosomes. This wouldn't have occurred if the majority of the peptide had been captured in F98 cells by a form of endocytosis such as macropinocytosis. We were not able to assess the relative volumes occupied by the cytoplasm and the nucleus. These values would however be meaningless to some extent as both compartments are themselves sub-compartmentalized. However, the values of cpm accumulation within these two compartments were closely related suggesting that most likely passive equilibrium was reached in the concentrations of the labeled peptide. In any case, the finding that the peptide is present in the nucleus contradicts other observations using dyes or proteins as cargoes, as in all cases MCa analogs were mostly confined to the cytoplasmic region presumably because of cargo-oriented trapping into endosomes [8–12,14]. In other cases, however, we found evidence for nuclear accumulation of doxorubicin as cargo [22,25–27], indicating that the matter of nuclear accumulation is cargo dependent. The reason for the accumulation of ¹²⁵I-Tyr-L-MCa in the nucleus has not been investigated. However, it may be argued that the peptide freely crosses nuclear pores and passively invades the nucleus. Because of its basic nature, it may then be stabilized there by ionic interactions with DNA. This matter may be studied later by using some of the small cell penetrating peptide variants derived from L-MCa that lack the basic nature of the full-length peptide [10,14].

The kinetics of accumulation within the plasma membrane and the cytoplasm deserve another comment. The time constant of a few minutes for the cell penetration of ¹²⁵I-Tyr-L-MCa is in apparent contrast with the second time scale required for L-MCa to trigger Ca²⁺ release after external application [6]. This difference is unlikely to be due to the extra-tyrosine residue or its labeling with iodine. The ryanodine receptor activation requires less than 10 nM internal concentration. However because of the peculiar location of the binding site of L-MCa on the ryanodine receptor [5], at the interface of the cytoplasm and the plasma membrane, it is possible that local L-MCa elevations may suffice to activate the ryanodine receptor. This would further be exaggerated by the presence of up to four binding sites of L-MCa on the ryanodine receptor, with a single occupancy being sufficient for activation. In addition, significant Ca²⁺ signals are expected with the activation of very few ryanodine receptors. Finally, considering the lipophilic environment of the L-MCa binding site, the reversibility of interaction between L-MCa and the ryanodine receptor is not evident. For all these reasons, we therefore believe that the kinetics of cell entry and Ca^m release activation cannot be easily compared.

Regarding peptide concentrations reached within the cell, we found values indicating near passive distribution between the outside and the inside of the cell. Precise estimation of cell concentration of ¹²⁵I-Tyr-L-MCa is also linked to the precise estimation of cell volume. We purposely used two techniques of cell volume investigation and found closely related values. The close to 2-fold difference suggests that our concentration values can be corrected by a factor of 2 as well. In the worst-case scenario, the global concentration of the peptide inside cells would match the outside concentration of ¹²⁵I-Tyr-L-MCa. The estimated cell volume is of course the total cell volume and does not take into account the volume loss that should be introduced by the volume of many organelles such as mitochondria, endoplasmic reticulum and the Golgi apparatus for instance, if the peptide does not accumulate into these organelles. If we take this assumption as correct, then we may assume that part of the peptide accumulation may occur against the concentration gradient. Voltage-driven accumulation may well represent one mechanism explaining how cells may cumulate higher peptide concentrations than the outside. Cells are negatively polarized. The net positively charged L-MCa should be attracted by the negative charges located underneath the plasma membrane. A second potential mechanism may be local increases of the peptide concentration at the external side of the plasma membrane. L-MCa interacts with negatively charged glycosaminoglycans [24] or negatively charged lipids [8] and the positive charges of L-MCa may contribute to greater

interactions, thereby locally increasing the peptide concentration. In any case, the finding that the labeled peptide can barely escape the intracellular environment is also evidence for the existence of an accumulation process that is not only linked to passive redistribution of the peptide into the cells. It indicates the existence of a strong asymmetry in the fluxes of Tyr-L-MCa through the membrane. This may be linked to the asymmetric lipid composition or the existence again of a voltage gradient across the plasma membrane.

Acknowledgements

We thank the following platforms (GAIA, Prométhée, and microscopie optique from Université Joseph Fourier) for their collaboration. C. Tisseyre has a fellowship from Région Rhône-Alpes (cluster 11 Handicap, Vieillessement et Neurosciences). MDW thanks the French Agence Nationale de la Recherche (program Nanofret2 and LabEx “Ion Channel Science and Therapeutics”, program number: ANR-11-LABX-0015) for financial support.

References

- [1] M. Mae, U. Langel, Cell-penetrating peptides as vectors for peptide, protein and oligonucleotide delivery, *Curr. Opin. Pharmacol.* 6 (2006) 509–514.
- [2] M. Pooga, U. Soomets, M. Hallbrink, A. Valkna, K. Saar, K. Rezaei, U. Kahl, J.X. Hao, X.J. Xu, Z. Wiesenfeld-Hallin, T. Hokfelt, T. Bartfai, U. Langel, Cell penetrating PNA constructs regulate galanin receptor levels and modify pain transmission *in vivo*, *Nat. Biotechnol.* 16 (1998) 857–861.
- [3] M. Rhee, P. Davis, Mechanism of uptake of C105Y, a novel cell-penetrating peptide, *J. Biol. Chem.* 281 (2006) 1233–1240.
- [4] A. Mosbah, R. Kharrat, Z. Fajloun, J.G. Renisio, E. Blanc, J.M. Sabatier, M. El Ayeb, H. Darbon, A new fold in the scorpion toxin family, associated with an activity on a ryanodine-sensitive calcium channel, *Proteins* 40 (2000) 436–442.
- [5] X. Altafaj, W. Cheng, E. Esteve, J. Urbani, D. Grunwald, J.M. Sabatier, R. Coronado, M. De Waard, M. Ronjat, Maurocalcine and domain A of the II–III loop of the dihydropyridine receptor Cav 1.1 subunit share common binding sites on the skeletal ryanodine receptor, *J. Biol. Chem.* 280 (2005) 4013–4016.
- [6] E. Esteve, K. Mabrouk, A. Dupuis, S. Smida-Rezgui, X. Altafaj, D. Grunwald, J.C. Platel, N. Andreotti, I. Marty, J.M. Sabatier, M. Ronjat, M. De Waard, Transduction of the scorpion toxin maurocalcine into cells. Evidence that the toxin crosses the plasma membrane, *J. Biol. Chem.* 280 (2005) 12833–12839.
- [7] S. Mouhat, B. Jouirou, A. Mosbah, M. De Waard, J.M. Sabatier, Diversity of folds in animal toxins acting on ion channels, *Biochem. J.* 378 (2004) 717–726.
- [8] S. Boisseau, K. Mabrouk, N. Ram, N. Garmy, V. Collin, A. Tadmouri, M. Mikati, J.M. Sabatier, M. Ronjat, J. Fantini, M. De Waard, Cell penetration properties of maurocalcine, a natural venom peptide active on the intracellular ryanodine receptor, *Biochim. Biophys. Acta* 1758 (2006) 308–319.
- [9] K. Mabrouk, N. Ram, S. Boisseau, F. Strappazzon, A. Rehaïm, R. Sadoul, H. Darbon, M. Ronjat, M. De Waard, Critical amino acid residues of maurocalcine involved in pharmacology, lipid interaction and cell penetration, *Biochim. Biophys. Acta* 1768 (2007) 2528–2540.
- [10] C. Poillot, H. Bichraoui, C. Tisseyre, E. Bahemberae, N. Andreotti, J.M. Sabatier, M. Ronjat, M. De Waard, Small efficient cell-penetrating peptides derived from scorpion toxin maurocalcine, *J. Biol. Chem.* 287 (2012) 17331–17342.
- [11] C. Poillot, K. Dridi, H. Bichraoui, J. Pecher, S. Alphonse, B. Douzi, M. Ronjat, H. Darbon, M. De Waard, D-Maurocalcine, a pharmacologically inert efficient cell-penetrating peptide analogue, *J. Biol. Chem.* 285 (2010) 34168–34180.
- [12] T.-N.L., N. Ram, K. Pernet-Gallay, C. Poillot, M. Ronjat, A. Andrieux, C. Arnoult, J. Daou, M. De Waard, *In vitro* and *in vivo* cell delivery of quantum dots by the cell penetrating peptide maurocalcine, *Int. J. Biomed. Nanosci. Nanotechnol.* 2 (2011) 12–32.
- [13] G.J. Stasiuk, S. Tamang, D. Imbert, C. Poillot, M. Giardiello, C. Tisseyre, E.L. Barbider, P.H. Fries, M. de Waard, P. Reiss, M. Mazzanti, Cell-permeable Ln(III) chelate-functionalized InP quantum dots as multimodal imaging agents, *ACS Nano* 5 (2011) 8193–8201.
- [14] C. Tisseyre, E. Bahemberae, L. Dardevet, J.M. Sabatier, M. Ronjat, M. De Waard, Cell penetration properties of a highly efficient mini maurocalcine Peptide, *Pharm. (Basel)* 6 (2013) 320–339.
- [15] S. Mitra, T.S. Banerjee, S.K. Hota, D. Bhattacharya, S. Das, P. Chattopadhyay, Synthesis and biological evaluation of dibenz[b, f][1,5]oxazocine derivatives for agonist activity at kappa-opioid receptor, *Eur. J. Med. Chem.* 46 (2011) 1713–1720.
- [16] E. Frampas, C. Maurel, P. Thedrez, P. Remaud-Le Saec, A. Faivre-Chauvet, J. Barbet, The intraportal injection model for liver metastasis: advantages of associated bioluminescence to assess tumor growth and influences on tumor uptake of radiolabeled anti-carcinoembryonic antigen antibody, *Nucl. Med. Commun.* 32 (2011) 147–154.
- [17] Z. Fajloun, R. Kharrat, L. Chen, C. Lecomte, E. Di Luccio, D. Bichet, M. El Ayeb, H. Rochat, P.D. Allen, I.N. Pessah, M. De Waard, J.M. Sabatier, Chemical synthesis and characterization of maurocalcine, a scorpion toxin that activates Ca(2+) release channel/ryanodine receptors, *FEBS Lett.* 469 (2000) 179–185.
- [18] R.B. Merrifield, Solid-phase peptide synthesis, *Adv. Enzymol. Relat. Areas Mol. Biol.* 32 (1969) 221–296.
- [19] E. Cuche, F. Bevilacqua, C. Depeursinge, Digital holography for quantitative phase-contrast imaging, *Opt. Lett.* 24 (1999) 291–293.
- [20] B. Rappaz, P. Marquet, E. Cuche, Y. Emery, C. Depeursinge, P. Magistretti, Measurement of the integral refractive index and dynamic cell morphology of living cells with digital holographic microscopy, *Opt. Express* 13 (2005) 9361–9373.
- [21] N. Ram, N. Weiss, I. Texier-Nogues, S. Aroui, N. Andreotti, F. Pirollet, M. Ronjat, J.M. Sabatier, H. Darbon, V. Jacquemond, M. De Waard, Design of a disulfide-less, pharmacologically-inert and chemically-competent analog of maurocalcine for the efficient transport of impermeant compounds into cells, *J. Biol. Chem.* 283 (2008) 27048–27056.
- [22] S. Aroui, N. Ram, F. Appaix, M. Ronjat, A. Kenani, F. Pirollet, M. De Waard, Maurocalcine as a non toxic drug carrier overcomes doxorubicin resistance in the cancer cell line MDA-MB 231, *Pharm. Res.* 26 (2009) 836–845.
- [23] A. Jayagopal, Y.R. Su, J.L. Blakemore, M.F. Linton, S. Fazio, F.R. Haselton, Quantum dot mediated imaging of atherosclerosis, *Nanotechnology* 20 (2009) 165102.
- [24] N. Ram, S. Aroui, E. Jaumain, H. Bichraoui, K. Mabrouk, M. Ronjat, H. Lortat-Jacob, M. De Waard, Direct peptide interaction with surface glycosaminoglycans contributes to the cell penetration of maurocalcine, *J. Biol. Chem.* 283 (2008) 24274–24284.
- [25] S. Aroui, S. Brahim, M. De Waard, J. Breard, A. Kenani, Efficient induction of apoptosis by doxorubicin coupled to cell-penetrating peptides compared to unconjugated doxorubicin in the human breast cancer cell line MDA-MB 231, *Cancer Lett.* 285 (2009) 28–38.
- [26] S. Aroui, S. Brahim, M. De Waard, A. Kenani, Cytotoxicity, intracellular distribution and uptake of doxorubicin and doxorubicin coupled to cell-penetrating peptides in different cell lines: a comparative study, *Biochem. Biophys. Res. Commun.* 391 (2010) 419–425.
- [27] S. Aroui, S. Brahim, J. Hamelin, M. De Waard, J. Breard, A. Kenani, Conjugation of doxorubicin to cell penetrating peptides sensitizes human breast MDA-MB 231 cancer cells to endogenous TRAIL-induced apoptosis, *Apoptosis* 14 (2009) 1352–1365.

Article 3:
**Chlorotoxin: A Helpful Natural
Scorpion Peptide to Diagnose Glioma and
Fight Tumor Invasion**

Article de revue publié dans le journal Toxins en 2015

Review

Chlorotoxin: A Helpful Natural Scorpion Peptide to Diagnose Glioma and Fight Tumor Invasion

Lucie Dardevet ^{1,2,3}, Dipti Rani ^{1,2}, Tarek Abd El Aziz ^{1,2,3,4}, Ingrid Bazin ⁵, Jean-Marc Sabatier ⁶, Mahmoud Fadl ⁴, Elisabeth Brambilla ^{2,7} and Michel De Waard ^{1,2,3,8,*}

¹ Grenoble Neuroscience Institute, Inserm U836, Team 3, Chemin Fortuné Ferrini, Bâtiment Edmond Safra, 38042 Grenoble Cedex 09, France;
E-Mails: lucie.dardevet@gmail.com (L.D.); diptidahiya@gmail.com (D.R.); tarek.mohamed@mu.edu.eg (T.A.E.A.)

² Science Technology Health, Université Joseph Fourier, BP53, 38041 Grenoble, France;
E-Mail: EBrambilla@chu-grenoble.fr

³ Labex Ion Channel Science and Therapeutics, 660 route des lucioles, 06560 Valbonne, France

⁴ Zoology Department, Faculty of Science, Minia University, 61519 Minia, Egypt;
E-Mail: mahmoudfs2000@yahoo.com

⁵ Ecole des Mines d'Ales, 6 av de Clavieres, 30100 Ales Cedex, France;
E-Mail: ingrid.bazin@mines-ales.fr

⁶ Inserm UMR 1097, 163, Avenue de Luminy, 13288 Marseille Cedex 09, France;
E-Mail: sabatier.jm1@libertysurf.fr

⁷ Institut Albert Bonniot, Inserm U823, Rond-Point de la Chantourne, 38706 La Tronche Cedex, France

⁸ Smartox Biotechnology, 570 Rue de la Chimie, Bâtiment Nanobio campus, 38400 Saint-Martin d'Hères, France

* Author to whom correspondence should be addressed; E-Mail: michel.dewaard@ujf-grenoble.fr; Tel.: +33-456-520-563; Fax: +33-456-520-637.

Academic Editor: Jean-Nicolas Tournier

Received: 12 November 2014 / Accepted: 20 February 2015 / Published: 27 March 2015

Abstract: Chlorotoxin is a small 36 amino-acid peptide identified from the venom of the scorpion *Leiurus quinquestriatus*. Initially, chlorotoxin was used as a pharmacological tool to characterize chloride channels. While studying glioma-specific chloride currents, it was soon discovered that chlorotoxin possesses targeting properties towards cancer cells including glioma, melanoma, small cell lung carcinoma, neuroblastoma and medulloblastoma. The investigation of the mechanism of action of chlorotoxin has been challenging because

its cell surface receptor target remains under questioning since two other receptors have been claimed besides chloride channels. Efforts on chlorotoxin-based applications focused on producing analogues helpful for glioma diagnosis, imaging and treatment. These efforts are welcome since gliomas are very aggressive brain cancers, close to impossible to cure with the current therapeutic arsenal. Among all the chlorotoxin-based strategies, the most promising one to enhance patient mean survival time appears to be the use of chlorotoxin as a targeting agent for the delivery of anti-tumor agents. Finally, the discovery of chlorotoxin has led to the screening of other scorpion venoms to identify chlorotoxin-like peptides. So far several new candidates have been identified. Only detailed research and clinical investigations will tell us if they share the same anti-tumor potential as chlorotoxin.

Keywords: chlorotoxin; glioma; cancer; targeting; diagnosis; treatment; therapy; chloride channel; Annexin A2; metalloprotease

1. Glioma, a Difficult to Cure Human Brain Cancer

Amongst primary brain tumors, gliomas can be considered as the most lethal malignant tumors. This is a family of central nervous system (CNS) tumors derived from differentiated glial cells or glioblastoma stem-like cells [1,2]. It is composed of glioblastoma multiforme (GBM), anaplastic astrocytoma, astrocytoma and oligodendroglioma. The two first gliomas occur at an incidence of 78% of all the primary brain tumors. Gliomas represent very aggressive brain cancers characterized with a fast cell proliferation rate and a strong tendency to invade healthy brain tissue (French Foundation for medical research). Even low-grade gliomas infiltrate the entire brain. The molecular mechanisms of brain tumor invasion are complex. They involve (i) modification of receptor-mediated adhesive properties of tumors cells; (ii) degradation and remodeling of the extracellular matrix by tumor-secreted metalloproteinases; and (iii) creation of an intercellular space for tumor cell invasion (See Box 1). Standard treatment involves surgery whenever the tumor mass is accessible, followed by chemoradiation and adjuvant chemotherapy with temozolomide. In spite of this therapeutic arsenal, the survival rate of patients rarely exceeds sixteen months [3]. At best, 3% of the patients may benefit of a five-year survival time. This fatal outcome points to other major issues with gliomas, which is their resistance to radiation and chemotherapy, and the difficulty to accurately localize them within the tissue. Although it is possible to roughly visualize the tumor with current imaging techniques, it is very tedious to determine the exact boundaries of tumor invasion. In addition, diagnosis of this cancer still requires tissue biopsy and histopathological analyses. Histological features of interest comprise vascular proliferation and focal necrosis.

Box 1. Mechanism of glioma cell invasion.

Cell invasion is a natural mechanism that plays an important role in embryonic development, wound healing, immune response and tissue repair. In this situation, the cell migrates on the influence of chemical signals, physical cues and physicochemical processes. Unfortunately, when this complex mechanism is affected by deleterious mutations, an uncontrolled cell invasion leads to the development of several pathologies (e.g., arthritis, atherosclerosis, aneurism, chronic obstructive pulmonary disease, etc.). In the case of cancer, it leads to metastasis or an infiltrative tumor [4]. One of the major characteristics of glioma cells is their propensity to invade healthy brain tissue. The principal mode of invasion of a glioma cell is a single cell invasion, which can be decomposed into five steps: (i) change in glioma cell morphology (formation of membrane protrusions); (ii) interaction between membrane protrusions and extracellular matrix (ECM) to obtain traction; (iii) degradation of ECM by matrix metalloprotease (MMP)-proteins among others; (iv) change of shape (contraction) for the cell to cross the “ECM hole”; (v) detachment of the rear end connection (the cell moves forward). The key abilities for glioma cells to invade healthy brain tissue are modification of cell adhesion property, degradation of ECM, and change of shape. The invading tumor cells do not spread anarchically in the brain, the degradation of ECM occurs at the border between the tumor and the healthy tissue [5]. The invading cells spread following existing anatomical structures such as nerves and blood vessels [6]. During the first steps of invasion, glioma cells will interact with ECM and its environment thanks to adhesion proteins, especially integrins, giving the cell traction points to displace. Then, using proteolytic enzymes, such as the MMP proteins, the cells begin to degrade the ECM, to create a space in which through which they can pass. In order to move through the newly created space, glioma cells need a change in shape and volume. At this point, glioma cells use ionic channels (Cl^- and K^+ channel) to shrink, and so fit the space to pursue the invasion. Because of adhesion molecules and specific cell surface receptors, cancer cells move forward in the invasive direction [4,6,7]. When the invasive cells reach a certain distance from the primary tumor mass, they re-enter the cell cycle and form a new tumor mass [8].

In this context, therefore, the identification of marker molecules, specifically binding to tumor cells, would represent a tremendous asset to researchers and clinicians aiming at precisely localizing the tumor mass. If, in addition, such a marker molecule could selectively deliver therapeutic agents to these cancer cells, this would enlarge the arsenal of chemical entities used in therapeutics to treat gliomas. Tumor-specific targeted therapies are increasingly used strategies that have demonstrated their potential through the emergence and development of antibodies, antibody-like ligands, proteins, peptides or chemical drugs to identify, localize or treat cancers [9]. The principle of targeted therapies is based on the identification of a suitable molecular target expressed at the surface of a given cell type. Most of the time, it is a membrane receptor that is over-expressed or preferentially expressed in cancer cells. Targeting the cancer cells ensures that the normal brain tissue is not affected by a cytotoxic drug that would be conjugated to the ligand that binds to the specific cell target. All of the targeting agents should have tolerable cell toxicities, fit mass production criteria, and have a high specificity or selectivity of binding to tumors cell or other tumor-related targets (vascular cells). For gliomas, in addition to these characteristics, the ability of the targeting agent to naturally cross the blood brain barrier (BBB) would be a desirable property. Alternatively, this targeting agent should at least cross the blood-brain tumor barrier (BBTB). This would prevent the need for a loco-regional injection to deliver the targeting agent to the tumor site within the brain. In spite of these evident advantages, investigators were unable to unequivocally identify glioma-specific markers so far. Reasons for this problematic deficit come from the great genetic and antigenic variability of gliomas. This further explains why the diagnosis of this

cancer type still requires tissue biopsy and histopathological analyses. This situation has recently changed with the identification of chlorotoxin (CTX) for glioma detection.

2. Animal Toxins, Wonderful Potent Natural Peptides for Therapy and Diagnosis

Peptides are increasingly considered as good drug candidates for therapeutic applications. In 2009, 438 peptides were considered by the pharmaceutical industry in their development programs. Of these candidates, 72 were in Phase III clinical trials. Forty-eight peptides are now on the market. In 2007, four of them reached global sales over 500 million dollars each: copaxane (\$3.33 billions), lupron (\$1.88 billions), byetta (\$967 millions) and forteo (\$709 millions). The majority of these peptides target G protein coupled receptors, although other targets are increasingly common, such as ion channels.

A complete report on the development of peptides as therapeutic drugs can be requested from <http://www.peptidetherapeutics.org>. Obviously, it may seem odd at first glance to consider animal toxins as potential drugs. However, animal venoms are enriched sources of biologically active peptides of about 100 to a 1000 different components. In addition, peptides issued from venoms are tailored by Nature to be extremely stable *in vivo*. Different from synthetic chemical libraries, all toxins present in venoms are active, often at nanomolar affinities. In addition, while venoms can be toxic, the toxicity is mainly due to a few peptide members or to the synergistic effect of a combination of peptides. As a matter of fact, the vast majority of venom components possesses interesting therapeutic potential that can be usefully exploited. Hence, several toxins are actually in various clinical phases for the treatment of pain, epilepsy, cancer, atherosclerosis and cardiac failure. It might be of interest that many of these natural peptides target ion channels, ionotropic receptors, transporters and G protein coupled receptors. They also have been found to target enzymes, all constituting major pharmacological classes for the treatment of pathological conditions. Other unusual cell targets have been reported. Disintegrins, a group of snake venom toxins, have the potential to block cancer cell migration and invasion *via* an RGD-dependent sequence that interacts with integrins, a class of membrane proteins required for cell immobilization through interaction with the extracellular matrix [10,11].

3. Chlorotoxin, a Natural Peptide Acting as a Potent Glioma Marker

CTX is a small neurotoxin of 36 amino acids, isolated in 1993 from the venom of the Israeli scorpion *Leiurus quinquestriatus* [12]. It holds great promise for the treatment of glioma and other solid tumors. CTX has a compact structure, which is maintained by four disulfide bonds that connect the eight cysteine residues present in the sequence. The amino acid sequence of this natural peptide is detailed in Figure 1A. The cysteine pattern adopted is of the type C₁-C₄, C₂-C₆, C₃-C₇ and C₅-C₈. Three small antiparallel β -sheets are packed against an α -helix [12] (Figure 1B). With its compact structure, CTX was proposed to cross the BBB (TransMolecular, Inc., Cambridge, MA, USA; unpublished data). However, the data were not sufficiently substantiated to firmly demonstrate that CTX crosses the BBB rather than the BBTB. Nevertheless, it was clear that CTX diffused deeply into the tumors while other targeting agents such as antibodies could not [9,13]. Another report showed that in transgenic mice that spontaneously develop brain medulloblastoma cancers, a fluorescently-tagged Cy5.5-CTX labeled cancer cells while no disruption of the BBB was observed (exclusion of blue Evans labeling of brain structures) [14]. Since this is the only study that investigates the issue of the BBB crossing by CTX and

that BBB disturbance by tumors may depend on the tumor type and the stage of progression, it remains cautious to state that CTX crosses at least the BBTB. As a component of the scorpion venom, CTX induces paralysis in small insects or other invertebrates that may be stung by the scorpion. When injected in vertebrates, however, no apparent signs of toxicity have been observed. This indicates that the binding of CTX on its cell surface receptor has no cell toxic or unwanted physiological consequences, as observed for many other animal toxins.

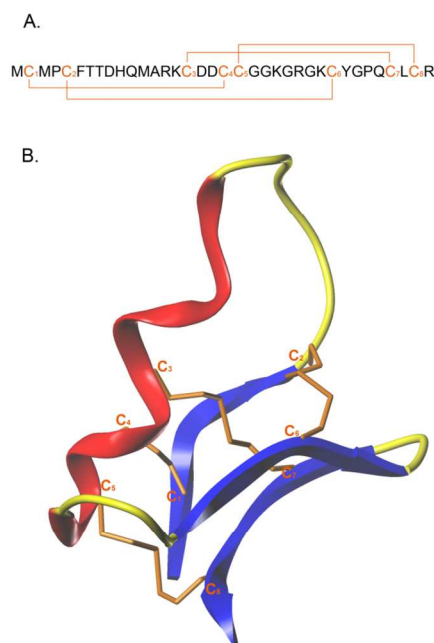


Figure 1. Amino acid sequence and 3D representation of CTX: **(A)** Amino acid sequence of CTX with the eight cysteine residues and the four disulfide bridge in orange; **(B)** 3D structure of CTX, obtain from 1CHL PDB file; α -helix in red, β sheet in blue and disulfide bridge in orange.

As developed in Section 4, none of the proposed receptors of CTX present important properties for cell survival, although they can be considered as pro-factors for glioma development.

The amino acid sequence of CTX presents several interesting features for its labeling by a number of compounds. Following chemical modification, CTX can then be used to (i) identify its receptor; (ii) characterize its pharmacological properties; and (iii) investigate its mode of action. Several types of chemical modifications have been performed. CTX contains a single tyrosine residue at position 29 that can be used successfully for iodination. ^{125}I -CTX has been used to determine the number of receptor binding sites and the affinity of CTX for these sites from cultured glioma cell lines [15]. ^{131}I -CTX was used instead of ^{125}I -CTX for *in vivo* approaches to obtain gamma-ray scintigram scans because of its higher γ emission properties. Intact activity after iodination of Tyr²⁹ demonstrates that this amino acid is not critical for CTX activity. Lysine residues can also be used to easily perform conjugation of active substances thanks to a wide range of cross-linking reagents. Finally, Oregon green-labeled CTX and a complex of biotin-CTX/avidin-rhodamine have been used for immunohistochemical detection of glioma

cells in culture, human glioma xenografts in SCID mice or in patients biopsies [15]. For the biopsies, the intensity of the labeling was found to increase with the malignancy grade of the tumors.

Table 1. Summary of various human tissues stained with CTX.

Tissues origin	Tissues types	Cases	Results
<i>Primary brain tumors (glioma)</i>	Glioblastoma multiforme WHO Grade IV	31	31 positive
	Anaplastic astrocytoma WHO Grade III	7	7 positive
	Low-grade astrocytoma WHO Grade II	4	4 positive
	Pilocytic astrocytoma WHO Grade I	14	13 positive, 1 negative
	Other ungraded gliomas	5	4 positive, 1 negative
	Oligodendroglioma	8	8 positive
	Gliosarcoma	2	2 positive
	Ganglioglioma	5	5 positive
	Meningioma	25	20 positive, 5 negative
	Ependymoma	3	3 positive
<i>Other normal or diseased brain tissue</i>	Alzheimer's brain	8	8 negative
	Parkinson's/schizophrenic brain	4	4 negative (2 each)
	Normal brain or uninvolved tissue of brain cancer patients	29	21 negative, 8 positive *
	Epilepsy/gliosis/stroke brain	6	6 negative ‡
<i>Neuroectodermal tumors</i>	Medulloblastoma	4	4 positive
	Neuroblastoma	9	8 positive 1 negative
	Ganglioneuroma	4	4 positive
	Melanoma (metastatic)	11	11 positive
	Melanoma (primary)	5	5 positive
	Pheochromocytoma	6	5 positive, 1 negative
	Ewing's sarcoma	2	2 positive
	Primitive neuroectodermal tumors	2	2 negative
	Small cell lung carcinoma	6	5 positive, 1 negative
	Schwannoma	4	4 positive
<i>Other brain tumors</i>	Epidermoid cysts	5	1 positive, 4 negative
	Brain tumors of unknown pathology	9	9 positive
	Pituitary gland of glioblastoma multiforme pt.	2	2 positive
	Metastatic tumors to brain	17	15 positive, 2 negative §
<i>Other tumors</i>	Breast cancer	14	13 positive, 1 negative
	Breast cancer metastases	11	11 positive
	Kidney cancer	3	3 positive
	Liver cancer	3	3 positive
	Lung cancer	3	3 positive
	Lymphoma	2	2 positive
	Ovarian cancer	3	3 positive
	Pancreatic cancer	3	3 positive
	Prostate cancer	9	8 positive, 1 negative
	<i>Normal human tissues</i>	Breast	2
Colon		2	2 negative
Endometrium/myometrium		3	3 negative
Eyeball (cross-section)		1	1 negative
Heart		2	2 negative
Kidney		3	3 negative ¶
Adrenal gland		3	3 negative
Liver		2	2 negative
Lung		3	3 negative
Lymph node		3	1 positive, 2 negative
Meninges		3	3 negative
Muscle (skeletal)		2	2 negative
Thyroid		1	1 negative
Pancreas		3	1 positive, 2 negative
Prostate		3	1 positive, 2 negative
Spleen		2	2 negative
Stomach		2	2 negative
Ovary		2	2 negative
Skin		6	6 negative
Testes		2	2 negative

*: samples from normal brains or from area of a glioblastoma multiforme patient's brain diagnosed not to be involved in glioblastoma multiforme; ‡: Areas of glial cell reactivity show a few cells binding bCITx; §: Metastatic tumors of unknown tissue origin; ¶: a few positive cells were observed.

Soroceanu *et al.* demonstrated that ^{125}I -labelled CTX has both high and low affinity binding sites on glioma cells and is able to label cancer cells on biopsies of human patients affected with glioma [15]. They also showed that injection of ^{131}I -CTX by IV route in SCID mice bearing human glioma tumor lead to specific peptide accumulation within the tumor. This study proves that CTX is able to label cancer cells *in situ* in the brain. A few years later, Lyons *et al.* showed that CTX binds to glioma cells as previously described but also to other tumors of the same neuroectodermal origin [16]. These additional studies, performed on over 200 tissue biopsies, include melanoma, small cell lung carcinoma, neuroblastoma, medulloblastoma, Ewing's sarcoma and pheochromocytoma. These findings further extend the range of applications in which CTX may be used (Table 1). All these properties highlight the fact that CTX is a very attractive peptide for targeted cancer therapy or imaging. As a matter of fact, these properties were exploited by TransMolecular Incorporation that launched CTX for clinical trials under its trade name TM-601. After completion of clinical Phase II, the intellectual property rights on the molecule were acquired by Morphotek Incorporation, a US-based subsidiary of Eisa Corporation. In order to facilitate phenotyping and histological staining, a full line of CTX-labeled derivatives has been produced by TransMolecular Incorporation under the terms TM602, TM604, *etc.* We will give more details on the interest of TM-601 later in the review. So far, TM-601 is the only derivative of CTX for which human clinical studies are partially published.

This review article provides an overview of the research progress that has been made on CTX, namely on its mechanism of action and the development of CTX-derived compounds for the detection and treatment of glioma. A small part of our analysis will also be devoted to the discovery of chlorotoxin-like peptides of therapeutic potential.

4. Mode of Action of CTX: Looking for a Glioma-Specific Receptor

Chloride channels—Originally, CTX holds its name from its pharmacological effect on rat colonic epithelial cell chloride channels as described by Debin *et al.* in 1993 [12]. Small conductance Cl^- channels were shown to be potently blocked by CTX when the latter was applied towards the intracellular face of the channel [12,17]. After this initial characterization, CTX has been used as a general pharmacological tool to investigate the function of chloride channels. It is through this procedure that Ullrich *et al.* discovered the existence of specific CTX-sensitive glioma chloride currents in acute slices of human gliomas [18]. To further identify this receptor/ion channel, ^{125}I -CTX binding to various malignant glioma cell lines (D54-MG, SK-1-MG, U87-MG, U105-MG, U251-MG and U373-MG) was investigated [15]. Using radioreceptor assays, the authors identified a 72 kDa band as the receptor of ^{125}I -CTX. This molecular weight is in agreement with the molecular weight of CLC, a family of chloride channels [19]. Prolonged exposure to CTX results in cell internalization of this channel type [20]. What may seem as the most promising result is the fact that although gliomas come with an amazing degree of antigenic variability, they all seem to over-express this CTX-sensitive chloride current [21,22]. These channels are absent or in low abundance in healthy tissues or in tumors of non-glial origin [23]. Interestingly, expression of this channel type appears to be correlated with the histopathological tumor grade. High-grade tumors express more chloride channels than low tumor grades. The role of this channel type in glioma is still obscure but one suggestion is that it may facilitate the modifications in cell volume and shape that accompany glioma cell migration and healthy brain tissue invasion [24].

Indeed, Cl^- ions movement across the plasma membrane controls the cell volume changes. In turn, the change in glioma cell shape is required for cell invasion within the novel extracellular spaces created between healthy cells. This CLC chloride channel is therefore of potential importance for glioma malignancy. In this context, CTX would act by inhibiting Cl^- flux and limiting the extent of glioma cell shape alteration, thereby hampering the glioma tissue invasion potency. Other chloride channel inhibitors have been tested and also shown to inhibit glioma migration [8]. This model fits well with the reported anti-invasive effects of CTX on glioma cells and the inhibition of metastasis [5,8,20,21,25,26]. More information about the role of ion channels in glioma invasion can be found in several excellent review articles [8,25,26]. From the literature, it can be inferred that chloride channels constitute a marker of interest for the diagnosis of glioma and, because of their role in tumor growth, they can be used as a potential target for therapeutic approaches. In any case, the data point to the fact that the chloride channel may constitute a marker of interest for the diagnosis of glioma, and, because of its function in tumor growth, a potential target for therapeutic approaches. Nevertheless, the arguments in favor of a chloride channel as the actual target of CTX need to be balanced with more negative findings: (i) patch-clamp reports showing that, in spite of CTX-mediated chloride current block, the functional inhibition of the channel occurs with a lower affinity than expected from binding experiments (600 nM) [18]; and (ii) CTX has no effect on the proliferative rate of C6 glioma cells *in vitro* [24]. In fact, in their binding studies, Soroceanu *et al.* found two binding sites for ^{125}I -CTX in glioma cell lines *in vitro*: a high affinity binding site with a K_d value of 4–9 nM and a low affinity one with a K_d in the 0.5–1 μM range. These findings may argue for the existence of more than one type of membrane receptors for CTX.

Matrix metalloprotease MMP-2—While searching for the molecular identity of the cell surface receptor of CTX, a 6His-tagged CTX analogue was designed and used to prepare an affinity column for mass spectrometry-mediated identification of CTX receptor from a solubilized human D54-MG glioma cell line. Surprisingly, the authors found that besides interacting with the CLC-3 chloride channel, CTX also brought along a complex of proteins that comprises membrane type 1 matrix metalloprotease MT1-MMP, matrix metalloprotease MMP-2 and tissue inhibitor of matrix metalloproteinase-2 TIMP-2 [5]. The matrix metalloprotease MMP-2 is expressed in glioma and other tumors but is not present in normal brain tissues. It is part of the larger family of metalloproteases that have been associated with the enzymatic degradation of the extracellular matrix (ECM). Excess matrix metalloprotease MMP-2 expression is therefore related to the easiness of the tissue invasion capability of glioma cells. All types of tumors reported to bind CTX were found to over-express the matrix metalloprotease MMP-2. This correlation between the expression level of MMP-2 and CTX binding supports the concept that the matrix metalloprotease MMP-2 may be part of the receptor complex of CTX. Within the protein complex interacting with CTX, the authors also identified the presence of $\alpha\text{v}\beta 3$ integrin [20]. How integrins, matrix metalloproteases and chloride channels come together to interact with CTX remains a difficult issue to solve. Obviously, more research has to be done in terms of biochemistry and cell biology to define with which protein exactly CTX may interact to pull-down such a large protein complex. Considering the size of the peptide, it may appear unlikely that CTX can interact with all these protein partners simultaneously. It is, however, not uncommon that an animal toxin lacks selectivity and is capable of binding to several types of membrane receptors. Of course, the matrix metalloprotease MMP-2 also appears to be an interesting target for explaining the effects of CTX. The matrix metalloprotease MMP-2 is involved in ECM degradation, and the local enzymatic activity of this protein

in the tumor environment should logically favor glioma cell division and migration. Interestingly, CTX has been observed to inhibit the enzymatic activity of the matrix metalloprotease MMP-2 and to promote endocytosis of this metalloprotease in glioma [5]. These two factors combined should reduce the extent of ECM degradation that can be sustained by the remaining matrix metalloprotease MMP-2 thereby providing another explanation of CTX-mediated inhibition of cell invasion. In any case, a compound that would prevent both ECM degradation and chloride channel-mediated cell shape alterations would be ideal. Conceptually, it is preferable to envision that Cl^- channels are associated with a complex of proteins formed by MMP-2, $\alpha\text{v}\beta 3$ integrin, MT1-MMP and TIMP-2. CTX would not bind to individual receptors, but instead to this complex of proteins, and this binding would produce internalization of the entire protein complex, thereby leading to reduction of the activity of both the chloride channel and the MMP-2 [20]. This CTX-mediated internalization process would occur in caveolar rafts. In agreement with this concept, it was found that the effect of CTX on Cl^- current took over 15 min, a time lapse more compatible with receptor internalization than with ion channel blockade. Interestingly, the observation that CTX is also co-internalized during this process explains why the iodinated analogue of CTX is still visualized within tumors eight days after administration in clinical trials [27]. Arguably, the existence of such a protein complex that comprises both metalloproteinases and chloride channels makes sense for cancer cells because of the imperious need to degrade ECM and concomitantly alter cell morphology to facilitate the infiltration of tiny intercellular spaces. A study further reports that CTX, coupled to iron nanoparticles, inhibits the invasive nature of glioma cells *in vitro*, deactivates membrane-bound metalloproteinase 2, produces receptor-mediated endocytosis and inhibits cell volume changes [13].

Annexin A2—As if things were not complex enough, another research group now claims that the CTX receptor is annexin A2. This study was prompted by a contradictory report about MMP-2 as CTX receptor [14]. The observation was made that CTX also bound to a non-tumor cell type (proliferating human vascular endothelial cells) which also makes CTX a potent anti-angiogenic agent [28]. Based on this observation, TransMolecular Inc. reinvestigated the identity of the endothelial/glioma CTX receptor using affinity columns, cross-linking reagents and mass spectrometry. Annexin A2 was identified as the common receptor component that binds TM602, the biotinylated derivative of CTX, in all cell lines [29]. Annexin A2 is a calcium-dependent phospholipid binding protein present on the extracellular side of the plasma membrane of various tumor cells and endothelial cell types. It has many roles in cellular functions such as angiogenesis, apoptosis, cell migration, proliferation, invasion and cohesion. siRNA knockout of annexin A2 results in reduced binding of a technetium-99m-labelled-TM601 in cell lines expressing annexin A2. Interestingly, the same siRNA-mediated knockout decreases the *in vitro* migration of glioma cells [30]. In any case, these studies promote the idea that annexin A2 is an interesting therapeutic target in angiogenesis and tumor progression [31], although they dramatically complicate the landscape with regard to the identity of the real CTX receptor. In addition, while annexin A2 is involved in cell proliferation, migration and invasion, not much is known about how CTX binding to annexin A2 may hamper glioma invasion in the brain.

All these potential CTX receptors appear to be over-expressed in other tumors. This is the case of MMP-2 in breast, colon, skin, lung, prostate and ovary cancers, but also for annexin A2 in colorectal, pancreatic prostate and lung cancers, and hepatocellular and squamous cell carcinomas. This may explain why CTX also targets other cancer types [5,9,14,15,18,21,32] (Table 1). The multiplicity of claimed “true” receptors of CTX may seem disturbing at once unless one considers that they are all part

of the same receptor complex. While MMP-2 and annexin-2 are all possible receptors at this stage, it is worth mentioning, however, that most animal toxins target ion channels. It may therefore come as a surprise that CTX may target (a) receptor(s) of a different nature than ion channels. Regardless of the nature of the true CTX receptor, the mechanism of CTX action on glioma needs refinement; most likely by a complete structure–function analysis that sorts out the structural determinants of CTX involved in binding on each one of these multiple potential receptors.

5. Targeted Imaging of Glioma by CTX

The first step in glioma treatment is surgical removal of the tumor mass if possible. Because of its great tendency to invade the normal brain tissue, it is very difficult for a surgeon to remove the entire tumor without leaving some cancerous cells located outside of the main tumor mass. Cancer cells that could not be removed by the surgeon will unavoidably cause the formation of new tumor mass(es) provoking the relapse of the patient. This is the reason why molecular tools for glioma detection and imaging are needed to provide efficient help to the surgeon and to evaluate the benefit of a different treatment than surgery. CTX is a small neurotoxin peptide that selectively binds to glioma cells. As it can be chemically synthesized and easily modified with appropriate imaging or therapeutic functions, several reports demonstrate that it can be used as a tool for glioma detection and imaging [14,27,33–41].

On the basis of this principle, three types of compounds have been designed. The first type is composed of CTX covalently coupled to a fluorescent indicator, Cy5.5. This tool should allow a surgeon to directly visualize cancer cells in real-time during tumor resection [14,33,34]. The second type of compound is composed of a Magnetic Resonance Imaging (MRI) contrast agent coupled to CTX as targeting ligand [27,35,36]. Finally, the third type of complex is composed of multifunctional nanoparticles, generally MRI contrast agents associated with optical imaging or therapeutic agents, together with CTX [37–41].

“Tumor paint” is a complex of CTX (as targeting agent) and Cy5.5, a near-infrared fluorescent (NIRF) molecule, first described by Veiseh *et al.* [14]. While CTX is able to specifically bind to glioma and related tumor cells, it cannot be detected in the absence of a convenient marker. Cy5.5 is an interesting marker because it emits photons in the near-IR spectrum. These types of photons have the particularity to be poorly absorbed by water and hemoglobin, making them compatible with intraoperative imaging. Bioconjugation of CTX to Cy5.5 was performed via NHS ester crosslinking. Cy5.5 NHS ester will react with CTX primary amines to form CTX-Cy5.5. The trouble with this approach is that there are four primary amines on CTX (three lysine residues (Lys¹⁵, Lys²³ and Lys²⁷) and the *N*-terminal amine group) that are all able to react with NHS ester Cy5.5, thus potentially yielding a mixture of mono-, di-, and tri-labeled peptides. Although it can be envisioned to use a mixture of labeled peptides to detect pathological tumor masses, it is technically challenging and costly to reproducibly preserve the exact ratio between these different labeled compounds [33]. A solution to this problem has been proposed by Akcan *et al.* [34]. In their report, they substituted the lysine residues at position 15 and 23 by alanine or arginine. These two lysine residues were targeted because they react minimally with Cy5.5 NHS esters. The conditions of labeling with Cy5.5 were chosen in such a way that the *N*-terminal primary amine was not labeled. According to this procedure, they obtained monolabeled CTX with Cy5.5 grafted onto Lys²⁷ only. Cy5.5 labeling of a non-mutated, but cyclized CTX surprisingly also yielded a monolabeled peptide [34]. All these generated compounds (the original tumor paint CTX-Cy5.5 multi-labeled compound, the

mono-labeled mutated CTX, and the cyclic labeled CTX) have kept their ability to target tumor cells. More studies have been conducted with the tumor paint CTX-Cy5.5 compound on both toxicity and biodistribution [14]. The bioconjugate is homogeneously distributed in mice upon IV injection. Renal accumulation could be observed, but not to abnormal levels since CTX itself is eliminated in the urine. No toxic effect was observed two weeks after exposure to CTX-Cy5.5 in mice. This compound will progress towards use in human clinical trials. It should ease the definition of glioma boundaries upon surgery and hopefully increase the mean survival time of the operated patients that may benefit of this technology.

MRI contrast agents are needed to visualize the precise glioma localization within the brain and determine the exact size of the tumors. Gadolinium ions (Gd(III)) are widely used MRI contrast agents when chelated in appropriate molecular cages (e.g., Gd(III)-diethylenetriaminepentaacetic acid (Gd-DTPA) from Magnevist and Gd(III)-N,N0,N00,N000-tetracarboxymethyl-1,4,7,10-tetraazacyclododecane (Gd-DOTA) [36]. They are stable and have low molecular weights. However, they are rapidly eliminated and do not possess intrinsic targeting abilities. In order to enhance the retention time of these Gd-based contrast agents in mice and add a targeting function to the contrast agent, Huang *et al.* created a dendrigraft poly-L-lysine (DGL) compound [36]. DGL is a L-lysine dendritic macromolecule that carries both Gd chelates and CTX. This compound allows a better uptake of the contrast agent by tumor cells and provides a targeting cancer cell property to the macromolecule. The retention time in the tumor was enhanced as expected and greater signal intensity was recorded. This compound shows no apparent toxicity, making it a good candidate as MRI contrast agent for glioma detection in the future.

Finally, nanoprobess have been used as MRI contrast agents as well. Contrary to Gd chelates, nanoprobess provide a better resolution of the edge of the tumor thanks to an improved cellular uptake and a slower clearance at the tumor site [35]. Nevertheless, they similarly do not possess any intrinsic tumor-targeting ability so that they seem to preferentially label the reticulo-endothelial system surrounding the tumor site. In order to overcome this problem, a new nanoprobe composed of an iron superoxide particle, coated with polyethylene glycol (PEG), and conjugated with CTX was designed [35]. The efficiency of this nanoprobe was evaluated *in vitro* and *in vivo* in mice. It shows a real improvement in tumor targeting efficiency compared to nanoprobess lacking CTX conjugation. These CTX-functionalized nanoprobess have no detectable toxic effects. The most interesting thing about these nanoprobess is that not all the PEG molecules are used to fix CTX. These nanoprobess can therefore be used as a conjugation platform not only to target and identify cancer cells, but also to fight cancer cells. It is with this view in mind that the same research group has designed improved nanoprobess [37,38]. This enhanced version of the nanoprobess [37] has better characteristics: (i) the probes pass the BBB or the BBTB and present reduced opsonisation properties; (ii) they are composed of biocompatible material and (iii) contain Cy5.5, an additional diagnostic component. This new nanoprobe offers combined MRI detectability and near-IR fluorescent detection. Because this compound has a demonstrated residency time exceeding five days in cancer cells, it would allow preoperative diagnostics, followed by intra-operating imaging during tumor resection and post-operative control. Moreover, with such a nanoprobe platform, there is additional room for further chemical functionalization in order to have other specific applications. Cy5.5 is not the only dye that has been used to create multifunctional superparamagnetic iron oxide nanoparticles. Fluorescein isothiocyanate (FITC) has also been successfully added to this type of nanoparticle [39]. Regarding the emission spectra of FITC, this nanoprobe can only be used *in vitro*. A good discrimination between glioma cells and healthy tissue has been described for this compound.

Table 2. Summary of various compound made with CTX.

Types of link	Cargos	Application	References
Covalently link to	<i>Iode</i> ¹²⁵ I, ¹³¹ I	Radiotherapy and Imaging	[3,9,15,28,32,35,40,42,43]
	<i>Fluorescent dyes</i>		
	Cy5.5	Imaging and detection	[14,15,29]
	Oregon green		
	<i>Drugs</i>		
	Platinum	Therapeutic	[44,45]
	Anticancer drugs		
	<i>Biotine</i>	Immunostaining detection	[15]
	<i>Nitric oxide</i>	Therapeutic adjuvant	[46]
	Covalently link to a vehicle	<i>Nanoparticle</i>	
Iron superoxides core		MRI contrast agent	[34]
Multifunctional nanoprobes + Fluorescent dyes (Cy5.5, FITC, Alexa fluor)		MRI contrast agent and imaging agent	[13,36,37]
Multifunctional nanoprobes + cDNA or siRNA		MRI contrast agent and therapeutic	[38,47]
Multifunctional nanoprobes + Methotrexate		Therapeutic and MRI contrast agent	[39]
PEI core + cDNA+ Fluorescent dyes		Therapeutic and imaging	[48,49]
<i>Liposome</i> Doxorubicine loaded		Therapeutic	[50]
<i>Dendrigrapt poly Lysine</i> With Gadelinium		MRI contrast agent	[33]
<i>Empty capsule of hepatitis B</i>	Future therapeutic vector	[51]	

Besides imaging tumors, multifunctional nanoparticles have also been designed for cancer treatment (Table 2). Instead of a dye or other markers, drugs or siRNA, DNA is being used. Since the main interest of this type of compound is the therapeutic area, more details will be given in the next section. Developing dual imaging/therapeutic molecules based on CTX is of course not exclusively limited to multifunctional nanoprobes since ¹³¹I-TM601, a radiolabeled CTX, designed at first for radiotherapy of glioma, has shown an evident efficacy to visualize brain tumors by SPECT [27]. More details on this compound will be provided in the following subsection.

6. Chlorotoxin as Therapeutic Targeting Peptides

After glioma surgery has been performed, the next step to treat glioma is radiotherapy with or without chemotherapy. In this area, CTX is also used as a targeting peptide to precisely deliver a therapeutic agent or radionuclides (Table 2).

The first CTX compound developed was ¹³¹I-TM601. It entered clinical trial in 2002 in the USA. This compound is made of a synthetic version of CTX named TM-601 on which iodination was performed on Tyr²⁹. ¹³¹I-TM601 is the subject of several publications [3,9,27–29,32,42,43,52], and many patents have been filled in to protect its use as a therapeutic drug. The Phase I study was conducted to determine the safety, biodistribution, tolerability and dosimetry of intracavitary injection of ¹³¹I-TM601 in adult patients affected with high grade glioma [42]. A single dose of intracavitary administration of

10 mCi of ^{131}I -TM601 (0.25 to 1 mg of product) seems to be well tolerated. This result demonstrated the safety and the good tolerance of the patients to the product over the 180-day period observation. However, three of the eighteen patients developed adverse effects that were imputed to the mode of administration (through an Ommaya reservoir) rather than to ^{131}I -TM601 itself. These adverse symptoms include high fever, chills, mild cerebral edema on computed tomography (CT), and infection of the tumor resection cavity. None of these secondary effects have impaired the continuation of the study. As expected, ^{131}I -TM-601 accumulated in the tumor cavity margin. As such, radiation doses to normal tissue organs were insignificant. As no major toxicity and no death due to ^{131}I -TM-601 have been reported, the FDA allowed the trial to go to Phase III [9,42,43]. An FDA approval has also been obtained to investigate the effect of TM601 on newly occurring glioma. According to TransMolecular Incorporation, TM601 is extremely stable, presents no immunogenicity and lacks toxicity in humans. This stability issue has been probed by the group of Olson that demonstrates that 70% of CTX remained intact after 24 h incubation in human serum at 37 °C, indicating the relative resistance of the peptide to peptidases [34]. The excretion route appears to be through the urinary tract. The benefit of the treatment with TM601 would be a two-fold increase in the patient's lifespan, which is by itself a considerable advance considering the devastating rapid progression of the disease when diagnosed. Parallel to this trial, the same team has worked on an intravenous injection protocol of this product but this time with an imaging application in perspective (described earlier in our review) [27]. Interestingly, intracranial injection of ^{131}I -CTX detects brain tumors by gamma-ray scintigram scans *in vivo*, but also labels the stomach, indicating that the molecular target of CTX is also expressed in this organ. So far, TM-601 is the only derivative of CTX for which human clinical studies are partially published.

Besides the clinical trial of ^{131}I -TM-601, many other CTX applications have been described that may be potentially useful to treat glioma. A large proportion of them rely on the administration of therapeutic agents, cDNA or siRNA to block oncogene expression, thanks to the use of nanoparticles [40,41,47–49,53]. The use of two types of nanoparticles has been reported: (i) with a polymer core or (ii) an iron superoxide core (multifunctional nanoparticles). Polymers such as polyethylenimine (PEI) or poly(amidoamine) (PAMAM) have been used to administer cDNA to cancer cells [48,49]. These vectors have shown some success for internalization and transfection of cancer cells, providing researchers with a viable alternative to viral infection. Many differences underlie nanoparticles formed with polymer or iron cores, such as size, surface charge and surface composition, but the most interesting one resides in the fact that the iron core particle can also be used for MRI. In addition also, superparamagnetic iron oxide nanoparticles can be used for hyperthermia therapy of cancer cells. Thus, Veisheh and collaborators have designed two new nanoproboscopes based on the same platform (coated iron superoxide particles conjugated to CTX) that can be used as MRI contrast agent and deliver therapeutic agents (such as methotrexate and siRNA) to glioma cells [40,41]. Both compounds accumulate in glioma cells with a concomitant increase in methotrexate toxicity for nanoparticles coated with this anti-tumor agent and a better knock-down for the siRNA nanoprobe. Another team has worked on targeted gene therapy thanks to this multifunctional nanoparticle and successfully showed cell transfection with a plasmid coding for Green Fluorescent Protein. They prove that the use of this vector induces an improved selective uptake by cancer cells and thereby a better gene expression [47]. With these nanoproboscopes, the effect of the glioma treatment can be followed by MRI by inspecting nanoprobe accumulation in tumor cells. Other nanovectors have been described that contain CTX [13,51]. In these studies, while CTX is used for its vectoring properties,

the complexes developed do not contain any cytotoxic agent. One first type of nanoparticle described has a rather classic composition since the iron nanoparticle is coated with PEG on which CTX and alexafluor 680 have been grafted [13]. A second type of study reports a particle with an original composition since it contains an empty capsule of hepatitis B virus on which a Fc antibody fragment was adsorbed [51]. It is on this antibody fragment that CTX has been conjugated. These types of particles show preferential binding onto glioma cells and the mere presence of CTX is sufficient to inhibit the invasion of these cancer cells. Further development of these compounds is needed to lead to new therapeutic vectors with CTX as targeting agent.

Nanoparticles are not the sole vectors useful to administer therapeutic agents to glioma. Xiang *et al.*, describes the administration of doxorubicin to cancer cells using liposomes labeled with CTX as a vehicle [50]. This vector leads to a better accumulation of doxorubicin in cancer cells and increases the toxic effect. Key results presented in this manuscript are of obvious interest since they circumvent the use of nanoparticles that have unknown effects in the human body following long-term administration.

Nanoparticle-based therapies are as a matter of fact less likely to enter clinical phase trials than more classical compounds. In other reports, making more direct use of the glioma targeting properties of CTX, the peptide has been covalently linked to active anti-tumor agents [45,46]. Graf *et al.* [45] describe the synthesis of a platinum (IV)-CTX conjugate. This compound was designed in order to create an equally effective analog of cisplatin. Cisplatin is one of the most widely used anticancer drugs that, unfortunately, has major negative side effects. This led researchers to find related analogues without the major drawbacks associated to cisplatin. Thus, in this report from Graf and collaborators, platinum (IV)-CTX conjugate has a cell toxicity closely related to the one of cisplatin with the add-on benefit of glioma targeting. Although the results look promising, additional studies have to be conducted to fully characterize this compound. Another recent report describes an innovative use of CTX [46]. This time, CTX is covalently bound to nitric oxide (NO) to form a diazeniumdiolate NO donor (the NO first reacts with free amines of CTX to form radicals which then react with another NO molecule to form the diazeniumdiolate compound) [54]. This compound is not meant to act as an anticancer drug but to induce chemo-sensitivity to the targeted cell. Thus, a subsequent administration of temozolomide or carmustine, two anti-tumor drugs, will improve the toxicity of these drugs towards glioma cells and, in any case, exceed the one observed in the absence of CTX-nitric oxide treatment. This compound is designed to locally enhance the toxic effect of known anticancer drugs. This article opens a new field of possibilities to treat cancer although the mechanism of action of NO has yet to be elucidated.

7. Chlorotoxin-Like Toxins

Although many studies have attempted to analyze the mechanisms of action of CTX, structure-activity relationship studies are still curiously lacking. As CTX seems a promising lead compound to fight solid cancer, researchers have looked for the existence of other venomous toxins that may have the same potential as CTX. While quite a few peptides were identified, based on sequence homology and/or mode of action [55–58] (Table 3), only four of them share the CTX-reported activity on chloride channels. This is the case for AaCtx from the venom of *Androctonus australis* scorpion [59], BmKCTa from the venom of *Buthus martenzii* scorpion [60,61] and GaTx1 and GaTx2 both originating from the venom of *Leiurus quinquestriatus* scorpion [62,63] (Figure 2).

Table 3. Primary sequence alignments of chlorotoxin-like peptides. Alignments were performed by using @TOME V2 [64]. Percentage sequence of identity is given as compared to chlorotoxin by using @TOME V2 [64]. Disulfide Bridge pattern is given when known. Cysteine residues involved in disulfide bridges appear in blue in the table and are numbered in order of appearance.

Toxin	Primary sequence	Length	Identity	Disulfide bridge pattern	Species
Chlorotoxin	MC ₁ MP ₂ C ₂ FTTDDHQM ₃ ARK ₃ DDC ₄ C ₅ G-GK-GRGK ₆ C ₆ YGPQC ₇ LC ₈ -R	36 AA	100%	C ₁ -C ₄ ,C ₂ -C ₆ ,C ₃ -C ₇ ,C ₅ -C ₈	<i>Leiturus quinquestriatus quinquestriatus</i>
I ₁	MC ₁ MP ₂ C ₂ FTTRPDMAQQ ₃ RAC ₄ C ₅ K-GR-GK--C ₆ FGPQC ₇ LC ₈ GYD-	36 AA	71%	C ₁ -C ₄ ,C ₂ -C ₆ ,C ₃ -C ₇ ,C ₅ -C ₈	<i>Buthus eupeus</i>
I ₃	MC ₁ MP ₂ C ₂ FTTDDHQTARRC ₃ RDC ₄ C ₅ G-GR-GR-KC ₆ FG-QC ₇ LC ₈ GYD-	36 AA	82%	C ₁ -C ₄ ,C ₂ -C ₆ ,C ₃ -C ₇ ,C ₅ -C ₈	<i>Buthus eupeus</i>
I ₄	MC ₁ MP ₂ C ₂ FTTDDHMAKK ₃ RDC ₄ C ₅ G-GN---GKC ₆ FGPQC ₇ LC ₈ NR	35 AA	82%	C ₁ -C ₄ ,C ₂ -C ₆ ,C ₃ -C ₇ ,C ₅ -C ₈	<i>Buthus eupeus</i>
I ₅	MC ₁ MP ₂ C ₂ FTTDDPNMANK ₃ RDC ₄ C ₅ G-GG-KK--C ₆ FGPQC ₇ LC ₈ NR--	35 AA	79%	C ₁ -C ₄ ,C ₂ -C ₆ ,C ₃ -C ₇ ,C ₅ -C ₈	<i>Buthus eupeus</i>
I _{5a}	MC ₁ MP ₂ C ₂ FTTDDPNMAKK ₃ RDC ₄ C ₅ G-GN-GK--C ₆ FGPQC ₇ LC ₈ NR--	35 AA	79%	C ₁ -C ₄ ,C ₂ -C ₆ ,C ₃ -C ₇ ,C ₅ -C ₈	<i>Buthus eupeus</i>
Bs-8	RC ₁ KPC ₂ FTTDDPQMSKK ₃ ADC ₄ C ₅ G-GK-GKGC ₆ YGPQC ₇ LC ₈ ----	35 AA	80%	C ₁ -C ₄ ,C ₂ -C ₆ ,C ₃ -C ₇ ,C ₅ -C ₈	<i>Buthus sindicus</i>
LqH-8/6	RC ₁ SPC ₂ FTTDDQMTKK ₃ YDC ₄ C ₅ G-GK-GKGC ₆ YGPQC ₇ LC ₈ APY-	38 AA	72%	C ₁ -C ₄ ,C ₂ -C ₆ ,C ₃ -C ₇ ,C ₅ -C ₈	<i>Leiturus quinquestriatus hebraeus</i>
PBITx1	RC ₁ KPC ₂ FTTDDPQMSKK ₃ ADX ₄ C ₅ G-GX--KX	25 AA	64%		<i>Parabuthus schlechteri</i>
Bs-14	-C ₁ GPC ₂ FTKDPETEKK ₃ ATC ₄ C ₅ G-GI-GR--C ₆ FGPQC ₇ LC ₈ NRGY	36 AA	61%	C ₁ -C ₄ ,C ₂ -C ₆ ,C ₃ -C ₇ ,C ₅ -C ₈	<i>Buthus sindicus</i>
Neurotoxin P2	-C ₁ GPC ₂ FTTDDPYTESK ₃ ATC ₄ C ₅ G-GR-GK--C ₆ VGPQC ₇ LC ₈ NRI-	35 AA	70%	C ₁ -C ₄ ,C ₂ -C ₆ ,C ₃ -C ₇ ,C ₅ -C ₈	<i>Androctonus mauretanicus mauretanicus</i>
AaCix	MC ₁ IPC ₂ FTTNPMAAK ₃ NAC ₄ C ₅ G-SRRGS--C ₆ RGPQC ₇ LC ₈ ----	34 AA	61%	C ₁ -C ₄ ,C ₂ -C ₆ ,C ₃ -C ₇ ,C ₅ -C ₈	<i>Androctonus australis</i>
GaTx1	-C ₁ GPC ₂ FTTDDHMQEK ₃ AEC ₄ C ₅ G-GI-GK--C ₆ YGPQC ₇ LC ₈ NR--	34 AA	79%	C ₁ -C ₄ ,C ₂ -C ₆ ,C ₃ -C ₇ ,C ₅ -C ₈	<i>Leiturus quinquestriatus hebraeus</i>
BmKCT	-C ₁ GPC ₂ FTTDDANMARK ₃ REC ₄ C ₅ G-GI-GK--C ₆ FGPQC ₇ LC ₈ NRI-	35 AA	76%	C ₁ -C ₄ ,C ₂ -C ₆ ,C ₃ -C ₇ ,C ₅ -C ₈	<i>Buthus martensii</i>
Bm12-b	-C ₁ GPC ₂ FTTDDANMARK ₃ REC ₄ C ₅ G-GN-GK--C ₆ FGPQC ₇ LC ₈ NRE-	35 AA	76%	C ₁ -C ₄ ,C ₂ -C ₆ ,C ₃ -C ₇ ,C ₅ -C ₈	<i>Buthus martensii</i>
Lepidopteran	RC ₁ GPC ₂ FTTDDPQTQAK ₃ SEC ₄ C ₅ G-RK-GG-VC ₆ KGPQC ₇ LC ₈ GIQ-	37 AA	63%	C ₁ -C ₄ ,C ₂ -C ₆ ,C ₃ -C ₇ ,C ₅ -C ₈	<i>Buthus tamulus</i>
BHTx3	RC ₁ PPC ₂ FTTNPMEADC ₃ RKC ₄ C ₅ G-GR--GY-C ₆ ASYQC ₇ LC ₈ PG--	35 AA	53%	C ₁ -C ₄ ,C ₂ -C ₆ ,C ₃ -C ₇ ,C ₅ -C ₈	<i>Buthus tamulus</i>
GaTx2	--VSC1-----EDC ₂ PDHC ₃ STQK-ARAKC ₄ DNDKC ₅ VC ₆ EPI	29 AA	38%	C ₁ -C ₄ ,C ₂ -C ₅ ,C ₃ -C ₆	<i>Leiturus quinquestriatus hebraeus</i>

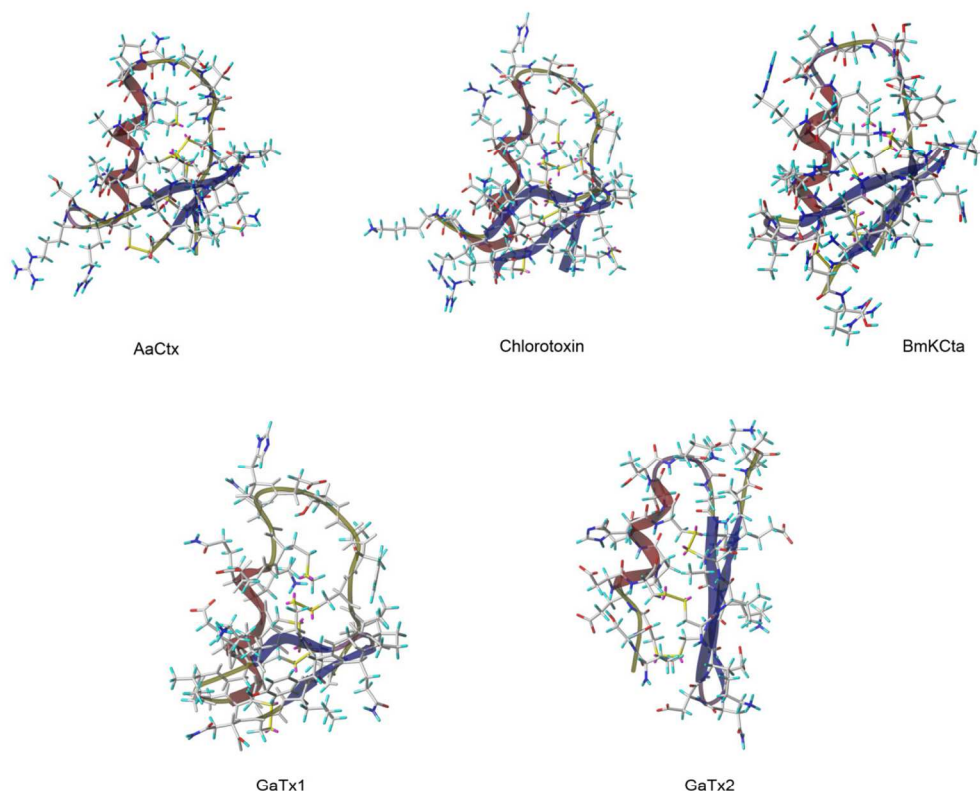


Figure 2. 3D Representation of CTX and the other chlorotoxin like peptide. 3D structure were obtain from pdb files for Chlorotoxin (1CHL), from model of *SWISS-MODEL Repository* [65–69] for BmKc1a, GaTx1 and GaTx2, and from model build by homology with CTX using @TOME V2 [64] and modeller for AaCtx.

AaCtx is a small peptide composed of 34 amino acid residues. It is present in a low concentration (0.05%) in the venom of *Androctonus australis*. It also contains eight cysteine residues, all engaged in disulfide bridges with a pairing pattern that is identical to the one observed in CTX. This toxin has 61% identity (75% sequence homology) with CTX. Overall, the amino acid sequence of AaCtx differs from that of CTX by 12 amino acids, which induce a change in the net charge of the peptide of +4 for AaCtx vs. +3 for CTX. Rjeibi *et al.*, characterized this peptide more precisely [59]. They investigated a potential neurotoxic effect in mice. Intra-cerebroventricular injection of 1 µg AaCtx produces no toxic symptoms. With regard of the high dose used in this study, these authors considered AaCtx as non-toxic for mammals. They also considered the effect of AaCtx on glioma cell migration and tissue invasion. They found a dose-dependent inhibition of migration and invasion with an IC_{50} of 125 µM and 10 µM, respectively. CTX acts on both processes at a lower concentration (600 nM) [8], indicating that AaCtx has a lower efficiency than CTX. A rapid screening for a mechanism of action of the peptide on migration and invasion of glioma cells did not reveal any evident effect on the extracellular matrix proteins (fibronectin, fibrinogen, vitronectin, laminin and collagen type IV). The authors made the assumption that AaCtx blocking effect on invasion and migration was due to a blockage of chloride channels. They linked the difference in net charges with CTX and also the substitution of acidic amino acid by

neutral ones to the lower activity of AaCtx. Obviously, and again, only complete structure-activity relationship studies will be able to confirm the relevance of chloride channels as therapeutic target of these scorpion toxins.

BmKCTa is a component of the Chinese scorpion *Buthus martenzii karsh*. The venom of this scorpion was shown to induce glioma cell apoptosis and inhibit glioma tumor growth *in vivo*. Many bioactive compounds have been identified in this venom and there are still more to come [70,71]. The first description of BmKCTa dates back to the characterization of the cDNA sequence encoding it [60]. This peptide is composed of 36 amino acids and shares a high 68% sequence identity with CTX. It was first expressed in a bacterial system, and acute toxicity assays in mice were performed in 2005. An LD₅₀ value of 4.3 mg/kg was determined in mice [61]. BmKCTa is, without any doubt, the most investigated CTX-like peptide. Comparative toxicity studies on glioma cells and astrocytes, patch-clamp experiments, and histological analyzes were conducted to further define the properties of this peptide and assess its potential as a therapeutic agent against human gliomas. BmKCTa inhibits SHG-44 glioma cell growth in a dose-dependent manner with an IC₅₀ of 0.28 μM while the IC₅₀ for normal astrocytes is 8 μM. This result indicates the extent of cell specificity in the toxicity of BmKCTa for glioma cells. In parallel, whole-cell patch-clamp recording shows the inhibiting effect of BmKCTa on chloride currents in SHG-44 cells. The histological analysis of BmKCTa in mice demonstrates that brain, skeletal and cardiac muscles are all target organs [72]. Similarly to CTX, BmKCTa is of potential interest as therapeutic agent against glioma and has also been found to bind to MMP-2 [73,74]. Both of these similitudes have led to the development of a compound based on BmKCTa to treat and image glioma [75]. An international patent has been filled in to use BmKCTa as an anti-tumor translocation peptide [76].

GaTx1 and GaTx2 are two toxins extracted from the venom of the *Leiurus quinquestriatus hebraeus* scorpion. GaTx1 is a peptide of 34 amino acid residues (79% homology sequence with CTX), which acts on cystic fibrosis transmembrane conductance regulator (CFTR). This receptor is a member of the ABC family but also possesses intrinsic Cl⁻ channel activity. It is known for its implication in cystic fibrosis. GaTx1 is a specific inhibitor of the CFTR channel that acts through reversible binding on a receptor site localized on the cytoplasmic side. It provides researchers with an interesting molecular tool for quantitatively dissecting the functional role of CFTR [62]. GaTx2 is a peptide of 29 amino acids that has poor sequence homology with CTX (38%). It is, however, also described to act on another Cl⁻ channel (CIC-2) than CTX (CIC-3) [63]. This channel is a member of the same family of chloride channels as CIC-3, and is also up-regulated on the glioma cell surface. Its physiological role, however, remains undefined although it can reasonably be assumed to play a similar role as CIC-3 in glioma cell invasion and migration [26]. GaTx2 inhibits CIC-2 by slowing its activation, and the resulting inhibition is voltage-dependent. Interestingly, the GaTx2 sequence was described earlier in 1997 under the name of leiuopeptide II without undergoing extensive characterization [77]. Nevertheless, GaTx2 can be used as a pharmacological tool to help determine the role and localization of CIC-2 channel in cells. It may serve as a scaffold/vector to design drugs that target CIC-2 channels. It is worth mentioning that because CIC-2 channels are also highly expressed in glioma cells [18] indicating that this toxin should also possess glioma-targeting properties. This remains to be tested of course.

Apart from these four toxins, two other animal toxins are worth mentioning here. First, Lqh-8/6 isolated from the venom of *Leiurus quinquestriatus hebraeus* scorpion, and Bs14 isolated from the

venom of *Buthus indicus* scorpion. Both are small peptides of 38 and 36 amino acids, respectively. They both share a high sequence and structure similarity with CTX (72% and 61% sequence identity, respectively). Each of them has eight cysteine residues in its sequence leading to the same compact folded structure and disulfide pairing pattern found in CTX. All of this evidence suggests that chloride channels should be their natural targets. However, at the current time, only the structures of these toxins have been studied, leaving us with the hope that new CTX toxin analogues, also possessing glioma targeting properties, will soon be discovered.

8. Conclusions

Since its discovery, CTX has been established as a promising tool to foster research on glioma. Although its mechanism of action is far from being fully elucidated, many applications have emerged to use its cancer-targeting properties. So far CTX has been linked to nanoparticles, radioisotopes and fluorescent molecules. In addition, it has been used to enhance the efficacy of already existing anti-tumor molecules and conjugated to active drugs to create new, more effective ones. One compound (¹³¹I-TM601) is already in Phase III of clinical trial. Other positive clinical perspectives for CTX or CTX-like toxins, include diagnosis by tumor paint using the reputed Cy5.5 dye or still more infrared-friendly dyes, tumor treatment with ¹³¹I and possibly the grafting onto CTX of other cytotoxic agents regularly used in clinics for cancer treatment such as cisplatin-like compounds, anthracyclines, or reactive oxygen species. All of this effervescence demonstrates the keen interest surrounding this toxin. CTX is one of the first target compounds that is not an antibody or an antibody fragment. Natural selection has made CTX very adapted to insects and other invertebrates but with only a small link to humans. This has led to a small, compact, highly diffusible peptide that can cross the BBB or the BBTB with so far no evident signs of toxicity for normal human cells. The issue of how well CTX crosses the BBB or the BBTB remains to be seriously investigated, as both proper cancer cell labeling and treatment will also require the targeting of cancer cells at the invasion front or at secondary tumor sites where the BBB may be well preserved. Obviously, CTX is not perfect. While it can inhibit tumor invasion, CTX cannot kill cancer cells on its own, obliging scientists to perform a complicated and costly work in designing and chemical grafting of compounds that provide this desired toxic property to the new molecules. Another point that needs to be addressed in the future is the absence of detailed structure activity relationship studies between CTX and its numerous potential targets. The absence of relevant information complicates the definitive identification of the real cell surface marker of glioma cells and will limit for some time the unambiguous identification of CTX-like toxins and their resulting characterization in the frame of glioma detection, diagnosis, imaging and treatment. Regarding the promising results obtained so far with CTX, there is no doubt, however, that more studies will be initiated in a few years to finalize the identification of the CTX target. Another source of hope consists of chlorotoxin-like toxins. It looks as if they are a promising reservoir of biologically active peptides with characteristics similar to or resembling those of CTX. In addition, since the vast majority of scorpion venoms remain to be characterized, there are still many more new compounds that will soon emerge with the same therapeutic promises, possibly targeting other ion channels of interest, such as Ca²⁺-activated small conductance K⁺ channels. Animal toxins may soon become an interesting source of promising therapeutic substances like plants have been before. CTX is on its way to definitively establish itself as a proof of concept of this emerging theory.

Acknowledgments

We acknowledge financial support from Inserm and the Région Rhône-Alpes for the “Fond d’Appui Labo”. This program is supported by an ANR financing to the LabEx Ion Channels, Science and Therapeutics under the code number ANR-11-LABX-0015. Tarek Abd El Aziz is a recipient of a scholarship of the Egyptian Government.

Author Contributions

Lucie Dardevet wrote the first draft of the manuscript as a PhD exercise; Dipti Rani performed the initial bibliography searches and conceptualized the review; Tarek Abd El Aziz, Jean-Marc Sabatier, Ingrid Bazin, Mahmoud Fadl and Elisabeth Brambilla brought in valuable corrections; Elisabeth Brambilla was also at the origin of many chlorotoxin projects in our laboratory; Michel De Waard wrote the manuscript, performed corrections and submitted the manuscript.

Conflicts of Interest

The authors declare no conflict of interest.

References

1. Yin, C.; Lv, S.; Chen, X.; Guo, H. The role of glioma stem cells in glioma tumorigenesis. *Front. Biosci.* **2014**, *19*, 818–824.
2. Singh, S.K.; Hawkins, C.; Clarke, I.D.; Squire, J.A.; Bayani, J.; Hide, T.; Henkelman, R.M.; Cusimano, M.D.; Dirks, P.B. Identification of human brain tumour initiating cells. *Nature* **2004**, *432*, 396–401.
3. Yin, L.T.; Fu, Y.J.; Xu, Q.L.; Yang, J.; Liu, Z.L.; Liang, A.H.; Fan, X.J.; Xu, C.G. Potential biochemical therapy of glioma cancer. *Biochem. Biophys. Res. Commun.* **2007**, *362*, 225–229.
4. Veisheh, O.; Kievit, F.M.; Ellenbogen, R.G.; Zhang, M. Cancer cell invasion: Treatment and monitoring opportunities in nanomedicine. *Adv. Drug Deliv. Rev.* **2011**, *63*, 582–596.
5. Deshane, J.; Garner, C.C.; Sontheimer, H. Chlorotoxin inhibits glioma cell invasion via matrix metalloproteinase-2. *J. Biol. Chem.* **2003**, *278*, 4135–4144.
6. Bølge Tysnes, B.; Mahesparan, R. Biological mechanisms of glioma invasion and potential therapeutic targets. *J. Neurooncol.* **2001**, *53*, 129–147.
7. Caruso, G.; Caffo, M.; Alafaci, C.; Raudino, G.; Cafarella, D.; Lucerna, S.; Salpietro, F.M.; Tomasello, F. Could nanoparticle systems have a role in the treatment of cerebral gliomas? *Nanomed. Nanotechnol. Biol. Med.* **2011**, *7*, 744–752.
8. Soroceanu, L.; Manning, T.J.; Sontheimer, H. Modulation of glioma cell migration and invasion using Cl(−) and K(+) ion channel blockers. *J. Neurosci.* **1999**, *19*, 5942–5954.
9. Mamelak, A.N.; Jacoby, D.B. Targeted delivery of antitumoral therapy to glioma and other malignancies with synthetic chlorotoxin (TM-601). *Expert Opin. Drug Deliv.* **2007**, *4*, 175–186.
10. Ritter, M.R.; Zhou, Q.; Markland, F.S., Jr. Contortrostatin, a snake venom disintegrin, induces alphavbeta 3-mediated tyrosine phosphorylation of CAS and FAK in tumor cells. *J. Cell. Biochem.* **2000**, *79*, 28–37.

11. Schmitmeier, S.; Markland, F.S.; Chen, T.C. Anti-invasive effect of contortrostatin, a snake venom disintegrin, and TNF-alpha on malignant glioma cells. *Anticancer Res.* **2000**, *20*, 4227–4233.
12. DeBin, J.A.; Maggio, J.E.; Strichartz, G.R. Purification and characterization of chlorotoxin, a chloride channel ligand from the venom of the scorpion. *Am. J. Physiol.* **1993**, *264*, C361–C369.
13. Veiseh, O.; Gunn, J.W.; Kievit, F.M.; Sun, C.; Fang, C.; Lee, J.S.H.; Zhang, M. Inhibition of tumor-cell invasion with chlorotoxin-bound superparamagnetic nanoparticles. *Small* **2009**, *5*, 256–264.
14. Veiseh, M.; Gabikian, P.; Bahrami, S.B.; Veiseh, O.; Zhang, M.; Hackman, R.C.; Ravanpay, A.C.; Stroud, M.R.; Kusuma, Y.; Hansen, S.J.; *et al.* Tumor paint: A chlorotoxin: Cy5.5 bioconjugate for intraoperative visualization of cancer foci. *Cancer Res.* **2007**, *67*, 6882–6888.
15. Soroceanu, L.; Gillespie, Y.; Khazaeli, M.B.; Sontheimer, H. Use of chlorotoxin for targeting of primary brain tumors. *Cancer Res.* **1998**, *58*, 4871–4879.
16. Lyons, S.A.; O’Neal, J.; Sontheimer, H. Chlorotoxin, a scorpion-derived peptide, specifically binds to gliomas and tumors of neuroectodermal origin. *Glia* **2002**, *39*, 162–173.
17. DeBin, J.A.; Strichartz, G.R. Chloride channel inhibition by the venom of the scorpion *Leiurus quinquestriatus*. *Toxicon* **1991**, *29*, 1403–1408.
18. Ullrich, N.; Bordey, A.; Gillespie, G.Y.; Sontheimer, H. Expression of voltage-activated chloride currents in acute slices of human gliomas. *Neuroscience* **1998**, *83*, 1161–1173.
19. Jentsch, T.J.; Günther, W.; Pusch, M.; Schwappach, B. Properties of voltage-gated chloride channels of the *CIC* gene family. *J. Physiol.* **1995**, *482*, 19S–25S.
20. McFerrin, M.B.; Sontheimer, H. A role for ion channels in glioma cell invasion. *Neuron Glia Biol.* **2006**, *2*, 39–49.
21. Olsen, M.L.; Schade, S.; Lyons, S.A.; Amaral, M.D.; Sontheimer, H. Expression of voltage-gated chloride channels in human glioma cells. *J. Neurosci.* **2003**, *23*, 5572–5582.
22. Ullrich, N.; Sontheimer, H. Cell cycle-dependent expression of a glioma-specific chloride current: Proposed link to cytoskeletal changes. *Am. J. Physiol.* **1997**, *273*, C1290–C1297.
23. Turner, K.L.; Sontheimer, H. Cl⁻ and K⁺ channels and their role in primary brain tumour biology. *Philos. Trans. R. Soc. Lond. B Biol. Sci.* **2014**, *369*, 20130095.
24. Rouzaire-Dubois, B.; Milandri, J.B.; Bostel, S.; Dubois, J.M. Control of cell proliferation by cell volume alterations in rat C6 glioma cells. *Pflügers Arch. Eur. J. Physiol.* **2000**, *440*, 881–888.
25. Sontheimer, H. An unexpected role for ion channels in brain tumor metastasis. *Exp. Biol. Med.* **2008**, *233*, 779–791.
26. Lui, V.C.H.; Lung, S.S.S.; Pu, J.K.S.; Hung, K.N.; Leung, G.K.K. Invasion of human glioma cells is regulated by multiple chloride channels including *CIC-3*. *Anticancer Res.* **2010**, *30*, 4515–4524.
27. Hockaday, D.C.; Shen, S.; Fiveash, J.; Raubitschek, A.; Colcher, D.; Liu, A.; Alvarez, V.; Mamelak, A.N. Imaging glioma extent with ¹³¹I-TM-601. *J. Nucl. Med.* **2005**, *46*, 580–586.
28. Jacoby, D.B.; Dyskin, E.; Yalcin, M.; Kesavan, K.; Dahlberg, W.; Ratliff, J.; Johnson, E.W.; Mousa, S.A. Potent pleiotropic anti-angiogenic effects of TM601, a synthetic chlorotoxin peptide. *Anticancer Res.* **2010**, *30*, 39–46.
29. Kesavan, K.; Ratliff, J.; Johnson, E.W.; Dahlberg, W.; Asara, J.M.; Misra, P.; Frangioni, J.V.; Jacoby, D.B. Annexin A2 is a molecular target for TM601, a peptide with tumor-targeting and anti-angiogenic effects. *J. Biol. Chem.* **2009**, *285*, 4366–4374.

30. Tatenhorst, L.; Rescher, U.; Gerke, V.; Paulus, W. Knockdown of annexin 2 decreases migration of human glioma cells *in vitro*. *Neuropathol. Appl. Neurobiol.* **2006**, *32*, 271–277.
31. Sharma, M.C.; Sharma, M. The role of annexin II in angiogenesis and tumor progression: A potential therapeutic target. *Curr. Pharm. Des.* **2007**, *13*, 3568–3575.
32. Shen, S.; Khazaeli, M.B.; Gillespie, G.Y.; Alvarez, V.L. Radiation dosimetry of ¹³¹I-chlorotoxin for targeted radiotherapy in glioma-bearing mice. *J. Neurooncol.* **2005**, *71*, 113–119.
33. Stroud, M.R.; Hansen, S.J.; Olson, J.M. *In vivo* bio-imaging using chlorotoxin-based conjugates. *Curr. Pharm. Des.* **2011**, *17*, 4362–4371.
34. Akcan, M.; Stroud, M.R.; Hansen, S.J.; Clark, R.J.; Daly, N.L.; Craik, D.J.; Olson, J.M. Chemical re-engineering of chlorotoxin improves bioconjugation properties for tumor imaging and targeted therapy. *J. Med. Chem.* **2011**, *54*, 782–787.
35. Sun, C.; Veiseh, O.; Gunn, J.; Fang, C.; Hansen, S.; Lee, D.; Sze, R.; Ellenbogen, R.G.; Olson, J.; Zhang, M. *In vivo* MRI detection of gliomas by chlorotoxin-conjugated superparamagnetic nanoprobes. *Small* **2008**, *4*, 372–379.
36. Huang, R.; Han, L.; Li, J.; Liu, S.; Shao, K.; Kuang, Y.; Hu, X.; Wang, X.; Lei, H.; Jiang, C. Chlorotoxin-modified macromolecular contrast agent for MRI tumor diagnosis. *Biomaterials* **2011**, *32*, 5177–5186.
37. Veiseh, O.; Sun, C.; Gunn, J.; Kohler, N.; Gabikian, P.; Lee, D.; Bhattarai, N.; Ellenbogen, R.; Sze, R.; Hallahan, A.; *et al.* Optical and MRI multifunctional nanoprobe for targeting gliomas. *Nano Lett.* **2005**, *5*, 1003–1008.
38. Veiseh, O.; Sun, C.; Fang, C.; Bhattarai, N.; Gunn, J.; Kievit, F.; Du, K.; Pullar, B.; Lee, D.; Ellenbogen, R.G.; *et al.* Specific targeting of brain tumors with an optical/magnetic resonance imaging nanoprobe across the blood-brain barrier. *Cancer Res.* **2009**, *69*, 6200–6207.
39. Meng, X.; Wan, J.; Jing, M.; Zhao, S.; Cai, W.; Liu, E. Specific targeting of gliomas with multifunctional superparamagnetic iron oxide nanoparticle optical and magnetic resonance imaging contrast agents. *Acta Pharmacol. Sin.* **2007**, *28*, 2019–2026.
40. Sun, C.; Fang, C.; Stephen, Z.; Veiseh, O.; Hansen, S.; Ellenbogen, R.G.; Olson, J.; Zhang, M. Tumor-targeted drug delivery and MRI contrast enhancement by chlorotoxin-conjugated iron oxide nanoparticles. *Nanomedicine* **2008**, *3*, 495–505.
41. Veiseh, O.; Kievit, F.M.; Fang, C.; Mu, N.; Jana, S.; Leung, M.C.; Mok, H.; Ellenbogen, R.G.; Park, J.O.; Zhang, M. Chlorotoxin bound magnetic nanovector tailored for cancer cell targeting, imaging, and siRNA delivery. *Biomaterials* **2010**, *31*, 8032–8042.
42. Mamelak, A.N.; Rosenfeld, S.; Bucholz, R.; Raubitschek, A.; Nabors, L.B.; Fiveash, J.B.; Shen, S.; Khazaeli, M.B.; Colcher, D.; Liu, A.; *et al.* Phase I single-dose study of intracavitary-administered iodine-131-TM-601 in adults with recurrent high-grade glioma. *J. Clin. Oncol.* **2006**, *24*, 3644–3650.
43. Wu, X.S.; Jian, X.C.; Yin, B.; He, Z.J. Development of the research on the application of chlorotoxin in imaging diagnostics and targeted therapies for tumors. *Chin. J. Cancer* **2010**, *29*, 626–630.
44. Nicolaidis, N.C.; Postema, M.; Multifunctional Agents. WO/2013/003507, 3 January 2013.
45. Graf, N.; Mokhtari, T.E.; Papayannopoulos, I.A.; Lippard, S.J. Platinum(IV)-chlorotoxin (CTX) conjugates for targeting cancer cells. *J. Inorg. Biochem.* **2012**, *110*, 58–63.
46. Safdar, S.; Payne, C.A.; Tu, N.H.; Taite, L.J. Targeted nitric oxide delivery preferentially induces glioma cell chemosensitivity via altered p53 and O6-Methylguanine-DNA Methyltransferase activity. *Biotechnol. Bioeng.* **2013**, *110*, 1211–1220.

47. Kievit, F.M.; Veiseh, O.; Fang, C.; Bhattarai, N.; Lee, D.; Ellenbogen, R.G.; Zhang, M. Chlorotoxin labeled magnetic nanovectors for targeted gene delivery to glioma. *ACS Nano* **2010**, *4*, 4587–4594.
48. Veiseh, O.; Kievit, F.M.; Gunn, J.W.; Ratner, B.D.; Zhang, M. A ligand-mediated nanovector for targeted gene delivery and transfection in cancer cells. *Biomaterials* **2009**, *30*, 649–657.
49. Huang, R.; Ke, W.; Han, L.; Li, J.; Liu, S.; Jiang, C. Targeted delivery of chlorotoxin-modified DNA-loaded nanoparticles to glioma via intravenous administration. *Biomaterials* **2011**, *32*, 2399–2406.
50. Xiang, Y.; Liang, L.; Wang, X.; Wang, J.; Zhang, X.; Zhang, Q. Chloride channel-mediated brain glioma targeting of chlorotoxin-modified doxorubicine-loaded liposomes. *J. Control. Release* **2011**, *152*, 402–410.
51. Kasai, T.; Nakamura, K.; Vaidyanath, A.; Chen, L.; Sekhar, S.; El-Ghlban, S.; Okada, M.; Mizutani, A.; Kudoh, T.; Murakami, H.; *et al.* Chlorotoxin fused to IgG-Fc inhibits glioblastoma cell motility via receptor-mediated endocytosis. *J. Drug Deliv.* **2012**, *2012*, 975763.
52. Zhai, H.; Acharya, S.; Gravanis, I.; Mehmood, S.; Seidman, R.J.; Shroyer, K.R.; Hajjar, K.A.; Tsirka, S.E. Annexin A2 promotes glioma cell invasion and tumor progression. *J. Neurosci.* **2011**, *31*, 14346–14360.
53. Fu, Y.; An, N.; Li, K.; Zheng, Y.; Liang, A. Chlorotoxin-conjugated nanoparticles as potential glioma-targeted drugs. *J. Neurooncol.* **2012**, *107*, 457–462.
54. Safdar, S.; Taite, L.J. Targeted diazeniumdiolates: Localized nitric oxide release from glioma-specific peptides and proteins. *Int. J. Pharm.* **2012**, *422*, 264–270.
55. Ali, S.A.; Stoeva, S.; Schütz, J.; Kayed, R.; Abassi, A.; Zaidi, Z.H.; Voelter, W. Purification and primary structure of low molecular mass peptides from scorpion (*Buthus sindicus*) venom. *Comp. Biochem. Physiol. A. Mol. Integr. Physiol.* **1998**, *121*, 323–332.
56. Tytgat, J.; Debont, T.; Rostoll, K.; Müller, G.J.; Verdonck, F.; Daenens, P.; van Der Walt, J.J.; Possani, L.D. Purification and partial characterization of a “short” insectotoxin-like peptide from the venom of the scorpion *Parabuthus schlechteri*. *FEBS Lett.* **1998**, *441*, 387–391.
57. Wudayagiri, R.; Inceoglu, B.; Herrmann, R.; Derbel, M.; Choudary, P.V.; Hammock, B.D. Isolation and characterization of a novel lepidopteran-selective toxin from the venom of South Indian red scorpion, *Mesobuthus tamulus*. *BMC Biochem.* **2001**, *2*, 16.
58. Wu, J.J.; Dai, L.; Lan, Z.D.; Chi, C.W. The gene cloning and sequencing of Bm-12, a Chlorotoxin-like peptide from the scorpion *Buthus martensi* Karsch. *Toxicon* **2000**, *38*, 661–668.
59. Rjeibi, I.; Mabrouk, K.; Mosrati, H.; Berenguer, C.; Mejdoub, H.; Villard, C.; Laffitte, D.; Bertin, D.; Ouafik, L.; Luis, J.; *et al.* Purification, synthesis and characterization of AaCtx, the first chlorotoxin-like peptide from *Androctonus australis* scorpion venom. *Peptides* **2011**, *32*, 656–663.
60. Zeng, X.C.; Li, W.X.; Zhu, S.Y.; Peng, F.; Zhu, Z.H.; Wu, K.L.; Yiang, F.H. Cloning and characterization of a cDNA sequence encoding the precursor of a chlorotoxin-like peptide from the Chinese scorpion *Buthus martensii* Karsch. *Toxicon Off. J. Int. Soc. Toxinology* **2000**, *38*, 1009–1014.
61. Fu, Y.; Yin, L.; Wang, W.; Chai, B.; Liang, A. Synthesis, expression and purification of a type of chlorotoxin-like peptide from the scorpion, *Buthus martensii* Karsch, and its acute toxicity analysis. *Biotechnol. Lett.* **2005**, *27*, 1597–1603.
62. Fuller, M.D.; Thompson, C.H.; Zhang, Z.-R.; Freeman, C.S.; Schay, E.; Szakács, G.; Bakos, E.; Sarkadi, B.; McMaster, D.; French, R.J.; *et al.* State-dependent inhibition of cystic fibrosis transmembrane conductance regulator chloride channels by a novel peptide toxin. *J. Biol. Chem.* **2007**, *282*, 37545–37555.

63. Thompson, C.H.; Olivetti, P.R.; Fuller, M.D.; Freeman, C.S.; McMaster, D.; French, R.J.; Pohl, J.; Kubanek, J.; MaCarty, N.A. Isolation and characterization of a high affinity peptide inhibitor of CIC-2 chloride channels. *J. Biol. Chem.* **2009**, *284*, 26051–26052.
64. Pons, J.L.; Labesse, G. @TOME-2: A new pipeline for comparative modeling of protein-ligand complexes. *Nucleic Acids Res.* **2009**, *37*, W485–W491.
65. Biasini, M.; Bienert, S.; Waterhouse, A.; Arnold, K.; Studer, G.; Schmidt, T.; Kiefer, F.; Cassarino, T.G.; Bertoni, M.; Bordoli, L.; *et al.* SWISS-MODEL: Modelling protein tertiary and quaternary structure using evolutionary information. *Nucleic Acids Res.* **2014**, *42*, doi:10.1093/nar/gku340.
66. Kopp, J.; Schwede, T. The SWISS-MODEL repository of annotated three-dimensional protein structure homology models. *Nucleic Acids Res.* **2004**, *32*, D230–D234.
67. Arnold, K.; Bordoli, L.; Kopp, J.; Schwede, T. The SWISS-MODEL workspace: A web-based environment for protein structure homology modelling. *Bioinformatics* **2006**, *22*, 195–201.
68. Kiefer, F.; Arnold, K.; Künzli, M.; Bordoli, L.; Schwede, T. The SWISS-MODEL Repository and associated resources. *Nucleic Acids Res.* **2009**, *37*, D387–D392.
69. Guex, N.; Peitsch, M.C.; Schwede, T. Automated comparative protein structure modeling with SWISS-MODEL and Swiss-PdbViewer: A historical perspective. *Electrophoresis* **2009**, *30*, doi:10.1002/elps.200900140.
70. Wang, W.X.; Ji, Y.H. Scorpion venom induces glioma cell apoptosis *in vivo* and inhibits glioma tumor growth *in vitro*. *J. Neurooncol.* **2005**, *73*, 1–7.
71. Goudet, C.; Chi, C.W.; Tytgat, J. An overview of toxins and genes from the venom of the Asian scorpion *Buthus martensi* Karsch. *Toxicon* **2002**, *40*, 1239–1258.
72. Fu, Y.J.; Yin, L.T.; Liang, A.H.; Zhang, C.F.; Wang, W.; Chai, B.F.; Yang, J.Y.; Fan, X.J. Therapeutic potential of chlorotoxin-like neurotoxin from the Chinese scorpion for human gliomas. *Neurosci. Lett.* **2007**, *412*, 62–67.
73. Fu, Y.J.; Yin, L.T.; Liang, A.H. Polyclonal antibody against a recombinant chlorotoxin-like peptide from the Chinese scorpion and detection of its putative receptors in human glioma cells. *Biotechnol. Lett.* **2006**, *28*, 1439–1443.
74. Fu, Y.J.; An, N.; Chan, K.G.; Wu, Y.B.; Zheng, S.H.; Liang, A.H. A model of BmK CT in inhibiting glioma cell migration via matrix metalloproteinase-2 from experimental and molecular dynamics simulation study. *Biotechnol. Lett.* **2011**, *33*, 1309–1317.
75. Fu, Y.; An, N.; Zheng, S.; Liang, A.; Li, Y. BmK CT-conjugated fluorescence nanodiamond as potential glioma-targeted imaging and drug. *Diam. Relat. Mater.* **2012**, *21*, 73–76.
76. Jiang, D.; Li, W.; Cao, Z.; Mao, X.; Fan, S.; Liu, H. Anti Tumor Translocation Peptide of Scorpion, Preparation Method and Application. CN101003788A, 25 July 2007.
77. Buisine, E.; Wieruszkeski, J.M.; Lippens, G.; Wouters, D.; Tartar, A.; Sautiere, P. Characterization of a new family of toxin-like peptides from the venom of the scorpion *Leiurus quinquestriatus* hebraeus. 1H-NMR structure of leiuropeptide II. *J. Pept. Res. Off. J. Am. Pept. Soc.* **1997**, *49*, 545–555.

© 2015 by the authors; licensee MDPI, Basel, Switzerland. This article is an open access article distributed under the terms and conditions of the Creative Commons Attribution license (<http://creativecommons.org/licenses/by/4.0/>).

Article 4:
**H-Rubies, a new family of red emitting
fluorescent pH sensors for living cells**

Article publiée dans le journal Chemical Science en 2015

Cite this: *Chem. Sci.*, 2015, 6, 5928

H-Rubies, a new family of red emitting fluorescent pH sensors for living cells†

Guillaume Despras,^{‡a} Alsu I. Zamaleeva,^{‡bf} Lucie Dardevet,^{cd} Céline Tisseyre,^{cd} Joao Gamelas Magalhaes,^f Charlotte Garner,^a Michel De Waard,^{cde} Sebastian Amigorena,^f Anne Feltz,^b Jean-Maurice Mallet^a and Mayeul Collot^{§*a}

Monitoring intracellular pH has drawn much attention due to its undeniably important function in cells. The widespread development of fluorescent imaging techniques makes pH sensitive fluorescent dyes valuable tools, especially red-emitting dyes which help to avoid the overcrowded green end of the spectral band. Herein, we present H-Rubies, a family of pH sensors based on a phenol moiety and a X-rhodamine fluorophore that display a bright red fluorescence upon acidification with pK_a values spanning from 4 to 9. Slight structural modifications led to dramatic changes in their physicochemical properties and a relationship between their structures, their ability to form *H*-aggregates, and their apparent pK_a was established. While molecular form H-Rubies can be used to monitor mitochondrial acidification of glioma cells, their functionalised forms were linked *via* click chemistry to dextrans or microbeads containing a near infrared Cy5 (Alexa-647) in order to provide ratiometric systems that were used to measure respectively the phagosomal and endosomal pH in macrophages (RAW 264.7 cells) using flow cytometry.

Received 27th March 2015
Accepted 13th July 2015

DOI: 10.1039/c5sc01113b

www.rsc.org/chemicalscience

Introduction

Intracellular pH plays many different and important roles in cellular activity and is especially involved in ion transport,¹ apoptosis,^{2,3} multidrug resistance⁴ and muscle contraction.^{5,6} Moreover, abnormal intracellular pH values are also associated with diseases such as Alzheimer's⁷ and cancer.^{8,9} Monitoring variations of intracellular pH in living cells is therefore of the utmost importance and is an essential parameter for studying phagocytosis,¹⁰ endocytosis¹¹ and consequently cellular

internalisation pathways. Fluorescence spectroscopy and fluorescence imaging techniques have many advantages including high sensitivity, high spatial and temporal resolution and are not destructive to the cells. As such, molecular fluorescent pH indicators have become indispensable tools for observing pH changes in cells. Although many fluorescent indicators have already been developed (for an extensive review see: Han and Burgess),¹² several factors have to be taken into account in order to achieve efficient use within cells, including solubility in biological media, hydrophobicity, photostability and brightness. Our recent efforts to develop functionalisable red emitting fluorescent sensors^{13–15} were driven by the increasing use of cells transfected with green or yellow fluorescent proteins (FPs), thus allowing multicolour imaging. Whilst recent progresses have been reported in the development of red emitting genetically encoded pH sensors,¹⁶ there is still a demand for efficient molecular red fluorescent indicators. Among red-shifted fluorescent pH sensors, cyanines suffer from a weak photo-stability. Benzoxanthene dyes like SNARF, act as ratiometric probes but generally suffer from weak quantum yields. In contrast, red-emitting BODIPYs have recently attracted special attention due to their photostability and high brightness.^{17,18} Having said this they tend to suffer from high lipophilicity making them inefficient for cellular experiments as their apparent pK_a shifts in lipophilic environment.¹⁹

In his review, Han *et al.*¹² pointed out that despite their advantageous spectral properties, pH probes based on rhodamine were not extensively developed.²⁰ Rhodamine-based pH

^aLaboratory of Biomolecules (LBM), UPMC Université Paris 06, Ecole Normale Supérieure (ENS), CNRS, UMR 7203, Paris F-75005, France. E-mail: mayeul.collot@unistra.fr

^bEcole Normale Supérieure, Institut de Biologie de l'ENS (IBENS), INSERM U1024, CNRS UMR 8197, Paris F-75005, France

^cINSERM U836, LabEx Ion Channels, Science and Therapeutics, Grenoble Institute of Neuroscience, chemin fortuné ferrini, bâtiment Edmond Safra, 38042 Grenoble Cedex 09, France

^dUniversité Joseph Fourier, Grenoble, France

^eSmartox Biotechnology, Saint Martin d'Hères, France

^fINSERM U932, Institute Curie, 75248, Paris, Cedex 05, France

† Electronic supplementary information (ESI) available: Details of the organic synthesis, characterisations (HPLC, NMR, mass spectra) as well as measurements of their photophysical properties can be found in the supplementary information. See DOI: 10.1039/c5sc01113b

‡ Contributed equally to this work.

§ Current address: Laboratoire de Biophotonique et Pharmacologie, UMR 7213 CNRS, Université de Strasbourg, Faculté de Pharmacie, 74, Route du Rhin, 67401, Illkirch, France.



probes mostly rely on the spirolactam ring opening principle, generally yielding pH sensors with high dynamic ranges but low pK_a values as well as high hydrophobicity due to their neutrally charged OFF state.^{21–26}

A key criteria for a pH sensor is its pK_a value, which should be in the physiological range. While the cytosol and some other cellular compartments, such as the nucleus and endoplasmic reticulum maintain their pH at ~ 7.2 , endosomes, lysosomes and secretory vesicles on the other hand are acidic environments with the pH ranging from 4.5 to 6.7. Conversely, alkaline pH can be found in mitochondria (~ 8),²⁷ phagosomes of dendritic cells^{28,29} and neutrophils.³⁰ As such, a collection of pH probes with a large range of pK_a values is required in order to extend the scope of their application and thus a straightforward method of tuning their pK_a values without tedious chemical modifications would be a necessity. Finally, the large majority of fluorescent pH sensors do not offer an orthogonal and specific site of attachment required for functionalisation. Many common pH probes are too lipophilic and tend to compartmentalise in hydrophobic domains of the cell, however, to date no alternative methods of functionalisation have been proposed. In this report we present the development of a new family of red-emitting pH probes based on X-rhodamines and a phenol moiety as the pH reporter (see abstract scheme). In addition to their pK_a values ranging from ~ 4 to ~ 9 , these ON–OFF type pH sensors, based on the PET (photoinduced electron transfer) quenching phenomena, exhibit high brightness in their acidic phenol form and can display very high turn ON of their fluorescence thanks to the formation of dark soluble *H*-aggregates in their OFF state. Among this new family, a number of H-Rubies were designed to bear a linker allowing the functionalisation of dextran and microbeads in order to measure the pH in living cells.

Results and discussion

Synthesis of phenolic X-rhodamines

ON–OFF pH probes generally require a pH-sensitive moiety whereby protonation/deprotonation modifies the quantum yield of a linked fluorophore either through PET (Photoinduced Electron Transfer) quenching phenomena or ICT (Internal Charge Transfer). Among these pH-sensitive moieties, phenol is the most popular as illustrated by the wide use of fluorescein and its derivatives: FITC, BCECF, *etc.* Moreover, the pK_a of phenols can be easily lowered and tuned to a biologically relevant range by introducing proper electron-withdrawing groups on the phenyl ring. Boens' group successfully converted an *ortho*-chlorophenol to obtain a pH-sensitive BODIPY with a pK_a of 7.6.³¹ Only few examples of phenolic rhodamines are given in the literature³² and none of those were exploited as pH probes, leading us to investigate the potential efficiency of these entities as fluorescent pH sensors. The red-emitting fluorophore X-rhodamine was chosen for its highly desirable spectral properties including a high molar absorption, high quantum yield and good photo-stability as well as its reduced hydrophobicity compared to BODIPY. Thus, an initial set of 9 X-rhodamines was synthesised from hydroxybenzaldehydes

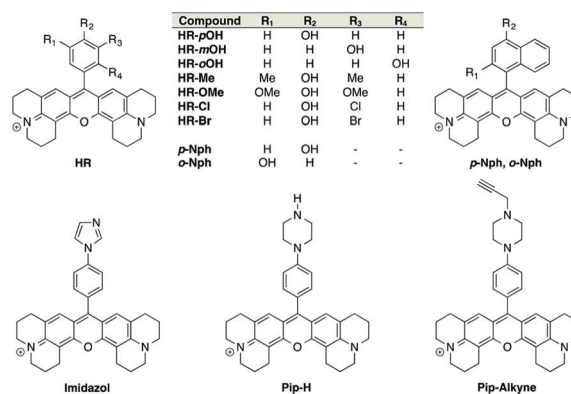


Fig. 1 Structures of the synthesised X-rhodamines and the first set of H-Rubies.

and hydroxynaphthaldehydes (for synthesis see ESI†). The use of phenyl-imidazol and (*N*-alkylated)-phenyl-piperazine^{33,34} as alternative pH-sensitive indicators was also explored giving rise to X-rhodamines: **Imidazole**, **Pip-H** and **Pip-Alkyne** (Fig. 1).

The spectral properties and pK_a values obtained for this first set of synthesised fluorophores are given in Table 1. Although X-rhodamine Imidazole did not behave as a fluorescent pH sensor (no significant variation of fluorescence intensity upon protonation), phenyl-piperazine and phenol-based X-rhodamines displayed clear pH sensitivity. Despite its physiologically relevant pK_a value and the capacity to be functionalised, **Pip-Alkyne** was not developed further as its dynamic range (3-fold) was found to be much lower than those obtained with phenol-based X-rhodamines.

Structure/properties relationship of H-Rubies

Absorption spectra of H-Rubies at different pH values provided us with information regarding their aggregation states (Fig. 2) since rhodamines can form different patterns of aggregations including *H*- and *J*-aggregates.^{35,36} The observed broadening of absorption spectra for **HR-pOH** clearly indicated the formation of non-defined aggregates at high pH values. This could be explained by the equilibrium between the zwitterionic phenolate form and the neutral, hydrophobic and planar quinone form (Fig. 2C). With regard to its isomers **HR-mOH** and **HR-oOH**, the neutral quinone forms cannot be formed due to the impossible delocalization of the electrons in the **HR-mOH** form and a twisted structure imposed by hindered sterical effect in **HR-oOH**; therefore, their absorption spectra only display slight changes upon deprotonation with no sign of aggregation (Fig. 2A and B). Interestingly, absorption spectra of **HR-Br** at pH values above its pK_a exhibited a second band indicating formation of soluble *H*-aggregates (Fig. 2D). Basic forms of **HR-Cl** and **HR-Br** both form *H*-aggregates, the stabilisation of which could be attributed to intermolecular halogen bonding^{37,38} between the electron-rich oxygen of the phenolate and the halogen atom forming typical head to head *H*-aggregate dimers. It is also noted that H-Rubies that forms *H*-aggregates in their



Table 1 Spectral and physico-chemical properties of the first set of synthesised X-rhodamines (5 μM in MOPS 30 mM, 100 mM KCl)^a

Compound		$\lambda_{\text{abs,max}}$ (nm)	λ_{em}^d (nm)	$\text{Log } \epsilon$ ($\lambda_{\text{abs,max}}$) ($\text{M}^{-1} \text{cm}^{-1}$)	Φ	$\Phi_{\text{ON}}/\Phi_{\text{OFF}}$	Dynamic range ^e	Dynamic range @ pH ± 1 pK _a ^f	pK _a
HR- <i>p</i> OH	ON ^b	576	587	4.78	0.55	9	34	30	8.97
	OFF ^c	579 ^f	598	4.53	0.06				± 0.05
HR- <i>m</i> OH	ON ^b	578	602	4.70	0.30	3	132	75	9.33
	OFF ^c	577	603	4.63	0.11				± 0.13
HR- <i>o</i> OH	ON ^b	581	603	4.89	0.75	3	866	460	9.68
	OFF ^c	579	603	4.69	0.27				± 0.17
HR-Me	ON ^b	574	597	4.71	0.09	High	955	833	8.75
	OFF ^c	N/A ^g	598	N/A ^g	N/A ^h				± 0.16
HR-OMe	ON ^b	577	598	4.72	0.22	8	302	N/A ⁱ	N/A ⁱ
	OFF ^c	576	600	4.74	0.03				
HR-Cl	ON ^b	579	601	4.68	0.47	High	753	512	6.17
	OFF ^c	544	599	4.52	N/A ^h				± 0.10
Hr-Br	ON ^b	581	601	4.39	0.55	High	384	291	6.51
	OFF ^c	544	600	4.40	N/A ^h				± 0.10
<i>p</i> -Nph	ON ^b	581	600	4.79	0.28	6	23	9.7	8.51
	OFF ^c	579	602	4.34	0.05				± 0.17
<i>o</i> -Nph	ON ^b	584	604	4.43	0.77	8	337	166	8.73
	OFF ^c	576	604	4.46	0.10				± 0.17
Pip-H	ON ^b	578	600	4.88	0.16	4	6	3.9	8.67
	OFF ^c	579	601	4.84	0.04				± 0.07
Pip-Alkyne	ON ^b	577	600	4.98	0.34	2	3	1.9	4.95
	OFF ^c	579	602	4.45	0.15				± 0.09
Imidazole	ON ^b	583	609	4.80	0.40	N/A ⁱ	N/A ⁱ	N/A ⁱ	N/A ⁱ
	OFF ^c	584	608	N/A ⁱ	N/A ⁱ				

^a ϵ = molar extinction coefficient, λ = wavelength, Φ = quantum yield. ^b Protonated form: pH 4. ^c Deprotonated form: pH 10. ^d Excitation at 535 nm. ^e $[(I_{\text{max}} - I_{\text{min}})/I_{\text{min}}]$ with I = fluorescence intensity. ^f Fluorescence enhancement between ± 1 pH unit around the pK_a value. ^g Broad absorbance. ^h Non-fluorescent. ⁱ pK_a value was too high. ^j No pH sensitivity.

basic forms have significantly enhanced acidity. For example, HR-Br is 1000-times more acidic than HR-*p*OH. This difference in acidity cannot be exclusively attributed to the electronic withdrawing effect of the bromine atom. These results tend to suggest that *H*-aggregation stabilises the basic forms of H-Rubies and hence, enhances their acidity. In this line of thought, since aggregation is concentration dependent, absorbance spectra and titration curves of HR-Br were measured at different concentrations of dye ranging from 500 nM to 5 μM (see Fig. S3 and S4[†]). The results showed that aggregation of basic form occurred at concentration above 500 nM and impacted the pK_a which varied from 6.5 at 5 μM to 7.3 at 500 nM. Moreover at a concentration of 500 nM where no aggregation of the basic form occurs the fluorescence enhancement was diminished as the OFF state was only due to the PET quenching phenomenon. *H*-aggregates are virtually non-fluorescent and thus, for the H-Rubies that are able to undergo this type of aggregation, this property can confer impressive levels of fluorescence enhancement (dynamic range) between their basic and acidic forms making them promising pH sensor for bio-imaging purposes. By controlling the *H*-aggregation of fluorophores one can achieve highly sensitive fluorogenic systems with a pronounced turning ON of fluorescence upon de-aggregation. This principle has been successfully used for bioimaging of ligand-receptor interactions³⁹ and was also applied in monitoring intracellular pH with fluorogenic polymers.⁴⁰

Synthesis of functionalised H-Rubies

Despite the first phenol-based X-rhodamines yielding excellent results as fluorescent pH probes, the importance of the ability to functionalise such fluorescent sensors must be emphasised and thus, the basic principle was pushed further in order to develop

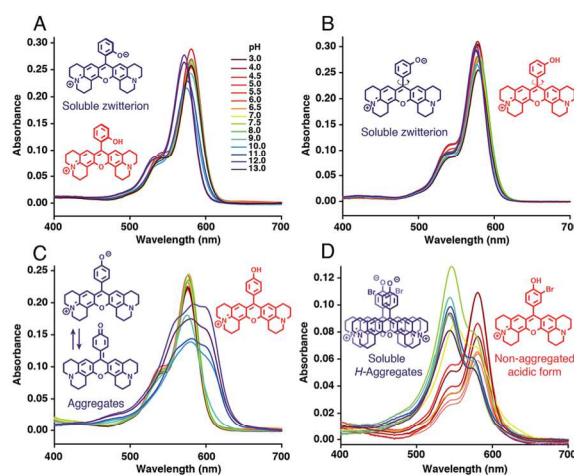


Fig. 2 Absorption spectra of (A) HR-*o*OH, (B) HR-*m*OH, (C) HR-*p*OH and (D) HR-Br at 5 μM in MOPS 30 mM, 100 mM KCl at different pH and their basic form (blue) and acidic form (red) structures.



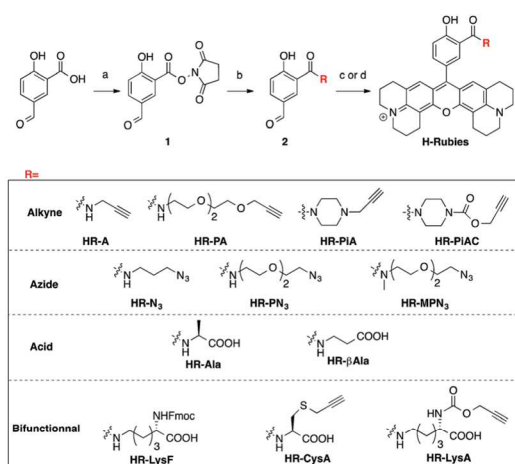


Fig. 3 Synthesis and structures of the functionalisable H-Rubies: (a) NHS, DCC, THF; (b) amine, DIEA, DMSO; (c) 8-hydroxyjulolidine, PTSA, propionic acid then *p*-chloranil, DCM/MeOH (1 : 1); (d) 8-hydroxyjulolidine, TfOH, DCM, then *p*-chloranil.

functionalisable H-Rubies. For this purpose, a linker was added at the *ortho* position of the phenol *via* an amide bond: a mild electron-withdrawing group that would ensure the conservation of a biologically relevant pK_a . For this new set of functionalisable H-Rubies, 5-formylsalicylic acid **1** was converted into its activated ester **2** onto which were condensed primary and

secondary amines bearing one or two orthogonal functions. Once the desirable aldehydes were obtained, they were transformed into their corresponding X-rhodamines with a custom optimized methodology allowing us to obtain the H-Rubies with yields of up to 93% (see ESI†). This new set of sensors can be categorised as follows: alkynes and azides, allowing linkage *via* bio-orthogonal Huisgen cycloaddition “click chemistry”; acids that can be coupled with amines and bifunctional H-Rubies, bearing two different functional groups (Fig. 3). Among the bifunctional H-Rubies that were developed is an Fmoc-protected Lysine H-Ruby (**HR-LysF**), which can be incorporated into a peptide sequence.

Structure/properties relationship of functionalisable H-Rubies

Once again, it was noticed that slight modifications of the base structure led to dramatic changes in the photophysical properties of H-Rubies such as epsilon, quantum yields and pK_a values which ranged from 4 to 8 (Table 2). The most notable differences were observed between secondary and tertiary amides whereby secondary amides appeared much more acidic than tertiary amides. To emphasise this phenomena, we synthesised **HR-PN₃** and its methylated tertiary amide equivalent **HR-MPN₃** and showed that the latter was 60-times less acidic. Moreover, absorption spectra of these functionalisable H-Rubies clearly showed different behaviours of their basic forms in water. While deprotonated tertiary amide H-Rubies showed

Table 2 Spectral and physicochemical properties of the functionalisable H-Rubies (5 μ M in MOPS 30 mM, 100 mM KCl)

Compound		$\lambda_{abs,max}$ (nm)	λ_{em}^c (nm)	$\text{Log } \epsilon$ ($\lambda_{abs,max}$) ($M^{-1} \text{ cm}^{-1}$)	ϕ	ϕ_{ON}/ϕ_{OFF}	Dynamic range ^d	Dynamic range @ pH ± 1 pK_a^e	pK_a
HR-A	ON ^a	574	600	4.26	0.09	6	6	4.2	5.33
	OFF ^b	534	598	4.58	0.02				± 0.13
HR-PA	ON ^a	580	602	4.87	0.46	1150	31	22	6.89
	OFF ^b	573	596	4.86	4×10^{-4}				± 0.04
HR-PIA	ON ^a	580	601	4.55	0.80	35	98	29	7.64
	OFF ^b	574	600	4.32	0.02				± 0.10
HR-PIAC	ON ^a	580	601	4.86	0.64	40	86	45	7.68
	OFF ^b	575	602	4.69	0.02				± 0.09
HR-N₃	ON ^a	580	600	4.43	0.25	28	88	74	3.96
	OFF ^b	523	596	4.43	0.01				± 0.03
HR-PN₃	ON ^a	578	603	4.72	0.41	21	21	19	6.20
	OFF ^b	573	597	4.74	0.02				± 0.03
HR-MPN₃	ON ^a	578	605	5.20	0.65	65	78	66	8.00
	OFF ^b	573	603	5.20	0.01				± 0.03
HR-Ala	ON ^a	577	601	4.81	0.15	8	9	8.3	7.85
	OFF ^b	573	597	5.03	0.019				± 0.03
HR-βAla	ON ^a	577	602	5.10	0.20	11	11	N/A ^f	N/A ^f
	OFF ^b	572	598	5.30	0.018				
HR-LysF	ON ^a	583	607	4.73	0.11	37	45	33	4.84
	OFF ^b	580	600	4.66	0.003				± 0.10
HR-CysA	ON ^a	577	602	4.69	0.09	N/A ^f	N/A ^f	N/A ^f	N/A ^f
	OFF ^b	572	597	5.08	0.014				
HR-LysA	ON ^a	577	602	4.75	0.25	13	13	11	7.51
	OFF ^b	572	596	4.96	0.02				± 0.04

^a Protonated form: pH 4. ^b Deprotonated form: pH 10. ^c Excitation at 535 nm. ^d $[(I_{max} - I_{min})/I_{min}]$ with I = fluorescence intensity. ^e Fluorescence enhancement between ± 1 pH unit around the pK_a value. ^f Complex titration curve.



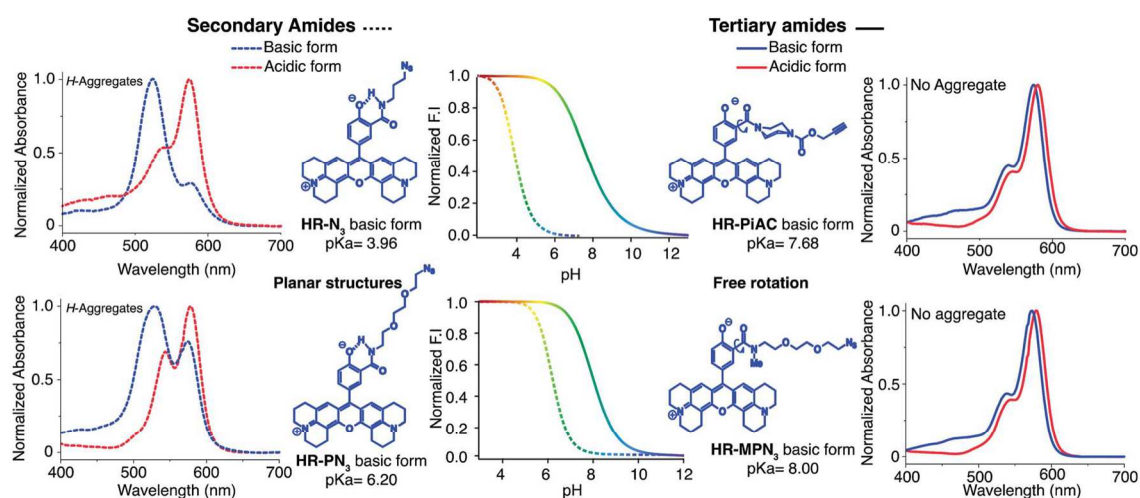


Fig. 4 Difference of acidity and *H*-aggregation capability between secondary amide H-Rubies (dashed lines) and tertiary amide H-Rubies (plain lines). Concentration of probes was 5 μM in MOPS 30 mM, 100 mM KCl, excitation wavelength at 535 nm.

slight hypsochromic shifts of their maximum absorption wavelengths (1–5 nm), absorption spectra of secondary amide H-Rubies displayed a second absorption band (530 nm) indicating typical formation of soluble *H*-aggregates.

These differences can be explained by the formation of a H-bond between the phenolate and the proton of the secondary amide whereby the former is stabilised and hence, the pK_a is lowered (Fig. 4). Moreover, the six membered ring formed *via* H-bonding leads to a constrained conformation which aids the formation of planar, head-to-head *H*-aggregates. As seen in our initial observations, the acidity of H-Rubies is enhanced by their ability to form *H*-aggregates in their OFF state (Fig. 4).

Imaging of acidic domains in living cells with molecular H-Rubies

The impressive physical and optical properties of H-Rubies lead us to investigate their ability to image acidic domains in living cells. After establishing their insensitivity towards biologically significant metals (Zn^{2+} , Mg^{2+} , Ca^{2+} , Fe^{3+} , Mn^{2+}) and their nontoxicity (see ESI Fig. S5† for LDH cytotoxicity assay), **HR-N₃**, **HR-Me**, **HR-Cl** and **HR-Br** were involved in cellular experiments (Fig. 5A). These probes were specifically chosen for their respective pK_a values: **HR-Me** served as a positive control since its pK_a is more than two units above maximum physiological pH, **HR-N₃** was expected to be a negative control since it has a pK_a of 4, whereas **HR-Cl** and **HR-Br** were expected to sense variations of pH within the cell (Fig. 5B). Firstly, Fischer's rat glioblastoma F98 cells (primary tumor) were incubated with the four dyes (1 μM) for only 20 min and visualised by confocal laser scanning microscopy. The obtained images indicated that these H-Rubies are cell-permeant and stain the mitochondria; this was confirmed by colocalisation experiments with mitotracker-green (see Fig. S6†). In a second time, flow cytometry assays with these cells showed a clear correlation between the observed fluorescence intensity of the cells and the measured pK_a of the

probes (Fig. 5B and C plain lines). Finally, we checked the pH sensitivity of these H-Rubies upon cytosolic acidification. The intracellular pH was decreased to pH 6 and flow cytometry assays were performed (Fig. 5C dashed lines). The results showed that albeit **HR-N₃** and **HR-Cl** displayed non-significant fluorescence enhancement (blue and green lines), **HR-Br** (orange line) displayed an impressive *in cellulo* response to this acidification ($\Delta\text{pH} = 1.4$, fluorescence enhancement: up to 13-fold). **HR-Me** also showed an interesting fluorescence enhancement (~ 5 -fold) but behaved in an inconsistent manner when the intracellular pH was alkalinised (Fig. S7†). Despite **HR-Br** cannot be used to determine absolute pH values *in cellulo* because of the effect of its concentration on its pK_a , its cell permeability combined with its high fluorescence enhancement in the physiological pH range make it an attractive tool for tracking mitochondrial acidification which is an important field in cell biology as it is involved in mitophagy that is associated to various pathologies including neurodegenerative and cardiovascular diseases.^{41,42}

Measurements of intraorganellar pH using functionalisable H-Rubies

To demonstrate the different biological applications of H-Rubies we developed two systems to measure sub-organellar pH in living cells. Our first approach aimed at the calibration of phagosomal pH in living cells using flow cytometry. As pH reporter, **HR-PiAC** was chosen for its useful properties in cellular experiments such as its high brightness, its high dynamic range (~ 80 -fold) and its pK_a value of 7.68 (Fig. 6A and B). 3 μm latex beads containing amino groups were combined with the bifunctional linker azido-PEG₄-NHS ester followed by double functionalisation using click chemistry with **HR-PiAC** and a pH-insensitive near infrared emitting dye, Alexa Fluor 647, to allow ratiometric measurements (Fig. 6C). It was noticed that the covalent binding of two dyes on the surface of the beads



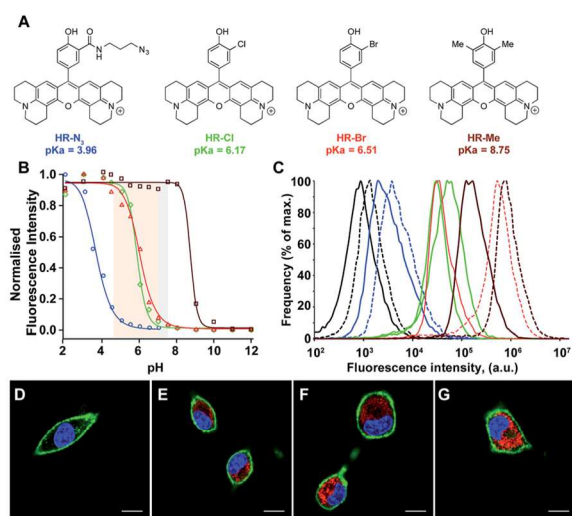


Fig. 5 (A) Structures and pK_a values of the H-Rubies used for cellular experiments. (B) pH titration curves (Hill equation fit) of HR- N_3 (blue), HR-Cl (green), HR-Br (red) and HR-Me (brown) at 5 μ M in MOPS (30 mM) KCl (100 mM), cytosolic and cellular acidic pH ranges are delimited with coloured areas. (C) Comparison of fluorescence intensity of F98 cells incubated for 20 min with 1 μ M of HR- N_3 (blue), HR-Cl (green), HR-Br (red) and HR-Me (brown) at pH 7.4 (plain lines) and pH 6 (dashed lines) assessed by flow cytometry. Each curve is an average of 3 independent measurements. The control corresponds to the intrinsic fluorescence of cells (black line). Bottom: laser scanning confocal microscopy images of F98 cells incubated for 20 min with 1 μ M of (D) HR- N_3 , (E) HR-Cl, (F) HR-Br, (G) HR-Me. The H-Rubies were visualized in red, the nuclei were stained with Hoechst (blue) and the membrane with Alexa 647-conjugated concanavalin A (green). Pictures show the three merged channels. Scale bars are 10 μ m.

influences the physicochemical properties of HR- PiAC , namely its dynamic range and its pK_a . This effect has already been noticed in our previous work involving a molecular fluorescent Ca^{2+} sensor linked to a quantum dot⁴³ and can be attributed to the proximity of the dye to the hydrophobic environment of the polystyrene bead that enhances the basal fluorescence of the sensor. Compared to the titration curve of the free dye, the fluorescence ratio of the two dyes obtained by flow cytometry shows an almost linear dependence when the pH is varied from 5 to 9. As a result, although these beads have a decreased sensitivity in the pH of physiological domain, it provides a ratiometric system which displays a pH sensitivity over a wider range when compared to a free HR- PiAC (Fig. 6D).

The dyes-modified beads were then added to a suspension of RAW 264.7 macrophages and incubated for 30 min at 37 °C to complete the process of phagocytosis. After several washes the cells were fixed and visualized by confocal microscopy to assess the efficiency of bead internalisation. Orthogonal view analysis of confocal sections shows partial internalisation of the beads by macrophages. As shown in Fig. 7, in addition to fully internalised beads, some beads are attached to the outer cell membrane. On average only 30% of beads were fully internalised by the cells. This could interfere with flow cytometric measurements of phagosomal pH because the laser-based

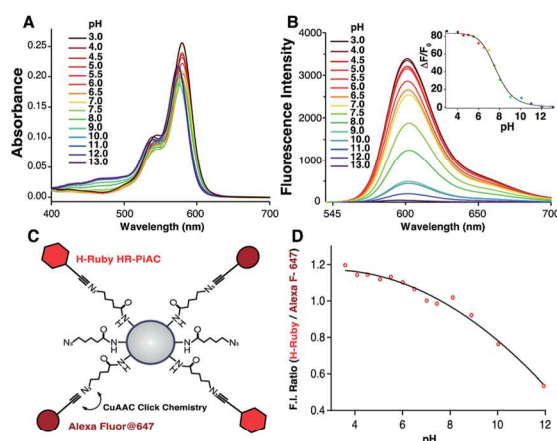


Fig. 6 Absorption (A) and emission spectra (B) of HR- PiAC (5 μ M, MOPS 30 mM, 100 mM KCl) at different pH (excitation wavelength = 535 nm), inset is the titration curve fitted with the Hill equation providing a pK_a of 7.68 ± 0.09 and an enhancement of fluorescence of ~ 80 -fold. Scheme of bead-based pH sensor, containing pH-sensitive dye HR- PiAC and pH-insensitive Alexa Fluor 647 (C); titration curve of the pH beads measured by flow cytometry (D).

technique in this case will identify all fluorescent objects, *i.e.* cells with internal and/or external beads. We, therefore, performed an additional modification of the beads by coating them with a biotinylated ovalbumin (OVA), *via* passive absorption. The coated beads, firstly, have a reduced non-specific binding to the cell surface and favour phagocytosis through the interaction between the mannosylated structure present on the surface of OVA⁴⁴ and the mannose receptors of macrophages.⁴⁵ Secondly, accessible biotin groups of OVA can be tagged by FITC-streptavidin.

For phagosomal pH measurement by flow cytometry, adherent RAW 264.7 macrophages were incubated for 30 min at 37 °C with the OVA-modified beads and let rest for 3 more hours for phagosomal maturation. Afterwards the cells were harvested and incubated with streptavidin-FITC that only binds to the non-internalised beads containing OVA-biotin. Two populations of phagocytic and non-phagocytic cells can be differentiated by the fluorescence intensity of Alexa Fluor 647 of the beads. A cell population with beads attached to the cell surface

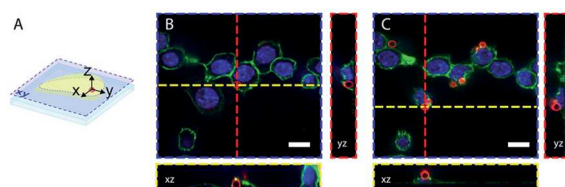


Fig. 7 Confocal microscopy images of fixed RAW 264.7 cells after bead phagocytosis. DAPI nuclear staining, concanavalin-Alexa 488 membrane staining and pH beads are in blue, green and red respectively. (A) illustrates the orthogonal views of the cell that allow differentiation of the internalized beads (B) and the beads attached to the cell surface (C). Scale bars are 10 μ m.



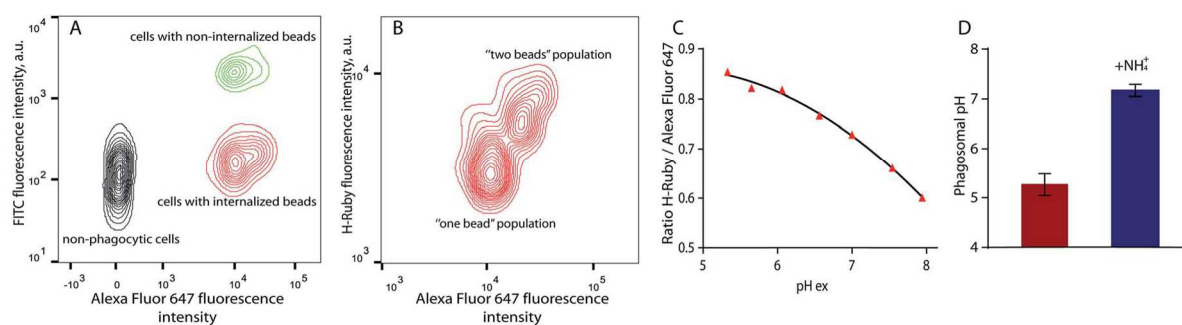


Fig. 8 Phagosomal pH measurement in RAW 264.7 cells by flow cytometry. (A) Density plot of the cells after bead internalisation showing three distinct populations: non-phagocytic cells, cells with internalised beads and cells with non-internalised beads on which a biotin – streptavidin – FITC interaction takes place; (B) the cells with only one internalised bead were used for analysis of phagosomal pH. (C) Typical calibration curve of H-Ruby/Alexa Fluor 647 ratio of the cells clamped at different pHs with the ionophore nigericin; (D) phagosomal pH (5.3 ± 0.2 , in red) in RAW 264.7 cells measured after 3 hours of phagosomes maturation NH_4Cl addition shows alkalisation of phagolysosomes (7.2 ± 0.1 , in blue). The data represent the mean of 3 independent experiments \pm SD.

can be separated by the higher fluorescence intensity of FITC at extracellular pH (Fig. 8A). Further detailed analysis of the phagocytic population shows the presence of subpopulations according to the fluorescence intensities of Alexa Fluor 647 and H-Ruby: cells that have internalised one bead per cell exhibit a lower fluorescence intensity (Fig. 8B). For precise analysis of phagosomal pH the cells were gated on one bead population and a ratiometric calibration curve of phagosomal pH was obtained changing the external pH over the 5 to 8 range using a citric acid/HEPES buffer and imposing the same pH intracellularly using nigericin, a K^+/H^+ ionophore (Fig. 8C). Finally, to determine the phagosomal pH, the ratio of the mean fluorescence intensities of HRuby vs. Alexa Fluor 647 obtained from the intact cells was interpolated to the calibration curve yielding a phagolysosomal pH of 5.3 ± 0.2 . This result is in a good agreement with a previously published study where authors showed a phagosomal pH value of 5.22 ± 0.03 in RAW cells using FITC-sRBC particles.⁴⁶ Addition of the weak base $\text{NH}_4^+/\text{NH}_3$ caused fast alkalisation, and demonstrated the intracellular localisation of the beads (Fig. 8D).

Another application of these newly synthesized H-Rubies is the calibration of endosomal pH by flow cytometry and to achieve this we used a polysaccharide dextran that is known to target the endolysosomal pathway.⁴⁷ 40 kDa dextran was converted to an alkyne containing dextran and was subsequently clicked to HR- PN_3 (Fig. 9A). In comparison to its parent molecular form HR- PN_3 , the fluorescent pH-sensitive dextran displayed a slightly shifted apparent pK_a value (respectively 6.20 ± 0.03 and 6.77 ± 0.02 ; Fig. 9B) with a virtually non-fluorescent OFF state (see ESI†). Functionalisation did not significantly affect the fluorescence enhancement between pH 10 and 4 (respectively 21- and 19-fold) making this water-soluble polymer a valuable tool for monitoring endosomal pH. To demonstrate this, adherent RAW 264.7 cells were incubated for 30 min with HR- PN_3 dextran conjugate and let rest for 3 more hours. As shown in Fig. 9C, vesicles of different shapes and sizes could be observed inside the cells due to the movement and segregation of the dextran molecules between the endocytic organelles.⁴⁸

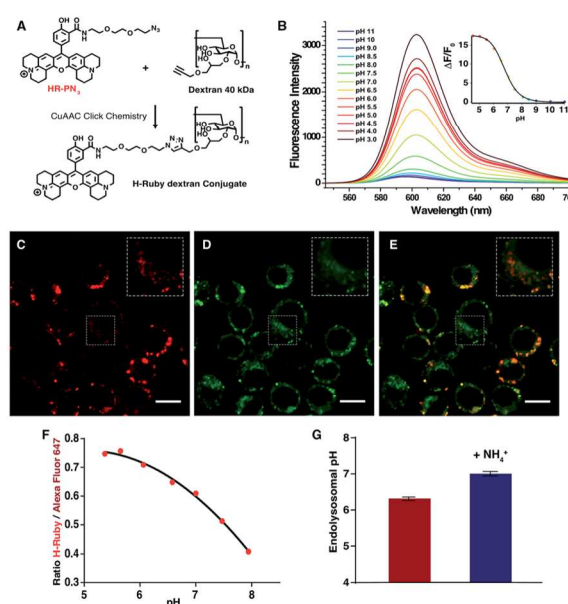


Fig. 9 (A) Synthesis of HR- PN_3 dextran conjugate via CuAAC Click Chemistry. (B) Emission spectra of HR- PN_3 dextran conjugate (MOPS 30 mM, 100 mM KCl) at different pH (excitation wavelength = 535 nm), inset is the titration curve fitted to the Hill equation yielding a pK_a of 6.77 ± 0.02 and an enhancement of fluorescence of ~ 18 -fold and 13 fold between ± 1 pH unit around the pK_a . (C–E) Confocal images of RAW 264.7 cells after incubation with 1 mg mL^{-1} HR- PN_3 dextran conjugate (C), co-stained by Lysotracker Green (D) and a merged image of two channels (E). HR- PN_3 dextran conjugate labels lysosomes (in red) that colocalises with Lysotracker, and endosomes that are shown in insets and do not colocalise with Lysotracker. Scale bars are 10 μm . (F) Typical calibration curve of H-Ruby/Alexa Fluor 647 ratio of the cells clamped at different pHs with the ionophore nigericin. (G) Endosomal pH (6.3 ± 0.05 , in red) in RAW 264.7 cells measured after 3 hours of incubation with HR- PN_3 dextran. NH_4Cl addition shows alkalisation of endosomal organelles (7.0 ± 0.06 , in blue). The data represent the mean of 3 independent experiments \pm SD.



Addition of LysoTracker Green led to its partial colocalisation with **HR-PN₃ dextran conjugate** (Fig. 9C–E) suggesting that **HR-PN₃ dextran** accumulates both in the more acidic lysosomes and in the mildly acidic vesicles of the endocytic pathway as well. This observation is consistent with the flow cytometry experiments where, applying the same strategy as described above, the pH value of 6.3 ± 0.04 was obtained (Fig. 9F–G).

Methods and materials

LDH-cytotoxicity assay

CHO-K1 cells (20 000 per well) were seeded in 96 multiple well plates 24 h before the experiment. Cells (40 000 per well) were incubated with the fluorescent compounds in 100 μ L DMEM for 2 hours at 37 °C. The incubation milieu was then replaced by 100 μ L fresh DMEM containing 10% of cell-counting solution (Dojindo Laboratories) and incubated for a further 2 h at 37 °C. The absorbance measured at 450 nm had a direct relationship to the number of viable cells. Experiments were conducted in triplicate and repeated twice.

Cell culture

Undifferentiated malignant glioma rat (F98) and Chinese Hamster Ovary (CHO) cell lines (from ATCC) were maintained at 37 °C in 5% CO₂ in DMEM/F-12 nutrient medium (Invitrogen, Cergy Pontoise, France) supplemented with 2% (v/v) heat-inactivated fetal bovine serum (Invitrogen) and 100 μ g mL⁻¹ streptomycin and 100 units per mL penicillin (Invitrogen). RAW 264.7 macrophages cell line was maintained at 37 °C in 5% CO₂ in DMEM nutrient medium (Gibco, Invitrogen) supplemented with 10% fetal calf serum (Eurobio, France).

Confocal microscopy

Cell cultures were incubated with the pH probes (in DMEM/F-12 nutrient medium only) for 20 min, and then washed twice with phosphate-buffered saline (PBS) alone. After 4 hours, the nucleus were stained with 60 μ g mL⁻¹ Hoechst 34580 for 15 min, the cell cultures were then washed with PBS and the plasma membrane was stained with 30 μ g mL⁻¹ Alexa 647-conjugated concanavalin A and the mitochondria stained with 50 nM mitotracker green for 5 min (stainings were purchased at Invitrogen, Cergy Pontoise, France). Cells were washed once more. Live cells were then immediately analysed by confocal laser scanning microscopy using a Zeiss LSM operating system. Alexa 647 (633 nm), Hoechst 34580 (405 nm), pH probes (561 nm) and mitotracker green (488 nm) were sequentially excited and emission fluorescence was collected.

To assess the efficiency of bead internalisation, the cells, after completing the process of phagocytosis (as described in “Organelle pH measurement by flow cytometry”), were plated on coverslips ($d = 12$ mm) coated with 10 μ g mL⁻¹ fibronectin and incubated at 37 °C in 5% CO₂: the cell membrane was stained with 25 μ g mL⁻¹ Alexa Fluor 488 – conjugated concanavalin (Invitrogen, USA) at 4 °C for 5 min and 4% paraformaldehyde was added for 20 min to fix the cells. The coverslips with the cells were then mounted on microscope

slides using a mounting medium DAPI-Fluoromount G (Southern Biotech, USA) and left at room temperature overnight. Imaging was performed on a spinning disk microscope. The pH-sensitive beads were excited with 561 nm laser line and detected with ET630/75 nm filter, DAPI was excited with 405 nm laser line and detected with ET460/50 nm band-pass filter and Concanavalin A-Alexa Fluor 488 was excited with 488 nm laser line and detected with D505/40 nm band-pass filter. Images were collected using microscope software Software: MetaMorph 7.8.2.0. The subsequent analysis of the images was conducted on an open source image processing program ImageJ.

Fluorescence activated cell sorting analyses – effect of the pH_i on the fluorescence intensity of the H-Rubies

For the dose-response curve, F98 cells were incubated with various concentrations of the H-Rubies in DMEM/F-12 culture medium without serum at 37 °C for 2 h. The cells were then washed with PBS to remove excess extracellular H-Ruby and were then treated with 0.05% Trypsin–EDTA for 2 min at 37 °C to detach cells from the surface, and centrifuged at 200 g in DMEM/F-12 culture medium before suspension in PBS. Flow cytometry analyses were performed with live cells using an Accuri C6 flow cytometer (BD Biosciences, Le Pont de Claix, France). For acquisition a 488 nm wavelength laser was used for H-Rubies excitation, the fluorescence emissions were recorded in a 584 ± 20 nm spectral detection channel. Data were obtained and analyzed using CFlow Sampler (BD Biosciences). Live cells were gated by forward/side scattering for a total of 10 000 events.

The pH_i of F-98 cells was modified using the pseudo-null calibration method describe by Chow *et al.*⁴⁹ F98 cells were incubated with 1 μ M of H-Rubies in DMEM/F-12 culture medium without serum at 37 °C for 20 min. The cells were then washed with PBS to remove excess extracellular probe and were then treated with 0.05% Trypsin–EDTA for 2 min at 37 °C to detach the cells from the surface, and centrifuged at 200 g in DMEM/F 12 culture medium before suspension in culture medium. Just before the analysis the pseudo null solution were added (ratio of culture medium: pseudo-null solution 1 : 1) and the data were acquired immediately (within 30 s). Pseudo-null solutions were made according to the method of Chow *et al.* Six times concentrated standard solution was made by adding 1 M ammonium hydroxide and 1 M acetic acid to the basal solution (culture medium). This provided a set of pseudo-null solution as shown in Table S1 (see ESI†). Flow cytometry analyses were performed with live cells using an Accuri C6 flow cytometer (BD Biosciences, Le Pont de Claix, France). Data were obtained and analyzed using CFlow Sampler (BD Biosciences). Live cells were gated by forward/side scattering for a total of 10 000 events.

Functionalisation of the beads by H-Ruby

Polybead® Amino Microspheres 3.00 μ m (Polysciences) were used. First the beads were washed with dH₂O. In order to convert the NH₂ groups on the beads surface to N₃ groups for further click chemistry reactions, 100 nmol of the bifunctional linker N₃–PEG₄–NHS was added to 100 μ L of the beads



containing ~20 nmol of NH₂ groups and incubated at room temperature for 2 h. The alkyne-modified H-Ruby **HR-PiAC** and alkyne-containing Alexa Fluor 647 (Molecular Probes®) were then mixed with the bead solution in a ratio 1 nmol of NH₂ group: 10 nmol of H-Ruby: 2.5 nmol of Alexa Fluor 647. 5 μL of 25 mM CuSO₄·5H₂O and 5 μL of 25 mM sodium ascorbate were added to initiate a click-reaction. The mixture was incubated overnight at room temperature. The dyes modified beads were successively washed with 0.1 M EDTA, 10% ethanol and PBS to remove non-reacted dyes.

Organellar pH measurement by flow cytometry

Measurement of phagosomal or endosomal pH was performed using macrophages cell line RAW 264. The cells were plated on a Petri dish and at 80% confluence pH beads in a 4 : 1 ratio or 0.7 mg mL⁻¹ 40 kDa **HR-PN₃ dextran conjugate** and 0.3 mg mL⁻¹ 40 kDa Alexa Fluor 647 dextran conjugate were added and incubated 30 min at 37 °C to complete internalisation. Afterwards the non-internalised beads/dextran were washed out, fresh medium was added and the cells were let rest at 37 °C, 5% CO₂ for 3 more hours. For FACS analysis the cells were harvested and resuspended in CO₂-independent medium (GIBCO, Invitrogen). For NH₄⁺/NH₃ tests, 20 mM NH₄Cl was added to the extracellular medium and let to incubate for 3 min.

The calibration of phagosomal and endosomal pH was performed using the K⁺/H⁺ ionophore nigericin that, together with a high concentration of potassium in the buffer, equalises the intracellular and extracellular pH.³⁰ The cells containing internalised pH beads or dextran were resuspended in buffers containing 143 mM KCl, 1.17 mM MgCl₂, 1.3 mM CaCl₂, 5 mM glucose and 10 μM nigericin with defined pH buffers ranging from pH 5.0 to pH 8.0 with 0.5 increments. 20 mM citric acid was used for a buffer range of pH 5.0–6.5 and 20 mM (4-(2-hydroxyethyl)-1-piperazineethanesulfonic acid) (HEPES) – for buffers in the pH range 7.0–8.0. 0.05 μM DAPI was added to exclude the dead cells. After incubation for 5 min at RT the samples were analyzed by a flow cytometer (BD LSR Fortessa, BD Biosciences). For acquisition, a 532 nm wavelength laser was used for H-Rubies excitation, and its emission fluorescence was recorded in a 610 ± 20 nm spectral detection channel. For Alexa Fluor 647 a 640 nm wavelength laser was used for excitation and a 670 ± 30 nm spectral detection channel to record its emission fluorescence. Each time 10 000 events were acquired. For analysis, a population of live cells was gated by forward/side scatter, and within this population only the cells which have phagocytosed one pH bead were selected for precise pH determination.

Conclusion

We have developed a new set of efficient red-emitting fluorescent pH sensors based on PET quenching phenomena. H-Rubies exhibit specific pK_a values and a structure/properties relationship based on their ability to form non-emissive dark H-aggregates was established. Four non-functionalizable H-Rubies were chosen for cellular experiments and were shown to

cross the plasma membrane to compartmentalise in mitochondria. Among them, **HR-Br** displays a strong fluorescence enhancement upon acidification of mitochondria in live cells. Functionalizable H-Rubies were linked to a dextran polymer or to microbeads that were also decorated with a pH-insensitive dye leading to ratiometric pH probe systems. These systems were successfully used to measure phagosomal and endocytic pHs in live cells. The authors believe that this new family of fluorescent indicators, with their large choice of pK_a values and spectral properties specifically adapted to cellular imaging, represents a valuable toolkit for imaging pH variations in living cells. Moreover, their diverse functionalizable side arms allows them to be attached to particles, polymers and biomolecules such as peptides or antibodies for accurate pH readout of subcellular micro-domains.

Acknowledgements

G. D. and A. Z. benefitted of post-doctoral fellowships from the Pierre Gilles de Gennes foundation. C.T. was supported by the Région Rhône Alpes by an emergence fellowship. We would like to thank Jean-Marie Carpier (Institute Curie, U932) for his help with imaging, Dr. Sandrine Sagan and Dr Fabienne Burlina (Laboratoire des biomolécules, UMR CNRS 7203) for the toxicity assays. We also acknowledge PICT-IBISA (Institute Curie), member of the France-BioImaging national research infrastructure. This work was supported by the Fondation Pierre-Gilles de Gennes (to S. A., A. F. and J. M. M.), the European Research Council (2013-AdG No. 340046), la Ligue Nationale contre le Cancer (EL 2014.LNCC/SA) and the French Agence National de la Recherche (ANR P3N, nanoFRET2 grant to A. F., M. D. W. and J. M. M., and ANR-11-LABX-0015 to M. D. W.). This work is the subject of a European patent EP 13 199 575.5 – 1451 “fluorescent red emitting functionalizable pH probes”.

Notes and references

- 1 S. Grinstein and S. Dixon, *Physiol. Rev.*, 1989, **69**, 417.
- 2 R. A. Gottlieb, H. A. Giesing, J. Y. Zhu, R. L. Engler and B. M. Babior, *Proc. Natl. Acad. Sci. U. S. A.*, 1995, **92**, 5965.
- 3 R. A. Gottlieb, J. Nordberg, E. Skowronski and B. M. Babior, *Proc. Natl. Acad. Sci. U. S. A.*, 1996, **93**, 654.
- 4 S. Simon, D. Roy and M. Schindler, *Proc. Natl. Acad. Sci. U. S. A.*, 1994, **91**, 1128.
- 5 G. Lamb and D. Stephenson, *J. Physiol.*, 1994, **478**, 331.
- 6 H. Westerblad and D. Allen, *J. Physiol.*, 1993, **466**, 611.
- 7 A. A. Golabek, E. Kida, M. Walus, W. Kaczmarek, M. Michalewski and K. E. Wisniewski, *Mol. Genet. Metab.*, 2000, **70**, 203.
- 8 H. Izumi, T. Torigoe, H. Ishiguchi, H. Uramoto, Y. Yoshida, M. Tanabe, T. Ise, T. Murakami, T. Yoshida, M. Nomoto and K. Kohno, *Cancer Treat. Rev.*, 2003, **29**, 541.
- 9 B. A. Webb, M. Chimenti, M. P. Jacobson and D. L. Barber, *Nat. Rev. Cancer*, 2011, **11**, 671.
- 10 M. Miksa, H. Komura, R. Wu, K. G. Shah and P. Wang, *J. Immunol. Methods*, 2009, **342**, 71.



- 11 R. J. Lee, S. Wang and P. S. Low, *Biochim. Biophys. Acta, Mol. Cell Res.*, 1996, **1312**, 237.
- 12 J. Han and K. Burgess, *Chem. Rev.*, 2010, **110**, 2709.
- 13 M. Collot, C. Loukou, A. V. Yakovlev, C. D. Wilms, D. Li, A. Evrard, A. Zamaleeva, L. Bourdieu, J.-F. Leger, N. Ropert, J. Eilers, M. Oheim, A. Feltz and J.-M. Mallet, *J. Am. Chem. Soc.*, 2012, **134**, 14923.
- 14 M. Collot, C. Wilms, A. Bentkayet, P. Marcaggi, K. Couchman, S. Charpak, S. Dieudonné, M. Hässler, A. Feltz and J.-M. Mallet, *elife*, 2015, **4**.
- 15 M. Collot, C. Wilms and J.-M. Mallet, *RSC Adv.*, 2014, **5**, 6993.
- 16 M. Tantama, Y. P. Hung and G. Yellen, *J. Am. Chem. Soc.*, 2011, **133**, 10034.
- 17 T. Jokic, S. M. Borisov, R. Saf, D. A. Nielsen, M. Kühl and I. Klimant, *Anal. Chem.*, 2012, **84**, 6723.
- 18 Y. Ni and J. Wu, *Org. Biomol. Chem.*, 2014, **12**, 3774.
- 19 X.-X. Zhang, Z. Wang, X. Yue, Y. Ma, D. O. Kiesewetter and X. Chen, *Mol. Pharmaceutics*, 2013, **10**, 1910.
- 20 Life technologies proposes a rhodamine based pH sensor, see <https://www.lifetechnologies.com/order/catalog/product/P36600>.
- 21 M. Tian, X. Peng, J. Fan, J. Wang and S. Sun, *Dyes Pigm.*, 2012, **95**, 112.
- 22 W. Zhang, B. Tang, X. Liu, Y. Liu, K. Xu, J. Ma, L. Tong and G. Yang, *Analyst*, 2009, **134**, 367.
- 23 H.-S. Lv, S.-Y. Huang, Y. Xu, X. Dai, J.-Y. Miao and B.-X. Zhao, *Bioorg. Med. Chem. Lett.*, 2014, **24**, 535.
- 24 L. Yuan, W. Lin and Y. Feng, *Org. Biomol. Chem.*, 2011, **9**, 1723.
- 25 Z. Li, S. Wu, J. Han and S. Han, *Analyst*, 2011, **136**, 3698.
- 26 A. Bender, Z. R. Woydziak, L. Fu, M. Branden, Z. Zhou, B. D. Ackley and B. R. Peterson, *ACS Chem. Biol.*, 2013, **8**, 636.
- 27 J. R. Casey, S. Grinstein and J. Orłowski, *Nat. Rev. Mol. Cell Biol.*, 2010, **11**, 50.
- 28 A. Savina, C. Jancic, S. Hugues, P. Guermontprez, P. Vargas, I. C. Moura, A.-M. Lennon-Duménil, M. C. Seabra, G. Raposo and S. Amigorena, *Cell*, 2006, **126**, 205.
- 29 A. Savina, A. Peres, I. Cebrian, N. Carmo, C. Moita, N. Hacohen, L. F. Moita and S. Amigorena, *Immunity*, 2009, **30**, 544.
- 30 A. W. Segal, *Annu. Rev. Immunol.*, 2005, **23**, 197.
- 31 W. Qin, M. Baruah, W. M. de Borggraeve and N. Boens, *J. Photochem. Photobiol., A*, 2006, **183**, 190.
- 32 I. C. S. Cardoso, A. L. Amorim, C. Queirós, S. C. Lopes, P. Gameiro, B. de Castro, M. Rangel and A. M. G. Silva, *Eur. J. Org. Chem.*, 2012, **2012**, 5810.
- 33 Y. Tian, F. Su, W. Weber, V. Nandakumar, B. R. Shumway, Y. Jin, X. Zhou, M. R. Holl, R. H. Johnson and D. R. Meldrum, *Biomaterials*, 2010, **31**, 7411.
- 34 N. V. Marinova, N. I. Georgiev and V. B. Bojinov, *J. Photochem. Photobiol., A*, 2011, **222**, 132.
- 35 I. López Arbeloa and P. Ruiz Ojeda, *Chem. Phys. Lett.*, 1982, **87**, 556.
- 36 K. Adachi, K. Watanabe and S. Yamazaki, *Ind. Eng. Chem. Res.*, 2014, **53**, 13046.
- 37 A. Priimagi, G. Cavallo, P. Metrangolo and G. Resnati, *Acc. Chem. Res.*, 2013, **46**, 2686.
- 38 P. Politzer, P. Lane, M. C. Concha, Y. Ma and J. S. Murray, *J. Mol. Model.*, 2006, **13**, 305.
- 39 I. A. Karpenko, M. Collot, L. Richert, C. Valencia, P. Villa, Y. Mély, M. Hibert, D. Bonnet and A. S. Klymchenko, *J. Am. Chem. Soc.*, 2014, **137**, 405.
- 40 K. Zhou, H. Liu, S. Zhang, X. Huang, Y. Wang, G. Huang, B. D. Sumer and J. Gao, *J. Am. Chem. Soc.*, 2012, **134**, 7803.
- 41 H. Chen and D. C. Chan, *Hum. Mol. Genet.*, 2009, **18**, R169.
- 42 R. A. Gottlieb and R. S. Carreira, *Am. J. Physiol.: Cell Physiol.*, 2010, **299**(2), C203.
- 43 A. I. Zamaleeva, M. Collot, E. Bahembera, C. Tisseyre, P. Rostaing, A. V. Yakovlev, M. Oheim, M. de Waard, J.-M. Mallet and A. Feltz, *Nano Lett.*, 2014, **14**, 2994.
- 44 M. Thaysen-Andersen, S. Mysling and P. Højrup, *Anal. Chem.*, 2009, **81**(10), 3933.
- 45 L. Martinez-Pomarez, *J. Leukocyte Biol.*, 2012, **92**, 1177.
- 46 B. E. Steinberg, N. Touret, M. Vargas-Caballero and S. Grinstein, *Proc. Natl. Acad. Sci. U. S. A.*, 2007, **104**(22), 9523.
- 47 C. J. Galloway, G. E. Dean, M. Marsh, G. Rudnick and I. Mellman, *Proc. Natl. Acad. Sci. U. S. A.*, 1983, **80**, 3334.
- 48 E. P. Berthiaume, C. Medina and J. A. Swanson, *JCB*, 1995, **4**, 989.
- 49 S. Chow, D. Hedley and I. Tannock, *Cytometry*, 1996, **24**(4), 360.
- 50 J. Bond and J. Varley, *Cytometry*, 2005, **64A**, 43.



Article 5:

In cellulo phosphorylation induces pharmacological reprogramming of maurocalcin, a cell-penetrating venom peptide.

Article publiée dans le PNAS en 2016

In cellulo phosphorylation induces pharmacological reprogramming of maurocalcin, a cell-penetrating venom peptide

Michel Ronjat^{a,b,1,2}, Wei Feng^{c,1}, Lucie Dardevet^{a,b}, Yao Dong^c, Sawsan Al Khoury^{a,b}, Franck C. Chatelain^{d,e}, Virginie Vialla^{a,b,f}, Samir Chahboun^{a,b}, Florian Lesage^{d,e}, Hervé Darbon^g, Isaac N. Pessah^c, and Michel De Waard^{a,b,f,2}

^aINSERM U836, LabEx Ion Channel, Science and Therapeutics, Grenoble Institute of Neuroscience, 38042 Grenoble, France; ^bUniversité Grenoble Alpes, 38042 Grenoble, France; ^cDepartment of Molecular Biosciences, School of Veterinary Medicine, University of California, Davis, CA 95616; ^dCNRS UMR 7275, LabEx Ion Channel, Science and Therapeutics, Institut de Pharmacologie Moléculaire et Cellulaire, F-06560 Valbonne, France; ^eUniversité de Nice Sophia Antipolis, F-06560 Nice, France; ^fSmartox Biotechnologies, 38400 Saint-Martin d'Hères, France; and ^gArchitecture et Fonction des Macromolécules Biologiques-CNRS UMR 7257, Aix-Marseille Université, 13009 Marseille, France

Edited by Andrew R. Marks, Columbia University College of Physicians & Surgeons, New York, NY, and approved February 25, 2016 (received for review August 31, 2015)

The venom peptide maurocalcin (MCa) is atypical among toxins because of its ability to rapidly translocate into cells and potently activate the intracellular calcium channel type 1 ryanodine receptor (RyR1). Therefore, MCa is potentially subjected to posttranslational modifications within recipient cells. Here, we report that MCa Thr²⁶ belongs to a consensus PKA phosphorylation site and can be phosphorylated by PKA both in vitro and after cell penetration in cellulo. Unexpectedly, phosphorylation converts MCa from positive to negative RyR1 allosteric modulator. Thr²⁶ phosphorylation leads to charge neutralization of Arg²⁴, a residue crucial for MCa agonist activity. The functional effect of Thr²⁶ phosphorylation is partially mimicked by aspartyl mutation. This represents the first case, to our knowledge, of both ex situ posttranslational modification and pharmacological reprogramming of a small natural cysteine-rich peptide by target cells. So far, phosphorylated MCa is the first specific negative allosteric modulator of RyR1, to our knowledge, and represents a lead compound for further development of phosphatase-resistant analogs.

maurocalcin | phosphorylation | pharmacology | toxin | ryanodine receptor

Animal venoms represent biolibraries that are natural sources for the discovery of a growing number of peptides with important pharmacological properties. These peptides have been instrumental in discriminating different subtypes of ion channels and membrane receptors (1–3). Several of them are now approved by the US Food and Administration for the treatment of various human pathological conditions (4). Maurocalcin (MCa) is a 33-amino acid peptide that belongs to the family of the calxin toxins characterized by their folding forming an inhibitor cystine knot motif (5, 6). After its initial purification from the venom of the scorpion *Scorpio maurus palmatus*, MCa was obtained as a synthetic peptide that exhibits structural and pharmacological properties identical to those of the natural peptide (7). Extensive characterization of MCa identified it as one of the most potent effectors of ryanodine receptor type 1 (RyR1) (8, 9). RyR1 is one of the three isoforms that make up the RyR intracellular calcium channels family. It was first identified in skeletal muscles (10) but is also broadly expressed in many other tissues such as pre- and postsynaptic sites within neurons of the brain (11). RyR calcium channels regulate Ca²⁺ release from intracellular stores, and therefore represent crucial players of a number of physiological and toxicological processes, from muscle contraction to gene expression (12). As a consequence, silencing of the gene encoding RyR1 is lethal at birth (13). Despite extensive studies of the RyR biophysical properties, only a few molecules specifically acting on these calcium channels have been identified. The only specific inhibitors of RyR1 known so far are ryanodine at high concentration (14), although this compound also exhibits agonist properties at low doses (15, 16), and dantrolene. Ruthenium

red lacks selectivity and cell permeability. On the agonist side, MCa is a very informative pharmacologic tool to investigate RyR properties because of its nanomolar potency and novel ability to stabilize long-lived subconductances of the channel. Accordingly, MCa increases specific binding of [³H]-ryanodine to RyR1 with an apparent affinity in the range of 10 to 50 nM (9). This effect results from the ability of MCa to convert RyR1 low-affinity ryanodine binding sites into high-affinity sites, increase RyR1 sensitivity to activating low Ca²⁺ concentrations (μM), and decrease RyR1 sensitivity to inhibiting high Ca²⁺ concentrations (mM), with the two latest effects probably requiring an allosteric mechanism. MCa binding onto RyR1 also induces Ca²⁺ release from sarcoplasmic reticulum vesicles (8). These effects correlate with the induction by MCa of long-lasting subconductance open transitions of purified RyR1 channels reconstituted in artificial lipid bilayers (7, 17, 18). This positive allosteric activity of MCa is the consequence of its interaction with a cytoplasmic RyR1 domain that directly controls the gating of this calcium channel (19). Production of MCa analogs after alanine scanning helped identifying critical residues involved in the positive allosteric activity of the peptide (9, 20). The pharmacophore of MCa was restricted to a few basic amino acid residues, among which Arg²⁴

Significance

Animal toxin peptides typically exhibit high affinity and selectivity for specific subclasses of cell receptors that account for their activity. Posttranslational modifications of toxin sequences may occur in the venom gland machinery, but there is no example so far of toxins being subjected to such modifications ex situ after delivery to target cells. Here, we provide evidence that the cell permeant maurocalcin (MCa), found in scorpion venom, undergoes PKA-mediated phosphorylation in cellulo, and that posttranslational modification leads to its complete pharmacological reprogramming activity toward ryanodine receptor type 1 (RyR1), a key player in Ca²⁺ homeostasis in excitable cells. Phosphorylation converts MCa from a potent stabilizer of RyR1 channel substates to a negative allosteric modulator that mitigates RyR1 channel Ca²⁺ leak.

Author contributions: M.R., I.N.P., and M.D.W. designed research; M.R., W.F., Y.D., S.A.K., V.V., S.C., H.D., and I.N.P. performed research; M.R., W.F., L.D., F.C.C., F.L., H.D., I.N.P., and M.D.W. analyzed data; and M.D.W. wrote the paper.

The authors declare no conflict of interest.

This article is a PNAS Direct Submission.

¹M.R. and W.F. contributed equally to this work.

²To whom correspondence may be addressed. Email: michel.dewaard@univ-nantes.fr or michel.ronjat@ujf-grenoble.fr.

This article contains supporting information online at www.pnas.org/lookup/suppl/doi:10.1073/pnas.1517342113/-DCSupplemental.

was the most important for activity (9). Despite these extensive studies, none of the mutations converted MCa into RyR1 antagonist peptide, but mostly lowered affinity or inhibited agonist effect.

It is highly unusual that a venom peptide targets an intracellular receptor. Several reports indicate that MCa binds cell surface glycosaminoglycans (21) and membrane lipids (20), and that it rapidly translocates into cells using mechanisms akin to cell-penetrating peptides (CPPs) (22). As a matter of fact, MCa and CPPs share interesting structural features, such as the presence of a strong dipole moment characterized by a heavily basic face opposing a far less charged one (23–25), with the latter being also quite hydrophobic. Similar to a CPP, MCa proved to be efficient in the transport of several types of cargoes ranging from drugs to peptides, proteins, and nanoparticles (22, 26–32). MCa is

the first natural CPP, to our knowledge, emerging from venom sources and whose cytoplasm delivery and activity could be straightforwardly examined through the activation of RyR channels (33). It is therefore conceivable that MCa may undergo posttranslational modifications by target cell enzymes on delivery into the cytoplasm.

In this report, we show that MCa is a substrate of PKA in vitro, leading to the phosphorylation of Thr²⁶. We also demonstrate that MCa phosphorylation happens in cellulo after translocation. Phosphorylation of MCa leads to a fine peptide structural modification responsible for its complete pharmacological reprogramming, thereby converting MCa into a RyR1 antagonist. We thus establish for the first time, to our knowledge, that the pharmacological properties of a small cell-penetrating toxin peptide can be dramatically modified by posttranslational modification, opening

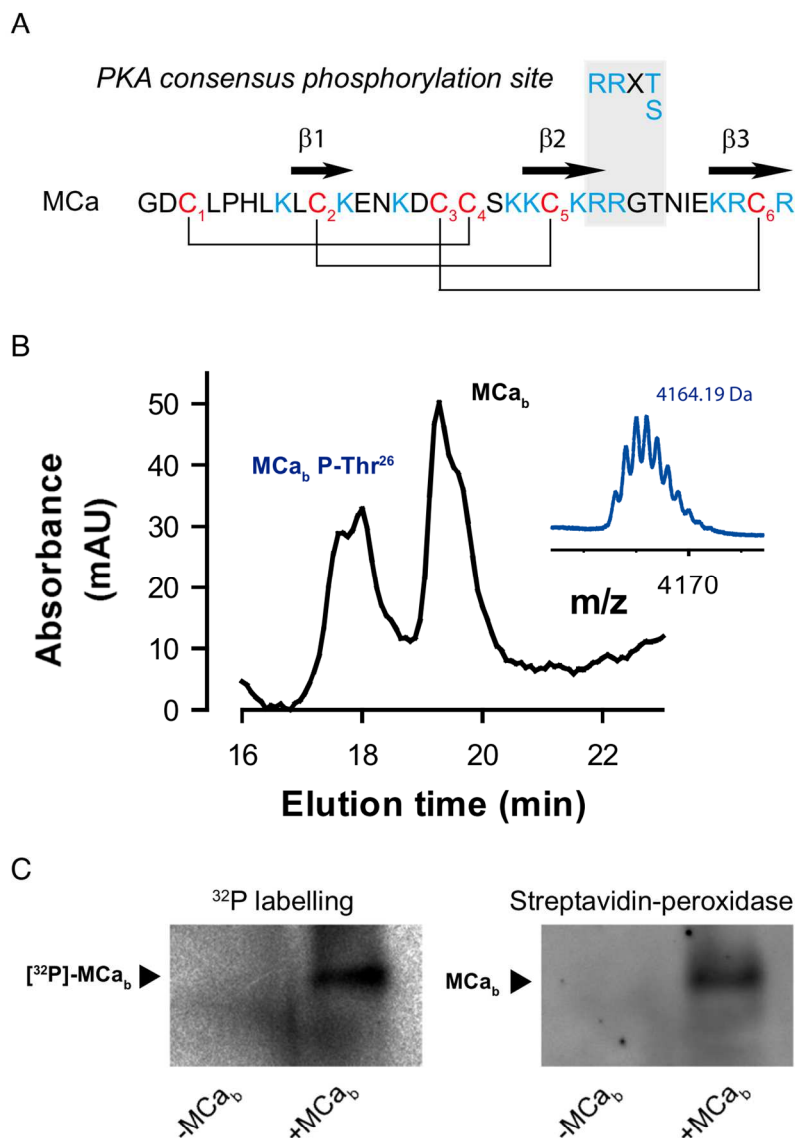


Fig. 1. MCa is phosphorylated by PKA. (A) Identification of a consensus phosphorylation site in MCa primary structure. (B) In vitro phosphorylation of MCa_b by the catalytic subunit of PKA. Shift in the HPLC profile of MCa_b induced by phosphorylation by PKA. (Inset) Mass spectrometry profile illustrating the appearance of the phosphorylated MCa_b variant. Representative of $n = 3$. (C) In cellulo phosphorylation of MCa_b. HEK293 cells were incubated with [³²P]-orthophosphoric acid in the presence or absence of MCa_b. (Left) Autoradiogram showing the appearance of [³²P]-MCA_b. (Right) Labeling of MCA_b with streptavidin-peroxidase. Representative of $n = 2$.

innovative approaches to develop negative allosteric modulators of the RyR1 channel, with M_{Ca} P-Thr²⁶ as a promising lead.

Results

M_{Ca} Is Phosphorylated by Protein Kinase A. Analysis of M_{Ca} sequence reveals a consensus R-R-X-T site of phosphorylation by PKA at position R²³R²⁴G²⁵T²⁶, indicating that Thr²⁶ may get phosphorylated (Fig. 1A). This phosphorylation site is conserved throughout the members of the calcein toxin family that include imperatoxin A (34), hemicalcein (35), opicalcein 1 (6), and hadrucalcin (36), indicating that phosphorylation may be a common feature of these toxins acting as RyR1 agonists. Opicalcein 2 is the only toxin of this family that lacks this consensus sequence (6). According to the 3D structure of M_{Ca} (23) and earlier alanine scan studies (9, 18, 20), the domain encompassing R²³R²⁴G²⁵T²⁶ lays in the pharmacophore region of the peptide, making this site both accessible to PKA phosphorylation (23) and of potential functional importance (SI Appendix, Fig. S1A). We first investigated in vitro M_{Ca} phosphorylation by the catalytic subunit of PKA. Phosphorylation was assessed by analytical HPLC and mass spectrometry (MS) (SI Appendix, Fig. S1B). As shown, phosphorylation induces a leftward shift in the HPLC profile of M_{Ca}, (N-terminal biotinylated version of M_{Ca}) indicative of reduced peptide hydrophobicity. MS spectra recording by MALDI-TOF of the resulting product shows the appearance of an experimental molecular mass of (M+H)⁺ 4,164.19 Da (Fig. 1B, inset) corresponding to the expected theoretical molecular mass of phosphorylated M_{Ca}, (M_{Ca} P-Thr²⁶ at 4,164.20 Da), in addition to the mass of the unphosphorylated one [(M+H)⁺ at 4,084.70 Da]. To confirm that phosphorylation takes place at Thr²⁶ residue, the mutated M_{Ca}, Thr²⁶Glu analog was used as negative control in the phosphorylation experiment. Both HPLC and MS analyses failed to detect the appearance of phosphorylated M_{Ca}, Thr²⁶Glu (SI Appendix, Fig. S1B). These data indicate that Ser¹⁸, the only other residue that could experimentally undergo phosphorylation in M_{Ca} sequence, is not targeted by PKA. Examination of MALDI-TOF spectra of crude *Maurus palmatus* venom, from which M_{Ca} was originally discovered, failed to uncover a mass corresponding to phosphorylated M_{Ca}. Thus, we investigated whether M_{Ca} could be phosphorylated after cell penetration into the cytoplasm of target cells. After 3 h of incubation of HEK293 cells with M_{Ca}, in the presence of [³²P]-orthophosphoric acid, cytoplasmic M_{Ca}, was isolated and phosphorylation witnessed by autoradiography. As shown, a ³²P-labeled band appeared in cells incubated with M_{Ca}, but not in the absence of M_{Ca} (Fig. 1C). The identification of this band was confirmed by streptavidin-peroxidase labeling. These data therefore constitute evidence that M_{Ca} phosphorylation can occur ex situ and in cellulo after cell penetration into recipient cells.

Interaction of M_{Ca} with RyR1 Is Preserved After Phosphorylation. To produce a fully phosphorylated M_{Ca}, the chemical synthesis of M_{Ca}, P-Thr²⁶ was performed [SI Appendix, Fig. S2 (37)]. Binding of purified RyR1 on variable concentrations of M_{Ca}, or P-M_{Ca}, Thr²⁶ was measured using streptavidin-covered beads. Bound RyR1 was then measured by immune staining, using antibody directed against RyR1 (38). As shown, the amount of bound RyR1 increases with the concentration of M_{Ca}, or P-M_{Ca}, Thr²⁶, reaching plateau at 100 nM for M_{Ca}, and 300 nM for P-M_{Ca}, Thr²⁶ (Fig. 2A). Apparent affinities of RyR1 are 58.2 nM for M_{Ca}, and 149.6 nM for P-M_{Ca}, Thr²⁶ (Fig. 2B). Binding of RyR1 on M_{Ca}, P-Thr²⁶ is strongly inhibited by an excess of nonbiotinylated M_{Ca} (Fig. 2C), indicating that M_{Ca} precludes phosphorylated M_{Ca} binding on RyR1.

M_{Ca} Pharmacological Reprogramming by Phosphorylation. M_{Ca} is a strong positive allosteric modulator of RyR1, and channel openings have been associated with a pronounced enhancement of [³H]-ryanodine binding (7–9, 18, 20, 39). In sharp contrast to

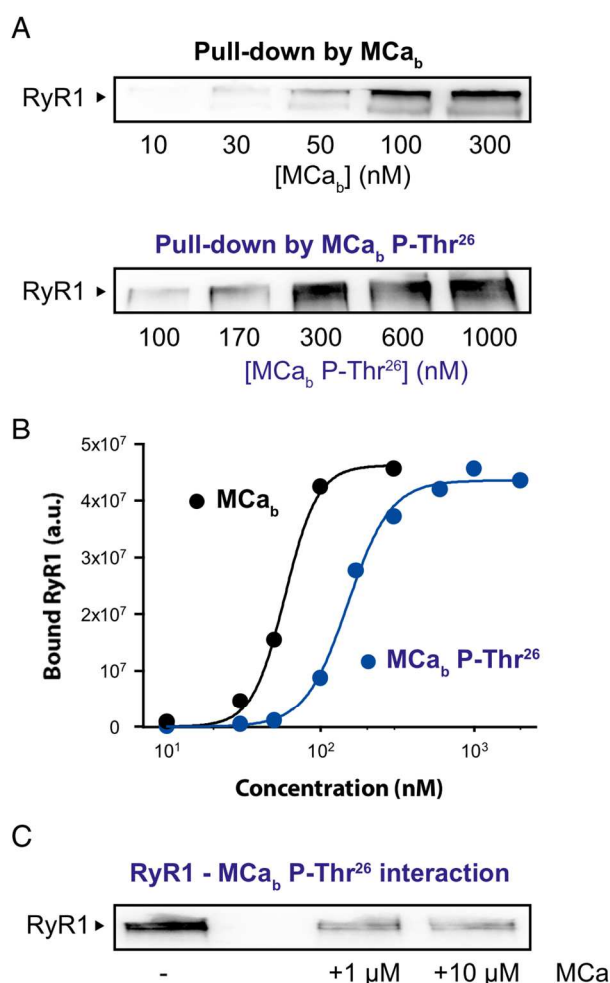


Fig. 2. Direct interaction of M_{Ca}, P-Thr²⁶ with purified RyR1. (A) Western blot analyses of RyR1 on interaction with variable concentrations of M_{Ca}, or M_{Ca}, P-Thr²⁶ immobilized on streptavidin-covered beads. (B) Concentration dependence of RyR1 pull-down by M_{Ca}, or M_{Ca}, P-Thr²⁶. Data were fitted by Hill-type sigmoid functions of the type $y = (a \cdot x^b) / (c^b + x^b)$, where $a = 4.6 \times 10^7 \pm 0.2 \times 10^7$ a.u. (M_{Ca}) and $4.4 \times 10^7 \pm 0.1 \times 10^7$ a.u. (M_{Ca}, P-Thr²⁶), $b = 4.0 \pm 0.6$ (M_{Ca}) and 3.1 ± 0.3 (M_{Ca}, P-Thr²⁶), and $c = 58.2 \pm 2.6$ nM (M_{Ca}) and 149.7 ± 5.8 nM (M_{Ca}, P-Thr²⁶). a.u. = arbitrary unit. (C) Western blot of RyR1 showing extent of pull-down by 170 nM M_{Ca}, P-Thr²⁶/streptavidin-coated beads in the absence and presence of an excess nonbiotinylated 1 μM M_{Ca}. Representative of $n = 2$.

the reported effects of M_{Ca}, 5–10 μM M_{Ca}, P-Thr²⁶ was found to inhibit the binding of [³H]-ryanodine onto RyR1, provided we used 1 nM [³H]-ryanodine and assessed binding for 30 min (Fig. 3A). Use of higher concentrations of [³H]-ryanodine and longer incubation times led to the loss of this inhibition ($n = 4$). These data indicate that M_{Ca} phosphorylation onto Thr²⁶ precludes the agonist effect and favors inhibition.

Next, the effect of M_{Ca}, P-Thr²⁶ was investigated on Ca²⁺ release from Ca²⁺-loaded sarcoplasmic reticulum (SR) vesicles. As expected from earlier reports (8, 9), 50 nM M_{Ca}, induces a strong Ca²⁺ release from Ca²⁺-loaded SR vesicles despite the maintained activity of the SR ATPase Ca²⁺ pump (Fig. 3B). In contrast, a 20-fold higher concentration of M_{Ca}, P-Thr²⁶ (1 μM) is unable to promote net Ca²⁺ release from SR vesicles, whereas a subsequent addition of 100 nM M_{Ca}, still induces a strong

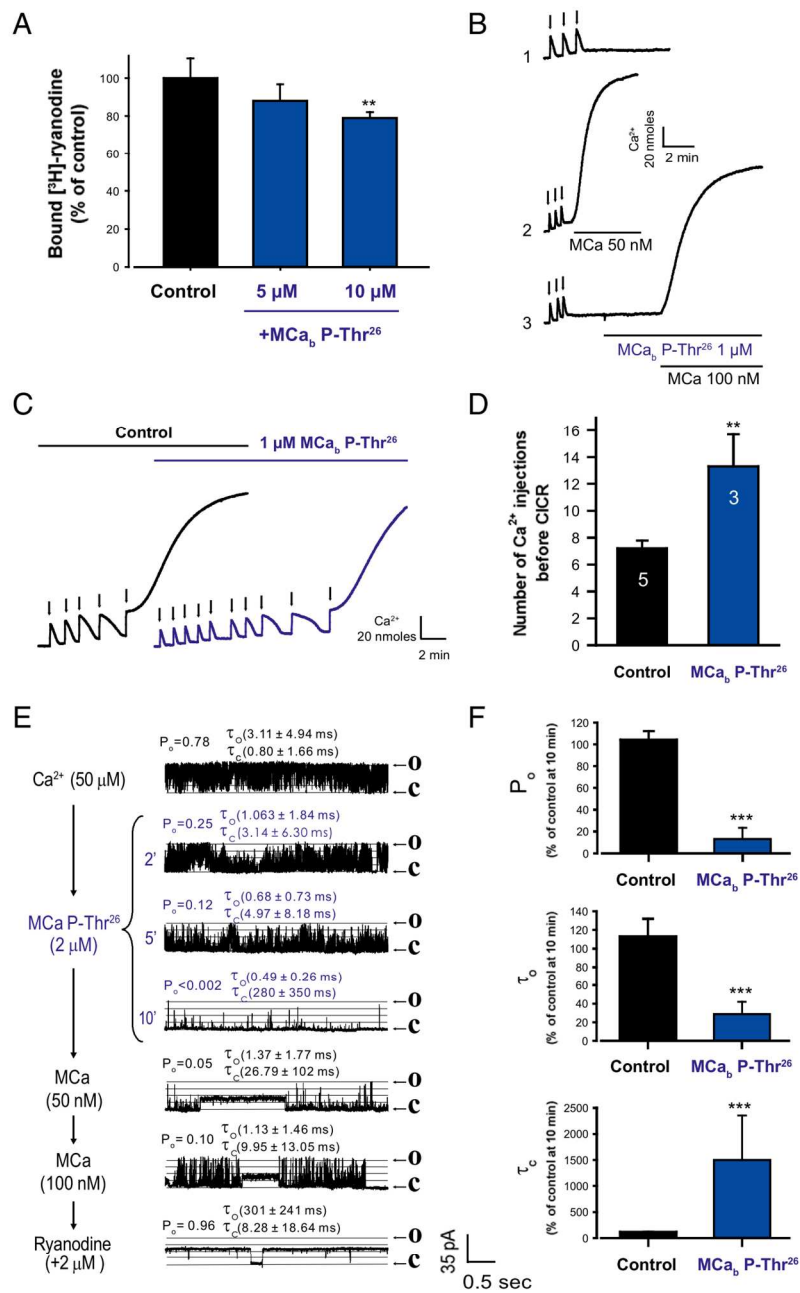


Fig. 3. Phosphorylation confers RyR1 antagonistic properties to MCa_b. (A) MCa_b P-Thr²⁶ produces a mild reduction in [³H]-ryanodine binding onto SR vesicles. SR, 100 μg/mL, pCa 5, SR pretreated at 25 °C with MCa_b P-Thr²⁶ before a 30-min incubation at 37 °C with 1 nM [³H]-ryanodine (mean ± SD, *n* = 5). (B) MCa_b P-Thr²⁶ does not induce Ca²⁺ release from SR vesicles. (1) Control experiments showing SR vesicle Ca²⁺ loading by three successive additions of 20 nmol Ca²⁺ (arrows). (2) Ca²⁺ release induced by 50 nM MCa after SR loading with three identical additions of Ca²⁺. (3) Addition of MCa_b P-Thr²⁶ (1 μM) to Ca²⁺-loaded SR vesicles does not induce Ca²⁺ release. Subsequent addition of 100 nM MCa efficiently releases Ca²⁺. (C) Inhibition of Ca²⁺-induced Ca²⁺ release by 1 μM MCa_b P-Thr²⁶. The presence of MCa_b P-Thr²⁶ doubles the number of Ca²⁺ additions required for CICR. (D) Number of Ca²⁺ injections required to trigger CICR in the presence of 1 μM MCa_b P-Thr²⁶ (*n* = 8 experiments). (E) MCa_b P-Thr²⁶ (2 μM) causes a time-dependent inhibition of RyR1 channel activity (traces 2–4) that can be reactivated by MCa. Sequential additions of ligands into the *cis* solution were denoted with downward arrows on the left side of each representative current trace. Open probability (P_o), mean open- and closed-dwelling time constants obtained for each recording condition were denoted above each representative trace. "O" and "C" in the figure indicate the full and zero conductance states when the channel fully opened and closed, respectively. Total *n* = 7 independent bilayer measurements under similar conditions produced consistent responses. (F) RyR1 gating parameters (P_o, τ_o, and τ_c) in the absence and presence of MCa_b P-Thr²⁶ (at 10 min after application) as percentage of control condition. Data are presented by mean ± SD; control group (vehicle), *n* = 3; group with MCa_b P-Thr²⁶, *n* = 4. ***P* < 0.005; ****P* < 0.001.

release of Ca²⁺, indicating the functionality of the SR vesicles (Fig. 3B). MCa_b P-Thr²⁶ does not act as a weak agonist by

producing a partial depletion from SR vesicles. Indeed, the slope of Ca²⁺ release from SR vesicles after loading was negative, on

average, in the presence of 1 μM M Ca_b P-Thr²⁶ (*SI Appendix, Fig. S3A*), and the total Ca^{2+} content in SR vesicles remained identical to the nontreated SR vesicles, as assessed by Ca^{2+} release, triggered by the application of 1 μM of the A23187 Ca^{2+} ionophore (*SI Appendix, Fig. S3 B and C*). These results indicate that M Ca should have the ability to displace M Ca_b P-Thr²⁶ from its binding site on RyR1. Similarly, the agonists caffeine (2 mM) and ryanodine (20 μM) were also found to keep their Ca^{2+} release-activating effects in the presence of 2 μM M Ca_b P-Thr²⁶ (*SI Appendix, Fig. S4 A and B*). A more physiological process of RyR1 activation is the process of calcium-induced calcium release (CICR), whereby cytoplasmic Ca^{2+} triggers RyR1 opening and Ca^{2+} release from SR (40). Sensitivity of SR vesicles to CICR can be measured by sequential addition of Ca^{2+} to the SR vesicle medium that will lead to CICR (41). Under control conditions, SR vesicle loading by seven additions of Ca^{2+} (280 nmol) is required to trigger CICR, whereas induction of CICR requires up to 13 additions of Ca^{2+} (520 nmol) in the presence of 1 μM M Ca_b P-Thr²⁶ (Fig. 3 C and D). This result indicates that M Ca_b P-Thr²⁶ attenuates the response of RyR1 to cytoplasmic activating Ca^{2+} .

To more directly explore the inhibitory effect of M Ca_b P-Thr²⁶, we measured single-channel gating activity of RyR1 reconstituted in bilayer lipid membranes. In the presence of optimal cytosolic (*cis*) Ca^{2+} concentration (50 μM), typical RyR1 channels exhibit a high open probability (P_o) of 0.78 with characteristic, very short-lived transitions to the full open state (Fig. 3E). The addition of 2 μM M Ca_b P-Thr²⁶ into the *cis* chamber produced a very strong channel gating inhibition in a time-dependent manner (Fig. 3E). This time-dependent reduction in P_o was invariably observed ($n = 7$ channels) and suggests that multiple sites on RyR1 may need to be occupied to see full inhibition. Kinetic analysis of RyR1 gating indicates a \sim fourfold decrease in mean open dwell time and a \sim 13-fold increase in mean closed dwell time, resulting in an eightfold decrease in P_o 10 min after addition of M Ca_b P-Thr²⁶ (Fig. 3F). Subsequent addition of 50 nM M Ca into the *cis* chamber resulted in reactivation of RyR1, as witnessed by the appearance of the M Ca -induced characteristic (7–9, 17, 18) long-lasting subconductance states (Fig. 3E). Moreover, M Ca -modified RyR1 channel remains responsive to 2 μM ryanodine, as witnessed by the appearance of a different long-lasting subconductance state (Fig. 3E). In addition to M Ca and ryanodine, RyR1 channels inhibited by 3 μM M Ca_b P-Thr²⁶ could also be reactivated by the addition of 2 mM caffeine to the *cis* chamber. In turn, these caffeine-reactivated channels remained responsive to 50 nM M Ca (*SI Appendix, Fig. S5A*). Altogether, evidence of reactivation of channel activity by the RyR1 agonists M Ca , ryanodine, and caffeine further illustrate the fact that M Ca , as well as ryanodine or caffeine, overcome the effect of M Ca_b P-Thr²⁶ on RyR1, explaining why the inhibition of [³H]-ryanodine binding by M Ca_b P-Thr²⁶ is difficult to observe. This overriding effect of caffeine on P_o suppression by M Ca_b P-Thr²⁶ probably occurs through an allosteric mechanism, considering that caffeine and calcins bind onto distinct sites. Finally, we also determined that application of 2 μM M Ca_b P-Thr²⁶ lowers the channel P_o without promoting the subconductance state of RyR1, indicating again that this analog is not a weak activator (*SI Appendix, Fig. S5B*). Altogether, these results lead to the hypothesis that M Ca_b P-Thr²⁶ decreases RyR1 sensitivity to activating Ca^{2+} concentrations; hence the term negative allosteric modulator for M Ca_b P-Thr²⁶.

Thr²⁶ Phosphorylation Leads to Neutralization of the Guanidinium Group of Arg²⁴. Preserving the 3D structure of M Ca is mandatory for its pharmacological activity (42). Although a pharmacophore has been mapped that is responsible for the agonist activity of M Ca (9, 20, 24), none of the analogs previously produced exhibit inhibitory activity. The consequences of Thr²⁶ phosphorylation on M Ca structure were thus expected to be subtle, and were therefore fully inspected using circular dichroism,

¹H-NMR, molecular modeling, and ¹H-2D-NMR. Nuclear Overhauser effects in the amide region of M Ca and M Ca P-Thr²⁶ are identical in intensity, showing that the backbone conformation was not altered by the phosphorylation. Both circular dichroism spectra of M Ca_b and M Ca_b P-Thr²⁶ were identical, indicating the preservation of the β -strands (Fig. 4A). However, the chemical shifts of several NH protons from backbone and side chains were altered in the region of the pharmacophore (Fig. 4B; *SI Appendix, Fig. S6A*). These chemical shift variations can be explained by alterations in the chemical environment of the atomic nuclei located in the immediate vicinity of the phosphate group now present onto the hydroxyl moiety of Thr²⁶ (43). Protons of amino acid residues 20–23 and 30–33 of M Ca_b P-Thr²⁶, close to the phosphoryl group, are indeed expected to shift orientation relative to the peptide backbone (23). A total of 25 3D projections of M Ca_b P-Thr²⁶ were modeled, using the 25 deposited structures of M Ca (Protein Data Bank ID code 1C6W). Twelve of the modeled 3D structures were found to be in agreement with the ¹H-NMR data acquired on M Ca_b P-Thr²⁶ and predicted a reorientation of the lateral chain of Arg²⁴ and an electrostatic interaction with the lateral chain of the phosphorylated Thr²⁶. Three of 25 modeled structures indicated a possible hydrogen bond interaction of the phosphate group of Thr²⁶ with the amine group of Asn²⁷, but were not compatible with the NMR data. To visualize the structural modifications, the average 3D structure of M Ca_b P-Thr²⁶ (on the basis of the 12 NMR-coherent structures) is superimposed to the corresponding average M Ca structure (*SI Appendix, Fig. S6B*). As illustrated, the predicted structural changes are observed for amino acid residues 22–33. Nevertheless, the main observation is that the phosphate group on Thr²⁶ induces a strong downfield chemical shift variation of the NH ϵ proton of the Arg²⁴ side chain (Fig. 4 B and C). This chemical shift is far more pronounced than the one observed for the NH δ proton of Asn²⁷, indicating that the side chain of Arg²⁴ was more likely to move than the one of Asn²⁷ in response to Thr²⁶ phosphorylation. To confirm the modeling data, the proximity of the guanidinium group of Arg²⁴ with the phosphoryl group of Thr²⁶ was experimentally measured by ¹H-2D-NMR (*SI Appendix, Fig. S7*). We compared the frequency resonance of Arg²⁴ guanidinium NH ϵ proton in M Ca_b P-Thr²⁶ and compared it with M Ca . A clear chemical shift variation of this guanidinium group was observed, indicating the vicinity with the phosphoryl group of Thr²⁶. Such an influence of the phosphoryl group was demonstrated earlier (44). Furthermore, results from these experiments show that the Asn²⁷ side chain is negligibly affected by the modification of Thr²⁶, further ruling out its contribution to the pharmacological reprogramming of M Ca_b P-Thr²⁶. The modeled structure of M Ca_b P-Thr²⁶ illustrating the arginine-phosphate electrostatic interaction is shown in Fig. 4D. This type of interaction has been described to present “covalent-like” stability (45), although geometry and distance should affect the stability of this interaction. The resulting structure is in agreement with the reported critical role of Arg²⁴ in M Ca activity (9). A functional role of Asn²⁷ in the pharmacological activity of M Ca_b P-Thr²⁶, through the formation of a hydrogen bond between the phosphate group of Thr²⁶ and the amine group of Asn²⁷ ($n = 3$ of 25 modeled structures) (*SI Appendix, Fig. S8A*), was further ruled out by chemically synthesizing and testing two new analogs, M Ca_b Asn²⁷Ala and M Ca_b P-Thr²⁶ Asn²⁷Ala. M Ca_b Asn²⁷Ala fully preserves the stimulating activity of M Ca on [³H]-ryanodine binding, indicating that Asn²⁷ is a priori not a residue of the pharmacophore (*SI Appendix, Fig. S8B*). In addition, M Ca_b P-Thr²⁶ Asn²⁷Ala was found to delay, but not inhibit, caffeine-induced Ca^{2+} release from SR vesicles (*SI Appendix, Fig. S8C*). On the basis of these data, we propose that the electrostatic interaction of Thr²⁶ phosphate with Arg²⁴ guanidinium represents the structural modification of M Ca that is involved in its pharmacological reprogramming.

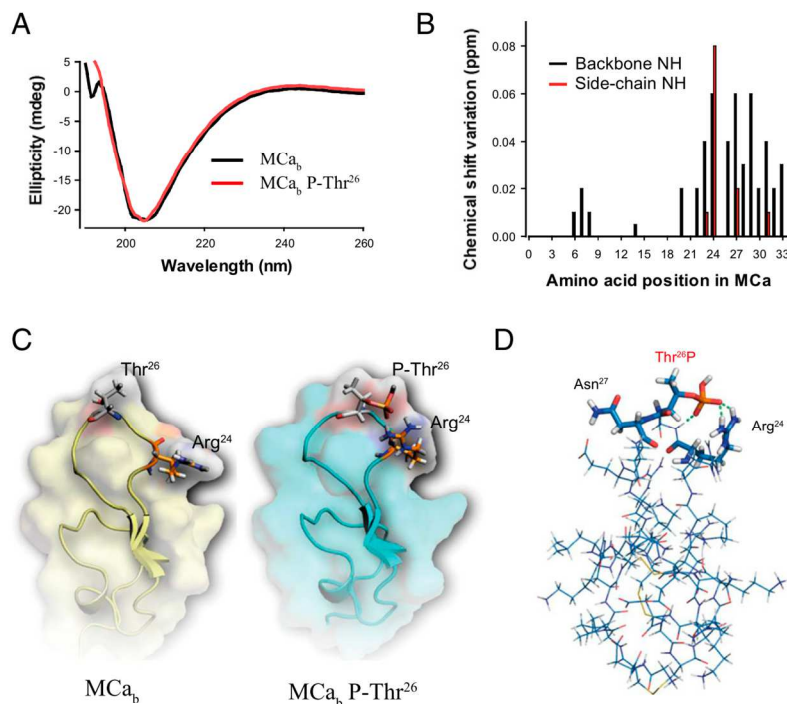


Fig. 4. Structural modifications induced by Thr²⁶ phosphorylation. (A) Circular dichroism data indicating the conservation of secondary structures of MCA_b after phosphorylation. (B) Chemical shift variation (in absolute values) in backbone NH and side-chain NH after Thr²⁶ phosphorylation. Note that major variations are observed within the loop encompassing residues 22–31. The structure of MCA P-Thr²⁶ was modeled starting with MCA as a structural basis (1C6W from the Protein Database Base). (C) 3D structural variations induced by Thr²⁶ phosphorylation. MCA structure is in transparency. (D) Zoom in on the ionic interaction occurring between the side chains of Thr²⁶ and Arg²⁴ residues of MCA P-Thr²⁶.

Thr²⁶ Substitution by the Negatively Charged Aspartyl Best Mimics Phosphorylation.

To test the importance of this intramolecular electrostatic interaction between phosphorylated Thr²⁶ and Arg²⁴ residues, we chemically synthesized and tested on RyR1 channel activity two closely resembling MCA_b analogs: MCA_b Thr²⁶Glu and MCA_b Thr²⁶Asp. Molecular modeling indicates that the negatively charged carboxylic function of glutamyl is unable to establish an electrostatic interaction with the positively charged guanidinium group of Arg²⁴ because of the structural constraints imposed by the rigid backbone of MCA and the superior side-chain length (SI Appendix, Fig. S9A). The opposite was found to be true for the aspartyl substitution (Fig. 5A). This is confirmed by ¹H-2D-NMR experiments that indicate a clear chemical shift variation of the Arg²⁴ guanidinium NHε proton of MCA_b Thr²⁶Asp compared with MCA, which was not observed for MCA_b Thr²⁶Glu (SI Appendix, Fig. S7). These data confirm the importance of peptide backbone geometry for the establishment of salt bridges (46). As shown, 2 μM MCA_b Thr²⁶Asp added into the *cis* chamber produced a time-dependent channel gating inhibition (Fig. 5B). However, this inhibition was less pronounced than the one observed with MCA_b P-Thr²⁶. A kinetic analysis of the MCA_b Thr²⁶Asp-modified RyR1 channel indicates a decrease in mean open dwell time (1.9-fold) and an increase in mean closed dwell time (1.6-fold), resulting in a 2.1-fold decrease in P_o 10 min after addition of MCA_b Thr²⁶Asp (Fig. 5C). As observed with MCA_b P-Thr²⁶, the MCA_b Thr²⁶Asp-modified RyR1 channel activity remains responsive to the sequential addition of 50 nM MCA and of 2 μM ryanodine (Fig. 5B). In contrast, 2 μM MCA_b Thr²⁶Glu increases P_o of RyR1 channels without stabilizing subconductances characteristic of MCA (SI Appendix, Fig. S9B), and recordings lasting several minutes fail to promote subsequent channel inhibition observed with either MCA_b P-Thr²⁶ or MCA_b Thr²⁶Asp. Finally, with regard to Ca²⁺

release from SR, MCA_b Thr²⁶Asp also does not trigger Ca²⁺ release but remains sensitive to 2 mM caffeine or 20 μM ryanodine, akin to MCA_b P-Thr²⁶ (SI Appendix, Fig. S10). Collectively, these data indicate that Thr²⁶ is critical for conferring nanomolar affinity and stabilizing channel subconductance behavior characteristic of MCA. Pharmacological reprogramming of MCA is highly dependent on both the precise electrostatic interaction between MCA_b P-Thr²⁶ or its phosphomimic MCA_b Thr²⁶Asp and Arg²⁴ and the distance of the negative charge on the Thr²⁶ side chain from the ridged MCA backbone (e.g., MCA_b Thr²⁶Asp vs. MCA_b Thr²⁶Glu).

Discussion

Posttranslational modifications such as phosphorylation control the function of a large number of proteins by modifying their ability to interact with their partners and/or by altering their activity (47). Often phosphorylation sites have been found to be located on binding interfaces and to modulate strength of interaction and function (48). Concerning toxins, a number of posttranslational modifications have been reported, all occurring *in situ* at the site of production within venom glands, and include proteolytic processing, disulphide bridge formation, carboxylation of glutamic acid, bromination of tryptophan, epimerization of some amino acids, cyclization of N-terminal glutamine, and O-glycosylation, to name a few (49). It is of interest that peptides from *Conus* venoms are among the most highly posttranslationally modified gene products (49). In this study, we investigated whether the venom peptide MCA could be phosphorylated *ex situ* within target cells and examined the consequences of this phosphorylation on its pharmacological properties. MCA presents an interesting combination of features, rarely encountered for peptide toxins, to cross the plasma membrane and to act on an intracellular ion channel target (i.e., RyR1). We report that MCA is a substrate of PKA *in vitro* and is

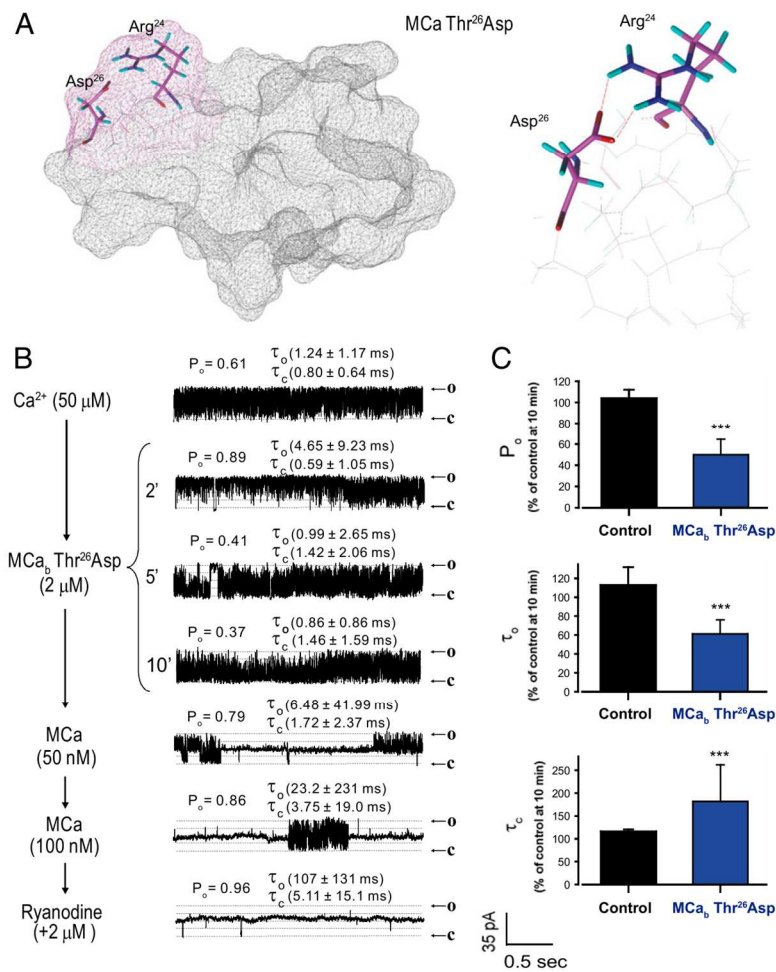


Fig. 5. The MCa_b Thr²⁶ Asp partially mimics the antagonist effect of MCa_b P-Thr²⁶. (A) 3D structure of MCa Thr²⁶ Asp with a zoom in on the ionic interaction occurring between the side chains of Asp²⁶ and Arg²⁴ residues of MCa Thr²⁶ Asp (Right). (B) MCa_b Thr²⁶ Asp (2 μ M) causes a time-dependent inhibition of RyR1 channel activity (traces 2–4) that can be reactivated by MCa. Sequential additions of ligands into the *cis* solution were denoted with downward arrows on the left side of each representative current traces. Open probability, mean open- and closed-dwelling time constants (P_o , τ_o , and τ_c) obtained for each recording condition were denoted above each representative trace. “O” and “C” in the figure indicate the full and zero conductance states when the channel fully opened and closed, respectively. Total $n = 11$ independent bilayer measurements under similar conditions produced consistent responses. (C) RyR1 gating parameters (P_o , τ_o , and τ_c) in the absence and presence of MCa_b Thr²⁶ Asp (at 10 min after application) as a percentage of control condition (control, $n = 3$; MCa_b Thr²⁶ Asp, $n = 3$).

also phosphorylated in cellulo after cell penetration. To our knowledge, this is the first reported case of an exogenous bioactive peptide that gets phosphorylated within host cells. Probably the most significant discovery is that phosphorylation of MCa provokes its complete pharmacological reprogramming, converting MCa toward an inhibitor of RyR1 activity. Earlier reports about cell phosphorylation of exogenous material concerned clostridial neurotoxins (botulinum neurotoxins A, B, and E and tetanus neurotoxin) (50), but these are very large proteins compared with MCa, and phosphorylation does not negate the activity of these toxins. We provide a clue on how phosphorylation may induce such a drastic change in pharmacological properties of MCa. It is shown here that the negative charge or charges introduced by the phosphate group contribute to both loss of positive allosteric modulation and neutralization of the guanidinium group of Arg²⁴, leading to the conversion toward negative allosteric modulation. The channel bilayer and Ca^{2+} release experiments indicate that MCa_b P-Thr²⁶ and MCa_b Thr²⁶ Asp reduce channel activity and

delay CICR without producing stable subconductances, which is a hallmark of nonphosphorylated MCa, and without fully blocking the channel even at high concentrations. Importantly, the observed MCa_b P-Thr²⁶ and MCa_b Thr²⁶ Asp effect is the result of forcing the channel to adopt a more “normal” activity, similar to that observed in low cytoplasmic Ca^{2+} , with classical characteristic rapid gating full transitions of RyR1 openings and closings. We thus propose that MCa_b P-Thr²⁶ and MCa_b Thr²⁶ Asp modify the agonist effect of Ca^{2+} on RyR1; hence the term negative allosteric modulators for these peptides. MCa itself remains a positive allosteric modulator for favoring the activating role of cytoplasmic Ca^{2+} (9). With regard to [³H]-ryanodine binding, we observed a mild inhibition by MCa_b P-Thr²⁶ only when performing binding in the presence of low concentrations of [³H]-ryanodine and for a short incubation time. Higher ryanodine concentrations (50 nM) and longer incubation times completely prevented the MCa_b P-Thr²⁶ effect. This might be explained by both possible dephosphorylation of MCa_b P-Thr²⁶ during the time course of the

experiment with dephosphorylated MCa overriding the effect of M_{Ca_b} P-Thr²⁶, and/or ryanodine itself precluding M_{Ca_b} P-Thr²⁶ effect, as supported by results obtained in bilayer experiments showing the persistence of ryanodine effect on the M_{Ca_b} P-Thr²⁶-modified RyR1.

The fact that MCa prevents M_{Ca_b} P-Thr²⁶ binding on RyR1 suggests their binding occurs on the same site between the clamp and handle domain of RyR1 (51, 52). Although the presence of distinct sites allosterically influencing each other remains possible, it seems, however, unlikely because of the structural similarities between the two ligands being very high and the notion that toxins interact with their receptors through multiple points. However, two binding sites have previously been identified for MCa (19) on RyR1, and therefore the ability of M_{Ca_b} P-Thr²⁶ to bind to these sites, as well as their respective roles in the effect of M_{Ca_b} P-Thr²⁶ on RyR1 modulation, remains to be established. In addition, the existence of an allosteric behavior between the MCa and/or M_{Ca_b} P-Thr²⁶ binding sites within the RyR1 tetramer is also a strong possibility. This could possibly explain the slow onset of action of M_{Ca_b} P-Thr²⁶, as well as the rapid overriding effect of MCa on M_{Ca_b} P-Thr²⁶. Alternatively, it remains possible that phosphorylation of MCa alters the K_{off} of binding on RyR1 sites, explaining why MCa so easily overrides M_{Ca_b} P-Thr²⁶. Interestingly, the reported binding site for imperatoxin A, a close homolog of MCa, is located near the proposed CaM binding site. Knowing that CaM can also act as activator or an inhibitor, depending on Ca²⁺ concentration, there is an interesting parallel to be made on the opposing effects of M_{Ca_b} P-Thr²⁶ and MCa on RyR1 behavior. These evidences highlight the crucial role of this RyR1 region in the control of channel gating properties. M_{Ca_b} P-Thr²⁶ will therefore represent an interesting tool to study the structural constraints that take place within the RyR1 MCa/M_{Ca_b} P-Thr²⁶ binding site and that control RyR1 channel gating. A particular important question will be to understand how Thr²⁶ of MCa interacts with RyR1 and what structural change is induced in RyR1 by the addition of a phosphate group or, more generally, a well-positioned negative charge on the lateral chain of the substituted residue at position 26 of MCa. Obviously, the recent resolution of the 3D structure of RyR1 (53–55) presents exciting perspectives on the understanding of the positive and negative allosteric modulation of this physiologically important ion channel. The data also need to be considered in the frame of an intriguing sequence homology between MCa and a cytoplasmic domain of the skeletal muscle voltage-gated calcium channel, the dihydropyridine receptor (DHPR) (9). Several studies have led to the proposal that MCa could mimic the action of this DHPR domain on RyR1 (56). Interestingly, this DHPR domain carries a Ser residue, Ser⁶⁸⁷, corresponding to Thr²⁶ of MCa, that has been previously shown to be phosphorylated in vitro by PKA (57, 58). In their study, the authors showed that a peptide corresponding to this sequence of DHPR completely loses its ability to activate RyR1 under phosphorylation of the Ser⁶⁸⁷ residue. Although DHPR II-III loop residues 681–690 do not seem essential for engaging physiological EC coupling in intact skeletal myotubes (59), our results suggest that MCa, and possibly the other calxin toxins with the inhibitor cystine knot motif, have evolved to mimic some aspect or aspects of interactions between the DHPR and RyR1, whose structures have been optimized for high affinity and efficacy toward functional modification of RyR1.

Both MCa P-Thr²⁶ and MCa Thr²⁶Asp can now be considered interesting lead inhibitors of RyR1 channel activity. Both of these compounds freely cross the plasma membrane and can therefore be readily used to silence RyR1 channel activity in vitro. In vivo use can also be programmed because of the extreme protease

resistance of MCa and important half-life in mice (24). Although M_{Ca_b} Thr²⁶Asp recapitulates some of the properties of MCa P-Thr²⁶, it does so only partially. Still better inhibitors may be designed that will not possess a phosphate group on the lateral chain. This is desirable if one wants to avoid dephosphorylation to occur in cellulo. Reasons why the aspartyl substitution only partially mimics the phosphate group on Thr²⁶ may include an imperfect charge neutralization of Arg²⁴, the absence of a second negative charge that the phosphate group may carry depending on pH, and a less perfect interaction with RyR1 site. Obviously, several more analogs need to be designed to sort these issues out, but the basic observations are there that will help us design better inhibitors that are also phosphatase-resistant. The present compounds will nevertheless be useful to silence RyR1, and probably other RyR isoforms, in a number of pathological conditions in which abnormal RyR1 channel activity is involved. These include skeletal and cardiac myopathies (60), neurodegenerative disorders (61, 62), and environmentally triggered disorders (12). Our results suggest that MCa P-Thr²⁶ is capable of normalizing two important dysfunctional properties of RyR1: by decreasing the sensitivity of RyR1 to cytoplasmic Ca²⁺, allowing a decrease of spontaneous CICR (Fig. 3 A–D), and by normalizing RyR1 channel activity in the presence of high (50 μM) cytoplasmic Ca²⁺ (Fig. 3 E and F), restoring P_o to near those measured at [Ca²⁺]_{rest} (~120 nM). Coordinated reduction of abnormal RyR1 opening mediated Ca²⁺ leak and normalization of RyR1 channel hyperactivity may have translational significance toward the development of new therapeutic strategies in treating the growing number of complex disorders that converge on RyR dysregulation.

In conclusion, these results represent the first demonstration, to our knowledge, that a small bioactive peptide toxin may undergo phosphorylation in cellulo at its site of delivery but also that such a modification has the ability to fully reprogram its pharmacological properties. Taking into account the growing list of active peptides isolated from venoms and the large spectra of posttranslational modifications, a systematic investigation of the effect of such toxin modification could lead to the characterization of new functionalities of these peptides. It is noteworthy that phosphorylated versions of bioactive peptides have also been detected in snake venoms (63), indicating that our observation may represent the first example, to our knowledge, of a larger list of peptides whose pharmacological activity is modulated by posttranslational modifications. Obviously, homologous peptides from the calxin family, which also bear the consensus phosphorylation site, are the next candidates for investigation of the effect of phosphorylation on pharmacology.

Materials and Methods

Detailed methods can be found in *SI Appendix, Materials and Methods*. Peptide syntheses were performed as previously described (7). The in cellulo phosphorylation was performed in HEK293 cells, using the PKA activator 8-bromoadenosine 3',5'-cyclic monophosphate. NMR recordings were performed at a peptide concentration of 1 mM, using a Bruker DRX500 Avance III equipped with a QX1 probe. Junctional SR was from skeletal muscle of New Zealand White rabbits. [¹H]-ryanodine binding and Ca²⁺ release experiments were performed at 0.1 mg/mL SR vesicles concentration. The interaction of M_{Ca_b} and M_{Ca_b} P-Thr²⁶ with RyR1 was performed with purified RyR1. All planar bilayer experiments were performed using junctional SR membrane vesicles on a bilayer clamp BC 525C apparatus.

ACKNOWLEDGMENTS. We acknowledge the assistance of Mr. Jing Jie with some of the Ca²⁺ flux measurements made during revision of the manuscript. We thank Gamma Imaging Applications, Prométhée, and microscopie optique from Université Joseph Fourier for their collaboration. This work was supported by the French Agence Nationale de la Recherche (LabEx "Ion Channel Science and Therapeutics," Program ANR-11-LABX-0015), the Association Française contre les Myopathies, and the National Institutes of Health (Grants 1P01 AR52354, 2P01 ES011269, P42 ES004699, and US EPA STAR R829388 and R833292 to I.N.P. and W.F.).

- Adams ME, Myers RA, Imperial JS, Olivera BM (1993) Toxotyping rat brain calcium channels with omega-toxins from spider and cone snail venoms. *Biochemistry* 32(47):12566–12570.
- Adams ME, Olivera BM (1994) Neurotoxins: Overview of an emerging research technology. *Trends Neurosci* 17(4):151–155.
- Calvete JJ (2013) Snake venomomics: From the inventory of toxins to biology. *Toxicon* 75:44–62.
- King GF (2011) Venoms as a platform for human drugs: Translating toxins into therapeutics. *Expert Opin Biol Ther* 11(11):1469–1484.
- Smith JJ, et al. (2011) Unique scorpion toxin with a putative ancestral fold provides insight into evolution of the inhibitor cystine knot motif. *Proc Natl Acad Sci USA* 108(26):10478–10483.
- Zhu S, Darbon H, Dyason K, Verdonck F, Tytgat J (2003) Evolutionary origin of inhibitor cystine knot peptides. *FASEB J* 17(12):1765–1767.
- Fajloun Z, et al. (2000) Chemical synthesis and characterization of maurocalcine, a scorpion toxin that activates Ca²⁺ release channel/ryanodine receptors. *FEBS Lett* 469(2–3):179–185.
- Chen L, et al. (2003) Maurocalcine and peptide A stabilize distinct subconductance states of ryanodine receptor type 1, revealing a proportional gating mechanism. *J Biol Chem* 278(18):16095–16106.
- Estève E, et al. (2003) Critical amino acid residues determine the binding affinity and the Ca²⁺ release efficacy of maurocalcine in skeletal muscle cells. *J Biol Chem* 278(39):37822–37831.
- Imagawa T, Smith JS, Coronado R, Campbell KP (1987) Purified ryanodine receptor from skeletal muscle sarcoplasmic reticulum is the Ca²⁺-permeable pore of the calcium release channel. *J Biol Chem* 262(34):16636–16643.
- Zimanyi I, Pessah IN (1991) Pharmacological characterization of the specific binding of [³H]ryanodine to rat brain microsomal membranes. *Brain Res* 561(2):181–191.
- Pessah IN, Cherednichenko G, Lein PJ (2010) Minding the calcium store: Ryanodine receptor activation as a convergent mechanism of PCB toxicity. *Pharmacol Ther* 125(2):260–285.
- Takeshima H, et al. (1994) Excitation-contraction uncoupling and muscular degeneration in mice lacking functional skeletal muscle ryanodine-receptor gene. *Nature* 369(6481):556–559.
- Zimanyi I, Buck E, Abramson JJ, Mack MM, Pessah IN (1992) Ryanodine induces persistent inactivation of the Ca²⁺ release channel from skeletal muscle sarcoplasmic reticulum. *Mol Pharmacol* 42(6):1049–1057.
- Buck E, Zimanyi I, Abramson JJ, Pessah IN (1992) Ryanodine stabilizes multiple conformational states of the skeletal muscle calcium release channel. *J Biol Chem* 267(33):23560–23567.
- Fleischer S, Ogunbunmi EM, Dixon MC, Fleer EA (1985) Localization of Ca²⁺ release channels with ryanodine in junctional terminal cisternae of sarcoplasmic reticulum of fast skeletal muscle. *Proc Natl Acad Sci USA* 82(21):7256–7259.
- Szappanos H, et al. (2005) Differential effects of maurocalcine on Ca²⁺ release events and depolarization-induced Ca²⁺ release in rat skeletal muscle. *J Physiol* 565(Pt 3):843–853.
- Lukács B, et al. (2008) Charged surface area of maurocalcine determines its interaction with the skeletal ryanodine receptor. *Biophys J* 95(7):3497–3509.
- Altafaj X, et al. (2005) Maurocalcine and domain A of the II-III loop of the dihydropyridine receptor Cav 1.1 subunit share common binding sites on the skeletal ryanodine receptor. *J Biol Chem* 280(6):4013–4016.
- Mabrouk K, et al. (2007) Critical amino acid residues of maurocalcine involved in pharmacology, lipid interaction and cell penetration. *Biochim Biophys Acta* 1768(10):2528–2540.
- Ram N, et al. (2008) Direct peptide interaction with surface glycosaminoglycans contributes to the cell penetration of maurocalcine. *J Biol Chem* 283(35):24274–24284.
- Poillot C, De Waard M (2011) [Potential of cell penetrating peptides for cell drug delivery]. *Med Sci (Paris)* 27(5):527–534.
- Mosbah A, et al. (2000) A new fold in the scorpion toxin family, associated with an activity on a ryanodine-sensitive calcium channel. *Proteins* 40(3):436–442.
- Tisseyre C, et al. (2014) Quantitative evaluation of the cell penetrating properties of an iodinated Tyr-L-maurocalcine analog. *Biochim Biophys Acta* 1843(10):2356–2364.
- Tisseyre C, et al. (2013) Cell penetration properties of a highly efficient mini maurocalcine Peptide. *Pharmaceuticals (Basel)* 6(3):320–339.
- Ram NT-NI, et al. (2011) In vitro and in vivo cell delivery of quantum dots by the cell penetrating peptide maurocalcine. *Int J Biomed Nanosci Nanotechnol* 2:12–32.
- Stasiuk GJ, et al. (2011) Cell-permeable Ln(III) chelate-functionalized InP quantum dots as multimodal imaging agents. *ACS Nano* 5(10):8193–8201.
- Zamaleeva AI, et al. (2014) Cell-penetrating nanobiosensors for pointillistic intracellular Ca²⁺-transient detection. *Nano Lett* 14(6):2994–3001.
- Aroui S, Brahim S, De Waard M, Bréard J, Kenani A (2009) Efficient induction of apoptosis by doxorubicin coupled to cell-penetrating peptides compared to unconjugated doxorubicin in the human breast cancer cell line MDA-MB 231. *Cancer Lett* 285(1):28–38.
- Aroui S, Brahim S, Waard MD, Kenani A (2010) Cytotoxicity, intracellular distribution and uptake of doxorubicin and doxorubicin coupled to cell-penetrating peptides in different cell lines: A comparative study. *Biochem Biophys Res Commun* 391(1):419–425.
- Aroui S, et al. (2009) Conjugation of doxorubicin to cell penetrating peptides sensitizes human breast MDA-MB 231 cancer cells to endogenous TRAIL-induced apoptosis. *Apoptosis* 14(11):1352–1365.
- Aroui S, et al. (2009) Maurocalcine as a non toxic drug carrier overcomes doxorubicin resistance in the cancer cell line MDA-MB 231. *Pharm Res* 26(4):836–845.
- Estève E, et al. (2005) Transduction of the scorpion toxin maurocalcine into cells. Evidence that the toxin crosses the plasma membrane. *J Biol Chem* 280(13):12833–12839.
- el-Hayek R, Lokuta AJ, Arévalo C, Valdivia HH (1995) Peptide probe of ryanodine receptor function. Imperatoxin A, a peptide from the venom of the scorpion *Pandinus imperator*, selectively activates skeletal-type ryanodine receptor isoforms. *J Biol Chem* 270(48):28696–28704.
- Shahbazzadeh D, et al. (2007) Hemicalcin, a new toxin from the Iranian scorpion *Hemiscorpius lepturus* which is active on ryanodine-sensitive Ca²⁺ channels. *Biochem J* 404(1):89–96.
- Schwartz EF, et al. (2009) Characterization of hadrucalcin, a peptide from *Hadrurus gertschi* scorpion venom with pharmacological activity on ryanodine receptors. *Br J Pharmacol* 157(3):392–403.
- Poillot C, et al. (2010) D-Maurocalcine, a pharmacologically inert efficient cell-penetrating peptide analogue. *J Biol Chem* 285(44):34168–34180.
- Marty I, Villaz M, Arlaud G, Bally I, Ronjat M (1994) Transmembrane orientation of the N-terminal and C-terminal ends of the ryanodine receptor in the sarcoplasmic reticulum of rabbit skeletal muscle. *Biochem J* 298(Pt 3):743–749.
- Boisseau S, et al. (2006) Cell penetration properties of maurocalcine, a natural venom peptide active on the intracellular ryanodine receptor. *Biochim Biophys Acta* 1758(3):308–319.
- Endo M, Tanaka M, Ogawa Y (1970) Calcium induced release of calcium from the sarcoplasmic reticulum of skinned skeletal muscle fibres. *Nature* 228(5266):34–36.
- Pessah IN, Zimanyi I (1991) Characterization of multiple [³H]ryanodine binding sites on the Ca²⁺ release channel of sarcoplasmic reticulum from skeletal and cardiac muscle: Evidence for a sequential mechanism in ryanodine action. *Mol Pharmacol* 39(5):679–689.
- Ram N, et al. (2008) Design of a disulfide-less, pharmacologically inert, and chemically competent analog of maurocalcine for the efficient transport of impermeant compounds into cells. *J Biol Chem* 283(40):27048–27056.
- Theillet FX, et al. (2013) Site-specific NMR mapping and time-resolved monitoring of serine and threonine phosphorylation in reconstituted kinase reactions and mammalian cell extracts. *Nat Protoc* 8(7):1416–1432.
- Lowry DF, Ahmadian MR, Redfield AG, Sprinzl M (1992) NMR study of the phosphate-binding loops of *Thermus thermophilus* elongation factor Tu. *Biochemistry* 31(11):2977–2982.
- Woods AS, Ferré S (2005) Amazing stability of the arginine-phosphate electrostatic interaction. *J Proteome Res* 4(4):1397–1402.
- Donald JE, Kulp DW, DeGrado WF (2011) Salt bridges: Geometrically specific, designable interactions. *Proteins* 79(3):898–915.
- Sims RJ, 3rd, Reinberg D (2008) Is there a code embedded in proteins that is based on post-translational modifications? *Nat Rev Mol Cell Biol* 9(10):815–820.
- Nishi H, Hashimoto K, Panchenko AR (2011) Phosphorylation in protein-protein binding: Effect on stability and function. *Structure* 19(12):1807–1815.
- Buczek O, Bulaj G, Olivera BM (2005) Conotoxins and the posttranslational modification of secreted gene products. *Cell Mol Life Sci* 62(24):3067–3079.
- Ferrer-Montiel AV, Canaves JM, DasGupta BR, Wilson MC, Montal M (1996) Tyrosine phosphorylation modulates the activity of clostridial neurotoxins. *J Biol Chem* 271(31):18322–18325.
- Samsó M, Trujillo R, Gurrola GB, Valdivia HH, Wagenknecht T (1999) Three-dimensional location of the imperatoxin A binding site on the ryanodine receptor. *J Cell Biol* 146(2):493–499.
- Zalk R, et al. (2015) Structure of a mammalian ryanodine receptor. *Nature* 517(7532):44–49.
- Yan Z, et al. (2015) Structure of the rabbit ryanodine receptor RyR1 at near-atomic resolution. *Nature* 517(7532):50–55.
- Efremov RG, Leitner A, Aebersold R, Raunser S (2015) Architecture and conformational switch mechanism of the ryanodine receptor. *Nature* 517(7532):39–43.
- Lau K, Van Petegem F (2014) Crystal structures of wild type and disease mutant forms of the ryanodine receptor SPRY2 domain. *Nat Commun* 5:5397.
- Pouvreau S, et al. (2006) Transient loss of voltage control of Ca²⁺ release in the presence of maurocalcine in skeletal muscle. *Biophys J* 91(6):2206–2215.
- Lu X, Xu L, Meissner G (1995) Phosphorylation of dihydropyridine receptor II-III loop peptide regulates skeletal muscle calcium release channel function. Evidence for an essential role of the beta-OH group of Ser687. *J Biol Chem* 270(31):18459–18464.
- Imagawa T, Leung AT, Campbell KP (1987) Phosphorylation of the 1,4-dihydropyridine receptor of the voltage-dependent Ca²⁺ channel by an intrinsic protein kinase in isolated triads from rabbit skeletal muscle. *J Biol Chem* 262(17):8333–8339.
- Pronza C, Wilkens CM, Beam KG (2000) Excitation-contraction coupling is not affected by scrambled sequence in residues 681–690 of the dihydropyridine receptor II-III loop. *J Biol Chem* 275(39):29935–29937.
- Bers DM (2014) Cardiac sarcoplasmic reticulum calcium leak: Basis and roles in cardiac dysfunction. *Annu Rev Physiol* 76:107–127.
- Del Prete D, Checler F, Chami M (2014) Ryanodine receptors: Physiological function and deregulation in Alzheimer disease. *Mol Neurodegener* 9:21.
- Paula-Lima AC, Adasme T, Hidalgo C (2014) Contribution of Ca²⁺ release channels to hippocampal synaptic plasticity and spatial memory: Potential redox modulation. *Antioxid Redox Signal* 21(6):892–914.
- Munawar A, et al. (2011) Venom peptide analysis of *Vipera ammodytes meridionalis* (Viperinae) and *Bothrops jararacussu* (Crotalinae) demonstrates subfamily-specificity of the peptidome in the family Viperidae. *Mol Biosyst* 7(12):3298–3307.

**Supplementary information manuscript “*In cellulo* phosphorylation-induced
pharmacological reprogramming of maurocalcine, a cell penetrating venom peptide”**

SI Materials and Methods

Materials. N- α -Fmoc-L-aminoacid, Wang-Tentagel resin and reagents used for peptide synthesis were obtained from Iris Biotech. Solvents were analytical grade products from Acros Organics. Acetonitrile was High Performance Liquid Chromatography (HPLC) gradient grade from Fischer Scientific and trifluoroacetic acid (purity \geq 98%) from Fluka.

Solid-phase peptide synthesis. Chemical syntheses of M_{Ca_b}, M_{Ca_b} P-Thr²⁶, M_{Ca_b} Thr²⁶Asp, M_{Ca_b} Thr²⁶Glu, M_{Ca_b} Asn²⁷Ala and M_{Ca_b} P-Thr²⁶ Asn²⁷Ala were performed as previously described (1) with the following modifications. Briefly, these peptides were chemically synthesized by the solid-phase peptide synthesis (SPPS) method using an automated peptide synthesizer (CEM© Liberty). The peptide chains were assembled stepwise on 0.24 mEq of Fmoc-L-Arg(Pbf)-Wang-Tentagel resin using 0.24 mmol of N- α -fluorenylmethyloxycarbonyl (Fmoc) L-amino-acid derivatives. The side-chain protecting groups were Trityl for Cys and Asn, tert-butyl for Ser and Tyr, Thr, Glu and Asp, Pbf for Arg, and tert-butylcarbonyl for Lys. Reagents were at the following concentrations: 0.2 M Fmoc-amino-acids (Fmoc-AA-OH in dimethylformamide (DMF)), 0.5 M activator (2-(1H-benzotriazole-1-yl)-1,1,3,3-tetramethyluronium hexafluorophosphate in DMF), 2 M activator base (diisopropylethylamine in N-methyl-pyrrolidone) and deprotecting agent (5% piperazine / 0.1 M 1-hydroxybenzotriazole in DMF), as advised by PepDriver (CEM©). After peptide chain assemblies, the resins were treated for 4 hours at room temperature with a mixture of trifluoroacetic acid/water/triisopropylsilane/1,4-dithiothreitol (92.5/2.5/2.5/2.5). The peptide mixture was then filtered to eliminate the resin and the filtrate precipitated by adding cold *t*-butylmethyl ether. The crude peptides were pelleted by centrifugation (10,000 \times g, 15 min) and the supernatants were discarded. The reduced peptides were submitted to oxidation for disulfide bridge formation in 0.1 M Tris / HCl buffer at pH 8.2 during 3 days at room temperature. Oxidized / folded peptides were then

purified by HPLC using a Vydac C18 column (218TP1010, 250 × 10 mm). Elution of the peptides were performed with a 10-60% acetonitrile linear gradient containing 0.1% trifluoroacetic acid (TFA) over 40 min. The purity of the collected fractions was analyzed by reversed phase (RP) - HPLC using analytical C18 column (Vydac, 218TP104, 10 μm, 250 × 4.6 mm). All peptides were characterized by MALDI-TOF mass spectrometry. Samples were mixed 1:1 (v/v) with 10 mg/mL α-cyano-4-hydroxycinnamic acid (HCCA) before spotted onto a MALDI target plate. Mass spectrometry analyses were performed on a 4800 MALDI-TOF/TOF instrument (ABSciex). MS spectra were acquired in positive ion reflector mode over a mass range of 800-6000 m/z.

In cellulo phosphorylation. HEK293 cells were incubated in the presence of M_{Ca_b}, PKA activator (8-bromoadenosine 3',5'-cyclic monophosphate salt) and 0.5-1.0 mCi/ml [³²P] orthophosphoric acid for 3 hr at 37°C in phosphate free media. Next, cells were washed twice to remove extracellular M_{Ca_b} and solubilized in the presence of phosphatase inhibitors (phosSTOP Roche) in buffer containing (in mM): Tris 15, KCl 60, NaCl 15, MgCl₂ 1.5, pH 7.0, Triton X-100 0.5%. M_{Ca_b} was collected using streptavidin-coated magnetic beads and [³²P]-labeled M_{Ca_b} visualized by autoradiography and streptavidin-peroxidase labeling after separation by 16.5% Tris-glycine gels (Bio-Rad) and transfer on nitrocellulose membrane (Bio-Rad). Control was performed in the absence of M_{Ca_b}.

NMR recordings and structure modeling. M_{Ca}, M_{Ca_b} P-Thr²⁶, M_{Ca_b} Thr²⁶Asp and M_{Ca_b} Thr²⁶Glu were solubilized in 500 μl of a mixture of H₂O and D₂O (9:1, v/v) at a final concentration of 1 mM. All ¹H-2D-NMR NOESY spectra (mixing time 80 ms) were recorded using the states-time-proportional phase increment method to achieve F1 quadrature detection. The spectrometer was a Bruker DRX500 Avance III equipped with a QX1 probe with z axis gradients. The temperature was set to 300 K, and the spectra were recorded with 2048 complex points in the directly acquired dimension and 400 points in the indirectly detected dimension. Solvent suppression was achieved using excitations sculpting with gradients. The obtained spectra were Fourier transformed (4096 × 1024 points) and analyzed with Topspin Bruker software.

The 3D structure of M_{Ca} P-Thr²⁶ was also modelled using the 25 conformations of M_{Ca} of the Protein

Database Bank structure (access code 1C6W). Using Sybyl X1.3, the energy of each conformation was minimized before introducing any modification into the structure. The parameter of the minimization were as follows: field force: MMFF94, charge: MMFF94, method: Powell without initial optimization, terminate point: gradient = 0.5 kcal/(mol.Å). Next, a phosphate group was added to Thr²⁶ for each of the 25 conformations using the phosphorylate tool of Sybyl X1.3. The energy was again minimized for each conformer using the same parameters as before, and each phosphorylated conformation compared to its unphosphorylated one. Twelve conformations were coherent with the NMR results on MCa_b P-Thr²⁶ and a mean structure of these conformations was represented and superimposed with the mean structure of the corresponding MCa conformations. The other 13 conformations show either no structural alterations or a modification of the orientation of the lateral chain of Asn²⁷ without (n=3) or with (n=3) an interaction with the phosphate group of Thr²⁶. For the twelve NMR-coherent conformations, there is an interaction between the phosphate group of Thr²⁶ and the guanidinium group of the lateral chain of Arg²⁴ with a distance between 1.53 and 2 Å that is fully compatible with an electrostatic interaction.

For MCa Thr²⁶Asp and MCa Thr²⁶Glu, the mutate tool from Sybyl X1.3 was used to replace the Thr²⁶ by the adequate amino acid on the 25 conformation. Then the energy was minimized using the same parameters as described for MCa P-Thr²⁶. Each MCa Thr²⁶Asp and MCa Thr²⁶Glu conformations were compared to their respective MCa and MCa P-Thr²⁶ counterparts. Concerning MCa Thr²⁶Asp, six conformations on 25 indicate an interaction between the lateral chains of Asp²⁶ and Arg²⁴ (distance varying between 1.93 and 2 Å), while 19 others provided no particular tendency. In contrast, none of the 25 conformations of MCa Thr²⁶Glu showed an interaction between the lateral chains of Glu²⁶ and Arg²⁴.

Preparation of junctional SR from rabbit skeletal muscle and purified RyR1. Junctional SR membrane vesicles enriched in RyR1 were prepared from skeletal muscle of New Zealand White rabbits according to the method of Saito *et al.* (2) with modifications described by Pessah and Zimanyi in 1991 (3). The preparations were stored in 10% sucrose, 10 mm HEPES, pH 7.4, at -80°C until

needed. Purified RyR1 was prepared from solubilized SR vesicles by separation on sucrose gradient according to Lay et al. (4).

[³H]-ryanodine binding on SR vesicles from skeletal muscle. SR vesicles (0.1 mg/mL) were incubated at 37°C for 30 min in a buffer composed of 100 mM KCl, 2 mM EGTA, 2 mM CaCl₂ (pCa 5), 20 mM MOPS, pH 7.4, 1 nM [³H]-ryanodine. [³H]-ryanodine bound to heavy SR vesicles was measured by filtration through Whatman GF/B glass filters followed by three washes with 5 ml of ice-cold washing buffer composed of 100 mM KCl, 20 mM MOPS, pH 7.4. Bound [³H]-ryanodine retained on the filters was measured by liquid scintillation. Nonspecific binding was measured in the presence of 80 μM unlabeled ryanodine. The data are presented as mean ± S.E. Each experiment was performed in triplicate.

MCa_b and MCa_b P-Thr²⁶ interaction with RyR1. Purified RyR1 was transferred in a buffer containing KCl 100 mM, 2 mM EGTA, CaCl₂ 1.84 mM (pCa 6), MOPS 20 mM pH 7.4 (buffer A) using Sephadex G-25 column. Constant amount of purified RyR1 was incubated for 2 hrs at room temperature in 200 μl of buffer A in presence of various concentration of MCa_b or MCa_b P-Thr²⁶ immobilized on streptavidin-covered beads. Total volume of beads was kept constant for each concentrations of MCa_b or MCa_b P-Thr²⁶ by adding naked beads. Beads were then collected and washed three times with 1 ml PBS-0.1% tween. Bound RyR1 was measured by immunolabelling after separation on SDS page gel and transfer onto nitrocellulose.

Ca²⁺ release measurements. Ca²⁺ release from SR vesicles (0.1 mg/mL) was measured through the absorbance at 650 nm of the Ca²⁺-sensitive indicator Arsenazo III (250 μM) in a buffer containing 100 mM KCl, 6 mM Na₄P₂O₇, 20 mM MOPS pH 7.4 and 1 mM ATP-Mg. On some occasions, antipyrylazo III (AP III, 250 μM, 710 nm) was used instead of Arsenazo III because it is less sensitive to the presence of Mg²⁺ (specified in the legends of the figures). A slightly different buffer was used: 92 mM KCl, 20 mM K-MOPS (pH 7.0), 7.5 mM Na-pyrophosphate, and a coupled enzyme system consisting of 1 mM MgATP, 20 μg/mL creatine phosphokinase, and 5 mM phosphocreatine. Ca²⁺

loading was achieved by successive additions of 40-45 nmoles of CaCl_2 (20-30 μM final concentration). Ca^{2+} signal was calibrated under the same conditions in the presence of Ca^{2+} ionophore A23187 (4 μM).

Recording and analysis of single RyR1 channels in bilayer lipid membrane (BLM). Junctional SR membrane vesicles (approximately 0.1 mg/ml) were used to induce fusion with the planar BLM. BLM was formed by 30 mg/ml phosphatidylethanolamine: phosphatidylserine: phosphatidylcholine in decane (5:3:2 by weight purchased from Avanti Polar Lipids, Inc., Alabaster, AL). A 10-fold Cs^+ concentration gradient (500 to 50 mM) was built from *cis* to *trans* compartment. The recording baths were buffered to pH 7.4 by 20 mM HEPES. The holding potential was held at -40 mV by bilayer clamp BC 525C (Warner Instruments, Hampden, CT) on the *trans* side, where *cis* was virtually grounded. The *cis* chamber was where membrane protein and indicated Ca^{2+} concentrations were added to ensure the sidedness of cytosolic face of the incorporated channels. The luminal (*trans*) side of the channel was always maintained at 100 μM Ca^{2+} . Immediately after a fusion of SR, the *cis* chamber was perfused with an identical buffer except no JSR protein to prevent additional channel incorporation. The current signals were filtered at 1 kHz (low pass Bessel Filter 8 Pole; Warner Instruments), digitized and acquired at a sampling rate of 10 kHz (Digidata 1440A, Molecular Devices (Sunnyvale, CA)). All current recordings were made with Axoscope 10 software (Molecular Devices) for at least 1 min under each defined experimental condition. The channel open probability (P_o), mean open and closed dwell times (τ_o and τ_c) and current amplitude histograms were calculated and obtained using pClamp software version 10.0 (Molecular Devices).

Results

Single channel activity Supplementary Figure 5b

Basal channel activity at optimal *cis* Ca^{2+} demonstrates a high frequency of transitions to the fully open state (O2; first histogram). Addition of MCa P-Thr²⁶ (3 μM) decreases probability of the fully open state (O2) measured at 2, 5 and 10 min post addition (2nd, 3rd and 4th histograms, respectively). Importantly, the dwell times for events to the open substate O1 (the characteristic MCa substate) does

not change despite the fact that channel P_o drops precipitously, i.e., there is no evidence that channel inhibition coincides with increased dwell time at the classic O1 MCa substate (the open dwell time of O1 transitions is no different than the unmodified channel during the baseline period). Moreover, when MCa is subsequently added to the cis chamber after 10 min the frequency of the MCa substate O1 increases (left panel-histograms 5 and 6, and right panel-summary P_o and mean dwell time at O1). MCa but not MCa P-Thr²⁶ elicits an increase in dwell time at O1 demonstrating that (i) MCa competes with MCa P-Thr²⁶ and (ii) MCa increases the dwell time of the channel at O1, as expected for MCa alone. Addition of ryanodine locks the channel in the classic ryanodine-modified substate that is distinct from the MCa substate as demonstrated by the current histogram 7 in the Left Panel, and reduces the mean dwell time at O1 (the MCa state) and decreases the P_o of the fully open state O2 to zero. Representative analyses are from N=4 channels.

References

1. Esteve E, *et al.* (2003) Critical amino acid residues determine the binding affinity and the Ca²⁺ release efficacy of maurocalcine in skeletal muscle cells. *J Biol Chem* 278(39):37822-37831.
2. Saito A, Seiler S, Chu A, & Fleischer S (1984) Preparation and morphology of sarcoplasmic reticulum terminal cisternae from rabbit skeletal muscle. *J Cell Biol* 99(3):875-885.
3. Pessah IN & Zimanyi I (1991) Characterization of multiple [3H]ryanodine binding sites on the Ca²⁺ release channel of sarcoplasmic reticulum from skeletal and cardiac muscle: evidence for a sequential mechanism in ryanodine action. *Mol Pharmacol* 39(5):679-689.
4. Lai FA, Erickson HP, Rousseau E, Liu QY, & Meissner G (1988) Purification and reconstitution of the calcium release channel from skeletal muscle. *Nature* 331(6154):315-319.

SI Supplementary Figures

Supplementary Fig. 1. (a) Consensus PKA phosphorylation site on MCa. Critical residues for recognition by PKA are highlighted in color by stick representation (blue/red). The potential residue undergoing phosphorylation (Thr²⁶) is in red. Surface representation of MCa (Fast Connolly) according to NMR structure (PDB 1C6W accession number). The consensus phosphorylation site is

located in the pharmacophore region of MCa. (b) MCa_b Thr²⁶Glu is not a PKA substrate. Lack of phosphorylation by PKA of MCa_b Thr²⁶Glu is evidenced by the absence of shift in HPLC profile. The mass spectra leads only to detection of the original non-phosphorylated synthetic analogue MCa_b Thr²⁶Glu (experimental (M+H)⁺ = 4116.82 Da (inset) in agreement with its theoretical mass.

Supplementary Fig. 2. Chemical synthesis of MCa_b P-Thr²⁶. Analytical C18 RP-HPLC profiles of crude reduced (a), crude folded/oxidized (b), and purified (c) MCa_b P-Thr²⁶ peptide. The phosphorylated Thr²⁶ substitutes the regular Thr²⁶ residue in the MCa sequence. Inset: MALDI-TOF mass spectrometry profile illustrating the correct mass of the folded/oxidized phosphorylated analogue.

Supplementary Fig. 3. MCa_b P-Thr²⁶ does not induce Ca²⁺ leak from SR vesicles. (a) SR vesicles were actively loaded with Ca²⁺ in the presence of 1 μM MCa_b P-Thr²⁶ by sequential addition of 40 nmoles of Ca²⁺. After the last injection, extra vesicular Ca²⁺ concentration was monitored for over 9 min. No significant change of the extra vesicular Ca²⁺ concentration level was observed as indicated by the linear fit of the slope (which turned out to be negative on average, n=9). (b) SR vesicles were actively loaded with five injection of Ca²⁺ in the absence (left panel) or presence (right panel) of 1 μM MCa_b P-Thr²⁶. SR Ca²⁺ content was then measured by the addition of the ionophore A23187 that fully empties the SR vesicles. (c) Average SR Ca²⁺ content measured as in (b) (n=5 experiments).

Supplementary Fig. 4. The agonist effects of caffeine and ryanodine are preserved in the presence of MCa_b P-Thr²⁶. (a) Macroscopic Ca²⁺ currents measured with the AP III dye showing that 2 mM caffeine still triggers Ca²⁺ release from SR vesicles in spite of the presence of 2 μM MCa_b P-Thr²⁶ (bottom trace). The top trace shows that 50 nM MCa is highly potent in triggering Ca²⁺ release from SR vesicles in conditions where MCa_b P-Thr²⁶ has no agonist activity (two challenges at 20- and 40-fold higher concentrations) (n=7 experiments). (b) Similar experiment as in (a) also using AP III as a dye to measure Ca²⁺ except using 100 nM MCa in top panel and 20 μM ryanodine after the two applications of MCa_b P-Thr²⁶ (n=2 experiments).

Supplementary Fig. 5. Properties of M_{Ca}_b P-Thr²⁶ RyR1 inhibition in lipid bilayers. **(a)** M_{Ca} P-Thr²⁶ (3 μM) inhibits single channel gating frequency and open probability (P_o) in the presence of optimal Ca²⁺ in the cytoplasmic (*cis*; 50 μM) and luminal (*trans*; 100 μM) chambers (trace 1 *versus* trace 2). Subsequent addition of caffeine (*cis*; 2 mM) overrides the suppression of P_o (3rd trace), restoring baseline P_o. Addition of M_{Ca} demonstrates that the channel remains responsive to the classic Calcein state, further indicating reversibility through competition with M_{Ca} P-Thr²⁶. **(b)** Analysis of substate frequencies (left panel), channel mean open dwell times at the M_{Ca} substate (O1), and their relationship to P_o at the full-open conductance (O2) before (grey, control period) and after sequential additions of M_{Ca} P-Thr²⁶ (2 μM; blue), M_{Ca} (50 nM; black) and ryanodine (black, 2 μM). The *cis/trans* Ca²⁺ conditions are as in **(a)**. The results shown are representative of n=2 experiments.

Supplementary Fig. 6. Structural modifications induced by M_{Ca} phosphorylation. **(a)** Parts of a noesy spectrum of M_{Ca}_b (in blue) and M_{Ca}_b P-Thr²⁶ (in red). Variations in chemical shifts are boxed and amino acid positions identified by numbers. Major shifts go from residues 23 to 31 and encompass the pharmacophore region. Correlations with the side chain amide proton of residues Arg²⁴ and Asn²⁷ are labelled with a star. The spectra were recorded on a Bruker DRX500 as previously described (36). **(b)** Superimposition of average M_{Ca} and modelled M_{Ca}_b P-Thr²⁶ structures. Stick representations of M_{Ca} (background plane) and M_{Ca} P-Thr²⁶ (front plane). Average M_{Ca} structure was recovered from the PDB and modelled structure of M_{Ca} P-Thr²⁶ was produced according to ONLINE METHODS. Carbon atoms of M_{Ca} residues in yellow are those that differ in positioning from M_{Ca} P-Thr²⁶. Green colour indicates identical position of carbon atoms. Representation of structures was performed using Sybyl-X1.3.

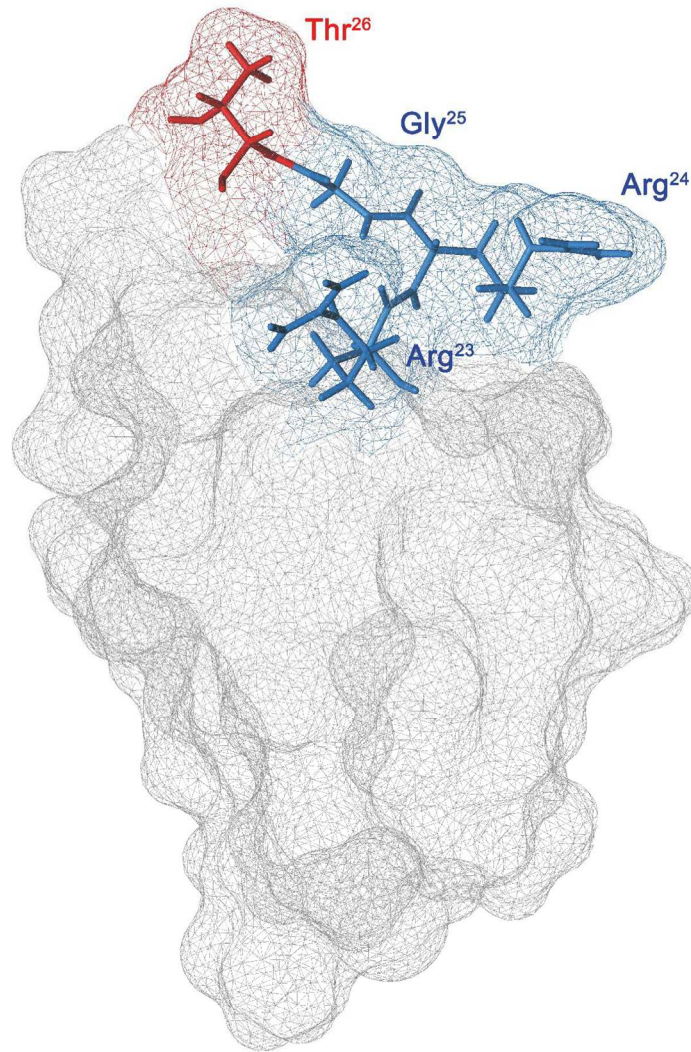
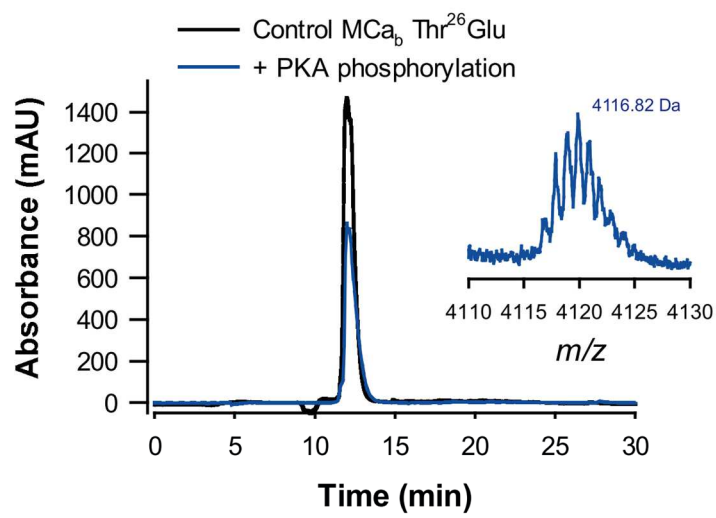
Supplementary Fig. 7. Structural evidence for the reorientation of the lateral chain of Arg²⁴. Zoom of overlaid ¹H-2D NMR Noesy spectra of M_{Ca}_b (in blue) and M_{Ca}_b P-Thr²⁶ (in red) in the region of CHd/NHe correlations of Arg²⁴. The spectra for M_{Ca}_b Thr²⁶Glu (in black) and M_{Ca}_b Thr²⁶Asp (in green) are shown for comparison. The spectra for Asn¹³ are shown as negative control.

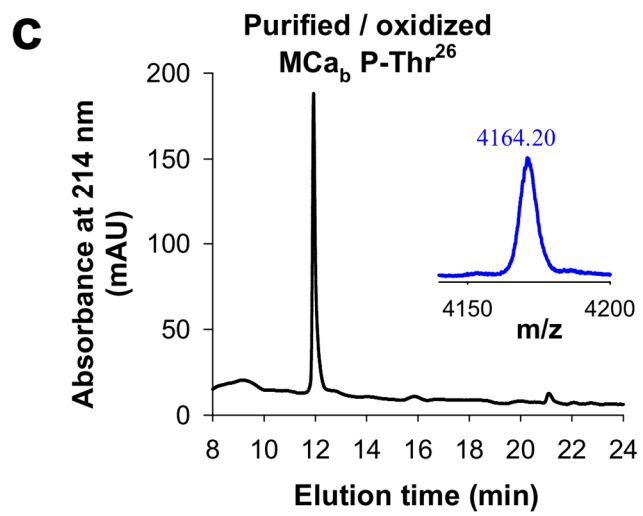
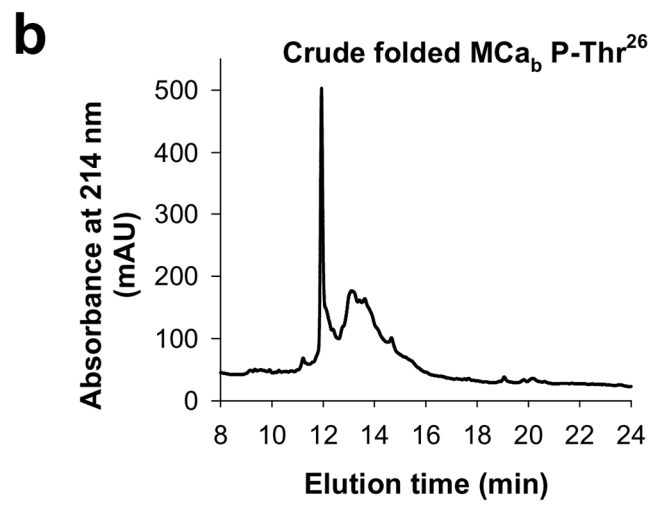
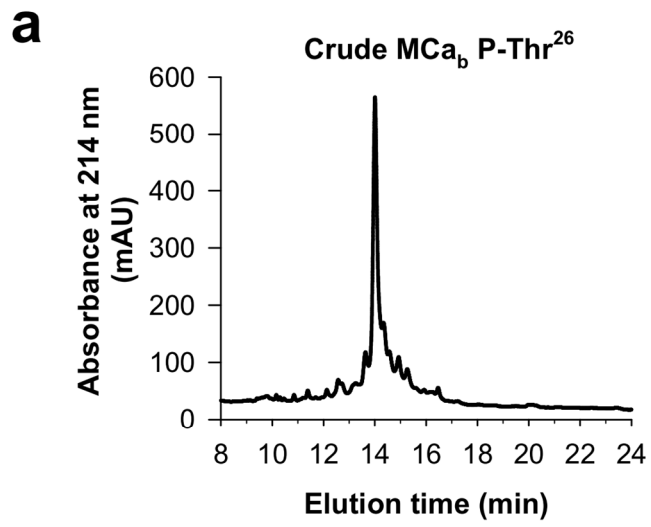
Supplementary Fig. 8. Asn²⁷ mutation does not affect MCa or MCa_b P-Thr²⁶ pharmacology. **(a)** Zoom on the hydrogen bond that was predicted to occur in n=3 out of 25 modelled structures between the side chains of Thr²⁶ and Asn²⁷ of MCa P-Thr²⁶. **(b)** Effect of MCa_b Asn²⁷Ala analogue on [³H]-ryanodine binding onto SR vesicles. Experimentally, binding was performed at pCa = 5. No significant differences were observed between the efficacies of MCa_b and MCa_b Asn²⁷Ala indicating that the Asn to Ala substitution at position 27 is non-disruptive of MCa pharmacology. **(c)** SR Ca²⁺ release illustrating the kinetics of Ca²⁺ release by 2 mM caffeine in the absence and presence of the double mutant MCa_b P-Thr²⁶ Asn²⁷Ala. The trace overlay (right panel) illustrates the delay introduced in caffeine-mediated Ca²⁺ release by MCa_b P-Thr²⁶ Asn²⁷Ala (n=7 experiments). AP III dye used in this set of experiments.

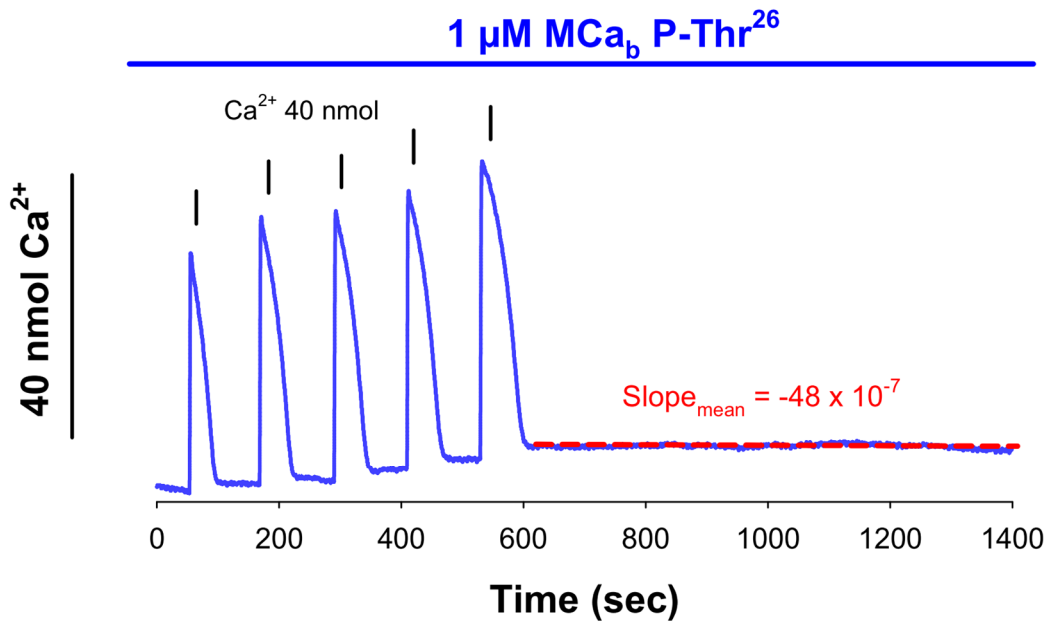
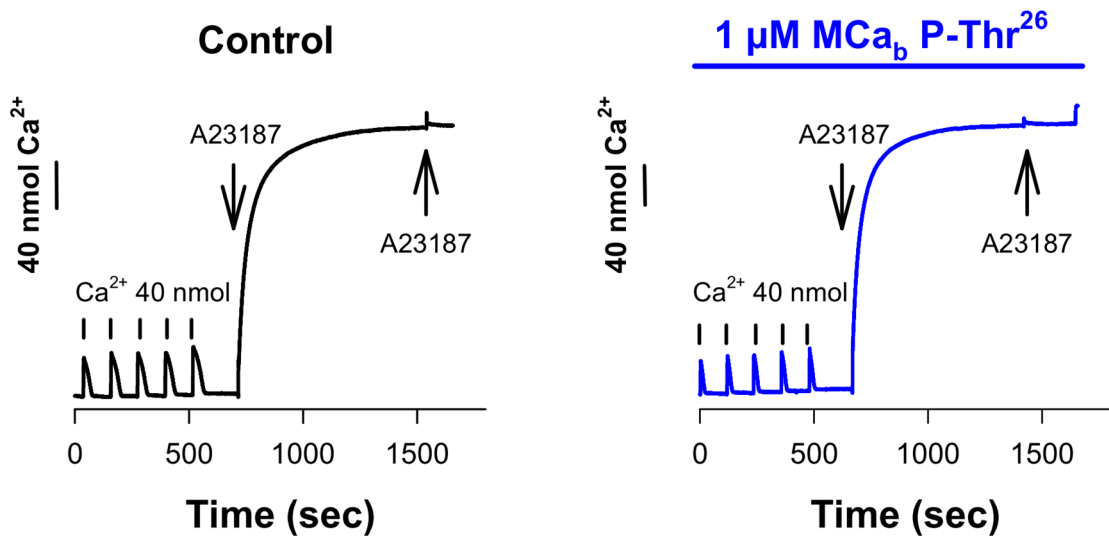
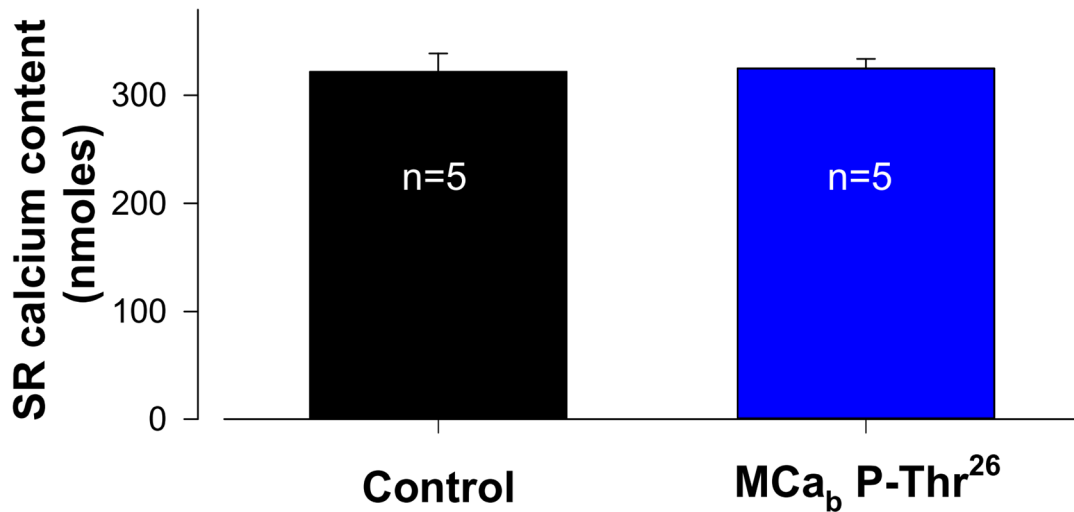
Supplementary Fig. 9. The MCa_b Thr²⁶Glu analogue does not mimic the antagonist effect of MCa_b P-Thr²⁶. **(a)** 3D structure of MCa Thr²⁶Glu (left panel) with a zoom in (right panel) illustrating the lack of ionic interaction between the side chains of Glu²⁶ and Arg²⁴ residues of MCa Thr²⁶Glu. **(b)** MCa_b Thr²⁶Glu (200 nM and 2 μM) causes a small time-dependent activation of RyR1 channel activity (traces 2-6). Sequential additions of ligands into the *cis* solution were denoted with downward arrows on the left side of each representative current traces. Mean open- and closed-dwelling time constants (τ_o and τ_c), obtained for each recording conditions, were denoted above each representative trace. “O” and “C” in the figure indicate the full and zero conductance states when the channel fully opened and closed, respectively. Total n=6 independent bilayer measurements under similar conditions produced consistent responses. The lower panel recapitulates the evolution of Po following the addition of MCa_b Thr²⁶Glu in the *cis* chamber.

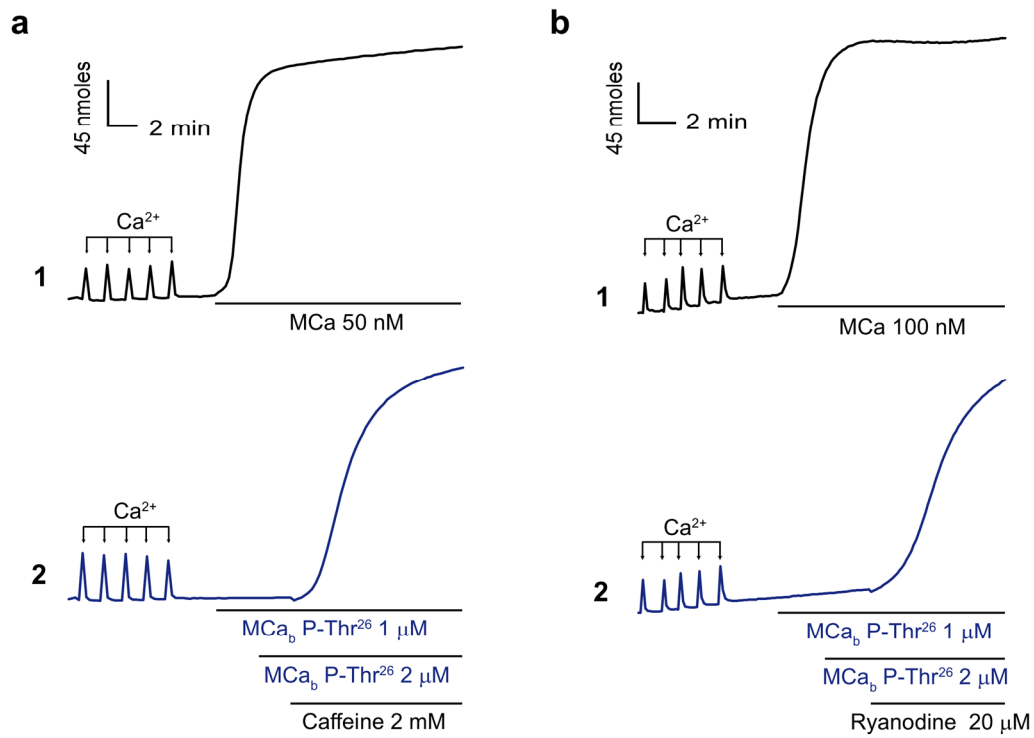
Supplementary Fig. 10. Caffeine and ryanodine override the effect of MCa_b Thr²⁶Asp. **(a)** 1 and 2 μM MCa_b Thr²⁶Asp has no effect on Ca²⁺ release from SR vesicles (trace 2) in conditions in which 50 nM MCa is active (trace 1). 2 mM caffeine reactivates the Ca²⁺ release in spite of the continuous

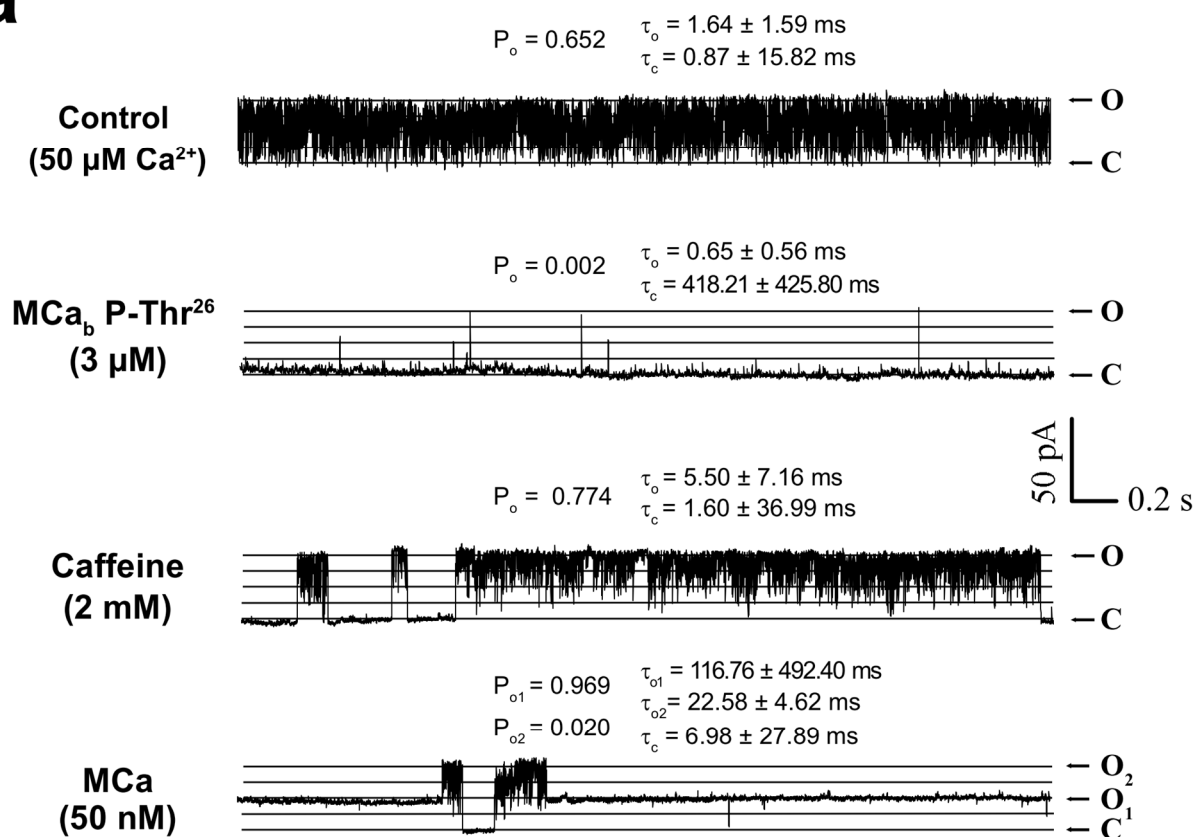
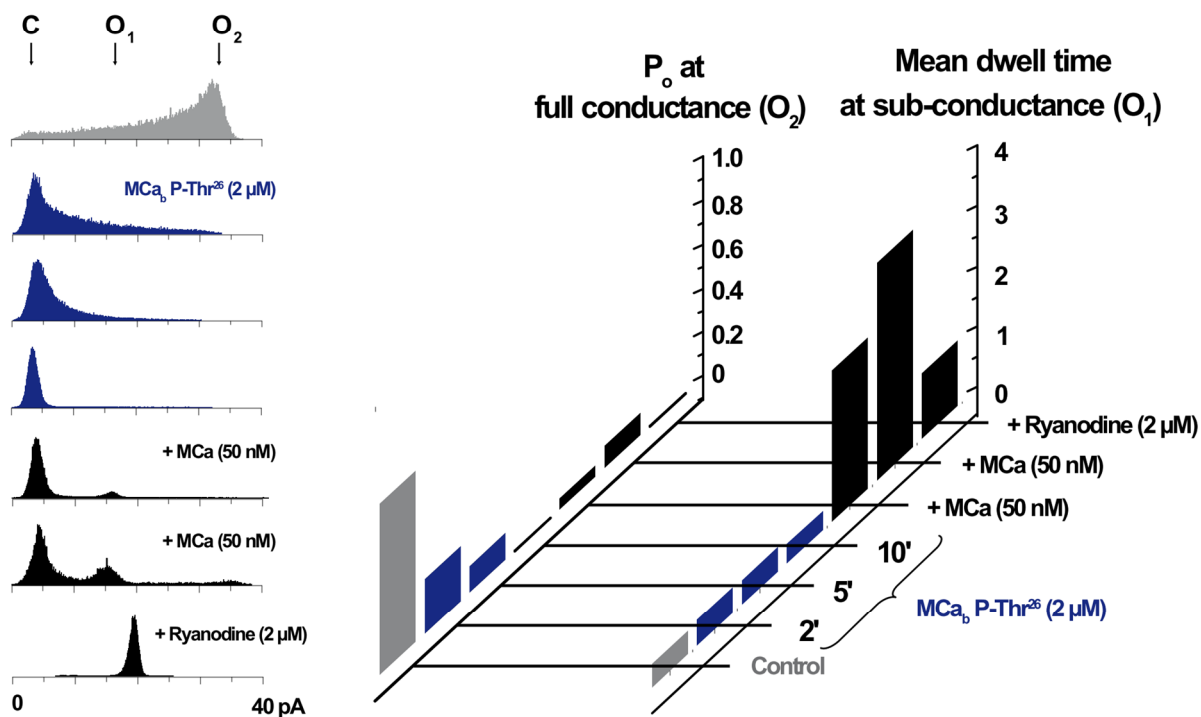
presence of M_{Ca}_v Thr²⁶ Asp. Representative example of n=5 using the AP III dye. **(b)** Similar as in **(a)** but using 20 μM ryanodine instead of 2 mM caffeine to show reactivation of Ca²⁺ release (n=2).

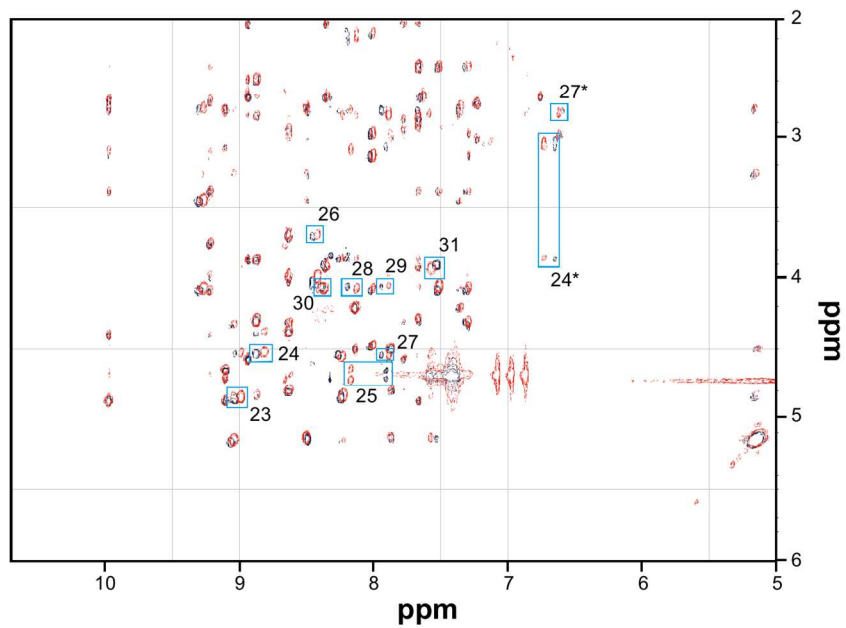
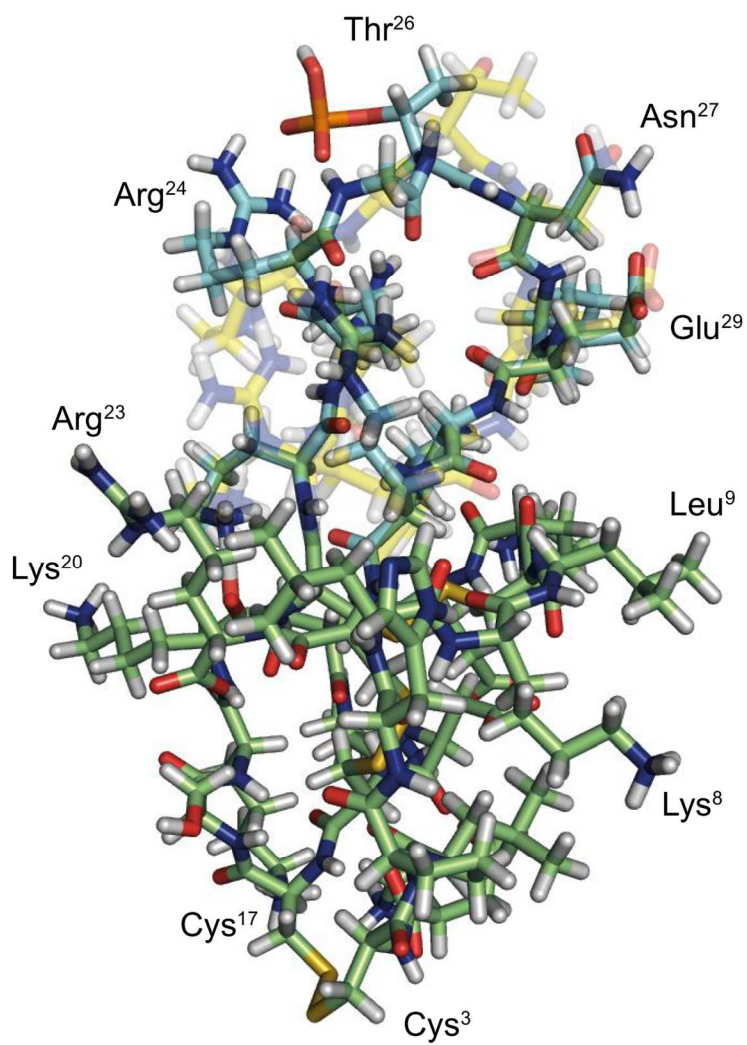
a**b**

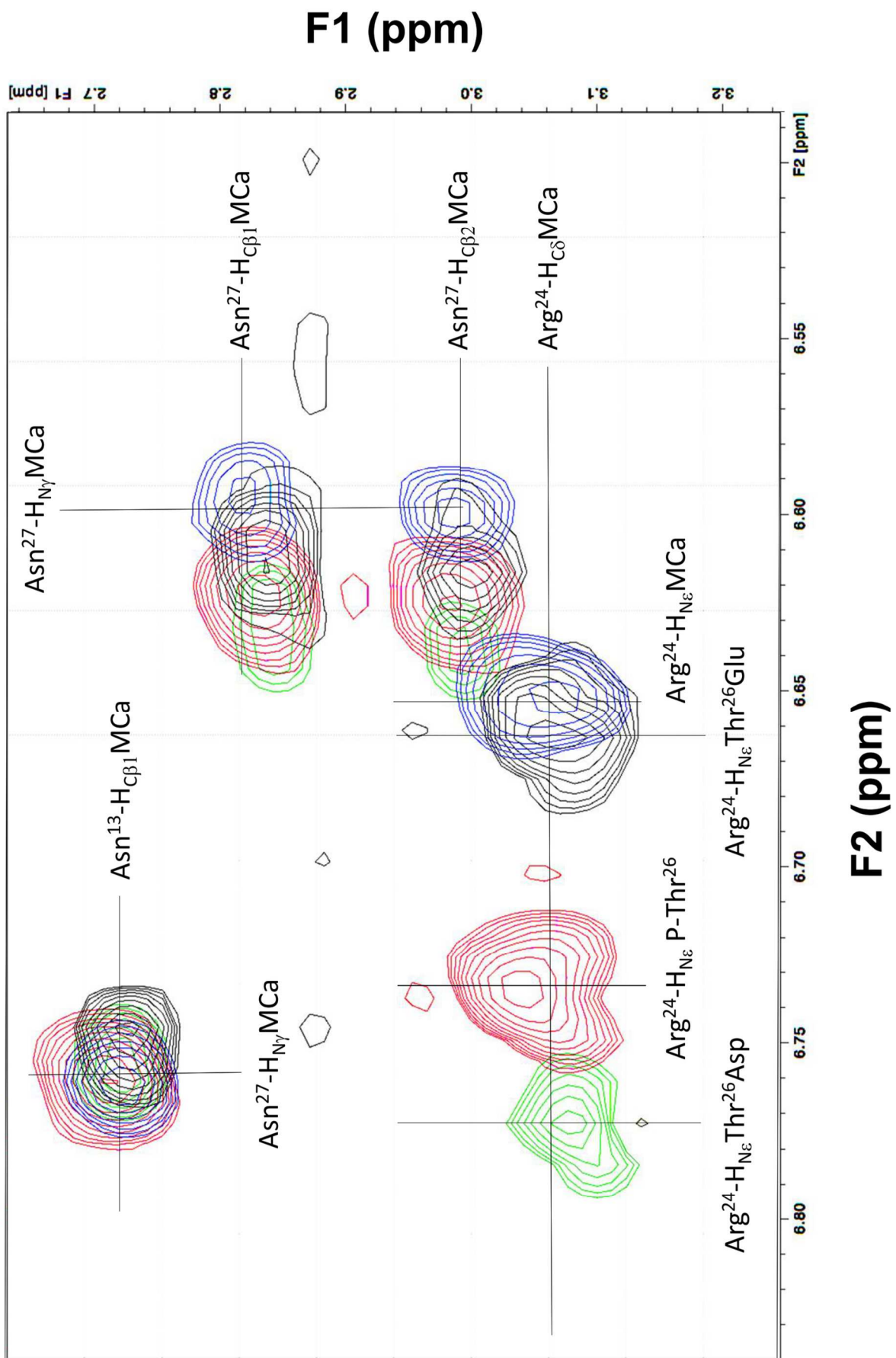


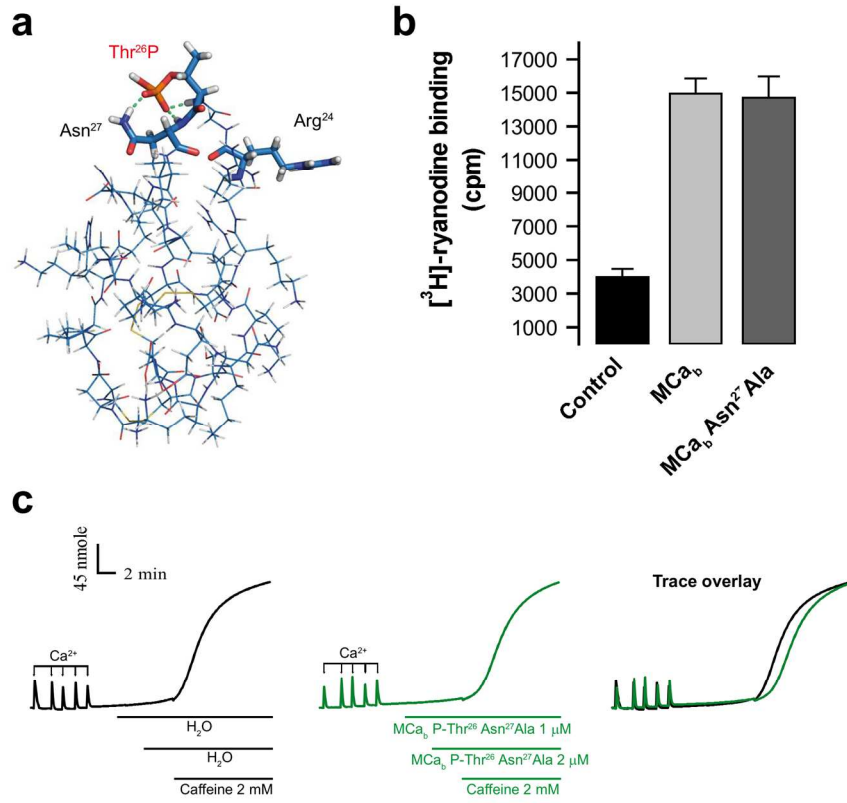
a**b****c**

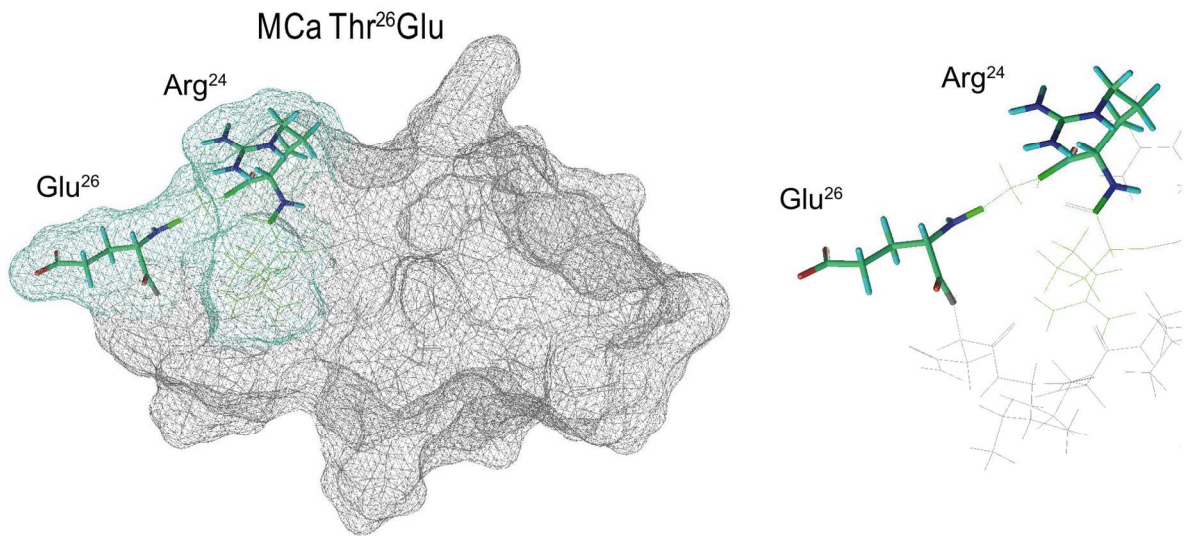
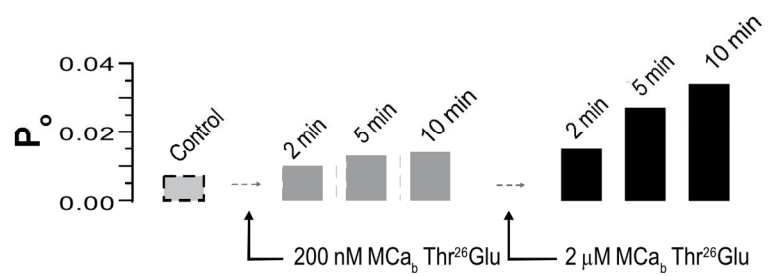
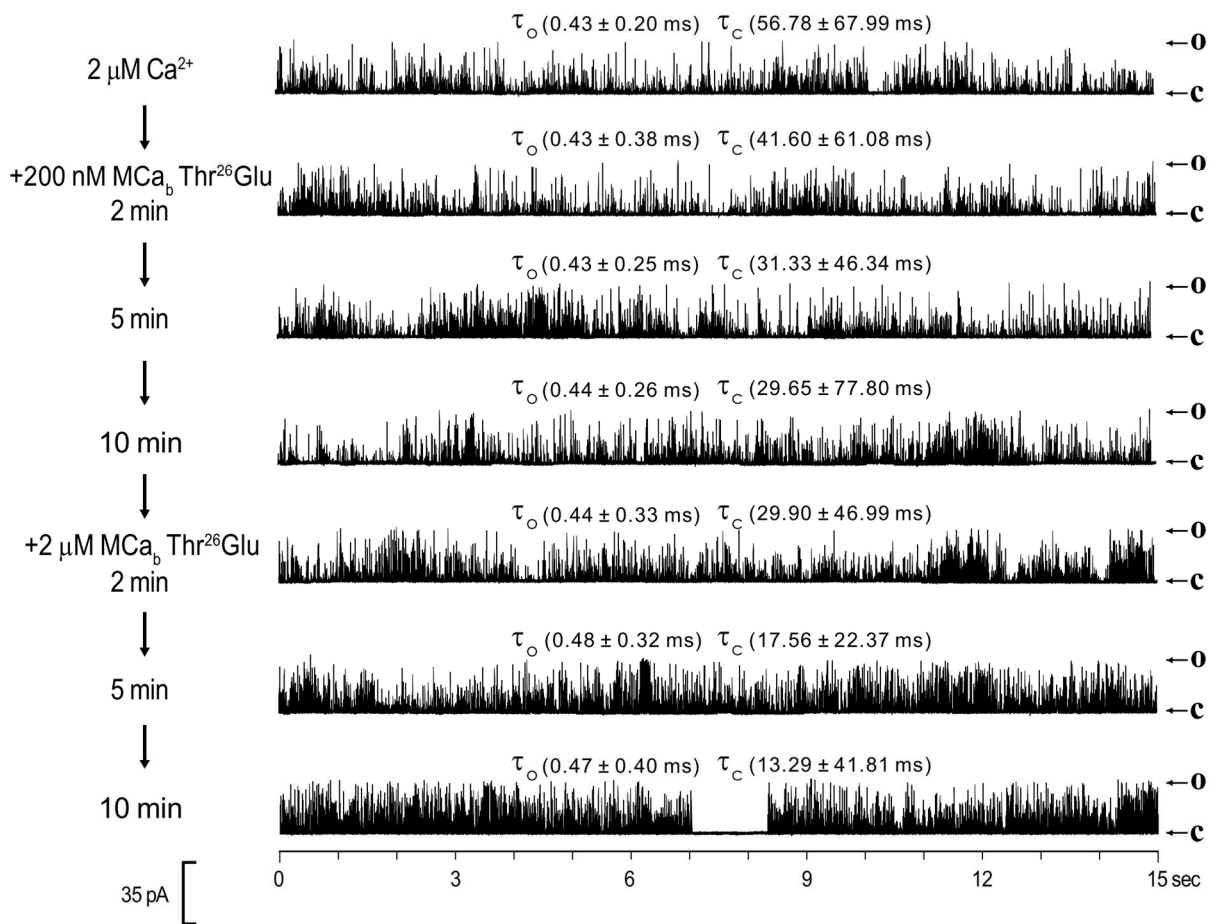


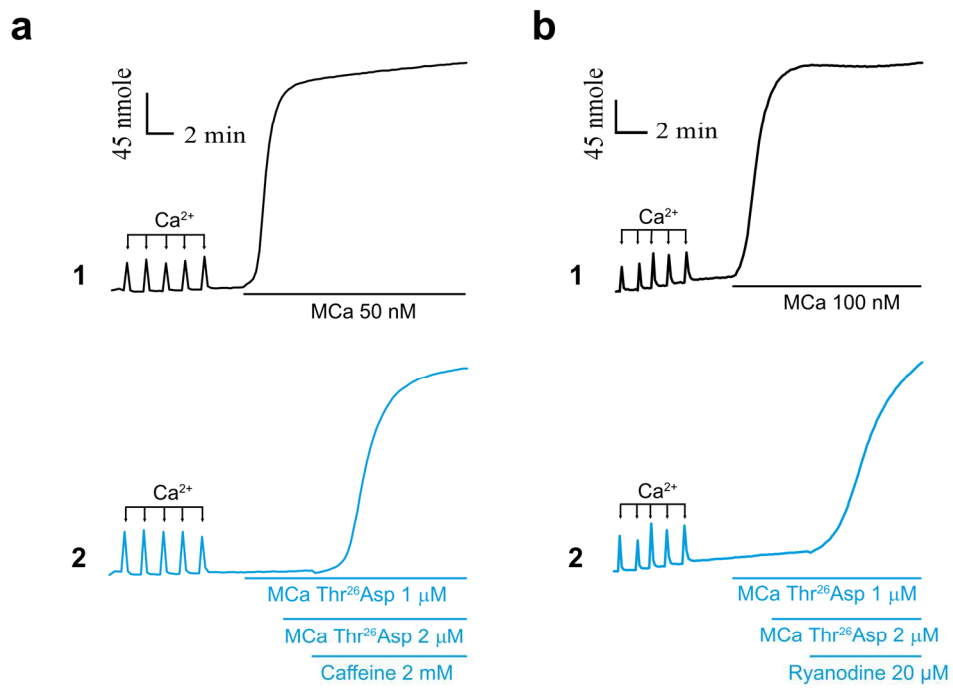
a**b**

a**b**





a**b**



Références

Adjadj, E.; Naudat, V.; Quiniou, E.; Wouters, D.; Sautière, P.; Craescu, C. T. Solution Structure of Lqh-8/6, a Toxin-like Peptide from a Scorpion Venom--Structural Heterogeneity Induced by Proline Cis/trans Isomerization. *Eur. J. Biochem.* **1997**, *246* (1), 218–227.

Ai, S.; Duan, J.; Liu, X.; Bock, S.; Tian, Y.; Huang, Z. Biological Evaluation of a Novel Doxorubicin-Peptide Conjugate for Targeted Delivery to EGF Receptor-Overexpressing Tumor Cells. *Mol. Pharm.* **2011**, *8* (2), 375–386.

Akcan, M.; Stroud, M. R.; Hansen, S. J.; Clark, R. J.; Daly, N. L.; Craik, D. J.; Olson, J. M. Chemical Re-Engineering of Chlorotoxin Improves Bioconjugation Properties for Tumor Imaging and Targeted Therapy. *J. Med. Chem.* **2011**, *54*, 782–787.

Alberici, L.; Roth, L.; Sugahara, K. N.; Agemy, L.; Kotamraju, V. R.; Teesalu, T.; Bordignon, C.; Traversari, C.; Rizzardi, G.-P. G.-P.; Ruoslahti, E. De Novo Design of a Tumor-Penetrating Peptide. *Cancer Res.* **2013**, *73* (2), 804–812.

Altafaj, X.; France, J.; Almassy, J.; Jona, I.; Rossi, D.; Sorrentino, V.; Mabrouk, K.; De Waard, M.; Ronjat, M. Maurocalcine Interacts with the Cardiac Ryanodine Receptor without Inducing Channel Modification. *Biochem. J.* **2007**, *406*, 309–315.

Ami, T.; Fujimoto, K. Click Chemistry as an Efficient Method for Preparing a Sensitive DNA Probe for Photochemical Ligation. *Chembiochem* **2008**, *9* (13), 2071–2074.

Ampie, L.; Woolf, E. C.; Dardis, C. Immunotherapeutic Advancements for Glioblastoma. *Front. Oncol.* **2015**, *5* (January), 12.

Apps, M.; Choi, E.; Wheate, N. The State-of-Play and Future of Platin Drugs. *Endocr. Relat. Cancer* **2015**.

Aroui, S.; Brahim, S.; Hamelin, J.; De Waard, M.; Bréard, J.; Kenani, A. Conjugation of Doxorubicin to Cell Penetrating Peptides Sensitizes Human Breast MDA-MB 231 Cancer Cells to Endogenous TRAIL-Induced Apoptosis. *Apoptosis* **2009a**, *14*, 1352–1365.

Aroui, S.; Brahim, S.; De Waard, M.; Bréard, J.; Kenani, A. Efficient Induction of Apoptosis by Doxorubicin Coupled to Cell-Penetrating Peptides Compared to Unconjugated Doxorubicin in the Human Breast Cancer Cell Line MDA-MB 231. *Cancer Lett.* **2009b**, *285*, 28–38.

Aroui, S.; Ram, N.; Appaix, F.; Ronjat, M.; Kenani, A.; Pirollet, F.; De Waard, M. Maurocalcine as a Non Toxic Drug Carrier Overcomes Doxorubicin Resistance in the Cancer Cell Line MDA-MB 231. *Pharm. Res.* **2009c**, *26* (4), 836–845.

Balayssac, S.; Burlina, F.; Convert, O.; Bolbach, G.; Chassaing, G.; Lequin, O. Comparison of Penetratin and Other Homeodomain-Derived Cell-Penetrating Peptides:

Interaction in a Membrane-Mimicking Environment and Cellular Uptake Efficiency. *Biochemistry* **2006**, *45*(5), 1408–1420.

Bechara, C.; Sagan, S. Cell-Penetrating Peptides: 20 Years Later, Where Do We Stand? *FEBS Lett.* **2013**, *587*(12), 1693–1702.

Behin, A.; Hoang-Xuan, K.; Carpentier, A. F.; Delattre, J.-Y. Primary Brain Tumours in Adults. *Lancet* **2003**, *361*, 323–331.

Billiet, L.; Fournier, D.; Du Prez, F. Step-Growth Polymerization and “Click” Chemistry: The Oldest Polymers Rejuvenated. *Polymer (Guildf).* **2009**, *50*(16), 3877–3886.

Binder, W. H.; Sachsenhofer, R. “Click” Chemistry in Polymer and Materials Science. *Macromol. Rapid Commun.* **2007**, *28*(1), 15–54.

Bock, V. D.; Hiemstra, H.; van Maarseveen, J. H. CuI-Catalyzed Alkyne-Azide “Click” Cycloadditions from a Mechanistic and Synthetic Perspective. *European J. Org. Chem.* **2006**, *2006*(1), 51–68.

Boisseau, S.; Mabrouk, K.; Ram, N.; Garmy, N.; Collin, V.; Tadmouri, A.; Mikati, M.; Sabatier, J. M.; Ronjat, M.; Fantini, J.; et al. Cell Penetration Properties of Maurocalcine, a Natural Venom Peptide Active on the Intracellular Ryanodine Receptor. *Biochim. Biophys. Acta - Biomembr.* **2006**, *1758*, 308–319.

Borst, P.; Evers, R.; Kool, M.; Wijnholds, J. A Family of Drug Transporters: The Multidrug Resistance-Associated Proteins. *J. Natl. Cancer Inst.* **2000**, *92*(16), 1295–1302.

Brandes, A. a.; Tosoni, A.; Franceschi, E.; Reni, M.; Gatta, G.; Vecht, C. Glioblastoma in Adults. *Crit. Rev. Oncol. Hematol.* **2008**, *67*, 139–152.

Brandt, F.; O’Connell, C.; Cazzaniga, A.; Waugh, J. M. Efficacy and Safety Evaluation of a Novel Botulinum Toxin Topical Gel for the Treatment of Moderate to Severe Lateral Canthal Lines. *Dermatologic Surg.* **2010**, *36*(SUPPL. 4), 2111–2118.

Brasseur, R.; Divita, G. Happy Birthday Cell Penetrating Peptides: Already 20years. *Biochim. Biophys. Acta - Biomembr.* **2010**, *1798*(12), 2177–2181.

Breinbauer, R.; Köhn, M. Azide-Alkyne Coupling: A Powerful Reaction for Bioconjugate Chemistry. *ChemBioChem* **2003**, *4*(11), 1147–1149.

Brennan, J. L.; Hatzakis, N. S.; Tshikhudo, T. R.; Dirvianskyte, N.; Razumas, V.; Patkar, S.; Vind, J.; Svendsen, A.; Nolte, R. J. M.; Rowan, A. E.; et al. Bionanoconjugation via Click Chemistry: The Creation of Functional Hybrids of Lipases and Gold Nanoparticles. *Bioconjug. Chem.* **2006**, *17*, 1373–1375.

Buisine, E.; Wieruszkeski, J. M.; Lippens, G.; Wouters, D.; Tartar, A.; Sautiere, P. Characterization of a New Family of Toxin-like Peptides from the Venom of the Scorpion *Leiurus Quinquestriatus Hebraeus*. 1H-NMR Structure of Leiuropeptide II. *J. Pept. Res. Off. J. Am. Pept. Soc.* **1997**, *49* (6), 545–555.

Burden, D. A.; Oshero, N. Mechanism of Action of Eukaryotic Topoisomerase II and Drugs Targeted to the Enzyme. **1998**, *1400*.

Chauffert, P. B. REFERENTIEL de L ' ANOCE F Pour Les GLIOMES de L ' ADULTE. **2012**, 1–59.

Ché, C.; Yang, G.; Thiot, C.; Lacoste, M.-C.; Currie, J.-C.; Demeule, M.; Régina, A.; Béliveau, R.; Castaigne, J.-P. New Angiopep-Modified Doxorubicin (ANG1007) and Etoposide (ANG1009) Chemotherapeutics with Increased Brain Penetration. *J. Med. Chem.* **2010**, *53* (7), 2814–2824.

Colombo, M.; Peretto, I. Chemistry Strategies in Early Drug Discovery: An Overview of Recent Trends. *Drug Discov. Today* **2008**, *13* (15-16), 677–684.

Conner, S. D.; Schmid, S. L. Regulated Portals of Entry into the Cell. *Nature* **2003**, *422* (6927), 37–44.

Cousins, M. J.; Pickthorn, K.; Huang, S.; Critchley, L.; Bell, G. The Safety and Efficacy of KAI-1678- an Inhibitor of Epsilon Protein Kinase C (ϵ PKC)-versus Lidocaine and Placebo for the Treatment of Postherpetic Neuralgia: A Crossover Study Design. *Pain Med.* **2013**, *14* (4), 533–540.

Dahe, li. Anti Tumor Translocation Peptide of Scorpion, Preparation Method and Application, July 25, 2007.

Damian, M. S.; Hedman, H. K.; Elmroth, S. K. C.; Diederichsen, U. Synthesis and DNA Interaction of Platinum Complex/peptide Chimera as Potential Drug Candidates. *European J. Org. Chem.* **2010**, 6161–6170.

Daniels, D. S.; Schepartz, A. Intrinsically Cell-Permeable Miniature Proteins Based on a Minimal Cationic PPII Motif. *J. Am. Chem. Soc.* **2007**, *129* (47), 14578–14579.

Dano, K. ACTIVE OUTWARD TRANSPORT OF DAUNOMYCIN IN RESISTANT EHRlich ASCITES TUMOR CELLS. *Biochim. Biophys. Acta* **1973**, *323*, 466–483.

Darlix, A.; Baumann, C.; Lorgis, V.; Ghiringhelli, F.; Blonski, M.; Chauffert, B.; Zouaoui, S.; Pinelli, C.; Rech, F.; Beauchesne, P.; et al. Prolonged Administration of Adjuvant Temozolomide Improves Survival in Adult Patients with Glioblastoma. *Anticancer Res.* **2013**, *33* (8), 3467–3474.

Debin, J. a; Strichartz, G. R. Short Communications Chloride Channel Inhibition By the Venom of the. *Toxicon* **1991**, 29 (II), 1403–1408.

DeBin, J. A.; Strichartz, G. R. Chloride Channel Inhibition by the Venom of the Scorpion *Leiurus Quinquestriatus*. *Toxicon Off. J. Int. Soc. Toxinology* **1991**, 29 (11), 1403–1408.

DeBin, J. A.; Maggio, J. E.; Strichartz, G. R. Purification and Characterization of Chlorotoxin, a Chloride Channel Ligand from the Venom of the Scorpion. *Am. J. Physiol.* **1993**, 264 (2 Pt 1), C361–C369.

Derossi, D.; Joliot, A. H.; Chassaing, G.; Prochiantz, A. The Third Helix of the Antennapedia Homeodomain Translocates through Biological Membranes. *J. Biol. Chem.* **1994**, 269 (14), 10444–10450.

Derossi, D.; Calvet, S.; Trembleau, A.; Brunissen, A.; Chassaing, G.; Prochiantz, A. Cell Internalization of the Third Helix of the Antennapedia Homeodomain Is Receptor-Independent. *J. Biol. Chem.* **1996**, 271 (30), 18188–18193.

Deshane, J.; Garner, C. C.; Sontheimer, H. Chlorotoxin Inhibits Glioma Cell Invasion via Matrix Metalloproteinase-2. *J. Biol. Chem.* **2003**, 278 (6), 4135–4144.

Desjardins, M. ER-Mediated Phagocytosis: A New Membrane for New Functions. *Nat. Rev. Immunol.* **2003**, 3 (4), 280–291.

Dijk, M. Van. *New Biodegradable Peptide-Based Polymer Constructs*; 2009.

Dingemans, A. M. C.; Pinedo, H. M.; Giaccone, G. Clinical Resistance to Topoisomerase-Targeted Drugs. *Biochim. Biophys. Acta - Gene Struct. Expr.* **1998**, 1400, 275–288.

Du, J.-Z.; Du, X.-J.; Mao, C.-Q.; Wang, J. Tailor-Made Dual pH-Sensitive Polymer-Doxorubicin Nanoparticles for Efficient Anticancer Drug Delivery. *J. Am. Chem. Soc.* **2011**, 133 (44), 17560–17563.

Duchardt, F.; Fotin-Mleczek, M.; Schwarz, H.; Fischer, R.; Brock, R. A Comprehensive Model for the Cellular Uptake of Cationic Cell-Penetrating Peptides. *Traffic* **2007**, 8 (7), 848–866.

Durzyńska, J.; Przysiecka, Ł.; Nawrot, R.; Barylski, J.; Nowicki, G.; Warowicka, A.; Musidlak, O.; Goździcka-Józefiak, A. Viral and Other Cell-Penetrating Peptides as Vectors of Therapeutic Agents in Medicine. *J. Pharmacol. Exp. Ther.* **2015**, 354 (1), 32–42.

Elmqvist, a; Lindgren, M.; Bartfai, T.; Langel U. VE-Cadherin-Derived Cell-Penetrating Peptide, pVEC, with Carrier Functions. *Exp. Cell Res.* **2001**, 269 (2), 237–244.

Estève, E.; Mabrouk, K.; Dupuis, A.; Smida-rezgui, S.; Altafaj, X.; Grunwald, D.; Platel,

J.; Andreotti, N.; Marty, I.; Ronjat, M.; et al. HAL Archives Ouvertes – France Author Manuscript Transduction of the Scorpion Toxin Maurocalcine into Cells . Evidence That the Toxin Crosses the Plasma Membrane HAL-AO Author Manuscript. **2005a**, *1* (1), 1–15.

Estève, E.; Mabrouk, K.; Dupuis, A.; Smida-Rezgui, S.; Altafaj, X.; Grunwald, D.; Platel, J.-C.; Andreotti, N.; Marty, I.; Sabatier, J.-M.; et al. Transduction of the Scorpion Toxin Maurocalcine into Cells. *J. Biol. Chem.* **2005b**, *280* (13), 12833–12839.

Fajloun, Z.; Kharrat, R.; Chen, L.; Lecomte, C.; Di, E. Chemical Synthesis and Characterization of Maurocalcine, a Scorpion Toxin That Activates Ca²⁺ Release Channel/ryanodine Receptors. *FEBS Lett.* **2000**, *469*, 179–185.

Fan, S.; Sun, Z.; Jiang, D.; Dai, C.; Ma, Y.; Zhao, Z.; Liu, H.; Wu, Y.; Cao, Z.; Li, W. BmKCT Toxin Inhibits Glioma Proliferation and Tumor Metastasis. *Cancer Lett.* **2010a**, *291* (2), 158–166.

Fan, S.; Sun, Z.; Jiang, D.; Dai, C.; Ma, Y.; Zhao, Z.; Liu, H.; Wu, Y.; Cao, Z.; Li, W. BmKCT Toxin Inhibits Glioma Proliferation and Tumor Metastasis. *Cancer Lett.* **2010b**, *291* (2), 158–166.

Feldhoff, P. W.; Mirski, S. E.; Cole, S. P.; Sullivan, D. M. Altered Subcellular Distribution of Topoisomerase II Alpha in a Drug-Resistant Human Small Cell Lung Cancer Cell Line. *Cancer Res* **1994**, *54* (3), 756–762.

Feron, O. Tumor-Penetrating Peptides : **2010**, *2* (34), 1–6.

Foerg, C.; Merkle, H. P. On the Biomedical Promise of Cell Penetrating Peptides: Limits versus Prospects. *J. Pharm. Sci.* **2008**, *97* (1), 144–162.

Frankel, a D.; Pabo, C. O. Cellular Uptake of the Tat Protein from Human Immunodeficiency Virus. *Cell* **1988**, *55* (6), 1189–1193.

Frederick, C. A.; Williams, L. D.; Ughetto, G.; Mare, I. I. G. A. Van Der; Boom, J. H. Van; Rich, A.; Wang, A. H. Structural Comparison of Anticancer Drug-DNA Complexes: Adriamycin and. **1990**, 2538–2549.

Fretz, M.; Jin, J.; Conibere, R.; Penning, N. A.; Al-Taei, S.; Storm, G.; Futaki, S.; Takeuchi, T.; Nakase, I.; Jones, A. T. Effects of Na⁺/H⁺ Exchanger Inhibitors on Subcellular Localisation of Endocytic Organelles and Intracellular Dynamics of Protein Transduction Domains HIV-TAT Peptide and Octaarginine. *J. Control. Release* **2006**, *116* (2), 247–254.

Fu, Y. J.; Yin, L. T.; Wang, W.; Chai, B. F.; Liang, A. H. Synthesis, Expression and Purification of a Type of Chlorotoxin-like Peptide from the Scorpion, *Buthus Martensii* Karsch, and Its Acute Toxicity Analysis. *Biotechnol. Lett.* **2005**, *27* (20), 1597–1603.

Fu, Y. J.; Yin, L. T.; Liang, A. H.; Zhang, C. F.; Wang, W.; Chai, B. F.; Yang, J. Y.; Fan, X. J. Therapeutic Potential of Chlorotoxin-like Neurotoxin from the Chinese Scorpion for Human Gliomas. *Neurosci. Lett.* **2007**, *412*, 62–67.

Fu, Y.; An, N.; Zheng, S.; Liang, A.; Li, Y. BmK CT-Conjugated Fluorescence Nanodiamond as Potential Glioma-Targeted Imaging and Drug. *Diam. Relat. Mater.* **2012a**, *21*, 73–76.

Fu, Y.; An, N.; Li, K.; Zheng, Y.; Liang, A. Chlorotoxin-Conjugated Nanoparticles as Potential Glioma-Targeted Drugs. *J. Neurooncol.* **2012b**, *107*, 457–462.

Fu, Y.-J. J.; Yin, L.-T. T.; Liang, A.-H. H. Polyclonal Antibody against a Recombinant Chlorotoxin-like Peptide from the Chinese Scorpion and Detection of Its Putative Receptors in Human Glioma Cells. *Biotechnol. Lett.* **2006**, *28*(18), 1439–1443.

Fu, Y.-J. J.; An, N.; Chan, K.-G. G.; Wu, Y.-B. B.; Zheng, S.-H. H.; Liang, A.-H. H. A Model of BmK CT in Inhibiting Glioma Cell Migration via Matrix Metalloproteinase-2 from Experimental and Molecular Dynamics Simulation Study. *Biotechnol. Lett.* **2011**, *33*(7), 1309–1317.

Fuller, M. D.; Thompson, C. H.; Zhang, Z.-R.; Freeman, C. S.; Schay, E.; Szakács, G.; Bakos, E.; Sarkadi, B.; McMaster, D.; French, R. J.; et al. State-Dependent Inhibition of Cystic Fibrosis Transmembrane Conductance Regulator Chloride Channels by a Novel Peptide Toxin. *J. Biol. Chem.* **2007**, *282*(52), 37545–37555.

Gazit, E.; Lee, W. J.; Brey, P. T.; Shai, Y. Mode of Action of the Antibacterial Cecropin B2: A Spectrofluorometric Study. *Biochemistry* **1994**, *33*(35), 10681–10692.

Gehring, W. J.; Van Qian, Q.; Billeter, M.; Furukubo-Tokunaga, K.; Schier, A. F.; Resendez-Perez, D.; Affolter, M.; Otting, G.; Wüthrich, K. Homeodomain-DNA Recognition. *Cell* **1994**, *78*(2), 211–223.

Gewirtz, D. a. A Critical Evaluation of the Mechanisms of Action Proposed for the Antitumor Effects of the Anthracycline Antibiotics Adriamycin and Daunorubicin. *Biochem. Pharmacol.* **1999**, *57*(7), 727–741.

Gold, S.; Monaghan, P.; Mertens, P.; Jackson, T. A Clathrin Independent Macropinocytosis-Like Entry Mechanism Used by Bluetongue Virus-1 during Infection of BHK Cells. *PLoS One* **2010**, *5*(6), e11360.

Gole, A.; Murphy, C. J. Azide-Derivatized Gold Nanorods: Functional Materials for “Click” Chemistry. *Langmuir* **2007**, *24*(1), 266–272.

Gomez, J. a; Gama, V.; Yoshida, T.; Sun, W.; Hayes, P.; Leskov, K.; Boothman, D.;

Matsuyama, S. Bax-Inhibiting Peptides Derived from Ku70 and Cell-Penetrating Pentapeptides. *Biochem. Soc. Trans.* **2007**, *35* (Pt 4), 797–801.

Gomez, J. A.; Chen, J.; Ngo, J.; Hajkova, D.; Yeh, I.-J.; Gama, V.; Miyagi, M.; Matsuyama, S. Cell-Penetrating Penta-Peptides (CPP5s): Measurement of Cell Entry and Protein-Transduction Activity. *Pharmaceuticals* **2010**, *3* (12), 3594–3613.

Goudet, C.; Chi, C. W.; Tytgat, J. An Overview of Toxins and Genes from the Venom of the Asian Scorpion *Buthus Martensi* Karsch. *Toxicon* **2002**, *40*, 1239–1258.

Goyenvalle, A.; Davies, K. E. Challenges to Oligonucleotides-Based Therapeutics for Duchenne Muscular Dystrophy. *Skelet. Muscle* **2011**, *1* (1), 8.

Graf, N.; Mokhtari, T. E.; Papayannopoulos, I. A.; Lippard, S. J. Platinum(IV)-Chlorotoxin (CTX) Conjugates for Targeting Cancer Cells. *J. Inorg. Biochem.* **2012**, *110*, 58–63.

Green, M.; Ishino, M.; Loewenstein, P. M. Mutational Analysis of HIV-1 Tat Minimal Domain Peptides: Identification of Trans-Dominant Mutants That Suppress HIV-LTR-Driven Gene Expression. *Cell* **1989**, *58* (1), 215–223.

Gregoritza, M.; Brandl, F. P. The Diels-Alder Reaction: A Powerful Tool for the Design of Drug Delivery Systems and Biomaterials. *Eur. J. Pharm. Biopharm.* **2015**, *97*, 438–453.

Hassane, F. S.; Frisch, B.; Schuber, F. Targeted Liposomes: Convenient Coupling of Ligands to Preformed Vesicles Using “click Chemistry.” *Bioconjug. Chem.* **2006**, *17* (3), 849–854.

Hein, C. D.; Liu, X.-M. X.-M.; Wang, D. Click Chemistry, A Powerful Tool for Pharmaceutical Sciences. *Pharm. Res.* **2008**, *25* (10), 2216–2230.

Heitz, F.; Morris, M. C.; Divita, G. Twenty Years of Cell-Penetrating Peptides: From Molecular Mechanisms to Therapeutics. *Br. J. Pharmacol.* **2009**, *157* (2), 195–206.

Hirose, T.; Sunazuka, T.; Sugawara, A.; Endo, A.; Iguchi, K.; Yamamoto, T.; Ui, H.; Shiomi, K.; Watanabe, T.; Sharpless, K. B.; et al. Chitinase Inhibitors: Extraction of the Active Framework from Natural Argifin and Use of in Situ Click Chemistry. *J. Antibiot. (Tokyo)*. **2009**, *62* (5), 277–282.

Hockaday, D. C.; Shen, S.; Fiveash, J.; Raubitschek, A.; Colcher, D.; Liu, A.; Alvarez, V.; Mamelak, A. N. Imaging Glioma Extent with 131I-TM-601. *J. Nucl. Med.* **2005**, *46* (4), 580–586.

Holzer, A. K.; Howell, S. B. The Internalization and Degradation of Human Copper Transporter 1 Following Cisplatin Exposure. *Cancer Res.* **2006**, *66* (22), 10944–10952.

Hopewell, J. W.; Duncan, R.; Wilding, D.; Chakrabarti, K. Preclinical Evaluation of the Cardiotoxicity of PK2: A Novel HPMA Copolymer–doxorubicin–galactosamine Conjugate Antitumour Agent. *Hum. Exp. Toxicol.* **2001**, *20* (9), 461–470.

Hosseini, A.; Lattanzio, F. a; Samudre, S. S.; DiSandro, G.; Sheppard, J. D.; Williams, P. B. Efficacy of a Phosphorodiamidate Morpholino Oligomer Antisense Compound in the Inhibition of Corneal Transplant Rejection in a Rat Cornea Transplant Model. *J. Ocul. Pharmacol. Ther.* **2012**, *28* (2), 194–201.

Hottinger, a. F.; Homicsko, K.; Negretti, L.; Lhermitte, B.; Stupp, R. Decision Making and Management of Gliomas: Practical Considerations. *Ann. Oncol.* **2012**, *23* (Supplement 10).

Huang, R.; Han, L.; Li, J.; Liu, S.; Shao, K.; Kuang, Y.; Hu, X.; Wang, X.; Lei, H.; Jiang, C. Chlorotoxin-Modified Macromolecular Contrast Agent for MRI Tumor Diagnosis. *Biomaterials* **2011a**, *32* (22), 5177–5186.

Huang, R.; Ke, W.; Han, L.; Li, J.; Liu, S.; Jiang, C. Targeted Delivery of Chlorotoxin-Modified DNA-Loaded Nanoparticles to Glioma via Intravenous Administration. *Biomaterials* **2011b**, *32* (9), 2399–2406.

Injac, R.; Strukelj, B. Recent Advances in Protection against Doxorubicin-Induced Toxicity. *Technol. Cancer Res. Treat.* **2008**, *7* (6), 497–516.

Ishida, S.; McCormick, F.; Smith-McCune, K.; Hanahan, D. Enhancing Tumor-Specific Uptake of the Anticancer Drug Cisplatin with a Copper Chelator. *Cancer Cell* **2010**, *17* (6), 574–583.

Jacoby, D. B.; Dyskin, E.; Yalcin, M.; Kesavan, K.; Dahlberg, W.; Ratliff, J.; Johnson, E. W.; Mousa, S. a. Potent Pleiotropic Anti-Angiogenic Effects of TM601, a Synthetic Chlorotoxin Peptide. *Anticancer Res.* **2010**, *30* (1), 39–46.

Jacquesson, T.; Ducray, F.; Maucort-Boulch, D.; Armoiry, X.; Louis-Tisserand, G.; Mbaye, M.; Pelissou-Guyotat, I.; Guyotat, J. [Surgery of High-Grade Gliomas Guided by Fluorescence: A Retrospective Study of 22 Patients]. *Neurochirurgie.* **2013**, *59* (1), 9–16.

Joliot, a; Pernelle, C.; Deagostini-Bazin, H.; Prochiantz, a. Antennapedia Homeobox Peptide Regulates Neural Morphogenesis. *Proc. Natl. Acad. Sci. U. S. A.* **1991**, *88* (5), 1864–1868.

Juliano, R. L.; Ling, V. A Surface Glycoprotein Modulating Drug Permeability in Chinese Hamster Ovary Cell Mutants. *Biochim. Biophys. Acta* **1976**, *455* (1), 152–162.

Kaplan, I. M.; Wadia, J. S.; Dowdy, S. F. Cationic TAT Peptide Transduction Domain Enters Cells by Macropinocytosis. *J. Control. Release* **2005**, *102* (1), 247–253.

Kartner, N.; Riordan, J. R.; Ling, V. Cell Surface P-Glycoprotein Associated with Multidrug Resistance in Mammalian Cell Lines. *Science* **1983**, *221* (4617), 1285–1288.

Kasai, T.; Nakamura, K.; Vaidyanath, A.; Chen, L.; Sekhar, S.; El-Ghlban, S.; Okada, M.; Mizutani, A.; Kudoh, T.; Murakami, H.; et al. Chlorotoxin Fused to IgG-Fc Inhibits Glioblastoma Cell Motility via Receptor-Mediated Endocytosis. *J. Drug Deliv.* **2012**, *2012*, 975763.

Keime-Guibert, F.; Chinot, O.; Taillandier, L.; Cartalat-Carel, S.; Frenay, M.; Kantor, G.; Guillamo, J.-S.; Jadaud, E.; Colin, P.; Bondiau, P.-Y.; et al. Radiotherapy for Glioblastoma in the Elderly. *N. Engl. J. Med.* **2007**, *356* (15), 1527–1535.

Keizer, H. G. FREE RADICAL-DEPENDENT MECHANISMS OF Y'. **1990**, *47*, 219–231.

Kelland, L. R.; Sharp, S. Y.; O'Neill, C. F.; Raynaud, F. I.; Beale, P. J.; Judson, I. R. Mini-Review: Discovery and Development of Platinum Complexes Designed to Circumvent Cisplatin Resistance. *J. Inorg. Biochem.* **1999**, *77*(1-2), 111–115.

Kelland, L. The Resurgence of Platinum-Based Cancer Chemotherapy. *Nat. Rev. Cancer* **2007**, *7*(July), 573–584.

Kerr, M. C.; Teasdale, R. D. Defining Macropinocytosis. *Traffic* **2009**, *10* (4), 364–371.

Kesavan, K.; Ratliff, J.; Johnson, E. W.; Dahlberg, W.; Asara, J. M.; Misra, P.; Frangioni, J. V.; Jacoby, D. B. Annexin A2 Is a Molecular Target for TM601, a Peptide with Tumor-Targeting and Anti-Angiogenic Effects. *J. Biol. Chem.* **2009**, *285* (7), 4366–4374.

Khalil, I. A.; Kogure, K.; Futaki, S.; Harashima, H. High Density of Octaarginine Stimulates Macropinocytosis Leading to Efficient Intracellular Trafficking for Gene Expression. *J. Biol. Chem.* **2006**, *281* (6), 3544–3551.

Kievit, F. M.; Veisoh, O.; Fang, C.; Bhattarai, N.; Lee, D.; Ellenbogen, R. G.; Zhang, M. Chlorotoxin Labeled Magnetic Nanovectors for Targeted Gene Delivery to Glioma. *ACS Nano* **2010**, *4* (8), 4587–4594.

Kolb, H. C.; Sharpless, K. B. The Growing Impact of Click Chemistry on Drug Discovery. *Drug Discov. Today* **2003**, *8* (24), 1128–1137.

Kolb, H. C.; Finn, M. G.; Sharpless, K. B. Click Chemistry: Diverse Chemical Function from a Few Good Reactions. *Angew. Chem. Int. Ed. Engl.* **2001**, *40* (11), 2004–2021.

Koren, E.; Apte, A.; Jani, A.; Torchilin, V. P. Multifunctional PEGylated 2C5-Immunoliposomes Containing pH-Sensitive Bonds and TAT Peptide for Enhanced Tumor Cell Internalization and Cytotoxicity. *J. Control. Release* **2012**, *160* (2), 264–273.

Krasiński, A.; Radić, Z.; Manetsch, R.; Raushel, J.; Taylor, P.; Sharpless, K. B.; Kolb, H.

C. In Situ Selection of Lead Compounds by Click Chemistry: Target-Guided Optimization of Acetylcholinesterase Inhibitors. *J. Am. Chem. Soc.* **2005**, *127*(18), 6686–6692.

Kumari, S.; Mg, S.; Mayor, S. Endocytosis Unplugged: Multiple Ways to Enter the Cell. *Cell Res.* **2010**, *20*(3), 256–275.

Larsen, A. K.; Skladanowski, A. Cellular Resistance to Topoisomerase-Targeted Drugs: From Drug Uptake to Cell Death. *Biochim. Biophys. Acta - Gene Struct. Expr.* **1998**, *1400*(1-3), 257–274.

Lebleu, B.; Moulton, H. M.; Abes, R.; Ivanova, G. D.; Abes, S.; Stein, D. a.; Iversen, P. L.; Arzumanov, A. a.; Gait, M. J. Cell Penetrating Peptide Conjugates of Steric Block Oligonucleotides. *Adv. Drug Deliv. Rev.* **2008**, *60*, 517–529.

Lévy, S.; Chapet, S.; Mazon, J.-J. Prise En Charge Des Gliomes. *Cancer/Radiothérapie* **2014**, *18*(5-6), 461–467.

Liang, J. F.; Yang, V. C. Synthesis of Doxorubicin-Peptide Conjugate with Multidrug Resistant Tumor Cell Killing Activity. *Bioorg. Med. Chem. Lett.* **2005**, *15*(22), 5071–5075.

Lin, Y. Z.; Yao, S. Y.; Veach, R. A.; Torgerson, T. R.; Hawiger, J. Inhibition of Nuclear Translocation of Transcription Factor NF-Kappa B by a Synthetic Peptide Containing a Cell Membrane-Permeable Motif and Nuclear Localization Sequence. *J Biol Chem* **1995**, *270*, 14255–14258.

Lopes, L. B.; Furnish, E. J.; Komalavilas, P.; Flynn, C. R.; Ashby, P.; Hansen, A.; Ly, D. P.; Yang, G. P.; Longaker, M. T.; Panitch, A.; et al. Cell Permeant Peptide Analogues of the Small Heat Shock Protein, HSP20, Reduce TGF-beta1-Induced CTGF Expression in Keloid Fibroblasts. *J. Invest. Dermatol.* **2009**, *129*(3), 590–598.

Lui, V. C. H.; Lung, S. S. S.; Pu, J. K. S.; Hung, K. N.; Leung, G. K. K. Invasion of Human Glioma Cells Is Regulated by Multiple Chloride Channels Including ClC-3. *Anticancer Res.* **2010**, *30*, 4515–4524.

Lundberg, P.; Langel, U. A Brief Introduction to Cell-Penetrating Peptides. *J. Mol. Recognit.* **2003**, *16*, 227–233.

Lundberg, P.; Magzoub, M.; Lindberg, M.; Hallbrink, M.; Jarvet, J.; Eriksson, L. E.; Langel, U.; Graslund, A. Cell Membrane Translocation of the N-Terminal (1-28) Part of the Prion Protein. *Biochem Biophys Res Commun* **2002**, *299*(1), 85–90.

Lyons, S. a.; O'Neal, J.; Sontheimer, H. Chlorotoxin, a Scorpion-Derived Peptide, Specifically Binds to Gliomas and Tumors of Neuroectodermal Origin. *Glia* **2002**, *39*(May), 162–173.

Ma, N.; Wang, Y.; Zhao, B.-X.; Ye, W.-C.; Jiang, S. The Application of Click Chemistry in the Synthesis of Agents with Anticancer Activity. *Drug Des. Devel. Ther.* **2015**, *9*, 1585–1599.

Mabrouk, K.; Ram, N.; Boisseau, S.; Strappazzon, F.; Reham, A.; Sadoul, R.; Darbon, H.; Ronjat, M.; De Waard, M. Critical Amino Acid Residues of Maurocalcine Involved in Pharmacology, Lipid Interaction and Cell Penetration. *Biochim. Biophys. Acta - Biomembr.* **2007**, *1768*, 2528–2540.

Madani, F.; Lindberg, S.; Langel, U.; Futaki, S.; Gräslund, A.; Madani, F.; Lindberg, S.; Langel, Ü.; Futaki, S.; Gräslund, A. Mechanisms of Cellular Uptake of Cell-Penetrating Peptides. *J. Biophys.* **2011**, *2011*, 1–10.

Malmström, A.; Grønberg, B. H.; Marosi, C.; Stupp, R.; Frappaz, D.; Schultz, H.; Abacioglu, U.; Tavelin, B.; Lhermitte, B.; Hegi, M. E.; et al. Temozolomide versus Standard 6-Week Radiotherapy versus Hypofractionated Radiotherapy in Patients Older than 60 Years with Glioblastoma: The Nordic Randomised, Phase 3 Trial. *Lancet Oncol.* **2012**, *13*(9), 916–926.

Mamelak, A. N.; Jacoby, D. B. Targeted Delivery of Antitumoral Therapy to Glioma and Other Malignancies with Synthetic Chlorotoxin (TM-601). *Expert Opin. Drug Deliv.* **2007**, *4*, 175–186.

Mamelak, A. N.; Rosenfeld, S.; Bucholz, R.; Raubitschek, A.; Nabors, L. B.; Fiveash, J. B.; Shen, S.; Khazaeli, M. B.; Colcher, D.; Liu, A.; et al. Phase I Single-Dose Study of Intracavitary-Administered Iodine-131-TM-601 in Adults with Recurrent High-Grade Glioma. *J. Clin. Oncol.* **2006**, *24*(22), 3644–3650.

Mamidyala, S. K.; Finn, M. G. In Situ Click Chemistry: Probing the Binding Landscapes of Biological Molecules. *Chem. Soc. Rev.* **2010**, *39*(4), 1252–1261.

Manetsch, R.; Krasieński, A.; Radić, Z.; Raushel, J.; Taylor, P.; Sharpless, K. B.; Kolb, H. C. In Situ Click Chemistry: Enzyme Inhibitors Made to Their Own Specifications. *J. Am. Chem. Soc.* **2004**, *126*(40), 12809–12818.

McLellan, L. I.; Wolf, C. R. Glutathione and Glutathione-Dependent Enzymes in Cancer Drug Resistance. *Drug Resist Updat* **1999**, *2*(3), 153–164.

McPherson, C. Glioma Brain Tumors. *Mayf. Clin. Spine Inst.* **2013**, 1–3.

Meng, X.; Wan, J.; Jing, M.; Zhao, S.; Cai, W.; Liu, E. Specific Targeting of Gliomas with Multifunctional Superparamagnetic Iron Oxide Nanoparticle Optical and Magnetic Resonance Imaging Contrast Agents. *Acta Pharmacol. Sin.* **2007**, *28*(12), 2019–2026.

Mercer, J.; Helenius, A. Virus Entry by Macropinocytosis. *Nat. Cell Biol.* **2009**, *11*(5), 510–520.

Meyer-Losic, F.; Quinonero, J.; Dubois, V.; Alluis, B.; Dechambre, M.; Michel, M.; Cailler, F.; Fernandez, A.-M.; Trouet, A.; Kearsley, J. Improved Therapeutic Efficacy of Doxorubicin through Conjugation with a Novel Peptide Drug Delivery Technology (Vectocell). *J. Med. Chem.* **2006**, *49* (23), 6908–6916.

Meyer-Losic, F.; Nicolazzi, C.; Quinonero, J.; Ribes, F.; Michel, M.; Dubois, V.; De Coupade, C.; Boukaissi, M.; Chéné, A. S.; Tranchant, I.; et al. DTS-108, a Novel Peptidic Prodrug of SN38: In Vivo Efficacy and Toxicokinetic Studies. *Clin. Cancer Res.* **2008**, *14* (7), 2145–2153.

Milletti, F. Cell-Penetrating Peptides: Classes, Origin, and Current Landscape. *Drug Discov. Today* **2012**, *17* (15-16), 850–860.

Millward, S. W.; Agnew, H. D.; Lai, B.; Lee, S. S.; Lim, J.; Nag, A.; Pitram, S.; Rohde, R.; Heath, J. R. In Situ Click Chemistry: From Small Molecule Discovery to Synthetic Antibodies. *Integr. Biol. (Camb)*. **2013**, *5* (1), 87–95.

Minotti, G.; Cairo, G.; Monti, E. Role of Iron in Anthracycline Cardiotoxicity: New Tunes for an Old Song? *FASEB J.* **1999**, *13* (2), 199–212.

Minotti, G.; Menna, P.; Salvatorelli, E.; Cairo, G.; Gianni, L. Anthracyclines: Molecular Advances and Pharmacologic Developments in Antitumor Activity and Cardiotoxicity. *Pharmacol. Rev.* **2004**, *56* (2), 185–229.

Miyaji, Y.; Walter, S.; Chen, L.; Kurihara, A.; Ishizuka, T.; Saito, M.; Kawai, K.; Okazaki, O. Distribution of KAI-9803, a Novel δ -Protein Kinase C Inhibitor, after Intravenous Administration to Rats. *Drug Metab. Dispos.* **2011**, *39* (10), 1946–1953.

Moorhouse, a. D.; Moses, J. E. Click Chemistry and Medicinal Chemistry: A Case of "Cyclo-Addiction." *ChemMedChem* **2008**, *3* (5), 715–723.

Morris, M. C.; Vidal, P.; Chaloin, L.; Heitz, F.; Divita, G. A New Peptide Vector for Efficient Delivery of Oligonucleotides into Mammalian Cells. *Nucleic Acids Res.* **1997**, *25* (14), 2730–2736.

Morris, M. C.; Depollier, J.; Mery, J.; Heitz, F.; Divita, G. A Peptide Carrier for the Delivery of Biologically Active Proteins into Mammalian Cells. *Nat. Biotechnol.* **2001**, *19* (12), 1173–1176.

Mosbah, A.; Kharrat, R.; Fajloun, Z.; Renisio, J. G.; Blanc, E.; Sabatier, J. M.; El Ayeb, M.; Darbon, H. A New Fold in the Scorpion Toxin Family, Associated with an Activity on a Ryanodine-Sensitive Calcium Channel. *Proteins* **2000**, *40* (3), 436–442.

Moses, J. E.; Moorhouse, A. D. The Growing Applications of Click Chemistry. *Chem. Soc.*

Rev. **2007**, *36* (8), 1249–1262.

Mouhat, S.; Jouirou, B.; Mosbah, A.; De Waard, M.; Sabatier, J.-M. Diversity of Folds in Animal Toxins Acting on Ion Channels. *Biochem. J.* **2004**, *378* (Pt 3), 717–726.

Mu, Q.; Lin, G.; Patton, V. K.; Wang, K.; Press, O. W.; Zhang, M. Gemcitabine and Chlorotoxin Conjugated Iron Oxide Nanoparticles for Glioblastoma Therapy. *J. Mater. Chem. B. Mater. Biol. Med.* **2016**, *4* (1), 32–36.

Mueller, J.; Kretzschmar, I.; Volkmer, R.; Boisguerin, P. Comparison of Cellular Uptake Using 22 CPPs in 4 Different Cell Lines Comparison of Cellular Uptake Using 22 CPPs in 4 Different Cell Lines. **2008**, *19* (November), 2363–2374.

Nakase, I.; Niwa, M.; Takeuchi, T.; Sonomura, K.; Kawabata, N.; Koike, Y.; Takehashi, M.; Tanaka, S.; Ueda, K.; Simpson, J. C.; et al. Cellular Uptake of Arginine-Rich Peptides: Roles for Macropinocytosis and Actin Rearrangement. *Mol. Ther.* **2004**, *10* (6), 1011–1022.

Nakase, I.; Tadokoro, A.; Kawabata, N.; Takeuchi, T.; Katoh, H.; Hiramoto, K.; Negishi, M.; Nomizu, M.; Sugiura, Y.; Futaki, S. Interaction of Arginine-Rich Peptides with Membrane-Associated Proteoglycans Is Crucial for Induction of Actin Organization and Macropinocytosis. *Biochemistry* **2007**, *46* (2), 492–501.

Nakayama, F.; Yasuda, T.; Umeda, S.; Asada, M.; Imamura, T.; Meineke, V.; Akashi, M. Fibroblast Growth Factor-12 (FGF12) Translocation into Intestinal Epithelial Cells Is Dependent on a Novel Cell-Penetrating Peptide Domain: Involvement of Internalization in the in Vivo Role of Exogenous FGF12. *J. Biol. Chem.* **2011**, *286* (29), 25823–25834.

Nicolaides, N. C.; Postema, M.; Morphotek USA, I. Multifunctional AGENTS. March 26, 2013.

Nielsen, D.; Maare, C.; Skovsgaard, T. Cellular Resistance to Anthracyclines. *Gen. Pharmacol.* **1996**, *27* (2), 251–255.

Oehlke, J.; Krause, E.; Wiesner, B.; Beyermann, M.; Bienert, M. Extensive Cellular Uptake into Endothelial Cells of an Amphipathic Beta-Sheet Forming Peptide. *FEBS Lett.* **1997**, *415* (2), 196–199.

Oehlke, J.; Scheller, A.; Wiesner, B.; Krause, E.; Beyermann, M.; Klauschenz, E.; Melzig, M.; Bienert, M. Cellular Uptake of an Alpha-Helical Amphipathic Model Peptide with the Potential to Deliver Polar Compounds into the Cell Interior Non-Endocytically. *Biochim. Biophys. Acta* **1998**, *1414* (1-2), 127–139.

Oglecka, K.; Lundberg, P.; Magzoub, M.; Göran Eriksson, L. E.; Langel, U.; Gräslund, A. Relevance of the N-Terminal NLS-like Sequence of the Prion Protein for Membrane Perturbation

Effects. *Biochim. Biophys. Acta* **2008**, *1778* (1), 206–213.

Okonogi, N.; Shirai, K.; Oike, T.; Murata, K.; Noda, S. E.; Suzuki, Y.; Nakano, T. Topics in Chemotherapy, Molecular-Targeted Therapy, and Immunotherapy for Newly-Diagnosed Glioblastoma Multiforme. *Anticancer Res* **2015**, *35* (3), 1229–1235.

Olsen, M. L.; Schade, S.; Lyons, S. a; Amaral, M. D.; Sontheimer, H. Expression of Voltage-Gated Chloride Channels in Human Glioma Cells. *J. Neurosci.* **2003**, *23* (13), 5572–5582.

Omotehara, Y.; Hakuba, N.; Hato, N.; Okada, M.; Gyo, K. Protection Against Ischemic Cochlear Damage by Intratympanic Administration of AM-111. *Otol. Neurotol.* **2011**, *32* (9), 1422–1427.

Opsteen, J. A.; van Hest, J. C. M. Modular Synthesis of ABC Type Block Copolymers by “click” Chemistry. *J. Polym. Sci. Part A Polym. Chem.* **2007**, *45* (14), 2913–2924.

Otvos, L.; Cudic, M.; Chua, B. Y.; Deliyannis, G.; Jackson, D. C.; Otvos, L. An Insect Antibacterial Peptide-Based Drug Delivery System. *Mol. Pharm.* **2004**, *1* (3), 220–232.

Pelkmans, L.; Kartenbeck, J.; Helenius, a. Caveolar Endocytosis of Simian Virus 40 Reveals a New Two-Step Vesicular-Transport Pathway to the ER. *Nat. Cell Biol.* **2001**, *3* (5), 473–483.

Perret, P.; Ahmadi, M.; Riou, L.; Bacot, S.; Pecher, J.; Poillot, C.; Broisat, A.; Ghezzi, C.; De Waard, M. Biodistribution, Stability, and Blood Distribution of the Cell Penetrating Peptide Maurocalcine in Mice. *Int. J. Mol. Sci.* **2015**, *16* (11), 27730–27740.

Poillot, C.; De Waard, M. Administration de Molécules Actives Dans Les Cellules. *Med Sci* **2011**, *27* (5), 527–534.

Poillot, C.; Dridi, K.; Bichraoui, H.; Pêcher, J.; Alphonse, S.; Douzi, B.; Ronjat, M.; Darbon, H.; De Waard, M. D-Maurocalcine, a Pharmacologically Inert Efficient Cell-Penetrating Peptide Analogue. *J. Biol. Chem.* **2010**, *285* (44), 34168–34180.

Poillot, C.; Bichraoui, H.; Tisseyre, C.; Bahemberae, E.; Andreotti, N.; Sabatier, J. M.; Ronjat, M.; De Waard, M. Small Efficient Cell-Penetrating Peptides Derived from Scorpion Toxin Maurocalcine. *J. Biol. Chem.* **2012**, *287* (21), 17331–17342.

Pons, J. L.; Labesse, G. @TOME-2: A New Pipeline for Comparative Modeling of Protein-Ligand Complexes. *Nucleic Acids Res.* **2009**, *37*.

Pooga, M.; Hällbrink, M.; Zorko, M.; Langel, U. Cell Penetration by Transportan. *FASEB J.* **1998**, *12* (1), 67–77.

Prabaharan, M.; Grailer, J. J.; Pilla, S.; Steeber, D. A.; Gong, S. Amphiphilic Multi-Arm-Block Copolymer Conjugated with Doxorubicin via pH-Sensitive Hydrazone Bond for Tumor-Targeted Drug Delivery. *Biomaterials* **2009**, *30* (29), 5757–5766.

Qian, Y. Q.; Billeter, M.; Otting, G.; Müller, M.; Gehring, W. J.; Wüthrich, K. The Structure of the Antennapedia Homeodomain Determined by NMR Spectroscopy in Solution: Comparison with Prokaryotic Repressors. *Cell* **1989**, *59* (3), 573–580.

Rabik, C. A.; Dolan, M. E. Molecular Mechanisms of Resistance and Toxicity Associated with Platinating Agents. *Cancer Treat. Rev.* **2007**, *33* (1), 9–23.

Ram, N.; Weiss, N.; Texier-Nogues, I.; Aroui, S.; Andreotti, N.; Pirolet, F.; Ronjat, M.; Sabatier, J. M.; Darbon, H.; Jacquemond, V.; et al. Design of a Disulfide-Less, Pharmacologically Inert, and Chemically Competent Analog of Maurocalcine for the Efficient Transport of Impermeant Compounds into Cells. *J. Biol. Chem.* **2008**, *283*, 27048–27056.

Reissmann, S. Cell Penetration: Scope and Limitations by the Application of Cell-Penetrating Peptides. *Journal of Peptide Science*. January 14, 2014, pp 760–784.

Rjeibi, I.; Mabrouk, K.; Mosrati, H.; Berenguer, C.; Mejdoub, H.; Villard, C.; Laffitte, D.; Bertin, D.; Ouafik, L.; Luis, J.; et al. Purification, Synthesis and Characterization of AaCtx, the First Chlorotoxin-like Peptide from *Androctonus Australis* Scorpion Venom. *Peptides* **2011**, *32*, 656–663.

Roa, W.; Brasher, P. M. a; Bauman, G.; Anthes, M.; Bruera, E.; Chan, a; Fisher, B.; Fulton, D.; Gulavita, S.; Hao, C.; et al. Abbreviated Course of Radiation Therapy in Older Patients with Glioblastoma Multiforme: A Prospective Randomized Clinical Trial. *J. Clin. Oncol.* **2004**, *22* (9), 1583–1588.

Roldán Urgoiti, G. B.; Singh, A. D.; Easaw, J. C. Extended Adjuvant Temozolomide for Treatment of Newly Diagnosed Glioblastoma Multiforme. *J. Neurooncol.* **2012**, *108* (1), 173–177.

Rousselle, C.; Clair, P.; Lefauconnier, J.-M.; Kaczorek, M.; Scherrmann, J.-M.; Tamsamani, J. New Advances in the Transport of Doxorubicin through the Blood-Brain Barrier by a Peptide Vector-Mediated Strategy. *Mol. Pharmacol.* **2000a**, *57* (4), 679–686.

Rousselle, C.; Clair, P.; Lefauconnier, J. M.; Kaczorek, M.; Scherrmann, J. M.; Tamsamani, J. New Advances in the Transport of Doxorubicin through the Blood-Brain Barrier by a Peptide Vector-Mediated Strategy. *Mol. Pharmacol.* **2000b**, *57* (4), 679–686.

Rouzaire-Dubois, B.; Milandri, J. B. B.; Bostel, S.; Dubois, J. M. M. Control of Cell Proliferation by Cell Volume Alterations in Rat C6 Glioma Cells. *Pflügers Arch. Eur. J. Physiol.* **2000**, *440* (6), 881–888.

Säälik, P.; Elmquist, A.; Hansen, M.; Padari, K.; Saar, K.; Viht, K.; Langel, U.; Pooga, M. Protein Cargo Delivery Properties of Cell-Penetrating Peptides. A Comparative Study. *Bioconj. Chem.* **15**(6), 1246–1253.

Sadler, K.; Eom, K. D.; Yang, J. L.; Dimitrova, Y.; Tam, J. P. Translocating Proline-Rich Peptides from the Antimicrobial Peptide Bactenecin 7. *Biochemistry* **2002**, *41* (48), 14150–14157.

Safdar, S.; Taite, L. J. Targeted Diazeniumdiolates: Localized Nitric Oxide Release from Glioma-Specific Peptides and Proteins. *Int. J. Pharm.* **2012**, *422* (1–2), 264–270.

Safdar, S.; Payne, C. a.; Tu, N. H.; Taite, L. J. Targeted Nitric Oxide Delivery Preferentially Induces Glioma Cell Chemosensitivity via Altered p53 and O6-Methylguanine-DNA Methyltransferase Activity. *Biotechnol. Bioeng.* **2013**, *110* (4), 1211–1220.

Sahay, G.; Alakhova, D. Y.; Kabanov, A. V. Endocytosis of Nanomedicines. *J. Control. Release* **2010**, *145* (3), 182–195.

Sanderson, J. M. Peptide-Lipid Interactions: Insights and Perspectives. *Org. Biomol. Chem.* **2005**, *3* (2), 201–212.

Savino, M.; Annibali, D.; Carucci, N.; Favuzzi, E.; Cole, M. D.; Evan, G. I.; Soucek, L.; Nasi, S. The Action Mechanism of the Myc Inhibitor Termed Omomyc May Give Clues on How to Target Myc for Cancer Therapy. *PLoS One* **2011**, *6* (7), e22284.

Scheller, A.; Oehlke, J.; Wiesner, B.; Dathe, M.; Krause, E.; Beyermann, M.; Melzig, M.; Bienert, M. Structural Requirements for Cellular Uptake of Alpha-Helical Amphipathic Peptides. *J. Pept. Sci.* **1999**, *5* (4), 185–194.

Seo, T. S.; Li, Z.; Ruparel, H. Click Chemistry to Construct Fluorescent Oligonucleotides for DNA Sequencing. **2003**, No. 16, 609–612.

Shai, Y.; Oren, Z. From “carpet” mechanism to de-Novo Designed Diastereomeric Cell-Selective Antimicrobial Peptides. *Peptides* **2001**, *22* (10), 1629–1641.

Shen, S.; Khazaeli, M. B.; Gillespie, G. Y.; Alvarez, V. L. Radiation Dosimetry of ¹³¹I-Chlorotoxin for Targeted Radiotherapy in Glioma-Bearing Mice. *J. Neurooncol.* **2005**, *71* (2), 113–119.

Shi, N.; Qi, X.; Xiang, B.; Zhang, Y. A Survey on “Trojan Horse” Peptides: Opportunities, Issues and Controlled Entry to “Troy.” *J. Control. Release* **2014**, *194*, 53–70.

Smertenko, A.; Omran, M. A. A.; Hussey, P. J.; McVean, A. TOXIN EVOLUTION IN SCORPION VENOM: EVIDENCE FOR TOXIN DIVERGENCE UNDER STRONG NEGATIVE SELECTION IN *LEIURUS QUINQUESTRIATUS* SUBSPECIES. *J. Toxicol. Toxin Rev.* **2001**, *20* (3–

4), 229–244.

Soman, N. R.; Baldwin, S. L.; Hu, G.; Marsh, J. N.; Lanza, G. M.; Heuser, J. E.; Arbeit, J. M.; Wickline, S. A.; Schlesinger, P. H. Molecularly Targeted Nanocarriers Deliver the Cytolytic Peptide Melittin Specifically to Tumor Cells in Mice, Reducing Tumor Growth. *J. Clin. Invest.* **2009**, *119* (9), 2830–2842.

Sontheimer, H. An Unexpected Role for Ion Channels in Brain Tumor Metastasis. *Exp. Biol. Med. (Maywood)*. **2008**, *233*, 779–791.

Sontheimer, M. B. M. and H.; McFerrin, M. B.; Sontheimer, H.; Sontheimer, M. B. M. and H. A Role for Ion Channels in Glioma Cell Invasion. *Neuron Glia Biol.* **2006**, *2* (1), 39–49.

Soomets, U.; Lindgren, M.; Gallet, X.; Hällbrink, M.; Elmquist, A.; Balaspiri, L.; Zorko, M.; Pooga, M.; Brasseur, R.; Langel, U. Deletion Analogues of Transportan. *Biochim. Biophys. Acta* **2000**, *1467* (1), 165–176.

Soroceanu, L.; Gillespie, Y.; Khazaeli, M. B.; Sontheimer, H. Use of Chlorotoxin for Targeting of Primary Brain Tumors. *Cancer Res.* **1998**, *58* (21), 4871–4879.

Soroceanu, L.; Manning, T. J.; Sontheimer, H. Modulation of Glioma Cell Migration and Invasion Using Cl(-) and K(+) Ion Channel Blockers. *J. Neurosci.* **1999**, *19* (14), 5942–5954.

Di Stefano, G.; Lanza, M.; Kratz, F.; Merina, L.; Fiume, L. A Novel Method for Coupling Doxorubicin to Lactosaminated Human Albumin by an Acid Sensitive Hydrazone Bond: Synthesis, Characterization and Preliminary Biological Properties of the Conjugate. *Eur. J. Pharm. Sci.* **2004**, *23* (4-5), 393–397.

Stroud, M. R.; Hansen, S. J.; Olson, J. M.; R. Stroud, M.; J. Hansen, S.; M. Olson, J. In Vivo Bio-Imaging Using Chlorotoxin-Based Conjugates. *Curr. Pharm. Des.* **2011**, *17* (38), 4362–4371.

Stummer, W.; Pichlmeier, U.; Meinel, T.; Wiestler, O. D.; Zanella, F.; Reulen, H. J. Fluorescence-Guided Surgery with 5-Aminolevulinic Acid for Resection of Malignant Glioma: A Randomised Controlled Multicentre Phase III Trial. *Lancet Oncol.* **2006**, *7* (5), 392–401.

Stummer, W.; van den Bent, M. J.; Westphal, M. Cytoreductive Surgery of Glioblastoma as the Key to Successful Adjuvant Therapies: New Arguments in an Old Discussion. *Acta Neurochir. (Wien)*. **2011**, *153* (6), 1211–1218.

Stupp, R.; Regg, C. New Drugs and Combinations for Malignant Glioma. *Forum (Genova)*. **2003**, *13* (1), 61–75.

Stupp, R.; Mason, W. P.; van den Bent, M. J.; Weller, M.; Fisher, B.; Taphoorn, M. J. B.; Belanger, K.; Brandes, A. A.; Marosi, C.; Bogdahn, U.; et al. Radiotherapy plus Concomitant and

Adjuvant Temozolomide for Glioblastoma. *N. Engl. J. Med.* **2005**, *352*(10), 987–996.

Stupp, R.; Hegi, M. E.; Mason, W. P.; van den Bent, M. J.; Taphoorn, M. J.; Janzer, R. C.; Ludwin, S. K.; Allgeier, A.; Fisher, B.; Belanger, K.; et al. Effects of Radiotherapy with Concomitant and Adjuvant Temozolomide versus Radiotherapy Alone on Survival in Glioblastoma in a Randomised Phase III Study: 5-Year Analysis of the EORTC-NCIC Trial. *Lancet Oncol.* **2009**, *10*(5), 459–466.

Sugahara, K. N.; Teesalu, T.; Karmali, P. P.; Kotamraju, V. R.; Agemy, L.; Girard, O. M.; Hanahan, D.; Mattrey, R. F.; Ruoslahti, E. Tissue-Penetrating Delivery of Compounds and Nanoparticles into Tumors. *Cancer Cell* **2009**, *16*(6), 510–520.

Sun, C.; Veiseh, O.; Gunn, J.; Fang, C.; Hansen, S.; Lee, D.; Sze, R.; Ellenbogen, R. G.; Olson, J.; Zhang, M. In Vivo MRI Detection of Gliomas by Chlorotoxin-Conjugated Superparamagnetic Nanoparticles. *Small* **2008a**, *4*(3), 372–379.

Sun, C.; Fang, C.; Stephen, Z.; Veiseh, O.; Hansen, S.; Ellenbogen, R. G.; Olson, J.; Zhang, M. Tumor-Targeted Drug Delivery and MRI Contrast Enhancement by Chlorotoxin-Conjugated Iron Oxide Nanoparticles. *Nanomedicine* **2008b**, *3*(4), 495–505.

Tamborini, M.; Locatelli, E.; Rasile, M.; Monaco, I.; Rodighiero, S.; Corradini, I.; Comes Franchini, M.; Passoni, L.; Matteoli, M. A Combined Approach Employing Chlorotoxin-Nanovectors and Low Dose Radiation To Reach Infiltrating Tumor Niches in Glioblastoma. *ACS Nano* **2016**, *10*(2), 2509–2520.

Thomas, F.; Chatelut, E. Les Dérivés Du Platine. *Oncologie* **2007**, *9*(11), 741–745.

Thompson, C. H.; Olivetti, P. R.; Fuller, M. D.; Freeman, C. S.; McMaster, D.; French, R. J.; Pohl, J.; Kubanek, J.; MaCarty, N. a. Isolation and Characterization of a High Affinity Peptide Inhibitor of CIC-2 Chloride Channels. *J. Biol. Chem.* **2009**, *284*(38), 26051–26052.

Tisseyre, C.; Bahembera, E.; Dardevet, L.; Sabatier, J. M.; Ronjat, M.; De Waard, M. Cell Penetration Properties of a Highly Efficient Mini Maurocalcine Peptide. *Pharmaceuticals* **2013**, *6*(3), 320–339.

Tisseyre, C.; Ahmadi, M.; Bacot, S.; Dardevet, L.; Perret, P.; Ronjat, M.; Fagret, D.; Usson, Y.; Ghezzi, C.; De Waard, M. Quantitative Evaluation of the Cell Penetrating Properties of an Iodinated Tyr-L-Maurocalcine Analog. *Biochim. Biophys. Acta - Mol. Cell Res.* **2014**, *1843*(10), 2356–2364.

Tollis, S.; Dart, A. E.; Tzircotis, G.; Endres, R. G. The Zipper Mechanism in Phagocytosis: Energetic Requirements and Variability in Phagocytic Cup Shape. *BMC Syst. Biol.* **2010**, *4*(1), 149.

Tron, G. C.; Pirali, T.; Billington, R. A.; Canonico, P. L.; Sorba, G.; Genazzani, A. A. Click Chemistry Reactions in Medicinal Chemistry: Applications of the 1,3-Dipolar Cycloaddition between Azides and Alkynes. *Med. Res. Rev.* **2008**, *28*(2), 278–308.

Tünnemann, G.; Ter-Avetisyan, G.; Martin, R. M.; Stöckl, M.; Herrmann, A.; Cardoso, M. C. Live-Cell Analysis of Cell Penetration Ability and Toxicity of Oligo-Arginines. *J. Pept. Sci.* **2008**, *14*(4), 469–476.

Turner, K. L.; Sontheimer, H. Cl⁻ and K⁺ Channels and Their Role in Primary Brain Tumour Biology. *Philos. Trans. R. Soc. Lond. B. Biol. Sci.* **2014**, *369*, 20130095.

Ullrich, N.; Sontheimer, H. Cell Cycle-Dependent Expression of a Glioma-Specific Chloride Current: Proposed Link to Cytoskeletal Changes. *Am. J. Physiol.* **1997**, *273* (4 Pt 1), C1290–C1297.

Ullrich, N.; Bordey, a.; Gillespie, G. Y.; Sontheimer, H. Expression of Voltage-Activated Chloride Currents in Acute Slices of Human Gliomas. *Neuroscience* **1998**, *83*(4), 1161–1173.

Veiseh, M.; Gabikian, P.; Bahrami, S. B.; Veiseh, O.; Zhang, M.; Hackman, R. C.; Ravanpay, A. C.; Stroud, M. R.; Kusuma, Y.; Hansen, S. J.; et al. Tumor Paint: A chlorotoxin: Cy5.5 Bioconjugate for Intraoperative Visualization of Cancer Foci. *Cancer Res.* **2007**, *67*, 6882–6888.

Veiseh, O.; Sun, C.; Gunn, J.; Kohler, N.; Gabikian, P.; Lee, D.; Bhattarai, N.; Ellenbogen, R.; Sze, R.; Hallahan, A.; et al. Optical and MRI Multifunctional Nanoprobe for Targeting Gliomas. *Nano Lett.* **2005**, *5*, 1003–1008.

Veiseh, O.; Kievit, F. M.; Gunn, J. W.; Ratner, B. D.; Zhang, M. A Ligand-Mediated Nanovector for Targeted Gene Delivery and Transfection in Cancer Cells. *Biomaterials* **2009a**, *30*(4), 649–657.

Veiseh, O.; Gunn, J. W.; Kievit, F. M.; Sun, C.; Fang, C.; Lee, J. S. H.; Zhang, M. Inhibition of Tumor-Cell Invasion with Chlorotoxin-Bound Superparamagnetic Nanoparticles. *Small* **2009b**, *5*(2), 256–264.

Veiseh, O.; Sun, C.; Fang, C.; Bhattarai, N.; Gunn, J.; Kievit, F.; Du, K.; Pullar, B.; Lee, D.; Ellenbogen, R. G.; et al. Specific Targeting of Brain Tumors with an Optical/magnetic Resonance Imaging Nanoprobe across the Blood-Brain Barrier. *Cancer Res.* **2009c**, *69*, 6200–6207.

Veiseh, O.; Kievit, F. M.; Fang, C.; Mu, N.; Jana, S.; Leung, M. C.; Mok, H.; Ellenbogen, R. G.; Park, J. O.; Zhang, M. Chlorotoxin Bound Magnetic Nanovector Tailored for Cancer Cell Targeting, Imaging, and siRNA Delivery. *Biomaterials* **2010**, *31*, 8032–8042.

Vercauteren, D.; Piest, M.; van der Aa, L. J.; Al Soraj, M.; Jones, A. T.; Engbersen, J. F. J.; De Smedt, S. C.; Braeckmans, K. Flotillin-Dependent Endocytosis and a Phagocytosis-like Mechanism for Cellular Internalization of Disulfide-Based Poly(amido amine)/DNA Polyplexes. *Biomaterials* **2011**, *32* (11), 3072–3084.

Vivès, E.; Schmidt, J.; Pèlegri, A. Cell-Penetrating and Cell-Targeting Peptides in Drug Delivery. *Biochim. Biophys. Acta - Rev. Cancer* **2008**, *1786* (2), 126–138.

Wadia, J. S.; Stan, R. V.; Dowdy, S. F. Transducible TAT-HA Fusogenic Peptide Enhances Escape of TAT-Fusion Proteins after Lipid Raft Macropinocytosis. *Nat. Med.* **2004**, *10* (3), 310–315.

Wang, a H.; Ughetto, G.; Quigley, G. J.; Rich, a. Interactions between an Anthracycline Antibiotic and DNA: Molecular Structure of Daunomycin Complexed to d(CpGpTpApCpG) at 1.2-Å Resolution. *Biochemistry* **1987**, *26* (4), 1152–1163.

Wang, G. W.; Kang, Y. J. Inhibition of Doxorubicin Toxicity in Cultured Neonatal Mouse Cardiomyocytes with Elevated Metallothionein Levels. *J. Pharmacol. Exp. Ther.* **1999**, *288* (3), 938–944.

Wang, J.; Van De Water, T. R.; Bonny, C.; de Ribaupierre, F.; Puel, J. L.; Zine, A. A Peptide Inhibitor of c-Jun N-Terminal Kinase Protects against Both Aminoglycoside and Acoustic Trauma-Induced Auditory Hair Cell Death and Hearing Loss. *J. Neurosci.* **2003**, *23* (24), 8596–8607.

Wang, W. X.; Ji, Y. H. Scorpion Venom Induces Glioma Cell Apoptosis in Vivo and Inhibits Glioma Tumor Growth in Vitro. *J. Neurooncol.* **2005**, *73*, 1–7.

Warso, M. A.; Richards, J. M.; Mehta, D.; Christov, K.; Schaeffer, C.; Rae Bressler, L.; Yamada, T.; Majumdar, D.; Kennedy, S. A.; Beattie, C. W.; et al. A First-in-Class, First-in-Human, Phase I Trial of p28, a Non-HDM2-Mediated Peptide Inhibitor of p53 Ubiquitination in Patients with Advanced Solid Tumours. *Br. J. Cancer* **2013**, *108* (5), 1061–1070.

Wick, W.; Platten, M.; Meisner, C.; Felsberg, J.; Tabatabai, G.; Simon, M.; Nikkhah, G.; Papsdorf, K.; Steinbach, J. P.; Sabel, M.; et al. Temozolomide Chemotherapy Alone versus Radiotherapy Alone for Malignant Astrocytoma in the Elderly: The NOA-08 Randomised, Phase 3 Trial. *Lancet Oncol.* **2012**, *13* (7), 707–715.

De Witt Hamer, P. C.; Robles, S. G.; Zwinderman, A. H.; Duffau, H.; Berger, M. S. Impact of Intraoperative Stimulation Brain Mapping on Glioma Surgery Outcome: A Meta-Analysis. *J. Clin. Oncol.* **2012**, *30* (20), 2559–2565.

Wold, L. E.; Aberle, N. S.; Ren, J. Doxorubicin Induces Cardiomyocyte Dysfunction via a p38 MAP Kinase-Dependent Oxidative Stress Mechanism. *Cancer Detect. Prev.* **2005**, *29* (3),

Wu, X. S.; Jian, X. C.; Yin, B.; He, Z. J. Development of the Research on the Application of Chlorotoxin in Imaging Diagnostics and Targeted Therapies for Tumors. *Chin. J. Cancer* **2010**, *29* (6), 626–630.

Xiang, Y.; Liang, L.; Wang, X.; Wang, J.; Zhang, X.; Zhang, Q. Chloride Channel-Mediated Brain Glioma Targeting of Chlorotoxin-Modified Doxorubicin-Loaded Liposomes. *J. Control. Release* **2011**, *152* (3), 402–410.

Xu, T.; Fan, Z.; Li, W.; Dietel, B.; Wu, Y.; Beckmann, M. W.; Wrosch, J. K.; Buchfelder, M.; Eyupoglu, I. Y.; Cao, Z.; et al. Identification of Two Novel Chlorotoxin Derivatives CA4 and CTX-23 with Chemotherapeutic and Anti-Angiogenic Potential. *Sci. Rep.* **2016**, *6*, 19799.

Yang, Y.; Yang, Y.; Xie, X.; Cai, X.; Zhang, H.; Gong, W.; Wang, Z.; Mei, X. PEGylated Liposomes with NGR Ligand and Heat-Activable Cell-Penetrating Peptide-Doxorubicin Conjugate for Tumor-Specific Therapy. *Biomaterials* **2014**, *35* (14), 4368–4381.

Yeaman, M. R.; Yount, N. Y. Mechanisms of Antimicrobial Peptide Action and Resistance. *Pharmacol. Rev.* **2003**, *55* (1), 27–55.

Yeung, T. K.; Hopewell, J. W.; Simmonds, R. H.; Seymour, L. W.; Duncan, R.; Bellini, O.; Grandi, M.; Spreafico, F.; Strohal, J.; Ulbrich, K. Reduced Cardiotoxicity of Doxorubicin given in the Form of N-(2-Hydroxypropyl) Methacrylamide Conjugates: An Experimental Study in the Rat. *Cancer Chemother. Pharmacol.* **1991**, *29* (2), 105–111.

Yin, L. T.; Fu, Y. J.; Xu, Q. L.; Yang, J.; Liu, Z. L.; Liang, A. H.; Fan, X. J.; Xu, C. G. Potential Biochemical Therapy of Glioma Cancer. *Biochem. Biophys. Res. Commun.* **2007**, *362*, 225–229.

Zeng, X.; Li, W.; Peng, F.; Zhu, Z. Original Research Article Cloning and Characterization of a Novel cDNA Sequence Encoding the Precursor of a Novel Venom Peptide (BmKbpp) Related to a Bradykinin-Potentiating Peptide from Chinese Scorpion *Buthus Martensii* Karsch. **2000**, *38*, 207–210.

Zhai, H.; Acharya, S.; Gravanis, I.; Mehmood, S.; Seidman, R. J.; Shroyer, K. R.; Hajjar, K. A.; Tsirka, S. E. Annexin A2 Promotes Glioma Cell Invasion and Tumor Progression. *J. Neurosci.* **2011**, *31* (40), 14346–14360.

Zhang, M.-M.; Green, B. R.; Catlin, P.; Fiedler, B.; Azam, L.; Chadwick, A.; Terlau, H.; McArthur, J. R.; French, R. J.; Gulyas, J.; et al. Structure/function Characterization of Micro-Conotoxin KIIIA, an Analgesic, Nearly Irreversible Blocker of Mammalian Neuronal Sodium Channels. *J. Biol. Chem.* **2007**, *282* (42), 30699–30706.

Zhang, S.; Liu, X.; Bawa-Khalfe, T.; Lu, L.-S.; Lyu, Y. L.; Liu, L. F.; Yeh, E. T. H. Identification of the Molecular Basis of Doxorubicin-Induced Cardiotoxicity. *Nat. Med.* **2012**, *18* (11), 1639–1645.

Zhao, L.; Shi, X.; Zhao, J. Chlorotoxin-Conjugated Nanoparticles for Targeted Imaging and Therapy of Glioma. *Curr. Top. Med. Chem.* **2015**, *15* (13), 1196–1208.

A Phase I Safety and Immunogenicity Preventive Vaccine Trial Based on the HIV-1 Tat and V2-deleted Env Proteins (ISS P-002) - Full Text View - ClinicalTrials.gov <https://www.clinicaltrials.gov/ct2/show/NCT01441193?term=ISS+P-002&rank=1> (accessed Jan 19, 2016).

Glioblastoma (GBM) | American Brain Tumor Association <http://www.abta.org/brain-tumor-information/types-of-tumors/glioblastoma.html> (accessed Jan 19, 2016).

Orphanet: Glioblastome http://www.orpha.net/consor/cgi-bin/OC_Exp.php?Lng=FR&Expert=360 (accessed Jan 19, 2016).

Résumé

Les glioblastomes sont des tumeurs cérébrales qui sont extrêmement agressives, et qui, en dépit de l'arsenal thérapeutique (chirurgie, radiothérapie ou chimiothérapie), ne laissent pas plus de 16 mois d'espérance de vie aux patients. Dans le cadre de cette thèse, nous proposons d'utiliser certaines toxines en tant que vecteurs pour l'administration de médicaments anticancéreux, et notamment pour le traitement du gliome. Les travaux présentés ici se concentrent sur l'utilisation de variants de la maurocalcine (M_{Ca}) et des analogues de la chlorotoxine (CTX). La M_{Ca} est une toxine issue du venin du scorpion *Scorpio Maurus palmatus*, qui est capable de pénétrer dans les cellules facilement et rapidement. Il a été prouvé que la M_{Ca} peut entrer dans la cellule avec une cargaison. C'est en exploitant cette capacité présente chez deux de ces variants, que nous avons synthétisé avec succès deux nouveaux composés à base de cette toxine avec de la doxorubicine et un dérivé du platine. Les études de toxicité et de caractérisation de ces composés, qui ont été réalisées, ont permis de mettre en évidence l'intérêt et le potentiel de la M_{Ca}. La seconde partie de ces travaux de thèse porte sur la CTX et des peptides semblables, également extraits de venin de scorpion. Ils ont la particularité de fixer / d'interagir uniquement avec les cellules cancéreuses d'origine gliale. Après une rapide caractérisation de ces analogues de la CTX, l'un d'eux la Lqh-8/6 a été utilisé avec succès pour l'administration ciblée de doxorubicine. L'ensemble des travaux menés durant cette thèse constitue une base de départ solide pour une amélioration des systèmes de vectorisation, surtout en cancérologie de molécules actives. De plus ces résultats mettent aussi en avant l'avantage de l'utilisation d'un système de couplage « universel » basé sur la chimie click.

Mots Clés : Maurocalcine, Chlorotoxine, Chimie click, Doxorubicine, Platine, Glioblastome

Abstract

Glioblastoma are cerebral tumors that are extremely aggressive, and that, in spite of a battery of therapeutic interventions (surgery, radiotherapy or chemotherapy), leave no more than 16 months life expectancy to the patients. As part of this thesis, we propose to use some selected toxins as vectors for the delivery of anticancer drugs, and namely for the treatment of glioma. The works presented here concentrate on the use of variants of maurocalcine (M_{Ca}) and the analogues of chlorotoxine (CTX). M_{Ca} is a toxin from the scorpion *Maurus palmatus* that has cell penetrating propriety. It has been proved that M_{Ca} can enter the cell with cargoes. While exploiting this present capacity to two of these variants, we synthesized successfully two new compounds with this toxin with the doxorubicine and a by-product of the platinum. Toxicity studies and characterization of these compounds that have been made, have permitted to highlight the interest and potential of the M_{Ca}. The second part of this thesis work focused on the CTX and similar peptides, also extracted from scorpion venom. They have the particularity to fix/ interact only with cancer cell from neuroectodermal origin. After a fast characterization of these analogues of CTX, one of them (Lqh-8/6) was successfully used for the targeted administration of doxorubicin. All work conducted during this thesis constitutes a solid starting point for an improvement of the systems of vectorization of active molecules, especially in cancer research. Moreover, these results also emphasize the advantage of the use of a system of "universal" coupling based on the click chemistry.

Keywords: Maurocalcine, Chlorotoxin, Click chemistry, Doxorubicin, Platin, Glioblastoma